UNIVERSITAT DE BARCELONA

Integrative analysis of endocrine disruption in zebrafish (*Danio rerio*)

Rubén Francisco Martínez López

Integrative analysis of endocrine disruption in zebrafish (*Danio rerio*)

Rubén Francisco Martínez López

UNIVERSITAT DE BARCELONA

CSIC
CONSEJO SUPERIOR DE INVESTIGACIONES CIENTÍFICAS

FACULTAT DE BIOLOGIA
Departament de Biologia Cel·lular, Fisiologia i Immunologia
Programa: Aqüicultura (HDK1B)

Integrative analysis of endocrine disruption in zebrafish (*Danio rerio*)

Tesi presentada per

Rubén Francisco Martínez López

per optar al títol de doctor per la Universitat de Barcelona (UB)

Doctorand:

Mr. Rubén Francisco Martínez López

Firmado digitalmente por MARTINEZ LOPEZ RUBEN FRANCISCO - 43174119Z
Fecha: 2020.06.10 11:11:15 +02'00'

Supervisors:

Dr. Benjamin Cayetano Piña Capó

PIÑA CAPO BENJAMIN CAYETANO - 42974340J
Digitally signed by PIÑA CAPO BENJAMIN CAYETANO - 42974340J
Date: 2020.06.10 11:58:55 +02'00'

Dra. Laia Navarro Martín

NAVARRO MARTIN LAIA - 46629187E
Digitally signed by NAVARRO MARTIN LAIA - 46629187E
Date: 2020.06.10 13:48:02 +02'00'

Centre Superior d'Investigacions Científiques (CSIC); Institut de diagnòstic ambiental i estudis de l'aigua (IDAEA); Departament de Química ambiental

Tutora:

Dra. M. Isabel Navarro Álvarez

MARIA ISABEL NAVARRO ALVAREZ - DNI 46225760S (AUT)
Firmado digitalmente por MARIA ISABEL NAVARRO ALVAREZ - DNI 46225760S (AUT)
Fecha: 2020.06.10 20:05:13 +02'00'

Universitat de Barcelona (UB); Departament de Biologia Cel·lular, Fisiologia i Immunologia Doctoral

Barcelona, Juny 2020

FACULTY OF BIOLOGY

Department of Cell Biology, Physiology and Immunology

Doctoral programme: Aquaculture (HDK1B)

Integrative analysis of endocrine disruption in zebrafish (*Danio rerio*)

Thesis presented by

Rubén Francisco Martínez López

to apply for PhD degree by the University of Barcelona (UB)"

PhD candidate:

Mr. Rubén Francisco Martínez López

Supervisors:

Dr. Benjamin Cayetano Piña Capó **Dr. Laia Navarro Martín**

Centre Superior d'Investigacions Científiques (CSIC); Institut de diagnòstic ambiental i estudis de l'aigua (IDAEA); Departament de Química ambiental

Tutor:

Dr. M. Isabel Navarro Álvarez

University of Barcelona (UB); Department of Cell Biology, Physiology and Immunology

Barcelona, June 2020

Acknowledgments

Ha llegado el momento de escribir los agradecimientos y he de decir que casi me han resultado más difíciles que algunas partes de la tesis, más por lo que guardarme que por lo que decir. Adaptando una frase de una conocida obra… no os podré agradecer a la mitad de vosotros la mitad de lo que desearía, y lo que os agradezco aquí es menos de la mitad de lo que la mitad merecéis. Ha sido mucha gente la que me ha brindado apoyo durante este período, y quiero disculparme de antemano si me dejo a cualquier persona que crea que se merezca estar aquí y no lo está, pues ha sido un mero fallo de memoria, la cual ha estado ejerciendo un duro trabajo durante estos últimos años, y no de voluntad.

Quiero empezar los agradecimientos con Jeroni, puesto que con él empecé mi andadura en el mundo de la investigación, siendo un gran mentor y apoyo, dándome a conocer la oportunidad de desarrollar el doctorado que he terminado realizando; y también a Neus, por su inestimable ayuda con los equipos durante ese tiempo.

A la Laia i al Benjamí, per absolutament tot, no puc imaginar millors supervisors que ells. Per haver-hi depositat la seva confiança en mi per a realitzar aquest projecte, pels seus consells, ànims, formació, ajuda (no solament professional), correccions en les anades i tornades del papers (incloses àrdues argumentacions per a decidir què deixar i que llevar)... Si he acabat finalment el doctorat ha estat gràcies a tot dos! De mica en mica, s'ha emplenat la pica! Gràcies també per la seva hospitalitat (calçotada, carnaval) així com al Jordi i a la Bàrbara. Molta sort per als petitets Guim i Roc!

A Isabel, por todo su apoyo tanto como tutora como coordinadora del doctorado, así como a Josep, con las clases de prácticas, en las cuales debo inestimable ayuda tanto al anterior, como a Laura, Borja, Ignasi, Norma, Albert, Sara, Miguel…

Al Carlos, al Demetrio i al Romà, per ajudar-nos en el nostre projecte.

Gracias a Laia (HN), Pilar y Ainhoa, por ayudarme a adaptarme y ayudarme tanto durante los primeros meses en el lab. Aún recuerdo mis primeros tumbos con los tanques y los "bichos" en el estabulario. A Alejandro, siempre con una sonrisa y dispuesto a apuntarse a cualquier plan, ¡menudas pelis que hemos ido a ver!

A todos los que habéis pasado en un momento u otro por el lab para realizar sus proyectos o para ayudarnos en el nuestro (Carla, Miquel, David, Núria, ambas Astrid, Yesenia, Juliana, Luis, Chiara, Nádia, Olga, Kaouthar, Albert…).

À Morgane, non seulement pour son aide au lab, mais aussi pour être une compagne fantastique et une personne merveilleuse.

A todos y todas que habéis venido de estancia por el idaea, y aunque fuera por otros grupos, hemos estado viviendo grandes aventuras juntos (Gilberto, Andrés, Marica, Fernando, Fátima, Helene, Laia, Lukas…)

També a la Alicia i a la Elena (C), pels moments al lab, i a la Elena (O).

A Marisa y a Guti, por las charlas de pasillo y su buen humor en cualquier momento.

A Edgar, Miriam, Anderson, Cristina, Bubu…por todas las excursiones que hicimos.

A Karen, por todos y cada uno de los grandes momentos que pasamos en Port Aventura, Monserrat, las fallas, las fiestas, calçotades, aquarium…, por su alegría, optimismo y sinceridad. ¡Fue increíble!

Als meus companys de pis però sobre tot, amics, Jordi, Joan i Toni, i Xera, i també al Pujol i Clement, amb vosaltres m'he sentit sempre com a casa, heu estat la meva segona família a Barcelona. Hem viscut de tot! El mateix puc dir per la Carme i el Clement (DEP), que m'han tractat com si fossi un més de la seva família. Gràcies per tot!

Same to Roger, John (M), John (A), Brigitte, Sean and Rose, who share in Canada with me more than a room, but advices and time. A Mari Carmen y Juan Carlos, quien me acogieron en Madrid durante el curso.

To Vance, who since the start, it was like we know each other. Thanks for accepting me in the lab, for your help, advices, patience (I still remember my English oral skills during my first weeks in Canada…), all the activities with the people of the lab, and your amazing hospitality. I really enjoyed the Wayward Sound! Thanks to Leslie too!

Danke an Jan, für das Vertrauen, das er mir entgegengebracht hat, für all seine Hilfe, sogar über die Arbeit hinaus, für seine Kameradschaft, für die großartigen Momente, die wir durchgemacht haben, und auch für die sehr lustigen Momente (¡es muy bueno!), für den deutschen Unterricht (ich bin sehr verrückt!). Er war wie mein großer Bruder in Kanada. Also to Hannah, for her kindly hospitality. Best wishes for the little one, keep kicking hard the ball, Johan!

To Sue and Juan, who became instantly friends of mine, for all our shared moments: the beach, the shows, the Canada Day, the ice skating just the last day of the season (so lucky)…

Same to Dan, for all his help, sport talks, advices, shared moments and common laughs… (remember, beard is +4 in axe throwing), as well to Mais, Reem and Zeinab and their friendship.

To Marilyn, Majd and Jess, for all their help, sometimes quite early or late in the lab, as well to Devina, Mel, Alley, Christine and Tyler. Thanks also to Federico, Kim, Di, Tu, Chunyu, Amin, Paige, Mónica, Izzy, Kinan, Elie, Nha-Thi, and Lucie.

To Christine (A) and Vishal, for their big help in the aquarium. Y del mismo modo, también a Eva y a Alejandro.

Al Francesc i al Marc, no sé exactament quan vàrem començar a fer coses junts i a "unir" els nostres labs però definitivament va ser una grandíssima idea. Hem fet un caramull de coses junts: el viatge a Paris, les festes i els xurros... Merci!

A todos mis compañeros de lab, con los que hemos vivido cumpleaños (la dieta en el lab es imposible), fiestas de Navidad, viajes, birras, calçotades, fiestas varias, escolabs y csics al aula, congresos, piscolabis, cafés, descansitos… (Anna, Inma, Claudia, Eli, Ale, Bruno, Claudia (R), María, Francisco, Juliette y Mel). ¡Gracias a tod@s!

A Anna e Inma, por el apoyo mutuo que nos hemos brindado los tres, que empezando las tesis con pocos meses de diferencia y teniendo la misma edad, hemos sido como trillizos a los que han separado a cada uno en un lab diferente.

A Marta, por su inestimable ayuda, no solamente en el lab, sino en todo lo demás. Y cuando decías que eras como la madre de todos los becarios que pasaban por el lab, yo me lo tomé a broma… ¡qué sería del lab sin ti!

A Claudia, por su alegría desbordante, por su amistad y apoyo desde que empezó en el lab. ¡No he conocido aún a nadie con tanto optimismo (en el buen sentido) y que genere tan buen ambiente a su alrededor!

A Miriam, por estar a mi lado siempre en cualquier locura que le propusiera hacer (incluido lanzar hachas contra una diana), por esas pelis comiendo cotufas, por los paseos en bici a orillas del mar, los museos, la carrera en Montmeló… Por tus sonrisas, apoyo y confianza durante todos estos años, y todo lo que hemos realizado juntos. ¡Espero poder leer algún día tu novela publicada!

A todos mis amigos "de toda la vida": Jose, Gus, Luis, Philipp, Pablo, Antonio, y también a Toni, Jasón, Dani, Juanjo, Javi, Jaume, Joan Àngel, Andreu… Hemos hecho muchísimas cosas juntos, sean tanto en grupos más grandes o más pequeños (playa, partidas de todo tipo, juegos, rol, fútbol, bici, baloncesto, cuevas, excursiones…). Con algunos de vosotros

he compartido hechos y pensamientos que nadie más saben, y ninguno de vosotros me ha fallado nunca. ¡Aún nos queda mucha cuerda y mucha caña que dar!

Y, por último, a toda mi familia, tanto de Palma como de Benizar, a mis tíos (Tete Martín, Tita Vicenta, Tito Juan, Susi, Manolo), mis primos (Alba, Ana, Adrián), prima Pura, Jorge… A mis Yayas, Ana y Antonia, Tata Paquita…

Y especialmente a mi mamá, papá, y mi hermano Alex, por TODO, en mayúsculas, no tengo palabras suficientes para agradeceros todo lo que habéis hecho por mí y no puedo revelar ya nada que no os haya dicho ya. Si soy lo que soy hoy en día, ¡es gracias a vosotros! GRACIAS.

Rubén

This thesis was supported temporarily by 2016FI-B 00159 AGAUR grant from the "Generalitat de Catalunya", and by a FPU predoctoral fellow from the Spanish Ministry of Education, Culture and Sport (ref. FPU15/03332), in addition to the travelling grants EST16/00695, EST17/00830 and EST18/00001 from the same ministry.

Contents

Thesis supervisors' report

Dr. Benjamin Cayetano Piña Capó, principal investigator at the Environmental Chemistry Department at IDAEA-CSIC (Institute of Environmental Assessment and Water Research – Spanish National Research Council), and Dr. Laia Navarro Martín, postdoctoral researcher in the same department,

State that:

- The current PhD thesis' report entitled "Integrative analysis of endocrine disruption in zebrafish (*Danio rerio*)" has been performed by Mr. Rubén Francisco Martínez López under our supervision in the Environmental Chemistry Department of the Institute of Environmental Assessment and Water Research (IDAEA-CSIC).
- All the results herein presented are consequence of his research as a PhD student, in the extension and contribution exposed below.

Research contributions:

- 1) Title: "**Dose-dependent transcriptomic responses of zebrafish eleutheroembryos to Bisphenol A**"
- Authors: R. Martínez, A. Esteve-Codina, L. Herrero-Nogareda, E. Ortiz-Villanueva, C. Barata, R. Tauler, D. Raldúa, B. Piña, L. Navarro-Martín
- Citation reference: *Environmental Pollution* 243 (2018) 988–997. Impact factor (2019): 5.714, quartile Q1 (decile D1)
- DOI: 10.1016/j.envpol.2018.09.043
- Contribution: conceptualization, data curation, formal analysis, investigation, visualization, writing - original draft, writing - review & editing.

- 2) Title: "**Unravelling the mechanisms of PFOS toxicity by combining morphological and transcriptomic analyses in zebrafish embryos**"
- Authors: R. Martínez, L. Navarro-Martín, C. Luccarelli, A.E. Codina, D. Raldúa, C. Barata, R. Tauler, B. Piña

- Citation reference: *Science of The Total Environment* 674 (2019) 462–471. Impact factor (2019): 5.589, quartile Q1 (decile D2)
- DOI: 10.1016/j.scitotenv.2019.04.200
- Contribution: conceptualization, data curation, formal analysis, investigation, visualization, writing - original draft, writing - review & editing.

- 3) Title: "**Morphometric signatures of exposure to endocrine disrupting chemicals in zebrafish eleutheroembryos**"
- Authors: R. Martínez, L. Herrero-Nogareda, M. Van Antro, M.P. Campos, M. Casado, C. Barata, B. Piña, L. Navarro-Martín
- Citation reference: *Aquatic Toxicology* 214 (2019) 105232. Impact factor (2019): 3.794, quartile Q1 (decile D2)
- DOI: 10.1016/j.aquatox.2019.105232
- Contribution: conceptualization, data curation, formal analysis, investigation, visualization, writing - original draft, writing - review & editing.

- 4) Title: "**Changes in lipid profiles induced by bisphenol A (BPA) in zebrafish eleutheroembryos during the yolk sac absorption stage**"
- Authors: R. Martínez, L. Navarro-Martín, M. van Antro, I. Fuertes, M. Casado, C. Barata, B. Piña
- Citation reference: *Chemosphere* 246 (2020) 125704. Impact factor (2019): 5.108, quartile Q1 (decile D2)
- DOI: 10.1016/j.chemosphere.2019.125704
- Contribution: conceptualization, data curation, formal analysis, investigation, methodology, visualization, writing - original draft, writing - review & editing.

- 5) Title: "**Acute and long-term metabolic consequences of early developmental Bisphenol A exposure in zebrafish (*Danio rerio*)**"
- Authors: R. Martínez, W. Tu, T. Eng, M. Allaire-Leung, B. Piña, L. Navarro-Martín, J. A. Mennigen
- Citation reference: *Chemosphere* 256 (2020) 127080. Impact factor (2019): 5.108, quartile Q1 (decile D2)

- DOI: 10.1016/j.chemosphere.2020.127080
- Contribution: conceptualization, data curation, formal analysis, investigation, methodology, resources, software, validation, visualization, writing – original draft, writing – review & editing.

- 6) Title: "**Transcriptomic effects of tributyltin (TBT) in zebrafish eleutheroembryos. A functional benchmark dose analysis**"
- Authors: R. Martínez, A. E. Codina, C. Barata, R. Tauler, B. Piña, L. Navarro-Martín
- Citation reference: J Hazard Mater. 398 (2020) 122881. Impact factor (2019): 7.650, quartile Q1 (decile D1)
- DOI: 10.1016/j.jhazmat.2020.122881
- Contribution: conceptualization, data curation, formal analysis, investigation, visualization, writing - original draft, writing - review & editing.

* Impact factors has been obtained from the Journal Citation Reports (2020).
* Research contributions has been categorized following the "CRediT author statement" guidelines used by several journals [1].

And, in order to certify it, we sign the current certificate.

Barcelona, June of 2020

Dr. Benjamin Cayetano Piña Capó

PIÑA CAPO BENJAMIN CAYETANO - 42974340J
Digitally signed by PIÑA CAPO BENJAMIN CAYETANO - 42974340J
Date: 2020.06.10 14:36:17 +02'00'

Dr. Laia Navarro Martín

NAVARRO MARTIN LAIA - 46629187E
Digitally signed by NAVARRO MARTIN LAIA - 46629187E
Date: 2020.06.10 13:53:59 +02'00'

- **OTHER PUBLICATIONS:**

- Title: "**Non-targeted approaches to endocrine disruption: omics for risk assessment**"
- Authors: B. Piña, L. Navarro-Martín, C. Barata, R. Martínez
- Citation reference: *Research Signpost*, 2018: pp. 1–28. Impact factor (2019): - (book chapter)
- ISBN: 978-81-308-0576-4
- Contribution: writing – original draft, writing – review & editing.

- Title: "**Omics in Zebrafish Teratogenesis**"
- Authors: B. Piña, L. Navarro, C. Barata, D. Raldúa, R. Martínez, M. Casado
- Citation reference: *Teratogenicity Testing* (*Methods in Molecular Biology*), 2018: pp. 421–441. Impact factor (2019): - (book chapter)
- DOI: doi.org/10.1007/978-1-4939-7883-0_23
- Contribution: writing – original draft, writing – review & editing.

- Title: "**Functional Data Analysis: Omics for Environmental Risk Assessment**"
- Authors: B. Piña, D. Raldúa, C. Barata, J. Portugal, L. Navarro-Martín, R. Martínez, I. Fuertes, M. Casado
- Citation reference: *Comprehensive Analytical Chemistry*, 2018: pp. 583–611. Impact factor (2019): - (book chapter)
- DOI: doi.org/10.1016/bs.coac.2018.07.007
- Contribution: writing – original draft, writing – review & editing.

- Title: "**Assessment of endocrine disruptors effects on zebrafish (*Danio rerio*) embryos by untargeted LC-HRMS metabolomic analysis**"
- Authors: E. Ortiz-Villanueva, J. Jaumot, R. Martínez, L. Navarro-Martín, B. Piña, R. Tauler
- Citation reference: *Science of The Total Environment* 635 (2018) 156–166. Impact factor (2019): 5.589, quartile Q1 (decile D2)
- DOI: 10.1016/j.scitotenv.2018.03.369
- Contribution: data curation, formal analysis and investigation (apical and morphological endpoints of the larvae); writing - review & editing.

* Dr. Elena Ortiz-Villanueva used this publication in her doctoral thesis.

- Title: "**Developmental fluoxetine exposure in zebrafish reduces offspring basal cortisol concentration via life stage-dependent maternal transmission**"
- Authors: R. Martinez, M.N. Vera-Chang, M. Haddad, J. Zon, L. Navarro-Martin, V.L. Trudeau, J.A. Mennigen
- Citation reference: *PLoS One* 14 (2019) e0212577. Impact factor (2019): 2.776, quartile Q2 (decile D4)
- DOI: doi.org/10.1371/journal.pone.0212577
- Contribution: conceptualization, data curation, formal analysis, investigation, methodology, resources, software, validation, visualization, writing – original draft, writing – review & editing.

- Title: "**Bioconcentration and metabolic effects of emerging PFOS alternatives in developing zebrafish**"
- Authors: W. Tu, R. Martínez, L. Navarro-Martin, D.J. Kostyniuk, C. Hum, J. Huang, M. Deng, Y. Jin, H.M. Chan, J.A. Mennigen
- Citation reference: *Environmental Science & Technology* 53 (2019) 13427–13439. Impact factor (2019): 7.149, quartile Q1 (decile D1)
- DOI: doi.org/10.1021/acs.est.9b03820
- Contribution: formal analysis, investigation and methodology (miRNAs, oxygen consumption and extracellular acidification rates; benchmark doses); writing - review & editing.

- Title: "**Genetic ablation of bone marrow beta-adrenergic receptors in mice modulates miRNA-transcriptome networks of neuroinflammation in the paraventricular nucleus**"
- Authors: C.J. Martyniuk, R. Martínez, D.J. Kostyniuk, J.A. Mennigen, J. Zubcevic
- Citation reference: *Physiological Genomics* 52 (2020) 169–177. Impact factor (2019): 2.581, quartile Q2 (decile D5)
- DOI: doi.org/10.1152/physiolgenomics.00001.2020
- Contribution: formal analysis and investigation (miRNAs).

Synopsis

Understanding the mode of action of different pollutants and xenobiotics in human and wildlife is a key step in environmental risk assessment. O*mic* technologies allow the study of the global status at different biological levels (transcriptome, metabolome, lipidome...) from a holistic and integrative point of view. The *omic* data fusion and integration of the effects at these different levels is an extremely useful method to elucidate the mode of action (MoA) of the pollutants and to propose adverse outcome pathways (AOPs). In this way, the aim of this thesis is to determine molecular and phenotypical signatures of exposure of several endocrine disrupting chemicals (EDCs) on zebrafish (*Danio rerio*) eleutheroembryos, which constitutes an excellent model for endocrine disruption. Morphometric and transcriptomic (RNA-Sequencing) studies were carried out in individuals exposed to bisphenol A (BPA), perfluorooctanesulfonate (PFOS) and tributyltin (TBT). Further metabolic, epigenetic (DNA methylation and miRNAs) and lipidomic (thin layer chromatography and high performance liquid chromatography – mass spectrometry) studies were performed only in BPA-exposed individuals. Main effects of BPA included lipid metabolism disruption, yolk sac malabsorption syndrome and lipid retention (obesogenicity), visual system alteration, and estrogenicity. Some of its effects were long-term persistent and could be mediated by epigenetic mechanisms. PFOS had immunosuppressive and anorexic-like properties, it disrupted the transcription of genes related to cell adhesion molecules (CAMs), and the exposed eleutheroembryos presented muscle-skeletal alterations (scoliosis and kyphosis). Finally, TBT disrupted the transcription of genes related to steroid and cell cycle metabolism, and elicited a general developmental delay (diapause-arrest effect) in the exposed individuals. Phenotypic observations were related to their transcriptomic alterations and their proposed molecular initiation event (MIE), allowing the design of an AOP for each of the studied EDCs. Overall, this thesis shows the usefulness of transcriptomics and of data integration at different biological levels to discern AOPs and MIE, therefore contributing to a deeper comprehension of the toxicity and the mode of action of BPA, PFOS and TBT. We consider that these results can be extrapolated to understand the toxic effects of these compounds in other animals, including humans.

Sinopsis

Comprender el modo de acción de los diferentes contaminantes y xenobióticos en humanos y en la vida silvestre constituye un paso clave en la evaluación del riesgo ambiental. Las tecnologías "ómicas" permiten el estudio global de los diferentes niveles biológicos (transcriptoma, metaboloma, lipidoma...) desde un punto de vista holístico e integrado. La fusión de datos ómicos y la integración de los efectos observados a estos diferentes niveles es un método extremadamente útil para dilucidar el modo de acción (MoA) de los contaminantes y proponer "mecanismos explicativos de efectos adversos" (AOP). De este modo, el objetivo de esta tesis es determinar las firmas moleculares y fenotípicas de exposición a varios disruptores endocrinos (EDC) en eleuteroembriones de pez cebra (*Danio rerio*), el cual constituye un excelente modelo para estudiar la disrupción endocrina. Se realizaron estudios morfométricos y transcriptómicos (RNA-Seq) en individuos expuestos a bisfenol A (BPA), perfluorooctanosulfonato (PFOS) y tributilestaño (TBT). Adicionalmente, otros estudios metabólicos, epigenéticos (metilación de ADN y miRNAs) y lipidómicos (mediante cromatografía de capa fina y cromatografía líquida de alta eficacia – espectrometría de masas) se realizaron específicamente en individuos expuestos a BPA. Los principales efectos causados por el BPA incluyeron la alteración del metabolismo de lípidos, síndrome de malabsorción del saco vitelino y retención de lípidos (obesogenicidad), alteración del sistema visual y estrogenicidad. Algunos de sus efectos fueron persistentes a largo plazo y podrían estar regulados por mecanismos epigenéticos. El PFOS presentó propiedades inmunosupresoras y pseudo-anoréxicas, alteró la transcripción de genes relacionados con las moléculas de adhesión celular (MAC) y los eleuteroembriones expuestos a él presentaron alteraciones músculo-esqueléticas (escoliosis y cifosis). Finalmente, el TBT alteró la transcripción de genes relacionados con el metabolismo de esteroides y del ciclo celular, y provocó un retraso general del desarrollo (efecto "pseudo-diapáusico") en los individuos expuestos. Las observaciones fenotípicas se pudieron relacionar con las alteraciones transcriptómicas y el evento molecular de iniciación (MIE) propuesto para cada EDC estudiado, permitiendo así el diseño de un AOP específico para cada uno de ellos. En conclusión, esta tesis muestra la utilidad de la transcriptómica y de la integración de datos a diferentes niveles biológicos para la propuesta de AOPs y MIEs, contribuyendo a una comprensión más profunda de la toxicidad y el modo de acción del BPA, PFOS y TBT. Consideramos que estos resultados pueden extrapolarse para comprender los efectos tóxicos de estos compuestos en otros animales, incluidos los humanos.

Sinopsi

Comprendre el mode d'acció dels diferents contaminants i xenobiòtics en humans i en la vida silvestre constitueix un pas clau en l'avaluació del risc ambiental. Les tecnologies "òmiques" permeten l'estudi global dels diferents nivells biològics (transcriptoma, metaboloma, lipidoma...) des d'un punt de vista holístic i integrat. La fusió de dades òmiques i la integració dels efectes observats a aquests diferents nivells és un mètode extremadament útil per dilucidar el mode d'acció (MoA) dels contaminants i proposar "mecanismes explicatius d'efectes adversos" (AOP). D'aquesta manera, l'objectiu d'aquesta tesi és determinar les signatures moleculars i fenotípiques d'exposició a diversos disruptors endocrins (EDC) a eleuteroembrions de peix zebra (*Danio rerio*), el qual constitueix un excel·lent model per estudiar la disrupció endocrina. Es van realitzar estudis morfomètrics i transcriptòmics (RNA-Seq) en individus exposats a bisfenol A (BPA), perfluorooctanosulfonat (PFOS) i tributilestany (TBT). Addicionalment, altres estudis metabòlics, epigenètics (metilació d'ADN i miRNAs) i lipidòmics (mitjançant cromatografia de capa fina i cromatografia líquida d'alta eficàcia - espectrometria de masses) es van realitzar específicament en individus exposats a BPA. Els principals efectes causats pel BPA van incloure l'alteració del metabolisme de lípids, síndrome de malabsorció del sac vitel·lí i retenció de lípids (obesogenicitat), alteració del sistema visual i estrogenicitat. Alguns dels seus efectes van ser persistents a llarg termini i podrien estar regulats per mecanismes epigenètics. El PFOS va presentar propietats immunosupressores i pseudo-anorèxiques, va alterar la transcripció de gens relacionats amb les molècules d'adhesió cel·lular (MAC) i els eleuteroembrions exposats a ell van presentar alteracions músculo-esquelètiques (escoliosi i cifosi). Finalment, el TBT va alterar la transcripció de gens relacionats amb el metabolisme d'esteroides i del cicle cel·lular, i va provocar un retard general de desenvolupament (efecte “pseudo-diapàusic”) en els individus exposats. Les observacions fenotípiques es van poder relacionar amb les alteracions transcriptòmiques i l'esdeveniment molecular d'iniciació (MIE) proposat per a cada EDC estudiat, permetent així el disseny d'un AOP específic per a cada un d'ells. En conclusió, aquesta tesi mostra la utilitat de la transcriptòmica i de la integració de dades a diferents nivells biològics per a la proposta d'AOPs i MIEs, contribuint a una comprensió més profunda de la toxicitat i el mode d'acció de l'BPA, PFOS i TBT. Considerem que aquests resultats poden extrapolar-se per comprendre els efectes tòxics d'aquests compostos en altres animals, inclosos els humans.

List of abbreviations

- 5hmC: hydroxymethylated cytosine
- 5mC: methylated cytosine
- 9cRA: 9-cis retinoic acid
- α-AT: acetylated alpha-tubulin
- ADHD: attention deficit hyperactivity disorder
- ANOVA-PLS: analysis of variance – partial least squares regression
- AOP: adverse outcome pathway
- APCI: atmospheric pressure chemical ionization
- AR: androgen receptor
- atRA: all-trans retinoic acid
- BHT: butilhydrotoluene
- BL: body length
- BMD: benchmark dose
- BMDL: benchmark dose lower limit
- BMDU: benchmark dose upper limit
- BMI: body mass index
- bp: nucleotide base pair
- BPA: bisphenol A
- BPAF: bisphenol AF
- BPS: bisphenol S
- BW: body weight
- CAM: cell adhesion molecule
- CAR: constitutive androstane receptor
- cDNA: DNA copy
- CE: cholesterol ester
- CEC: contaminant of emerging concern
- Ch: cholesterol
- Cl-PFESA: chlorinated polyfluoroalkyl ether sulfonic acid
- C_p: crossing point
- C_q: quantification cycle
- C_t: cycle threshold
- DAVID: database for annotation, visualization and integrated discovery
- DBE: double-bond equivalent
- DBT: dibutyltin
- DDT: cichlorodiphenyltrichloroethane
- DEG: differentially expressed gene
- DG: diglyceride
- DHA: docosahexaenoic fatty acid
- DMC: differentially methylated CpG
- DMR: differentially methylated region
- DMSO: dimethyl sulfoxide
- dpf: days post-fertilization
- E1: estrone
- E2: 17-β-estradiol
- E3: estriol
- EC: emerging contaminant
- EC_{50}: half maximal effective concentration
- ECAR: extracellular acidification rate
- EDC: endocrine disrupting chemical
- EDTA: ethylenediaminetetraacetic acid
- EE2: 17α-ethynylestradiol
- EL: eye length
- EP: emerging pollutant
- EPA: eicosapentaenoic acid
- ER: estrogen receptor
- ERA: environmental risk assessment
- ERE: estrogen response element
- ERK/MAPK: kinase/mitogen-activated protein kinase
- ERR: estrogen-related receptor
- ESD: eye-snout distance
- ESI: electrospray ionization
- EW: eye width
- F53-B: chlorinated polyfluorinated ether sulfonate
- FBA: flux balance analysis
- FC: fold-change
- FDR: false discovery ratio
- FFA: free fatty acid
- FT-ICR-MS: Fourier transform ion cyclotron resonance – mass spectrometry
- FXR: farnesoid X receptor
- Gb: gigabase

- GC: gas chromatography
- gDNA: genomic DNA
- GH: growth hormone
- GO: gene ontology
- GR: glucocorticoid receptor
- HDL: high-density lipoprotein
- HFD: high feeding diet
- hpf: hours post-fertilization
- HPG: hypothalamus-pituitary gland-gonads axis
- HPI: hypothalamus-pituitary gland-interrenal axis
- HPLC-MS: high performance liquid chromatography - mass spectrometry
- HPT: hypothalamus-pituitary gland-thyroid axis
- HSP: heat-shock protein
- HTA: head-trunk angle
- HT-NGS: high-throughput next generation sequencing
- HW: head width
- ICP-MS: inductively coupled plasma – mass spectrometry
- IDL: intermediate-density lipoprotein
- IgG: imunoglobulin G
- IOD: inter-ocular distance
- ITIS: integrated taxonomic information system
- KE: key event
- KEGG: Kyoto encyclopedia of genes and genomes
- KER: key event relationship
- KO: knockout model
- LC_{50}: median lethal concentration
- LC-PUFA: long chain – polyunsaturated fatty acid
- LDL: low-density lipoprotein
- LOAEC: lowest observed adverse effect concentration
- LOD: limit of detection
- LOEC: lowest observed effect concentration
- LOQ: limit of quantification
- LPE: lysophosphatidylethanolamine
- LRT: likelihood ratio test
- LXR: liver X receptors
- m/z: mass-to-charge ratio
- MALDI: matrix assisted laser desorption ionization
- MAPQ: mapping qualities
- MEHP: mono-(2-ethylhexyl)phthalate
- MIE: molecular initiation event
- miRNA: microRNA
- MoA: mode of action
- mpf: months post-fertilization
- NC: normalized copies
- ND: normal diet
- NGS: next generation sequencing
- NMR: nuclear magnetic resonance
- NOAEC: no observed adverse effect concentration
- NOEC: no observed effect concentration
- NR: nuclear receptor
- OCR: oxygen consumption rate
- PAH: polycyclic aromatic hydrocarbon
- PAM: partition around medoids
- Parv: anti-parvalbumin
- PBS: phosphate-buffered saline
- PC: phosphatidylcholine
- PCA: principal component analysis
- PCB: polychlorinated biphenyl
- PC-O: ether phosphatidylcholine
- PC-P: phosphatidylcholine plasmalogen
- PCR: polymerase chain reaction
- PDB: protein data base
- PE: phosphatidylethanolamine
- PE-O: ether phosphatidylethanolamine
- PE-P: phosphatidylethanolamine plasmalogen
- PFA: paraformaldehyde
- PFAS: perfluoroalkyl substance
- PFOA: perfluorooctanoic acid
- PFOS: perfluorooctanesulfonate
- PG: phosphatidylglycine

- PI: phosphatidylinositol
- PI3K/AKT: phosphatidyl-inositol-3-kinase/AKT
- PL: phospholipid
- PM_x: particulate matter
- PoD: point of departure
- POP: persistent organic pollutant
- PPAR: peroxisome proliferator-activated receptor
- ppb: part per billion
- PPI: protein - protein interaction
- ppm: part per million
- PPP: pentose phosphate pathway
- PPRE: peroxisome proliferators response element
- ppt: part per trillion
- PS: phosphatidylserine
- PXR: pregnane X receptor
- qPCR: quantitative polymerase chain reaction
- RA: retinoic acid
- RAR: retinoid acid receptor
- R_f: retardation factor
- RIN: RNA integrity number
- RISC: RNA-induced silencing complex
- RMSD: root-mean-square deviation of atomic positions
- RMSE: root mean squared error
- ROI: region of interest
- ROS: reactive oxygen species
- RXR: retinoid X receptor
- SB: swim bladder
- SBA: swim bladder area
- SBI: swim bladder inflation
- SDS-PAGE: sodium dodecyl sulfate polyacrylamide gel electrophoresis
- SEM: standard error of the mean
- SM: sphingomyelin
- SMRT: single molecule real-time sequencing
- SSRI: selective serotonin reuptake inhibitor
- T3: thyroid hormone (triiodothyronine)
- TAE: tris-acetate-EDTA
- TBBPA: tetrabromobisphenol A
- TBP: 2,4,6-tribromophenol
- TBT: tributyltin
- TCBPA: tetrachlorobisphenol A
- TDI: tolerable daily intake
- TG: triglyceride
- TLC: thin layer chromatography
- T_m: melting temperature
- TNF: tumor necrosis factor
- TOF: time of flight
- TR: thyroid hormone receptor
- TSS: transcription starting site
- UHPLC: ultra high-performance liquid chromatography
- VDR: vitamin D receptor
- VIP: variable importance in projection score
- VLDL: very low-density lipoprotein
- WE: wax ester
- WGBS: whole genome bisulfite sequencing
- Y2H: yeast two-hybrid screening
- YS: yolk sac
- YSA: yolk sac area
- YSL: yolk syncytial layer
- ZE: zebrafish eleutheroembryos
- ZFET: zebrafish embryo toxicity test
- ZFIN: zebrafish information network
- ZMWs: zero-mode waveguides

* Gene names abbreviations are not included

List of figures

List of tables

List of text boxes

I. General introduction

"The saddest aspect of life right now is that science gathers knowledge faster than society gathers wisdom"

Isaac Asimov

I.1. Pollution and emerging contaminants

Pollution can be understood both as the introduction of a new substance into the environment and as the artificial alteration of the concentration of naturally present compounds, like the anthropogenic increase of the CO_2. The history of the anthropogenic pollution can be considered almost as long as the history of humankind at local or global scales. It probably started with soot contamination at the caves in prehistoric times [2], followed by massive forest clearance during the agricultural expansion [3–5] and heavy metal pollution due to the development of mining and metallurgy [6–8], the air and water pollution linked to the industrial revolution at 18th century [9], and, finally, the current global pollution associated to present-time industrialization, manufacturing, and transport activities. This represents a historical continuum that leads to the actual global contamination of air, soil and water bodies [10–12].

Although pollution can also be biological (pathogenic viruses and bacteria, invasive species…) or physical (noise, visual and light, thermal, and radioactive pollution), is the chemical pollution the one that currently acquire more diverse forms. Chemical contamination has been traditionally linked to inorganic elements and compounds. For example, to heavy metals (from industrial uses, mining, or electronic waste [13]), or to by-products of different combustion processes (mostly related to energy production) including several gases (NO_x, SO_x, CO, CO_2…) [14,15] and particulate matter ($PM_{0.1}$, $PM_{2.5}$, PM_{10}…) [16], which are becoming relevant pollution agents. The development of organic chemistry during the last two centuries added several large families of organic compounds (drugs, pesticides, fertilizers, plastics and microplastics, dioxins and furans, hydrocarbons, surfactants…) [17–23], which also end up in the environment, affecting the biosphere in new and unsuspected forms. Pollution has deep consequences for both health and economy. European Commission estimated in approximately 9 million the global deaths caused by total pollution in 2015 [24] while its global welfare economical losses were estimated in US$4.6 trillion per year (6.2% of global economic output) by the *Lancet* Commission on Pollution and Health [25].

Several of these organic pollutants are persistent in the environment as they resist chemical, biological, and photolytic degradation: the so-called POPs, or persistent organic pollutants. Several POPs are known to be transported through air and water [26] and to bioaccumulate and to biomagnify throughout the food chain. These bioaccumulative compounds may exert several toxic effects in the exposed wildlife, including neurotoxicity, behavioural changes, endocrine disruption, effects upon reproduction, immune dysfunction and genotoxicity [27]. Due to this potential risk for environmental and human health, their production and use have been restricted or banned in different international treaties, starting with the Stockholm Convention on Persistent Organic Pollutants in 2004, which mandates the cease or the limitation of the production of 12 POPs known as the "dirty dozen" [26]. Since then, more POPs have been added to the diverse annexes of the Convention, with different levels of restriction, which eventually include global bans.

Text box I.1.

· Bioconcentration: Process by which internal levels of a given compounds in an organism become higher than the environmental loads due to an imbalance between its passive intake (by respiration or skin absorption) and excretion rates. [28–30].

· Bioaccumulation: Similar process as bioconcentration, but including all possible routes of chemical exposure (diet, respiration, absorption…) [28–30].

· Biomagnification: Process by which the compound concentration increases through the trophic chain due to the dietary input and the accumulation in the organisms [28–30].

During the last decades, priority pollutants, including POPs, have been monitored in the environment, specifically in water bodies. Given to their known potential deleterious effects over the organisms, their modes of action (MoAs) have been well characterized. Oppositely to these "well-known villains" [31], a new group of contaminants of emerging concern (a.k.a. CECs) have arose during the last years. The categorization of a compound as "emerging" pollutant can be controversial. In general, they can be associated to two

groups: either new compounds for which no adequate toxicological data is available, or already known compounds for which either their environmental levels or toxic effects were insufficiently characterized. There are several circumstances that are fueling the growing concern for CECs. On one side, the restriction of undoubtedly toxic and hazardous chemicals results in their substitution by new compounds designed to have the same industrial properties, commonly with a lack of ecotoxicological information about their risks. In addition, the improvement of analytical chemistry technologies pushed the levels of detection of many CECs in the range of part per trillion (ppt) (ng/L) or even pg/L, allowing the monitoring of harmful chemical compounds that were certainly known but that remained undetected due to their low concentration. Finally, there is a growing list of pollutants already known to be environmentally present, but for which new information about their ecotoxicological risks, effects, or mode of action as xenobiotics is being discovered [31–34].

Text box I.2.

· POPs: persistent organic pollutants. Organic chemicals resistant to environmental degradation (chemical, biological or photolytic) which exert adverse impacts on exposed individuals [26].

· Contaminants of emerging concern (CECs) or emerging pollutants (EPs) / contaminants (ECs): pollutants of all chemical nature that have been recently detected in the environment or for which new adverse effects have been recently described [31–34].

· Xenobiotic: non-natural chemical present within an organism, or a natural one in much higher concentrations than physiological levels.

All these sets of compounds' classifications are not mutually exclusive and a specific chemical can be categorized or not at the same time as POP, CEC… considering its properties. Regardless that, xenobiotics exert a huge variety of effects, at different biological levels, in the organisms exposed to them [35] (see figure I.1.). The study of these adverse effects is a main subject of the modern environmental toxicology.

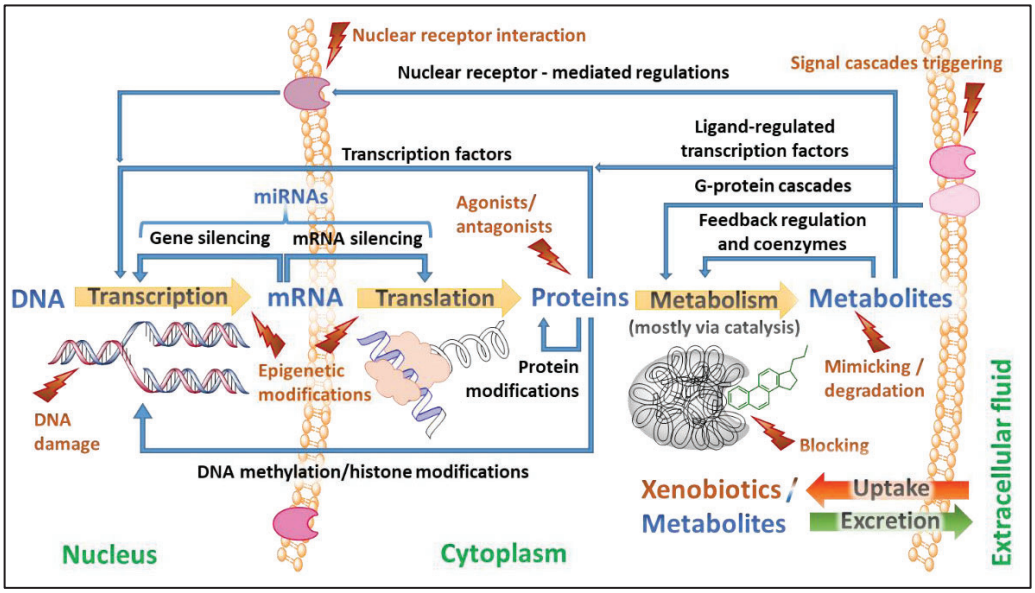

Figure I.1. (adapted from [36]): central dogma of biology including main regulatory mechanisms. Possible effects of xenobiotics (at different biological levels) are marked with a brown lightning. The environmental risk of a xenobiotic will mainly be determined by its concentration, its toxicity/mode of action, and its persistence/chemical reactivity/biodegradability.

I.2. Environmental toxicology and risk assessment

Text box I.3.

· Environmental toxicology: multidisciplinary science that mainly focuses on the effects assessment of pollutants at organismal, organ, tissue, cell, organelle and biochemical pathway levels ("from organism to below") [37,38].

· Ecotoxicology: multidisciplinary science that mainly focuses on the effects of the pollutants on individual organisms, species, populations, communities and ecosystems ("from organism to above") [37,38].

· Environmental risk assessment (ERA): multidisciplinary science that not only studies the mode of action of xenobiotics in the living organisms and their dose-response adverse effects, but also the environment biomonitoring of the pollutants, the assessment of all possible hazards derived from the contamination (at the wildlife, human, economic... levels), the implementation of legal safe benchmark doses, and the identification of preventive and remediation measures (to avoid or remediate the detrimental effects of a possible contamination, respectively) [39–41].

Environmental toxicology is the multidisciplinary science that study all these adverse effects of the pollutants, or of their mixes, on the living organisms. Environmental toxicology and ecotoxicology terms are often confused and equally used, although a main difference is accepted to exist between them (see box I.3.). Environmental toxicology is considered a relatively new field that is receiving particular public attention since the publication by Rachel Carson of the book *Silent Spring* [42,43]. It constitutes a substantial part of the environmental risk assessment (ERA), which includes all the steps in the hazard identification, risk characterization (MoAs, environmental levels, etc.), risk management and communication plans [39].

Xenobiotics usually exert their effects through their interaction with one or more biological targets. For example, endocrine disruptors are known to interact with different nuclear receptors [44]; some psychotic drugs, like selective serotonin reuptake inhibitors or SSRIs, interact with neurotransmitter receptors and/or transporters [45]; and several genotoxic chemicals bind to DNA either covalently or non-covalently [46].
The first interaction of a xenobiotic with the organism at molecular level is the so-called molecular initiation event (MIE), which triggers different signalling cascades and alterations in several biological or physiological levels (key events or KEs) [47] that ultimately lead to a specific adverse outcome.

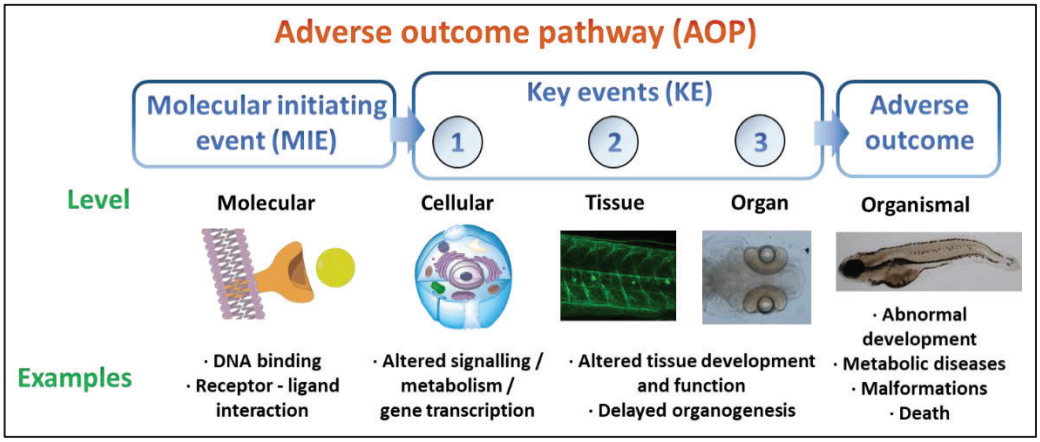

Figure I.2. (based on [48,49]): general scheme of an adverse outcome pathway framework. Zebrafish larvae images (5 days post fertilization) are used in the examples.

Once these KEs, together with their relationships (KER), are strongly supported by several evidences, they may be further structured into an adverse outcome pathway (AOP) [47]. AOP is a framework that explains the mechanism of action of a given xenobiotic, including all the sequence of events from the MIE, the propagation of the signalling cascade across the affected pathways, up to all adverse outcomes across the different organization levels [47,50] (figure I.2.). The comprehension of the AOP of a xenobiotic is extremely useful in environmental risk assessment and its adequate regulation [51].

Text box I.4.

· Adverse outcome pathway (AOP): "conceptual construct that portrays existing knowledge concerning the linkage between a direct molecular initiating event and an adverse outcome at a biological level of organization relevant to risk assessment" [51].

· Key event (KE): "An alteration in biological or physiological state that is essential to the progression of a perturbation leading to a specific adverse outcome" [48].

· Key event relationship (KER): causal and predictive linkage between one key event to another. It describes the likelihood and conditions by which a particular KE trigger the next KE [52,53].

· Molecular initiating event (MIE): "initial interaction between a molecule and a biomolecule or biosystem that can be causally linked to an outcome via a pathway" [50].

The characterization of the consequences of exposure to pollutants can be based either in qualitative and quantitative observations of macroscopic phenotypes (to determine KEs and adverse outcomes), or in metabolic measurements and targeted biochemical determinations of different biomolecules (for MIE and KEs). Classical phenotypic parameters include lethality, weight, length, reproductive impairment and morphological deformations in adults and hatching, teratogenesis, and delays in development for developing embryos. In fish embryos, specific parameters include timing of swim bladder inflation, edemas, heartbeat, and others [54,55]. Metabolic and

molecular markers of toxicity include changes in metabolic rate, feeding or blood parameters, and alterations in protein and metabolite levels, in transcript abundance, in enzyme activities, and in the endocrine systems.

Determination of these biomarkers that serve as warning indicators of exposure to certain pollutants has been extremely useful for environmental toxicology [56,57]. Nevertheless, the discovery of specific biomarkers for each pollutant has been traditionally a slow and meticulous process when the MoA of the xenobiotic is unknown. The common approach consists on linkages between qualitative and quantitative observations of phenotypes of exposed animals or humans and biochemical characteristics that would be consequently identified as biomarkers. The complexity of the identification of mechanisms of action for each pollutant, and the extremely large number of metabolic pathways, genes, proteins… makes the selection of potential biomarkers of exposure difficult for the environmental agencies. For that reason, hazard testing is based in rather general adverse effects complemented with a limited number of specific toxicological endpoints. For example, the OECD test guideline nº 236 (zebrafish embryo toxicity test; ZFET [58]), widely used for acute toxicity testing, adds to the standard LC_{50} determination four specific indicators of lethality: coagulation of fertilized eggs, lack of somite formation, detachment of the tail-bud from the yolk sac, and heartbeat. The median lethal concentration (LC_{50}), or the concentration required to kill 50% of exposed individuals after a specified time [59], has been traditionally used to evaluate the toxicity of different compounds due to its simplicity, and the possibility to compare pollutants with very different mechanism of action. Although LC_{50} is still very useful to characterize the acute toxicity, other specific effects are also tested (using different model organisms) by several guidelines as the OECD test guideline nº 234 for sexual development [60], nº 424 for neurotoxicity [61], nº 451 for carcinogenicity [62], nº 493 for estrogenicity [63], or nº 456 for effects on steroidogenesis [64].

Nevertheless, the “targeted” design of these macroscopic and metabolic phenotypic assays limits the spectrum of toxic effects that can be covered. This can make the estimation of the mechanism of action of the pollutant difficult, since some toxic effects

could be overlooked if they occur at some biological level non-considered in the assays. In addition, these assays may not be adequate to characterize the biological effects at low environmentally relevant concentrations. At this point, the use of integrative and untargeted assays covering a wider range of endpoints at different biological levels could be considered as a milestone in environmental toxicology, especially with the development of non-targeted, high-throughput (a.k.a. *omic*) technologies [36,65] (see section I.6.). In this way, they are excellent approaches to study and characterize the AOP of a xenobiotic [36], including KEs and MIE. Although further targeted studies are usually required to truly confirm the key events [66], it extremely facilitates the multi-scale assessment of the environmental risks derived from the exposure to xenobiotics.

Text box I.5.

· Targeted analytical method: a method in which the number of biological measured molecules are limited (usually in the order of tens of molecules). These molecules are pre-selected and their biochemical information is known (for example, the chemical structure in case of metabolites or lipids, or the sequence in case of genes or transcripts). In a targeted study, all information about non-pre-selected biomolecules is lost although the sensitivity of the measured ones can be increased compared with an untargeted method.

· Untargeted analytical method: a method in which nearly the totality of a certain type of biomolecules present in the samples are measured. This usually represents tens to hundreds of metabolites [67,68], hundreds of lipid species [69], hundreds to thousands of proteins [70], or tens of thousands of transcripts and genes [36,71,72]). The complexity of the obtained data requires a highly-extensive computational processing although it allows to detect both known and unknown molecules.

· Semi-targeted analytical method: in this case, a high-throughput methodology is used, obtaining the complete raw data of both known and unknown samples. Nevertheless, for simplicity, only the information of known pre-selected molecules are extracted. This strategy is usually performed in lipidomics and metabolomics [73–75] and, based on the analysis depth, it allows the determination of a number of biomolecules between one order below or the same order of magnitude that an untargeted method.

A wide knowledge about all the biological levels of the studied species is essential to perform a proper functional analysis and AOP prediction of toxicological data (particularly from *omic* datasets). For that reason, environmental toxicology usually perform their assays in mice (*Mus musculus*) [76–78], or in zebrafish (*Danio rerio*) and their embryos [79–81] (see I.4. section) to determine MoA and draw AOPs for emerging pollutants. These species rank among the ones with better characterized and annotated genome, and for which more information about the transcriptome and the metabolome are available. In addition, the possibility to link xenobiotics' effects and molecular functions across species and to humans increased enormously the utility of these model animals.

I.3. Endocrine disruption and obesogenicity

Both xenobiotics and their biotransformation-derived metabolites (mostly via cytochromes P450 [82]) can exert an enormous spectrum of effects in the exposed organisms. Among them, endocrine disrupting chemicals (EDCs) are particularly relevant as they are able to dysregulate the endocrine system, which includes all the biological pathways that regulates the biosynthesis, release and homeostasis of endogenous hormones. This negative effects can be brought about by a number of different mechanisms, being one of special concern the ability of many EDCs to mimic, inhibit or interfere with the action of natural hormones [83]. EDCs may be very structurally diverse, as compounds like organochlorines, polybrominated flame retardants, perfluorinated substances, alkylphenols, phthalates, pesticides, polycyclic aromatic hydrocarbons, solvents, and some metals were shown to have endocrine-disrupting properties [84]. In turn, the phenomenon of endocrine disruption can affect many different physiological activities, presenting properties and provoking effects/disorders as estrogenicity; androgenicity; obesity, and lipid and adipogenesis dysregulation; thyroid dysregulation; steroid-related pathways alteration; infertility; developmental problems; and several metabolic syndromes [84].

EDCs effects in the endocrine system have been reported not only as metabolism alterations and disorders in studied animals, but also in human epidemiological studies [84,85]. As specific examples of putative EDC effects in humans, bisphenol A (BPA) exposure has been linked to obesity and diabetes [86]; organophosphate pesticides to cognitive and behavioral deficits [87]; PCBs (polychlorinated biphenyls) to neurodevelopmental problems [88]; some phthalates to reproductive disorders [88]; perfluoroalkyl substances (PFASs) to fetal growth delays and immunosuppression [89]; and brominated flame retardants to lower IQ and increased attention deficit hyperactivity disorder (ADHD) [88]. It has been also postulated that the exposure to some endocrine disruptors increased the incidence of some types of cancer [88].

Classically, the mode of action of the EDCs has been attributed to their binding with nuclear receptors (NRs) related with the endocrine system, as androgen receptors (ARs), estrogen receptors (ERs), estrogen-related receptors (ERRs), pregnane X receptors (PXRs), glucocorticoid receptors (GRs), retinoid X receptors (RXRs), thyroid hormone receptors (TRs), peroxisome proliferator-activated receptors (PPAR), constitutive androstane receptors (CARs) or farnesoid X receptors (FXRs) [90,91]. At the time of the discovery of these nuclear receptors, most of their endogenous ligands were unknown and they were categorized as “orphan receptors” [65]. After the binding of an EDC to a nuclear receptor, it can act as a total or partial agonist or as an antagonist of the receptor, depending on whether the physiological response is the same or the opposite effect of the natural endogenous ligand(s). Nevertheless, although this is the most common and well-known mechanism of EDCs, they are also other MoAs that potentially lead to endocrine disruption [90,92–94] as: 1) interference with the biosynthesis, transport and/or elimination of the natural hormones; 2) direct disruption of the enzymes’ action; or 3) deregulation of the NRs transcription, increasing or decreasing in this way the concentration of nuclear receptor sites, a MoA that can be mediated via epigenetic mechanisms.

Regardless of the MoA, the exposure to endocrine disruptors is a matter of concern, especially when occurring during sensitive time windows, like early developmental

stages, when several systems are still forming. It has been proposed that some of the consequences of exposure to EDC can be transmitted not only later in life but even inter/transgenerationally via epigenetic mechanisms [85,90,95].

Among the several alterations in the metabolism, behaviour, neural system and others induced by EDCs, those related with the lipid metabolism are of particular interest [96]. It has been reported that some EDCs can disrupt energy metabolic homeostasis, lipid accumulation, the adipose tissue and even the appetite and satiety in fish, rodents and humans [90,95,97]. These EDCs are called obesogens, a group of compounds that can exert lipid accumulation or induce obesity, regardless of their exact phenotypic manifestations (see text box I.6.). These different observed phenotypes rely in the different MoAs, receptor interactions, etc., exerted by each obesogen.

Text box I.6. (adapted from [98]): possible phenotypic manifestation of obesogens

· Increased number and/or size of adipocytes (fat cells that store energy as lipids: mainly triglycerides and cholesterol esters).

· Decreased energy expenditure: reduced basal metabolic rate, movement…

· Altered energy balance: increased adipogenesis and/or decreased lipolysis.

· Increased body weight and/or body mass index.

Classical phenotypic manifestations of humans exposed to obesogens are increased body weight and hunger, decreased satiety and other disorders related with obesity as type 2 diabetes, high blood pressure or increased risk of heart diseases [95,99,100]. In the aquatic crustacean *Daphnia magna*, the considered obesogen tributyltin (TBT) exert the accumulation of triacylglycerols in adults and impairment of their transfer to the eggs [101]. Similar accumulation of triacylglycerols were observed in the liver of exposed zebrafish [102]. In mammals, as rats and mice, exposure to different obesogens lead to higher body weight (both in adults and in their offspring), decreased mobilization of fat depots under fasting conditions, increased adiposity and food consumption [99,103–106]. Studies in zebrafish, a novel preferred animal model in ecotoxicology, reported

several endpoints; for example: TBT seems to increase adipocyte differentiation in zebrafish larvae and modulate the gene expression of key lipid metabolism' transcripts in liver and brain of chronic developmental exposed adults [102,107]; halogenated-BPAs (TBBPA and TCBPA) induced lipid accumulation in larvae and weight increase in juveniles [108]; and phthalates, triclosan and perfluorinated compounds reduced metabolic rate in embryos, and stimulates adipogenesis and increases the adipose tissue in larvae [109].

Regarding the key events that characterize the obesogens, it has been proposed that most of them act through the activation of the nuclear peroxisome proliferator activated receptors (PPARs) [94], which are key regulators in several processes related with lipid metabolism [110] and to be activated naturally by lipophilic hormones, fatty acids, and their metabolites [94]. Regardless of their involvement in different aspects of the lipid metabolism [111–114], the different isoforms of PPAR (PPAR-α/β/ϒ) form heterodimers with the 9-cis retinoic acid receptor (RXR) to become functionally active. The activation of PPAR-ϒ/RXR complex seems to be the master regulator of adipogenesis [94], as it binds to the peroxisome proliferators response elements (PPREs) in several target genes (apolipoproteins among them) to regulate their transcription [94,115,116]. The activation of PPAR-ϒ/RXR complex leads the increase of transcripts that encode for several apolipoproteins, therefore increasing the levels of lipoproteins after binding to different phospholipids [117], as it has been shown in different model organisms [113,118,119]. A general overview is shown in figure I.3.

Lipoproteins encapsulate neutral lipids as triglycerides or cholesterol esters. They present several physiological roles [120] that are at least partially related to their density: high-density lipoproteins (HDL), intermediate-density lipoproteins (IDL), low-density lipoproteins (LDL) or very low-density lipoproteins (VLDL). Nevertheless, their main biological function is to transport lipid molecules through the plasma to the different organs and tissues of the organism. They also play a key role at different developmental stages of development. For example, in fish embryos and eleutheroembryos, when endogenous feeding is still taking place, the production and secretion of lipoproteins by the yolk syncytial layer (YSL; membrane that enclose the yolk

cell) is essential for the transport of the yolk lipids to the rest of the organism and their utilization [121,122]. This function has been conserved among different fish species [117]. In adult stages, lipoproteins mainly transport the lipids either obtained in the digestive tract from the diet (exogenous pathway) or synthetized in the liver (endogenous pathway) [123]. Obesity has been related to a deregulation in apolipoproteins that could regulate the satiety, decreased levels of high-density lipoproteins (the ones that contain high levels of protein and low levels of triglycerides) and increased levels of low-density lipoproteins (low levels of protein and high levels of triglycerides) [123,124].

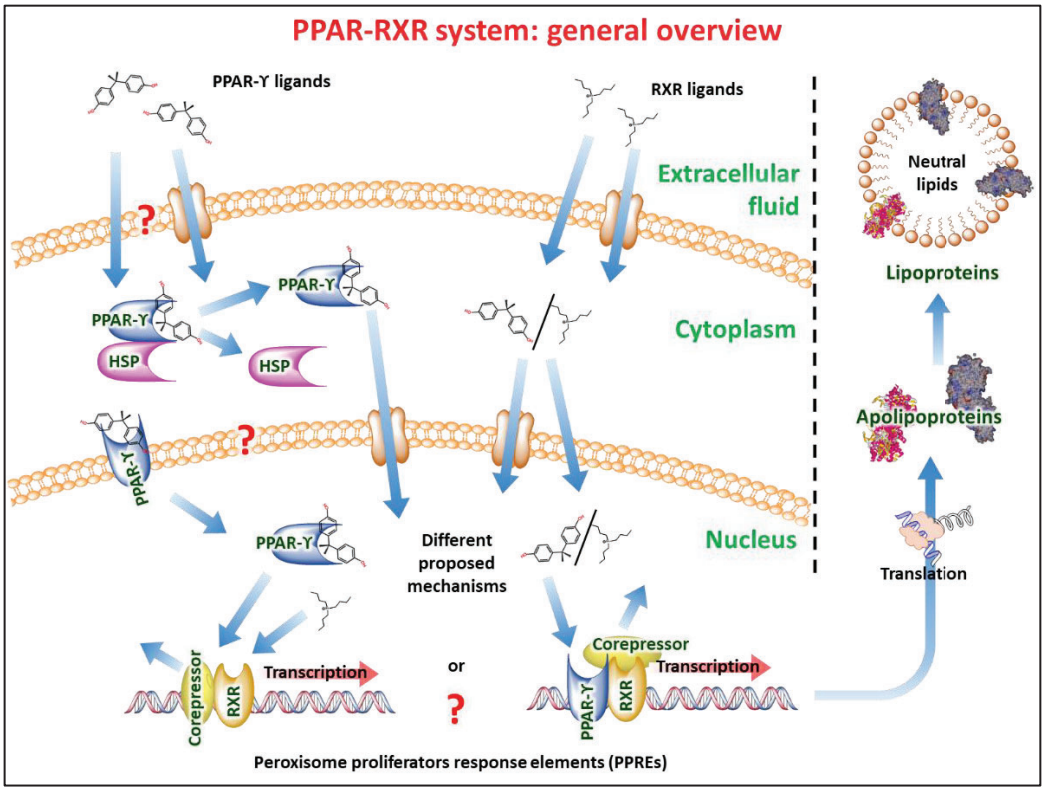

Figure I.3.: general overview of the action of PPAR-RXR system in the proliferation of lipoproteins. Proteins are named in green. HSP: heat-shock protein. Interrogation marks indicate different possible transport and mechanisms of ligands and receptors.

Among the different animal models, zebrafish (*Danio rerio*) is becoming a wide used option in ecotoxicology in the study of endocrine disruption (as exposed in section I.4.). MoAs and relevant KEs have bend defined in zebrafish for many potential EDCs, including perfluorooctanesulfonate (PFOS), 17α-ethinylestradiol (EE2), methoxychlor, endosulfan, heptachlor, DDT, bisphenol A (BPA), tetrabromobisphenol A (TBBPA), 2,4,6-tribromophenol (TBP), tributyltin (TBT), octylphenol, nonylphenol, several polycyclic aromatic hydrocarbons (PAHs), mono-(2-ethylhexyl)phthalate (MEHP) [125]… among others. Characteristically, toxicological data from zebrafish can be usually generalized to other vertebrates, including humans. The main endocrine system of zebrafish is shown in figure I.4.

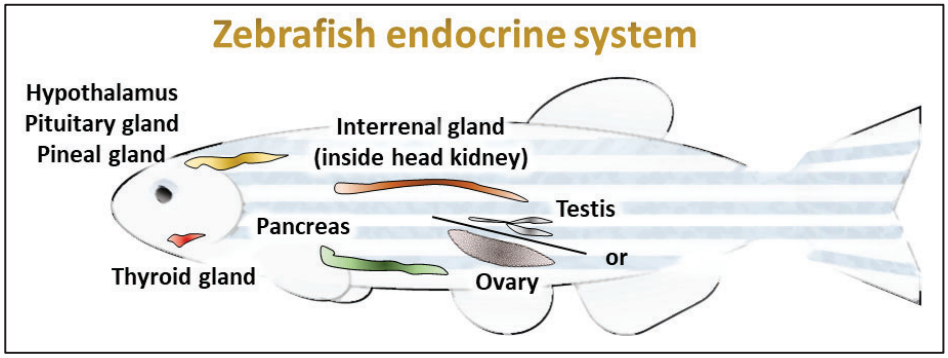

Figure I.4. (modified from [125]): zebrafish endocrine system. Although hypothalamus-pituitary gland-thyroid (HPT), hypothalamus-pituitary gland-gonads (HPG), and hypothalamus-pituitary gland-interrenal (HPI) axes represent the main targets of EDCs, other systems can be targeted [90].

I.4. Zebrafish as model organism

The choice of an appropriate model organism in environmental toxicology is a crucial step, as the lack of information and references can trigger additional difficulties during data processing and functional interpretation of the results. For example, *de novo* assembly is much more demanding that mapping against a reference sequence [126], and functional annotation of deregulated genes is much easier if the reference genome is annotated in functionally-oriented databases as GO (http://geneontology.org/) or

KEGG (https://www.genome.jp/kegg/) [127]. In addition, the use of a well-characterized model allows extrapolating the observed effects to other species, including humans. Taking that into consideration, as previously mentioned, zebrafish represents an excellent animal model for this purpose.

Zebrafish (*Danio Rerio*), first described by Francis Hamilton at 1822 [128], is an small freshwater teleost fish (adults of 3 - 5 cm and embryos of 3.5 - 4.0 mm) and natural of South Asia, that has been used in research since 80s and represent one of the most studied vertebrate animal models.

Text box I.7.

The taxonomic classification of zebrafish (*Danio Rerio*), retrieved (27/01/2020) from the Integrated Taxonomic Information System (ITIS) (http://www.itis.gov) is the next:

- Kingdom: Animalia
  - Subkingdom: Bilateria
    - Infrakingdom: Deuterostomia
      - Phylum: Chordata
        - Subphylum: Vertebrata
          - Infraphylum: Gnathostomata
            - Superclass: Actinopterygii
              - Class: Teleostei
                - Superorder: Ostariophysi
                  - Order: Cypriniformes
                    - Superfamily: Cyprinoidea
                      - Family: Cyprinidae
                        - Subfamily: Danioninae
                          - Genus: Danio
                            - Species: Danio rerio

Its use in environmental toxicology (as well as in other fields as medical research) has been extremely increased during these last decades due to great advantages as:

1) Zebrafish genome is totally or almost totally characterized, and it has been studied at many *omic* levels as genomics [129], epigenomics/epigenetics [130], transcriptomics [131,132], proteomics [133,134], metabolomics [135,136], lipidomics [74], glycomics [137], interactomics [138], morphometrics [139,140] and even proposed for fluxomics [141].

2) Its rearing and manipulation are effortless, due to its small size, allowing its aquatic facilities to be more cost-affordable, compact, and efficient.

3) Their large offspring (usually in the range of 150-250 eggs per female [142,143]) and relatively short life cycle (see text box I.8.), allow to feasibly obtain high number of replicates and to reasonably easily perform inter/transgenerational studies.

4) Even taking into consideration that zebrafish is not a mammal, their biological systems are very similar to human ones, allowing the extrapolation of the results and being considered as a model organism for several levels. As example, zebrafish is considered as an animal model for endocrine disruption [144,145], lipid metabolism [146], epigenetic mechanisms [130], general and environmental toxicology [58,79,147,148], and it shares the 70% of genes with humans [149].

5) Several knockout models (KO) has been generated [150–152]. This technique has been applied in the study of many pathologies in clinical research, and in the determination of MoA of different xenobiotics in environmental toxicology.

6) Transparency of zebrafish larvae allows the non-invasive live observation of the internal organs and of their morphometrics [130,140].

Text box I.8.: zebrafish developmental stages

· Zebrafish individuals are considered as embryos while they remain inside the chorion [153–155]). After hatching, between 48 and 72 hpf [156–160], remain as free swimming, non-feeding embryos, the so-called eleutheroembryo stage, during which swim bladder inflates (4-5 dpf) [159,161]. Yolk sac gets completely resorbed at 5-6 dpf, when the animal starts exogenous feeding, being therefore considered as early larvae [156,159].

· Zebrafish larvae suffer “metamorphosis processes” by which some of their organs develop to the “adult structure” between 15 and 30 dpf [156,159,162,163], being considered as juveniles [159–161].

· Zebrafish juveniles continue to growth and are considered as totally functional adults when they are able to have offspring, approximately at 3-4 months after fertilization [158–161]. Zebrafish adults can live usually up to 2-3 years [160].

Comparing the general use of zebrafish as animal model during the last 5 years to other species used in environmental toxicology as *Daphnia* or fish key species proposed by OECD [164], zebrafish achieves the highest number of scientific publications (based on Scopus -https://www.scopus.com/-): approximately 3400 per year. Their use is still far behind the numbers achieved by mice (*Mus musculus*; approximately 80000/y), largely and traditionally employed in drug development and pre-clinical assays, although the relative tendencies of their use seemed to be in opposite direction: for first time since 90’s, the number of scientific publications on *Mus musculus* during past year (2019) was smaller than the previous year, while scientific publications on zebrafish is rapidly increasing (figure I.5.).

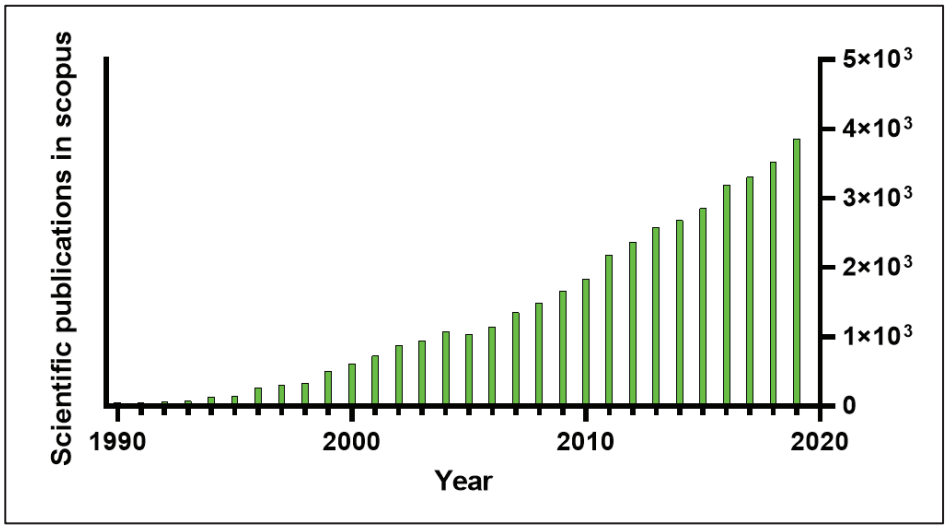

Figure I.5.: total number of scientific documents (published per year) containing in the title, in the keywords or in the abstract, the terms zebrafish and/or *Danio rerio*. Based in Scopus document search (-https://www.scopus.com/-).

In summary, zebrafish is becoming a preferred animal model for experimentation, and specifically for environmental toxicology [79–81]. The Zebrafish Information Network (ZFIN; https://zfin.org/) has been stablished as a "central repository […] for zebrafish genetic, genomic, phenotypic and developmental data" [165].

I.5. Epigenetic mechanisms

Epigenetics studies the heritable changes that do not involve DNA sequence modifications. Although epigenetics can study any heritable phenotypic change, it mainly focuses on the mechanisms by which gene activity and expression are regulated. These epigenetic mechanisms can take place before the transcription (pretranscriptional regulations, as DNA methylation or histone modifications) or after it (posttranscriptional regulations, as miRNAs expression) [166,167].

These are not only the main mechanisms by which the cells of an organism (which contain exactly the same genetic material) are able to present an extremely different characteristics at all biological levels (functions, shapes, sizes, gene expression, metabolites and protein amount…), but they also play a key role in the inheritance of this information allowing indeed the cellular differentiation and their "cellular memory" [168]. In addition to this somatic epigenetic inheritance, spontaneous and environment-related epigenetic changes have been proposed to occur [169]. Environmental factors such as temperature, stress and nutrition or even exposures to certain xenobiotics are known to mediate epigenetic changes [169,170]. Indeed, these epigenetic changes contribute to the phenotypical plasticity that allow the organisms to better adapt to certain environmental conditions. In the last decades, researches have described a new concept named toxicoepigenetics to refer to the study of epigenetic mechanisms responsible of toxicological effects [65,171–173]. It has been proposed that modifications in the epigenome during exposures to xenobiotics are responsible, not only for the effects later in life when organisms are not exposed to xenobiotics any longer (so called long-term effects), but also for inter- and trans-generationally inherited

effects, affecting the next and unexposed generations of individuals [130,170,174,175]. For example, epigenetic effects are involved in the transgenerational inheritance of obesogenic properties in rats [176] or in heart disorders in zebrafish [177], both due to an exposure to bisphenol A (BPA). For that reason, it has been suggested the use of "epigenetic footprint" as a tool to evaluate the exposure of a given organisms to toxicants [65].

Text box I.9.

· Inter- and trans-generational effects: those effects caused by different sources (stress, xenobiotic exposure…) mediated by one or more epigenetic mechanisms that affect the offspring of the exposed individuals. While intergenerational effects take place when the environmental exposure of first generation (F_0) exerts a direct effect in the germinal cells that will become the offspring (F_1), transgenerational effects are truly inherited across generations, being transmitted to F_2, F_3 or even more [175,178].

I.5.1. miRNAs

MicroRNAs (miRNAs) are small non-coding RNAs (with a usual length of 22 nucleotides) that inhibit the expression of specific transcripts (mRNAs) by binding to certain regions in their sequence [179]. The miRNA-mRNA union usually starts with an exact base complementary of 8, 7 or 6 bases (called 8mer, 7mer, and 6mer, respectively) [180]. In animals, a relatively high number of miRNAs are high conserved and a full factorial pattern between miRNAs-mRNAs can be observed: a specific mRNA can be inhibited by several miRNAs at the same time, having different binding regions; and a specific miRNA can bind to more than one mRNA.

When they attach to an mRNA, they cannot only repress their translation initiation by inhibiting the assembly with 80S complex in the ribosome, by promoting mRNA deadenylation or by other mechanisms [181], but they also trigger the degradation of the mRNA by forming the RNA-induced silencing complex (RISC) with the *argonaute* protein, which cleaves the mRNA.

Inter/transgenerational inheritance via miRNAs can be exerted via the parental deposition in the gametes, regulating the expression of certain transcripts at crucial early developmental stages. In addition, other epigenetic mechanisms may regulate the expression or maturation of the different pri-miRNAs [182–184]. Injection of miRNA has been used to assess the modification of gene expression during the first developmental stages, and the technique has been even proposed as possible therapy [185–187]. General overview of miRNA synthesis and action is shown in figure I.6.

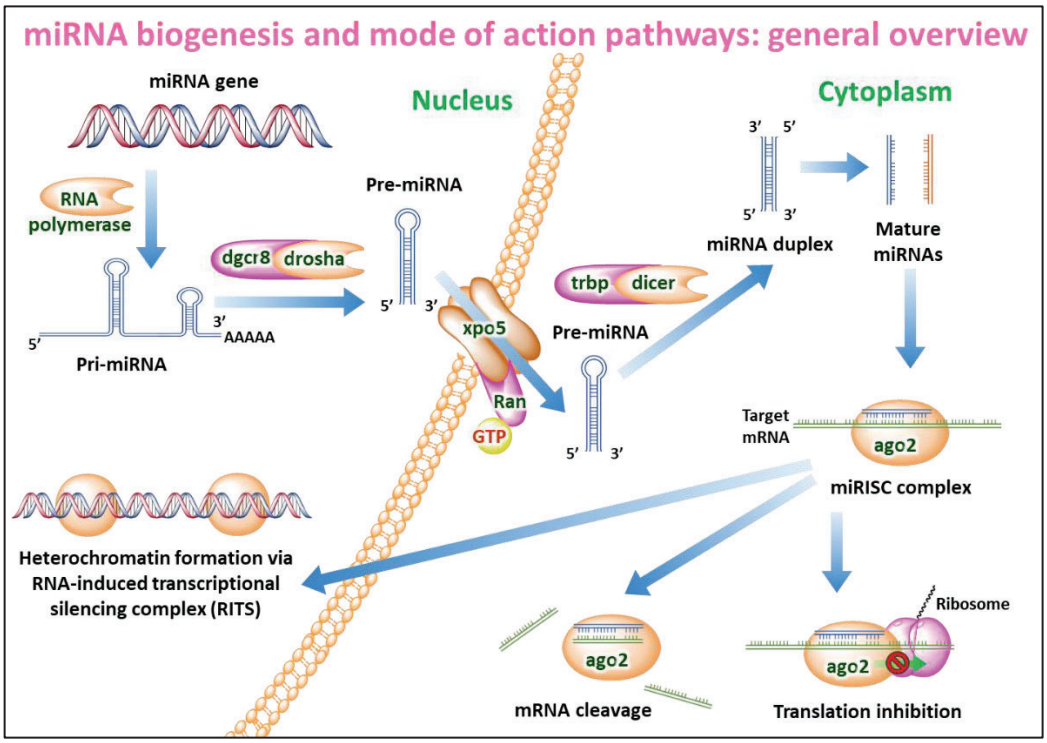

Figure I.6.: general overview of the biogenesis and mode of action of miRNAs. Enzymes are named in green. miRISC: miRNA-containing RNA-induced silencing complex.

I.5.2. DNA methylation

DNA methylation, which take place in the carbon 5 of the pyrimidine ring of cytosines (by DNA methyltransferases or DNMTs), can regulate DNA transcription. In mammals and zebrafish, this methylation mostly take place in the CG dinucleotides [188,189] (CpG

sites) constituting the “CpG Islands” when their frequency at certain genome region is notably high. Methylation mostly interferes with the binding of transcription factors in the promoter regions of the genes, which usually comprise 100-1000 base pairs and are placed close upstream to the transcription starting sites (TSSs) of its gene. Thus, the binding is inhibited and indeed, the transcription. In addition, highly methylated regions can also promoting their packaging and compacting, preventing in this way the access to them by polymerase [188,190]. The methylation level of the promoter and/or its surroundings and the gene expression are consistently inversely correlated [191].

Some compounds can trigger different methylation status at the DNA of several organisms [192]. For example, it has been reported that BPA exposure can change the methylation levels of zebrafish embryos, and of brain and testis in rats [193–195]. Toxicoepigenomics frequently takes advantage of the whole genome bisulfite sequencing (WGBS) to detect differentially methylated regions (DMRs) induced by the exposure [171,196] (see section II. Methodology). The transgenerational inheritance of DNA methylation status is other key point to be highlighted. It has been reported that in some organisms, like mammals, several reprogramming windows take place in germlines, allowing a totally new methylation status in the next generation. Thus, these processes of global erasure and re-establishment of the methylation should not allow toxicoepigenetic inheritances via DNA methylation. Conversely, it has been reported that the germline of other organisms, like zebrafish, does not suffer a global genome erasure of DNA methylation during development [197] so examples of epigenetic transmission via DNA methylation could be expected in zebrafish exposed to different environmental stressors.

Nevertheless, toxicoepigenetic inheritances via DNA methylation take place both in mammals and zebrafish [174,198–200]. For those organisms where global erasure and re-establishment of the methylation take place, it has been proposed that complex mechanisms allow certain sequences to resist these waves of reprogramming (as the imprinting marks). In this way, they can act as the “carriers of epigenetic information across generations, leading to transgenerational epigenetic inheritance” [169,201,202].

I.6. Integrated assays and *omic* technologies for environmental toxicology

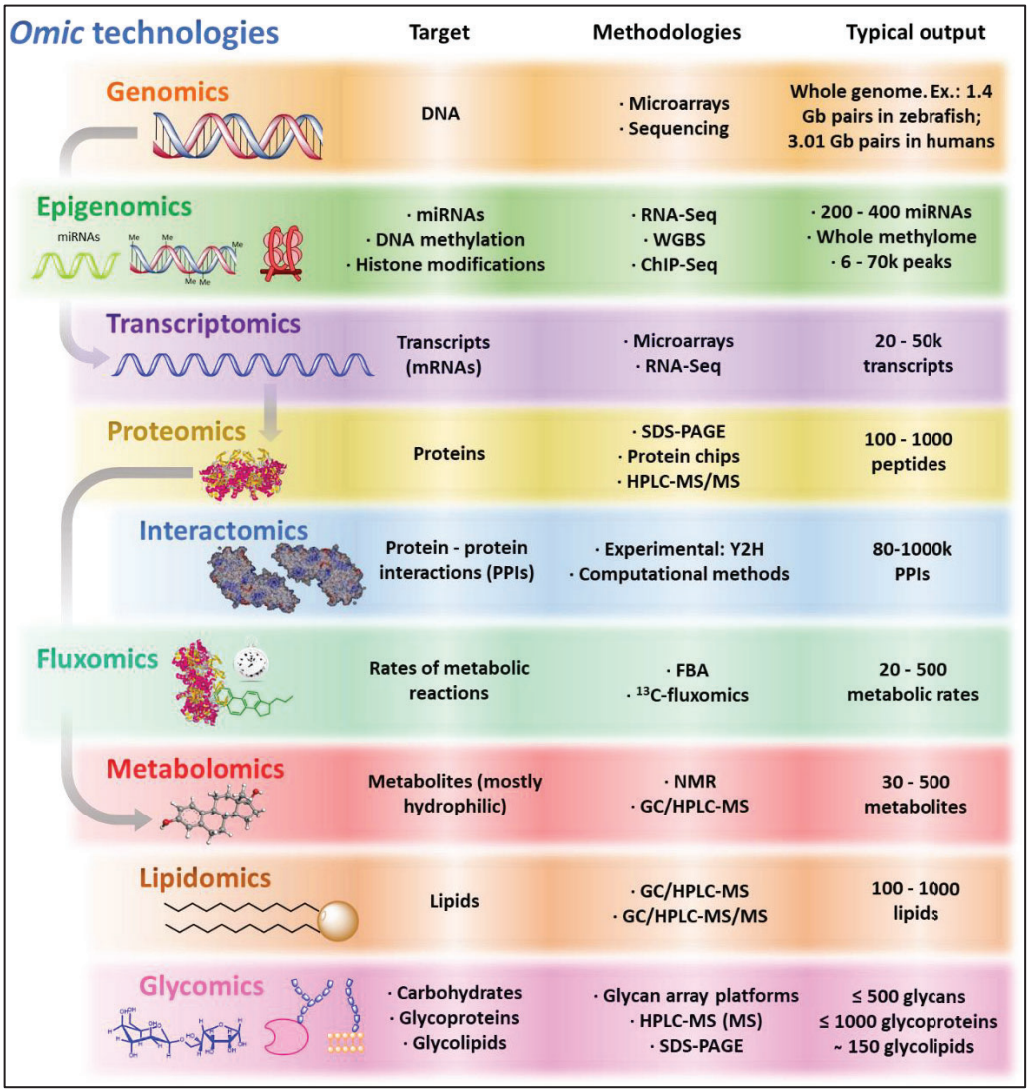

Figure I.7. (adapted from [36,203]): *omic* technologies, their target molecules, examples of the main methodologies used by each one and their typical measurements. Gb: gigabase; WGBS: whole genome bisulphite sequencing; SDS-PAGE: sodium dodecyl sulfate polyacrylamide gel electrophoresis; HPLC-MS: high performance liquid chromatography - mass spectrometry; Y2H: yeast two-hybrid screening; FBA: flux balance analysis; NMR: nuclear magnetic resonance; GC: gas chromatography.

During the last decades, different untargeted technologies that allow an integrated analysis and fully characterization of biological samples have been developed for,

improved or applied to environmental toxicology. As the neo-suffix "-ome" was widely used in biology to describe the totality of certain entities at some biological level (for example genome, to refer to the set of all genes of an organism), these technologies received the name of *omics* (see figure I.7.).

Different *omics* have already been, or are proposed to be, applied in environmental toxicological studies as genomics [204], epigenomics/epigenetics [205], transcriptomics [206], proteomics [207,208], metabolomics [66,209], lipidomics [210,211], and glycomics [212]. Other biological aspects related to biological processes have been aimed for their fully comprehension in an *in toto* approach. This is the case of interactomics [213], that seeks to describe the complete set of molecular interactions (usually focused in the protein - protein interactions or PPIs) or fluxomics [214], the goal of which is the determination of the metabolic rates of all the different reactions that take place in a particular biological system.

These “relatively new” and fully comprehensive *omics* technologies have even inspired the adaptation of traditional qualitative and quantitative observations of animal phenotypes into integrated morphometric assays where all possible morphologic changes are combined to stablish a linkage between the macroscopic phenotype and the different *omic* changes in organisms exposed to several xenobiotics [139,140,215].

In this way, these different untargeted and holistic approaches not only triggered a revolution when applied to environmental toxicology (allowing to better characterize the mode of action of several xenobiotics and to detect effects or mechanisms previously uncharted) but also permitted to achieve a higher comprehension of all the set of xenobiotics’ effects in a biological system when the information was combined [36,65].

Data fusion of different *omics* that covers several organization levels (genes, transcripts, proteins, metabolites…) raise itself as an excellent method to characterize and construct the adverse outcome pathway of a xenobiotic [36]. Several studies have already performed this omic integration [216–221], which can be carried out at three different levels [36]:

1) Integration at high level: the data management, clustering and functional analysis are performed individually for each individual *omic* dataset. At the end, the obtained information is integrated to develop a mechanistic interpretation. It is probably the easiest integration.

2) Integration at medium level: data analyses are performed individually and their outputs are integrated to perform the functional analysis (and the mechanistic interpretation). It requires a compatible codification of the outputs. Performing a functional analysis from protein and transcripts datasets in DAVID (Database for Annotation, Visualization and Integrated Discovery), or from metabolites, proteins and metabolites in KEGG (Kyoto Encyclopedia of Genes and Genomes) are examples of this integration level.

3) Integration at low level: in this case, the integration is performed from the first step (data integration and analysis). Although it could seem the preferred option for data fusion, it requires the same name of replicates (and preferably coming from the same sample), higher computational knowledge and a careful normalization of each dataset to consider the variability and structure of each biological level (for example, the up- or down-expression of a transcript can be even higher than 3 or 4 orders of magnitude while changes in lipids or metabolites amount usually only achieve 1 or 2 orders).

II. Methodology

"Science, in the immediate, produces knowledge and, indirectly, means of action. It leads to methodical action if definite goals are set up in advance [...]"

Albert Einstein

II.1. Applied *omics*/integrative assays and background information

This section is devoted to describe *omic* technologies and integrative analyses used in this thesis. It also provide background information beyond each technology and biological aspects involved in it.

II.1.1. Transcriptomics

Transcriptomic technologies are based mainly in the polymerase chain reaction (PCR) and DNA sequencing, processes both totally integrated in the prevailing two main actual techniques (microarrays and RNA-Seq).

II.1.1.1. Polymerase chain reaction (PCR) and qPCR

The practical application of the PCR, already envisaged by Kjell Kleppe in 1971, started in the middle 80's, when Kary Mullis introduced the use of thermostable DNA polymerases [222], therefore allowing the replication of a DNA template into millions or billions of copies. The PCR is based in a thermal cycling process, as illustrated in figure II.1.

Each cycle (denaturation, alignment, and elongation) duplicates the number of copies of the DNA template, following the equation:

$$N = N_0 \cdot (1 + E)^n$$

being N the number of cDNA strand copies after certain number of thermal cycles (n), N_0 the original number of copies, and E the efficiency (0-1) of the amplification.
The introduction of a thermostable DNA polymerase (such as the widely used Taq polymerase) which was not needed to be added in each cooling-heating cycle, promoted the use of the technique. Moreover, the use of reverse transcriptases, already isolated during the 70's [223], allowed the amplification of cDNA (DNA copy from a RNA molecule), therefore permitting the quantification of specific mRNA molecules by PCR.

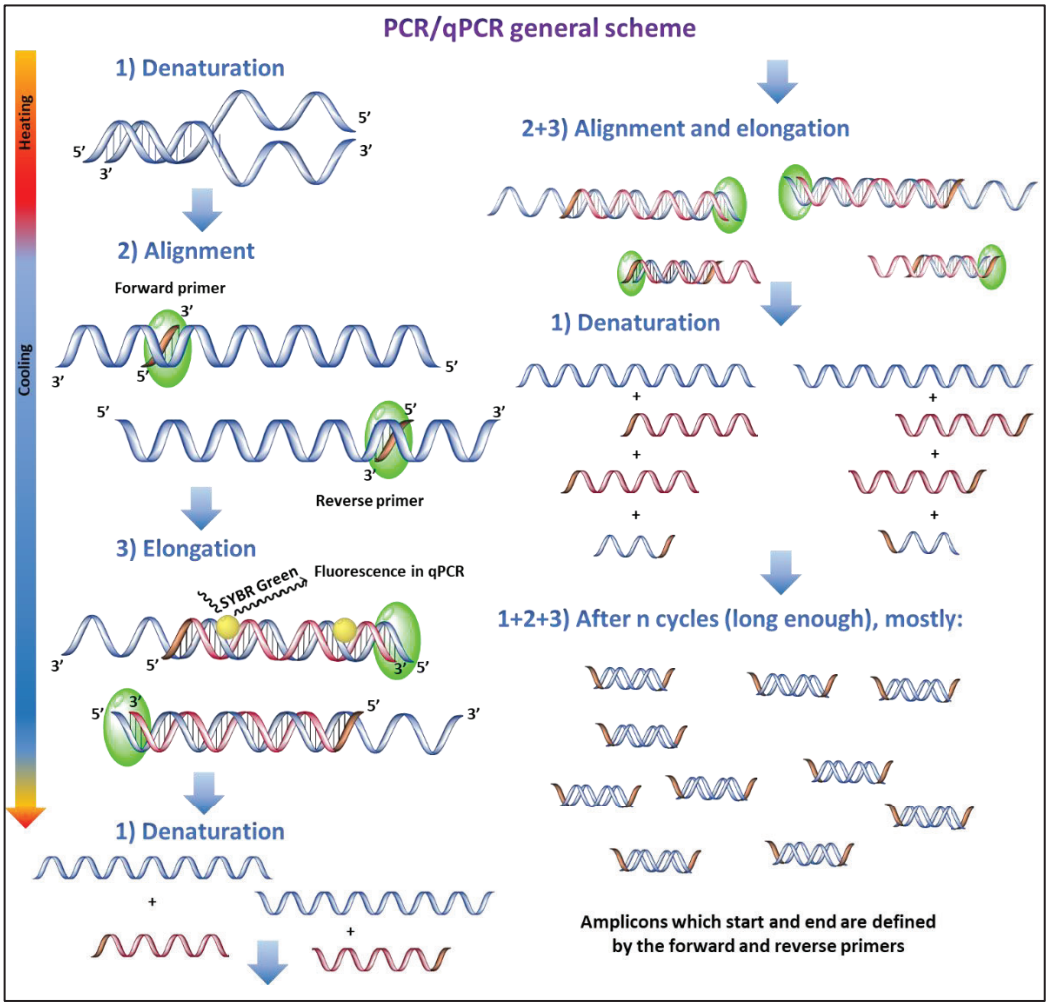

Figure II.1.: General scheme of PCR (polymerase chain reaction) basics. Fluorescent DNA-intercalating dye is used only in real time PCR.

While classical PCR is essentially a preparative technique that allows the synthesis of a given DNA molecule, several protocols allow a semi-quantitative estimation of the concentration of the template DNA (or cDNA). These protocols rely in the quantification of amplicon bands separated by agarose gel electrophoresis, stained with appropriated dyes (e.g., ethidium bromide, RedSafe or GelGreen) and quantification of the fluorescence by densitometry. The quantitative real-time PCR (qPCR), uses a fluorophore, either in solution (as the SYBR Green) or attached to specific primers (as

the TaqMan probes) to monitor the amplification of the template DNA at each thermal cycle [224]. By this mechanism, the fluorescence exponentially increases in each thermal cycle, which can be measured to calculate the template DNA/cDNA amount. This measurement needs to be performed in the exponential phase of the amplification curve (see figure II.2.), since it is the only range in which the fluorescence is directly proportional to the original input transcript amount. Indeed, the quantification cycle (see box II.1.) of each sample is indicative of its DNA/cDNA concentration and could be used for comparisons.

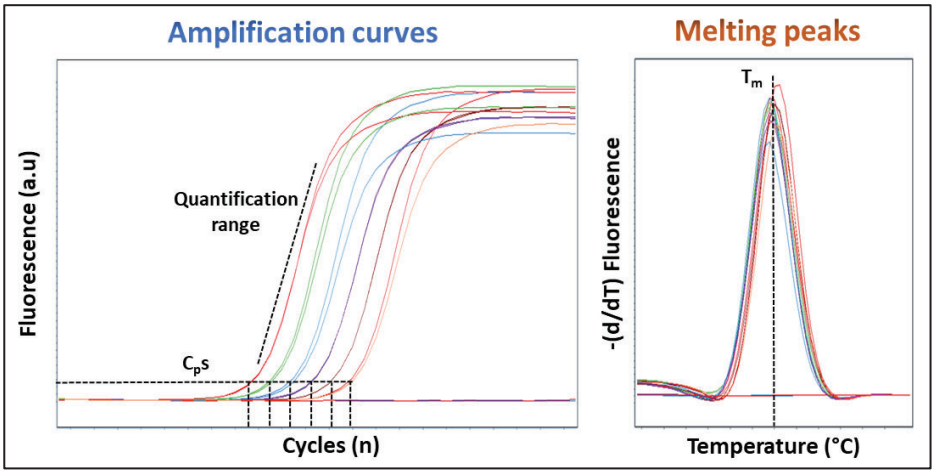

Figure II.2.: conventional amplification curves and melting peaks obtained in a real time quantitative PCR (qPCR). C_ps: quantification cycles; T_m: melting temperatures; a.u.: arbitrary units.

Text box II.1.

· cDNA: copy DNA, obtained from the retrotranscription of RNA.

· qPCR: real-time quantitative polymerase chain reaction. It allows the monitoring of the amplification reaction using a fluorophore, in contrast with the classical PCR.

· Primer: short single-stranded oligonucleotide, complementary to a certain region of the target cDNA, which allows the adhesion of the DNA polymerase to this double strand and the initiation of the replication and elongation processes.

· Fluorophore: fluorescent molecule that intercalates in any double-stranded DNA and allows the real time monitoring of the amplifications in a qPCR.

· Amplicon: a.k.a. PCR product, it is the cDNA fragment amplified by PCR/qPCR.

· Reference gene: a.k.a. housekeeping gene, it is a gene which is involved in basic cell functions and which expression (transcript amount) are basically constant across all the tested conditions. It is commonly used for data normalization in qPCR but not in high-throughput transcriptomics.

· C_q (quantitation/quantification cycle) / C_t (cycle threshold) / C_p (crossing point): cycle number at which the signal intensity rises above the threshold in a qPCR.

· T_m (melting temperature): maximum temperature obtained in the fusion peak. It represents the denaturation of the double strand of the amplified PCR product.

When the amplification of whole template DNA/cDNA is required, classical PCR (or a next generation sequencing technology; it depends on the final goal) is commonly used; meanwhile real time qPCR usually is kept for the amplification of only specific short regions of the DNA/cDNA, the so-called "amplicons". With this goal, knowing the sequence, the use of a specific pair of primers (one forward and one reverse), purposely designed to be complementary to each cDNA strand, allow us to selectively amplify this specific region. In qPCR, each amplicon usually cover between 70 and 200 bp (nucleotide base pairs), although longer amplicons (up to 400-500 bp) can be also generated [225]. The specific and correct amplification of the desired amplicon can be qualitatively assessed in qPCR by the efficiency and the melting peak. On the one hand, the efficiency of the amplification needs to be ideally between 0.9 (90 %; to assure that the efficiency is not too low) and 1.1 (110%; to assure that only the desired amplicon is being amplified). On the other hand, qPCR performs a fusion curve at the end of the cycles, at which the temperature is increasing and the denaturation of the double strand take place. As each amplicon has a specific melting point (single peak), the observation of several melting peaks could indicate the amplification of undesired amplicons.

Due to the fact that the C_q values are directly proportional to N_0, and considering that not all the samples have the same initial total RNA amount (different extraction efficiency, number and size of individuals from which RNA is extracted…), these values needs to be normalized. If an absolute quantification is required (for example, in studies

of wild populations, to compare the amount of each specie), a standard is used (for example, a plasmid DNA of absolute known concentration). If only a relative quantification of any desired mRNA is needed (usually the goal of the studies based in exposure to different xenobiotics and concentrations), different normalization methods are used: ΔΔCp, Pffafl or AccuCal-D methods, sigmoidal models, NORMA-Gene approach [226–231] … among others. The two different normalization methods used in this thesis (ΔΔCp and NORMA-gene) are explained below:

· ΔΔCp method [230] is widely used and relies on the measurement of a reference gene among all the others target genes. In this way, at specific C_p, the number of copies are:

$$N_{target} = N_0^{target} \cdot (1 + E_{target})^{Cp^{target}}$$

$$N_{ref} = N_0^{ref} \cdot (1 + E_{ref})^{Cp^{ref}}$$

Thereby, the relationship between the copies of target and reference genes is:

$$\frac{N_{target}}{N_{ref}} = \frac{N_0^{target} \cdot (1 + E_{target})^{Cp^{target}}}{N_0^{ref} \cdot (1 + E_{ref})^{Cp^{ref}}} = K$$

And normalized copies (NC) regarding the reference gene:

$$NC = \frac{N_0^{target}}{N_0^{ref}} = \frac{N_{target} \cdot (1 + E_{ref})^{Cp^{ref}}}{N_{ref} \cdot (1 + E_{target})^{Cp^{target}}} = K \cdot \frac{(1 + E_{ref})^{Cp^{ref}}}{(1 + E_{target})^{Cp^{target}}}$$

If the efficiencies of the amplification of both genes are similar between them and close to 1 (100 %), then 1 + E ≈ 2, and:

$$NC = K \cdot \frac{2^{Cp^{ref}}}{2^{Cp^{target}}} = K \cdot 2^{Cp^{ref} - Cp^{target}} = K \cdot 2^{\Delta Cp}$$

where $\Delta C_p = C_p^{ref} - C_p^{target}$

Then, to calculate the relationship (fold-change; FC) between the mRNAs copies of two experimental groups (usually performed for control versus treatment), and assuming a uniform PCR amplification efficiency across all samples ($K_1 \approx K_2$):

$$FC = \frac{NC_{treated}}{NC_{control}} = \frac{K_1 \cdot 2^{\Delta Cp_{treated}}}{K_2 \cdot 2^{\Delta Cp_{control}}} = 2^{\Delta Cp_{treated} - \Delta Cp_{control}} = 2^{\Delta\Delta Cp}$$

where $\Delta\Delta C_p = \Delta C_p^{treated} - \Delta C_p^{control}$

This method is useful for the measure of any number of genes although requires a reference gene (stable among the experimental conditions tested).

· NORMA-Gene approach [231] is based on a data-driven normalization, which takes into account the variation and amount of the several genes across all samples (for example, considering that a sample with a double amount of RNA would have an apparent double expression of all measured genes, at normal conditions). It is similar to the normalization performed with high-throughput data (see section II.1.1.3.1. RNA-Seq) although with a much more limited number of genes, relying on the assumption that a small sub-set of genes is representative of the whole transcriptome of a sample. Being less known and used than the $\Delta\Delta C_p$ method, NORMA-Gene approach requires at least the measurement of 5 or more target genes although it does not need any reference gene.

II.1.1.2. Sequencing

The term sequencing includes any process by which the order of the nucleotides in a nucleic chain of DNA or RNA is determined. Both history of RNA and DNA sequencing started and developed during the 70's, with the first sequenced gene (the one that codifies for bacteriophage MS2 coat protein) [232] and genome [233], and DNA sequencing with location-specific primers [234], adapted and enhanced by Frederick Sanger [235].

The methodologies used for sequencing have been changing during the years, from the first sequences obtained by two-dimensional chromatography, up to radioactive labeling, fluorescence labeling and pyrosequencing, among others [236–239].

Fluorescent Sanger's method (a general scheme is shown in figure II.3.) was commonly used until the arrival of the next generation sequencing (NGS) techniques and was useful for DNA and also RNA sequencing, after conversion of the RNA into cDNA. It was fully

automatized using computerized base calling, process by which the fluorescence of the chromatogram peaks are assigned to the nucleobases.

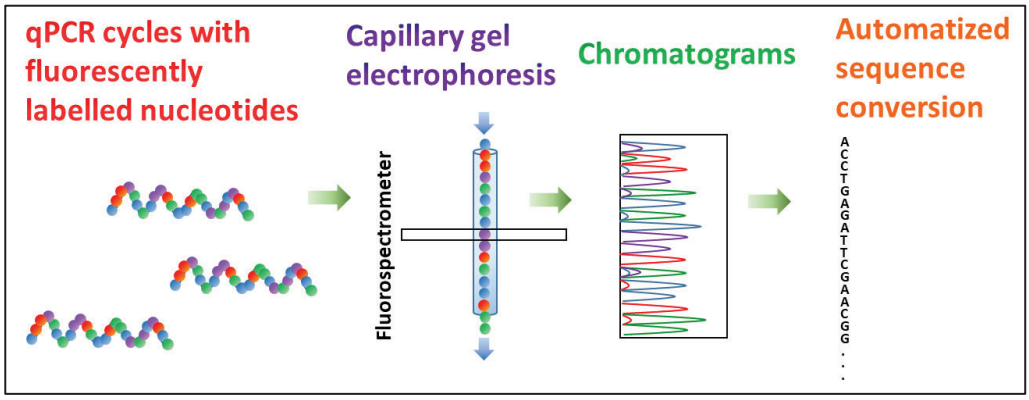

Figure II.3.: general scheme of automatized fluorescent Sanger's method for sequencing. Different nucleotides are differently coloured.

Nowadays, the sequencing process is integrated together with the amplification process in the next generation sequencing techniques, which has become not only easier and faster, but also economically more affordable. DNA sequencing prices fell faster than predicted by Moore's law due to the introduction of NGS. As an example, while the sequencing price of a whole human genome was $100 million in 2001, it decreased up to $10 million in 2007, to $340,000 in 2008 and $4200 in 2015 and to $1000 in the past year (2019) [240–242]. Some commercial companies have even claimed to be ready to reach the price of $100 for a human genome [242,243]. As a result, the number of sequenced genomes and transcriptomes of different species have been rapidly increasing during the last years [240,244,245].

II.1.1.3. Next generation sequencing

Transcriptome (as a whole set of transcripts) concept was introduced in late 90's [65,246] and the possibility to measured it by NGS (90's-2000's) opened a new era, which can be considered to be opened by the introduction of the microarrays which are nowadays being substituted by RNA-Seq methods [247].

II.1.1.3.1. RNA-Seq

While microarrays are based on short specific oligonucleotides ("probes") attached to a solid-surface ("chip") with a specific pattern, that allow the amplification of already known transcripts by relative fluorescence, RNA-Seq technologies allow the amplification of every possible strand in the samples and are based on a wider spectrum of methods that present many advantages: 1) no pre-knowledge of the sample is required; 2) an absolute count of the transcripts (after amplification) can be performed allowing a higher precision; 3) it allows the identification and quantification of rare transcripts, alternative splicing, mutations, etc. without previous knowledge; 4) lower amount of total RNA is needed; 5) it present a higher dynamic range (between very low and high expressed transcripts) [248].

Four of the most common RNA-Seq technologies are shown in the figure II.4. Among them, Illumina sequencing has been the method predominantly used during the last years. Advances of high throughput NGS technologies allow nowadays even the transcriptome sequencing of a single cell [249,250].

Text box II.2.

· NGS: high-throughput next generation sequencing technology.

· "Chip": device based on a solid-surface with a collection of designed primers (attached to the surface) for a large number of different genes. It is used in microarrays technologies and usually only allows one sample per chip [251].

· RNA-Seq library: set of oligonucleotides (originally from the sample's RNA) which have been cleaned (from gDNA contamination), retrotranscribed, fragmented and amplified. During the amplification process, certain adapters (designed to interact with a specific sequencing platform) are added to the fragments.

· "Flow cell": device used in RNA-Seq technologies. Similar to a microarray chip although it uses random primers (or primers complementary to the adapters added to the fragments in the amplification process) to bind every possible DNA/cDNA strand in the samples, which are introduced in different lanes, allowing the measurement of several samples per flow cell [248].

· Transcriptome assembly: reconstruction of the transcripts sequence from the generated reads, either with a reference sequence (genome or transcriptome guided; usually called mapping or alignment) or without it (d*e novo* assembly) [248,252].

· Multiplexing/demultiplexing: addition of barcodes (multiplexing or indexing) during the library preparation to each fragment regarding its origin (sample), to allow its identification and sort (demultiplexing) during the data analysis. It allows the measurement of different samples in the same flow-cell [253].

· Trimming: computational removal of adaptors sequences and low quality bases of the reads before the assembly [254].

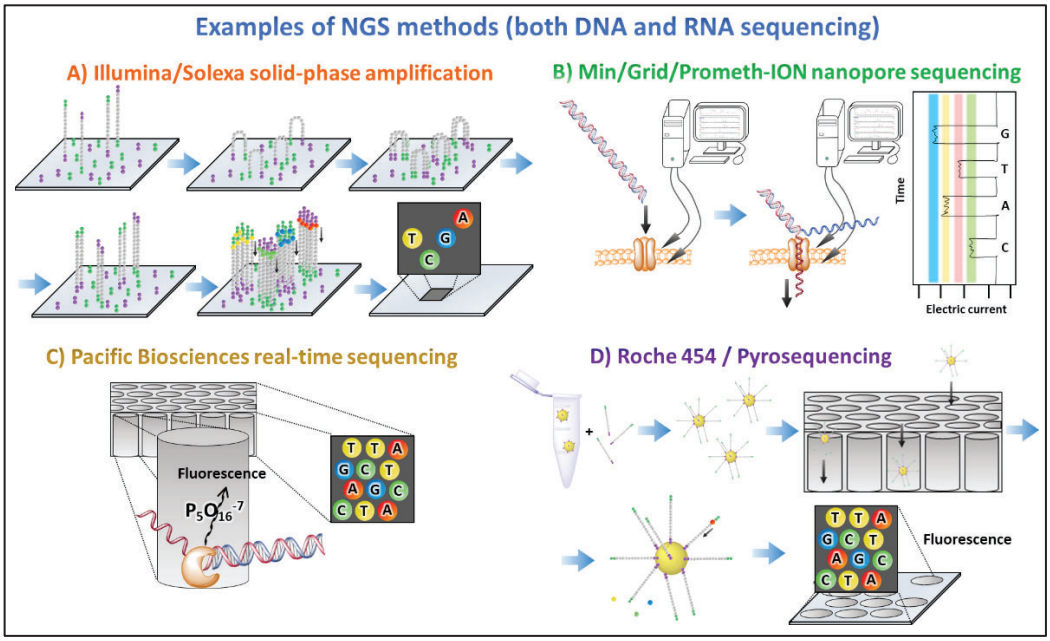

Figure II.4.: four common examples of next generation sequencing methods. A) Illumina/Solexa technology is based on the amplification on a solid surface, forming several clusters (each one of a specific amplicon that has been locally amplified via bridge formation). B) Nanopore sequencing is based on the unwound of the DNA helix by a biological solid-state nanopore and the application of an electric current (which change will be used to identify the nucleotide). C) Pacific Biosciences single molecule real-time sequencing (SMRT) is based on the attachment of a polymerase at the bottom of a very small wells (ZMWs or zero-mode waveguides) where a single molecule is sequenced at a time. D) Roche 454 pyrosequencing is based on the attachment of the fragments to solid spheres which are deposited in holes, where sequencing will take place.

Different steps as the transcript enrichment (amplification), their fragmentation and library preparation, the sequencing reads (long or short, single o paired) and other characteristics can slightly vary between the different existing methods.

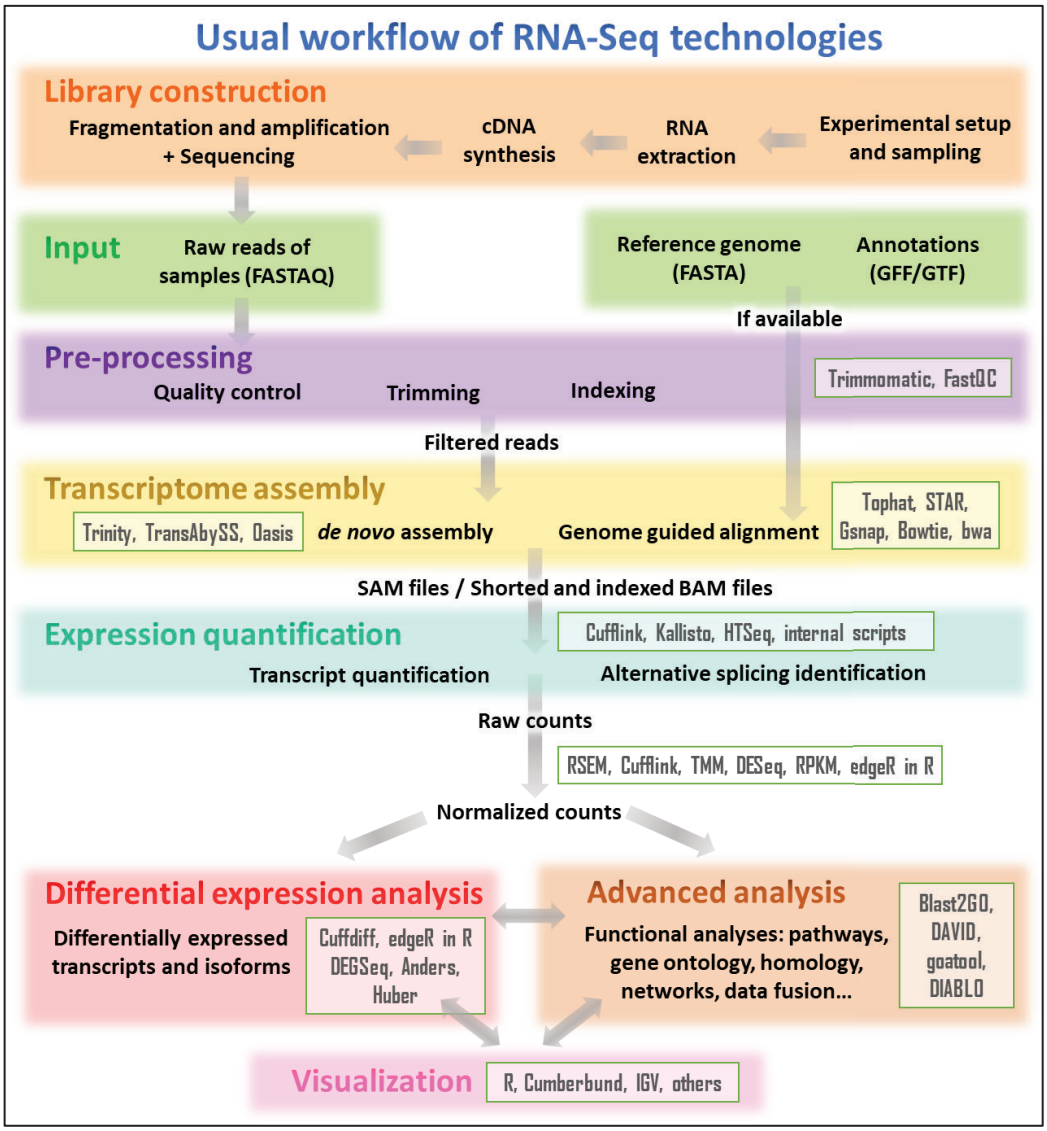

Figure II.5.: common experimental and computational workflow of RNA-Seq technologies. In grey (inside green boxes), common softwares used in each computational step. Computation time from the raw FASTAQ reads until the obtaining of normalized counts can last several weeks depending on the total information amount generated in the sequencing and the complexity of the assembly.

The ability of RNA-Seq technologies to rapidly and cheaply produce enormous amounts of sequencing data also triggered the apparition of new methodologies and workflows necessary to process all this "big data", which can reach the order of gigabytes-terabytes per run [248,255]. The usual workflow is schematized in figure II.5. [252,256].

II.1.2. Lipidomics

II.1.2.1. Lipids

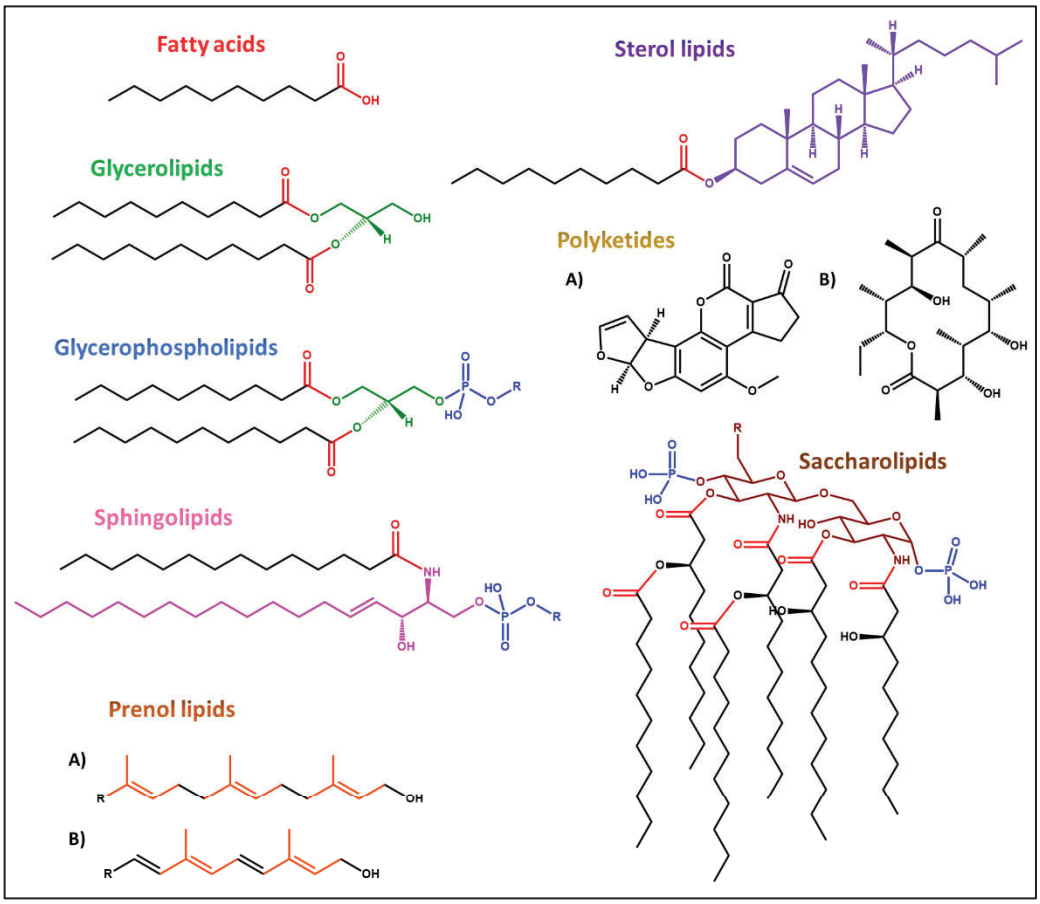

Figure II.6.: the eight main lipid families. Fatty acids, glycerolipids, glycerophospholipids, sphingolipids, saccharolipids, and polyketides are derived from condensation of ketoacyl subunits. Sterol and prenol lipids are derived from condensation of isoprene subunits. Characteristic functional groups or sub-structures of each lipid family are differently coloured.

Study of lipids by environmental toxicology becomes particularly relevant when studying obesogens or endocrine disruptors able to deregulate lipid metabolism. Lipids are hydrophobic or amphiphilic small metabolites which can be dissolved in non-polar solvents. The main eight lipid families [257–259] are reported in the figure II.6.

Their own chemical structure (most of them are amphiphilic and present one or more long non-polar hydrocarbon chains and a polar head) impedes their simultaneous extraction with other small and hydrophilic metabolites (as aminoacids or very small peptides, ATP, hormones, vitamins, hexoses, other amines, signaling molecules…) [260]. For this reason, although in metabolomic studies usually some lipids can be also measured, this term is kept for the high-throughput technology focused in the measurement in small and polar metabolites, while the term lipidomics are used for the exclusive study of lipids. Similarly, these different chemical characteristics among lipid families (figure II.6.) induce relevant biases in their quantification due both to the extraction and detection processes.

They present several biological functions (with all range of importance and outreach) [261,262], which can be summarized in table II.1.

Lipid family or subfamily	**Cellular, tissue and/or organismal functions**
Free fatty acids (FFA)	- Main class, they are used for energy obtainment (via oxidation) or lipid synthesis (via esterification) [263]. - Second messengers and signalling [264].
Phospholipids (PL) as phosphatidylethanolamines (PE); phosphatidylglycines (PG); phosphatidylinositols (PI); phosphatidylserines (PS) or phosphatidylcholines (PC)	- Main cell membrane lipids (PC and PE are the most abundant) [265]; including lipoproteins membrane lipids (PC is essential) [266]. - Calcium binding in bone growth (PS) [267]. - Protein anchorage and signalling molecules precursor (PI) [268,269]. - Activator of protein kinase C family, and precursor of cardiolipins (PG) [270]. - Implication in correct protein folding and chaperon-like processes (PE) [271].
Triglycerides (TG)	- Main form of energy storage [272]. - Involved in thermal insulation [272].

Diglycerides (DG)	- Signalling functions [273].
Sphingolipids as sphingomyelins (SM)	- Electric insulation: myelinisation by the Schwann cells [274]. - Lipid rafts (involved in many signal transduction processes) are enriched in sphingolipids, among others [275].
Prenol lipids	- Precursors of vitamins [276].
Sterol lipids	- Precursors of vitamins and steroids, including hormones (like estrogens, androgens…) [277]. - Signalling processes [277].
Cholesterol (Ch)	- Essential cell membrane lipid: fluidity regulation [278]. - Precursor of sterol lipids [278]. - Lipid rafts are enriched in cholesterol, among others [278].
Cholesterol esters (CE)	- Cholesterol homeostasis [279]. - Important in adrenal cortex steroid production [280].
Polyketides	- Antibiotic, antifungal and cytostatic properties [276].
Saccharolipids	- Cell membrane lipids in bacteria [276].

Table II.1.: Main lipid families and sub-families and examples of their functions at different biological levels.

Chromatographic techniques have been extremely useful for the integrative analysis of lipids in a holistic approach. In this thesis we used two methods for lipid analysis, thin layer chromatography (TLC) and liquid chromatography coupled to mass spectrometry (LC-MS). They present different characteristics regarding the lipid identification and applications and have been widely used for lipidomic studies in aquatic organisms [121,281].

II.1.2.2. Thin layer chromatography (TLC)

Thin layer chromatography (TLC), which has been in use for several decades [282], allows the separation of the different lipid families based on their different partitioning between the mobile and stationary phases. In TLC, the usual stationary phase is silica and the partition coefficient mostly depends on the hydrophobicity of the lipids. It allows the separation of the different lipid families, but not the individual lipid species. Indeed, after the loading, elution and charring of the plate, each individual spot represents a lipid family, whose relative amount can be calculated by densitometry [283,284]. Regarding

classical TLC, high performance TLC (HPTLC) incorporates a smaller silica particle size, thinner layer, plate loading automation and/or double plate elution (with different eluents), providing low-diffused, clean and better separated bands and increased sensitivity [283,285,286]. For aquatic organisms, modified Folch lipid extraction methods and double plate elution with polar and non-polar solvents are performed to measure all main lipid families [75,287,288]. An example of double eluted HPLTC is shown in figure II.7.

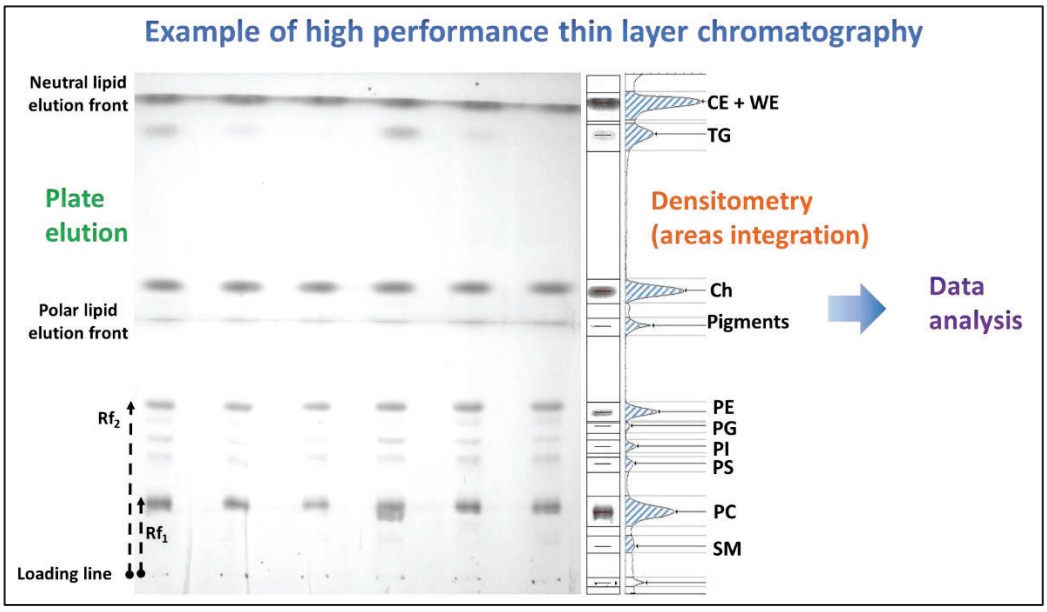

Figure II.7.: example of a double eluted high performance thin layer chromatography (HPLTC) of lipids extracted from zebrafish eleutheroembryos and peak densitometric integration. CE: cholesterol esters; WE: wax esters; TG: triacylglycerols; Ch: cholesterol; PE: phosphatidylethanolamines; PG: phosphatidylglycines; PI: phosphatidylinositols; PS: phosphatidylserines; PC: phosphatidylcholines; SM: sphingomyelins.

Indeed, HPTLC it is a powerful screening method for determination of xenobiotics' effects over each lipid family, usually before engaging in a more exhaustive but cost- and time-expensive high-performance liquid chromatography - mass spectrometry (HPLC-MS) study. Although its low economic and time cost, minimal sample cleaning

requirements, and high number or replicates per run, HPTLC can show higher matrix effects than HPLC-MS, and very low concentrated lipid families cannot be quantified.

Text box II.3.

· Stationary phase: adsorbent substance fixed in an inert solid surface. In HP/TLC plates composed by a thin layer of silica gel disposed on a glass surface are widely used.

· Mobile phase: eluent used to carry the analytes (in this case, the lipids). In HP/TLC plates, it is in liquid state and usually a non-polar, polar and mixes of organic solvents are used (hexane, methyl acetate, diethyl ether, chloroform, isopropanol…). The partition coefficient of each analyte between stationary and mobile phase will define its elution across the plate.

· Plate elution: process by which the mobile phase progresses across the plate, by capillarity, separating analytes by their properties.

· Retardation factor (R_f): in HPLTC, it is defined (for each analyte) as the ratio between its migration distance (distance traveled by the analyte in the plate) and the migration distance of the eluent front.

· Plate charring: in lipid HPTLC, is the process by which the plate is heated and lipids oxidized, revealing its position by the apparition of a brown spot in the plate. Classical charring reagents (which are sprayed on the plate surface before the charring) usually involve copper (II) salts in acid aqueous medium [75,289].

II.1.2.3. High-performance liquid chromatography - mass spectrometry (HPLC-MS)

A TLC version using columns instead of plates was developed in the 60s. The system, based on the gravity force to let a mobile phase go through the stationary phase, placed inside the column, was rapidly improved during the 70s, using smaller size particles in the stationary phase and higher pressures for the elution process, marking the birth of high-pressure liquid chromatography (HPLC) [290]. Further refinements as even higher pressures, smaller particle size, use of pumps and autosamplers, detector coupling, and

other improvements, allow actualizing the term to high-performance liquid chromatography and even to ultra high-performance liquid chromatography (UHPLC), which uses chromatographic columns with particle size lower than 2 µm and pressures higher than 400 bars (≈ 395 atm). This drastically reduces the time of analysis and increases the compounds separation [291,292]. UHPLC-MS couples the UHPLC to a mass spectrometer for detection, identification and quantification of the lipids. Although being more cost-expensive, it also presents lower limits of detection and quantification (LOD/LOQ, respectively), and also reduces sample matrix effects [75,293–295]. Moreover, the main advantage of the HPLC-MS is the possibility to detect the different individual lipid species inside a specific family (because of the different chain length of the fatty acids), due to the mass analyzer (which allow the separation of the analytes by their *m/z* ratio) and the detector. A scheme of UHPLC-MS is shown in figure II.8.

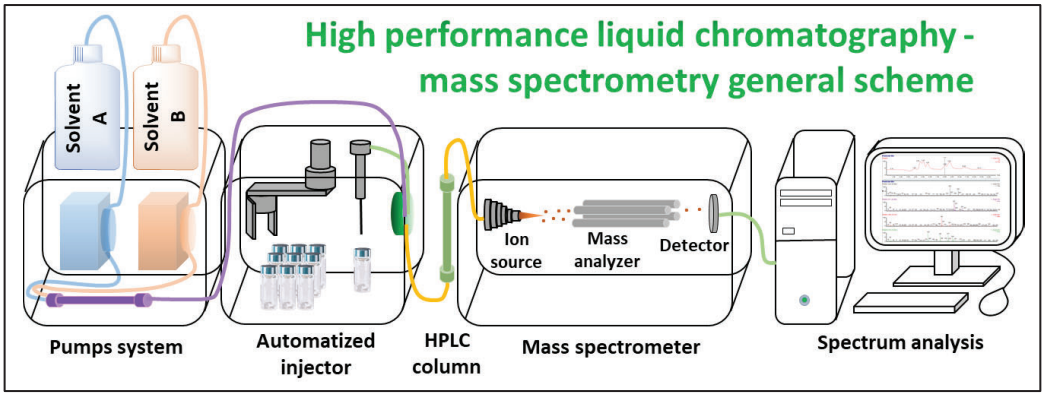

Figure II.8.: scheme of the main components of a high performance liquid chromatography - mass spectrometry system. For clarification purposes, disposal waste is not represented. HPLC column is commonly placed in a column heater, for temperature control.

Very briefly, when the sample is injected, it passes along with the mobile phase (methanol, acetonitrile, mixes…) through the chromatographic column (silica C8 or C18, HILIC…) where the analytes are separated. Due to the action of one or several pumps, the flow can be controlled as well as the composition of the solvent (being isocratic if it remains constant or using a gradient elution if it changes over time). When the separated analytes exit from the column, they are ionized by an ion source (matrix assisted laser

desorption ionization (MALDI), electrospray ionization (ESI) or atmospheric pressure chemical ionization (APCI), among others). Once ionized, these ions have a specific mass-to-charge ratio (*m/z*) and can be separated/selected by the mass analyzer (quadrupole mass filter, several ion traps, Fourier transform ion cyclotron resonance (FT-ICR-MS), time of flight (TOF)…) depending on this *m/z*. When the ions arrive to the detector (electron multiplier, Faraday cup, microchannel plate…), electric signals are produced which will be computerized to intensities, generating the total ion current chromatogram and mass spectra, from which several software could extract the peak areas of each analyte. Data analysis can be untargeted (for example, using the regions of interest (ROI) [296]) or semi-targeted (searching for specific *m/z* values of known lipids) [74,75]. The last approach is indeed still considered as *omic* as long as the number of measured lipids would be considerably high and representative of the sample.

Text box II.4.

· *m/z*: mass-to-charge ratio of the ionized lipids (or analytes, in general). Relationship between its molecular mass (in unified atomic mass units (u)) and its electric charge.

· Elution time: time that each lipid (or analyte, in general) requires to pass through the column, from injection to detection. Similar to R_f in HPTLC.

· Mass analyzer: mass spectrometer component that uses static or dynamic electric and/or magnetic fields to separate ions by their different m/z ratio. MS instruments are usually called by the name of its mass analyzer.

· Normal and reverse phase chromatography: in normal phase HPLC, stationary phase is polar and mobile phase is non-polar. Non-polar analytes will be the first to be eluted. Reverse phase HPLC uses a non-polar stationary phase and a polar mobile phase. Polar analytes will be the first to be eluted.

II.1.3. Epigenomics

Epigenomics represent the holistic approach of epigenetics (see section I.5. in the introduction). The study of chromatin modifications, DNA methylome or miRNAome are the common approaches for the identification of the epigenetic footprints, at different

levels. The two techniques used during this thesis (analysis of DNA methylation and of miRNAs) are briefly explained below.

Text box II.5.

· DNA methylome: set of all cytosine methylations of the complete genome of an organism (or specific tissue or cell).

· miRNAome: set of all miRNAs expressed in an organism (or specific tissue or cell).

II.1.3.1. miRNAs

The prediction of possible miRNAs candidates to be both affected by a xenobiotic or to mediate its effects can be difficult considering the complex multiple mRNAs-miRNAs interactions (see section I.5.1.). Indeed, the *omic* approach i.e. the measurement of the complete miRNAome (via RNA-Seq [297,298]) can be a powerful tool in toxicoepigenomics for stablishing the effects of a xenobiotic at this epigenetic level.

Nevertheless, the development during the last years of some predictions tools to both predict the transcripts targeted by a specific miRNA and the miRNAs that can target a specific mRNA, in several organisms [299] (http://www.targetscan.org/vert_72/), allows to perform the study of several miRNAs via "classical" targeted real time qPCR approach (analogously as mRNAs). Essentially, same protocols are used although an addition of polyadenylation step is required for the amplification of miRNAs. In opposition to an mRNA qPCR, where a pair of primers are designed, in miRNAs qPCRs, a universal reverse primer is used for the polyA tail while the forward primer consists in the same miRNA sequence.

II.1.3.2. DNA methylation

Toxicoepigenomics frequently takes advantage of the whole genome bisulfite sequencing (WGBS) to detect differentially methylated regions (DMRs) induced by the exposure [171,196]. WGBS relies in the same high-throughput sequencing technologies explained in section II.1.1.3.1. although a previous genomic DNA treatment with bisulfite

is added. Bisulfite treatment converts all unmethylated cytosines to uracils but not both methylated cytosines (5mC) nor hydroxymethylated cytosines (5hmC) [300,301]. Thus, uracils will be converted to thymines in the amplification and sequencing process meanwhile 5mC and 5hmC will remain as cytosines after the amplification [300,301]. Indeed, the comparison of the obtained sequences with a reference genome and/or with a non-bisulfite-treated genome, allow us to determine the methylation status of each individual CpG position. Taking into account all the obtained reads, their percentage of methylation could be evaluated.

Considering the sequence depth and the genome length, usually only few tens or hundreds of reads are obtained per each position. Thus, this approach only allow to detect changes in methylation higher than an specific percentage and usually 10% or higher values are used as cut-offs [193,302]. On the other hand, targeted analysis are also commonly performed, amplifying and sequencing only certain genome regions. That allows to achieve a higher sequence depth (thousands or tens of thousands of reads per position) and detect smaller percentage methylation changes [303].

II.1.4. Morphometrics

Morphometrics, which assess morphological abnormalities using automatable and repeatable methods, have been proposed to study phenotypic effects of exposure to pollutants in a holistic manner [139,215,304]. Transparent organisms (as zebrafish larvae) that allow the uncomplicated visualization of internal organs are extremely useful for morphometrics. In this way, as macroscopical phenotypes showed by the exposed individuals can be correlated with the effects of a given xenobiotic at different biological levels [139,215], morphometrics represents a powerful fast, cost-effective and easy method for screening. Indeed, the use of these integrative morphometric analyses has been proposed for the study of possible pathways or MoA of different xenobiotics [139]. Multivariate tests as principal components analyses (PCAs) are used to assess the “degree of affection” of each individual due to the exposure [305–307]. An example of morphometric and PCA analyses performed in zebrafish larvae is shown in figure II.9.

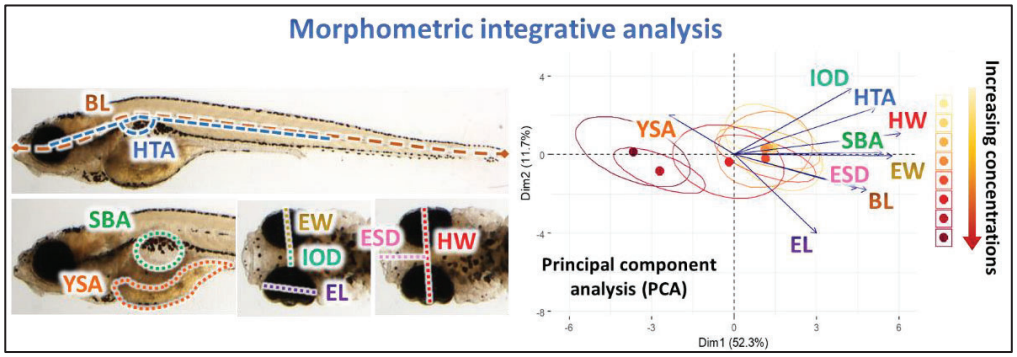

Figure II.9. (modified from [140]): example of morphometrics performed in zebrafish larvae and principal component analysis (PCA) for multivariate integration purpose.

II.2. Selected endocrine disrupting chemicals (EDCs) used in this study

Integrative analysis and *omics* technologies were used in this thesis to study the effects of a delimited set of compounds (figure II.10), reported to be endocrine disruptors, in zebrafish individuals, mainly at their first stages of development. BPA (bisphenol A) was chosen as a representative of a loose family of EDC that includes other bisphenols and alkylphenols, mainly used as plasticizers, polymer precursors and flame retardants. PFOS (perfluorooctanesulfonate) was studied among the perfluorinated compounds, which are used in fire-fighting foams, metal electroplating industry or *teflon* production. TBT (tributyltin) was studied as an example of organotins, used as stabilizers in polyvinyl chloride, anti-fouling paints, antifungal agents, and wood preservatives.

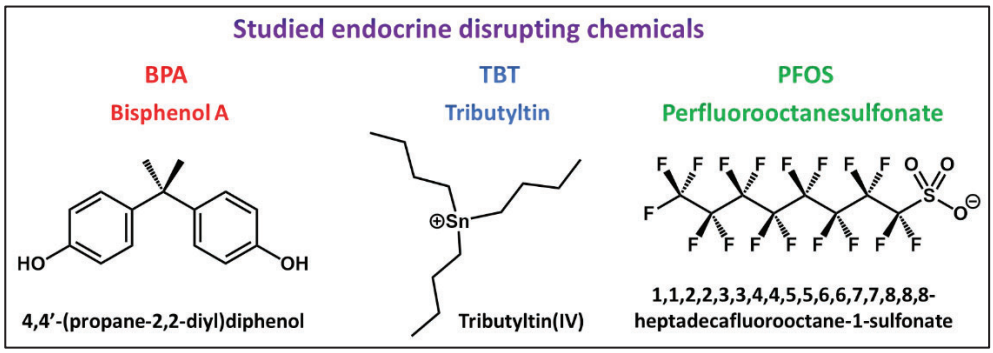

Figure II.10.: chemical structure of the three main EDCs studied in this thesis (BPA, TBT and PFOS). Abbreviations and common names are coloured in red, blue and green (for each compound). Systematic IUPAC names are expressed in black.

Even the legal restrictions in the production and uses of BPA, PFOS and TBT issued by many international agencies [308–314], they are still present in the environment, which can be explained by their low degradation (long half-lives), illegal uses, and wastes from their still authorized applications [315–319]. For that reason, environmental levels (at least, in some parts of the world) are found to be at the same order of magnitude that those found to exert certain adverse effects in living organisms, which is a cause of concern [320–322]. Table II.2. describes ranges of environmental concentrations found in water bodies.

	BPA [320,323–325]	**TBT** [317,326,327]	**PFOS** [328–330]
Surface and effluents waters	0-56 ppb	Rivers: 0.10-0.16 ppb Coastal waters: 0.02-4.6 ppb	0.00-0.3 ppb
Landfill leachates and wastewaters	0.001-17 ppm	0.06-0.22 ppb	0.00-0.64 ppb

Table II.2.: environmental levels of bisphenol A (BPA), perfluorooctanesulfonate (PFOS) and tributyltin (TBT). Parts per million: ppm (mg/L); parts per billion: ppb (µg/L).

While showing very different chemical structures, BPA, PFOS and TBT have been not only reported to have endocrine disrupting effects but specifically, to show obesogenic properties or affect lipid metabolism in some vertebrate models, including zebrafish [102,107–109,331–333]. Nevertheless, as they have been proposed to interact with different nuclear receptors [97,334–338], both their modes of action and their phenotypic manifestations probably differ. Several effects of BPA, TBT and PFOS in zebrafish have been reported during last decades, most of them derived from the measurement of a reduced dataset of analytes (transcripts, metabolites…) or phenotypic observations [339–344]. Although the implementation of *omic* technologies in some of these environmental toxicology studies took place, they were mostly limited to a single-dose exposure, or on adult differentiated tissue, or using unhatched eggs, when several developmental processes were not yet taken place [341,344–350].

To our knowledge, to date, only a couple of studies had integrated a dose-response design with a full *omic* technology (regardless of the *omic* used) to study the effects of BPA, TBT or PFOS during zebrafish embryogenesis (0-5 dpf) [351,352]. Indeed, the novelty of this thesis relies on the use and combination of several *omics* and integrative analyses and a dose-response design exposure in the study of effects of BPA, TBT and PFOS in the zebrafish during its embryogenesis; and the implementation of the benchmark dose approach [353] to compare both the different *omics* (and/or integrative analyses) and the different EDCs.

Text box II.6.

· Benchmark dose (BMD): threshold reference value at which it can be considered that biological effects start to take place. It is computationally calculated adjusting the effects to different mathematical models and substitutes traditionally used values as NOEC (no observed effect concentration) or LOEC (lowest observed effect concentration).

III. Hypothesis and objectives

"I have steadily endeavored to keep my mind free so as to give up any hypothesis [...] as soon as the facts are shown to be opposed to it"

Charles Darwin

The fact that some EDCs can act as obesogens is well stablished. Although many advances have been reached to determine their mode of action, several aspects remain unclear as if all obesogens act through disruption of the same pathways, if they behave similarly under a dose-response scenario, or if there are any molecular signatures that could be used as biomarkers of exposure to any obesogen-like compound, independently of its nature. To answer these fundamental questions, we selected three compounds, BPA, PFOS, and TBT, known by their obesogenic properties in different systems, and zebrafish eleutheroembryos as animal model. In this context, the main hypothesis and goals in this thesis are:

- General hypotheses

- Obesogenic effects can be studied in zebrafish embryos at stages in which no proper adipose tissue is developed yet, by integrating morphometric, biochemical, lipidomic, and transcriptomic data.

- At least some of the obesogenic-related alterations in zebrafish embryos can propagate to later developmental stages (eventually, up to the adult stage).

- Despite their fundamental structural differences, BPA, PFOS and TBT should have common dysregulatory effects that account for their alleged obesogenic properties.

- General objectives

- To study the endocrine disruption and other effects of BPA, PFOS and TBT at different biological levels in exposed zebrafish eleutheroembryos using *omic* technologies and integrative analyses.

- To integrate the results from the different biological levels to increase the knowledge of the mode of action of BPA, PFOS and TBT in zebrafish eleutheroembryos exposed to these endocrine disruptors.

- Specific objectives

- To evaluate the morphological alterations exerted by BPA, PFOS and TBT in zebrafish eleutheroembryos and to define non-lethal concentrations to be used in transcriptomic studies.

> Article I: “Morphometric signatures of exposure to endocrine disrupting chemicals in zebrafish eleutheroembryos”.

- To evaluate (through RNA-Seq) and functionally interpret transcriptomic dose-response effects of BPA, PFOS and TBT in zebrafish eleutheroembryos and to link them to other biological levels.

Article II: “Dose-dependent transcriptomic responses of zebrafish eleutheroembryos to Bisphenol A”.

Article III: “Unravelling the mechanisms of PFOS toxicity by combining morphological and transcriptomic analyses in zebrafish embryos”.

Article IV: “Transcriptomic effects of tributyltin (TBT) in zebrafish eleutheroembryos. A functional benchmark dose analysis”.

- To study lipid dysregulation in zebrafish eleutheroembryos through advanced lipidomic methodologies.

Article V: “Changes in lipid profiles induced by bisphenol A (BPA) in zebrafish eleutheroembryos during the yolk sac absorption stage”.

- To study long-term effects of obesogenic disruption and to investigate the possible role of epigenetic mechanisms.

Article VI: “Acute and long-term metabolic consequences of early developmental Bisphenol A exposure in zebrafish (*Danio rerio*)”.

Article VII: “Alterations of DNA methylation levels of key genes related to BPA exposures in zebrafish embryos”

- To use advanced integrative techniques to propose an adverse outcome pathway (AOP) for BPA, PFOS and TBT in zebrafish eleutheroembryos, and to identify both common and specific mechanisms of toxicity.

Discussion section.


Transcriptomics
Morphometrics
Metabolism
Epigenetics
Lipidomics

IV. Results

"That all our knowledge begins with experience there can be no doubt"

Immanuel Kant

Chapter I:

Morphometric alterations in zebrafish eleutheroembryos induced by bisphenol A (BPA), perfluorooctanesulfonic acid (PFOS), tributyltin chloride (TBT), and 17-β-estradiol (E2).

Morphological phenotypes of exposure to bisphenol A (BPA), perfluorooctanesulfonic acid (PFOS), tributyltin chloride (TBT), and 17-β-estradiol (E2) in zebrafish (Danio rerio) eleutheroembryos were assessed. The goal was to identify morphometric signatures that could be linked with the mode of action (MoA) of the above mentioned compounds as understanding the MoAs of the different pollutants in human and wildlife health is a key step in environmental risk assessment. At this point, these methodized morphometric analyses in zebrafish embryo model could represent an inexpensive and easy screening tool to predict these MoAs. Using a dose-response setup, morphological equitoxicity at equilethal concentrations were also assessed. No observed adverse effect levels (NOAELs) and lowest observed adverse effect levels (LOAELs) were determined, with the objective to perform the next transcriptomic assays at one of those concentrations.

Morphometric analysis

Measurement of 9 morphological parameters from dorsal and lateral images

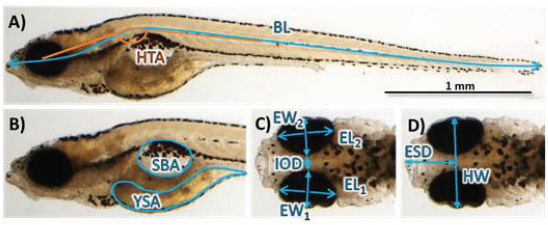

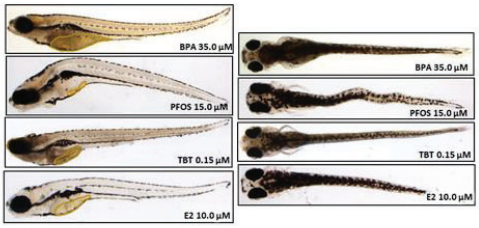

Data integration and characterization of specific morphological phenotypes

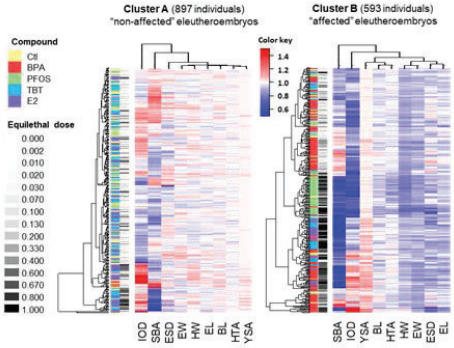

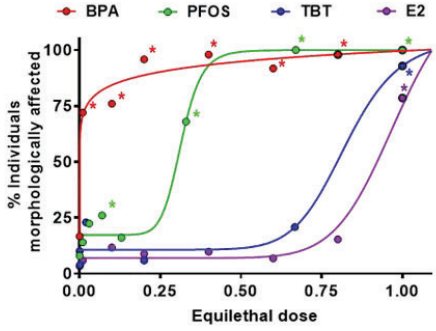

Main results

- Common non-specific adverse effects: increased larvae pigmentation and decreased swim bladder area.
- BPA: yolk sac malabsorption syndrome and altered craniofacial parameters.
- PFOS: notochord malformations (scoliosis and kyphosis).
- TBT: mere developmental delay.
- E2: increased body length.
- Rates of malformations in terms of equilethality: BPA >> PFOS >> TBT > E2.

Scientific article I

Morphometric signatures of exposure to endocrine disrupting chemicals in zebrafish eleutheroembryos

Authors: R. Martínez, L. Herrero-Nogareda, M. Van Antro, M.P. Campos, M. Casado, C. Barata, B. Piña, L. Navarro-Martín

Status: Published

Journal: Aquat. Toxicol. 214 (2019) 105232.

DOI: 10.1016/j.aquatox.2019.105232

Aquatic Toxicology 214 (2019) 105232

Contents lists available at ScienceDirect

Aquatic Toxicology

journal homepage: www.elsevier.com/locate/aqtox

Morphometric signatures of exposure to endocrine disrupting chemicals in zebrafish eleutheroembryos

Rubén Martínez[a,b], Laia Herrero-Nogareda[a], Morgane Van Antro[c,1], Maria Pilar Campos[a], Marta Casado[a], Carlos Barata[a], Benjamin Piña[a], Laia Navarro-Martín[a,*]

[a] Institute of Environmental Assessment and Water Research, IDAEA-CSIC, Barcelona, Catalunya, 08034, Spain
[b] Universitat de Barcelona (UB), Barcelona, Catalunya, 08007, Spain
[c] Laboratory of Evolutionary and Adaptive Physiology, Institute of Life, Earth and Environment, University of Namur, 61 Rue de Bruxelles, B5000, Namur, Belgium

ARTICLE INFO

Keywords:
EDCs
Dose-response
Morphology
Zebrafish
Endocrine disruption
Eleutheroembryo

ABSTRACT

Understanding the mode of action of the different pollutants in human and wildlife health is a key step in environmental risk assessment. The aim of this study was to determine signatures that could link morphological phenotypes to the toxicity mechanisms of four Endocrine Disrupting Chemicals (EDCs): bisphenol A (BPA), perfluorooctanesulfonate potassium salt (PFOS), tributyltin chloride (TBT), and 17-ß-estradiol (E2). Zebrafish (*Danio rerio*) eleutheroembryos were exposed from 2 to 5 dpf to a wide range of BPA, PFOS, TBT and E2 concentrations. At the end of the exposures several morphometric features were assessed. Common and non-specific effects on larvae pigmentation or swim bladder area were observed after exposures to all compounds. BPA specifically induced yolk sac malabsorption syndrome and altered craniofacial parameters, whereas PFOS had specific effects on the notochord formation presenting higher rates of scoliosis and kyphosis. The main effect of E2 was an increase in the body length of the exposed eleutheroembryos. In the case of TBT, main alterations on the morphological traits were related to developmental delays. When integrating all morphometrical parameters, BPA showed the highest rates of malformations in terms of equilethality, followed by PFOS and, distantly, by TBT and E2. In the case of BPA and PFOS, we were able to relate our results with effects on the transcriptome and metabolome, previously reported. We propose that methodized morphometric analyses in zebrafish embryo model can be used as an inexpensive and easy screening tool to predict modes of action of a wide-range number of contaminants.

1. Introduction

In the last decades contaminants of emerging concern have attracted the attention of many researchers due to their novelty and not yet fully understood effects (Diamanti-Kandarakis et al., 2009; Elliott et al., 2017; Jorgenson et al., 2018; Meador et al., 2018), publishing a wide spectrum of studies during the last years (Bieber et al., 2016; Shin and Schideman, 2015; Sousa et al., 2019). This is the case of the Endocrine Disrupting Chemicals (EDCs), which are able to disrupt the hormonal status of exposed individuals, both in animals and humans (Diamanti-Kandarakis et al., 2009; Kinch et al., 2016; Waye and Trudeau, 2011). Nowadays, there is a need to further study the wide range of chemicals that integrate the EDCs (National Research Council (US), 1999; Okkerman P.C, 2000). These include many compounds with different structures and composition, such as polychlorinated organic compounds (*e.g.,* dioxins and PCBs), phthalates, organic solvents (*e.g., xylene and toluene*), brominated flame retardants, parabens, biocides (*e.g.,* carbamates and tributyltin, TBT), perfluoroalkyls (*e.g.,* perfluorooctanoic (PFOA) and perfluorooctanesulfonic (PFOS) acids), alkyl- and bis- phenols (*e.g.,* bisphenol A (BPA) and bisphenol S (BPS)). Moreover other natural compounds, like estrone (E1), estradiol (E2) and estriol (E3), which are accidentally released into the environment (Adeel et al., 2017; Belhaj et al., 2015; Shore and Shemesh, 2016), are also considered EDCs.

EDCs have been linked to alterations of the reproductive success, fertility disruption (Fusani et al., 2007), feminization (Gross-Sorokin

* Corresponding author at: Institute of Environmental Assessment and Water Research, IDAEA-CSIC, Jordi Girona 18, 08034, Barcelona, Spain.
E-mail addresses: rmlqam@cid.csic.es (R. Martínez), laia@plen.ku.dk (L. Herrero-Nogareda), M.vanantro@nioo.knaw.nl (M. Van Antro), mpilarcj@gmail.com (M.P. Campos), mcbbmc@cid.csic.es (M. Casado), cbmqam@cid.csic.es (C. Barata), bpcbmc@cid.csic.es (B. Piña), laianavarromartin@gmail.com (L. Navarro-Martín).
[1] Current address: Department of Terrestrial Ecology, Netherlands Institute of Ecology (NIOO-KNAW), Wageningen, 6708 PB, The Netherlands.

https://doi.org/10.1016/j.aquatox.2019.105232
Received 13 May 2019; Received in revised form 21 June 2019; Accepted 21 June 2019
Available online 24 June 2019
0166-445X/

et al., 2006), neurodevelopmental problems (Kinch et al., 2015), behavior changes (Barrett and Patisaul, 2017; Ottinger et al., 2001) and even morphological abnormalities (Kinch et al., 2016; Sharma et al., 2016). The disruption of the steroidogenic pathway by EDCs is well-known and has been widely reported (Benninghoff et al., 2011; Carpenter, 2013; Lyssimachou et al., 2006; McGinnis and Crivello, 2011; Sanderson, 2006; Shi et al., 2008; Vandenberg et al., 2009). However, it has been shown that EDCs disrupt other hormonal pathways, pointing out the need of more complex and integrative interpretations (Martínez et al., 2018; Regnier and Sargis, 2014; Soto et al., 2009; Vandenberg et al., 2009). In the past, the study of EDCs has focused on lethality, effects at the phenotype level and/or identification and measurement of biomarkers of exposure (Kashiwada et al., 2002; Kinch et al., 2016; Scholz and Mayer, 2008). In the recent years the development of modern omics techniques allowed an advance in the study of EDCs identifying alterations at the molecular level studying the transcriptome, epigenome, proteome, metabolome or lipidome as a whole (Baker and Hardiman, 2014; Fuertes et al., 2018; Helsley and Zhou, 2017; Oliveira et al., 2016; Ortiz-Villanueva et al., 2018; Shrader et al., 2003).

Traditionally qualitative and quantitative observations of animal phenotypes had been related to genetic information contained in the genome. For example, this approach has been performed in human medicine not only to characterize several diseases (Baser et al., 2003; Beheshtian et al., 2008; Costantine et al., 2008; Trebo et al., 2008; Usta et al., 2014) but also to predict them (Listgarten et al., 2014; Mccabe and Mccabe, 2013; Si and Best, 2017; West et al., 2006; Weston and Hood, 2004). The development of next generation sequencing (NGS) technologies has provided new tools to establish genotype-phenotype correlations (Birtel et al., 2018; Huang et al., 2014; Lu et al., 2014; Tafazoli et al., 2018). On the other hand, morphological measures have been classically carried out, but recent studies have shown that the integration of several morphometric parameters permits a better description of different phenotypes (Lantz-Mcpeak et al., 2015; Teixidó et al., 2019). For that reason, it has recently been proposed to use these integrative morphometric analyses as a useful tool to screen possible pathways or modes of action of different pollutants (Teixidó et al., 2019). Recent efforts have been placed to describe and include all the related steps involved in the 'central dogma of the biology' (from DNA to protein) (Benfey and Mitchell-Olds, 2008; Biémont, 2010; Nassiri and McCall, 2018). In this regard, several studies have determined correlations between phenotypic alterations in animal models exposed to pollutants and the effects of those exposures at different biological levels. For example, it has been shown that transcriptomic and metabolomic alterations of exposures to some EDCs concur with the morphological alterations induced by them (Lee et al., 2017; Martínez et al., 2018; Orlando et al., 2004; Ortiz-Villanueva et al., 2018).

The aim of our study was to determine morphological signatures that could link phenotypes to the toxicity mechanisms of EDCs. We used the extensively studied zebrafish (*Danio rerio*), since it is considered a vertebrate model for human and environmental toxicology (Raldúa and Piña, 2014; Segner, 2009; Strähle et al., 2012), it has a highly conserved endocrine system compared to humans (Kimmel et al., 1995; Löhr and Hammerschmidt, 2011) and it has been pointed out as a model organism for the study of the endocrine disruptors in vertebrates (Scholz and Mayer, 2008; Stegeman et al., 2010). In addition, the development of zebrafish embryos (from fertilization up to hatching) and eleutheroembryos (from hatching up to 5 days post-fertilization, dpf) is well known, they can easily be observed using a wide variety of optical methods and their transparency facilitates morphological measures to study possible malformations caused by toxicants (Kimmel et al., 1995; Parichy et al., 2009; Truong et al., 2011). In the present study, we have exposed zebrafish eleutheroembryos from 2 to 5 dpf to different EDCs that have shown estrogenic properties and effects in lipid metabolism/obesity even with a very different chemical structure: BPA, a plastic monomer widely used in bottles (vom Saal et al., 2012); TBT, an antifouling compound used in boats (Penza et al., 2011); perfluorooctanesulfonate potassium salt (PFOS), a fluorosurfactant used in frying pans and fire-fighting foams (Chen et al., 2016); and 17-ß-estradiol (E2), one of the natural estrogenic hormones (Hao et al., 2013). The integration of morphometric parameters was used to analyze the effects of EDCs exposure identifying common and specific morphometric signatures of exposure to each EDC studied.

2. Materials and methods

2.1. Animals and rearing conditions

Adult wild-type zebrafish (*Danio rerio,* 12–18 months old) were maintained under standard conditions (28 ± 1 °C, 12L:12D photoperiod) and fed twice per day with dry flakes (TetraMin, Tetra, Germany). Fish water was composed by Instant Ocean (90 μg/ml, Aquarium Systems, Sarrebourg, France) and $CaSO_4{\cdot}2H_2O$ (100 μg/ml, Sigma-Aldrich, St.Louis. MO- USA), dissolved in reverse-osmosis purified water. Zebrafish eggs were obtained in 4-L breeding tanks by natural mating of the adults (2:1 males:females). A bottom mesh was used to separate adults and eggs. Eggs were collected and rinsed at 2 h post fertilization (hpf) and fertilized ones were placed in 6-well multiplates at a density of 3.3 embryos/ml (10 individuals per well in 3.0 ml of fish water; n = 5–6 replicate wells per group distributed in different 6-well multiplates to account for possible "tank" effects). All procedures were carried out in accordance with the institutional guidelines under a license from the local government (DAMM 7669, 7964) and were approved by the Institutional Animal Care and Use Committees at the Research and Development Centre of the Spanish National Research Council (CID-CSIC).

2.2. Zebrafish larvae exposures

2.2.1. Stocks solutions preparation

Bisphenol A (BPA, CAS-RN: 80-05-7, ≥99.0% purity), perfluorooctanesulfonate potassium salt (PFOS, CAS-RN: 2795-39-3, ≥98.0% purity), tributyltin chloride (TBT, CAS-RN: 1461-22-9, ≥96.0% purity) and 17-ß-estradiol (E2, CAS-RN: 50-28-2, ≥98.0% purity) were provided by Sigma-Aldrich (St. Louis, MO, USA). Stock solutions of each compound covering a wide concentration range were prepared in dimethyl sulfoxide (DMSO) and stored at −20 °C. During the exposure period, fresh experimental solutions (**Supplemental Table ST1**) were prepared every day, dissolving the stock solutions in fish water (final DMSO concentration: 0.2% (v/v)). The pH of the working solutions was found to be between the tolerated range: 6.0–8.5 ensuring its stability after the compound dilution (Avdesh et al., 2012; Reed and Jennings, 2011). Moreover, measured pH after 24 h was found to be stable and there was no need to correct it. Final working solutions for each compound covered a wide concentration range, being the highest tested concentrations enough to achieve 100% mortality of the embryos and the lowest concentrations similar or at the same level as concentrations found for example in harbors waters in case of TBT (Antizar-Ladislao, 2008), human internal circulating fluids levels in case of BPA (Teeguarden et al., 2013), human serum or wild fish eggs concentrations in case of PFOS (Alexander et al., 2008; Kannan et al., 2005) or agricultural effluent and slurries discharges in case of E2 (Adeel et al., 2017; Lecomte et al., 2017).

2.2.2. Zebrafish eleutheroembryos EDC exposures

Zebrafish eleutheroembryos (n = 50–60 individuals per group) were exposed from 2 to 5 days post-fertilization (dpf) to the above mentioned EDCs to the following concentrations: BPA (control (0.2% DMSO), 0.44, 4.4, 8.8, 17.5, 26.3, 35.0, 43.8, 219.0 and 438.0 μM); PFOS (control (0.2% DMSO), 0.2, 0.5, 1.0, 2.0, 5.0, 10.0, 15.0, 20.0 and 200.0 μM); TBT (control (0.2% DMSO), $3.0{\cdot}10^{-4}$, $3.0{\cdot}10^{-3}$, 0.03, 0.10, 0.15, 0.20, 0.25 and 0.30 μM); and E2 (control (0.2% DMSO), 0.1, 1.0,

2.0, 4.0, 6.0, 8.0, 10.0 and 100.0 μM). Exposures started at 2 dpf to avoid confounding factors due to the interference of the pollutants with the processes at very early embryonic stages, to focus in their effects in the already differentiated tissues of the larvae and to avoid the interaction factor due to their different crossing trough the chorion as the hatching of the zebrafish embryos take place between 48 and 72 hpf (Kimmel et al., 1995). Chemical analyses of the solutions were not required as BPA, PFOS, TBT and E2 have been shown to be stable and/or have half-lives of days in absence of catalyzed chemical degradation, specific bacteria or special conditions (Adeel et al., 2017; Cruz et al., 2015; Jordão et al., 2016; Jürgens et al., 2002; Kato et al., 2013; Meng et al., 2017). In any case, and due to the uptake and bioaccumulation of the compounds by the eleuthero/embryos (Souder and Gorelick, 2018) that could decrease the chemicals concentration in the water, the exposure medium was renewed every day to assure that zebrafish eleutheroembryos were exposed appropriately to each compound concentration.

2.2.3. Survival, hatching and swim bladder inflation rates

Survival, hatching and swim bladder inflation rates were assessed during the exposures by visual observation. Survival (at 3, 4 and 5 dpf), hatching rates (at 3, 4 and 5 dpf) and presence of inflated swim bladder (at 4 and 5 dpf) were recorded for each concentration with a dichotomous classification (live or death, hatched or not hatched, and SB inflated or not inflated).

2.2.4. Embryo collection, fixation and annotation of morphological traits

The annotation of morphological traits during normal development was determined to assess possible developmental delays due to the compound's exposure. Control eleutheroembryos (DMSO 0.2%) were collected and fixed at 3, 4, 5 and 6 dpf (30 individuals per day). At the end of the exposures (5 dpf), 50 eleutheroembryos per condition were also sampled and fixed to study the effects of the selected compounds on different morphological traits. Eleutheroembryos were fixed in 4% paraformaldehyde in PBS overnight at 4°°C (in darkness, to avoid different pigmentations due to different light conditions during the fixation process) and then washed several times with PBS. Fixed embryos were gradually transferred to 90% glycerol for conservation and facilitation of embryo placement under the microscope (Raldúa et al., 2008). The eleutheroembryos were stored during few weeks at room temperature and all the conditions from the same tested compound (including its control) were photographed in less than 2–3 days. With the aim of comparing the effects of the different tested compounds without any interfering morphometric alterations due to death processes, experimental conditions with statistical differences in survival rates at 5 dpf (compared to their respective control groups) were discarded for further morphological analysis. Furthermore, equilethal doses for each compound were calculated assigning the equilethal dose of 1.0 to the highest concentration that did not statistically affect survival at 5 dpf: the NOAEC (no observed adverse effect concentration) in terms of lethality. In the case of BPA, we observed a 24% of unhatched larvae and a 38% of larvae exhibiting gross malformations, such as the presence of semi-unrolled tail, at the highest BPA concentration sampled for morphometrics (43.8 μM, 1.0 of equilethal dose). Thus, their positioning under the microscope was not appropriated to ensure the correct measurement of the different morphological parameters. For that reason, this experimental group was excluded from the morphometric analyses.

In order to report morphological effects, lateral and dorsal images of each fixed eleutheroembryo were taken using a stereomicroscope Nikon SMZ1500 (Nikon Co., Tokyo, Japan) coupled with a Nikon digital Sight DS-Ri1 camera. Dorsal overall pigmentation was measured by densitometry. The colour intensity of a parallelogram taken between the middle of the head and the end of the tail (in the dorsal images) was measured using the imaging free software GelAnalyzer 2010a (http://www.gelanalyzer.com/). Background colour intensity was subtracted from each image and fold-changes were calculated respect each control group. In addition, the presence or the absence of scoliosis was annotated for each eleutheroembryo. Using dorsoventral images, a larva was considered to have scoliosis if it had spine malformations in, at least, two different directions presenting a 'zigzag' pattern. Finally, nine morphological traits were measured (**Supplementary Figure S1**) using the free graphical image analysis software ImageJ (National Institutes of Health, Bethesda, MD, USA) (Raldúa et al., 2008). These included: body length (BL), head-trunk angle (HTA), yolk sac area (YSA), swim bladder area (SBA), eye length (EL), eye width (EW), head width (HW), inter-ocular distance (IOD) and eye-snout distance (ESD). In the case of EL and EW, reported values reflect the mean of the size of both eyes. Craniofacial measurements (El, EW, HW, IOD and ESD) were chosen because of the evidences that BPA and TBT can alter visual and/or retinoic pathways (Martínez et al., 2018; Thayer et al., 2012); HTA, due to the possible effects of PFOS in the eleutheroembryos column (Hagenaars et al., 2014; Huang et al., 2010); YSA, because of the effects of the four compounds (BPA, PFOS, TBT and E2) over the lipid metabolism or obesity (Chen et al., 2016; Hao et al., 2013; Penza et al., 2011; vom Saal et al., 2012); and SBA, by virtue of its relationship with the YSA (Raldúa et al., 2008). To distinguish specific malformations caused by the pollutants from mere developmental delays, the length of the eleutheroembryos (BL) was measured as it has been defined as a good indicator of the developmental progress (Kimmel et al., 1995; Parichy et al., 2009; Teixidó et al., 2019).

2.3. Statistical analysis

2.3.1. Survival, hatching, swim bladder inflation rates and morphometric parameters

Differences between treatments in survival, hatching, swim bladder inflation, pigmentation and the nine morphological traits were analyzed using the non-parametric Kruskal-Wallis test with pairwise multiple comparisons (considering $p < 0.05$ as significance level). LC_{50} values were calculated by interpolation on the fitted curves (Hill equations with variable slope) over the survival data. All the raw morphometric measures except for the YSA were normalized to the mean control value ($measure_{Control} = 1.0$). Yolk sac area was expressed in mm^2 using a baseline correction subtracting the YSA mean of the control group to the rest of YSA individual values, avoiding mathematical artifacts due to the fact that YSA mean in the control group was near zero (most control larvae had reabsorbed their yolk sack at 5 dpf). Differences between treatments in the percentage of incidence of scoliosis was analyzed using a Fisher's exact test against the control group (considering $p < 0.05$ as significance level). Correlations between YSA and SBA, and between BL and YSA were performed with Pearson correlation tests ($p < 0.05$). All the statistical analyses were carried out with SPSS 24.0 (Armonk, NY: IBM Corp., 2016) and the associated graphs were performed using GraphPad Prism (v. 6.07, GraphPad Software, La Jolla, CA, USA).

2.3.2. PAM clustering and principal component analyses (PCAs)

With the aim of performing an integrative analysis of all variables and samples, hierarchical clustering and PAM (partition around medoids) clustering analyses were performed using the BPA, PFOS, TBT and E2 exposure morphological traits (normalized and scaled data). After performing a principal component analysis (PCA), the PAM algorithm analyzes the covariance matrix (obtained from the variables) to search k representative objects (medoids) that explain the structure of the data. Each medoid will represent one cluster and is constructed by assigning the nearest observations to it. The number of k medoids is selected to minimize the dissimilarities of the observations to their nearest medoids and accordingly, each observation is assigned to a cluster that represents the general structure of all the variables of this specific observation (sample). Therefore, after the clustering and PAM analysis, the samples of our study were classified in groups (clusters),

depending on the general pattern of all its nine measured parameters. Afterwards, we determined the number of larvae classified in each cluster for the different compound concentrations to establish a general degree of morphological impact produced by each condition (concentration and compound). Fisher's exact tests against each compound control group ($p < 0.05$) were used to establish statistical differences between groups in the percentage of affected individuals.

Two principal component analysis were also used as an unsupervised tool for exploratory data analysis using the nine measured morphological traits. Normalized data was also scaled before performing the PCAs. First PCA was carried out over the developmental data from a total of 128 non-exposed individuals at 3, 4, 5 and 6 dpf. Second PCA was performed over BPA, PFOS, TBT and E2 exposures data from a total of 1490 exposed individuals at different concentrations at 5 dpf. PCA and PAM clustering analyses were both performed and plotted with the packages *stats*, *factoextra*, *FactoMineR, gplots*, *ggplot2, corrplot, fpc*, *fmsb* and *cluster* in R (Hennig, 2014; Kassambara and Mundt, 2017; Lê et al., 2008; Maechler et al., 2019; Mevik and Wehrens, 2015; Nakazawa, 2018; R Development Core Team, 2008; Warnes et al., 2015; Wei et al., 2017; Wickham, 2011).

2.3.3. Polynomial regressions between morphological traits and body length

To study possible alterations on morphological traits due to changes on developmental rates, a polynomial regression was performed for each morphological trait using the non-exposed individuals. Each morphological feature ("y") and body length ("x") of the age developmental controls (3, 4, 5 and 6 dpf) were used to build a second degree polynomial regression ($y = a + b{\cdot}x + c{\cdot}x^2$) which minimized the variance of the coefficients estimators in the model (Ostertagová, 2012; Ziegel et al., 2006). In the regression, an iterative method was used to assure that the multiple variable residuals minimization achieves the global and not a local minimum. Then, body length of each exposed individual was used to estimate predicted values for the different morphological traits of each larvae. Multiple *t*-test (Bonferroni correction) comparing predicted (using the polynomial prediction as a model) versus observed experimental (measured) values was performed for each group and parameter. All the statistical analyses were carried out with SPSS 24.0 (Armonk, NY: IBM Corp., 2016) and the associated graphs were performed using GraphPad Prism (v. 6.07, GraphPad Software, La Jolla, CA, USA).

2.3.4. PLS (partial least squares) analyses

To explore and identify possible morphologic signatures that drive the differences between the ages (3, 4, 5 and 6 dpf) in the developmental controls and between the compounds (BPA, PFOS, TBT and E2) in the exposures, multivariate Partial Least Squares analyses were performed. A Partial Least Squares analysis is a supervised statistical method that finds a linear regression model by projecting observable variables (matrix X) and predicted variables (matrix Y) to a new space. The model is built to find the multidimensional direction that explains the maximum multidimensional variances. In case of the developmental age controls, a PLS1 was performed with 1D vector containing the age of the individuals used as the predicted variable. In case of the exposed data, a PLS2 was performed with a 2D matrix containing both the compound and its concentration as predicted variables (matrix Y). In both cases, the nine morphometric variables were used as predictors (matrix X). Normalized data was log-transformed after adding a negligible value (0.0001) to avoid zeros in the YSA data. In both cases, the features (variables) that best described the differences between groups were identified. Latent variable selection (number of selected components) was performed using cross validation (leave-one-out method) and based on cumulated R^2 (cumulative % of predictable variance), RMSE (Root Mean Squared Error) and cumulated Q^2 index (a statistic calculated from the cross validation that gives an estimate of the predictive power of a PLS model). PLS1 and PLS2 analyses were both performed and plotted with the packages *factoextra*, *FactoMineR, gplots*, *ggplot2 and pls* in R (Kassambara and Mundt, 2017; Lê et al., 2008; Mevik and Wehrens, 2015; R Development Core Team, 2008; Warnes et al., 2015; Wickham, 2011).

2.4. Open data

Raw data as well as analyzed data were submitted to the open repository https://digital.csic.es. The DOI https://doi.org/10.20350/digitalCSIC/8645 was assigned.

3. Results

3.1. Survival, hatching and swim bladder inflation

Survival, hatching and swim bladder inflation rates during and after the exposure are shown as fold change respect the control group in **Supplemental Table ST2** (Kruskal-Wallis non-parametric test, $p < 0.05$). TBT was the tested compound that showed higher lethality at the end of the exposures (5 dpf), with lethal concentrations causing the death of 50% of tested animals (LC_{50}) at 0.17 μM, followed by PFOS with LC_{50} of 18.2 μM. E2 and BPA were the compounds showing higher survival rates, with LC_{50} of 62.4 and 79.9 μM, respectively **(Supplemental Figure SF2)**. To compare the effects of the different tested compounds, equilethal doses were calculated as explained in Section 2.2.4. (**Supplemental Table ST1**, **Supplemental Figure SF2**). Equilethal doses of 1.0 were 43.8 μM for BPA, 15.0 μM in case of PFOS, 10.0 μM for E2 and 0.15 μM for TBT. A decrease in hatching rates was observed at 3, 4 and 5 dpf only at the BPA concentrations ≥ 35.0 μM and at 100 μM E2 (Kruskal-Wallis non-parametric test, $p < 0.05$). Effects on swim bladder inflation appeared at 4 dpf at lower concentrations than the ones affecting survival and hatching in all compounds. A significant decrease in swim bladder inflation was detected at concentrations ≥ 0.10 μM for TBT, 2.0 μM for E2, 5.0 μM for PFOS and 17.5 μM for BPA (Kruskal-Wallis non-parametric test, $p < 0.05$).

3.2. Analysis of the morphological traits

Visual inspection of the fixed larvae (Fig. 1) revealed two major morphological effects. We observed that larvae exposed to high concentrations of all compounds presented darker skin phenotypes compared to their respective controls (**Supplementary Fig. 3**). The same phenotype was also observed prior fixation and indicated an increase on the number and/or the area of the pigment cells. The densitometric results showed that exposed larvae presented a significant increase in pigmentation intensity than their control counterparts (between 12–29%, Kruskal-Wallis non-parametric test, $p < 0.05$). On the other hand, only the exposure to PFOS triggered the appearance of scoliosis at the two highest analyzed concentrations, i.e., 10.0 μM (18% of exposed individuals) and 15.0 μM (40%) (Fisher's exact test, $p < 0.05$; **Supplemental Table ST3**).

Fig. 2 shows fold changes (or differences) in the measured morphological traits at different equilethal doses for all tested compounds. Mean measurements for body length (BL), yolk sac area (YSA), swim bladder area (SBA), head-trunk angle (HTA), eye-snout distance (ESD), eye length (EL), eye width (EW), head width (HW) and inter-ocular distance (IOD) of each compound concentration are shown in **Supplemental Table ST4**. We observed a significant decrease in BL between 3–9% after exposure to the highest analyzed concentrations of BPA, PFOS and TBT (Kruskal-Wallis non-parametric test with pairwise multiple comparisons, $p < 0.05$). Conversely, eleutheroembryos exposed to E2 were statistically bigger (˜3%) than controls at middle concentrations (Kruskal-Wallis non-parametric test with pairwise multiple comparisons, $p < 0.05$). YSA of the exposed eleutheroembryos increased significantly with increasing concentrations in all tested pollutants (Kruskal-Wallis non-parametric test with pairwise multiple comparisons, $p < 0.05$). BPA induced the highest effect with YSA

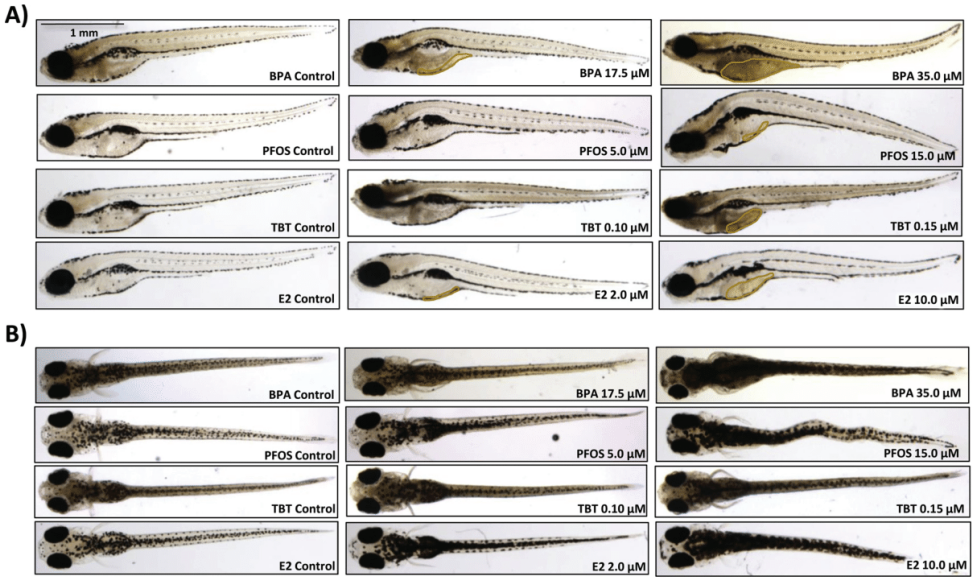

Fig. 1. Lateral (A) and dorsal (B) images of 5 dpf zebrafish eleutheroembryos exposed to BPA, PFOS, TBT and E2. Morphologically-representative images of the control, low observed effect concentration (LOEC, in terms of survival, hatching and swim bladder inflation) and maximum concentration used for the morphometric analysis are shown. Scale bar =1 mm. Yolk sacs are encircled by a yellow line for easier viewing.

reaching 0.125 mm^2 (a size of the YSA equivalent to a control eleutheroembryo at the age of 3.4 dpf) at the highest analyzed dose (35.0 µM). In the case of the E2 and TBT, treated eleutheroembryos at the highest concentrations increased their YSA to 0.048 and 0.039 mm^2, respectively (equivalent to a 4.1 and 4.2 dpf eleutheroembryo). PFOS was by far the compound with the least effect on YSA, reaching 0.011 mm^2 at its highest concentration (equivalent to a 4.6 dpf eleutheroembryo). On the other hand, all pollutants decreased the SBA in a similar dose-response pattern achieving a reduction of 50–64 % at the highest concentrations (Kruskal-Wallis non-parametric test with pairwise multiple comparisons, $p < 0.05$). While PFOS at the two highest concentrations reduced HTA by 12%, the rest of the compounds only affected by approximately 4%. (Kruskal-Wallis non-parametric test with pairwise multiple comparisons, $p < 0.05$).

To establish possible alterations in the head and/or visual perception, craniofacial features were measured. A significant decrease in eye-snout distance (ESD) was observed in all tested pollutants, reaching a maximum difference of 12–17% between the controls and the highest concentration analyzed (Kruskal-Wallis non-parametric test with pairwise multiple comparisons, $p < 0.05$). Similarly, a decrease in eye length (EL), was observed in exposed individuals with reductions of up to 9%, 7%, 12% and 16% for PFOS, E2, TBT and BPA, respectively (Kruskal-Wallis non-parametric test with pairwise multiple comparisons, $p < 0.05$). From all tested compounds, PFOS and BPA presented up to 15% decrease in eye width (EW), but interestingly, BPA significantly decrease of 9% in EW was observed even at the lowest concentration tested (Kruskal-Wallis non-parametric test with pairwise multiple comparisons, $p < 0.05$). Compared to BPA and PFOS, the effects of E2 and TBT in EW was moderate showing a decrease of 7–8 % compared to their respective control groups (Kruskal-Wallis non-parametric test with pairwise multiple comparisons, $p < 0.05$). Similar to the effects on EW, PFOS exposure significantly decreased the head width of exposed eleutheroembryos, reaching a maximum of 20% at the highest concentrations. E2 and TBT only reduced HW significantly between 5–9% at their highest concentration. The response of HW after BPA exposures presented a hormetic shape with intermediate BPA concentrations decreasing HW up to 14%, while highest concentrations decreased it only by 7–8%. Finally, the inter-ocular distance (IOD), together with the YSA and SBA, was one of the traits that was most affected specially by exposure to PFOS and BPA showing opposite effects (Kruskal-Wallis non-parametric test with pairwise multiple comparisons, $p < 0.05$). Interestingly, the effects of exposure on IOD were different for each of the tested pollutants. Following a monotonic dose-response, PFOS exposure reduced IOD up to 35% at the two highest concentrations. Conversely, BPA exhibited a hormetic dose-response pattern with a decrease of the IOD at middle concentrations (up to 24%) and an increase at the high concentrations (up to 23%). TBT and E2 only exhibited significant changes at one of the tested concentrations, with a 7% decrease in IOD at the highest TBT concentration (0.15 µM), and a 14% increase in IOD at intermediate E2 concentrations (6 µM).

3.3. Morphological traits integration analysis

With the aim to integrate the nine morphological parameters, a PCA linked to a partition around medoids (PAM) clustering analysis was performed. The first two components of the PCA explained more than 63% of the data variability and the PAM clustering defined two groups of samples (cluster A and B), including 897 and 593 larvae, respectively (Fig. 3**A** and **B**). Cluster A is integrated by eleutheroembryos from control or low concentration groups with no changes or mild effects in the morphometric parameters compared to controls (Fig. 3B). On the other hand, most of the individuals exposed to high concentrations and almost all BPA exposed individuals clustered together in cluster B (Fig. 3B) and were characterized by moderate and high effects in the morphometric measurements. Accordingly, 91% of the eleutheroembryos of the control groups were classified in the cluster A and 98% of the highest analyzed concentrations were classified in the cluster B. Therefore, we assigned individuals from cluster A as “unaffected” and the ones from cluster B as “affected” by the exposures. Afterwards, we determined the number of larvae classified in each cluster for all the different conditions (compound and concentration) to establish a general degree of morphological impact produced by them (Fig. 3C).

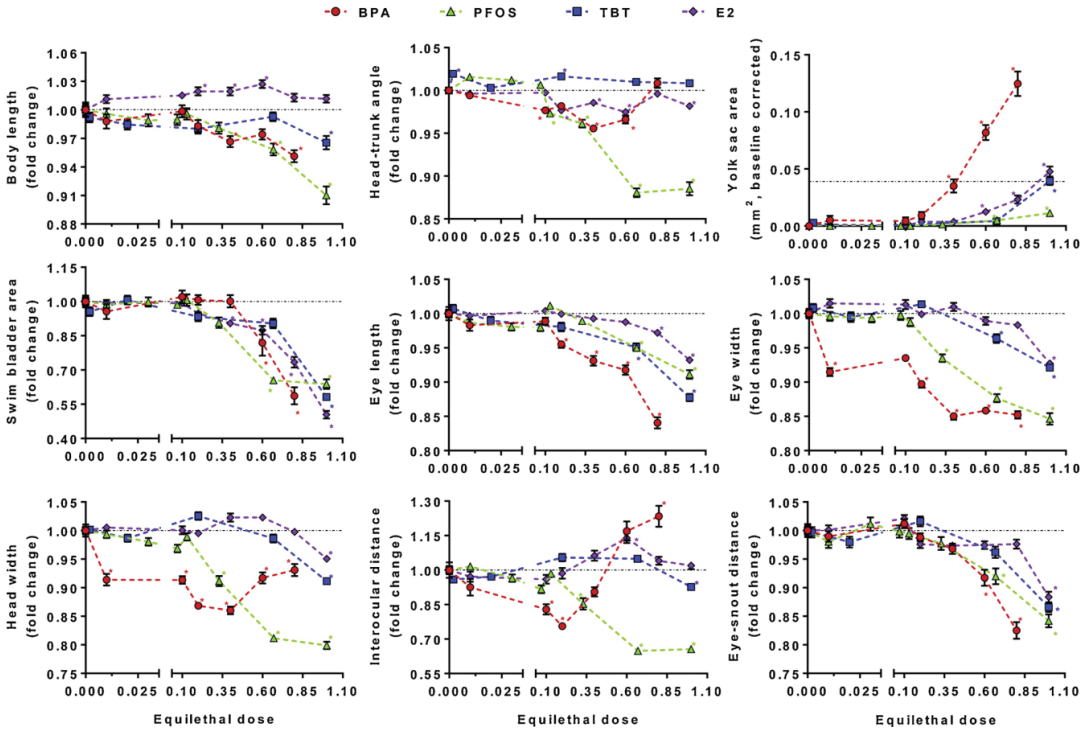

Fig. 2. Morphometric measurements of 5 dpf eleutheroembryos exposed from 2 to 5 dpf to different concentrations of BPA (red), PFOS (green), TBT (blue) and E2 (purple). Represented values per condition are relative to the average of the control group for each of the tested compounds (control average = 1.0), except for YSA which value was corrected by the control baseline (YSA of the control = 0.0). In order to compare the effects of the different tested pollutants, equilethal doses were calculated assigning to each compound the equilethal dose of 1.0 to the highest concentration that did not affected survival at 5 dpf. For each group, the mean (of the relative values) ± SEM (standard error of the mean) is shown (n = 50–60 individuals per group). Non-parametric test (Kruskal-Wallis with all possible pairwise multiple comparisons, $p < 0.05$) was performed. Colored asterisks indicate statistical differences respect each compound control. The morphometric parameters at the BPA equilethal dose = 1.0 were not determined because of the presence of high rates of malformations at this BPA concentration. Data represents a total of 1490 eleutheroembryos. In each sub-graph, control mean value (1.0) is shown at the x-axis with a black dotted line, except for the YSA where it represents the mean value of the 4 dpf control group (0.039 mm^2).

Considering equilethal concentrations, BPA and FPOS morphologically affected larvae at much lower concentrations than TBT and E2. In the case of BPA, the percentage of affected eleutheroembryos was statistically significant in all tested concentrations, reaching almost 75% of affected individuals at much lower concentrations than the rest of tested pollutants (equilethal concentration of 0.01 and 0.1, respectively, Fisher's exact test, $p < 0.05$). These concentrations were far away from the BPA doses where it starts to affect the larvae survival (morphometric $EC_{50} \sim 0.001\%$ of the equilethal dose) indicating that the BPA is the most morphological-affecting compound regarding its lethality, compared with the other three pollutants. After BPA, we observed that PFOS was the pollutant with the second highest morphological impact with almost 70% of the individuals affected at 5 μM PFOS (equilethal concentration of 0.33, Fisher's exact test, $p < 0.05$). The EC_{50} of PFOS was approximately at 30% of its equilethal dose, indicating that it had a mild effect in the morphology. Much higher concentrations were needed for TBT and E2 to produce significant differences in the percentage of affected individuals (93 and 79%, respectively): only their highest equilethal doses (1.0) had significant differences (Fisher's exact test, $p < 0.05$). The EC_{50} of TBT and E2 were at 80 and 92% of theirs equilethal doses, respectively. Therefore, TBT and E2 were the compounds with slighter effect in morphology, only showing morphometric changes at concentrations close to lethality.

3.4. Toxicity in development versus specific morphological effects of exposures

The developmental effects of the pollutants that triggered the morphological alterations that were observed could be caused by a mere effect of the EDCs in the developmental pace (growth and development) or by specific morphological alterations over a certain tissue/s (dysmorphogenesis). In order to distinguish toxicity in the development from specific morphological alterations caused by exposure to the different pollutants, a morphometric analysis was carried out in control samples at 3, 4, 5 and 6 dpf. As expected, we observed that during normal development: BL increased while HTA decreased; YSA decreased because larvae started to consume the yolk sac reservoir reaching a complete depletion at 5 dpf; SBA increased due to the start of swim bladder inflation at this age; ESD, EL and EW distances increased with age and IOD and HW presented different trends at different ages (**Supplementary Table ST4).** As a way to visualize how morphometric parameters changed with development, we carried out a PCA using morphometric data from 3, 4, 5 and 6 dpf non-exposed eleutheroembryos. Results indicate that although only two components had Eigenvalues higher than 1, three components were necessary to have a quality of representation of all variables between 60 and 95% (**Supplementary Figure SF4**). These 3 components explained up to 75.8% of the data variability. Representation of the selected components is showed in Fig. 4**A**, **B** and **C**. We observed that component 1

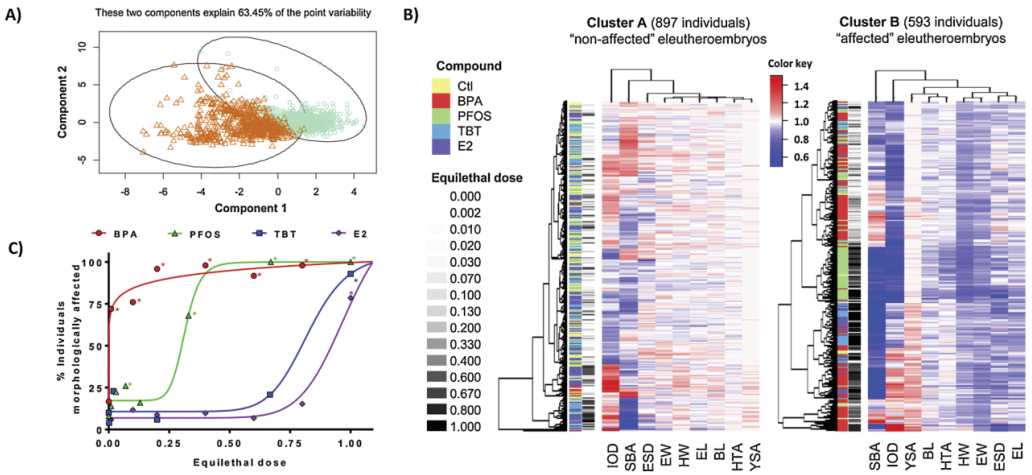

Fig. 3. A) Medoid PAM clustering of the measured morphometric traits from all eleutheroembryos exposed to BPA, PFOS, TBT and E2 (n = 50–60 individuals per group) by PCA analysis. The first two components of the PCA explained 63.45% of the data variability and defined two groups of individuals: cluster A with 897 individuals assigned as "non-affected" eleutheroembryos (cyan) and cluster B with 593 individuals assigned as "affected" eleutheroembryos (orange). **B)** Heatmaps of measurements of morphometric traits of "non-affected" and "affected" eleutheroembryos after exposure to BPA, PFOS, TBT and E2. Values were normalized by each control group parameter (control average = 1.0). Exceptionally, for the yolk sac area and to avoid the bias due to the proximity of its values to zero, data was base-corrected and centered to 1.0 respect the control group and used as input value. Color scale ranges from red to blue (increase or decrease, respectively, in the measure of the parameter, respect the mean value of the control group). Both rows (individuals) and columns (parameters) were grouped by hierarchical clustering and the corresponding dendrograms are shown at the left and the top of the panel, respectively. Color legends indicate both the equilethal dose (in grey scale) and the compound (yellow: control; red: BPA; green: PFOS; blue: TBT; purple: E2). **C)** Percentage of eleutheroembryos morphologically affected by the exposures (assigned to cluster B) for each condition (type of pollutant and equilethal dose). Experimental groups are represented in different colors: BPA in red, PFOS in green, TBT in blue and E2 in purple. Dose-response patterns were adjusted by a sigmoidal model.

reflected mainly the contribution of YSA, SBA, BL, ESD, EL and EW and differentiated samples with different ages. On the other hand, component 2 was mainly driven by IOD and HW while component 3 had a clear and unique influence of HTA contribution. With the aim to select the morphometric variables statistically relevant for the age development (drivers), a Partial Least Squares (PLS1) analysis was performed (Fig. 4D). Three components were selected which explained 70.1 and 83.1% of the variability in the X (predictors, morphometric data) and y (responses, age of the individuals) matrices, respectively. It could be observed that BL, YSA, SBA, EL and ESD were the morphologic signatures (VIP score > 1.0) that mainly drove the changes in the development. Although EW had a VIP score higher than IOD, HW and HTA, and had a reasonably contribution in the first component of the PCA, its VIP score was lower than 1.0 so it couldn't be considered as a driver for the growth in these early developmental stages. Thus, these results indicate that IOD, EW, HW and HTA are parameters that are not directly related to changes in development and growth at the analyzed ages (3–6 dpf).

It is also well known that larvae body length is a trait that perfectly follows growth and developmental progress in zebrafish, in some cases even better than age (Kimmel et al., 1995; Parichy et al., 2009; Teixidó et al., 2019). Fig. 5 represents the mean measurements of the different morphological traits respect to the mean body length for all experimental groups at 5 dpf, as well as for the control groups at different developmental ages (3, 4, 5 and 6 dpf). Results indicated that some of the observed effects (at least at the low doses) could be due to a general effect of the pollutants on developmental rates and growth. Consequently, with the objective to differentiate the morphometrical changes that were driven by a compound specific effect and not related to a delay or advance in the development, the experimental morphological values of each larvae (all conditions considered) were compared with its predicted values (calculated using a polynomial regression performed using the developmental control individuals (3–6 dpf) and their individual body length). We observed that in most cases, when the effects of the pollutants on the different morphological traits were compared with those ones tacking into account differences in body length (BL), results did not substantially change (Fig. 6**A** and **B**). Although some could be attributed to changes in growth, these results indicate a prevalence of a specific mode of action of the pollutants over a general effect on the eleutheroembryos development.

One of the most distinct effects observed between the different compounds tested in the present study was the effect of the exposures on YSA. We observed that in some cases retention of yolk sac reservoir was partially attributable to the fact that eleutheroembryos size was affected. For example, an increase in YSA was observed in medium doses of BPA and E2 (15.5 and 6.0–8.0 μM, respectively), but this was found to be related to eleutheroembryos size (Figs. 5 and 6B, observed-predicted difference: $p > 0.01$ in both cases). Similarly, the YSA increase in embryos exposed to the highest TBT concentration could be attributable to the fact that eleutheroembryos were smaller in size (Fig. 5 and 6B, observed-predicted difference: $p > 0.01$). Interestingly, different tendencies were observed between compounds after considering observed effects on development. Eleutheroembryos exposed to the highest BPA and E2 doses (26.3–35.0 and 10.0 μM, respectively) retained more yolk sac ($p < 0.001$ in both cases) than the predicted for individuals of their size (Fig. 6B, observed-predicted difference: $p < 0.001$-0.01 for BPA and $p < 0.0001$ for E2). In contrast, results demonstrated that after considering eleutheroembryo size, disruption of yolk sac consumption by exposure to PFOS was affected in a completely different way than for BPA (and highest E2 dose). Although exposed eleutheroembryos to highest concentrations of PFOS presented higher YSA than their control counterparts at 5 dpf (Fig. 2 and 6B, $p < 0.01$ and $p < 0.001$ at 10.0 and 15.0 μM, respectively), eleutheroembryos showed to have lower YSA values than the ones corresponding to their size (Fig. 6B, observed-predicted difference: $p < 0.01$ for 5.0 μM and $p < 0.0001$ for 10.0 and 15.0 μM).

In relation to changes observed in SBA our results showed that those were mostly not correlated to changes in growth. Despite of the fact

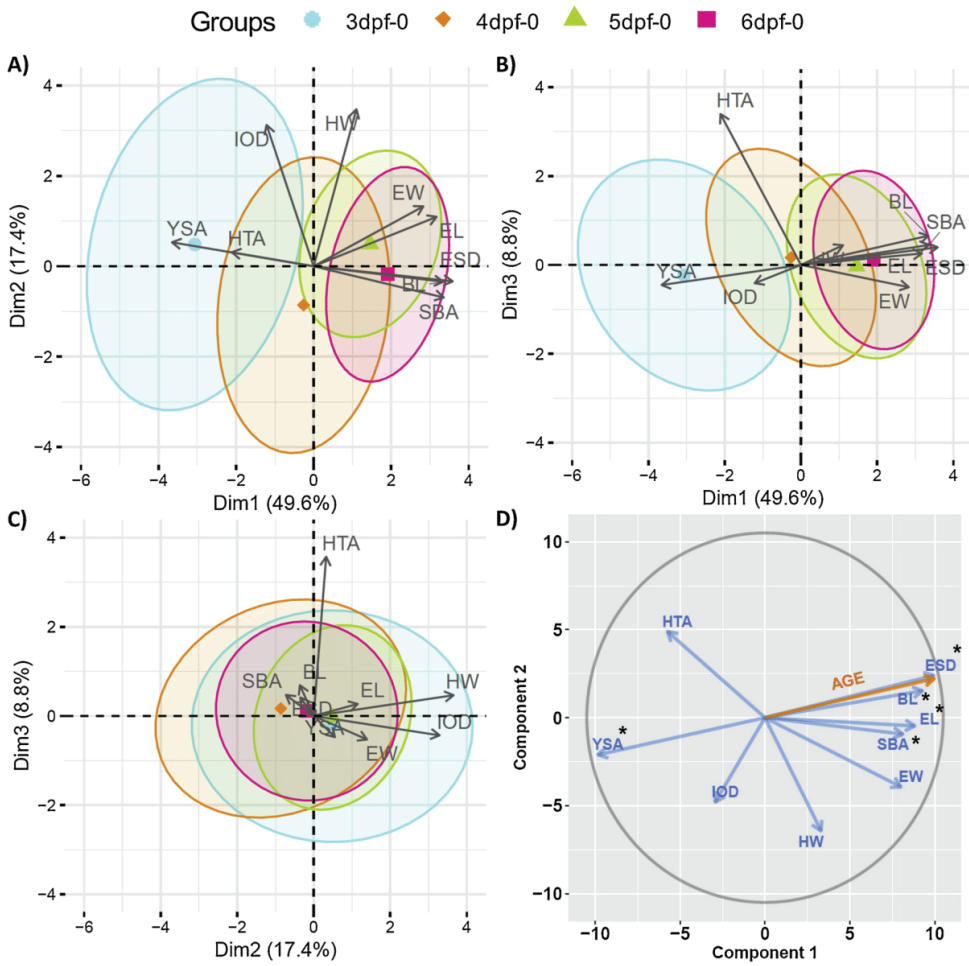

Fig. 4. A, B, C) Representation of the selected components from a Principal Component Analysis (PCA) using morphometric data from 3 (cyan), 4 (orange), 5 (green) and 6 dpf (pink) non-exposed eleutheroembryos (n = 29–35 individuals per group). Standardized values (normalized by the average of the control group and centered to zero) were used as input data, except for the YSA, which was corrected by the control baseline (being also zero the average of the control group). The three first components represented up to 75.8% of the data variability. Arrows represent variable (morphological traits) loadings indicating contribution of each variable to differentiate between individuals. The centroid of each group is shown as a color sphere to avoid oversaturation of the graph. **D)** First two components of a Partial Least Squares (PLS1) analysis using the control developmental age morphometric data (3, 4, 5 and 6 dpf). The nine morphometric variables were used as predictors (matrix X), normalized and log-transformed after adding a negligible value (0.0001) to avoid the zeros in the YSA. Unidimensional vector containing the age of the individuals was used as responses (matrix y). Three components were selected to construct the model which explain 70.1 and 83.1% of the variability in the X- and y-matrix, respectively. First two graphed components explain 57.8 and 82.1% of the variability in the X- and y-matrix, respectively. Blue and orange arrows represent the loadings of X-matrix (morphological traits) and y-matrix (age) variables. The morphologic signatures that drive the changes in the development (BL, YSA, SBA, EL and ESD) are marked with an asterisk and were selected based on their VIP score values (VIP score > 1.0).

that BL and SBA were both decreased by BPA, PFOS and TBT exposures (Fig. 6A, $p < 0.01$), differences between observed and predicted values on SBA were even observed when eleutheroembryo size was considered (Fig. 6B, $p < 0.01$). In the case of E2, whereas an increase in size was observed at intermediate concentrations ($p < 0.05$), a decrease in SBA was detected ($p < 0.01$) with increasing concentrations (Fig. 6A) and that observation was maintained after accounting for eleutheroembryo size (Fig. 6B, $p < 0.001$). We also observed that effects on YSA and SBA seem to be related (Fig. 6). Our results supported that observation and we found a significant inverse correlation between YSA and SBA (**Supplementary Figure SF5**, Pearson correlation: $p = 0.0003$). The decrease in HTA observed after exposures to increasing concentrations of BPA, PFOS and E2 (Fig. 6A, $p < 0.05$), was also observed when BL was considered. That indicates a specific effect of the exposures over this morphometric parameter, which barely exhibit any changes in control animals from different ages (and consequently different sizes) and was not considered as a driver for the development (Fig. 4C). In the case of observed effects of exposures on eye-snout distance (ESD) we found that those were mostly related to changes in BL. The decrease on ESD observed at the highest TBT concentration was related to lower eleutheroembryo BL (Fig. 6B, $p > 0.01$). In the case of BPA and PFOS, observed effects on ESD were mostly found to be related also to changes in BL, except for the highest tested concentrations, where animals showed lower and higher ESD, respectively, than what corresponded for their size (Fig. 6B, $p < 0.001$ and $p < 0.0001$, respectively). Interestingly, E2 treated individuals presented significant lower ESD at

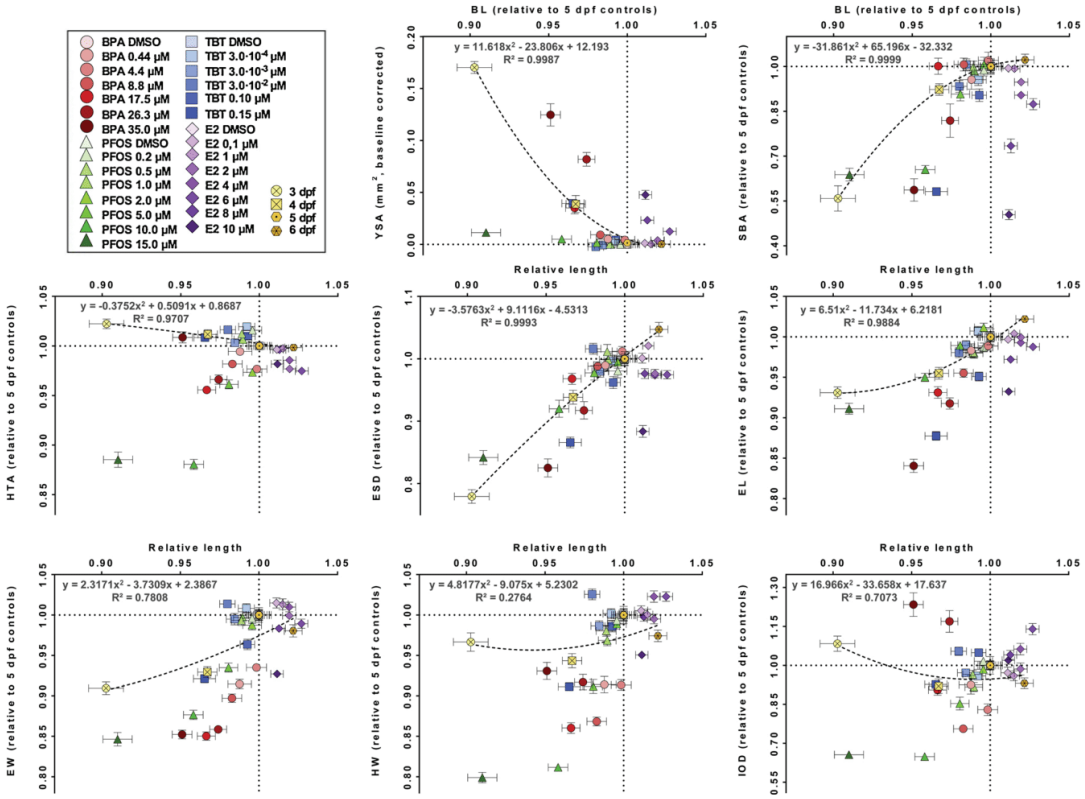

Fig. 5. Graphic representation of the relative body length (BL) versus the relative values of the different morphometric parameters measured in control eleutheroembryos at different ages (3, 4, 5 and 6 dpf) and exposed eleutheroembryos to different concentrations of BPA, PFOS, TBT and E2 at 5 dpf. Represented morphological traits are the following: yolk sac area (YSA), swim bladder area (SBA), head-trunk angle (HTA), eye-snout distance (ESD), eye length (EL), eye width (EW), head width (HW) and inter-ocular distance (IOD). Represented values for control eleutheroembryos at different ages (3 dpf, triangles; 4 dpf, squares; 5 dpf, dots; and 6 dpf, rhombus) are displayed in yellow. Dashed lines represent a polynomial regression performed for each morphological trait using non-exposed individuals measured from 3 to 6 dpf (regression parameters are indicted in the figure. Represented values for exposed eleutheroembryos are relative to the average of the control groups at 5 dpf for each of the tested compounds (control average = 1.0), except for YSA which value was corrected by the control baseline (YSA of the control = 0.0). Exposures to different pollutants are displayed in different colors: BPA in red, PFOS in green, TBT in blue and E2 in purple. Dotted lines (x = 1.0, y = 1.0) represents control averages at 5 dpf. The color scale for each individual compound increase in intensity/darkness with the increasing concentrations. For each experimental condition, the mean (of the relative values) ± SEM (standard error of the mean) is shown (data represent n = 29–35 individuals per group for the age controls and 50–60 individuals for the exposed groups).

relatively low concentrations (2 µM or higher, Fig. 6B) that did not appear significant when body length was not considered (Fig. 6A) due to the fact that E2 increased BL at moderate concentrations.

On the other hand, eye length (EL), eye width (EW) and head width (HW) were mostly not related to changes in body size during the 3–6 dpf stage and the significant alterations over them caused by the tested compounds corresponded to specific effects of the pollutants. In all cases, individuals exposed to increasing concentrations showed lower EL than the predicted value considering their size (Fig. 6B, $p < 0.001$). Changes in eye width (EW) and head width (HW) responded in a similar way, with BPA and PFOS showing observed measures smaller than the predicted ones (considering the animal size). On the other hand, TBT and E2 were dependent on the concentration tested (Fig. 6B) exhibiting generally highest EW and HW than their predicted, except for their highest concentration (15.0 and 10.0 µM, respectively) when they exhibit an opposite pattern. Finally, while TBT showed no specific effect on inter-ocular distance (IOD) (Fig. 6B, $p > 0.01$), opposite trends were observed for PFOS and E2, where individuals exposed to increasing concentrations of PFOS presented smaller IOD (Fig. 6B, $p < 0.0001$) and the ones exposed to intermediated concentrations of E2 presented bigger IOD (Fig. 6B, $p < 0.0001$) than what was expected for their size, respectively. Interestingly, a pronounced hormetic effect in IOD was observed in exposed BPA eleutheroembryos (Fig. 6A), characterized by a decrease of this parameter at low-intermediated BPA concentrations and an increase at high BPA concentrations (Fig. 2, **Supplementary Figure SF6**). This hormetic response was found to be unrelated to changes in BL, since same behavior was observed after considering BL (Fig. 6B, $p < 0.0001$).

3.5. Morphological signatures of BPA, PFOS, TBT and E2 exposures

Unsupervised PCA analysis performed on the exposed individuals' morphometric data indicate that although only two components had Eigenvalues higher than 1, five components were necessary to include major contribution of all variables. Selecting 5 components the quality of representation of all variables were found to be higher than 75% (**Supplementary Figure SF7**). These 5 components explained up to 87.7% of the data variability. Representation of the selected components is showed in **Supplementary Figure SF8**. We observed that component 1 reflected mainly the contribution of HW, EW, EL, BL, SBA

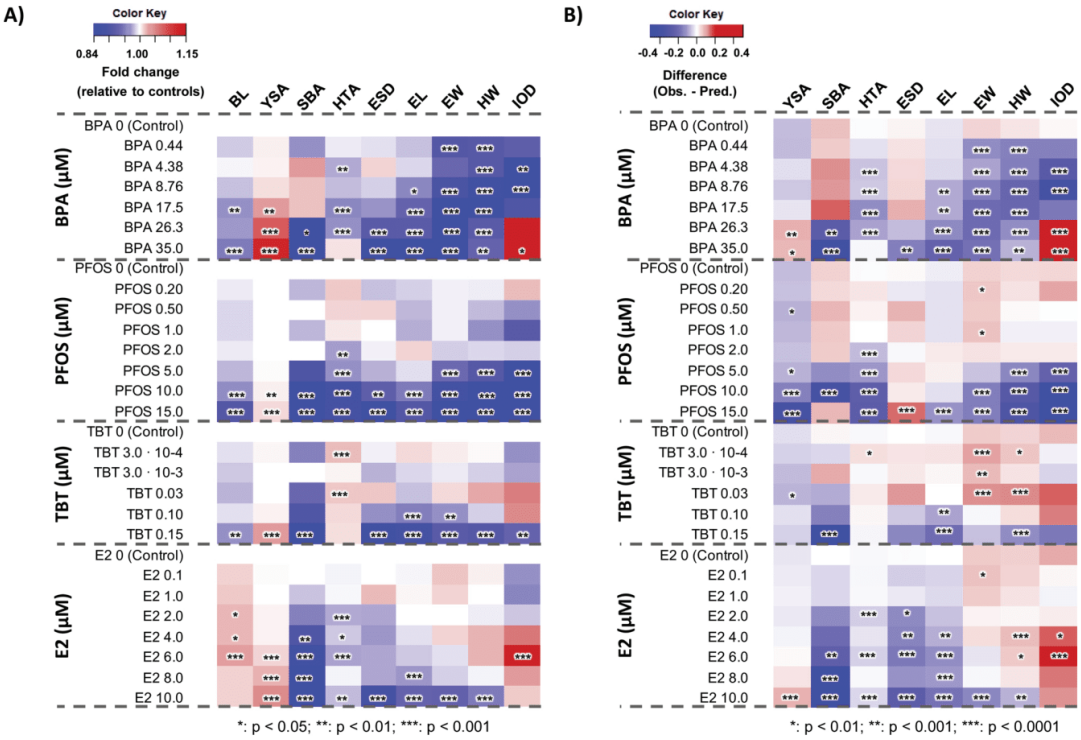

Fig. 6. A) Heatmap corresponding to relative average measurements of all morphological traits at 5 dpf for each of the tested compounds (n = 50–60 individuals per group). Values represent relative average values with respect the average of the control groups at 5 dpf. Represented morphological traits are the following: yolk sac area (YSA), swim bladder area (SBA), head-trunk angle (HTA), eye-snout distance (ESD), eye length (EL), eye width (EW), head width (HW) and inter-ocular distance (IOD). Color scale ranges from red (increase respect to controls) to blue (decrease respect to controls). White represents values similar to controls (control average = 1.0). Non-parametric Kruskal-Wallis test was performed for each group and parameter to determine significant differences from the control group. Asterisks mark groups statistically different from the control: * ($p < 0.05$), ** ($p < 0.01$), *** ($p < 0.001$). **B)** Heatmap corresponding to the difference between the observed experimental values of the morphometric parameters and their predicted values when considering eleutheroembryo body length. Predicted values for each morphometric trait were estimated from individuals body length using the polynomial regressions indicated in Fig. 5. Then, predicted values were subtracted from observed values (observed - predicted) and averages calculated and represented for each experimental group. Color scale ranges from red (higher than the expected value) to blue (lower than the expected value). White represents no differences between observed and predicted. Multiple *t*-test (Bonferroni correction) was performed for each group and parameter using each predicted value as a reference group to determine significant differences. Asterisks mark groups where the experimental value was statistically different from its predicted one: * ($p < 0.01$), ** ($p < 0.001$), *** ($p < 0.0001$).

and ESD to differentiated individuals exposed to increasing concentrations. The rest of components helped to visualize differences between compounds. Component 2 was mainly driven by YSA and IOD differentiating individuals exposed to BPA and PFOS. Component 3 driven by BL, HTA and YSA differentiate TBT from the rest of compounds. Component 4 driven by HTA and SBA separated E2 and PFOS from TBT and BPA. Results were not evident in the case of component 5, mainly driven by SBA, suggesting that this component could include only biological variation.

Finally, we performed a multivariate partial least square regression (PLS2) with the aim to predict morphological features that characterizes each compound exposure and that differentiate it from the others. Based on cumulated RMSE and Q^2 coefficients we selected 4 components that explained up to 80.2 and 36.1% of the X-block (morphometric variables) and the Y-block (tested compounds and concentrations) variance, respectively (**Supplementary Figure SF9**). To explain the contribution of each morphological trait to differentiate between components in each of the model components, variables with VIP (Variable Importance in Projection) scores higher than 1 were selected and therefore are the only ones described below (Fig. 7). The first component reflected the general dose-response effect of all tested compounds in HTA, EL, EW and HW (Fig. 7). In particular, it can be observed that component 1 explained the large decrease in EL, EW and HW produced by BPA and PFOS compared with those produced by TBT and E2 (Fig. 6B). Moreover, it also described a higher decrease in HTA produced at the highest equilethal concentrations of PFOS and BPA (followed by E2). It is remarkable at this point that the nine morphological traits play a role over the compound loading so, for example, although E2 produced a reduction in the HTA, its loading have still the same sign (and not the opposite) due to its lack of effects on the EL, EW and HW. This principle that related loadings with the morphometric effects of each pollutant applies for all the components. Subsequently, component 2 helped us to explain the main differences between PFOS treated individuals and the rest. It was clear that loadings for PFOS in this component had opposite sign than for the other compounds (Fig. 7). Meanwhile results showed a large increase in the YSA produced by BPA and followed by TBT, E2 and PFOS (which was slighter than the other three compounds, Fig. 2), we observed that individuals exposed to PFOS presented less YSA than what corresponded to their size (the opposite behaviour that was found for BPA, and E2, with animals showing bigger YSA than their predicted value; Fig. 6B). Furthermore, separation of PFOS from the rest of the compounds could be

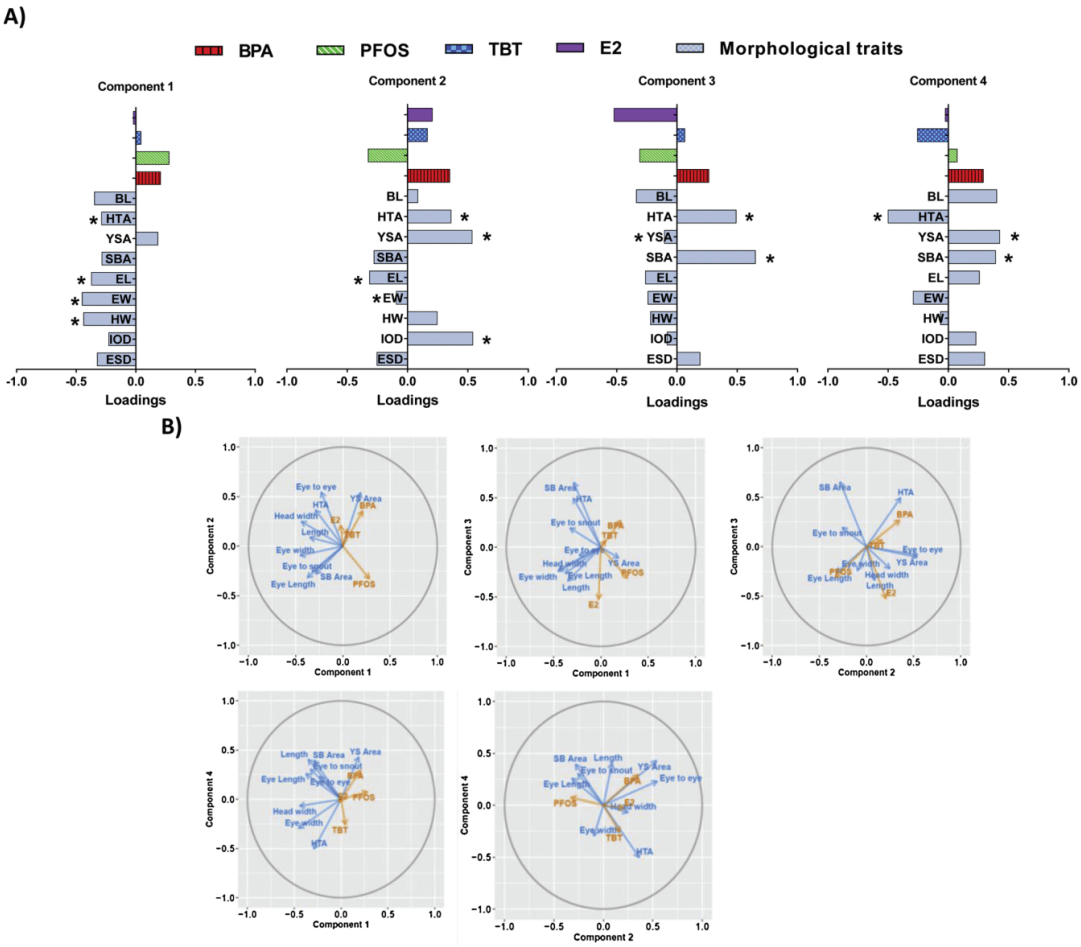

Fig. 7. Multivariate Partial Least Squares (PLS2) model performed with the exposed eleutheroembryo morphometric data using morphometric variables as predictors (X-block matrix) and a 2D matrix containing both the compound and its concentration as responses (Y-block matrix). A total of 9 morphological traits measured in 1490 eleutheroembryos (n = 50–60 individuals per condition) were analyzed from eleutheroembryos exposed to BPA, PFOS, TBT and E2. Normalized data were log-transformed after adding a negligible value (0.0001) to avoid the zeros in the YSA. **A)** PLS loadings of the compounds and the morphological traits for the four first components (C1, 2, 3 and 4) of the PLS2 analysis, which explained up to 80.2 and 36.1% of the X-block (morphometric variables) and the Y-block (tested compounds and concentrations), respectively. Asterisks mark the variables with a VIP score > 1.0. **B)** Loadings representation for each pair of components. Compounds and morphological traits loadings are colored in orange and blue, respectively.

explained by the fact that it was the only compound that showed a high decrease in the IOD with increasing concentrations (Figs. 2 and 6A). Although IOD showed a statistically hormetic behaviour only in BPA, it presented a similar pattern in TBT and E2 (albeit at different concentrations and opposite trend than observed for BPA), but not at PFOS, helping the separation of PFOS in this component. The contribution of a major decrease of HTA in PFOS exposed animals (compared to the other 3 compounds) is also present in this component (Fig. 7). Component 2 also helped to explain differences that differentiate BPA from TBT and E2. For example, it can be also observed how EL and EW enhanced BPA loading due to the major effect of this compound on these morphological traits (Fig. 6A). Both component 3 and 4 basically defined the effects of the four compounds over the HTA, YSA and SBA. In the case of component 3, major morphometric variables were HTA and SBA and the corresponding loadings for each compound point out that this component reflected differences between the effects of BPA from the ones caused by exposures to PFOS and E2. In particular, the compound with a higher negative loading in component 3 was E2 because of the fact that was the compound with highest decreases on SBA (Figs. 2 and 6A) at the same time that reduced HTA. PFOS showed a similar negative correlation, due to their decrease (Figs. 2 and 6A) at both parameters at the same time. Conversely, BPA and TBT increases SBA and HTA, respectively, at some concentrations (although it is not statistically significative in the case of the BPA) which produces an annulment with the other parameter and made positive their loading at component 3. On the other hand, results showed that component 4 differentiate TBT (the only compound that significantly increased HTA) mainly from BPA. In this component, HTA, YSA and SBA presented VIP scores > 1 and their loadings are similar to each other so an explanation regarding all these three morphometrical data is needed: HTA (negative loading value) is increased in TBT (-), YSA (positive loading value) is slightly increased (+), and SBA (positive loading value) is decreased (-) so the final loading of TBT is negative. In case of BPA: YSA (+), HTA (+, double negative) and SBA (=, hormetic behaviour) so its compound

loading is positive. In case of PFOS and E2, the final value is close to zero due to the annulment of the respective morphological traits.

4. Discussion

Zebrafish embryo morphologic malformations can be used to study the effects of exposure to different compounds and model the underlying etiological mechanisms involved in the response to pollutant exposures (Raghunath and Perumal, 2018; Truong et al., 2011; Zhang et al., 2017). Traditionally, researchers have focused in the study of singular morphological effects and/or effects on development (such as hatching delays or growth effects on embryos), demonstrating the potential of morphometric analysis to assess specific effects of some toxicants (Teixido et al., 2017; Teixidó et al., 2019). In the present study, we have not only evaluated and compared individual morphological effects of BPA, TBT, PFOS and E2, but also have integrated all the studied parameters to elucidate and determine general and specific morphometric signatures of exposure to BPA, TBT, PFOS and E2.

Our study determined that the compound that was most toxic in terms of lethality was the TBT followed by PFOS, E2 and BPA, with LC_{50} values of 0.17, 18.2, 62.4 and 79.9 μM, respectively. These results are very similar and in the same order of magnitude of previously reported LC_{50} for zebrafish larvae exposed to TBT (0.17-0.34 μM) (Dong et al., 2006; Kalasekar et al., 2015), PFOS (25 μM) (Jantzen et al., 2016) and BPA (12–25 ppm, i.e. 53–110 μM) (Chen et al., 2011; Moreman et al., 2017; Saili and Tanguay, 2013). Although no specific LC_{50} values for E2 (17β-estradiol) were found for other studies, its lethality in zebrafish embryos was found to be between 10 and 100 μM (Chandrasekar et al., 2010; Kishida et al., 2001), a similar range to that found in this study. In contrast, we observed that in general the tested compounds affected most of the studied morphological parameters in an inverse manner regarding its lethal toxicity: for example, BPA was the compound with higher malformation rates at comparable equilethal concentrations but the one with lower toxicity (higher LC_{50}); and TBT presented the highest toxicity (lowest LC_{50}) but a low rate of morphological alterations. E2, the only natural compound (endogenous estrogen) studied, did not present the same trend. In terms of survival, hatching and swim bladder inflation rates, we established LOECs (lowest observed effect concentrations) of 0.1 μM for TBT, 2.0 μM for E2, 5.0 μM for PFOS and 17.5 μM for BPA, results that were very similar to other previous studies (Lam et al., 2011; Martínez et al., 2018; Ortiz-Villanueva et al., 2018).

Our results showed an increase in pigmentation intensity in the individuals exposed to increasing concentrations of the four pollutants (BPA, PFOS, TBT and E2). This general effect is well described and has been previously reported by other researchers when fish larvae are exposed to several contaminants (Fushimi et al., 2009; Huang et al., 2010; Lam et al., 2011; Ortiz-Villanueva et al., 2018), but also when those are reared under stress conditions (Backström and Winberg, 2017; Nilsson Sköld et al., 2013), indicating that the observed changes in pigmentation were a non-specific response to stress. In general, we also observed a dose-response pattern when looking at the effect of the exposures on animal body length (BL), with PFOS being the compound that most affected growth. Although PFOS caused scoliosis and kyphosis (reduced HTA), the measured effects on growth were not due to these phenomena, since BL was measured across the larvae notochord (**Supplementary Figure SF1**) and not from the snout to the tail following a straight line. We also observed a reduction of BL in eleutheroembryos exposed to BPA as well as for TBT (although only detected at the highest tested concentration), suggesting that it could be caused by a general toxic effect and/or developmental delay, as shown in other studies (Qiu et al., 2018; Teraoka et al., 2002). On the other hand, our results showed that exposures to intermediate E2 concentrations significantly increased eleutheroembryos length. This is in concordance with other studies that have shown acceleration and increased growth (BL) in fish and amphibia exposed to estrogens (reviewed by Bulaeva et al., 2015). This effect has found to be related to the role of estrogens in growth hormone regulation (Cook, 2004; Fernández-Pérez et al., 2013; Leung et al., 2004).

Previous studies have proposed that GH also regulates lipid storage and control adipocyte lipolysis in other fish species (Albalat, 2005; Company et al., 1999; Mingarro et al., 2002) suggesting a possible role of the growth hormone in the yolk sac during the fish development (Di Prinzio et al., 2010), considering that the yolk sac is a main reservoir of lipids in the eleutheroembryo. One of the most remarkable findings of our study was the general effects on YSA after exposure to BPA, PFOS, TBT and E2, suggesting that lipid disruption may occur. This is in concordance with the fact that the tested compounds in this study are considered potential obesogens by the world health organization (WHO, (Bergman et al., 2013)). Interestingly, we found that there were differences in YSA response to the different compounds tested. At first, we observed that exposure to all tested compounds induced yolk sac retention with increasing concentrations, partially attributable to the fact that eleutheroembryos size was also affected by the exposures. However, our results also showed differences between compounds with 3 clear responses: 1) BPA specially, but also E2, exposures triggered eleutheroembryos to retain more yolk sac than what corresponded for their size; 2) PFOS exposed eleutheroembryos retained less yolk sac than the corresponded for their size; and 3) TBT exposed eleutheroembryos showing YSA that corresponded to their body size. We observed that E2 exposed eleutheroembryos accelerated growth at intermediated concentrations (2–4 μM) with complete consumption of the yolk sac, suggesting that eleutheroembryos were capable to use all the energy stored in the yolk sac. However, between 6–8 μM the YSA was increased and at 10 μM yolk malabsorption syndrome was observed (with larvae retaining more yolk sac that the one corresponding to animals of the same size (Raldúa et al., 2008)). Animals exposed to 26.3–35 μM BPA clearly showed yolk sac malabsorption syndrome, as smaller individuals retained greater YSA. Several studies have reported that the obesogenic effects of BPA can be explained by its binding to ERs (estrogen receptors) (Heindel and Schug, 2014; Mu et al., 2018), PPAR-ϒ (peroxisome proliferator-activated receptor gamma) (Martínez et al., 2018), RXR (retinoid X receptor) (Martínez et al., 2018), and ERR-ϒ (estrogen-related receptor gamma) (Bergman et al., 2013; Tohmé et al., 2014), inducing adipogenesis and obesity. The fact that both E2 and BPA are known to disrupt estrogen receptor (Bhandari et al., 2015; Moreman et al., 2017; Zhao et al., 2017), together with the recently published results that demonstrate that exposures to BPA and E2 in zebrafish eleutheroembryo trigger similar transcriptomic effects on genes linked to lipid metabolism (Martínez et al., 2018), suggest that both compounds might have similar modes of action and that interact simultaneously with different cellular targets, causing the observed macroscopic effects on YSA. Conversely, retention of yolk sac in PFOS exposed eleutheroembryos was very low. Interestingly, and as mentioned previously, PFOS exposures decreased eleutheroembryo BL, but contrary to BPA, exposed animals had less yolk sac reservoir than what should be expected for their size. PFOS and other perfluorinated compounds interaction with different PPAR receptors have also been reported (Holtcamp, 2012; Martínez et al., 2019) and obesogenic effects assessed (Bergman et al., 2013). In this regard, we have recently published that exposure to PFOS at 0.03 mg/L (0.1 μM), a concentration below the lowest dose tested in the present study, significantly increased transcripts related to lipid transport and metabolism (Martínez et al., 2019). Therefore, we conclude that observed effects on YSA are due to disruption of lipid transport and metabolism pathways. Finally, we observed that changes in yolk sac area in TBT exposed eleutheroembryos were associated mostly to changes in growth, demonstrating that the observed increase in YSA was mainly due to delays in growth, probably associated to a decrease in energy needs, and in consequence, to yolk sac consumption. It has been proposed that the effects of TBT in lipid metabolism (Bergman et al., 2013) are related to its interaction with the PPAR-ϒ and the RXR receptors (Heindel and Schug, 2014; Thayer et al., 2012; Zang et al., 2018). Nevertheless, we suggest that in

our study, the relationship between observed increases in YSA by TBT exposures and any possible observed effect at the transcriptomic level, could be more related to a delay in development rather than a direct disruption of the lipid metabolism pathway related to yolk sac reabsorption. From all the exposed above, we conclude that observed differences on the eleutheroembryo YSA response after exposures to BPA, PFOS, TBT and E2 are mostly due to the differences in their mode of action. Other researchers have linked EDCs dysregulation of energy consumption and metabolism with obesity (reviewed by Petrakis et al., 2017). Therefore, considering that the YSA is the principal energy reservoir of the zebrafish larvae up to 5 dpf, from which the nutrient uptake occurs, we suggest that the observed effects in this study on YSA could also be related to dysregulation of energy consumption and metabolism.

Results from our study showed that exposures to BPA, PFOS, TBT and E2 to increasing concentrations affected eleutheroembryos swim bladder area (SBA) indicating an impairment of swim bladder inflation. To elucidate if this impairment was related to developmental delays, eleutheroembryo body size was considered. We observed that in general, SBA experimental values of exposed eleutheroembryos were lower than the predicted ones by their body size, indicating that the observed effects in SBA were not due to developmental delays caused by the exposures. During development, inflation of the swim bladder naturally occurs after the depletion of the yolk sac (Robertson et al., 2007) and it has been suggested that swim bladder inflation delays can be a consequence of the mechanical pressure carried out by voluminous yolk sac remnants (Raldúa et al., 2008). Our results showed a strong relation between YSA and SBA suggesting that impairment of swim bladder inflation was related to mechanical pressure from the yolk ball and not directly related to effects on development and growth. Other negative effects in the SB inflation have been proposed as the thyroid disruption (Stinckens et al., 2018), which could be the case of all our four compounds (Sharan et al., 2014; Šošić-Jurjevic et al., 2015; Stinckens et al., 2018). Moreover decreases in the heart rate related to SB inflation have been also described by others (Yue et al., 2015). Particularly, previous studies showed that exposures to BPA and TBT reduced heart rates (Mu et al., 2018) while E2 increased them (Romano et al., 2017). In the case of PFOS, other studies showed contradictory results (Dang et al., 2018; Ding et al., 2011). For that reason, although effects in SB inflation in BPA and TBT exposed animals could be related to heart rate alterations in our study, opposite (for E2) or contradictory (for PFOS) effects suggest that this generalized effect on SB inflation could be more related to the observed alterations in yolk sac absorption.

One of the most specific effects of the exposures to PFOS was the high impact of this compound in the notochord formation and body length (Huang et al., 2010; Shi et al., 2008). Our results showed that eleutheroembryos exposed to PFOS presented much higher rates of scoliosis and also a much higher reduction of head-trunk angle (HTA), a.k.a. kyphosis, than the other compounds. This specificity was also denoted by the fact that HTA barely changed in control animals at these developmental stages (3–6 dpf), pointing out that any observable effects in this morphological trait was completely unrelated to developmental or growth delays. Similar spinal deformities in zebrafish larvae exposed to PFOS have been hypothesized to be related to dysregulations in myosin and others muscle fibers (Huang et al., 2010). That is coincident in our studies, with transcriptomic dysregulations in myosin, actin and tropomyosin transcripts showing a dose-response pattern according to increasing PFOS concentrations (Martínez et al., 2019).

Interestingly, another result that drew our attention was the observed alterations of craniofacial features caused more specifically by BPA (even at the lowest tested concentrations). Since the observed effects of head width was a combination of eye width and inter-ocular distance, we will only discuss these two craniofacial features. From one side, our results demonstrated that increasing concentrations of BPA provoked a decrease in eye size (microphtalmia) that was not found to be directly related to developmental delays. Similar or related effects in visual functions as visual behavior alterations, dysruption in opsin transcripts expression or craniofacial abnormalities were also observed in zebrafish exposed to BPA and its derivatives (Kinch et al., 2016; Liu et al., 2018; Pelayo et al., 2012). Moreover, we have recently shown that exposing eleutheroembryos to BPA during the same concentrations and developmental period caused dysregulation of genes related to vision (Martínez et al., 2018). However, whether gene disruption is a cause or a consequence of a reduction of eye size remains unknown, since both effects were observed at the same BPA concentrations. We therefore suggest that alterations in visual functions could be related to the eye malformations observed in the present study, but further studies that include BPA doses that do not affect eye size are needed to understand the underlying mechanism. On the other hand, several studies had proposed the interaction of BPA with the thyroid and retinoid pathways, as one mode of action of this compound not only for zebrafish but also in other species, via binding with the TR and RXR receptors (Boucher et al., 2014; Iwamuro et al., 2006; Martínez et al., 2018; Pelayo et al., 2012). Retinoid pathway plays a key role during the eye development and microphtalmia has been also reported during thyroid hormone T3 exposures (Pelayo et al., 2012). In this regard, we also previously reported dysregulation of the retinoid pathway in eleutheroembryos after BPA exposures, but not for the thyroid pathway (Martínez et al., 2018). Although further studies are necessary to make any conclusions, we suggest that is probable that the disruption of the retinoid pathway by exposure to BPA might be altering eye formation and development. Another remarkable result from our study was the hormetic response of the zebrafish eleutheroembryo inter-ocular distance (IOD) after BPA exposures, with intermediated concentrations decreasing IOD and higher concentrations triggering its increase. Other studies reported an increase in IOD after 15.0 μM BPA exposures during 7 days (Mccormick et al., 2010). Although at the same concentration eleutheroembryos exposed in our study presented similar IODs than their control counterparts and higher concentrations were required to observe increased IODs, these results aren't contradictory since the previous study exposed the larvae for a longer period. It has been proved that BPA exposures affected the development of the midbrain structure of developing zebrafish larvae via *otx* (orthodenticle homeobox) genes (Mercier et al., 1995; Tse et al., 2013). Furthermore, microphthalmia is a disease that has been associated with alterations in the *otx* human orthologues ((Howe et al., 2012), http://zfin.org), indicating that *otx* disruption by BPA could be not be only responsible for the effects on IOD but also on eye size, in conjunction with the via RXR, above explained. Another study demonstrated that BPA altered zebrafish larvae behavior by reducing their movements (Olsvik et al., 2019). With all the exposed above in mind, another question that remains unknown is whether alterations in behavior by BPA could be due to vision impairment caused by BPA-induced microphthalmia and cranial malformations. This could explain BPA specific effects in yolk sac consumption and lipid metabolism already discussed since a reduced movement phenotype could be linked to less energy requirements and consequently, less lipid reservoir expenditure. Accordingly with previous results (Jantzen et al., 2016), we observed that PFOS exposures also affected craniofacial features of exposed zebrafish eleutheroembryos (shown as decreases in EW and IOD at highest concentrations, even when considering body length reduction). Although others have found alterations of the thyroid system (Ghassabian and Trasande, 2018; Lee and Choi, 2017; Wang et al., 2014) by PFOS exposures, we haven't found in our recent study any alterations at the molecular level associated to vision, thyroid or retinoic pathways (Martínez et al., 2019), suggesting that exposures to PFOS might not alter vision function at the tested concentrations.

In summary, we have found that TBT, with higher lethality (lower LC_{50}) than PFOS, BPA and E2, produced less morphological effects (and those were mainly observed at the highest equilethal doses) and that BPA, with less toxicity (highest LC_{50}), induced higher morphological effects (even at the lowest doses). We can also conclude that

morphological effects of both TBT and E2 were mostly related to alterations in developmental rates and can be assigned to non-specific effects of the pollutant. This was particularly true for the case of TBT. In the case of E2, we also reported a clear effect on growth, with exposed animals showing higher body lengths. This was contrary to what we observed for the rest of the compounds, where exposed individuals were smaller than their control counterparts. On the other hand, the higher degree of morphological malformations observed in eleutheroembryos exposed to BPA (even at its lowest concentrations) and in the ones exposed to the medium-high PFOS concentrations were mostly related to specific effects and not to general alterations in developmental rates. Exposure to BPA induced the yolk sac malabsorption syndrome and also characterized by alterations on craniofacial traits. On the other hand, it was remarkable that malformations of eleutheroembryo notochord (appearance of scoliosis and kyphosis) was one of the main alterations produced in PFOS exposures. In general, the results indicate that the four studied compounds, with different chemical structure but common related effects in the estrogenic and lipid pathways (according to the bibliography), trigger different specific and non-estrogenic related morphological alterations most likely due to different ligand-receptor interactions. Results obtained in the present study will be very useful to establish linkages between effects at the transcriptome (Martínez et al., 2018) and metabolome (Ortiz-Villanueva et al., 2018) levels with observed morphological effects after exposures to the tested compounds. Further studies involving gene expression and gain and loss of functions (i.e. knockout experiments (Cornet et al., 2018; Housden et al., 2016; Varshney et al., 2013)) should be performed to establish correlations between the above mentioned phenotypic and transcriptomic changes. The combination of all available information at the different organizational levels will help us to understand and better characterize modes of action of the studied compounds in an integrative and a holistic manner.

5. Conclusion

It is known that the toxicity of the different pollutants does not underlie only in a general oxidative stress mechanism by reactive oxygen species (ROS), but also in specific ligand-receptor interactions, which are different in each case and explain the distinctive effects of each toxicant. In this scenario, we think that integration analysis of morphometric data can be used as a useful tool to study specific morphological effects in zebrafish embryo model which can be related to the underlying mode of action of the compound and, thereby, be an inexpensive and easy screening to predict modes of action of a wide-range number of contaminants. Integration of these morphometrics analyses with further biomolecular *omics* studies will allow us to elucidate and better understand pollutants modes of action, a main component of the toxicity characterization, one of the central elements of the environmental risk assessment, together with the environmental exposure characterization.

Acknowledgments

This work was supported by a grant from the Spanish Ministry of Economy and Competitiveness (ref. CTQ2014-56777-R). LNM was supported by a H2020-Marie Skłodowska-Curie Action MSCA-IF-RI-2017 awarded by the European Commission (ref. 797725-EpiSTOX). RM was supported by an FPU predoctoral fellow from the Spanish Ministry of Education and Science (ref. FPU15/03332). We thank Chiara Luccarelli for helping with eleutheroembryos measurements.

Appendix A. Supplementary data

Supplementary material related to this article can be found, in the online version, at doi:https://doi.org/10.1016/j.aquatox.2019.105232.

References

Adeel, M., Song, X., Wang, Y., Francis, D., Yang, Y., 2017. Environmental impact of estrogens on human, animal and plant life: a critical review. Environ. Int. 99, 107–119. https://doi.org/10.1016/j.envint.2016.12.010.

Albalat, A., 2005. Nutritional and hormonal control of lipolysis in isolated gilthead seabream (Sparus aurata) adipocytes. AJP Regul. Integr. Comp. Physiol. 289, R259–R265. https://doi.org/10.1152/ajpregu.00574.2004.

Alexander, J., Atli Auðunsson, G., Benford, D., Cockburn, A., Cravedi, J.-P., Dogliotti, E., Di Domenico, A., Luisa Fernández-Cruz, M., Fink-Gremmels, J., Fürst, P., Galli, C., Grandjean, P., Gzyl, J., Heinemeyer, G., Johansson, N., Mutti, A., Schlatter, J., van Leeuwen, R., van Peteghem, C., Verger, P., 2008. Perfluorooctane sulfonate (PFOS), perfluorooctanoic acid (PFOA) and their salts Scientific Opinion of the Panel on Contaminants in the Food chain. EFSA J. 6, 1–131. https://doi.org/10.2903/j.efsa.2008.653.

Antizar-Ladislao, B., 2008. Environmental levels, toxicity and human exposure to tributyltin (TBT)-contaminated marine environment. A review. Environ. Int. https://doi.org/10.1016/j.envint.2007.09.005.

Avdesh, A., Chen, M., Martin-Iverson, M.T., Mondal, A., Ong, D., Rainey-Smith, S., Taddei, K., Lardelli, M., Groth, D.M., Verdile, G., Martins, R.N., 2012. Regular care and maintenance of a zebrafish (Danio rerio) laboratory: an introduction. J. Vis. Exp. e4196. https://doi.org/10.3791/4196.

Backström, T., Winberg, S., 2017. Serotonin coordinates responses to social stress-What we can learn from fish. Front. Neurosci. https://doi.org/10.3389/fnins.2017.00595.

Baker, M.E., Hardiman, G., 2014. Transcriptional analysis of endocrine disruption using zebrafish and massively parallel sequencing. J. Mol. Endocrinol. https://doi.org/10.1530/JME-13-0219.

Barrett, E.S., Patisaul, H.B., 2017. Endocrine disrupting chemicals and behavior: re-evaluating the science at a critical turning point. Horm. Behav. 96, A1–A6. https://doi.org/10.1016/j.yhbeh.2017.09.010.

Baser, M.E., Kuramoto, L., Joe, H., Friedman, J.M., Wallace, A.J., Ramsden, R.T., Evans, D.G.R., 2003. Genotype-phenotype correlations for cataracts in neurofibromatosis 2. J. Med. Genet. 40, 758–760.

Beheshtian, A., Baranzini, S.E., Okuda, D.T., Zamvil, S.S., Cree, B.A.C., Caillier, S., Qualley, P., Nelson, S.J., Pelletier, D., Wang, J., Hauser, S.L., George, M., Leppert, D., Goodin, D.S., Gomez, R., Lincoln, R., Srinivasan, R., Waubant, E., Oksenberg, J.R., 2008. Genotype–phenotype correlations in multiple sclerosis: HLA genes influence disease severity inferred by 1HMR spectroscopy and MRI measures. Brain 132, 250–259. https://doi.org/10.1093/brain/awn301.

Belhaj, D., Baccar, R., Jaabiri, I., Bouzid, J., Kallel, M., Ayadi, H., Zhou, J.L., 2015. Fate of selected estrogenic hormones in an urban sewage treatment plant in Tunisia (North Africa). Sci. Total Environ. 505, 154–160. https://doi.org/10.1016/j.scitotenv.2014.10.018.

Benfey, P.N., Mitchell-Olds, T., 2008. From genotype to phenotype: systems biology meets natural variation. Science 80. https://doi.org/10.1126/science.1153716.

Benninghoff, A.D., Bisson, W.H., Koch, D.C., Ehresman, D.J., Kolluri, S.K., Williams, D.E., 2011. Estrogen-like activity of perfluoroalkyl acids in vivo and interaction with human and rainbow trout estrogen receptors in vitro. Toxicol. Sci. 120, 42–58. https://doi.org/10.1093/toxsci/kfq379.

Bergman, Å., Heindel, J.J., Jobling, S., Kidd, K.A., Zoeller, R.T., 2013. State of the science of endocrine disrupting chemicals 2012 - summary for decision makers. WHO. https://doi.org/10.1590/S1414-462X2013000100003.

Bhandari, R.K., Deem, S.L., Holliday, D.K., Jandegian, C.M., Kassotis, C.D., Nagel, S.C., Tillitt, D.E., vom Saal, F.S., Rosenfeld, C.S., 2015. Effects of the environmental estrogenic contaminants bisphenol A and 17α-ethinyl estradiol on sexual development and adult behaviors in aquatic wildlife species. Gen. Comp. Endocrinol. 214, 195–219. https://doi.org/10.1016/j.ygcen.2014.09.014.

Bieber, S., Rauch-Williams, T., Drewes, J.E., 2016. An assessment of international management strategies for CECs in water. ACS Symposium Series 11–22. https://doi.org/10.1021/bk-2016-1241.ch002.

Biémont, C., 2010. From genotype to phenotype. What do epigenetics and epigenomics tell us? Heredity (Edinb). 105, 1–3. https://doi.org/10.1038/hdy.2010.66.

Birtel, J., Gliem, M., Mangold, E., Müller, P.L., Holz, F.G., Neuhaus, C., Lenzner, S., Zahnleiter, D., Betz, C., Eisenberger, T., Bolz, H.J., Issa, P.C., 2018. Next-generation sequencing identifies unexpected genotype-phenotype correlations in patients with retinitis pigmentosa. PLoS One 13, e0207958. https://doi.org/10.1371/journal.pone.0207958.

Boucher, J.G., Husain, M., Rowan-Carroll, A., Williams, A., Yauk, C.L., Atlas, E., 2014. Identification of mechanisms of action of bisphenol A-induced human preadipocyte differentiation by transcriptional profiling. Obesity 22, 2333–2343. https://doi.org/10.1002/oby.20848.

Bulaeva, E., Lanctôt, C., Reynolds, L., Trudeau, V.L., Navarro-Martín, L., 2015. Sodium perchlorate disrupts development and affects metamorphosis- and growth-related gene expression in tadpoles of the wood frog (Lithobates sylvaticus). Gen. Comp. Endocrinol. 222, 33–43. https://doi.org/10.1016/j.ygcen.2015.01.012.

Carpenter, D.O., 2013. Effects of Persistent and Bioactive Organic Pollutants on Human Health. Wiley.

Chandrasekar, G., Archer, A., Gustafsson, J.Å., Lendahl, M.A., 2010. Levels of 17β-estradiol receptors expressed in embryonic and adult zebrafish following in vivo treatment of natural or synthetic ligands. PLoS One 5, e9678. https://doi.org/10.1371/journal.pone.0009678.

Chen, J., Wang, X., Ge, X., Wang, D., Wang, T., Zhang, L., Tanguay, R.L., Simonich, M., Huang, C., Dong, Q., 2016. Chronic perfluorooctanesulphonic acid (PFOS) exposure produces estrogenic effects in zebrafish. Environ. Pollut. 218, 702–708. https://doi.org/10.1016/j.envpol.2016.07.064.

Chen, X.N., Hang, X.M., Ke, W.B., Ma, Z.Y., Sun, Y.Q., 2011. Acute and Subacute Toxicity of Bisphenol A on Zebrafish (Danio rerio). Adv. Mater. Res. 356–360, 138–141. https://doi.org/10.4028/www.scientific.net/amr.356-360.138.

Company, R., Calduch-Giner, J.A., Kaushik, S., Pérez-Sánchez, J., 1999. Growth performance and adiposity in Gilthead sea bream (Sparus aurata): risks and benefits of high energy diets. Aquaculture. https://doi.org/10.1016/S0044-8486(98)00495-5.

Cook, D.M., 2004. Growth hormone and estrogen: a clinician's approach. J. Pediatr. Endocrinol. Metab. 17 (Suppl. 4), 1273–1276.

Cornet, C., Di Donato, V., Terriente, J., 2018. Combining Zebrafish and CRISPR/Cas9: toward a more efficient drug discovery pipeline. Front. Pharmacol. https://doi.org/10.3389/fphar.2018.00703.

Costantine, M., Toutain, A., Aït Yahya-Graison, E., Taine, L., Bottani, A., Sinet, P.-M., Florentin-Arar, L., Kitsiou, S., Dahoun, S., Gehrig, C., Lespinasse, J., Doco-Fenzy, M., Gagos, S., Lyle, R., Antonarakis, S.E., Pelet, A., Cornillet-Lefèbvre, P., Lopez, G., Delabar, J.M., Colleaux, L., Wakamatsu, N., Lyonnet, S., Horst, J., Schinzel, A., Kennerknecht, I., Béna, F., Franklin, J.C., Descartes, M., 2008. Genotype–phenotype correlations in Down syndrome identified by array CGH in 30 cases of partial trisomy and partial monosomy chromosome 21. Eur. J. Hum. Genet. 17, 454–466. https://doi.org/10.1038/ejhg.2008.214.

Cruz, A., Anselmo, A.M., Suzuki, S., Mendo, S., 2015. Tributyltin (TBT): a review on microbial resistance and degradation. Crit. Rev. Environ. Sci. Technol. 45, 970–1006. https://doi.org/10.1080/10643389.2014.924181.

Dang, Y., Wang, F., Liu, C., 2018. Real-time PCR array to study the effects of chemicals on the growth hormone/insulin-like growth factors (GH/IGFs) axis of zebrafish embryos/larvae. Chemosphere 207, 365–376. https://doi.org/10.1016/j.chemosphere.2018.05.102.

Di Prinzio, C.M., Botta, P.E., Barriga, E.H., Ríos, E.A., Reyes, A.E., Arranz, S.E., 2010. Growth hormone receptors in zebrafish (Danio rerio): adult and embryonic expression patterns. Gene Expr. Patterns 10, 214–225. https://doi.org/10.1016/j.gep.2010.03.001.

Diamanti-Kandarakis, E., Bourguignon, J.-P., Giudice, L.C., Hauser, R., Prins, G.S., Soto, A.M., Zoeller, R.T., Gore, A.C., 2009. Endocrine-disrupting chemicals: an endocrine society scientific statement. Endocr. Rev. 30, 293–342. https://doi.org/10.1210/er.2009-0002.

Ding, G.H., Zhang, J., Chen, Y.H., Luo, G.Y., Mao, C.H., 2011. Acute toxicity effect of PFOS on zebrafish embryo. Adv. Mater. Res. 356–360, 603–606. https://doi.org/10.4028/www.scientific.net/amr.356-360.603.

Dong, W., Muramoto, W., Nagai, Y., Takehana, K., Stegeman, J.J., Teraoka, H., Hiraga, T., 2006. Retinal neuronal cell is a toxicological target of tributyltin in developing zebrafish. J. Vet. Med. Sci. 68, 573–579.

Elliott, S.M., Brigham, M.E., Lee, K.E., Banda, J.A., Choy, S.J., Gefell, D.J., Minarik, T.A., Moore, J.N., Jorgenson, Z.G., 2017. Contaminants of emerging concern in tributaries to the Laurentian Great Lakes: I. Patterns of occurrence. PLoS One 12, e0182868. https://doi.org/10.1371/journal.pone.0182868.

Fernández-Pérez, L., Guerra, B., Díaz-Chico, J.C., Flores-Morales, A., 2013. Estrogens regulate the hepatic effects of growth hormone, a hormonal interplay with multiple fates. Front. Endocrinol. (Lausanne) 4, 66. https://doi.org/10.3389/fendo.2013.00066.

Fuertes, I., Jordão, R., Casas, F., Barata, C., 2018. Allocation of glycerolipids and glycerophospholipids from adults to eggs in Daphnia magna: perturbations by compounds that enhance lipid droplet accumulation. Environ. Pollut. 242, 1702–1710. https://doi.org/10.1016/j.envpol.2018.07.102.

Fusani, L., Della Seta, D., Dessì-Fulgheri, F., Farabollini, F., 2007. Altered reproductive success in rat pairs after environmental-like exposure to xenoestrogen. Proc. R. Soc. B Biol. Sci. 274, 1631–1636. https://doi.org/10.1098/rspb.2007.0064.

Fushimi, S., Wada, N., Nohno, T., Tomita, M., Saijoh, K., Sunami, S., Katsuyama, H., 2009. 17β-Estradiol inhibits chondrogenesis in the skull development of zebrafish embryos. Aquat. Toxicol. 95, 292–298. https://doi.org/10.1016/J.AQUATOX.2009.03.004.

Ghassabian, A., Trasande, L., 2018. Disruption in thyroid signaling pathway: a mechanism for the effect of endocrine-disrupting chemicals on child neurodevelopment. Front. Endocrinol. (Lausanne). https://doi.org/10.3389/fendo.2018.00204.

Gross-Sorokin, M.Y., Roast, S.D., Brighty, G.C., 2006. Assessment of feminization of male fish in English rivers by the Environment Agency of England and Wales. Environ. Health Perspect. 114, 147–151. https://doi.org/10.1289/ehp.8068.

Hagenaars, A., Stinckens, E., Vergauwen, L., Bervoets, L., Knapen, D., 2014. PFOS affects posterior swim bladder chamber inflation and swimming performance of zebrafish larvae. Aquat. Toxicol. 157, 225–235. https://doi.org/10.1016/j.aquatox.2014.10.017.

Hao, R., Bondesson, M., Singh, A.V., Riu, A., McCollum, C.W., Knudsen, T.B., Gorelick, D.A., Gustafsson, J.Å., 2013. Identification of estrogen target genes during zebrafish embryonic development through transcriptomic analysis. PLoS One 8, e79020. https://doi.org/10.1371/journal.pone.0079020.

Heindel, J.J., Schug, T.T., 2014. The obesogen hypothesis: current status and implications for human health. Curr. Environ. Heal. Reports 1, 333–340. https://doi.org/10.1007/s40572-014-0026-8.

Helsley, R.N., Zhou, C., 2017. Epigenetic impact of endocrine disrupting chemicals on lipid homeostasis and atherosclerosis: a pregnane X receptor-centric view. Environ. Epigenetics 3. https://doi.org/10.1093/eep/dvx017.

Hennig, C., 2014. fpc: flexible procedures for clustering [WWW Document]. URL. http://cran.r-project.org/package=fpc.

Holtcamp, W., 2012. Obesogens: an environmental link to obesity. Environ. Health Perspect. 120, a62–a68. https://doi.org/10.1289/ehp.120-a62.

Housden, B.E., Muhar, M., Gemberling, M., Gersbach, C.A., Stainier, D.Y.R., Seydoux, G., Mohr, S.E., Zuber, J., Perrimon, N., 2016. Loss-of-function genetic tools for animal models: cross-species and cross-platform differences. Nat. Rev. Genet. https://doi.org/10.1038/nrg.2016.118.

Howe, D.G., Bradford, Y.M., Conlin, T., Eagle, A.E., Fashena, D., Frazer, K., Knight, J., Mani, P., Martin, R., Moxon, S.A.T., Paddock, H., Pich, C., Ramachandran, S., Ruef, B.J., Ruzicka, L., Schaper, K., Shao, X., Singer, A., Sprunger, B., Van Slyke, C.E., Westerfield, M., 2012. ZFIN, the Zebrafish Model Organism Database: increased support for mutants and transgenics. Nucleic Acids Res. 41, D854–D860. https://doi.org/10.1093/nar/gks938.

Huang, H., Huang, C., Wang, L., Ye, X., Bai, C., Simonich, M.T., Tanguay, R.L., Dong, Q., 2010. Toxicity, uptake kinetics and behavior assessment in zebrafish embryos following exposure to perfluorooctanesulphonicacid (PFOS). Aquat. Toxicol. 98, 139–147. https://doi.org/10.1016/j.aquatox.2010.02.003.

Huang, X.-F., Qu, J., Jin, Z.-B., Lu, F., Wu, K.-C., Chen, J., Huang, F., Pang, C.-P., Wu, J., 2014. Genotype–phenotype correlation and mutation spectrum in a large cohort of patients with inherited retinal dystrophy revealed by next-generation sequencing. Genet. Med. 17, 271–278. https://doi.org/10.1038/gim.2014.138.

Iwamuro, S., Yamada, M., Kato, M., Kikuyama, S., 2006. Effects of bisphenol A on thyroid hormone-dependent up-regulation of thyroid hormone receptor α and β and down-regulation of retinoid X receptor γ in Xenopus tail culture. Life Sci. 79, 2165–2171. https://doi.org/10.1016/j.lfs.2006.07.013.

Jantzen, C.E., Annunziato, K.A., Bugel, S.M., Cooper, K.R., 2016. PFOS, PFNA, and PFOA sub-lethal exposure to embryonic zebrafish have different toxicity profiles in terms of morphometrics, behavior and gene expression. Aquat. Toxicol. 175, 160–170. https://doi.org/10.1016/j.aquatox.2016.03.026.

Jordão, R., Garreta, E., Campos, B., Lemos, M.F.L., Soares, A.M.V.M., Tauler, R., Barata, C., 2016. Compounds altering fat storage in Daphnia magna. Sci. Total Environ. 545–546, 127–136. https://doi.org/10.1016/j.scitotenv.2015.12.097.

Jorgenson, Z.G., Thomas, L.M., Elliott, S.M., Cavallin, J.E., Randolph, E.C., Choy, S.J., Alvarez, D.A., Banda, J.A., Gefell, D.J., Lee, K.E., Furlong, E.T., Schoenfuss, H.L., 2018. Contaminants of emerging concern presence and adverse effects in fish: a case study in the Laurentian Great Lakes. Environ. Pollut. 236, 718–733. https://doi.org/10.1016/j.envpol.2018.01.070.

Jürgens, M.D., Holthaus, K.I.E., Johnson, A.C., Smith, J.J.L., Hetheridge, M., Williams, R.J., 2002. The potential for estradiol and ethinylestradiol degradation in English rivers. Environ. Toxicol. Chem. 21, 480–488. https://doi.org/10.1002/etc.5620210302.

Kalasekar, S.M., Zacharia, E., Kessler, N., Ducharme, N.A., Gustafsson, J.Å., Kakadiaris, I.A., Bondesson, M., 2015. Identification of environmental chemicals that induce yolk malabsorption in zebrafish using automated image segmentation. Reprod. Toxicol. 55, 20–29. https://doi.org/10.1016/j.reprotox.2014.10.022.

Kannan, K., Tao, L., Sinclair, E., Pastva, S.D., Jude, D.J., Giesy, J.P., 2005. Perfluorinated compounds in aquatic organisms at various trophic levels in a Great Lakes food chain. Arch. Environ. Contam. Toxicol. 48, 559–566. https://doi.org/10.1007/s00244-004-0133-x.

Kashiwada, S., Ishikawa, H., Miyamoto, N., Ohnishi, Y., Magara, Y., 2002. Fish test for endocrine-disruption and estimation of water quality of Japanese rivers. Water Res. 36, 2161–2166. https://doi.org/10.1016/S0043-1354(01)00406-7.

Kassambara, A., Mundt, F., 2017. Factoextra: Extract and Visualize the Results of Multivariate Data Analyses [WWW Document]. URL. https://cran.r-project.org/web/packages/factoextra/index.html.

Kato, K., Wong, L.-Y., Basden, B.J., Calafat, A.M., 2013. Effect of temperature and duration of storage on the stability of polyfluoroalkyl chemicals in human serum. Chemosphere 91, 115–117. https://doi.org/10.1016/j.chemosphere.2012.11.013.

Kimmel, C.B., Ballard, W.W., Kimmel, S.R., Ullmann, B., Schilling, T.F., 1995. Stages of embryonic development of the zebrafish. Dev. Dyn. 203, 253–310. https://doi.org/10.1002/aja.1002030302.

Kinch, C.D., Ibhazehiebo, K., Jeong, J.-H., Habibi, H.R., Kurrasch, D.M., 2015. Low-dose exposure to bisphenol A and replacement bisphenol S induces precocious hypothalamic neurogenesis in embryonic zebrafish. Proc. Natl. Acad. Sci. 112, 1475–1480. https://doi.org/10.1073/pnas.1417731112.

Kinch, C.D., Kurrasch, D.M., Habibi, H.R., 2016. Adverse morphological development in embryonic zebrafish exposed to environmental concentrations of contaminants individually and in mixture. Aquat. Toxicol. 175, 286–298. https://doi.org/10.1016/j.aquatox.2016.03.021.

Kishida, M., McLellan, M., Miranda, J.A., Callard, G.V., 2001. Estrogen and xenoestrogens upregulate the brain aromatase isoform (P450aromB) and perturb markers of early development in zebrafish (Danio rerio). Comp. Biochem. Physiol. B Biochem. Mol. Biol. 129, 261–268. https://doi.org/10.1016/S1096-4959(01)00319-0.

Lam, S.H., Hlaing, M.M., Zhang, X., Yan, C., Duan, Z., Zhu, L., Ung, C.Y., Mathavan, S., Ong, C.N., Gong, Z., 2011. Toxicogenomic and phenotypic analyses of bisphenol-a early-life exposure toxicity in zebrafish. PLoS One 6, e28273. https://doi.org/10.1371/journal.pone.0028273.

Lantz-Mcpeak, S., Guo, X., Cuevas, E., Dumas, M., Newport, G.D., Ali, S.F., Paule, M.G., Kanungo, J., 2015. Developmental toxicity assay using high content screening of zebrafish embryos. J. Appl. Toxicol. 35, 261–272. https://doi.org/10.1002/jat.3029.

Lê, S., Josse, J., Husson, F., 2008. FactoMineR: an r package for multivariate analysis. J. Stat. Softw. 25, 1–18. https://doi.org/10.18637/jss.v025.i01.

Lecomte, S., Habauzit, D., Charlier, T.D., Pakdel, F., 2017. Emerging estrogenic pollutants in the aquatic environment and breast cancer. Genes (Basel) 8. https://doi.org/10.3390/genes8090229.

Lee, J.E., Choi, K., 2017. Perfluoroalkyl substances exposure and thyroid hormones in humans: epidemiological observations and implications. Ann. Pediatr. Endocrinol. Metab. 1012, 6–14. https://doi.org/10.6065/apem.2017.22.1.6.

Lee, S.L.J., Horsfield, J.A., Black, M.A., Rutherford, K., Fisher, A., Gemmell, N.J., 2017. Histological and transcriptomic effects of 17α-methyltestosterone on zebrafish gonad development. BMC Genomics 18, 557. https://doi.org/10.1186/s12864-017-3915-z.

Leung, K.C., Johannsson, G., Leong, G.M., Ho, K.K.Y., 2004. Estrogen regulation of growth hormone action. Endocr. Rev. https://doi.org/10.1210/er.2003-0035.

Listgarten, J., Stegle, O., Morris, Q., Brenner, S.E., Parts, L., 2014. Personalized medicine: from genotypes and molecular phenotypes towards therapy- session introduction. Pac. Symp. Biocomput. 19, 224–228. https://doi.org/10.1142/9789814583220_0022.

Liu, W., Zhang, X., Wei, P., Tian, H., Wang, W., Ru, S., 2018. Long-term exposure to bisphenol S damages the visual system and reduces the tracking capability of male zebrafish (Danio rerio). J. Appl. Toxicol. 38, 248–258. https://doi.org/10.1002/jat.3519.

Löhr, H., Hammerschmidt, M., 2011. Zebrafish in endocrine systems: recent advances and implications for human disease. Annu. Rev. Physiol. 73, 183–211. https://doi.org/10.1146/annurev-physiol-012110-142320.

Lu, J.T., Campeau, P.M., Lee, B.H., 2014. Genotype-phenotype correlation–promiscuity in the era of next-generation sequencing. N. Engl. J. Med. 371, 593–596. https://doi.org/10.1056/NEJMp1400788.

Lyssimachou, A., Munro Jenssen, B., Arukwe, A., 2006. Brain cytochrome P450 aromatase gene isoforms and activity levels in atlantic salmon after waterborne exposure to nominal environmental concentrations of the pharmaceutical ethynylestradiol and antifoulant tributyltin. Toxicol. Sci. 91, 82–92. https://doi.org/10.1093/toxsci/kfj136.

Maechler, M., Rousseeuw, P., Struyf, A., Hubert, M., Hornik, K., Studer, M., Roudier, P., Gonzalez, J., Kozlowski, K., Schubert, E., 2019. cluster: "Finding Groups in Data": Cluster Analysis Extended Rousseeuw et al. [WWW Document]. URL. https://cran.r-project.org/web/packages/cluster/index.html.

Martínez, R., Esteve-Codina, A., Herrero-Nogareda, L., Ortiz-Villanueva, E., Barata, C., Tauler, R., Raldúa, D., Piña, B., Navarro-Martín, L., 2018. Dose-dependent transcriptomic responses of zebrafish eleutheroembryos to Bisphenol A. Environ. Pollut. 243, 988–997. https://doi.org/10.1016/J.ENVPOL.2018.09.043.

Martínez, R., Navarro-Martín, L., Luccarelli, C., Codina, A.E., Raldúa, D., Barata, C., Tauler, R., Piña, B., 2019. Unravelling the mechanisms of PFOS toxicity by combining morphological and transcriptomic analyses in zebrafish embryos. Sci. Total Environ. 674, 462–471. https://doi.org/10.1016/j.scitotenv.2019.04.200.

Mccabe, L.L., Mccabe, E.R.B., 2013. Down syndrome and personalized medicine: changing paradigms from genotype to phenotype to treatment. Congenit. Anom. (Kyoto). https://doi.org/10.1111/cga.12000.

Mccormick, J.M., Paiva, M.S., Häggblom, M.M., Cooper, K.R., White, L.A., 2010. Embryonic exposure to tetrabromobisphenol A and its metabolites, bisphenol A and tetrabromobisphenol A dimethyl ether disrupts normal zebrafish (Danio rerio) development and matrix metalloproteinase expression. Aquat. Toxicol. 100, 255–262. https://doi.org/10.1016/j.aquatox.2010.07.019.

McGinnis, C.L., Crivello, J.F., 2011. Elucidating the mechanism of action of tributyltin (TBT) in zebrafish. Aquat. Toxicol. 103, 25–31. https://doi.org/10.1016/j.aquatox.2011.01.005.

Meador, J.P., Yeh, A., Gallagher, E.P., 2018. Adverse metabolic effects in fish exposed to contaminants of emerging concern in the field and laboratory. Environ. Pollut. 236, 850–861. https://doi.org/10.1016/j.envpol.2018.02.007.

Meng, P., Deng, S., Du, Z., Wang, B., Huang, J., Wang, Y., Yu, G., Xing, B., 2017. Effect of hydro-oleophobic perfluorocarbon chain on interfacial behavior and mechanism of perfluorooctane sulfonate in oil-water mixture. Sci. Rep. 7, 44694. https://doi.org/10.1038/srep44694.

Mercier, P., Simeone, A., Cotelli, F., Boncinelli, E., 1995. Expression pattern of two otx genes suggests a role in specifying anterior body structures in zebrafish. Int. J. Dev. Biol. 39, 559–573.

Mevik, B.-H., Wehrens, R., 2015. The pls package: principal component and partial least squares regression in R. J. Stat. Softw. 18, 1–23. https://doi.org/10.18637/jss.v018.i02.

Mingarro, M., Vega-Rubín De Celis, S., Astola, A., Pendón, C., Valdivia, M.M., Pérez-Sánchez, J., 2002. Endocrine mediators of seasonal growth in gilthead sea bream (Sparus aurata): the growth hormone and somatolactin paradigm. Gen. Comp. Endocrinol. 128, 102–111. https://doi.org/10.1016/S0016-6480(02)00042-4.

Moreman, J., Lee, O., Trznadel, M., David, A., Kudoh, T., Tyler, C.R., 2017. Acute toxicity, teratogenic, and estrogenic effects of bisphenol A and its alternative replacements bisphenol S, bisphenol F, and bisphenol AF in zebrafish embryo-larvae. Environ. Sci. Technol. 51, 12796–12805. https://doi.org/10.1021/acs.est.7b03283.

Mu, X., Huang, Y., Li, Xuxing, Lei, Y., Teng, M., Li, Xuefeng, Wang, C., Li, Y., 2018. Developmental effects and estrogenicity of bisphenol A alternatives in a zebrafish embryo model. Environ. Sci. Technol. 52, 3222–3231. https://doi.org/10.1021/acs.est.7b06255.

Nakazawa, M., 2018. Fmsb: Functions for Medical Statistics Book with Some Demographic Data [WWW Document]. URL. https://cran.r-project.org/web/packages/fmsb/index.html.

Nassiri, I., McCall, M.N., 2018. Systematic exploration of cell morphological phenotypes associated with a transcriptomic query. Nucleic Acids Res. https://doi.org/10.1093/nar/gky626.

National Research Council (US), 1999. Effects on Reproduction and Development; Hormonally Active Agents in the Environment, Hormonally Active Agents in the Environment. National Academies Press, Washington, D.C. https://doi.org/10.17226/6029.

Nilsson Sköld, H., Aspengren, S., Wallin, M., 2013. Rapid color change in fish and amphibians - function, regulation, and emerging applications. Pigm.t Cell Melanoma Res. https://doi.org/10.1111/pcmr.12040.

Okkerman P.C, C.G., 2000. Towards the establishment of a priority list of substances for further evaluation of their role in endocrine disruption. Eur. Comm. Dg Environ https://doi.org/M0355008/1786Q/10/11/00.

Oliveira, E., Barata, C., Piña, B., 2016. Endocrine disruption in the omics Era: new views, new hazards, new approaches. Open Biotechnol. J. 10, 20–35. https://doi.org/10.2174/1874070701610010020.

Olsvik, P.A., Whatmore, P., Penglase, S.J., Skjærven, K.H., Anglès d'Auriac, M., Ellingsen, S., 2019. Associations between behavioral effects of bisphenol A and DNA methylation in zebrafish embryos. Front. Genet. 10, 184. https://doi.org/10.3389/fgene.2019.00184.

Orlando, E.F., Kolok, A.S., Binzcik, G.A., Gates, J.L., Horton, M.K., Lambright, C.S., Gray, L.E., Soto, A.M., Guillette, L.J., 2004. Endocrine-disrupting effects of cattle feedlot effluent on an aquatic sentinel species, the fathead minnow. Environ. Health Perspect. 112, 353–358. https://doi.org/10.1289/ehp.6591.

Ortiz-Villanueva, E., Jaumot, J., Martínez, R., Navarro-Martín, L., Piña, B., Tauler, R., 2018. Assessment of endocrine disruptors effects on zebrafish (Danio rerio) embryos by untargeted LC-HRMS metabolomic analysis. Sci. Total Environ. 635, 156–166. https://doi.org/10.1016/j.scitotenv.2018.03.369.

Ostertagová, E., 2012. Modelling Using Polynomial Regression, Procedia Engineering. Elsevier, pp. 500–506. https://doi.org/10.1016/j.proeng.2012.09.545.

Ottinger, M.A., Abdelnabi, M.A., Henry, P., McGary, S., Thompson, N., Wu, J.M., 2001. Neuroendocrine and behavioral implications of endocrine disrupting chemicals in quail. Hormones and Behavior. Academic Press, pp. 234–247. https://doi.org/10.1006/hbeh.2001.1695.

Parichy, D.M., Elizondo, M.R., Mills, M.G., Gordon, T.N., Engeszer, R.E., 2009. Normal table of postembryonic zebrafish development: staging by externally visible anatomy of the living fish. Dev. Dyn. 238, 2975–3015. https://doi.org/10.1002/dvdy.22113.

Pelayo, S., Oliveira, E., Thienpont, B., Babin, P.J., Raldúa, D., André, M., Piña, B., 2012. Triiodothyronine-induced changes in the zebrafish transcriptome during the eleutheroembryonic stage: implications for bisphenol A developmental toxicity. Aquat. Toxicol. 110–111, 114–122. https://doi.org/10.1016/j.aquatox.2011.12.016.

Penza, M., Jeremic, M., Marrazzo, E., Maggi, A., Ciana, P., Rando, G., Grigolato, P.G., Di Lorenzo, D., 2011. The environmental chemical tributyltin chloride (TBT) shows both estrogenic and adipogenic activities in mice which might depend on the exposure dose. Toxicol. Appl. Pharmacol. 255, 65–75. https://doi.org/10.1016/j.taap.2011.05.017.

Petrakis, D., Vassilopoulou, L., Mamoulakis, C., Psycharakis, C., Anifantaki, A., Sifakis, S., Docea, A.O., Tsiaoussis, J., Makrigiannakis, A., Tsatsakis, A.M., 2017. Endocrine disruptors leading to obesity and related diseases. Int. J. Environ. Res. Public Health. https://doi.org/10.3390/ijerph14101282.

Qiu, W., Shao, H., Lei, P., Zheng, C., Qiu, C., Yang, M., Zheng, Y., 2018. Immunotoxicity of bisphenol S and F are similar to that of bisphenol A during zebrafish early development. Chemosphere. https://doi.org/10.1016/j.chemosphere.2017.11.125.

R Development Core Team, 2008. R: a Language and Environment for Statistical Computing. R Foundation for Statistical Computing.

Raghunath, A., Perumal, E., 2018. Analysis of Lethality and Malformations during Zebrafish (Danio rerio) Development. Teratogenicity Testing, pp. 337–363. https://doi.org/10.1007/978-1-4939-7883-0_18.

Raldúa, D., André, M., Babin, P.J., 2008. Clofibrate and gemfibrozil induce an embryonic malabsorption syndrome in zebrafish. Toxicol. Appl. Pharmacol. 228, 301–314. https://doi.org/10.1016/j.taap.2007.11.016.

Raldúa, D., Piña, B., 2014. In vivo zebrafish assays for analyzing drug toxicity. Expert Opin. Drug Metab. Toxicol. 10, 685–697. https://doi.org/10.1517/17425255.2014.896339.

Reed, B., Jennings, M., 2011. Guidance on the housing and care of Zebrafish. Res. Anim. Dep.

Regnier, S.M., Sargis, R.M., 2014. Adipocytes under assault: environmental disruption of adipose physiology. Biochim. Biophys. Acta Mol. Basis Dis. https://doi.org/10.1016/j.bbadis.2013.05.028.

Robertson, G.N., McGee, C.A.S., Dumbarton, T.C., Croll, R.P., Smith, F.M., 2007. Development of the swimbladder and its innervation in the zebrafish, Danio rerio. J. Morphol. 268, 967–985. https://doi.org/10.1002/jmor.10558.

Romano, S.N., Edwards, H.E., Souder, J.P., Ryan, K.J., Cui, X., Gorelick, D.A., 2017. G protein-coupled estrogen receptor regulates embryonic heart rate in zebrafish. PLoS Genet. 13. https://doi.org/10.1371/journal.pgen.1007069.

Saili, K.S., Tanguay, R.L., 2013. Developmental Neurobehavioral Toxicity of Bisphenol a in Zebrafish (Danio Rerio). Oregon State University.

Sanderson, J.T., 2006. The steroid hormone biosynthesis pathway as a target for endocrine-disrupting chemicals. Toxicol. Sci. https://doi.org/10.1093/toxsci/kfl051.

Scholz, S., Mayer, I., 2008. Molecular biomarkers of endocrine disruption in small model fish. Mol. Cell. Endocrinol. 293, 57–70. https://doi.org/10.1016/j.mce.2008.06.008.

Segner, H., 2009. Zebrafish (Danio rerio) as a model organism for investigating endocrine disruption. Comp. Biochem. Physiol. Part C Toxicol. Pharmacol. 149, 187–195. https://doi.org/10.1016/j.cbpc.2008.10.099.

Sharan, S., Nikhil, K., Roy, P., 2014. Disruption of thyroid hormone functions by low dose exposure of tributyltin: an in vitro and in vivo approach. Gen. Comp. Endocrinol. 206, 155–165. https://doi.org/10.1016/j.ygcen.2014.07.027.

Sharma, P., Grabowski, T.B., Patiño, R., 2016. Thyroid endocrine disruption and external body morphology of zebrafish. Gen. Comp. Endocrinol. 226, 42–49. https://doi.org/10.1016/j.ygcen.2015.12.023.

Shi, X., Du, Y., Lam, P.K.S., Wu, R.S.S., Zhou, B., 2008. Developmental toxicity and alteration of gene expression in zebrafish embryos exposed to PFOS. Toxicol. Appl. Pharmacol. 230, 23–32. https://doi.org/10.1016/j.taap.2008.01.043.

Shin, Y.H., Schideman, L.C., 2015. Characterizing the fate and transport of Chemicals of emerging Concerns (CECs) from integrated bioenergy and manure management system. Am. Soc. Agric. Biol. Eng. Annu. Int. Meet. 2015 (4), 3050–3057.

Shore, L.S., Shemesh, M., 2016. Estrogen as an environmental pollutant. Bull. Environ. Contam. Toxicol. 97, 447–448. https://doi.org/10.1007/s00128-016-1873-9.

Shrader, E.A., Henry, T.R., Greeley, M.S., Bradley, B.P., 2003. Proteomics in zebrafish exposed to endocrine disrupting chemicals. Ecotoxicology 12, 485–488. https://doi.org/10.1023/B:ECTX.0000003034.69538.eb.

Si, Y., Best, D.H., 2017. Molecular diagnosis of cystic fibrosis. Diagnostic Molecular

Pathology. Academic Press, pp. 235–243. https://doi.org/10.1016/B978-0-12-800886-7.00019-4.
Šošić-Jurjevic, B., Filipović, B., Renko, K., Miler, M., Trifunović, S., Ajdžanovič, V., Köhrle, J., Milošević, V., 2015. Testosterone and estradiol treatments differently affect pituitary-thyroid axis and liver deiodinase 1 activity in orchidectomized middle-aged rats. Exp. Gerontol. 72, 85–98. https://doi.org/10.1016/j.exger.2015.09.010.
Soto, A.M., Rubin, B.S., Sonnenschein, C., 2009. Interpreting endocrine disruption from an integrative biology perspective. Mol. Cell. Endocrinol. https://doi.org/10.1016/j.mce.2009.02.020.
Souder, J.P., Gorelick, D.A., 2018. Assaying uptake of endocrine disruptor compounds in zebrafish embryos and larvae. Comp. Biochem. Physiol. Part C Toxicol. Pharmacol. 208, 105–113. https://doi.org/10.1016/j.cbpc.2017.09.007.
Sousa, J.C.G., Ribeiro, A.R., Barbosa, M.O., Ribeiro, C., Tiritan, M.E., Pereira, M.F.R., Silva, A.M.T., 2019. Monitoring of the 17 EU Watch List contaminants of emerging concern in the Ave and the Sousa rivers. Sci. Total Environ. 649, 1083–1095. https://doi.org/10.1016/j.scitotenv.2018.08.309.
Stegeman, J.J., Goldstone, J.V., Hahn, M.E., 2010. Perspectives on zebrafish as a model in environmental toxicology. Fish Physiol. Biochem. 29, 367–439. https://doi.org/10.1016/S1546-5098(10)02910-9.
Stinckens, E., Vergauwen, L., Ankley, G.T., Blust, R., Darras, V.M., Villeneuve, D.L., Witters, H., Volz, D.C., Knapen, D., 2018. An AOP-based alternative testing strategy to predict the impact of thyroid hormone disruption on swim bladder inflation in zebrafish. Aquat. Toxicol. 200, 1–12. https://doi.org/10.1016/j.aquatox.2018.04.009.
Strähle, U., Scholz, S., Geisler, R., Greiner, P., Hollert, H., Rastegar, S., Schumacher, A., Selderslaghs, I., Weiss, C., Witters, H., Braunbeck, T., 2012. Zebrafish embryos as an alternative to animal experiments - a commentary on the definition of the onset of protected life stages in animal welfare regulations. Reprod. Toxicol. 33, 128–132. https://doi.org/10.1016/j.reprotox.2011.06.121.
Tafazoli, A., Eshraghi, P., Pantaleoni, F., Vakili, R., Moghaddassian, M., Ghahraman, M., Muto, V., Paolacci, S., Golyan, F.F., Abbaszadegan, M.R., 2018. Novel mutations and their genotype-phenotype correlations in patients with Noonan syndrome, using next-generation sequencing. Adv. Med. Sci. 63, 87–93. https://doi.org/10.1016/j.advms.2017.07.001.
Teeguarden, J., Hanson-Drury, S., Fisher, J.W., Doerge, D.R., 2013. Are typical human serum BPA concentrations measurable and sufficient to be estrogenic in the general population? Food Chem. Toxicol. https://doi.org/10.1016/j.fct.2013.08.001.
Teixido, E., Kießling, T., Leuthold, D., Scholz, S., 2017. Effect signatures in zebrafish embryos exposed to compounds with potential developmental toxicity. Reprod. Toxicol. 72, 49. https://doi.org/10.1016/j.reprotox.2017.06.179.
Teixidó, E., Kießling, T.R., Krupp, E., Quevedo, C., Muriana, A., Scholz, S., 2019. Automated morphological feature assessment for zebrafish embryo developmental toxicity screens. Toxicol. Sci. 167, 438–449. https://doi.org/10.1093/toxsci/kfy250.
Teraoka, H., Muramoto, W., Hiraga, T., Shirato, R., Kumagai, Y., 2002. Toxic effects of tributyltin on early zebrafish embryos. J. Rakuno Gakuen Univ. Nat. Sci. 26, 315–325.
Thayer, K.A., Heindel, J.J., Bucher, J.R., Gallo, M.A., 2012. Role of environmental chemicals in diabetes and obesity: a national toxicology program workshop review. Environ. Health Perspect. https://doi.org/10.1289/ehp.1104597.
Tohmé, M., Prud'Homme, S.M., Boulahtouf, A., Samarut, E., Brunet, F., Bernard, L., Bourguet, W., Gibert, Y., Balaguer, P., Laudet, V., 2014. Estrogen-related receptor γ is an in vivo receptor of bisphenol A. FASEB J. 28, 3124–3133. https://doi.org/10.1096/fj.13-240465.
Trebo, M., Wojcik, D., Zecca, M., Locatelli, F., Stary, J., Bergstrasser, E., Flotho, C., Niemeyer, C.M., Hasle, H., van den Heuvel-Eibrink, M.M., Kratz, C.P., 2008. Genotype-phenotype correlation in cases of juvenile myelomonocytic leukemia with clonal RAS mutations. Blood 111, 966–967. https://doi.org/10.1182/blood-2007-09-111831.
Truong, L., Harper, S.L., Tanguay, R.L., 2011. Evaluation of embryotoxicity using the zebrafish model. Methods Mol. Biol. https://doi.org/10.1007/978-1-60761-849-2_16.
Tse, W.K.F., Yeung, B.H.Y., Wan, H.T., Wong, C.K.C., 2013. Early embryogenesis in zebrafish is affected by bisphenol A exposure. Biol. Open 2, 466–471. https://doi.org/10.1242/bio.20134283.
Usta, J., Wehbeh, A., Rida, K., El-Rifai, O., Estiphan, T.A., Majarian, T., Barada, K., 2014. Phenotype-genotype correlation in Wilson disease in a large Lebanese family: association of c.2299insC with hepatic and of p. Ala1003Thr with neurologic phenotype. PLoS One 9, e109727. https://doi.org/10.1371/journal.pone.0109727.
Vandenberg, L.N., Maffini, M.V., Sonnenschein, C., Rubin, B.S., Soto, A.M., 2009. Bisphenol-a and the great divide: a review of controversies in the field of endocrine disruption. Endocr. Rev. https://doi.org/10.1210/er.2008-0021.
Varshney, G.K., Lu, J., Gildea, D.E., Huang, H., Pei, W., Yang, Z., Huang, S.C., Schoenfeld, D., Pho, N.H., Casero, D., Hirase, T., Mosbrook-Davis, D., Zhang, S., Jao, L.E., Zhang, B., Woods, I.G., Zimmerman, S., Schier, A.F., Wolfsberg, T.G., Pellegrini, M., Burgess, S.M., Lin, S., 2013. A large-scale zebrafish gene knockout resource for the genome-wide study of gene function. Genome Res. 23, 727–735. https://doi.org/10.1101/gr.151464.112.
vom Saal, F.S., Nagel, S.C., Coe, B.L., Angle, B.M., Taylor, J.A., 2012. The estrogenic endocrine disrupting chemical bisphenol A (BPA) and obesity. Mol. Cell. Endocrinol. https://doi.org/10.1016/j.mce.2012.01.001.
Wang, L., Wang, Y., Liang, Y., Li, J., Liu, Y., Zhang, J., Zhang, A., Fu, J., Jiang, G., 2014. PFOS induced lipid metabolism disturbances in BALB/c mice through inhibition of low density lipoproteins excretion. Sci. Rep. 4, 4582. https://doi.org/10.1038/srep04582.
Warnes, G.R., Bolker, B., Bonebakker, L., Gentleman, R., Huber, W., Liaw, A., Lumley, T., Maechler, M., Magnusson, A., Moeller, S., Schwartz, M., Venables, B., 2015. Gplots: various R programming tools for plotting data. Compr. R Arch. Netw.
Waye, A., Trudeau, V.L., 2011. Neuroendocrine disruption: more than hormones are upset. J. Toxicol. Environ. Heal. Part B 14, 270–291. https://doi.org/10.1080/10937404.2011.578273.
Wei, T., Simko, V., Levy, M., Xie, Y., Jin, Y., Zemla, J., 2017. corrplot: Visualization of a Correlation Matrix [WWW Document]. URL. https://cran.r-project.org/web/packages/corrplot/index.html.
West, M., Ginsburg, G.S., Huang, A.T., Nevins, J.R., 2006. Embracing the complexity of genomic data for personalized medicine. Genome Res. https://doi.org/10.1101/gr.3851306.
Weston, A.D., Hood, L., 2004. Systems biology, proteomics, and the future of health care: toward predictive, preventative, and personalized medicine. J. Proteome Res. 3, 179–196. https://doi.org/10.1021/pr0499693.
Wickham, H., 2011. ggplot2. Wiley Interdiscip. Rev. Comput. Stat. 3, 180–185. https://doi.org/10.1002/wics.147.
Yue, M.S., Peterson, R.E., Heideman, W., 2015. Dioxin inhibition of swim bladder development in zebrafish: is it secondary to heart failure? Aquat. Toxicol. 162, 10–17. https://doi.org/10.1016/j.aquatox.2015.02.016.
Zang, L., Maddison, L.A., Chen, W., 2018. Zebrafish as a model for obesity and diabetes. Front. Cell Dev. Biol. 6, 91. https://doi.org/10.3389/fcell.2018.00091.
Zhang, G., Roell, K.R., Truong, L., Tanguay, R.L., Reif, D.M., 2017. A data-driven weighting scheme for multivariate phenotypic endpoints recapitulates zebrafish developmental cascades. Toxicol. Appl. Pharmacol. 314, 109–117. https://doi.org/10.1016/j.taap.2016.11.010.
Zhao, F., Wei, P., Wang, J., Yu, M., Zhang, X., Tian, H., Wang, W., Ru, S., 2017. Estrogenic effects associated with bisphenol a exposure in male zebrafish (Danio rerio) is associated with changes of endogenous 17β-estradiol and gene specific DNA methylation levels. Gen. Comp. Endocrinol. 252, 27–35. https://doi.org/10.1016/j.ygcen.2017.07.032.
Ziegel, E.R., Massart, D.L., Vandeginste, B.G.M., Buydens, L.M.C., de Jong, S., Lewi, P.J., Verbeke, J.S., 2006. Chapter 10 Multiple and Polynomial Regression, in: Handbook of Chemometrics and Qualimetrics, Part B (Data Handling in Science and Technology). Elsevierhttps://doi.org/10.2307/1271476. p. 218.

Supplemental information: scientific article I

Morphometric signatures of exposure to endocrine disrupting chemicals in zebrafish eleutheroembryos

Authors: R. Martínez, L. Herrero-Nogareda, M. Van Antro, M.P. Campos, M. Casado, C. Barata, B. Piña, L. Navarro-Martín

Status: Published

Journal: Aquat. Toxicol. 214 (2019) 105232.

DOI: 10.1016/j.aquatox.2019.105232

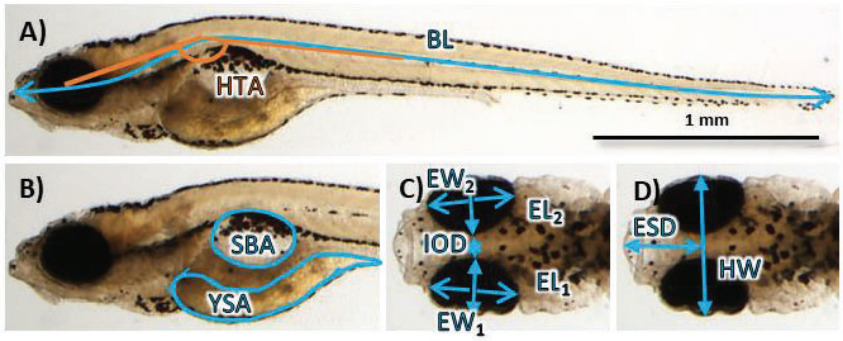

Supplementary Figure 1. Summary of the measured morphometric parameters taken sagitally (**A and B**) and dorsally (**C and D**). BL = body length; HTA = head-trunk angle; YSA = yolk sac area; SBA = swim bladder area; EL = eye length; EW = eye width; HW = head width; IOD = inter-ocular distance; ESD = eye-snout distance. Scale bar = 1 mm. Measurements were taken using the free graphical image analysis software ImageJ (National Institutes of Health, Bethesda, MD, USA) (Raldúa et al., 2008).

Raldúa, D., André, M., Babin, P.J., 2008. Clofibrate and gemfibrozil induce an embryonic malabsorption syndrome in zebrafish. Toxicol. Appl. Pharmacol. 228, 301–314. https://doi.org/10.1016/j.taap.2007.11.016

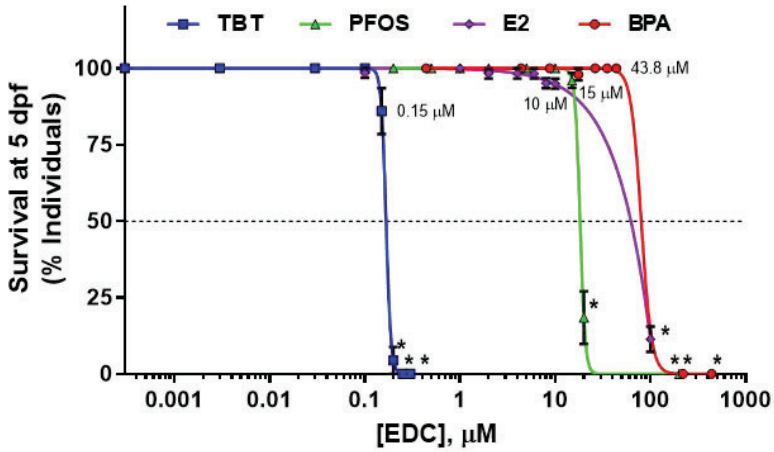

Supplementary Figure SF2. Survival rates in 5 dpf eleutheroembryos exposed to increasing concentrations of BPA, PFOS, TBT and E2 from 2 to 5 dpf. The mean value ± SD (standard deviation) is shown for each group (n=50-60 individuals per group). Non-parametric test (Kruskal-Wallis with multiple comparisons against the reference group (DMSO, control), $p < 0.05$) was performed. Asterisks mark the groups that are statistically different from the control group. From this data and regarding the highest concentration groups with no significant effect in lethality, we derived a maximum equilethal doses (1.0), of 43.8 µM for BPA, 15.0 µM in case of PFOS, 0.15 µM for TBT and 10.0 µM for E2. These concentrations were the highest exposure groups measured in the morphometric study.

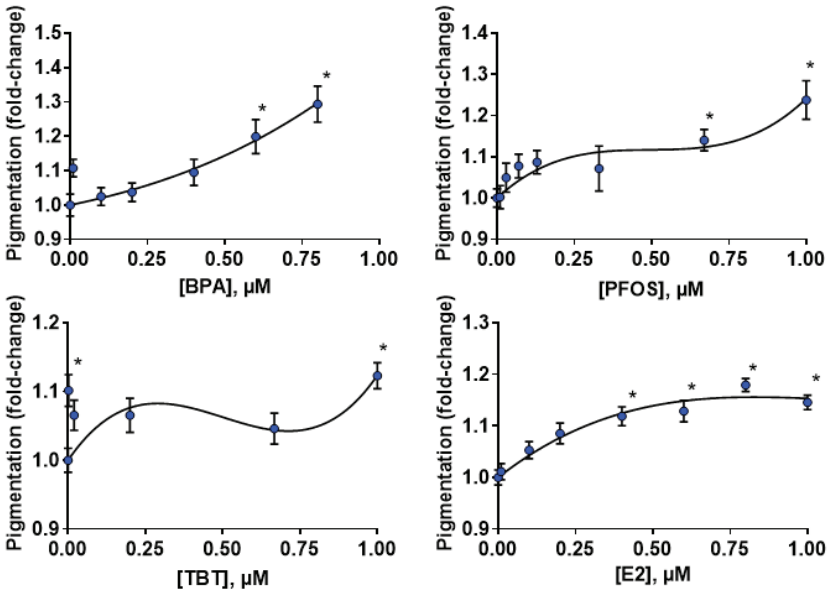

Supplementary Figure SF3. Pigmentation increase in the eleutheroembryos exposed to BPA, PFOS, TBT and E2. Kruskal-Wallis non-parametric tests ($p < 0.05$, n=11) were performed to establish the groups statistically different from each control group (marked with asterisks).

A)

Components	Eigenvalue	Variance (%)	Cumulative Variance (%)
Dim.1	4.46	49.56	49.56
Dim.2	1.56	17.36	66.92
Dim.3	0.80	8.85	75.77
Dim.4	0.67	7.45	83.22
Dim.5	0.45	4.97	88.19
Dim.6	0.33	3.70	91.89
Dim.7	0.30	3.35	95.24
Dim.8	0.25	2.75	97.99
Dim.9	0.18	2.01	100.00

B)

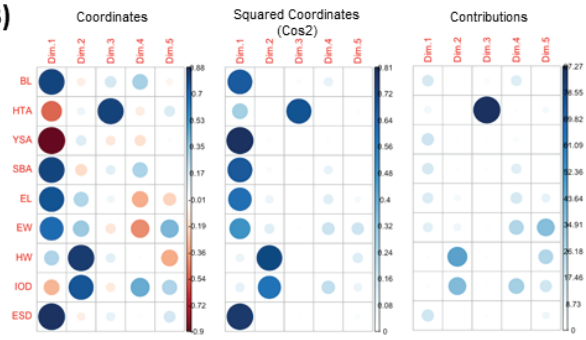

C)

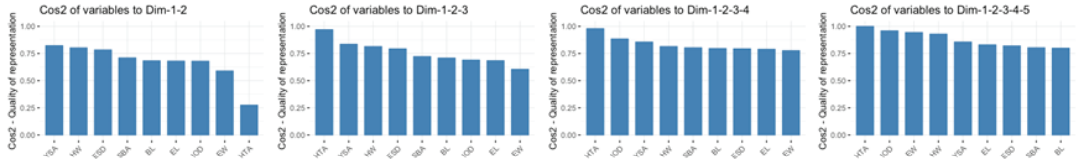

Supplementary Figure SF4. Selection of Principal Component Analysis (PCA) components to visualize morphometric data from 3, 4, 5 and 6 dpf non-exposed eleutheroembryos (n=29-35 individuals per condition). **A)** Table showing eigenvalues, explained variance and cumulative explained variable for the resulting PCA components. **B)** Variable coordinates, squared coordinates (cos2) and contributions for each of the resulting components. **C)** Accumulated cos2 values when considering the selection of different number of components.

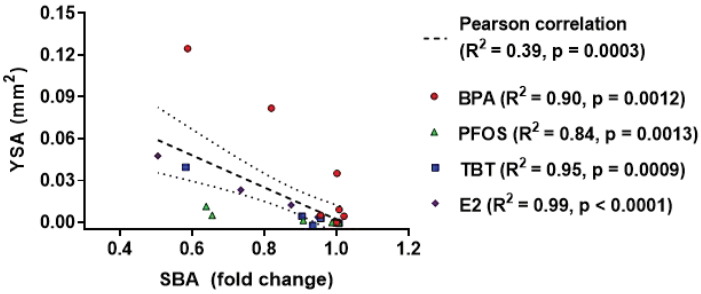

Supplementary Figure SF5. Correlation between yolk sac area and swim bladder area in the eleutheroembryos exposed to BPA, PFOS, TBT and E2. Pearson correlation coefficients were both calculated for general data and each compound particularly. The average of YSA and SBA of each condition (n=50-60 individuals per group) is represented.

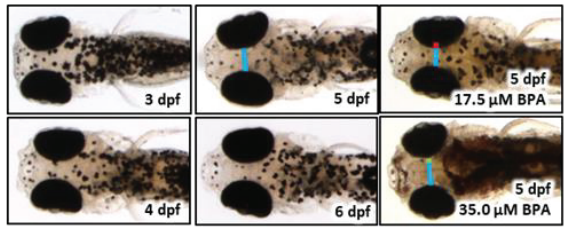

Supplementary Figure SF6. Hormetic behavior in IOD (inter-ocular distance) observed during the exposure to BPA. For comparison, representative images of the IOD distance in the age developmental controls are shown. The blue line indicates the length of the control; the red and green line represents a decrease and an increase, respectively, of that distance.

A)

Components	Eigenvalue	Variance (%)	Cumulative Variance (%)
Dim.1	3.85	42.78	42.78
Dim.2	1.86	20.67	63.45
Dim.3	0.84	9.33	72.78
Dim.4	0.73	8.06	80.84
Dim.5	0.62	6.88	87.72
Dim.6	0.43	4.74	92.46
Dim.7	0.36	3.98	96.45
Dim.8	0.27	2.98	99.42
Dim.9	0.05	0.58	100.00

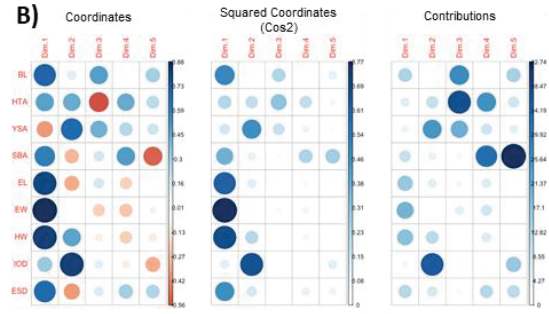

Supplementary Figure SF7. Selection of Principal Component Analysis (PCA) components to visualize morphometric data of 5 dpf exposed eleutheroembryos (n=50-60 individuals per condition) to increasing concentrations of BPA, PFOS, TBT and E2. **A)** Table showing eigenvalues, explained variance and cumulative explained variable for the resulting PCA components. **B)** Variable coordinates, squared coordinates (cos2) and contributions for each of the resulting components. **C)** Accumulated cos2 values when considering the selection of different number of components.

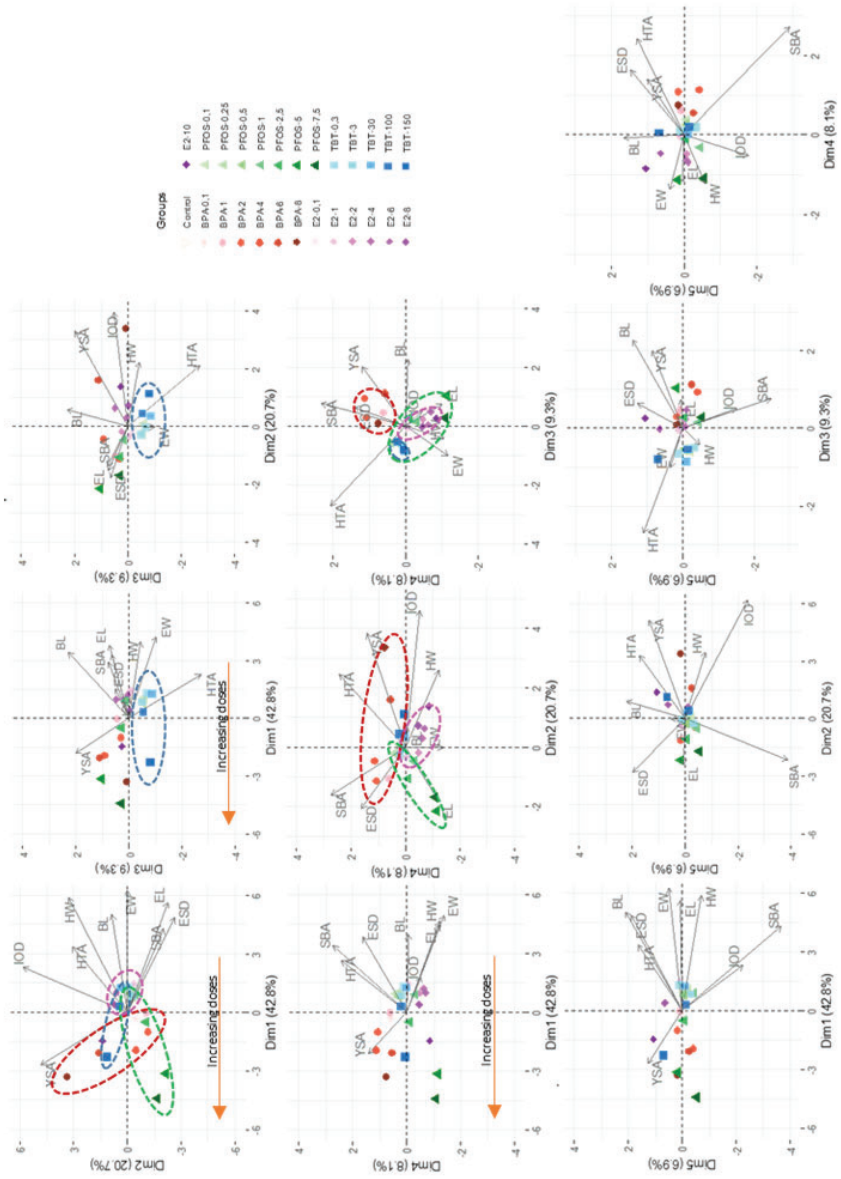

Supplementary Figure SF8. Representation of the selected components from a Principal Component Analysis (PCA) using morphometric data from the eleutheroembryos exposed to BPA (in red), PFOS (in green), TBT (in blue) and E2 (in purple). The color scale for each condition increase in intensity/darkness with the increasing concentrations. Standardized values (normalized by the average of the control group and centered to zero) were used as input data, except for the YSA, which was corrected by the control baseline (being also zero the average of the control group). The first 5 components of the model were chosen, which explained up to 87.7% of the data variability. Arrows represent variable (morphological traits) loadings indicating contribution of each variable to differentiate between individuals. The centroid of each group (n=50-60 individuals per group) is shown as a color sphere to avoid oversaturation of the graph. Dotted line circles are graph to help the visualization of some of the groups separation.

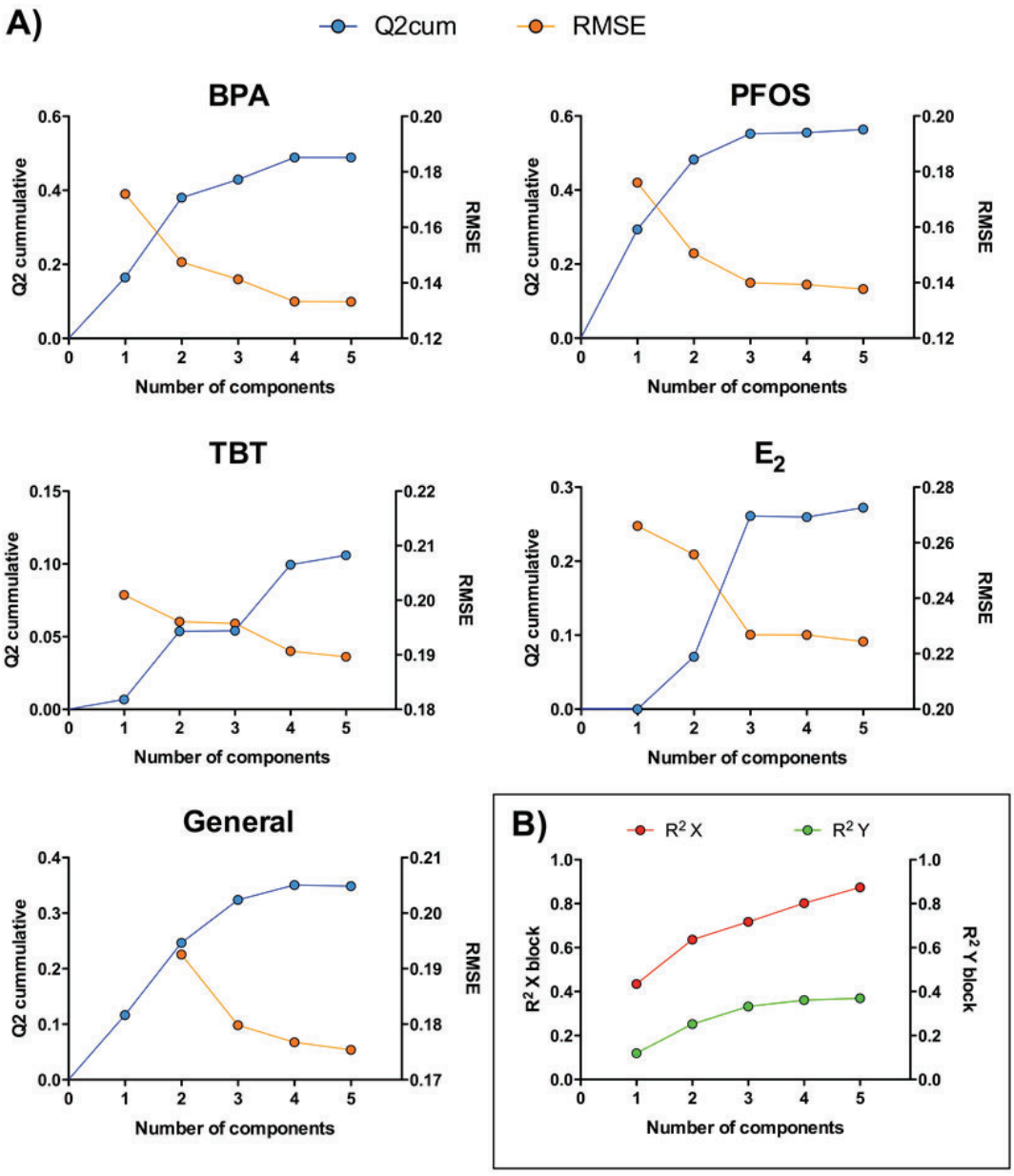

Supplementary Figure SF9. Selection of multivariate Partial Least Square (PLS2) model latent variables of 5 dpf exposed eleutheroembryos to increasing concentrations of BPA, PFOS, TBT and E2 (n=50-60 individuals per group). Latent variable selection (number of selected components) was performed using cross validation (leave-one-out method) and based on **A)** RMSE (Root Mean Squared Error) and cumulated Q^2 index (a statistic calculated from the cross validation than gives an estimate of the predictive power of a PLS model) and **B)** cumulated R^2 (cumulative % of variance explained) for the X- and Y- blocks.

Supplemental table ST1. Summary of the stocks solutions and the exposures doses (µM and its equivalence in equilethality) used in this study.

	Stock solution (mM)	Experimental solution (dose) (µM)	Equilethal dose (relative)
BPA	(DMSO)	0 (Control)	0 (Control)
	0.22	0.44	0.01
	2.19	4.38	0.10
	4.38	8.76	0.20
	8.76	17.5	0.40
	13.14	26.3	0.60
	17.52	35.0	0.80
	21.90	43.8	1.00
	109.50	219.0	5.00
	219.00	438.0	10.00
PFOS	(DMSO)	0 (Control)	0 (Control)
	0.10	0.20	0.01
	0.25	0.50	0.03
	0.50	1.00	0.07
	1.00	2.00	0.13
	2.50	5.00	0.33
	5.00	10.0	0.67
	7.50	15.0	1.00
	10.00	20.0	1.33
	100.00	200.0	13.33
TBT	(DMSO)	0 (Control)	0 (Control)
	$1.5 \cdot 10^{-4}$	$3.0 \cdot 10^{-4}$	$2.0 \cdot 10^{-3}$
	$1.5 \cdot 10^{-3}$	$3.0 \cdot 10^{-3}$	0.02
	0.015	0.03	0.20
	0.050	0.10	0.67
	0.075	0.15	1.00
	0.100	0.20	1.33
	0.125	0.25	1.67
	0.150	0.30	2.00
E2	(DMSO)	0 (Control)	0 (Control)
	0.05	0.1	0.01
	0.50	1.0	0.10
	1.00	2.0	0.20
	2.00	4.0	0.40
	3.00	6.0	0.60
	4.00	8.0	0.80
	5.00	10.0	1.00
	50.00	100.0	10.00

Supplemental table ST2 (part I). Summary of the survival, hatching and swim bladder inflation rates. Mean values ± SD (standard deviation) of each group are shown. Fold-change regarding the control group (1.0) are shown. Non-parametric Kruskal-Wallis test against the control group (p<0.05) were performed. Significant differences are marked with an asterisk (*); n/a: not applicable.

			Survival									Hatching…		
			3 dpf			4 dpf			5 dpf			3 dpf		
	Experimental dose (µM)	Equilethal dose (relative)	Fold-change (Mean ± SD)	n/ total n	St. sign.	Fold-change (Mean ± SD)	n/ total n	St. sign.	Fold-change (Mean ± SD)	n/ total n	St. sign.	Fold-change (Mean ± SD)	n/ total n	St. sign.
BPA	**0 (Control)**	0 (Control)	1.00 ± 0.05	49/50	n/a	1.00 ± 0.00	49/49	n/a	1.00 ± 0.00	49/49	n/a	1.00 ± 0.06	48/50	n/a
	0.44	0.01	1.02 ± 0.00	50/50		1.00 ± 0.00	50/50		1.00 ± 0.00	50/50		1.00 ± 0.09	48/50	
	4.38	0.10	1.02 ± 0.00	50/50		1.00 ± 0.00	50/50		1.00 ± 0.00	50/50		1.02 ± 0.05	49/50	
	8.76	0.20	1.02 ± 0.00	50/50		1.00 ± 0.00	49/49		1.00 ± 0.00	49/49		0.98 ± 0.09	47/50	
	17.5	0.40	1.02 ± 0.00	50/50		1.00 ± 0.00	50/50		0.98 ± 0.04	49/50		0.88 ± 0.12	42/50	
	26.3	0.60	1.02 ± 0.00	50/50		1.00 ± 0.00	49/49		1.00 ± 0.00	49/49		0.90 ± 0.06	43/50	
	35.0	0.80	1.02 ± 0.00	50/50		1.00 ± 0.00	51/51		1.00 ± 0.00	51/51		0.60 ± 0.14	29/50	*
	43.8	1.00	1.02 ± 0.00	50/50		1.00 ± 0.00	50/50		1.00 ± 0.00	50/50		0.46 ± 0.16	22/50	*
	219.0	5.00	0.00 ± 0.00	0/50	*	0.00 ± 0.00	0/0	*	0.00 ± 0.00	0/0	*	0.00 ± 0.00	0/50	*
	438.0	10.00	0.00 ± 0.00	0/50	*	0.00 ± 0.00	0/0	*	0.00 ± 0.00	0/0	*	0.00 ± 0.00	0/50	*
PFOS	**0 (Control)**	0 (Control)	1.00 ± 0.00	50/50	n/a	1.00 ± 0.00	50/50	n/a	1.00 ± 0.00	50/50	n/a	1.00 ± 0.05	49/50	n/a
	0.20	0.01	1.00 ± 0.00	50/50		1.00 ± 0.00	50/50		1.00 ± 0.00	50/50		0.98 ± 0.06	48/50	
	0.50	0.03	1.00 ± 0.00	50/50		0.98 ± 0.04	49/50		1.00 ± 0.00	49/49		0.98 ± 0.06	48/50	
	1.00	0.07	1.00 ± 0.00	50/50		1.00 ± 0.00	50/50		1.00 ± 0.00	50/50		1.02 ± 0.00	50/50	
	2.00	0.13	1.00 ± 0.00	50/50		1.00 ± 0.00	50/50		1.00 ± 0.00	50/50		0.96 ± 0.06	47/50	
	5.00	0.33	1.00 ± 0.00	50/50		1.00 ± 0.00	50/50		1.00 ± 0.00	50/50		0.96 ± 0.06	47/50	
	10.0	0.67	1.00 ± 0.00	50/50		1.00 ± 0.00	50/50		1.00 ± 0.00	50/50		0.96 ± 0.06	47/50	
	15.0	1.00	1.00 ± 0.00	50/50		1.00 ± 0.00	50/50		0.96 ± 0.05	46/48		0.96 ± 0.06	47/50	
	20.0	1.33	0.98 ± 0.04	49/50		1.00 ± 0.00	49/49		0.18 ± 0.19	9/49	*	0.96 ± 0.06	47/50	
	200.0	13.33	1.00 ± 0.00	50/50		0.94 ± 0.13	47/50		0.00 ± 0.00	0/47	*	0.94 ± 0.05	46/50	
TBT	**0 (Control)**	0 (Control)	1.00 ± 0.00	50/50	n/a	1.00 ± 0.00	50/50	n/a	1.00 ± 0.00	50/50	n/a	1.00 ± 0.00	50/50	n/a
	$3.0 \cdot 10^{-4}$	$2.0 \cdot 10^{-3}$	1.00 ± 0.00	50/50		1.00 ± 0.00	50/50		1.00 ± 0.00	50/50		1.00 ± 0.00	50/50	
	$3.0 \cdot 10^{-3}$	0.02	0.98 ± 0.04	49/50		1.00 ± 0.00	49/49		1.00 ± 0.00	49/49		1.00 ± 0.00	50/50	
	0.03	0.20	0.98 ± 0.04	50/51		1.00 ± 0.00	50/50		1.00 ± 0.00	50/50		1.00 ± 0.00	51/51	
	0.10	0.67	0.98 ± 0.04	49/50		1.00 ± 0.00	49/49		1.00 ± 0.00	49/49		1.00 ± 0.00	50/50	
	0.15	1.00	0.98 ± 0.04	49/50		1.00 ± 0.00	49/49		0.86 ± 0.17	42/49		1.00 ± 0.00	50/50	
	0.20	1.33	1.00 ± 0.00	50/50		1.00 ± 0.00	50/50		0.04 ± 0.10	2/49	*	1.00 ± 0.00	50/50	
	0.25	1.67	1.00 ± 0.00	50/50		1.00 ± 0.00	50/50		0.00 ± 0.00	0/50	*	1.00 ± 0.00	50/50	
	0.30	2.00	1.00 ± 0.00	50/50		0.78 ± 0.24	39/50	*	0.00 ± 0.00	0/39	*	1.00 ± 0.00	50/50	
E2	**0 (Control)**	0 (Control)	1.00 ± 0.00	61/61	n/a	1.00 ± 0.03	60/60	n/a	1.00 ± 0.03	60/60	n/a	1.00 ± 0.16	51/61	n/a
	0.1	0.01	1.00 ± 0.00	61/61		1.01 ± 0.03	60/60		1.01 ± 0.03	60/60		1.12 ± 0.06	57/61	
	1.0	0.10	1.00 ± 0.00	60/60		1.02 ± 0.00	60/60		1.00 ± 0.00	60/60		1.12 ± 0.06	56/60	
	2.0	0.20	1.00 ± 0.00	60/60		1.00 ± 0.03	59/59		1.00 ± 0.03	59/59		1.10 ± 0.04	55/60	
	4.0	0.40	0.98 ± 0.03	59/60		1.00 ± 0.03	59/59		1.00 ± 0.03	59/59		1.13 ± 0.04	57/60	
	6.0	0.60	0.98 ± 0.03	59/60		1.00 ± 0.03	59/59		1.00 ± 0.03	59/59		1.04 ± 0.15	52/60	
	8.0	0.80	1.00 ± 0.00	62/62		0.97 ± 0.03	59/59		0.97 ± 0.03	58/59		1.02 ± 0.03	53/62	
	10.0	1.00	1.00 ± 0.00	60/60		0.98 ± 0.04	58/59		0.97 ± 0.03	57/58		1.04 ± 0.06	52/60	
	100.0	10.00	1.00 ± 0.00	36/36		0.54 ± 0.11	19/36	*	0.11 ± 0.08	4/19	*	0.00 ± 0.00	0/36	*

Supplemental table ST2 (part II). Summary of the survival, hatching and swim bladder inflation rates. Mean values ± SD (standard deviation) of each group are shown. Fold-change regarding the control group (1.0) are shown. Non-parametric Kruskal-Wallis test against the control group (p<0.05) were performed. Significant differences are marked with an asterisk (*); n/a: not applicable.

			...Hatching						Inflated swim bladder						Selected groups for morphometric analysis
			4 dpf			5 dpf			4 dpf			5 dpf			
	Experimental dose (µM)	Equilethal dose (relative)	Fold-change (Mean ± SD)	n/ total n	St. sign.	Fold-change (Mean ± SD)	n/ total n	St. sign.	Fold-change (Mean ± SD)	n/ total n	St. sign.	Fold-change (Mean ± SD)	n/ total n	St. sign.	
BPA	**0 (Control)**	0 (Control)	1.00 ± 0.00	49/49	n/a	1.00 ± 0.00	49/49	n/a	1.00 ± 0.49	16/49	n/a	1.00 ± 0.04	48/49	n/a	✓
	0.44	0.01	1.00 ± 0.00	50/50		1.00 ± 0.00	50/50		1.03 ± 0.46	17/50		0.98 ± 0.06	48/50		✓
	4.38	0.10	1.00 ± 0.00	50/50		1.00 ± 0.00	50/50		1.15 ± 0.40	19/50		1.00 ± 0.05	49/50		✓
	8.76	0.20	1.00 ± 0.00	49/49		1.00 ± 0.00	49/49		0.60 ± 0.74	10/49		0.96 ± 0.06	46/49		✓
	17.5	0.40	1.00 ± 0.00	50/50		1.00 ± 0.00	50/50		0.12 ± 0.17	2/50	*	0.90 ± 0.11	44/50		✓
	26.3	0.60	0.98 ± 0.05	48/49		1.00 ± 0.00	49/49		0.19 ± 0.17	3/49	*	0.37 ± 0.18	18/49	*	✓
	35.0	0.80	0.90 ± 0.07	46/51	*	0.92 ± 0.04	47/51	*	0.00 ± 0.00	0/51	*	0.02 ± 0.04	1/51	*	✓
	43.8	1.00	0.76 ± 0.18	38/50	*	0.82 ± 0.15	41/50	*	0.00 ± 0.00	0/50	*	0.00 ± 0.00	0/50	*	x
	219.0	5.00	0.00 ± 0.00	0/0	*	0.00 ± 0.00	0/0	*	0.00 ± 0.00	0/0	*	0.00 ± 0.00	0/0	*	x
	438.0	10.00	0.00 ± 0.00	0/0	*	0.00 ± 0.00	0/0	*	0.00 ± 0.00	0/0	*	0.00 ± 0.00	0/0	*	x
PFOS	**0 (Control)**	0 (Control)	1.00 ± 0.05	49/50	n/a	1.00 ± 0.00	50/50	n/a	1.00 ± 0.14	45/50	n/a	1.00 ± 0.00	50/50	n/a	✓
	0.20	0.01	1.02 ± 0.00	50/50		1.00 ± 0.00	50/50		1.04 ± 0.10	47/50		1.00 ± 0.00	50/50		✓
	0.50	0.03	1.00 ± 0.05	49/50		0.98 ± 0.05	48/49		1.02 ± 0.05	46/50		0.98 ± 0.05	48/49		✓
	1.00	0.07	1.02 ± 0.00	50/50		1.00 ± 0.00	50/50		1.02 ± 0.14	46/50		1.00 ± 0.00	50/50		✓
	2.00	0.13	1.00 ± 0.05	49/50		1.00 ± 0.00	50/50		0.87 ± 0.21	39/50		0.98 ± 0.05	49/50		✓
	5.00	0.33	1.02 ± 0.00	50/50		1.00 ± 0.00	50/50		0.58 ± 0.16	26/50	*	0.66 ± 0.17	33/50	*	✓
	10.0	0.67	1.02 ± 0.00	50/50		1.00 ± 0.00	50/50		0.02 ± 0.05	1/50	*	0.02 ± 0.05	1/50	*	✓
	15.0	1.00	1.02 ± 0.00	50/50		1.00 ± 0.00	48/48		0.00 ± 0.00	0/50	*	0.00 ± 0.00	0/48	*	✓
	20.0	1.33	1.02 ± 0.00	49/49		1.00 ± 0.00	49/49		0.00 ± 0.00	0/49	*	0.00 ± 0.00	0/49	*	x
	200.0	13.33	1.00 ± 0.05	49/50		1.00 ± 0.00	47/47		0.00 ± 0.00	0/50	*	0.00 ± 0.00	0/47	*	x
TBT	**0 (Control)**	0 (Control)	1.00 ± 0.00	50/50	n/a	1.00 ± 0.00	50/50	n/a	1.00 ± 0.26	39/50	n/a	1.00 ± 0.00	50/50	n/a	✓
	$3.0 \cdot 10^{-4}$	$2.0 \cdot 10^{-3}$	1.00 ± 0.00	50/50		1.00 ± 0.00	50/50		0.97 ± 0.27	38/50		1.00 ± 0.00	50/50		✓
	$3.0 \cdot 10^{-3}$	0.02	1.00 ± 0.00	49/49		1.00 ± 0.00	49/49		1.15 ± 0.09	44/49		1.00 ± 0.00	49/49		✓
	0.03	0.20	1.00 ± 0.00	50/50		1.00 ± 0.00	50/50		1.11 ± 0.17	43/50		0.98 ± 0.04	49/50		✓
	0.10	0.67	1.00 ± 0.00	49/49		1.00 ± 0.00	49/49		0.50 ± 0.24	19/49	*	0.88 ± 0.13	43/49		✓
	0.15	1.00	1.00 ± 0.00	49/49		1.00 ± 0.00	49/49		0.00 ± 0.00	0/49	*	0.00 ± 0.00	0/49	*	✓
	0.20	1.33	1.00 ± 0.00	50/50		1.00 ± 0.00	49/49		0.00 ± 0.00	0/50	*	0.00 ± 0.00	0/49	*	x
	0.25	1.67	1.00 ± 0.00	50/50		1.00 ± 0.00	50/50		0.00 ± 0.00	0/50	*	0.00 ± 0.00	0/50	*	x
	0.30	2.00	1.00 ± 0.00	50/50		1.00 ± 0.00	39/39		0.00 ± 0.00	0/50	*	0.00 ± 0.00	0/39	*	x
E2	**0 (Control)**	0 (Control)	1.00 ± 0.03	60/60	n/a	1.00 ± 0.03	60/60	n/a	1.00 ± 0.07	56/60	n/a	1.00 ± 0.03	60/60	n/a	✓
	0.1	0.01	1.00 ± 0.03	60/60		1.00 ± 0.03	60/60		1.02 ± 0.08	57/60		0.98 ± 0.04	59/60		✓
	1.0	0.10	1.02 ± 0.00	60/60		1.02 ± 0.00	60/60		1.03 ± 0.04	57/60		1.00 ± 0.03	59/60		✓
	2.0	0.20	1.00 ± 0.03	59/59		1.00 ± 0.03	59/59		0.82 ± 0.15	45/59	*	0.97 ± 0.07	57/59		✓
	4.0	0.40	1.00 ± 0.03	59/59		1.00 ± 0.03	59/59		0.74 ± 0.14	41/59	*	0.98 ± 0.07	58/59		✓
	6.0	0.60	1.00 ± 0.03	59/59		1.00 ± 0.03	59/59		0.44 ± 0.16	24/59	*	0.93 ± 0.03	55/59	*	✓
	8.0	0.80	0.97 ± 0.03	59/59		0.97 ± 0.03	59/59		0.23 ± 0.15	13/59	*	0.66 ± 0.11	40/59	*	✓
	10.0	1.00	1.00 ± 0.03	59/59		0.98 ± 0.04	58/58		0.00 ± 0.00	0/59	*	0.03 ± 0.07	2/58	*	✓
	100.0	10.00	0.06 ± 0.07	2/36	*	0.09 ± 0.10	3/19	*	0.00 ± 0.00	0/36	*	0.00 ± 0.00	0/19	*	x

Supplemental table ST3. Scoliosis presence in the eleutheroembryos exposed to BPA, PFOS, TBT and E2. Fisher's exact tests were performed to detect statistical differences between each group and its control group: * ($p < 0.05$), ** ($p < 0.01$), * ($p < 0.001$), **** ($p < 0.0001$).**

Treatment	Concentration	total nº of larvae	nº of larvae with scoliosis	% of larvae with scoliosis	Significance
BPA	DMSO	48	2	4.2	
	0.44 µM	50	0	0.0	
	4.4 µM	50	2	4.0	
	8.8 µM	49	1	2.0	
	17.5 µM	49	4	8.2	
	26.3 µM	49	2	4.1	
	35.0 µM	50	8	16.0	
	43.8 µM	-	-	-	
PFOS	DMSO	50	0	0.0	
	0.2 µM	50	0	0.0	
	0.5 µM	49	0	0.0	
	1.0 µM	50	0	0.0	
	2.0 µM	50	0	0.0	
	5.0 µM	50	1	2.0	
	10.0 µM	50	9	18.0	**
	15.0 µM	45	18	40.0	****
TBT	DMSO	50	2	4.0	
	$3.0 \cdot 10^{-4}$ µM	50	0	0.0	
	$3.0 \cdot 10^{-3}$ µM	48	1	2.1	
	$3.0 \cdot 10^{-2}$ µM	51	0	0.0	
	0.10 µM	48	1	2.1	
	0.15 µM	42	6	14.3	
E2	DMSO	58	1	1.7	
	0.1 uM	52	2	3.8	
	1 uM	60	1	1.7	
	2 uM	57	1	1.8	
	4 uM	61	1	1.6	
	6 uM	59	3	5.1	
	8 uM	59	1	1.7	
	10 uM	56	5	8.9	

Supplemental table ST4 (part I). Summary of the morphometric features measured in the eleutheroembryos. Absolute mean values ± SD (standard deviation) of each group are shown. Distances are measured in mm, HTA in arc degrees, and areas in mm^2. In the case of EL and EW, values reflect the mean of the size of both eyes. Superscript letters indicate statistically different distributions (Kruskal-Wallis non-parametric test with pairwise multiple comparisons, $p < 0.05$). Fold changes regarding the control group are represented except for YSA (which change is shown as equivalent area regarding the age control). Equivalent area refers to the age (dpf) when eleutheroembryos show a similar value of YSA in absence of any pollutant) and it was calculated interpolating the YSA value in the polynomic regression explained in section 2.3. Arrows help the visualization of the direction (increase or decrease) of the fold change.

		BL (body length)			YSA (yolk sac area)			SBA (swim bladder area)		
	Dose (µM)	Mean ± SD (mm)	Fold change (%)		Mean ± SD (mm^2)	Equivalent Area		Mean ± SD (mm^2)	Fold change (%)	
BPA	0 (Control)	3.56 ± 0.19 ^{a}	0.0	–	0.000 ± 0.017 ^{a}	5.0	–	0.056 ± 0.01 ^{a}	0.0	–
	0.44	3.51 ± 0.19 ^{ab}	-1.4	↓	0.005 ± 0.027 ^{a}	4.8	↓	0.054 ± 0.013 ^{ab}	-3.6	↓
	4.38	3.55 ± 0.16 ^{a}	-0.3	↓	0.004 ± 0.023 ^{a}	4.8	↓	0.058 ± 0.011 ^{a}	3.6	↑
	8.76	3.50 ± 0.15 ^{ab}	-1.7	↓	0.009 ± 0.021 ^{ab}	4.6	↓	0.057 ± 0.008 ^{a}	1.8	↑
	17.5	3.44 ± 0.14 ^{bc}	-3.4	↓	0.035 ± 0.040 ^{b}	4.2	↓	0.057 ± 0.011 ^{a}	1.8	↑
	26.3	3.46 ± 0.13 ^{abc}	-2.8	↓	0.082 ± 0.044 ^{c}	3.7	↓	0.046 ± 0.021 ^{b}	-17.9	↓
	35.0	3.38 ± 0.15 ^{c}	-5.1	↓	0.125 ± 0.069 ^{c}	3.4	↓	0.033 ± 0.013 ^{c}	-41.1	↓
	43.8	-	-	–	-	-	–	-	-	–
PFOS	0 (Control)	3.63 ± 0.17 ^{a}	0.0	–	0.000 ± 0.000 ^{a}	5.0	–	0.051 ± 0.008 ^{a}	0.0	–
	0.20	3.61 ± 0.15 ^{a}	-0.6	↓	0.000 ± 0.000 ^{a}	5.0	–	0.050 ± 0.007 ^{a}	-2.0	↓
	0.50	3.59 ± 0.16 ^{a}	-1.1	↓	0.000 ± 0.000 ^{a}	5.0	–	0.051 ± 0.007 ^{a}	0.0	–
	1.00	3.59 ± 0.14 ^{a}	-1.1	↓	0.000 ± 0.000 ^{a}	5.0	–	0.050 ± 0.005 ^{a}	-2.0	↓
	2.00	3.61 ± 0.15 ^{a}	-0.6	↓	0.000 ± 0.000 ^{a}	5.0	–	0.051 ± 0.009 ^{a}	0.0	–
	5.00	3.56 ± 0.15 ^{ab}	-1.9	↓	0.001 ± 0.004 ^{ab}	4.9	↓	0.046 ± 0.008 ^{a}	-9.8	↓
	10.0	3.48 ± 0.16 ^{bc}	-4.1	↓	0.005 ± 0.011 ^{bc}	4.8	↓	0.033 ± 0.005 ^{b}	-35.3	↓
	15.0	3.30 ± 0.22 ^{c}	-9.1	↓	0.011 ± 0.017 ^{c}	4.6	↓	0.032 ± 0.007 ^{b}	-37.3	↓
TBT	0 (Control)	3.47 ± 0.13 ^{a}	0.0	–	0.000 ± 0.010 ^{a}	5.0	–	0.063 ± 0.008 ^{a}	0.0	–
	$3.0 \cdot 10^{-4}$	3.44 ± 0.13 ^{a}	-0.9	↓	0.003 ± 0.016 ^{a}	4.8	↓	0.060 ± 0.008 ^{a}	-4.8	↓
	$3.0 \cdot 10^{-3}$	3.42 ± 0.13 ^{ab}	-1.4	↓	0.000 ± 0.008 ^{a}	5.0	–	0.063 ± 0.008 ^{a}	0.0	–
	0.03	3.40 ± 0.12 ^{ab}	-2.0	↓	0.000 ± 0.004 ^{a}	5.0	–	0.059 ± 0.009 ^{a}	-6.3	↓
	0.10	3.44 ± 0.11 ^{a}	-0.9	↓	0.004 ± 0.014 ^{a}	4.8	↓	0.057 ± 0.009 ^{a}	-9.5	↓
	0.15	3.35 ± 0.16 ^{b}	-3.5	↓	0.039 ± 0.023 ^{b}	4.2	↓	0.037 ± 0.005 ^{b}	-41.3	↓
E2	0 (Control)	3.77 ± 0.10 ^{a}	0.0	–	0.000 ± 0.004 ^{a}	5.0	–	0.063 ± 0.006 ^{a}	0.0	–
	0.1	3.82 ± 0.12 ^{ab}	1.3	↑	0.001 ± 0.01 ^{a}	4.9	↓	0.063 ± 0.006 ^{a}	0.0	–
	1.0	3.83 ± 0.10 ^{ab}	1.6	↑	0.000 ± 0.004 ^{a}	5.0	–	0.062 ± 0.006 ^{a}	-1.6	↓
	2.0	3.85 ± 0.12 ^{b}	2.1	↑	0.004 ± 0.015 ^{a}	4.8	↓	0.060 ± 0.005 ^{ab}	-4.8	↓
	4.0	3.85 ± 0.12 ^{b}	2.1	↑	0.004 ± 0.011 ^{a}	4.8	↓	0.057 ± 0.006 ^{b}	-9.5	↓
	6.0	3.88 ± 0.12 ^{b}	2.9	↑	0.012 ± 0.021 ^{b}	4.6	↓	0.055 ± 0.009 ^{b}	-12.7	↓
	8.0	3.82 ± 0.12 ^{ab}	1.3	↑	0.023 ± 0.026 ^{b}	4.4	↓	0.046 ± 0.011 ^{c}	-27.0	↓
	10.0	3.82 ± 0.11 ^{ab}	1.3	↑	0.048 ± 0.032 ^{c}	4.1	↓	0.032 ± 0.008 ^{d}	-49.2	↓
Age control	3 dpf	3.23 ± 0.22 ^{a}	-9.7	↓	0.170 ± 0.032 ^{a}	3.0	↓	0.031 ± 0.013 ^{a}	-44.2	↓
	4 dpf	3.46 ± 0.12 ^{b}	-3.3	↓	0.039 ± 0.047 ^{b}	4.0	↓	0.050 ± 0.007 ^{b}	-9.1	↓
	5 dpf	3.57 ± 0.14 ^{c}	0.0	–	0.000 ± 0.004 ^{c}	5.0	–	0.055 ± 0.005 ^{bc}	0.0	–
	6 dpf	3.65 ± 0.11 ^{c}	2.2	↑	0.000 ± 0.001 ^{c}	6.0	↑	0.056 ± 0.006 ^{c}	2.2	↑

Supplemental table ST4 (part II). Summary of the morphometric features measured in the eleutheroembryos. Absolute mean values ± SD (standard deviation) of each group are shown. Distances are measured in mm, HTA in arc degrees, and areas in mm^2. In the case of EL and EW, values reflect the mean of the size of both eyes. Superscript letters indicate statistically different distributions (Kruskal-Wallis non-parametric test with pairwise multiple comparisons, $p < 0.05$). Fold changes regarding the control group are represented except for YSA (which change is shown as equivalent area regarding the age control). Equivalent area refers to the age (dpf) when eleutheroembryos show a similar value of YSA in absence of any pollutant) and it was calculated interpolating the YSA value in the polynomic regression explained in section 2.3. Arrows help the visualization of the direction (increase or decrease) of the fold change.

...		ESD (eye-snout distance)			HW (head width)			EL (eye length)		
	Dose (µM)	Mean ± SD (mm)	Fold change (%)		Mean ± SD (mm)	Fold change (%)		Mean ± SD (mm)	Fold change (%)	
BPA	0 (Control)	0.240 ± 0.018^{ab}	0.0	–	0.509 ± 0.036^{a}	0.0	–	0.293 ± 0.019^{a}	0.0	–
	0.44	0.238 ± 0.015^{ab}	-0.8	↓	0.465 ± 0.036^{b}	-9.8	↓	0.288 ± 0.017^{ab}	-1.7	↓
	4.38	0.243 ± 0.013^{a}	1.3	↑	0.465 ± 0.024^{b}	-9.8	↓	0.290 ± 0.011^{a}	-1.0	↓
	8.76	0.237 ± 0.012^{ab}	-1.3	↓	0.442 ± 0.019^{c}	-13.7	↓	0.280 ± 0.010^{bc}	-4.4	↓
	17.5	0.233 ± 0.015^{bc}	-2.9	↓	0.438 ± 0.023^{c}	-13.7	↓	0.273 ± 0.014^{c}	-6.8	↓
	26.3	0.220 ± 0.023^{c}	-8.3	↓	0.467 ± 0.034^{b}	-7.8	↓	0.269 ± 0.014^{c}	-8.2	↓
	35.0	0.198 ± 0.024^{d}	-17.5	↓	0.474 ± 0.037^{b}	-7.8	↓	0.246 ± 0.017^{d}	-16.0	↓
	43.8	-	-	–	-	-	–	-	-	–
PFOS	0 (Control)	0.233 ± 0.017^{a}	0.0	–	0.596 ± 0.029^{a}	0.0	–	0.320 ± 0.014^{ab}	0.0	–
	0.20	0.229 ± 0.018^{ab}	-1.7	↓	0.593 ± 0.027^{a}	-1.7	↓	0.316 ± 0.011^{ab}	-1.3	↓
	0.50	0.236 ± 0.019^{a}	1.3	↑	0.585 ± 0.028^{a}	-3.3	↓	0.314 ± 0.012^{b}	-1.9	↓
	1.00	0.233 ± 0.017^{a}	0.0	–	0.578 ± 0.028^{a}	-3.3	↓	0.313 ± 0.012^{b}	-2.2	↓
	2.00	0.232 ± 0.016^{a}	-0.4	↓	0.590 ± 0.027^{a}	-1.7	↓	0.324 ± 0.011^{a}	1.3	↑
	5.00	0.228 ± 0.018^{ab}	-2.1	↓	0.544 ± 0.037^{b}	-10.0	↓	0.317 ± 0.011^{ab}	-0.9	↓
	10.0	0.215 ± 0.023^{b}	-7.7	↓	0.484 ± 0.016^{c}	-20.0	↓	0.304 ± 0.011^{c}	-5.0	↓
	15.0	0.197 ± 0.017^{c}	-15.5	↓	0.477 ± 0.025^{c}	-20.0	↓	0.291 ± 0.013^{c}	-9.1	↓
TBT	0 (Control)	0.243 ± 0.014^{ab}	0.0	–	0.541 ± 0.025^{ab}	0.0	–	0.290 ± 0.012^{a}	0.0	–
	$3.0 \cdot 10^{-4}$	0.242 ± 0.015^{ab}	-0.4	↓	0.542 ± 0.023^{ab}	0.0	–	0.293 ± 0.012^{a}	1.0	↑
	$3.0 \cdot 10^{-3}$	0.238 ± 0.016^{ab}	-2.1	↓	0.534 ± 0.023^{b}	-1.9	↓	0.287 ± 0.011^{a}	-1.0	↓
	0.03	0.247 ± 0.015^{a}	1.6	↑	0.555 ± 0.025^{a}	3.7	↑	0.285 ± 0.013^{a}	-1.7	↓
	0.10	0.234 ± 0.016^{b}	-3.7	↓	0.534 ± 0.026^{b}	-1.9	↓	0.276 ± 0.011^{b}	-4.8	↓
	0.15	0.211 ± 0.013^{c}	-13.2	↓	0.493 ± 0.018^{c}	-9.3	↓	0.255 ± 0.010^{c}	-12.1	↓
E2	0 (Control)	0.248 ± 0.013^{ab}	0.0	–	0.597 ± 0.023^{ab}	0.0	–	0.350 ± 0.011^{a}	0.0	–
	0.1	0.248 ± 0.014^{ab}	0.0	–	0.600 ± 0.026^{ab}	0.0	–	0.349 ± 0.011^{a}	-0.3	↓
	1.0	0.253 ± 0.012^{a}	2.0	↑	0.597 ± 0.031^{ab}	0.0	–	0.351 ± 0.010^{a}	0.3	↑
	2.0	0.242 ± 0.013^{b}	-2.4	↓	0.594 ± 0.026^{b}	-1.7	↓	0.350 ± 0.008^{a}	0.0	–
	4.0	0.241 ± 0.011^{b}	-2.8	↓	0.610 ± 0.033^{ab}	1.7	↑	0.347 ± 0.012^{a}	-0.9	↓
	6.0	0.242 ± 0.013^{b}	-2.4	↓	0.610 ± 0.027^{a}	1.7	↑	0.345 ± 0.009^{ab}	-1.4	↓
	8.0	0.242 ± 0.015^{b}	-2.4	↓	0.595 ± 0.025^{ab}	0.0	–	0.340 ± 0.010^{b}	-2.9	↓
	10.0	0.219 ± 0.017^{c}	-11.7	↓	0.567 ± 0.019^{c}	-5.0	↓	0.326 ± 0.011^{c}	-6.9	↓
Age control	3 dpf	0.185 ± 0.015^{a}	-22.1	↓	0.541 ± 0.036^{a}	-3.3	↓	0.306 ± 0.013^{a}	-6.9	↓
	4 dpf	0.222 ± 0.015^{b}	-6.2	↓	0.528 ± 0.028^{a}	-5.6	↓	0.314 ± 0.013^{a}	-4.5	↓
	5 dpf	0.237 ± 0.011^{bc}	0.0	–	0.559 ± 0.027^{b}	0.0	–	0.328 ± 0.009^{b}	0.0	–
	6 dpf	0.248 ± 0.014^{c}	4.7	↑	0.545 ± 0.022^{ab}	-2.6	↓	0.336 ± 0.008^{b}	2.2	↑

Supplemental table ST4 (part III). Summary of the morphometric features measured in the eleutheroembryos. Absolute mean values ± SD (standard deviation) of each group are shown. Distances are measured in mm, HTA in arc degrees, and areas in mm^2. In the case of EL and EW, values reflect the mean of the size of both eyes. Superscript letters indicate statistically different distributions (Kruskal-Wallis non-parametric test with pairwise multiple comparisons, $p < 0.05$). Fold changes regarding the control group are represented except for YSA (which change is shown as equivalent area regarding the age control). Equivalent area refers to the age (dpf) when eleutheroembryos show a similar value of YSA in absence of any pollutant) and it was calculated interpolating the YSA value in the polynomic regression explained in section 2.3. Arrows help the visualization of the direction (increase or decrease) of the fold change.

...		EW (eye width)			IOD (interocular distance)			HTA (head-trunk angle)		
	Dose (µM)	Mean ± SD (mm)	Fold change (%)		Mean ± SD (mm)	Fold change (%)		Mean ± SD (degrees)	Fold change (%)	
BPA	0 (Control)	0.202 ± 0.009^{a}	0.0	–	0.105 ± 0.023^{bc}	0.0	–	162.3 ± 3.9^{ab}	0.0	–
	0.44	0.184 ± 0.008^{bc}	-8.9	↓	0.097 ± 0.027^{cd}	-7.6	↓	161.4 ± 3.5^{ab}	-0.6	↓
	4.38	0.189 ± 0.007^{ab}	-6.4	↓	0.087 ± 0.016^{de}	-17.1	↓	158.6 ± 2.9^{c}	-2.3	↓
	8.76	0.181 ± 0.007^{c}	-10.4	↓	0.080 ± 0.009^{e}	-23.8	↓	159.4 ± 3.3^{bc}	-1.8	↓
	17.5	0.171 ± 0.007^{d}	-15.3	↓	0.095 ± 0.015^{cd}	-9.5	↓	155.1 ± 4.3^{d}	-4.4	↓
	26.3	0.173 ± 0.007^{d}	-14.4	↓	0.123 ± 0.031^{ab}	17.1	↑	156.8 ± 5.2^{cd}	-3.4	↓
	35.0	0.172 ± 0.008^{d}	-14.9	↓	0.130 ± 0.033^{a}	23.8	↑	163.7 ± 5.9^{a}	0.9	↑
	43.8	-	-	–	-	-	–	-	-	–
PFOS	0 (Control)	0.222 ± 0.011^{a}	0.0	–	0.156 ± 0.013^{ab}	0.0	–	163.6 ± 2.8^{a}	0.0	–
	0.20	0.221 ± 0.010^{a}	-0.5	↓	0.159 ± 0.014^{a}	1.9	↑	166.2 ± 2.6^{a}	1.6	↑
	0.50	0.221 ± 0.009^{a}	-0.5	↓	0.151 ± 0.017^{abc}	-3.2	↓	165.6 ± 2.6^{a}	1.2	↑
	1.00	0.221 ± 0.010^{a}	-0.5	↓	0.143 ± 0.019^{bc}	-8.3	↓	164.7 ± 2.4^{a}	0.6	↑
	2.00	0.219 ± 0.009^{a}	-1.4	↓	0.154 ± 0.015^{ab}	-1.3	↓	159.2 ± 2.8^{b}	-2.7	↓
	5.00	0.208 ± 0.009^{b}	-6.3	↓	0.133 ± 0.027^{c}	-14.7	↓	157.3 ± 5.0^{b}	-3.9	↓
	10.0	0.195 ± 0.009^{c}	-12.2	↓	0.101 ± 0.011^{d}	-35.3	↓	144.1 ± 5.8^{c}	-11.9	↓
	15.0	0.188 ± 0.012^{c}	-15.3	↓	0.103 ± 0.011^{d}	-34.0	↓	144.8 ± 7.9^{c}	-11.5	↓
TBT	0 (Control)	0.194 ± 0.009^{a}	0.0	–	0.160 ± 0.016^{ab}	0.0	–	168.4 ± 2.4^{a}	0.0	–
	$3.0 \cdot 10^{-4}$	0.195 ± 0.008^{a}	0.5	↑	0.154 ± 0.014^{ab}	-3.8	↓	171.7 ± 2.6^{b}	1.9	↑
	$3.0 \cdot 10^{-3}$	0.193 ± 0.010^{a}	-0.5	↓	0.156 ± 0.012^{bc}	-2.5	↓	169.0 ± 2.6^{a}	0.3	↑
	0.03	0.196 ± 0.007^{a}	1.0	↑	0.169 ± 0.018^{a}	5.6	↑	171.2 ± 2.6^{b}	1.6	↑
	0.10	0.187 ± 0.009^{b}	-3.6	↓	0.168 ± 0.014^{a}	5.0	↑	170.1 ± 3.5^{ab}	1.0	↑
	0.15	0.178 ± 0.006^{c}	-8.2	↓	0.149 ± 0.013^{c}	-6.9	↓	169.9 ± 3.9^{ab}	0.8	↑
E2	0 (Control)	0.232 ± 0.010^{ab}	0.0	–	0.133 ± 0.018^{ab}	0.0	–	160.0 ± 2.8^{a}	0.0	–
	0.1	0.236 ± 0.010^{a}	1.7	↑	0.129 ± 0.021^{ab}	-3.0	↓	159.4 ± 3.2^{abc}	-0.4	↓
	1.0	0.235 ± 0.012^{a}	1.3	↑	0.127 ± 0.019^{a}	-4.5	↓	159.6 ± 3.1^{ab}	-0.3	↓
	2.0	0.232 ± 0.008^{ab}	0.0	–	0.131 ± 0.023^{ab}	-1.5	↓	156.3 ± 3.3^{d}	-2.3	↓
	4.0	0.235 ± 0.011^{ab}	1.3	↑	0.141 ± 0.023^{bc}	6.0	↑	157.7 ± 3.9^{bcd}	-1.4	↓
	6.0	0.230 ± 0.010^{ab}	-0.9	↓	0.151 ± 0.022^{c}	13.5	↑	156.0 ± 4.3^{d}	-2.5	↓
	8.0	0.229 ± 0.008^{b}	-1.3	↓	0.138 ± 0.017^{abc}	3.8	↑	159.4 ± 4.1^{abc}	-0.4	↓
	10.0	0.215 ± 0.007^{c}	-7.3	↓	0.135 ± 0.015^{ab}	1.5	↑	157.1 ± 4.7^{cd}	-1.8	↓
Age control	3 dpf	0.208 ± 0.010^{a}	-9.1	↓	0.120 ± 0.018^{a}	8.4	↑	164.0 ± 6.2^{a}	1.7	↑
	4 dpf	0.213 ± 0.009^{a}	-7.1	↓	0.102 ± 0.017^{b}	-8.0	↓	163.1 ± 4.3^{ab}	1.2	↑
	5 dpf	0.229 ± 0.013^{b}	0.0	–	0.110 ± 0.011^{ab}	0.0	–	161.2 ± 3.1^{b}	0.0	–
	6 dpf	0.224 ± 0.009^{b}	-2.0	↓	0.103 ± 0.012^{b}	-6.9	↓	161.0 ± 3.2^{b}	-0.2	↓

Chapter II:

Transcriptomic deregulation in zebrafish eleutheroembryos induced by BPA, PFOS and TBT. High-throughput sequencing analyses of the transcriptome: RNA-Seq.

Once morphometric signatures of BPA, PFOS and TBT were assessed and their toxicity and lethality studied, zebrafish eleutheroembryos were exposed from 2 to 5 days post fertilization (dpf) to sub-lethal concentrations, far from their general toxicity, and transcriptomic analyses were performed. RNA-sequencing technology was used to sequence the whole transcriptome. Dose-response exposures ranged from 0.44 to 17.5 µM of BPA, from 0.06 to 2.0 µM of PFOS, and from 0.0017 to 0.056 µM of TBT. Differentially expressed genes (DEGs) were determined, and functional analyses performed, with the goal to increase the knowledge of the mode of action of BPA, PFOS and TBT in the zebrafish eleutheroembryos. Most affected biological pathways were assessed. Transcriptomic dysregulations were compared and correlated with the morphometric signatures that took place at higher concentrations.

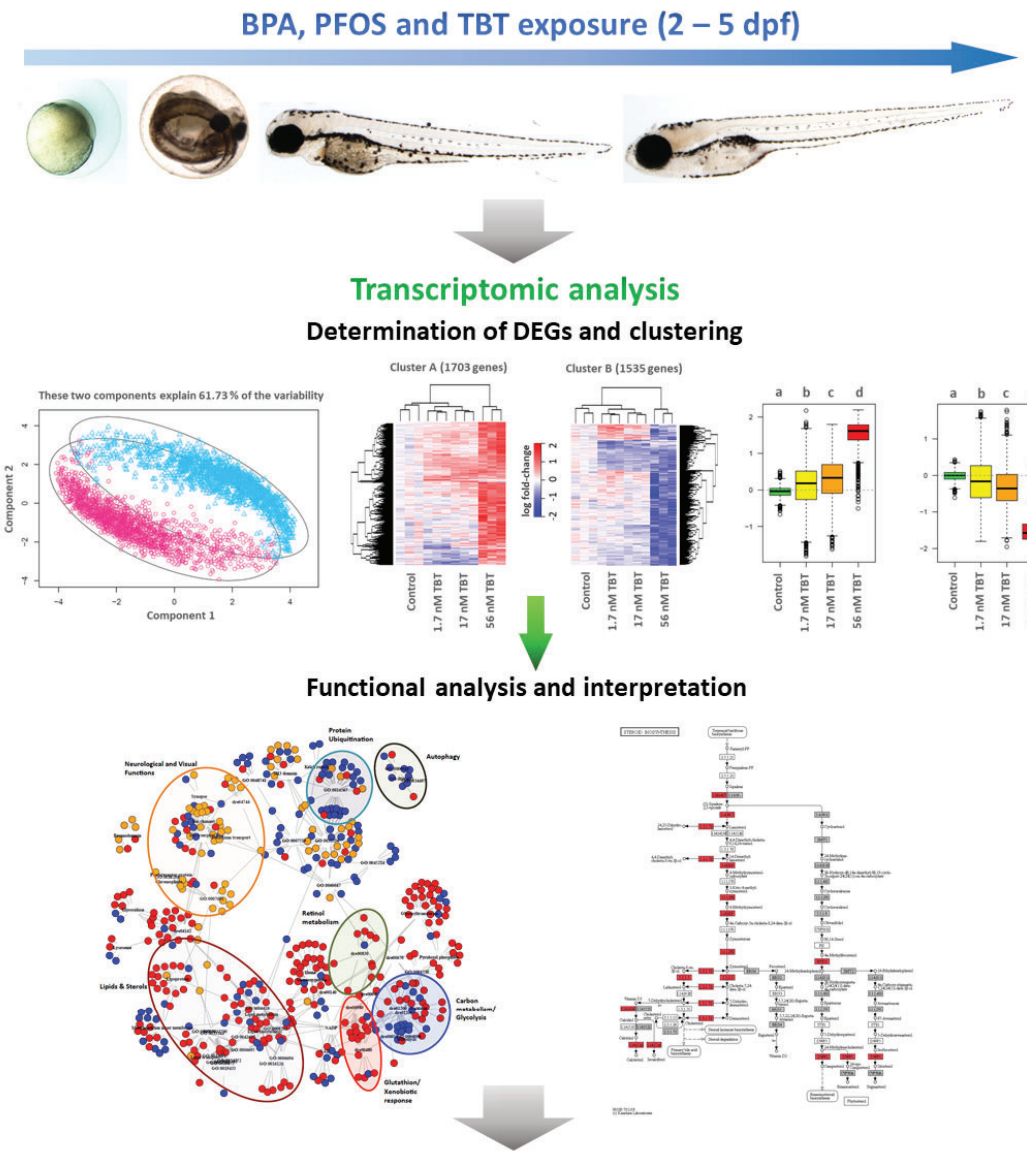

Main results

Main transcriptomic pathways disrupted by:

- BPA: lipid transport and metabolism, retinol and sterols metabolism, visual perception, energy homeostasis.

- PFOS: lipid transport and metabolism, immune system, and pathways related to cell adhesion molecules (CAMs).

- TBT: steroid metabolism, cholesterol and vitamin D_3 biosynthesis, cell division and development.

Scientific article II

Dose-dependent transcriptomic responses of zebrafish eleutheroembryos to Bisphenol A

Authors: R. Martínez, A. Esteve-Codina, L. Herrero-Nogareda, E. Ortiz-Villanueva, C. Barata, R. Tauler, D. Raldúa, B. Piña, L. Navarro-Martín

Status: Published

Journal: Environ. Pollut. 243 (2018) 988–997.

DOI: doi.org/10.1016/j.envpol.2018.09.04

Environmental Pollution 243 (2018) 988–997

Contents lists available at ScienceDirect

Environmental Pollution

journal homepage: www.elsevier.com/locate/envpol

Dose-dependent transcriptomic responses of zebrafish eleutheroembryos to Bisphenol A☆

Rubén Martínez [a, b], Anna Esteve-Codina [c, d], Laia Herrero-Nogareda [a], Elena Ortiz-Villanueva [a], Carlos Barata [a], Romà Tauler [a], Demetrio Raldúa [a], Benjamin Piña [a], Laia Navarro-Martín [a, *]

[a] Institute of Environmental Assessment and Water Research, IDAEA-CSIC, Barcelona, Catalunya, 08034, Spain
[b] Universitat de Barcelona (UB), Barcelona, Catalunya, 08007, Spain
[c] CNAG-CRG, Centre for Genomic Regulation (CRG), Barcelona Institute of Science and Technology (BIST), Barcelona, Catalunya, 08028, Spain
[d] Universitat Pompeu Fabra (UPF), Barcelona, Catalunya, 08003, Spain

ARTICLE INFO

Article history:
Received 7 May 2018
Received in revised form
20 August 2018
Accepted 7 September 2018
Available online 11 September 2018

Keywords:
BPA
Hormone-response
Obesogens
RNA-Seq
Differentially expressed genes (DEGs)
ANOVA-PLS

ABSTRACT

Despite the abundant literature on the adverse effects of Bisphenol A (BPA) as endocrine disruptor, its toxicity mechanisms are still poorly understood. We present here a study of its effects on the zebrafish eleutheroembryo transcriptome at concentrations ranging from 0.1 to 4 mg L^{-1}, this latter representing the lowest observed effect concentration (LOEC) found in our study at three different macroscopical endpoints (survival, hatching and swim bladder inflation). Multivariate data analysis methods identified both monotonic and bi-phasic patterns of dose-dependent responses. Functional analyses of genes affected by BPA exposure suggest an interaction of BPA with different signaling pathways, being the estrogenic and retinoid receptors two likely targets. In addition, we identified an apparently unrelated inhibitory effect on, among others, visual function genes. We interpret our data as the result of a sum of underlying, independent molecular mechanisms occurring simultaneously at the exposed animals, well below the macroscopic LOEC, but related to at least some of the observed morphological alterations, particularly in eye size and yolk sac resorption. Our data supports the idea that the physiological effects of BPA cannot be only explained by its rather weak interaction with the estrogen receptor, and that multivariate analyses are required to analyze the effects of toxicants like BPA, which interact with different cellular targets producing complex phenotypes.

1. Introduction

Bisphenol A (BPA) is a key monomer used in the production of certain kind of plastics with wide household uses. It can be found in drink containers, food packaging, adhesives or beverage cans (among many others), as it is amply used in the manufacture of polycarbonate plastics and epoxy resins (Huang et al., 2012; Wang et al., 2015). Many studies have demonstrated that BPA leaks from the original plastics over time, and, as a consequence, it is continuously released in large amounts into the environment. According to the United States Environmental Protection Agency (EPA), the annual release of BPA into the environment exceeded 500 tons in 2012. BPA is ubiquitous in the environment, typically showing parts per billion (ppb) level concentrations in surface waters (from non-detectable to 56.0 μg L^{-1}) and plastic items leachates (0.1–7.7 μg L^{-1}) (Corrales et al., 2015; Le et al., 2008; Talsness et al., 2009) and parts per million (ppm) levels in landfill leachates (0.001–17.2 mg L^{-1}) and mill effluents (0.0002–0.4 mg L^{-1}) (Canesi and Fabbri, 2015; Flint et al., 2012; Kolpin et al., 2002).

BPA is considered an important threat to the human health, wildlife and environment, owing to its estrogenic activity at environmentally relevant concentrations (0.1–1000 μg L^{-1}) (Arase et al., 2011; Cabaton et al., 2011; Careghini et al., 2015; Crain et al.,

☆ This paper has been recommended for acceptance by Dr. Harmon Sarah Michele.

* Corresponding author. Institute of Environmental Assessment and Water Research, IDAEA-CSIC, Jordi Girona 18, 08034, Barcelona, Spain.
E-mail addresses: rmlqam@cid.csic.es (R. Martínez), anna.esteve@cnag.crg.eu (A. Esteve-Codina), fjr181@alumni.ku.dk (L. Herrero-Nogareda), elena.ortiz@idaea.csic.es (E. Ortiz-Villanueva), cbmqam@cid.csic.es (C. Barata), roma.tauler@idaea.csic.es (R. Tauler), drpqam@cid.csic.es (D. Raldúa), bpcbmc@cid.csic.es (B. Piña), laianavarromartin@gmail.com (L. Navarro-Martín).

https://doi.org/10.1016/j.envpol.2018.09.043
0269-7491/

2007; Kang et al., 2006; Villeneuve et al., 2012; Xu et al., 2013). BPA alters gonadal functions at 0.2 μg L^{-1} - 2.2 mg L^{-1} (Chen et al., 2017; Ekman et al., 2012; Lee et al., 2003; Richter et al., 2007b), and affects hepatic vitellogenin production in fish and other organisms at 0.5–22.8 mg L^{-1} (Lindholst et al., 2000; Rankouhi et al., 2002). In addition to these effects on reproductive functions, exposure to BPA caused metabolic alterations in different animal models, including disruption of glucose homeostasis in rodents at 10–100 μg/kg/day (Alonso-Magdalena et al., 2010), disruption of lipid metabolism, increasing lipid storage and adipogenesis, and affecting body weight later in life at 0.25–250 μg/kg/day (Rubin and Soto, 2009; Ryan et al., 2010; Somm et al., 2009). These metabolic effects seem to be related to fundamental cell functions and they have been reported not only in mammals, but also in fish (1.0–4.0 mg L^{-1}) (Ortiz-Villanueva et al., 2017b) and even in crustaceans, like *Daphnia magna* (5.1–32.0 mg L^{-1}) (Jordão et al., 2016b; Nagato et al., 2013). Due to the demonstrated window of sensitivity to BPA exposure during early development, the European Union and Canadian Authorities have banned the use of BPA in baby bottles and toys. EPA and the European Food Safety Agency (EFSA) established a tolerable daily intake (TDI) of 50 and 4 μg/kg/day, respectively, derived from the no-observed-adverse-effect level (NOAEL) on liver and reproductive toxicity endpoints. This level of exposure, which can be reached from exclusively environmental, non-dietary exposures (EFSA, 2016; Lejonklou et al., 2017), may even be too high to protect consumers and wildlife, as environmentally relevant BPA doses below this TDI are already able to alter reproductive and metabolic functions in exposed animals (Richter et al., 2007a).

Zebrafish (*Danio rerio*) is becoming a preferred model for the analysis of sublethal effects of toxicants in vertebrates (Scholz and Mayer, 2008; Stegeman et al., 2010). It is easy to maintain, it has a short life cycle, and readily produce relatively large quantities of transparent embryos, the development of which has been extensively studied and can be observed using a variety of optical methods. Characteristically, zebrafish embryos hatch only 48–72 h after fertilization (hpf), continuing its development as free-swimming eleutheroembryos until reaching the larval, self-feeding stage at about 120 hpf (Kimmel et al., 1995; Strähle et al., 2012). Zebrafish has been deeply studied at least at four *-omic* levels: genomics, transcriptomics, proteomics and metabolomics (Mushtaq et al., 2013), and it is considered a convenient vertebrate model for human and environmental toxicology (Raldúa and Piña, 2014; Strähle et al., 2012).

During the last decade, both genomics and transcriptomics have large enhanced their performance specially with the development of high-throughput next generation sequencing (HT-NGS) technologies (Churko et al., 2013; Mortazavi et al., 2008; Reuter et al., 2015). Although both main HT-NGS technologies (microarrays and RNA-seq) have become powerful tools to analyze the transcriptome of many organisms, it has been the last one which has shown better advantages (Wang et al., 2009; Zhao et al., 2014). The use of HT-NGS to examine the effects of endocrine disrupting chemicals (EDCs) in zebrafish is becoming popular (Baker and Hardiman, 2014; Caballero-Gallardo et al., 2016). Nevertheless, most of the studies focus on a reduced dataset of genes, on adult tissues, on a single-dose exposure or on the effects during the first hours when the embryos still haven't developed most organs (Chen et al., 2018; Lam et al., 2011; Renaud et al., 2017; Saili et al., 2013; Tse et al., 2013; Wang et al., 2018).

The aim of the present study was to analyze transcriptome changes in zebrafish eleutheroembryos exposed to BPA and to examine the underlying regulatory mechanisms responsible for the multiple toxic effects of BPA both in aquatic, terrestrial animals and in humans.

2. Materials and methods

2.1. Animals and rearing conditions

Adult zebrafish (12–18 months old, wild-type *Danio rerio*) were maintained under standard conditions (28 ± 1 °C, 12L:12D photoperiod) and fed twice daily with dry flakes (TetraMin, Tetra, Germany). Eggs were obtained by natural mating and collected and rinsed 2 h after fertilization (hpf). Fertilized viable eggs were transferred to fish water (90 μg/ml of Instant Ocean -Aquarium Systems, Sarrebourg, France-, 0.58 mM $CaSO_4 \cdot 2H_2O$, dissolved in reverse osmosis purified water) and kept under standard conditions. All procedures were conducted in accordance with the institutional guidelines under a license from the local government (DAMM 7669, 7964) and were approved by the Institutional Animal Care and Use Committees at the Research and Development Centre of the Spanish Research Council (CID-CSIC).

2.2. Zebrafish eleutheroembryo exposure to BPA

2.2.1. BPA solutions preparation

Bisphenol A (BPA, Sigma-Aldrich, St. Louis, MO, USA) stock solutions (50, 500 and 2000 mg L^{-1}) were prepared in DMSO (dimethyl sulfoxide) and stored at −20 °C. During exposures fresh working solutions were prepared everyday by dissolving the stock solutions in fish water, with a final concentration of DMSO of 0.2% (v/v). Chemical analyses of these solutions were not performed as BPA has been shown to be stable for up to 48 h in water solutions (Jordão et al., 2016b). Preparing and changing water solutions every day until the end of the exposures assured continuous exposure to BPA.

2.2.2. Preliminary range-finding test

A preliminary exposure to BPA concentrations ranging from 0 to 100 mg L^{-1} was carried out from 2 to 5 days post-fertilization (dpf). During the first 48 h, embryos were kept in clean water to avoid alterations in the very early embryonic process, and to focus in the responses of the already differentiated tissues to BPA. Two dpf embryos were randomly distributed in 6-well microplates at a density of 3 embryos/mL. During the range-finding test, the experimental groups included a vehicle control (0.2% DMSO), 0.1, 1, 2, 4, 6, 8, 10, 50 and 100 mg L^{-1} BPA. Previous studies done in our laboratory have resulted in 0% survival rates of embryos exposed to environmentally relevant high BPA concentrations (1000 mg L^{-1}) found in landfill leachate and sewage treatment effluent sources (Crain et al., 2007; Kang et al., 2007). For that reason we set up our experiments to span from 100 mg L^{-1} to the range of a recent proposed total allowable concentration of BPA for drinking water (100 μg L^{-1}) (Willhite et al., 2008). For each experimental condition, at least 50 embryos were assessed for survival, hatching, swim bladder inflation rates and sub-lethal and teratogenic effects. Survival (3, 4 and 5 dpf), hatching rates (3, 4 and 5 dpf) and presence of inflated swim bladder (4 and 5 dpf) were recorded for each concentration.

2.2.3. Embryo fixation and morphological traits

Zebrafish eleutheroembryos exposed in the preliminary range-finding test during the period 2–5 dpf were fixed in 4% paraformaldehyde (PFA) in PBS overnight at 4 °C and washed several times with PBS. Fixed eleutheroembryos were gradually transferred to 90% glycerol for preservation and facilitation of eleutheroembryo positioning. Lateral and dorsoventral images of the fixed eleutheroembryos were then taken in order to report morphological effects using a stereomicroscope Nikon SMZ1500 and a Nikon digital Sight DS-Ri1 camera. Embryo standard length, yolk sac area

(YSA) and eye size (width) were measured using the free graphical image analysis software ImageJ (National Institutes of Health, Bethesda, MD, USA) (Raldúa et al., 2008). Values (length or width) were normalized by control group mean. Yolk sac area was expressed in mm^2, with baseline correction by subtracting YSA mean value of the control group.

2.2.4. Zebrafish eleutheroembryo exposure to BPA and sample collection

A second experiment was set up to collect samples for transcriptomic analysis. The concentrations used in the transcriptomic study were chosen to avoid molecular events directly related to alterations in development or embryo viability. In the preliminary range-finding test we determined 4 mg L^{-1} of BPA as the lowest observed effect concentration (LOEC) (see section 3.1.). For that reason, 4 mg L^{-1} was used as the highest BPA concentration to carry out the exposures for the transcriptomic study. Therefore, eleutheroembryos were exposed to Control (0.2% DMSO), 0.1, 1, and 4 mg L^{-1} BPA for three days from 2 to 5 dpf. BPA solutions were prepared as indicated above and changed every day. The anatomical development of embryos was followed daily during the exposure (Kimmel et al., 1995). Survival (3, 4 and 5 dpf), hatching rates (3, 4 and 5 dpf) and presence of inflated swim bladder (4 and 5 dpf) were recorded for each concentration. Replicate pools of 10 zebrafish eleutheroembryos were collected per condition from each replicate plate. Samples were snap-frozen in dry ice and stored at −80 °C until further analysis.

2.2.5. Statistical analysis

Differences between treatments in survival, hatching and swim bladder inflation (sections 2.2.2 and 2.2.4.) and in standard length, eye width and yolk sac area (section 2.2.3.) were analyzed using the non-parametric Kruskal-Wallis test with pairwise multiple comparisons since the data did not meet parametric assumptions. Analyses were performed using SPSS 24.0 (Armonk, NY: IBM Corp., 2016). Differences were considered to be significant when $p < 0.05$. Graphs (Fig. 1, Supplementary Figures 1 and 2) were performed using GraphPad Prism (v. 6.07, GraphPad Software, La Jolla, CA, USA).

2.3. RNA isolation, library preparation and RNA sequencing

Total RNA was isolated from the pools of 10 whole zebrafish eleutheroembryos using AllPrep DNA/RNA Mini Kit (Qiagen, CA, USA) as described by the manufacturer. Extracted RNA was reconstituted in RNAse-free water. Then, total RNA was assayed for quantity and quality using Qubit® RNA BR Assay kit (Thermo Fisher Scientific) and RNA 6000 Nano Assay on a Bioanalyzer 2100 (Agilent Technologies). Three high-quality RNA biological replicates per condition were sent for sequencing to the National Centre for Genomic Analysis (CNAG, Barcelona, Spain). In all cases, RNA concentrations ranged between 50 and 200 ng μL^{-1}, free of DNA and with RNA integrity number (RIN) > 8.

Libraries for RNA-Seq were prepared from total RNA using KAPA Stranded mRNA-Seq Kit Illumina® Platforms (Kapa Biosystems) with minor modifications. Briefly, after poly-A based mRNA enrichment with oligo-dT magnetic beads and 500 ng of total RNA as the input material, the mRNA was fragmented (resulting RNA fragment size was 80–250 nt, with the major peak at 130 nt). The second strand cDNA synthesis was performed in the presence of dUTP instead of dTTP, to achieve the strand specificity. The blunt-ended double stranded cDNA was 3′adenylated and Illumina indexed adapters (Illumina) were added by ligation. The ligation product was enriched through 15 PCR cycles and the final library was validated on an Agilent 2100 Bioanalyzer with the DNA 7500 assay.

Each library was sequenced using TruSeq SBS Kit v3-HS, in paired-end mode with a read length of 2 × 76bp. We generated on average 40 million paired-end reads for each sample in a fraction of a sequencing lane on HiSeq 2000 (Illumina) following the manufacturer's protocol. Image analysis, base calling and quality scoring of the run were processed using the manufacturer's software Real Time Analysis (RTA 1.13.48) and followed by generation of FASTQ sequence files by CASAVA software. More than 90% of the obtained reads mapped properly to the reference genome. The majority mapped to exonic regions and to protein-coding genes, with a total of 25,000 genes detected per sample.

The data discussed in this publication have been deposited in NCBI's Gene Expression Omnibus (Edgar et al., 2002) and are accessible through GEO Series accession number GSE113676 (https://www.ncbi.nlm.nih.gov/geo/query/acc.cgi?acc=GSE113676). Full description of mapping quality statistics can be found in Supplementary Table 1.

2.4. Data processing and differentially expressed genes (DEGs) analysis

RNA-seq reads were aligned to the *D. rerio* reference genome (GRCz10) using STAR version 2.5.1b (Dobin et al., 2013). Genes annotated in GRCz10.84 were quantified using RSEM version 1.2.28 (Li and Dewey, 2011) with default parameters. Data normalization was performed with the DESeq2 (v.1.10.1) R package (Li and Dewey, 2011; Love et al., 2014), which uses a variant of scaling factor normalization based on the assumption that most genes are not differentially expressed. In our case, we devised a dose-response experiment and decided to analyze both monotonic and non-monotonic responses, as both types of responses have been reported for many endocrine disruptors, including BPA (Vandenberg et al., 2012). For this reason, we chose the supervised ANOVA-PLS (Analysis Of Variance-Partial Least Square) analysis (*lmdme* package in R v. 1.0.136, R Core Team (Fresno et al., 2014)) to perform the differential expression analysis between all experimental conditions. ANOVA decomposes first the data matrix with the transcriptomic information of all samples (normalized and scaled) through a linear model, which takes into account the existence of different levels of exposure to BPA, but without requiring any assumption on the behavior of the different genes among these experimental subsets. In a second step, a PLS regression model is built between the matrices obtained in this linear decomposition (X) and the vector (y) that defines the class membership of the samples (control and BPA treated samples). The analysis determines if the experimental groups are different from each other, and it identifies features (variables) that describe best the differences between groups. We preferred this supervised, multi-level, multivariant method of data analysis as it reflects our experimental setup better than paired tests, like the Student's T test or the PLS-DA (Partial Least Square-Discriminant Analysis), in which a sample (usually, the control) is taken as a reference for all remaining conditions (Fresno et al., 2014). Thereby, ANOVA-PLS was performed on the normalized data scaled to the control set and log2 transformed, considering each one of the BPA concentrations (including controls) as a class. Genes showing significant variations among the classes were selected as DEGs for further analysis. The observed variations in selected DEGs were further confirmed by Real-time qRT-PCR (details presented as supplementary material).

Hierarchical clustering and PAM (partition around medoids) clustering analysis were performed using the packages *gplots*, *fpc*, and *cluster* in R. The PAM implementation in these packages performs a principal component analysis (PCA), to analyze the covariance matrix of the entered variables and to produce a two-

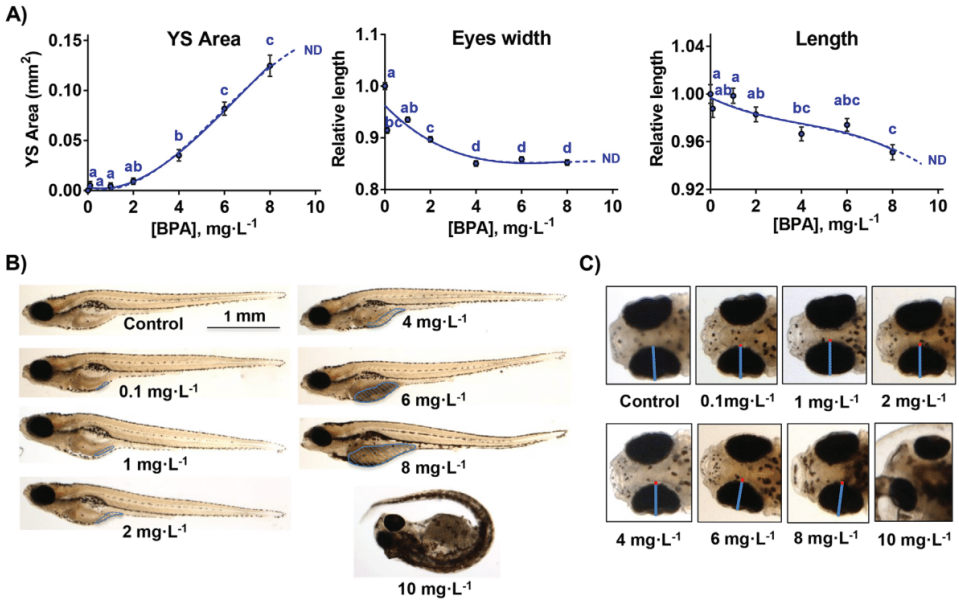

Fig. 1. Morphological results from the preliminary range-finding test. **A)** Effects of the BPA exposure in the area of the yolk sac remnants, relative eyes width and relative embryo standard length. The size of the yolk sac (YS Area) is expressed in mm^2, with baseline subtraction. Relative eyes width and standard length is expressed in relative values (normalized by control group mean). Low-case letters in each graph indicate statistically different distributions (Kruskal-Wallis non-parametric test with pairwise multiple comparisons, $p < 0.05$). Mean ± SEM values are shown (SEM = standard error of the mean). **B-C)** Representative images of yolk sac area (B) and relative eye width (C) means for each BPA condition are shown. In C), the blue line indicates the length of the control; the red line represents a decrease of that distance. The parameters at 10 mg L^{-1} were not determined (ND) due to the high rates of malformations at this BPA concentration. Survival rates at 50 and 100 mg L^{-1} were 0% and in consequence no data exists for both treatment groups. (For interpretation of the references to color in this figure legend, the reader is referred to the Web version of this article.)

dimension plot (two first components) that helps on visualization of how separable the defined clusters were. Samples from each cluster are differentially colored and marked with ellipses (https://www.rdocumentation.org/packages/cluster/versions/2.0.6/topics/pam). Significant differences between scaled values of all genes included in each cluster were assessed by one-way ANOVA followed by post hoc Tukey's B tests ($p < 0.05$) to identify statistically different subsets of samples, using *foreign* and *agricolae* R packages. Further graphs, including heatmaps, were performed with the *gplots* package, also in R.

Functional analysis of DEGs was performed using DAVID Bioinformatic Resources 6.8 Gene enrichment analysis was estimated in DAVID using the default zebrafish (*Danio rerio*) background; enrichment significances were set to a false discovery ratio (FDR) ≤5%. The analysis was limited to GO:Biological Function and KEGG datasets, for simplification. Identified modules with at least five hits were included in the network analysis, using the *reshape2* and *igraph* packages in R (R Development Core Team (2008), 2008). Bipartite graphs were drawn from an incidence table of genes (represented by their official gene names, ZFIN.org), using *igraph*. Any two given genes were considered linked if they share at least one common KEGG or GO (Gene Ontology) module. Metabolic pathways were obtained from the KEGG database.

3. Results

3.1. Survival hatching and swim bladder (SB) inflation rates

At the end of the preliminary range-finding test no significant differences in survival rates (ranging from 98 to 100%) were observed in BPA concentrations up to 10 mg L^{-1}. In contrast survival rates at higher concentrations were found to be 0% (Supplementary Figure 1). Gross malformations (Fig. 1) appeared at BPA concentrations of 10 mg L^{-1}. The first statistically significant effects (Kruskal-Wallis non-parametric test, $p < 0.05$) on hatching and swim bladder (SB) inflation appeared at 8 and 4 mg L^{-1}, respectively. We used the lowest concentration where, at least, one of these parameters was statistically different from the control (4 mg L^{-1}) as the LOEC to perform the next BPA exposure (section 2.2.4.). Similar LOEC value and alterations in development, malformations or larvae viability found in the present study are coincident with previous data (Lam et al., 2011; Ortiz-Villanueva et al., 2017a, 2017b; Pelayo et al., 2012).

During the exposure carried out for the transcriptomic study, mortality was negligible and lethal endpoints such as coagulated embryos, lack of somite formation, non-detachment of the tail, or lack of heartbeat were not observed. The fraction of non-hatched eggs was only episodic for all concentrations, whereas as expected a significant lower rate of inflated swim bladder was observed at the highest concentration group (4 mg L^{-1}, Kruskal-Wallis, $p < 0.05$, Supplementary Figure 2).

3.2. Analysis of BPA-induced morphological changes

Total embryo length showed a 2–4% reduction at the highest concentration tested that did not presented gross malformations (8 mg L^{-1}) together with a 10–15% reduction of eye width (Fig. 1), indicating a mild effect on general embryo development. The most relevant macroscopic effect at this concentration range was the presence of yolk sac remains at 5 dpf, a period at which its resorption by the developing embryo should be essentially complete in normal conditions (Fig. 1A and B). The effect was significant

at BPA concentrations above 2 mg L^{-1} following a linear dose-response effect (Fig. 1A and B).

3.3. Determination and classification of DEGs

The ANOVA-PLS analysis identified 2539 genes differentially expressed in at least one of the experimental subsets (Control, 0.1 mg L^{-1}, 1 mg L^{-1}, or 4 mg L^{-1}) relative to the rest. Hierarchical clustering showed that the expression profiles of the selected DEGs closely reflected the experimental setup, as the different biological replicates for all treatment groups fell into the same hierarchical cluster, except for the 1 mg L^{-1} class, which appeared divided into two subclusters (Fig. 2, note that the 0 value -white- corresponds to the averaged control levels). PAM clustering defined three groups of genes, A, B, and C, including 960, 1132 and 447 genes, respectively, corresponding to three different expression patterns among treatment groups (Fig. 3). Cluster A corresponds to genes whose mRNA levels steadily decreased as the BPA concentration increased, whereas transcripts included in Cluster B showed the opposite behavior. Conversely to the monotonic responses shown in Clusters A and B, genes in Cluster C display a bimodal response, with a maximum in untreated controls, a minimum value at the two middle concentrations, and an intermediate value at 4 mg L^{-1} (Fig. 3). Supplementary Figure 3 shows a very strong correlation between RNA-seq values and Real Time qRT-PCR estimation of mRNA levels for several selected genes ($r^2 = 0.68$, $p \leq 10^{-4}$).

3.4. DEGs functional characterization

DAVID functional analysis was carried out by both all DEGs together and for each of the three PAM clusters defined in Fig. 3. Functional modules, either from the GO datasets or from the KEGG dataset with false discovery ratio (FDR) $\leq$ 5% were selected for further study. Fig. 4A shows a network representation of modules from both GO:Biological Function and KEGG datasets in which transcripts (dots) are labeled by the cluster they belong; a quantitative representation of the same network is shown in Fig. 4B. The results show different functional categories particularly enriched in Cluster B (genes upregulated by BPA), which included liver development; lipid transport; lysosome and protein glycosylation; cytochrome P450-mediated metabolism; and different metabolic pathways for lipids, glutathione, retinol, and steroid hormones. Clusters A and C shared most of their principal functional categories, although protein ubiquitination and glycolysis/gluconeogenesis pathways' genes were overrepresented in Cluster A, and Cluster C included a large subset of genes related to visual perception (Fig. 4, note the colored areas in Fig. 4A). Fig. 5 shows graphic representations of relative mRNA levels of the genes included in some of these functional modules; the actual output of the DAVID analysis is shown in Supplementary Table 2.

3.5. Analysis of putative modes of action of BPA

Comparison between the observed BPA-induced transcriptomic changes with published results of zebrafish eleutheroembryos treated with *all-trans* Retinoic Acid (*at*RA), *9-cis* Retinoic Acid (9*c*RA) (Navarro-Martín et al., 2018), or 17-β-estradiol (E2) (Hao et al., 2013) revealed similar effects on several functional clusters (Fig. 5, three bottom lanes). For example, the BPA-induced general up-regulation of genes codifying for the enzymes of the retinol and glutathione metabolic pathways (dre00830 and dre00480, Fig. 5) was also observed in retinoic acid-treated eleutheroembryos. On the other hand, BPA induced changes in genes typically associated to the estrogenic response, like steroid hormone biosynthesis genes (dre00140), including *cyp19a1b*, the brain aromatase (Fig. 5) (Kishida et al., 2001; Mouriec et al., 2009; Petersen et al., 2013; Puy-Azurmendi et al., 2014). The similarity between BPA- and E2-induced changes extends to at least another functional category,

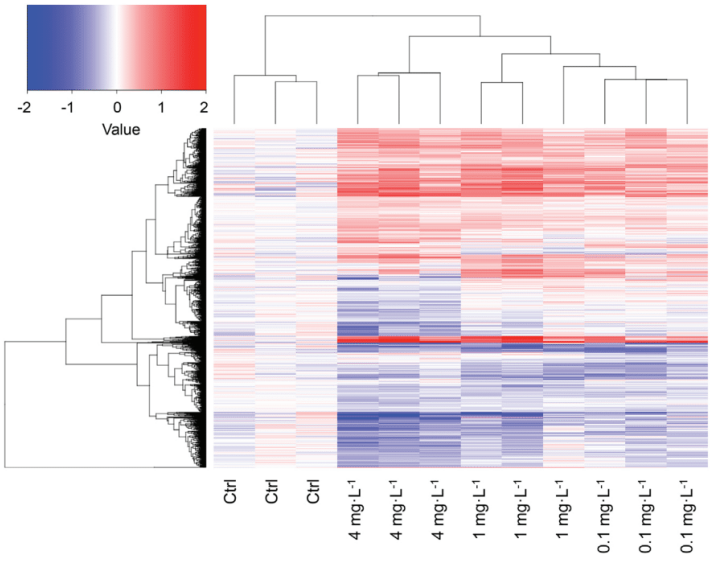

Fig. 2. Heatmap corresponding to 2539 genes identified by ANOVA-PLS as differentially expressed in at least one of the experimental subsets (Control, 0.1 mg L^{-1}, 1 mg L^{-1}, or 4 mg L^{-1}, color bars at the bottom of the map) relative to the rest, hereafter referred to as DEGs, differentially expressed genes. Values were centered to the average of Control samples and then log2 transformed. Color scale ranges from blue (strongly underrepresented relative to controls) to red (strongly overrepresented); white cells correspond to control values. Both rows (genes) and columns (samples) were grouped by hierarchical clustering; the corresponding dendrograms are shown at the left and the top of the panel, respectively. (For interpretation of the references to color in this figure legend, the reader is referred to the Web version of this article.)

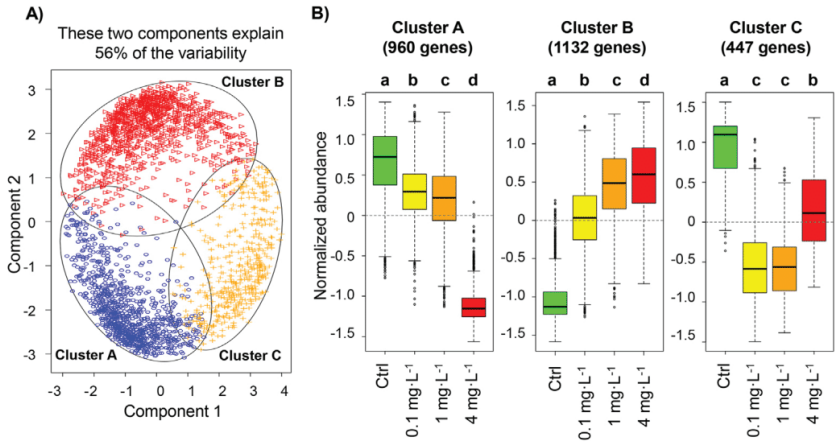

Fig. 3. Results from PAM clustering of DEGs. **A)** PCA analysis showing the three defined clusters labeled in blue, red and yellow (Clusters A, B and C, respectively), as identified by the PAM function in R. The two displayed components explain 56% of total point variability. **B)** Distribution of normalized abundance values for genes included in each of the three clusters. Low-case letters at the top of each graph indicate statistically different distributions (ANOVA + Tukey's B ($p \leq 0.05$) post-hoc test (all possible pairwise comparisons) was used to determine differences between groups). Thick bars indicate average values, boxes include values between the 1st and 3rd quartiles, whiskers cover the total distribution, except for outliers (circles). (For interpretation of the references to color in this figure legend, the reader is referred to the Web version of this article.)

lipid transport (GO:0006869), as three lipid-transport protein genes (*apoa1a, apobb.1, and apoa4a*) showed increased levels of mRNA upon exposure to both BPA and E2 (Fig. 5). Similar correlations could be also seen, although in a less convincing extend, for the Glucolysis/gluconeogenesis pathway (dre00010). In contrast, the general decrease of visual-perception genes (GO:0007601) was not observed in E2-treated eleutheroembryos, but the same functional cluster showed a general upregulation in both *at*RA and 9*c*RA treatments (Fig. 5).

4. Discussion

Transcriptome analyses create large datasets that are multivariate in nature, as each gene can be considered as a variable that can be explored to elucidate its relationship with physiological outcomes or with the experimental conditions. These analyses require multivariate analytical tools that reflect the experimental setup, which may vary notably from one experiment to another, depending on the experimental factors that have to be introduced in the model. In our case, we devised a dose-response experiment and decided to analyze both monotonic and non-monotonic responses, as both types of responses have been reported for many endocrine disruptors, including BPA. For this reason, we chose the supervised ANOVA-PLS method (Fresno et al., 2014) as a multivariate analysis that incorporates the existence of different levels of exposure to BPA, but without requiring any assumption on the behavior of the different genes among these experimental subsets. By combining this analysis with the robust, non-supervised PAM clustering, we defined three patterns of expression, two of them reflecting a quasi-linear, monotonic dose-response to BPA, and a third one with a bi-phasic profile. The functional analysis of the genes included in these three clusters revealed that they participate in different biological functions, and that they may reflect the interaction of BPA with different regulatory signals (Murata and Kang, 2018). We observed a strong effect in many metabolic pathways, as shown in Supplementary Figure 4. Note that essentially all enzymes involved in testosterone metabolism to estradiol and other steroid hormones became overexpressed upon BPA treatment (Supp. Figure 4A), and so were most of the genes involved in the retinol metabolism (Supp. Figure 4B). Those results are coincident with the effects shown by BPA in zebrafish and other animal models (Lam et al., 2011; Lindholst et al., 2000; Morales et al., 2018; Ortiz-Villanueva et al., 2017b; Shmarakov et al., 2017). For the carbon metabolism module (Suppl. Figure 4C), there is a clear division between the genes codifying glycolytic enzymes (central pathway), which became downregulated, and those from the pentose-phosphate or the C-1 metabolic pathways, which became mostly upregulated (Suppl. Figure 4C).

Most current legal limitations for BPA use in food and baby items are rooted in its alleged estrogenic potency, for which there is abundant information, at least from *in vitro* or *in culture* experiments (Chapin et al., 2008; Vandenberg et al., 2009). This is consistent with the alteration of several estrogen-related genes in BPA-treated samples, including the activation of the brain aromatase, one of the best-known E2-regulated genes in fish embryos, and considered as a specific biomarker of exposure to estrogens (Kishida et al., 2001; Mouriec et al., 2009; Petersen et al., 2013; Puy-Azurmendi et al., 2014). However, most whole-animal toxicological data, either from fish or from mammals, suggest a pleiotropic mode of action that cannot be directly related to BPA estrogenicity (Le Corre et al., 2015; Murata and Kang, 2018; Nishizawa et al., 2003; Wetherill et al., 2007; Zoeller et al., 2005). BPA has profound effects in zebrafish metabolome, affecting lipid, retinol and sugar metabolism (Ortiz-Villanueva et al., 2017a). Our data are consistent with the well-known interaction of BPA with the estrogen receptor, but it also suggests that at least part of the effects observed in BPA treated zebrafish embryo can be explained by the simultaneous activation of other receptors. For example, cytochrome *cyp26* genes become upregulated upon exposure to retinoids (Navarro-Martín et al., 2018), and its activation by BPA strongly suggest an interaction with the retinoic acid and/or the 9-*cis* retinoic acid receptors (RAR, RXR) (Acconcia et al., 2015; Navarro-Martín et al., 2018). The simultaneous activation of both receptors may explain the general upregulation of genes codifying enzymes involved in steroid hormone biosynthesis, glutathione metabolism, or lipid transport, as several of them appear to respond to the presence of one or both effectors. However, some of the observed responses to BPA appear to be unrelated to either estrogen or retinoid pathways, like the

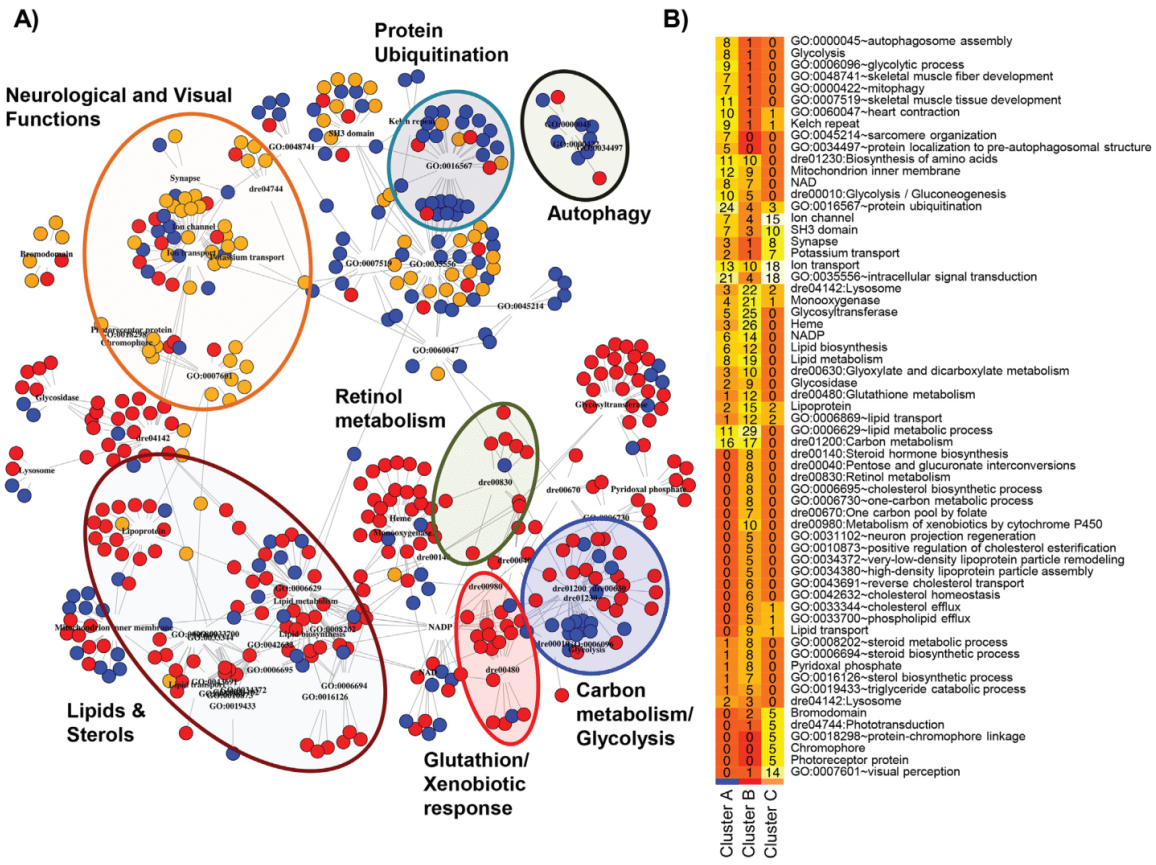

Fig. 4. Functional analyses of DEGs, distributed in clusters as shown in Fig. 3. **A)** Network representation of DEGs according to their adscription to functional modules (GO:biological process and KEGG databases, codes for each module are given as nodes). DEGs are represented by dots, colored by clusters as in Fig. 3. Color areas indicate groups of functional modules considered of particular relevance (see the text). **B)** Distribution of DEGs among the different functional modules (rows) and clusters (columns). Only modules with at least 5 hits in one of the clusters are represented; redundant modules were simplified to the one with the highest number of hits. Numbers indicate the absolute number of DEGs for each module and clusters, colors (heat code, from red -few- to white -most-) represent the relative importance of metabolites associated to each pathway for each cluster; two squares of the same shade of color correspond to identical fraction of DEGs for each cluster. (For interpretation of the references to color in this figure legend, the reader is referred to the Web version of this article.)

simultaneous increase of C1 metabolism and pentose phosphate pathway (PPP) genes, and the decrease of the glycolytic pathway. These effects may be related to reported BPA-mediated alterations in glucose and lipid homeostasis in mammals, putatively linked to estrogenic effects (Le Corre et al., 2015).

The decrease on different genes related to visual perception can be regarded as the transcriptional counterpart of the observed reduction in eye size. Effects on visual functions have been reported in zebrafish embryos linked to both BPA and bisphenol S, although the underlying mechanism of action is still to be determined (Kinch et al., 2016; Liu et al., 2018; Pelayo et al., 2012). Microphthalmia also was observed in zebrafish eleutheroembryos treated with the thyroid hormone T3, which altered expression of opsin genes (Pelayo et al., 2012), a similar effect, but not identical, to the one observed here. BPA can act as a weak T3 agonist and as potentiator of T3 action, although the very low levels of thyroid function at these specific embryonic stages probably reduce the contribution of this pathway to the observed effects of BPA (Pelayo et al., 2012). It is more likely that the microphthalmia is due to alterations on the retinoid pathway, a key function in early eye development. The bimodal response to visual perception genes to BPA probably indicates a rather complex toxic interaction, as very low doses of BPA reduced significantly their mRNA levels, an effect that became partially reverted by exposure to the highest tested concentration, which showed a strong inhibitory effect in many metabolic and energy-related transcripts. Exposure to BPA has been related with changes in larvae behavior in light-dark tests (Saili et al., 2012) and with alterations in the ability to discriminate color in adult zebrafish (Li et al., 2017). For that reason, we think that further studies are needed to elucidate if the BPA effects observed in the present study on eye width could be related to vision impairments and in consequence produce alterations in larvae behavioral responses.

Yolk sac resorption appears as a sensitive macroscopic endpoint for embryonic toxicity in zebrafish. Persistence of yolk sac remains beyond 5 dpf has been linked to metabolic alterations in lipid use and energy metabolism in zebrafish (Raldúa et al., 2008; Sant and Timme-Laragy, 2018). Our data suggest that BPA alters both lipid and energy metabolism, by increasing expression of lipid transport-related genes while reducing the expression of the glycolytic pathway. While this suggests a shift from sugar utilization to lipid

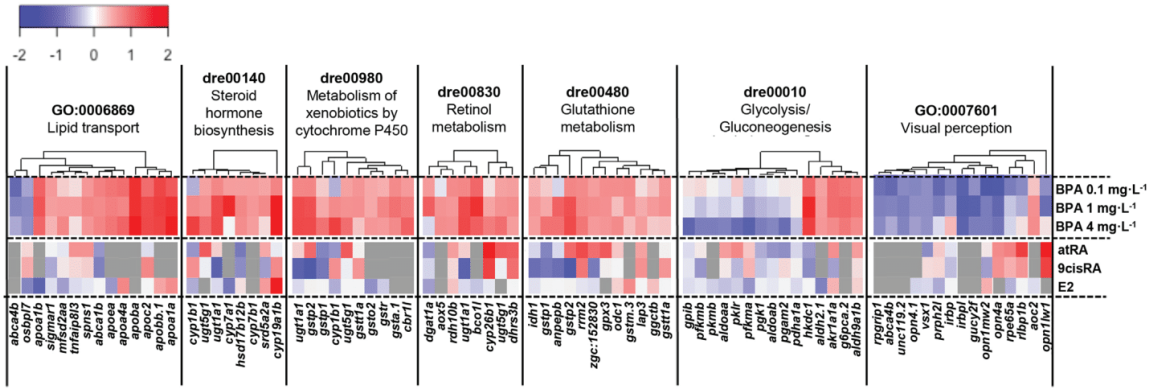

Fig. 5. Graphic representation of mRNA abundance changes of DEGs associated to relevant functional modules, as defined in Fig. 4. The three upper rows of each heatmap correspond to relative values for samples treated with 0.1, 1, and 4 mg L^{-1} BPA (averages of the three biological replicates), respectively. Color scale from blue (underexpression) to red (overexpression) as in Fig. 2; note that white represents control values. The three lower rows correspond to microarray data of zebrafish eleutheroembryos treated with either *all-trans* retinoic, *9-cis* retinoic acid [45] or 17-β-estradiol [46]. Color scale is the same as for BPA-treated samples, although in this case, additional grey sectors correspond to genes not present or not quantified in the corresponding microarray. (For interpretation of the references to color in this figure legend, the reader is referred to the Web version of this article.)

degradation, it is unclear which biological mechanism lies behind this effect. Recent reports indicate that a potential candidate is the PPAR/RXR system (Peroxisome Proliferator-Activated Receptor), especially considering the implication of this complex in the regulation of multiple metabolic pathways, and particularly of those related to sugar and lipid metabolism (Huang and Chen, 2017; Lempradl et al., 2015). It is presently unclear whether or not BPA directly interacts with any of the known PPARs, or whether at least part of the effect may be mediated through the co-activator RXR, the 9-*cis* retinoic acid receptor. RXR interacts with many other cellular receptors, and this will at least partially explain the pleiotropic effects of exposure to BPA. For example, this mechanism was suggested to explain the BPA interaction with thyroid hormone regulation, also in zebrafish (Pelayo et al., 2012). In addition, the observed changes produced by BPA in the pattern of energy utilization in zebrafish are reminiscent to the observed accumulation of storage lipids into lipid droplets in the crustacean *D. magna*. As no convincing homolog for PPARs have been found in Crustaceans yet, this effect has been attributed to the putative interaction with RXR and other receptors (Jordão et al., 2016a). Finally, the presence of yolk sac remains at 5 dpf may also be a side effect of the estrogenic activity. E2-treated embryos show at least some of the transcriptomic effects of BPA linked to lipid metabolism (Fig. 5), and they also show similar macroscopic effects when exposed to high concentrations of E2 (unpublished results). Finally, recent studies using molecular pathway analysis tools suggest multiple effects of BPA on cell signaling, including Fox and MapK pathways in mammals (Murata and Kang, 2018), which could be related to the observed effects on liver, and perhaps also eye, development.

5. Conclusion

The dose-response setup of our data allows drawing some conclusions about the cause-effect relationship between transcriptomic and morphological responses. While several of the observed changes in transcript abundances can be functionally related to the persistence of yolk sac remains and the shrinkage of eyes, they appeared at exposure levels 5–10 fold lower than the observed LOEC for these specific macroscopic alterations (Figs. 1 and 5). In addition, significant changes on embryo length that could be attributed to a general systemic disruption, only occurred at the highest range of BPA concentrations used in this work (4 mg L^{-1} and higher). We therefore consider that the transcriptomic changes are directly related with the primary action of BPA (e.g. receptor interaction or enzyme inhibition) rather than a consequence of the alteration of the embryo development (e.g. changes in tissue formation and composition). We have described transcriptomic alterations reflecting the molecular events implicated in BPA toxicity, which most likely transcend its well-known, but rather weak estrogenic activity. The present study contributes understanding of the environmental and human health hazards associated to the ubiquitous presence of BPA in the environment.

Conflicts of interest

The authors declare that they have no conflicts of interest.

Acknowledgments

This work was supported by the European Research Council under the European Union's Seventh Framework Programme (FP/2007–2013)/ERC Grant Agreement n. 320737. Some part of this study was also supported by a grant from the Spanish Ministry of Economy and Competitiveness (CTQ2014-56777-R) and by a grant (PT17/0009/0019) from ISCIII (Carlos III Health Institute), part of the Spanish Ministry of Economy and Competitiveness, and cofinanced by the European Regional Development Fund (ERDF). LNM was supported by a Beatriu de Pinos Postdoctoral Fellow (2013BP-B-00088) awarded by the Secretary for Universities and Research of the Ministry of Economy and Knowledge of the Government of Catalonia and the Cofund programme of the Marie Curie Actions of the 7th R&D Framework Programme of the European Union. RM was supported by a FPU predoctoral fellow from the Spanish Ministry of Education, Culture and Sport (ref. FPU15/03332). We would like to thank Ms. Elia Martinez-Prats and David Angelats for helping with the real time qRT-PCRs measurements.

Appendix A. Supplementary data

Supplementary data related to this article can be found at https://doi.org/10.1016/j.envpol.2018.09.043.

References

Acconcia, F., Pallottini, V., Marino, M., 2015. Molecular mechanisms of action of BPA. Dose. Response. 13 https://doi.org/10.1177/1559325815610582, 1559325815610582.

Alonso-Magdalena, P., Vieira, E., Soriano, S., Menes, L., Burks, D., Quesada, I., Nadal, A., 2010. Bisphenol A exposure during pregnancy disrupts glucose homeostasis in mothers and adult male offspring. Environ. Health Perspect. 118, 1243–1250. https://doi.org/10.1289/ehp.1001993.

Arase, S., Ishii, K., Igarashi, K., Aisaki, K., Yoshio, Y., Matsushima, A., Shimohigashi, Y., Arima, K., Kanno, J., Sugimura, Y., 2011. Endocrine disrupter bisphenol A increases in situ estrogen production in the mouse urogenital sinus. Biol. Reprod. 84, 734–742. https://doi.org/10.1095/biolreprod.110.087502.

Baker, M.E., Hardiman, G., 2014. Transcriptional analysis of endocrine disruption using zebrafish and massively parallel sequencing. J. Mol. Endocrinol. 52, R241–R256. https://doi.org/10.1530/JME-13-0219.

Caballero-Gallardo, K., Olivero-Verbel, J., Freeman, J.L., 2016. Toxicogenomics to evaluate endocrine disrupting effects of environmental chemicals using the zebrafish model. Curr. Genom. 17, 515–527. https://doi.org/10.2174/1389202917666160513105959.

Cabaton, N.J., Wadia, P.R., Rubin, B.S., Zalko, D., Schaeberle, C.M., Askenase, M.H., Gadbois, J.L., Tharp, A.P., Whitt, G.S., Sonnenschein, C., Soto, A.M., 2011. Perinatal exposure to environmentally relevant levels of bisphenol A decreases fertility and fecundity in CD-1 mice. Environ. Health Perspect. 119, 547–552. https://doi.org/10.1289/ehp.1002559.

Canesi, L., Fabbri, E., 2015. Environmental effects of BPA: focus on aquatic species. Dose. Response. 13 https://doi.org/10.1177/1559325815598304, 1559325815598304.

Careghini, A., Mastorgio, A.F., Saponaro, S., Sezenna, E., 2015. Bisphenol A, nonylphenols, benzophenones, and benzotriazoles in soils, groundwater, surface water, sediments, and food: a review. Environ. Sci. Pollut. Res. 22, 5711–5741. https://doi.org/10.1007/s11356-014-3974-5.

Chapin, R.E., Adams, J., Boekelheide, K., Gray, L.E., Hayward, S.W., Lees, P.S.J., McIntyre, B.S., Portier, K.M., Schnorr, T.M., Selevan, S.G., Vandenbergh, J.G., Woskie, S.R., 2008. NTP-CERHR expert panel report on the reproductive and developmental toxicity of bisphenol A. Birth Defects Res. Part B Dev. Reproductive Toxicol. 83, 157–395. https://doi.org/10.1002/bdrb.20147.

Chen, J., Saili, K.S., Liu, Y., Li, L., Zhao, Y., Jia, Y., Bai, C., Tanguay, R.L., Dong, Q., Huang, C., 2017. Developmental bisphenol A exposure impairs sperm function and reproduction in zebrafish. Chemosphere 169, 262–270. https://doi.org/10.1016/j.chemosphere.2016.11.089.

Chen, M., Zhang, J., Pang, S., Wang, C., Wang, L., Sun, Y., Song, M., Liang, Y., 2018. Evaluating estrogenic and anti-estrogenic effect of endocrine disrupting chemicals (EDCs) by zebrafish (Danio rerio) embryo-based vitellogenin 1 (vtg1) mRNA expression. Comp. Biochem. Physiol. C Toxicol. Pharmacol. 204, 45–50. https://doi.org/10.1016/j.cbpc.2017.11.010.

Churko, J.M., Mantalas, G.L., Snyder, M.P., Wu, J.C., 2013. Overview of high throughput sequencing technologies to elucidate molecular pathways in cardiovascular diseases. Circ. Res. 112, 1613–1623. https://doi.org/10.1161/CIRCRESAHA.113.300939.

Corrales, J., Kristofco, L.A., Steele, W.B., Yates, B.S., Breed, C.S., Williams, E.S., Brooks, B.W., 2015. Global assessment of bisphenol A in the environment: review and analysis of its occurrence and bioaccumulation. Dose. Response 13. https://doi.org/10.1177/1559325815598308, 1559325815598308.

Crain, D.A., Eriksen, M., Iguchi, T., Jobling, S., Laufer, H., LeBlanc, G.A., Guillette, L.J., 2007. An ecological assessment of bisphenol-A: evidence from comparative biology. Reprod. Toxicol. 24, 225–239. https://doi.org/10.1016/j.reprotox.2007.05.008.

Dobin, A., Davis, C.A., Schlesinger, F., Drenkow, J., Zaleski, C., Jha, S., Batut, P., Chaisson, M., Gingeras, T.R., 2013. STAR: ultrafast universal RNA-seq aligner. Bioinformatics 29, 15–21. https://doi.org/10.1093/bioinformatics/bts635.

Edgar, R., Domrachev, M., Lash, A.E., 2002. Gene Expression Omnibus: NCBI gene expression and hybridization array data repository. Nucleic Acids Res. 30, 207–210. https://doi.org/10.1093/nar/30.1.207.

EFSA, 2016. Overview of existing methodologies for the estimation of non-dietary exposure to chemicals from the use of consumer products and via the environment. EFSA J 14, e04525. https://doi.org/10.2903/j.efsa.2016.4525.

Ekman, D.R., Hartig, P.C., Cardon, M., Skelton, D.M., Teng, Q., Durhan, E.J., Jensen, K.M., Kahl, M.D., Villeneuve, D.L., Gray, L.E., Collette, T.W., Ankley, G.T., 2012. Metabolite profiling and a transcriptional activation assay provide direct evidence of androgen receptor antagonism by bisphenol A in fish. Environ. Sci. Technol. 46, 9673–9680. https://doi.org/10.1021/es3014634.

Flint, S., Markle, T., Thompson, S., Wallace, E., 2012. Bisphenol A exposure, effects, and policy: a wildlife perspective. J. Environ. Manag. 104, 19–34. https://doi.org/10.1016/j.jenvman.2012.03.021.

Fresno, C., Balzarini, M.G., Fernández, E.A., 2014. lmdme : linear models on designed multivariate experiments in R. J. Stat. Software 56. https://doi.org/10.18637/jss.v056.i07.

Hao, R., Bondesson, M., Singh, A.V., Riu, A., McCollum, C.W., Knudsen, T.B., Gorelick, D.A., Gustafsson, J.-Å., 2013. Identification of estrogen target genes during zebrafish embryonic development through transcriptomic analysis. PLoS One 8, e79020. https://doi.org/10.1371/journal.pone.0079020.

Huang, Q., Chen, Q., 2017. Mediating roles of PPARs in the effects of environmental chemicals on sex steroids. PPAR Res. 2017, 1–8. https://doi.org/10.1155/2017/3203161.

Huang, Y.Q., Wong, C.K.C., Zheng, J.S., Bouwman, H., Barra, R., Wahlström, B., Neretin, L., Wong, M.H., 2012. Bisphenol A (BPA) in China: a review of sources, environmental levels, and potential human health impacts. Environ. Int. 42, 91–99. https://doi.org/10.1016/j.envint.2011.04.010.

Jordão, R., Campos, B., Piña, B., Tauler, R., Soares, A.M.V.M., Barata, C., 2016a. Mechanisms of action of compounds that enhance storage lipid accumulation in Daphnia magna. Environ. Sci. Technol. 50, 13565–13573. https://doi.org/10.1021/acs.est.6b04768.

Jordão, R., Garreta, E., Campos, B., Lemos, M.F.L., Soares, A.M.V.M., Tauler, R., Barata, C., 2016b. Compounds altering fat storage in Daphnia magna. Sci. Total Environ. 545–546, 127–136. https://doi.org/10.1016/j.scitotenv.2015.12.097.

Kang, J.-H., Asai, D., Aasi, D., Katayama, Y., 2007. Bisphenol A in the aquatic environment and its endocrine-disruptive effects on aquatic organisms. Crit. Rev. Toxicol. 37, 607–625. https://doi.org/10.1080/10408440701493103.

Kang, J.-H., Kondo, F., Katayama, Y., 2006. Human exposure to bisphenol A. Toxicology 226, 79–89. https://doi.org/10.1016/j.tox.2006.06.009.

Kimmel, C.B., Ballard, W.W., Kimmel, S.R., Ullmann, B., Schilling, T.F., 1995. Stages of embryonic development of the zebrafish. Dev. Dynam. 203, 253–310. https://doi.org/10.1002/aja.1002030302.

Kinch, C.D., Kurrasch, D.M., Habibi, H.R., 2016. Adverse morphological development in embryonic zebrafish exposed to environmental concentrations of contaminants individually and in mixture. Aquat. Toxicol. 175, 286–298. https://doi.org/10.1016/j.aquatox.2016.03.021.

Kishida, M., McLellan, M., Miranda, J.A., Callard, G.V., 2001. Estrogen and xenoestrogens upregulate the brain aromatase isoform (P450aromB) and perturb markers of early development in zebrafish (Danio rerio). Comp. Biochem. Physiol. B Biochem. Mol. Biol. 129, 261–268. https://doi.org/10.1016/S1096-4959(01)00319-0.

Kolpin, D.W., Furlong, E.T., Meyer, M.T., Thurman, E.M., Zaugg, S.D., Barber, L.B., Buxton, H.T., 2002. Pharmaceuticals, hormones, and other organic wastewater contaminants in U.S. streams, 1999-2000: a national reconnaissance. Environ. Sci. Technol. 36, 1202–1211. https://doi.org/10.1021/es011055j.

Lam, S.H., Hlaing, M.M., Zhang, X., Yan, C., Duan, Z., Zhu, L., Ung, C.Y., Mathavan, S., Ong, C.N., Gong, Z., 2011. Toxicogenomic and phenotypic analyses of bisphenol-a early-life exposure toxicity in zebrafish. PLoS One 6. https://doi.org/10.1371/journal.pone.0028273.

Le, H.H., Carlson, E.M., Chua, J.P., Belcher, S.M., 2008. Bisphenol A is released from polycarbonate drinking bottles and mimics the neurotoxic actions of estrogen in developing cerebellar neurons. Toxicol. Lett. 176, 149–156. https://doi.org/10.1016/j.toxlet.2007.11.001.

Le Corre, L., Besnard, P., Chagnon, M.-C., 2015. BPA, an energy balance disruptor. Crit. Rev. Food Sci. Nutr. 55, 769–777. https://doi.org/10.1080/10408398.2012.678421.

Lee, H.J., Chattopadhyay, S., Gong, E.-Y., Ahn, R.S., Lee, K., 2003. Antiandrogenic effects of bisphenol A and nonylphenol on the function of androgen receptor. Toxicol. Sci. 75, 40–46. https://doi.org/10.1093/toxsci/kfg150.

Lejonklou, M.H., Dunder, L., Bladin, E., Pettersson, V., Rönn, M., Lind, L., Waldén, T.B., Lind, P.M., 2017. Effects of low-dose developmental bisphenol A exposure on metabolic parameters and gene expression in male and female Fischer 344 rat offspring. Environ. Health Perspect. 125, 67018. https://doi.org/10.1289/EHP505.

Lempradl, A., Pospisilik, J.A., Penninger, J.M., 2015. Exploring the emerging complexity in transcriptional regulation of energy homeostasis. Nat. Rev. Genet. 16, 665–681. https://doi.org/10.1038/nrg3941.

Li, B., Dewey, C.N., 2011. RSEM: accurate transcript quantification from RNA-Seq data with or without a reference genome. BMC Bioinf. 12, 323. https://doi.org/10.1186/1471-2105-12-323.

Li, X., Sun, M.-Z., Li, X., Zhang, S.-H., Dai, L.-T., Liu, X.-Y., Zhao, X., Chen, D.-Y., Feng, X.-Z., 2017. Impact of low-dose chronic exposure to Bisphenol A (BPA) on adult male zebrafish adaption to the environmental complexity: disturbing the color preference patterns and reliving the anxiety behavior. Chemosphere 186, 295–304. https://doi.org/10.1016/j.chemosphere.2017.07.164.

Lindholst, C., Pedersen, K.L., Pedersen, S.N., 2000. Estrogenic response of bisphenol A in rainbow trout (Oncorhynchus mykiss). Aquat. Toxicol. 48, 87–94. https://doi.org/10.1016/S0166-445X(99)00051-X.

Liu, W., Zhang, X., Wei, P., Tian, H., Wang, W., Ru, S., 2018. Long-term exposure to bisphenol S damages the visual system and reduces the tracking capability of male zebrafish (Danio rerio). J. Appl. Toxicol. 38, 248–258. https://doi.org/10.1002/jat.3519.

Love, M.I., Huber, W., Anders, S., 2014. Moderated estimation of fold change and dispersion for RNA-seq data with DESeq2. Genome Biol. 15, 550. https://doi.org/10.1186/s13059-014-0550-8.

Morales, M., Martínez-Paz, P., Sánchez-Argüello, P., Morcillo, G., Martínez-Guitarte, J.L., 2018. Bisphenol A (BPA) modulates the expression of endocrine and stress response genes in the freshwater snail Physa acuta. Ecotoxicol. Environ. Saf. 152, 132–138. https://doi.org/10.1016/j.ecoenv.2018.01.034.

Mortazavi, A., Williams, B.A., McCue, K., Schaeffer, L., Wold, B., 2008. Mapping and quantifying mammalian transcriptomes by RNA-Seq. Nat. Methods 5, 621–628. https://doi.org/10.1038/nmeth.1226.

Mouriec, K., Lareyre, J.J., Tong, S.K., Le Page, Y., Vaillant, C., Pellegrini, E., Pakdel, F., Chung, B.C., Kah, O., Anglade, I., 2009. Early regulation of brain aromatase (cyp19a1b) by estrogen receptors during zebrafish development. Dev. Dynam. 238, 2641–2651. https://doi.org/10.1002/dvdy.22069.

Murata, M., Kang, J.-H., 2018. Bisphenol A (BPA) and cell signaling pathways. Biotechnol. Adv. 36, 311–327. https://doi.org/10.1016/j.biotechadv.2017.12.002.

Mushtaq, M.Y., Verpoorte, R., Kim, H.K., 2013. Zebrafish as a model for systems biology. Biotechnol. Genet. Eng. Rev. 29, 187–205. https://doi.org/10.1080/02648725.2013.801238.

Nagato, E.G., D'eon, J.C., Lankadurai, B.P., Poirier, D.G., Reiner, E.J., Simpson, A.J., Simpson, M.J., 2013. (1)H NMR-based metabolomics investigation of Daphnia magna responses to sub-lethal exposure to arsenic, copper and lithium. Chemosphere 93, 331–337. https://doi.org/10.1016/j.chemosphere.2013.04.085.

Navarro-Martín, L., Oliveira, E., Casado, M., Barata, C., Piña, B., 2018. Dysregulatory effects of retinoic acid isomers in late zebrafish embryos. Environ. Sci. Pollut. Res. 25, 3849–3859. https://doi.org/10.1007/s11356-017-0732-5.

Nishizawa, H., Manabe, N., Morita, M., Sugimoto, M., Imanishi, S., Miyamoto, H., 2003. Effects of in utero exposure to bisphenol A on expression of RARalpha and RXRalpha mRNAs in murine embryos. J. Reprod. Dev. 49, 539–545.

Ortiz-Villanueva, E., Benavente, F., Piña, B., Sanz-Nebot, V., Tauler, R., Jaumot, J., 2017a. Knowledge integration strategies for untargeted metabolomics based on MCR-ALS analysis of CE-MS and LC-MS data. Anal. Chim. Acta 978, 10–23. https://doi.org/10.1016/j.aca.2017.04.049.

Ortiz-Villanueva, E., Navarro-Martín, L., Jaumot, J., Benavente, F., Sanz-Nebot, V., Piña, B., Tauler, R., 2017b. Metabolic disruption of zebrafish (Danio rerio) embryos by bisphenol A. An integrated metabolomic and transcriptomic approach. Environ. Pollut. 231, 22–36. https://doi.org/10.1016/j.envpol.2017.07.095.

Pelayo, S., Oliveira, E., Thienpont, B., Babin, P.J., Raldúa, D., André, M., Piña, B., 2012. Triiodothyronine-induced changes in the zebrafish transcriptome during the eleutheroembryonic stage: implications for bisphenol A developmental toxicity. Aquat. Toxicol. 110–111, 114–122. https://doi.org/10.1016/j.aquatox.2011.12.016.

Petersen, K., Fetter, E., Kah, O., Brion, F., Scholz, S., Tollefsen, K.E., 2013. Transgenic (cyp19a1b-GFP) zebrafish embryos as a tool for assessing combined effects of oestrogenic chemicals. Aquat. Toxicol. 138–139, 88–97. https://doi.org/10.1016/j.aquatox.2013.05.001.

Puy-Azurmendi, E., Olivares, A., Vallejo, A., Ortiz-Zarragoitia, M., Piña, B., Zuloaga, O., Cajaraville, M.P., 2014. Estrogenic effects of nonylphenol and octylphenol isomers in vitro by recombinant yeast assay (RYA) and in vivo with early life stages of zebrafish. Sci. Total Environ. 466–467, 1–10. https://doi.org/10.1016/j.scitotenv.2013.06.060.

R Development Core Team, 2008. R: a Language and Environment for Statistical Computing. R Foundation for Statistical Computing, 2008.

Raldúa, D., André, M., Babin, P.J., 2008. Clofibrate and gemfibrozil induce an embryonic malabsorption syndrome in zebrafish. Toxicol. Appl. Pharmacol. 228, 301–314. https://doi.org/10.1016/j.taap.2007.11.016.

Raldúa, D., Piña, B., 2014. In vivo zebrafish assays for analyzing drug toxicity. Expet Opin. Drug Metabol. Toxicol. 10, 685–697. https://doi.org/10.1517/17425255.2014.896339.

Rankouhi, T.R., van Holsteijn, I., Letcher, R., Giesy, J.P., van Den Berg, M., 2002. Effects of primary exposure to environmental and natural estrogens on vitellogenin production in carp (Cyprinus carpio) hepatocytes. Toxicol. Sci. 67, 75–80. https://doi.org/10.1093/toxsci/67.1.75.

Renaud, L., Silveira, W.A. da, Hazard, E.S., Simpson, J., Falcinelli, S., Chung, D., Carnevali, O., Hardiman, G., 2017. The plasticizer bisphenol A perturbs the hepatic epigenome: a systems level analysis of the miRNome. Genes 8, 269. https://doi.org/10.3390/genes8100269.

Reuter, J.A., Spacek, D.V., Snyder, M.P., 2015. High-throughput sequencing technologies. Mol. Cell. https://doi.org/10.1016/j.molcel.2015.05.004.

Richter, C.A., Birnbaum, L.S., Farabollini, F., Newbold, R.R., Rubin, B.S., Talsness, C.E., Vandenbergh, J.G., Walser-Kuntz, D.R., vom Saal, F.S., 2007a. In vivo effects of bisphenol A in laboratory rodent studies. Reprod. Toxicol. 24, 199–224. https://doi.org/10.1016/j.reprotox.2007.06.004.

Richter, C.A., Taylor, J.A., Ruhlen, R.L., Welshons, W.V., Vom Saal, F.S., 2007b. Estradiol and Bisphenol A stimulate androgen receptor and estrogen receptor gene expression in fetal mouse prostate mesenchyme cells. Environ. Health Perspect. 115, 902–908. https://doi.org/10.1289/ehp.9804.

Rubin, B.S., Soto, A.M., 2009. Bisphenol A: perinatal exposure and body weight. Mol. Cell. Endocrinol. 304, 55–62. https://doi.org/10.1016/j.mce.2009.02.023.

Ryan, K.K., Haller, A.M., Sorrell, J.E., Woods, S.C., Jandacek, R.J., Seeley, R.J., 2010. Perinatal exposure to bisphenol-a and the development of metabolic syndrome in CD-1 mice. Endocrinology 151, 2603–2612. https://doi.org/10.1210/en.2009-1218.

Saili, K.S., Corvi, M.M., Weber, D.N., Patel, A.U., Das, S.R., Przybyla, J., Anderson, K.A., Tanguay, R.L., 2012. Neurodevelopmental low-dose bisphenol A exposure leads to early life-stage hyperactivity and learning deficits in adult zebrafish. Toxicology 291, 83–92. https://doi.org/10.1016/j.tox.2011.11.001.

Saili, K.S., Tilton, S.C., Waters, K.M., Tanguay, R.L., 2013. Global gene expression analysis reveals pathway differences between teratogenic and non-teratogenic exposure concentrations of bisphenol A and 17β-estradiol in embryonic zebrafish. Reprod. Toxicol. 38, 89–101. https://doi.org/10.1016/j.reprotox.2013.03.009.

Sant, K.E., Timme-Laragy, A.R., 2018. Zebrafish as a model for toxicological perturbation of yolk and nutrition in the early embryo. Curr. Environ. Heal. reports 5, 125–133. https://doi.org/10.1007/s40572-018-0183-2.

Scholz, S., Mayer, I., 2008. Molecular biomarkers of endocrine disruption in small model fish. Mol. Cell. Endocrinol. 293, 57–70. https://doi.org/10.1016/j.mce.2008.06.008.

Shmarakov, I.O., Borschovetska, V.L., Blaner, W.S., 2017. Hepatic detoxification of bisphenol A is retinoid-dependent. Toxicol. Sci. 157, 141–155. https://doi.org/10.1093/toxsci/kfx022.

Somm, E., Schwitzgebel, V.M., Toulotte, A., Cederroth, C.R., Combescure, C., Nef, S., Aubert, M.L., Hüppi, P.S., 2009. Perinatal exposure to bisphenol a alters early adipogenesis in the rat. Environ. Health Perspect. 117, 1549–1555. https://doi.org/10.1289/ehp.11342.

Stegeman, J.J., Goldstone, J.V., Hahn, M.E., 2010. Perspectives on zebrafish as a model in environmental toxicology. In: Zebrafish, vol. 29, pp. 367–439. https://doi.org/10.1016/S1546-5098(10)02910-9.

Strähle, U., Scholz, S., Geisler, R., Greiner, P., Hollert, H., Rastegar, S., Schumacher, A., Selderslaghs, I., Weiss, C., Witters, H., Braunbeck, T., 2012. Zebrafish embryos as an alternative to animal experiments—a commentary on the definition of the onset of protected life stages in animal welfare regulations. Reprod. Toxicol. 33, 128–132. https://doi.org/10.1016/j.reprotox.2011.06.121.

Talsness, C.E., Andrade, A.J.M., Kuriyama, S.N., Taylor, J.A., vom Saal, F.S., 2009. Components of plastic: experimental studies in animals and relevance for human health. Philos. Trans. R. Soc. B Biol. Sci. 364, 2079–2096. https://doi.org/10.1098/rstb.2008.0281.

Tse, W.K.F., Yeung, B.H.Y., Wan, H.T., Wong, C.K.C., 2013. Early embryogenesis in zebrafish is affected by bisphenol A exposure. Biol. Open 2, 466–471. https://doi.org/10.1242/bio.20134283.

Vandenberg, L.N., Colborn, T., Hayes, T.B., Heindel, J.J., Jacobs, D.R., Lee, D.-H., Shioda, T., Soto, A.M., vom Saal, F.S., Welshons, W.V., Zoeller, R.T., Myers, J.P., 2012. Hormones and endocrine-disrupting chemicals: low-dose effects and nonmonotonic dose responses. Endocr. Rev. 33, 378–455. https://doi.org/10.1210/er.2011-1050.

Vandenberg, L.N., Maffini, M.V., Sonnenschein, C., Rubin, B.S., Soto, A.M., 2009. Bisphenol-A and the great divide: a review of controversies in the field of endocrine disruption. Endocr. Rev. 30, 75–95. https://doi.org/10.1210/er.2008-0021.

Villeneuve, D.L., Garcia-Reyero, N., Escalon, B.L., Jensen, K.M., Cavallin, J.E., Makynen, E.A., Durhan, E.J., Kahl, M.D., Thomas, L.M., Perkins, E.J., Ankley, G.T., 2012. Ecotoxicogenomics to support ecological risk assessment: a case study with bisphenol A in fish. Environ. Sci. Technol. 46, 51–59. https://doi.org/10.1021/es201150a.

Wang, P., Xia, P., Yang, J., Wang, Z., Peng, Y., Shi, W., Villeneuve, D.L., Yu, H., Zhang, X., 2018. A reduced transcriptome approach to assess environmental toxicants using zebrafish embryo test. Environ. Sci. Technol. 52, 821–830. https://doi.org/10.1021/acs.est.7b04073.

Wang, S., Wang, L., Hua, W., Zhou, M., Wang, Q., Zhou, Q., Huang, X., 2015. Effects of bisphenol A, an environmental endocrine disruptor, on the endogenous hormones of plants. Environ. Sci. Pollut. Res. 22, 17653–17662. https://doi.org/10.1007/s11356-015-4972-y.

Wang, Z., Gerstein, M., Snyder, M., 2009. RNA-Seq: a revolutionary tool for transcriptomics. Nat. Rev. Genet. 10, 57–63. https://doi.org/10.1038/nrg2484.

Wetherill, Y.B., Akingbemi, B.T., Kanno, J., McLachlan, J.A., Nadal, A., Sonnenschein, C., Watson, C.S., Zoeller, R.T., Belcher, S.M., 2007. In vitro molecular mechanisms of bisphenol A action. Reprod. Toxicol. 24, 178–198. https://doi.org/10.1016/j.reprotox.2007.05.010.

Willhite, C.C., Ball, G.L., McLellan, C.J., 2008. Derivation of a bisphenol A oral reference dose (RfD) and drinking-water equivalent concentration. J. Toxicol. Environ. Health Part B 11, 69–146. https://doi.org/10.1080/10937400701724303.

Xu, H., Yang, M., Qiu, W., Pan, C., Wu, M., 2013. The impact of endocrine-disrupting chemicals on oxidative stress and innate immune response in zebrafish embryos. Environ. Toxicol. Chem. 32, 1793–1799. https://doi.org/10.1002/etc.2245.

Zhao, S., Fung-Leung, W.-P., Bittner, A., Ngo, K., Liu, X., 2014. Comparison of RNA-Seq and microarray in transcriptome profiling of activated T cells. PLoS One 9, e78644. https://doi.org/10.1371/journal.pone.0078644.

Zoeller, R.T., Bansal, R., Parris, C., 2005. Bisphenol-A, an environmental contaminant that acts as a thyroid hormone receptor antagonist in vitro, increases serum thyroxine, and alters RC3/neurogranin expression in the developing rat brain. Endocrinology 146, 607–612. https://doi.org/10.1210/en.2004-1018.

Supplemental information: scientific article II

Dose-dependent transcriptomic responses of zebrafish eleutheroembryos to Bisphenol A

Authors: R. Martínez, A. Esteve-Codina, L. Herrero-Nogareda, E. Ortiz-Villanueva, C. Barata, R. Tauler, D. Raldúa, B. Piña, L. Navarro-Martín

Status: Published

Journal: Environ. Pollut. 243 (2018) 988–997.

DOI: doi.org/10.1016/j.envpol.2018.09.043

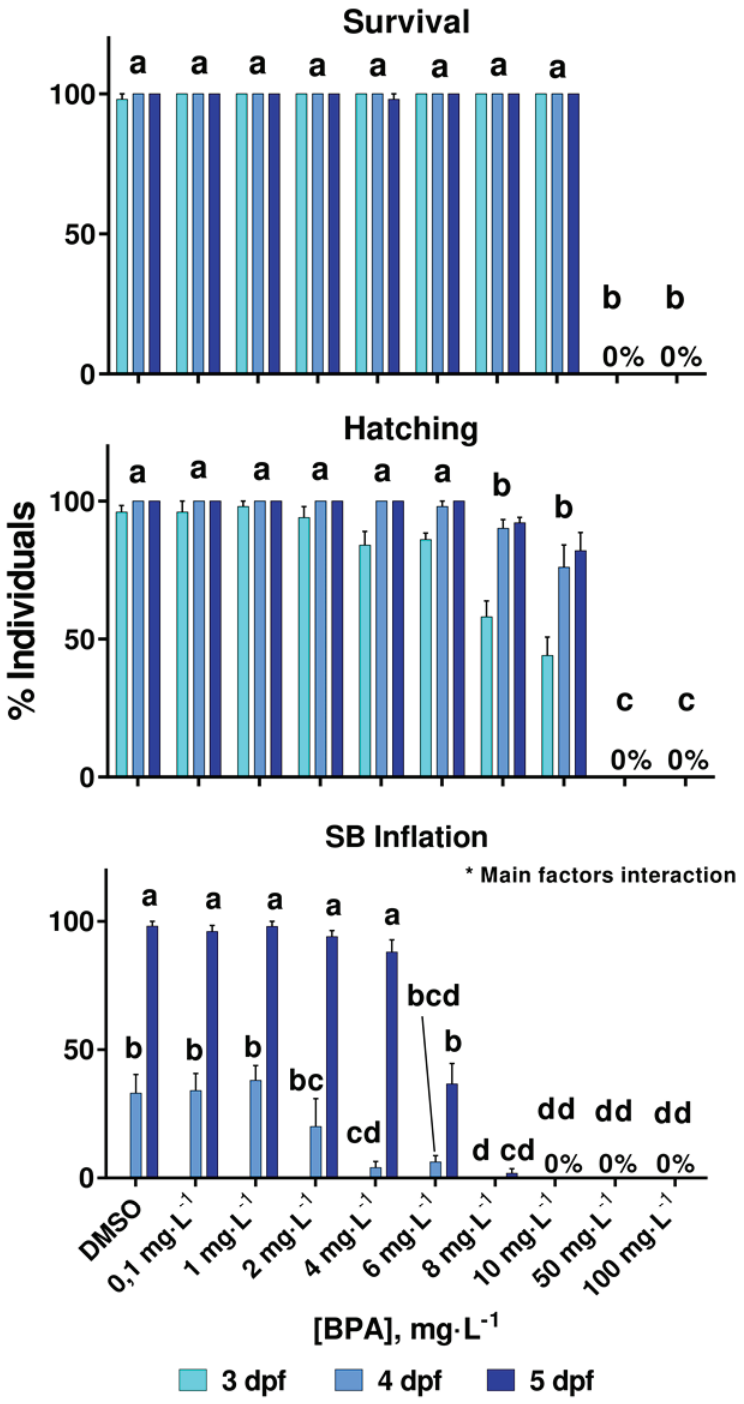

Supplementary Figure SF1. Survival, hatching and swim bladder (SB) inflation results at 3, 4 and 5 dpf for the used concentrations in the preliminary range finding test. Letters indicate statistically different sets of values (non-parametric Kruskal-Wallis test, $p < 0.05$). From these data, we derived a BPA concentration of 4 mg·L^{-1} as the macroscopic LOEC (lowest observed effect concentration).

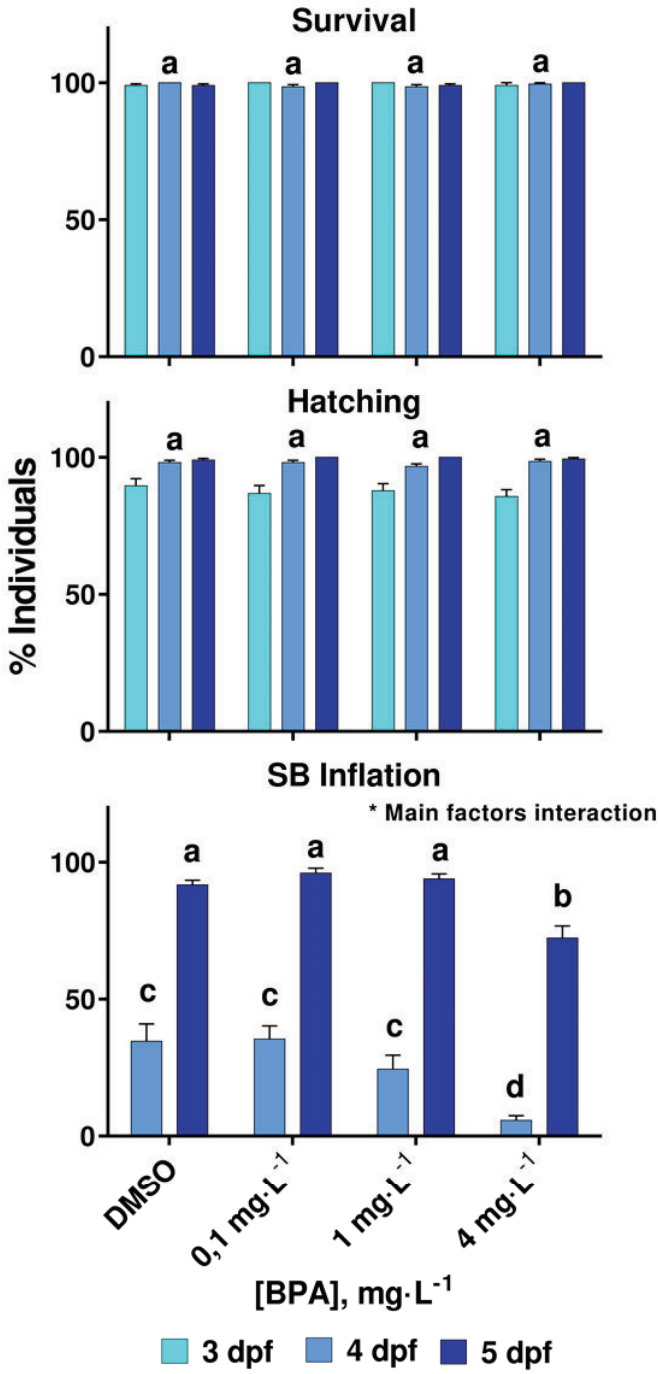

Supplementary Figure SF2. Survival, hatching and swim bladder (SB) inflation results at 3, 4 and 5 dpf for the used concentrations in the transcriptomic study (control, 0.1, 1 and 4 mg·L^{-1} of BPA). Non-parametric test (Kruskal-Wallis, $p < 0.05$) was performed. Letters indicate statistically different sets of values. LOEC value obtained (4 mg·L^{-1}) is coincident with the preliminary range finding test results.

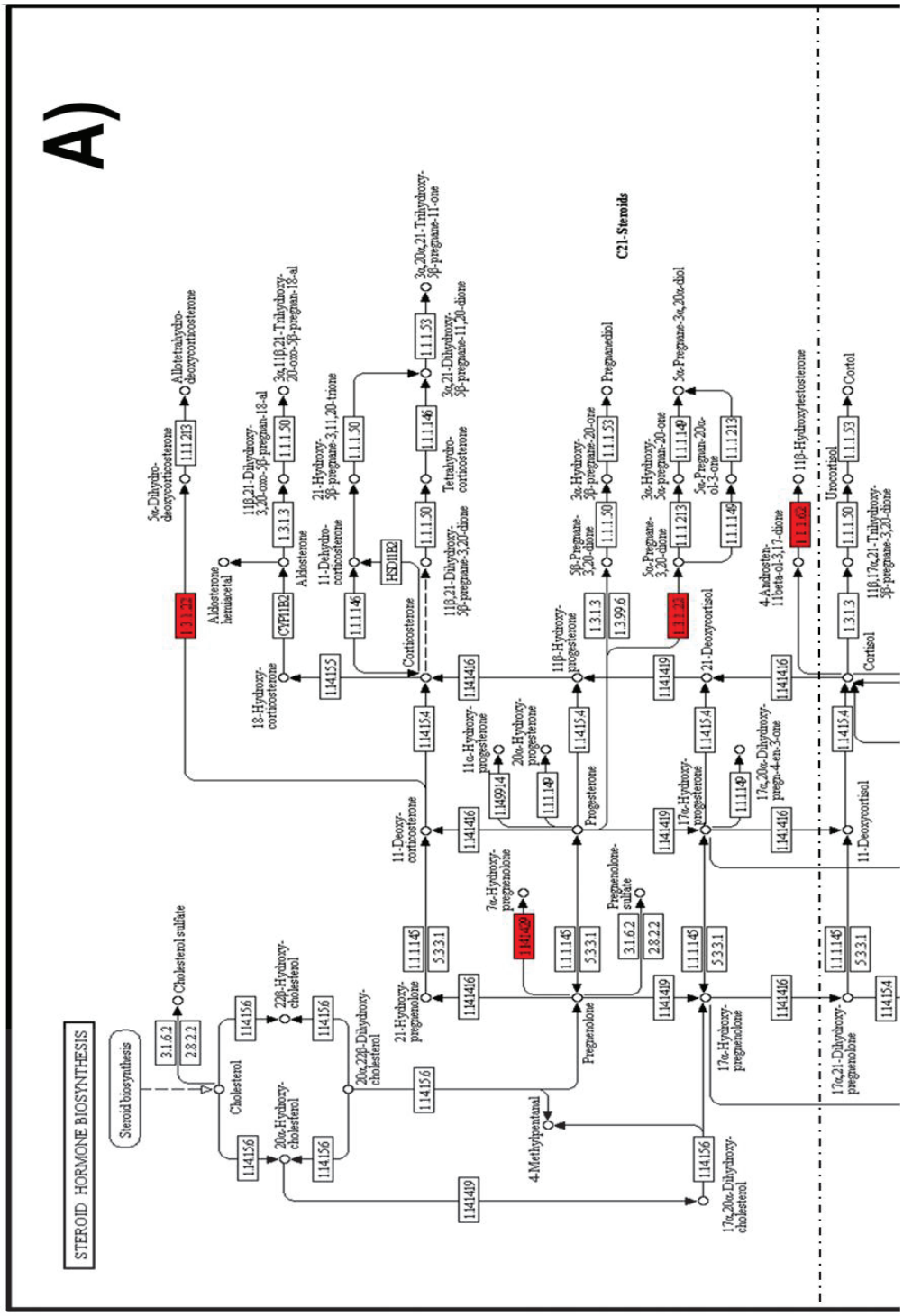

Supplementary Figure SF4 (part A-I). KEGG metabolic maps corresponding to modules dre00140 (Steroid hormone biosynthesis, **A**), dre00830 (Retinol metabolism, **B**) or dre01200 (Carbon metabolism, **C**). DEGs are cluster-colored in blue (Cluster A) or red (Cluster B). Glycolytic pathway (Gly, blue), pentose phosphate cycle (PPP, orange), C1 metabolism (C1, brown) and Krebs' cycle (TCA, purple) are highlighted in panel C.

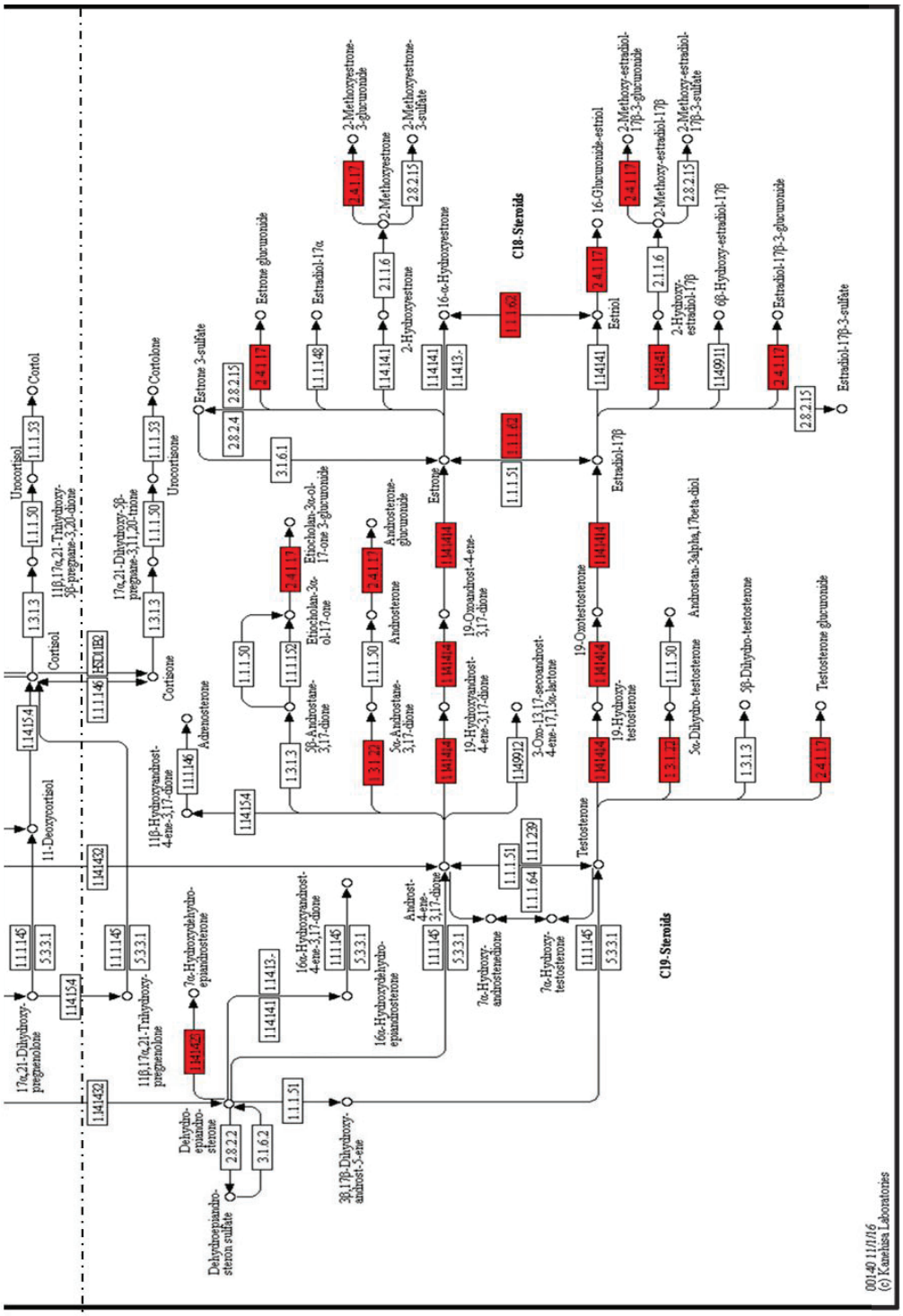

Supplementary Figure SF4 (part A-II). KEGG metabolic maps corresponding to modules dre00140 (Steroid hormone biosynthesis, **A**), dre00830 (Retinol metabolism, **B**) or dre01200 (Carbon metabolism, **C**). DEGs are cluster-colored in blue (Cluster A) or red (Cluster B). Glycolytic pathway (Gly, blue), pentose phosphate cycle (PPP, orange), C1 metabolism (C1, brown) and Krebs' cycle (TCA, purple) are highlighted in panel C.

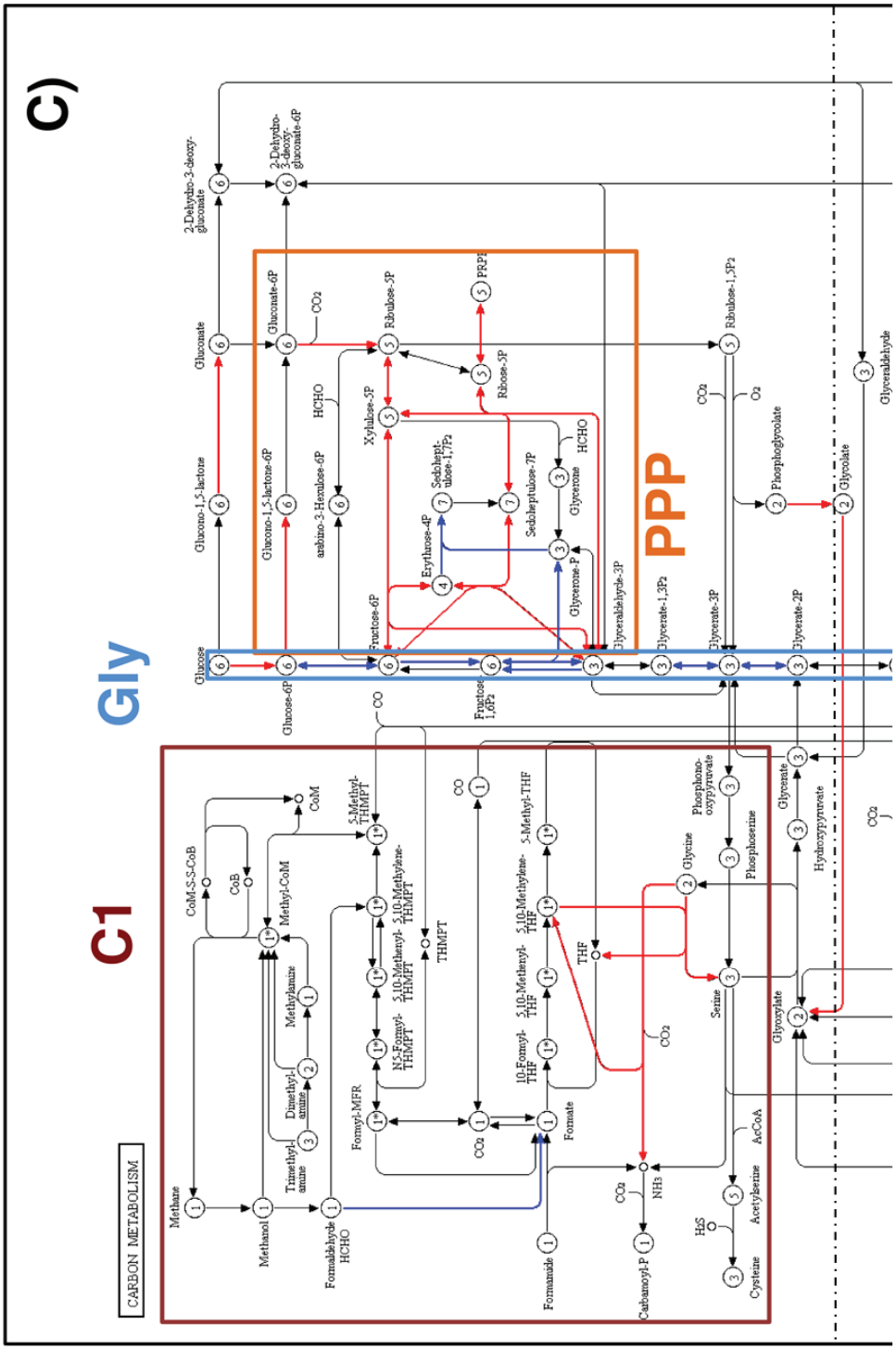

Supplementary Figure SF4 (part C-I). KEGG metabolic maps corresponding to modules dre00140 (Steroid hormone biosynthesis, **A**), dre00830 (Retinol metabolism, **B**) or dre01200 (Carbon metabolism, **C**). DEGs are cluster-colored in blue (Cluster A) or red (Cluster B). Glycolytic pathway (Gly, blue), pentose phosphate cycle (PPP, orange), C1 metabolism (C1, brown) and Krebs' cycle (TCA, purple) are highlighted in panel C.

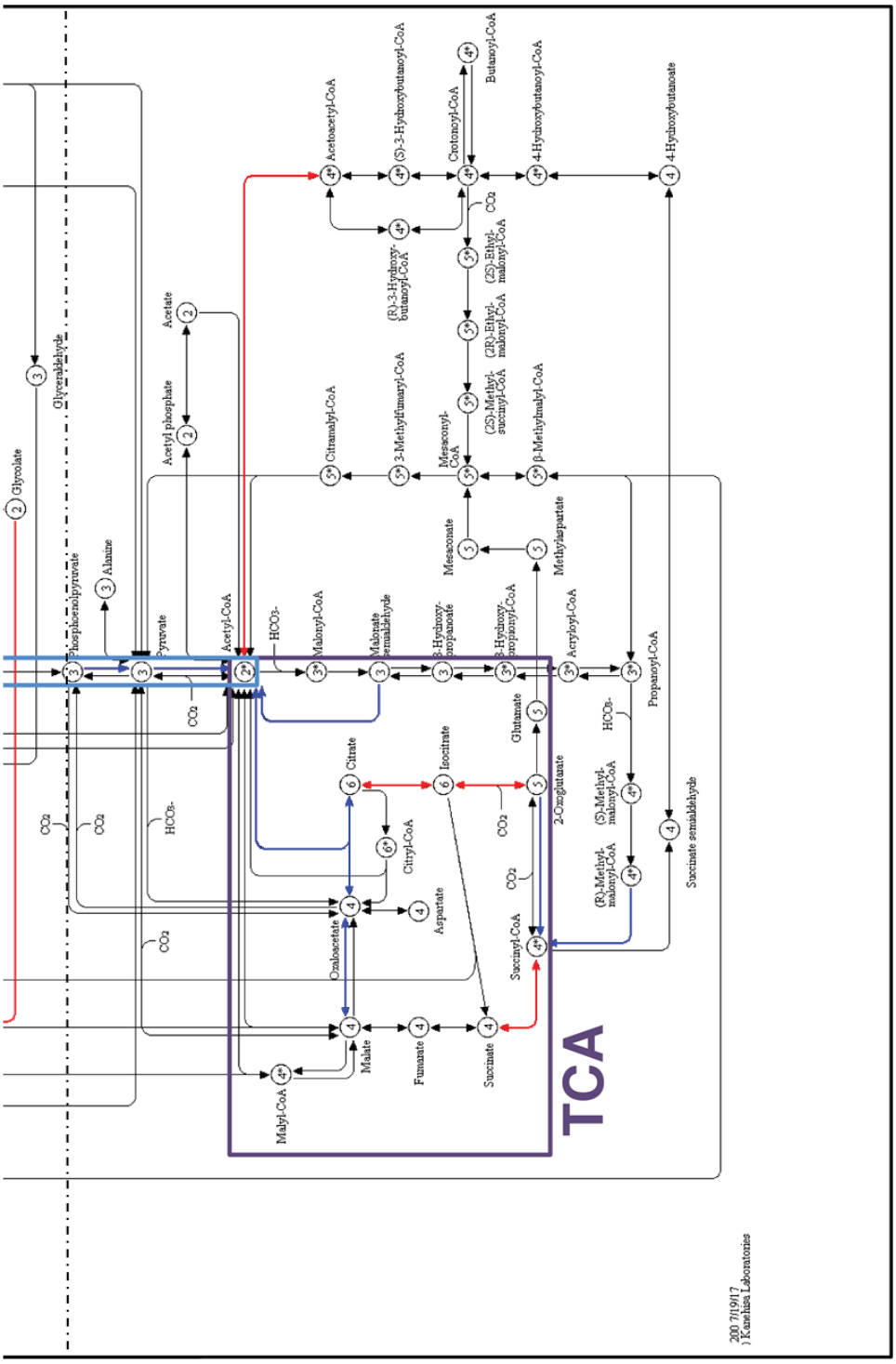

Supplementary Figure SF4 (part C-II). KEGG metabolic maps corresponding to modules dre00140 (Steroid hormone biosynthesis, **A**), dre00830 (Retinol metabolism, **B**) or dre01200 (Carbon metabolism, **C**). DEGs are cluster-colored in blue (Cluster A) or red (Cluster B). Glycolytic pathway (Gly, blue), pentose phosphate cycle (PPP, orange), C1 metabolism (C1, brown) and Krebs' cycle (TCA, purple) are highlighted in panel C.

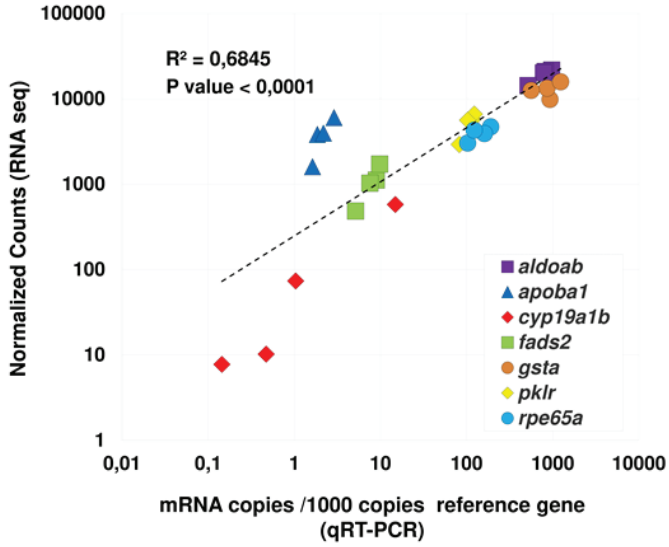

Supplementary Figure SF3. Correlation between RNA-seq values and Real Time qRT-PCR estimation of mRNA levels for several selected genes ($r^2 = 0.68$, $p \leq 10^{-4}$).

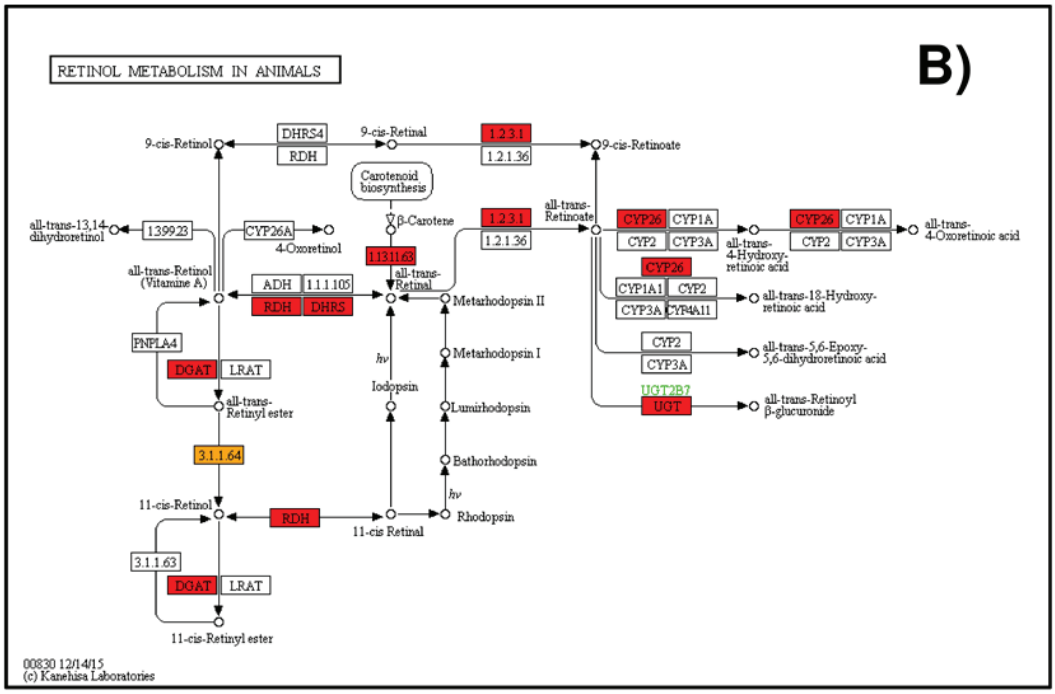

Supplementary Figure SF4 (part B). KEGG metabolic maps corresponding to modules dre00140 (Steroid hormone biosynthesis, **A**), dre00830 (Retinol metabolism, **B**) or dre01200 (Carbon metabolism, **C**). DEGs are cluster-colored in blue (Cluster A) or red (Cluster B). Glycolytic pathway (Gly, blue), pentose phosphate cycle (PPP, orange), C1 metabolism (C1, brown) and Krebs' cycle (TCA, purple) are highlighted in panel C.

Supplementary Table ST1. RNA-seq readings and mapping quality statistics.

Sample Barcode	Sample Name	Number of FLIs	Million read-pairs (or reads)	Yield (Gb)	Trimmed yield (Gb)	Avg PhiX error r1	Avg PhiX error r2	Organism	Reference	Avg % unique	Avg % unmapped	Avg % duplicate	Avg % difference r1	Avg % difference r2	Avg alignment insert size
AB3116	BPA (2-5) 0,1ppm R1	1	39,310	5,975	5,975	0.19	0.33	Danio rerio	drerio.GRCz10	82.52	1.28	27.07	1.18	1.20	147.00
AB3124	BPA (2-5) 0,1ppm R3	2	40,088	6,093	6,088	0.19	0.36	Danio rerio	drerio.GRCz10	81.82	1.64	22.25	1.26	1.33	145.00
AB3120	BPA (2-5) 0,1ppmR2	1	47,272	7,185	7,185	0.20	0.33	Danio rerio	drerio.GRCz10	80.22	1.48	28.14	1.22	1.23	142.00
AB3117	BPA (2-5) 1ppm R1	1	46,017	6,995	6,994	0.20	0.33	Danio rerio	drerio.GRCz10	80.44	1.39	26.67	1.14	1.14	149.00
AB3121	BPA (2-5) 1ppm R2	1	42,797	6,505	6,498	0.16	0.33	Danio rerio	drerio.GRCz10	79.45	1.32	24.31	1.21	1.33	142.00
AB3125	BPA (2-5) 1ppm R3	1	30,301	4,606	4,605	0.19	0.33	Danio rerio	drerio.GRCz10	82.95	1.43	26.25	1.24	1.26	146.00
AB3118	BPA (2-5) 4ppm R1	1	44,598	6,779	6,778	0.20	0.33	Danio rerio	drerio.GRCz10	80.63	1.32	24.69	1.16	1.17	151.00
AB3122	BPA (2-5) 4ppm R2	1	40,353	6,134	6,133	0.25	0.36	Danio rerio	drerio.GRCz10	81.42	1.32	23.27	1.22	1.20	154.00
AB3126	BPA (2-5) 4ppm R3	1	41,617	6,326	6,325	0.19	0.33	Danio rerio	drerio.GRCz10	81.90	1.50	26.38	1.18	1.18	148.00
AB3115	BPA (2-5) Ctrl R1	1	44,793	6,809	6,802	0.16	0.32	Danio rerio	drerio.GRCz10	79.87	1.76	25.01	1.18	1.28	144.00
AB3119	BPA (2-5) Ctrl R2	1	43,816	6,660	6,653	0.16	0.32	Danio rerio	drerio.GRCz10	81.09	1.61	27.74	1.22	1.32	143.00
AB3123	BPA (2-5) Ctrl R3	1	31,446	4,780	4,779	0.19	0.33	Danio rerio	drerio.GRCz10	81.17	1.49	26.66	1.25	1.25	144.00

Column description	
Sample Barcode	Unique internal CNAG identifier of the sample
Sample Name	Sample name provided by the collaborator
Number of FLIs	Number of sequencing Flowcell Lane Index units for this sample (equivalent to the number of times the sample has been sequenced)
Million read-pairs (or reads)	Total million read-pairs (or reads for single-end runs) that passed Illumina filter
Yield (Gb)	Total yield in Gigabases from the read-pairs (or reads for single-end runs) that passed Illumina filter
Trimmed yield (Gb)	Trimmed yield in Gigabases from the read-pairs (or reads for single-end runs) that passed Illumina filter
Avg PhiX error r1	Average % mismatches between the spiked-in PhiX read 1 and the PhiX reference
Avg PhiX error r2	Average % mismatches between the spiked-in PhiX read 2 and the PhiX reference
Organism	Sample's organism according to submitter
Reference	Reference sequence (genome, transcriptome, contigs...) to which the reads have been mapped
Avg % unique	Average % of reads aligning to a single location in the reference
Avg % unmapped	Average % of reads not aligning to any location in the reference
Avg % duplicate	Average % of read-pairs (or reads, for single-end runs) that map exactly at the same location in the reference as another read-pair
Avg % difference r1	Average % mismatches between read 1 and the reference
Avg % difference r2	Average % mismatches between read 2 and the reference
Avg alignment insert size	Average mapping distance between read 1 and read 2

Supplementary Table ST2. Results from DAVID Functional Analysis[a)], FDR≤5%

See annexes

Supplementary Table ST3. Primers, efficiency and accession number for the genes measured with qRT-PCR (ppiaa, aldoab, apoba1, cyp19a1b, fads2, gsta.1, pklr, and rpe65a).

Gene Name	Accesion nº	Description	Upper-primer (5'-3')	Lower primer (5'-3')	Efficiency	R^2
aldoab	NM_213215.1	aldolase a, fructose-bisphosphate, b	CCTCCGCTCTTAAAGCCTGG	TGTTCACGGCTCTCTTGACG	96%	0.987
apoba	XM_689735.9	apolipoprotein Ba	GCTAAAATTAAGTGCCCGGTTCT	TTTCGATTATGGGCAAATCATAAG	94%	0.981
cyp19a1b	NM_131642.2	cytochrome P450, family 19, subfamily A, polypeptide 1b	ACATTGGACGCATGCATAAGAC	CTGGGAACAGTGTTCTCGAAGTT	95%	0.989
fads2	NM_131645.2	fatty acid desaturase 2	TCTTCATTGGTCCTCCCCTG	CCCACATGCCATGACTGATC	99%	0.997
gsta.1	NM_213394.1	glutathione S-transferase, alpha tandem duplicate 1	GCAGAAAGTGTGAGTCTGTCCG	GATGTTTGTCCTCTTTCAGCCTC	99%	0.994
pklr	NM_201289.1	pyruvate kinase L/R	ATCGTCCTCGTTGTCCGATC	GGAAAACTCCACGCAGCAG	99%	0.989
rpe65a	NM_200751.1	retinal pigment epithelium -specific protein 65a	CCCTGACAGGATTTGCAAGC	GGCTCCGAAGGGTACGAGTC	97%	0.995
ppiaa	NM_212758.1	peptidylprolyl isomerase Aa (cyclophilin A)	GGGTGGTAATGGAGCTGAGA	AATGGACTTGCCACCAGTTC	98%	0.999

Scientific article III

Unravelling the mechanisms of PFOS toxicity by combining morphological and transcriptomic analyses in zebrafish embryos

Authors: R. Martínez, L. Navarro-Martín, C. Luccarelli, A.E. Codina, D. Raldúa, C. Barata, R. Tauler, B. Piña

Status: Published

Journal: Sci. Total Environ. 674 (2019) 462–471.

DOI: 10.1016/j.scitotenv.2019.04.200

Science of the Total Environment 674 (2019) 462–471

Contents lists available at ScienceDirect

Science of the Total Environment

journal homepage: www.elsevier.com/locate/scitotenv

Unravelling the mechanisms of PFOS toxicity by combining morphological and transcriptomic analyses in zebrafish embryos

Rubén Martínez [a,b], Laia Navarro-Martín [a], Chiara Luccarelli [a], Anna E. Codina [c,d], Demetrio Raldúa [a], Carlos Barata [a], Romà Tauler [a], Benjamin Piña [a,*]

[a] IDAEA-CSIC, Jordi Girona, 18, 08034 Barcelona, Spain
[b] Universitat de Barcelona (UB), Barcelona 08007, Spain
[c] CNAG-CRG, Centre for Genomic Regulation (CRG), Barcelona Institute of Science and Technology (BIST), Barcelona 08028, Spain
[d] Universitat Pompeu Fabra (UPF), Barcelona 08003, Spain

HIGHLIGHTS

- Zebrafish embryos show macroscopic alterations at PFOS concentrations >1 mg/L.
- Transcriptomic changes occur at concentrations 1/10 to 1/100 the macroscopic LOEC.
- Transcript analyses suggest alterations on lipid metabolism and the immune system.
- Some of the observed changes occur at concentrations already detected in humans.
- We propose tighter regulations limiting human and environmental exposure to PFOS.

GRAPHICAL ABSTRACT

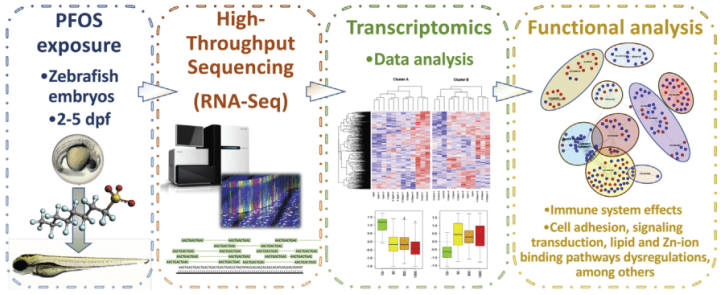

ARTICLE INFO

Article history:
Received 15 February 2019
Received in revised form 12 April 2019
Accepted 12 April 2019
Available online 15 April 2019

Editor: Henner Hollert

Keywords:
Endocrine disrupting chemicals
High-throughput sequencing
Differentially expressed genes (DEGs)
ANOVA-PLS
Immune system
Lipid disruption
Benchmark doses

ABSTRACT

Exposure to PFOS (perfluorooctanesulfonate) has been related to toxic effects on lipid metabolism, immunological response, and different endocrine systems. We present here a transcriptomic analysis of zebrafish embryos exposed to different concentrations of PFOS (0.03–1.0 mg/L) from 48 to 120 hpf. No major survival or morphological alterations (swimming bladder inflation, kyphosis, eye separation and size…) were observed below the 1.0 mg/L mark. Conversely, we observed significant increase in transcripts related to lipid transport and metabolism even at the lowest used concentration. In addition, we observed a general decrease on transcripts related to natural immunity and defense again infections, which adds to the recent concerns about PFOS as immunotoxicant, particularly in humans. Derived PoD (Point of Departure) values for transcriptional changes (0.011 mg/L) were about 200-fold lower than the corresponding PoD values for morphometric effects (2.53 mg/L), and close to levels observed in human blood serum or bird eggs. Our data suggest that currently applicable tolerable levels of PFOS in commercial goods should be re-evaluated, taking into account its potential effects on lipid metabolism and the immune system.

* Corresponding author at: Institute of Environmental Assessment and Water Research, IDAEA-CSIC, Jordi Girona 18, 08034 Barcelona, Spain.
E-mail addresses: rmlqam@cid.csic.es (R. Martínez), anna.esteve@cnag.crg.eu (A.E. Codina), drpqam@cid.csic.es (D. Raldúa), cbmqam@cid.csic.es (C. Barata), rtaqam@cid.csic.es (R. Tauler), bpcbmc@cid.csic.es (B. Piña).

https://doi.org/10.1016/j.scitotenv.2019.04.200
0048-9697/

1. Introduction

Polyfluoroalkyl and perfluoroalkyl substances (PFASs) consist of fully fluorinated hydrophobic alkyl chains attached to different hydrophilic ending groups. Their unique thermal stability and oxidation resistance have fueled their use for >50 years in different industrial and domestic applications, as surfactants, surface treatment, fire retardants, and coating materials (OECD, 2002). However, these same properties make PFAS very bioaccumulative and persistent in the environment, with the capability for long range transport through the atmosphere and water (Ahrens and Bundschuh, 2014). Perfluorooctane sulfonate (PFOS) is one of the most frequently detected PFASs in the environment, and the first one to be added to Annex B of the Stockholm Convention on Persistent Organic Pollutants list, which resulted in a global restriction, but not a ban, on its production and use (Paul et al., 2009). Like other PFAS, exposure to PFOS is known to induce adverse effects on growth, birth weight, fertility, carcinogenesis, immunity, lipid metabolism, and the thyroid system (Chaparro-Ortega et al., 2018; Du et al., 2013; Jensen and Leffers, n.d.; Lau, 2015). Nevertheless, neither PFOS nor any other PFAS has been yet categorized as endocrine disrupting chemical (EDC) by the European Commission (European Commission, 2000) or by other regulatory agencies. PFOS is found at relatively high levels (ng/L, μg/g and mg/L) in wastewaters, wastewater treatment plants' sludge, and exposed aquatic biota, respectively, showing an extremely high bioaccumulation potential (Ahrens and Bundschuh, 2014; Arvaniti and Stasinakis, 2015; Loos et al., 2013). In humans, blood serum levels of PFOS and other PFAS ranged from 1 to 10 μg/L in multiple surveys of general populations, and from 100 to 1000 μg/L for highly exposed populations (Kato et al., 2015; Olsen, 2015). Toxicological studies revealed potential toxic effects of these substances ranging from growth and reproductive functions to lipid metabolism and oxidative stress (Ankley et al., 2005; Lau et al., 2007; Rodriguez-Jorquera et al., 2019). The effect of the exposure to PFOS and other related compounds on the immunologic system is a matter of increasing concern, as it has been observed both in fish and in mammals, but its significance for human health is largely unknown (Corsini et al., 2011; DeWitt et al., 2009; DeWitt et al., 2016). Moreover, a recent report on the effect of PFOS on mice gut microbiome suggests an until now unexplored potentially harmful interactions between PFOS and microbial and animal metabolisms (Lai et al., 2018).

In the present study, we aimed to characterize and to describe the mechanisms of PFOS toxicity using zebrafish embryos as a model. Zebrafish characteristics (easy maintenance, small size, short life cycle, embryo transparency, large offspring, etc.) made it a preferred animal model for toxicity studies during the last decades (Hill et al., 2005; Scholz and Mayer, 2008; Stegeman et al., 2010). The study of zebrafish at least at genomic, transcriptomic, proteomic and metabolomic levels (Mushtaq et al., 2013) and its recognition as an acceptable vertebrate model for human and environmental toxicology (Raldúa and Piña, 2014; Strahle et al., 2012), make it an excellent election for ecotoxicological studies. During the last years, high-throughput next generation sequencing (HT-NGS) technologies facilitated the improvement and achievements of the transcriptomic studies (Mortazavi et al., 2008; Reuter et al., 2015), and showed its usefulness in the study of transcriptomic effects of several toxicants (Baker and Hardiman, 2014; Caballero-Gallardo et al., 2016). Although transcriptomics effects of PFOS over zebrafish larvae have been previously assessed, these studies were centered in a targeted dataset of transcripts (Jantzen et al., 2016; Shi et al., 2008) or based in a single PFOS dose (Chen et al., 2014; Fai Tse et al., 2016). The aim of this work was to analyze the toxic effects of PFOS in zebrafish embryos at sub-lethal concentrations, using a combination of morphometric and transcriptomic techniques. For that reason, we have designed dose-response assays using different PFOS concentrations to unravel the different mechanisms underlying the different toxic effects and to contribute to the risk assessment analysis of these currently ubiquitous pollutants.

2. Materials and methods

2.1. Zebrafish maintenance and rearing conditions

Adult wild-type zebrafish (*Danio rerio*, 12–18 months old) were maintained under controlled standard conditions (28 ± 1 °C, 12 L:12D photoperiod, ≤ 5 fish/L) in fish water. Fish water was composed of 90 μg/mL of Instant Ocean (Aquarium Systems, Sarrebourg, France) and 0.58 mM of $CaSO_4 \cdot 2H_2O$, dissolved in reverse osmosis purified water. Zebrafish were fed twice a day with dry flakes (TetraMin, Tetra, Germany). Eggs were obtained by natural mating of the adults, placing in breeding tanks males and females in a 2:1 proportion, respectively. A mesh was placed in each breeding tank to avoid zebrafish access to eggs, which were collected and rinsed at 2 hpf (hours post fertilization). Fertilization rate was assessed to be at least 70% (OECD, 2013) and fertilized eggs were randomly placed in 6 well plates with fish water (under standard conditions) at a density of 3 embryos/mL. Fish water was changed daily until the start of the PFOS exposure at 48 hpf (Sections 2.2.2 and 2.2.3). All procedures were performed accordingly with the institutional guidelines under a license from the local government (DAMM 7669, 7964) and were approved by the Institutional Animal Care and Use Committees at the Research and Development Centre of the Spanish National Research Council (CID-CSIC).

2.2. Zebrafish eleutheroembryo exposure to PFOS

2.2.1. PFOS solutions preparation

PFOS (perfluorooctanesulfonate (PFOS, CAS-RN: 2795-39-3) potassium salt) was purchased from Sigma-Aldrich (St. Louis, MO, USA, ≥98% purity). Five hundred-fold stock solutions (50–5000 mg/L, depending on the experiment, see Sections 2.2.2 and 2.2.3) were prepared in dimethyl sulfoxide (DMSO) and stored at −20 °C. Experimental solutions were prepared every day by dilution of the stock with fish water, with a final DMSO concentration of 0.2% (v/v) in all exposed and control groups. The pH of the working solutions was in the recommended range (6.8–7.5) (Avdesh et al., 2012). Concentrations are given as nominal values. Since the stability of PFOS in water solutions for at least 24 h have been previously assessed (Kato et al., 2013; Lyu et al., 2015), daily water changes were considered sufficient to ensure constant PFOS concentrations.

2.2.2. Exposures for morphometric tests

Zebrafish eleutheroembryos were exposed from 2 dpf to 5 dpf to a wide range of PFOS concentrations to stablish a suitable LOAEC (Lowest Observed Adverse Effect Concentration) below which transcriptomics studies should take place. We did not expose embryos during the first 48 hpf to avoid confounding factors due to the interference of PFOS with the early embryonic processes and to focus in the effect of PFOS in the already differentiated tissues of the larvae. PFOS concentrations ranged from 0 (control, 0.2% of DMSO) to PFOS solutions containing 0.10, 0.25, 0.50, 1.0, 2.5, 5.0, 7.5, 10 and 100 mg/L of PFOS (all of them in the presence of 0.2% of DMSO). Anatomical development of embryos was followed daily during the exposure as described (Kimmel et al., 1995). Survival (3, 4 and 5 dpf), hatching (3, 4 and 5 dpf) and swim bladder inflation rates (4 and 5 dpf) were assessed in at least 50 larvae per each experimental group.

2.2.3. Exposure for transcriptome analysis

Using the morphometric data, a second round of PFOS exposure was performed, avoiding PFOS concentrations that could affect embryo viability. Therefore, the highest used concentration was 1.0 mg/L of PFOS, as determined as LOAEC for morphometric effects (see Section 3.2.). Zebrafish eleutheroembryos were exposed to control (0.2% DMSO), 0.03, 0.3 and 1.0 mg/L of PFOS during 72 h from 2 to 5 dpf. The experimental design was selected to minimize all possible covariates. All animals belonged to the same batch and were simultaneously incubated in

6-well plates, each one containing control and exposed groups for each concentration (no batch- or plate-bias). Fresh working solutions were daily prepared from the stocks and renewed as previously described. For each experimental group, anatomical development of embryos (Kimmel et al., 1995), sub-lethal and developmental effects, survival and hatching rates at 3, 4 and 5 dpf, and swim bladder inflation rates at 4 and 5 dpf were reported, according to the OECD 236 guidelines (OECD, 2013). Replicates of 10 eleutheroembryos per experimental condition were collected, snap-frozen in dry ice and stored at −80 °C until further analysis (RNA extraction for high-throughput sequencing and RT-qPCR confirmation purposes).

2.3. Eleutheroembryo fixation, morphological and immunochemical measurements

Zebrafish eleutheroembryos were collected and fixed overnight at 4 °C in a phosphate buffered saline 1× solution (PBS) with 4% PFA (paraformaldehyde) as previously described (Martínez et al., 2018; Raldua et al., 2008). For morphological measurements, fixed eleutheroembryos were then washed several times with PBS and gradually transferred to 90% glycerol (10% PBS 1×) for long-term preservation and positioning facilitation under the microscope. A stereomicroscope Nikon SMZ1500 equipped with a Nikon digital Sight DS-Ri1 camera was used to acquire lateral and dorsoventral images of the fixed embryos (Fig. 1A). Afterwards the following morphological parameters were measured using the free graphical image analysis software ImageJ (National Institutes of Health, Bethesda, MD, USA): Body length (BL), head-trunk angle (HTA), yolk sac area (YSA), swim bladder area (SBA), eye length (EL), eye width (EW), head width (HW), inter-ocular distance (IOD) and eye-snout distance (ESD) (Fig. 1C). For immunochemical determinations, fixed eleutheroembryos were washed several times with PBS, gradually transferred to methanol 100%, and stored at −80 °C for at least 24 h. After rehydration of the larvae, a 50 min depigmentation step (3% H_2O_2 and 1% KOH in water) was included before the permeabilization steps. Whole mount immunohistochemistry was performed as previously described with minor modifications (Thienpont et al., 2011). Larvae were then incubated overnight at 4 °C in either anti-parvalbumin monoclonal antibody (Sigma-Aldrich, St. Louis, MO) at 1:2000 and anti-acetylated alpha-tubulin monoclonal antibody (Sigma-Aldrich, St. Louis, MO) at 1:1000. The above primary antibodies were used to detect ciliated and microvillous olfactory sensory neurons (anti-parvalbumin, *Parv*) and cilia from olfactory epithelium and

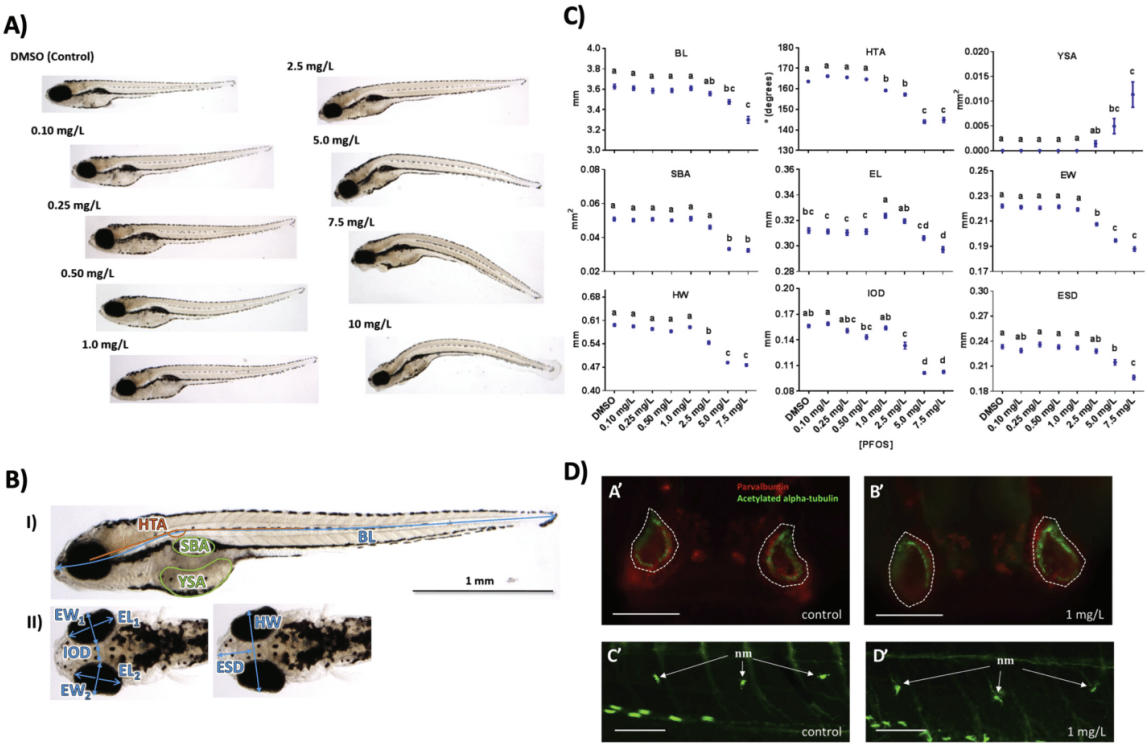

Fig. 1. Morphometric measurements of zebrafish embryos treated with different concentrations of PFOS from 2 to 5 dpf. A) Representative pictures of eleutheroembryos at 5 dpf exposed to different concentrations of PFOS. B) Description of morphological traits measured from lateral (I) and dorsoventral (II) images. Measured traits were the following: body length (BL), head-trunk angle (HTA), yolk sac area (YSA), swim bladder area (SBA), eye length (EL), eye width (EW), head width (HW), inter-ocular distance (IOD) and eye-snout distance (ESD). Scale bar: 1.0 mm. C) Quantitative analyses of the effects of PFOS on the morphological parameters shown in Panel C (n = 50 larvae/group). All measures are expressed in mm except YSA and SBA (expressed in mm^2), and HTA (expressed in arc degrees). Different low-case letters in each graph indicate statistically differences between experimental groups (Kruskal-Wallis tests plus Dunn's pairwise multiple comparisons with Bonferroni correction $p < 0.05$). Means and SEM (standard error of the mean) are represented. Morphological parameters were not determined at the highest concentrations in the exposure (10 and 100 mg/L) due to their high rates of mortality (82 and 100%, respectively). D) Immunofluorescent analyses of olfactory epithelium (A', B') and neuromasts (C', D') structures in 5 dpf eleutheroembryos after exposure to 1 mg/L PFOS. A'–B': Dorsal view of the head of a representative control (A') and 1 mg/L PFOS-exposed (B') eleutheroembryo immunolabeled with a double whole-mount immunofluorescence using anti-parvalbumin (*Parv*) and anti-acetylated alpha tubulin (*α-AT*) primary antibodies. The former antibody labels ciliated and microvillous neurons in the sensory olfactory epithelium, whereas the later labels kinocilia of ciliated nonsensory cells and the cilia of the ciliated sensory neurons. The region encircled by a dashed line corresponds with the olfactory pits. C'–D': Lateral view (head on the left side) of a representative control (C') and PFOS-exposed (D') eleutheroembryo immunolabeled with anti-acetylated alpha tubulin primary antibody, labeling the neuromasts (nm). Scale bars: 100 μm.

neuromast hair cells (acetylated alpha-tubulin, *α-AT*), respectively. The secondary antibodies used were Alexa Fluor 488 and 555 goat anti-rabbit IgG and goat anti-mouse IgG (1:300; Molecular Probes).

2.4. RNA extraction, library construction and high-throughput sequencing

Total RNA was isolated from independent pools of 10 eleutheroembryos (three pools for each condition, separately exposed and treated) using AllPrep DNA/RNA Mini Kit (Qiagen, CA, USA) as described by the manufacturer. Extracted RNA was reconstituted in RNAse-free water and its quantity and quality were determined by a Qubit® RNA BR Assay kit (Thermo Fisher Scientific) and RNA 6000 Nano Assay on a Bioanalyzer 2100 (Agilent Technologies), respectively. RNA preparations were sent to the National Center for Genomic Analysis (CNAG, Barcelona, Spain) for high-throughput sequencing (RNA-Seq). All replicates showed RNA concentrations between 50 and 200 ng/μL, were free of genomic DNA and had an RNA integrity number (RIN) > 8. The RNA-Seq libraries were prepared using KAPA Stranded mRNA-Seq Kit Illumina® Platforms (Kapa Biosystems) with minor modifications. A poly-A based mRNA enrichment with oligo-dT magnetic beads was performed over 500 ng of total RNA as input material. The mRNA was fragmented (resulting RNA fragment size: 80-250 nt; major peak: 130 nt). The second strand cDNA synthesis was carried out in the presence of dUTP instead of dTTP, to enhance strand specificity. The blunt-ended double-stranded cDNA was 3′ adenylated and Illumina indexed adapters (Illumina) were ligated. Ligation product was enriched with 15 PCR cycles and validated on an Agilent 2100 Bioanalyzer with the DNA 7500 kit. Each final library was sequenced using TruSeq SBS Kit v3-HS (paired-end mode; 2x76bp as read length). An average of 39 million paired-end reads for each sample was generated in a fraction of a sequencing lane on HiSeq 2000 (Illumina). Image analysis, base calling and quality scoring of the run were processed using the manufacturer's software Real Time Analysis (RTA 1.13.48) and FASTQ sequence files were generated by the sequencing analysis software CASAVA. Obtained reads mapped properly to the reference genome in more than a 95%. The majority mapped to exonic regions and to protein-coding genes, with a total of 24,425 genes detected. The transcriptomic data discussed in this publication have been deposited in NCBI's Gene Expression Omnibus (Edgar et al., 2002) and are accessible through GEO Series accession number GSE125072 (https://www.ncbi.nlm.nih.gov/geo/query/acc.cgi?acc=GSE125072). A full description of mapping quality statistics can be found in Supplementary Table ST1.

2.5. Data analysis

2.5.1. Morphometric statistical analysis

Differences between experimental groups in survival, hatching and swim bladder inflation rates (Sections 2.2.2 and 2.2.3.) and morphological measurements (Section 2.3.) were analyzed by non-parametric Kruskal-Wallis tests plus Dunn's pairwise multiple comparisons (significance level at $p < 0.05$, Bonferroni correction). SPSS 24.0 (Armonk, NY: IBM Corp., 2016) was used to carry out statistical tests whereas GraphPad Prism (v. 6.07, GraphPad Software, La Jolla, CA, USA) was used to perform the graphs (Fig. 1C and Supplementary Figs. SF1, SF2, SF3).

2.5.2. RNA-Seq data analysis

RNA-Seq reads were aligned to the *D. rerio* reference genome (GRCz10) using the STAR software version 2.5.1b (Dobin et al., 2013). The quantification of the genes annotated in GRCz10.84 was performed using RSEM version 1.2.28 (Li and Dewey, 2011) with default parameters. Data normalization was carried out using the DESeq2 (v.1.10.1) R package (Li and Dewey, 2011; Love et al., 2014), which uses a variant of scaling factor normalization based on the assumption that most genes are not differentially expressed. Differential expression analysis between all experimental conditions was analyzed using the ANOVA-PLS (Analysis of Variance-Partial Least Square) analysis using the *lmdme* package in R v. 1.0.136, R Core Team (Fresno et al., 2014). First, ANOVA decomposed the transcriptomic data matrix of all samples (normalized and scaled) through a linear model that considers the experimental design (PFOS treatment). Secondly, a PLS regression model was built between the matrices obtained in this linear decomposition (X) and a vector (y) that defined the class membership of the samples (control, 0.03, 0.3 and 1.0 mg/L). The analysis identified the features (variables) that described best the differences between groups and it determined if the experimental groups were different from each other. ANOVA-PLS was performed on the normalized data scaled to the control set and log2 transformed, considering each one of the PFOS concentrations (including controls) as a class. Genes showing significant variations among the classes ($p \leq 0.05$; 1434 transcripts in total) were selected as DEGs (differentially expressed genes) for further analysis. Hierarchical and PAM (partition around medoids) clustering analysis were performed using the packages *gplots*, *fpc*, and *cluster* in R. The PAM implementation in these packages allowed performing a principal components analysis (PCA) to analyze the covariance matrix of the entered variables and to produce a 2D plot showing the goodness of separation of the defined clusters (https://www.rdocumentation.org/packages/cluster/versions/2.0.6/topics/pam). Statistically significant differences between genes included in each cluster were assessed by one-way ANOVA followed by post hoc Tukey's B tests ($p < 0.05$) using the *foreign* and *agricolae* packages in R. Further graphs were carried out using the *gplots* package, also in R environment. DAVID Bioinformatic Resources 6.8 was used for the functional analysis of DEGs. Gene enrichment analysis was estimated in DAVID using the default zebrafish background setting the enrichment significances to a false discovery ratio (FDR) ≤ 5%. Identified modules with at least four hits were included in the network analysis, using the *reshape2* and *igraph* packages in R (R_Development_Core_Team, 2008). Graphs were elaborated from an incidence table of genes (represented by their official gene names, ZFIN.org) using the *igraph* package. Any two given genes were considered linked if they shared at least one common KEGG or GO (Gene Ontology) module. Metabolic pathways were obtained from the KEGG (Kyoto Encyclopedia of Genes and Genomes) database.

2.5.3. Benchmark dose and point of departure determination

Benchmark doses (BMD) for both morphometric and RNAseq data were calculated using the BMDExpress 2.2 sofware (https://www.sciome.com/bmdexpress/)(Phillips et al., 2018; Yang et al., 2007). Benchmark dose lower confidence limits (BMDLs) were calculated to stablish a reference dose or point of departure (PoD) for both datasets (Bhat et al., 2013; EPA, 2012; Farmahin et al., 2017; Webster et al., 2015).

3. Results and discussion

3.1. Survival and morphometric analyses

No statistically significant differences (non-parametric Kruskal-Wallis test, $p > 0.05$) were observed in hatching rates at PFOS concentrations up to 100 mg/L (Supplementary Fig. SF1A). On the other hand, we observed a significant increase in mortality rates at 5 dpf when embryos were exposed to 7.5, 10 and 100 mg/L and estimated LC50 at 9.1 mg/L. Swim bladder inflation was reduced at PFOS concentrations equal or higher than 2.5 mg/L, at both 4 and 5 dpf. Other lethal endpoints such as lack of heartbeat, coagulated embryos, lack of somite formation, or non-detachment of the tail, were not observed.

Several sublethal morphological changes, like appearance of spinal deformities (bent spine) and scoliosis, reduction of body length (BL), reduction of eye-snout distance (ESD), decrease in swim bladder area (SBA) or increases in yolk sac area (YSA) were observed at 5 dpf at PFOs concentrations equal or higher than 5 mg/L (Fig. 1A–C,

Supplementary Table ST2). This result was in concordance with previous reports of skeletal deformations (scoliosis and kyphosis) induced by PFOS and other perfluorinated compounds in zebrafish embryos (Hagenaars et al., 2014). Other quantitative morphological parameters, like eye and head width (EW and HW, respectively) and inter-ocular distance (IOD), were reduced respect to the controls at concentrations equal or higher than 2.5 mg/L of PFOS (6–15%, 9–20% and 15–35% respectively, Fig. 1B, C), whereas reductions of the head-trunk angle (HTA) and eye length (EL) showed some significant variations at the 1 mg/L of PFOS concentration (Fig. 1B, C). Note that morphological parameters could not be determined at the highest concentrations (10 and 100 mg/L) due to their high rates of mortality (82 and 100%, respectively). Using the BMDExpress software we calculated PFOS BMDLs for all measured morphological features and found HTA and YSA as the most and less affected parameters, respectively ($BMDL_{HTA}$ = 1.27 mg/L, $BMDL_{YSA}$ = 5.78 mg/L). Taking this into account, we used the median BMDL of all morphological features to estimate 2.53 mg/L of PFOS as the morphologic point of departure (PoD) for our study. These results were consistent with previously reported LOAEC values of 1.0 mg/L for activity/behavior (Spulber et al., 2014), 1.0–2.0 mg/L for morphometric alterations (Hagenaars et al., 2014; Shi et al., 2008) or 1.66 mg/L for PFOS ototoxicity (Stengel et al., 2017). We also tested effects on olfactory epithelium and lateral line neuromasts, since they are considered as sensitive markers for neurotoxic or cytotoxic effects of PFOS and other toxicants in zebrafish (Chen and Reese, 2013; de Esch et al., 2012; EPA, 2018; Hirose et al., 2011; Sato et al., 2009). Using immunochemical techniques, we observed no evident effects on the olfactory epithelium or on lateral line neuromasts at PFOS concentrations up to 1.0 mg/L, indicating lack of neurotoxicity at this PFOS concentration range (Fig. 1D). Taking into consideration all the above exposed reasons, we selected 1.0 mg/L as the maximum PFOS concentration used for the exposures in the transcriptomic study.

3.2. Transcriptome analyses

The ANOVA-PLS analysis identified 1434 transcripts as DEGs in at least one of the exposure groups with respect to the others. Hierarchical clustering of DEGs showed that the expression profiles of the selected DEGs closely reflected the experimental setup, as the different biological replicates for all treatment groups fell into the same hierarchical cluster (Fig. 2A, note that the white cells corresponds to the averaged control levels and red and blue cells, correspond to over- and under-

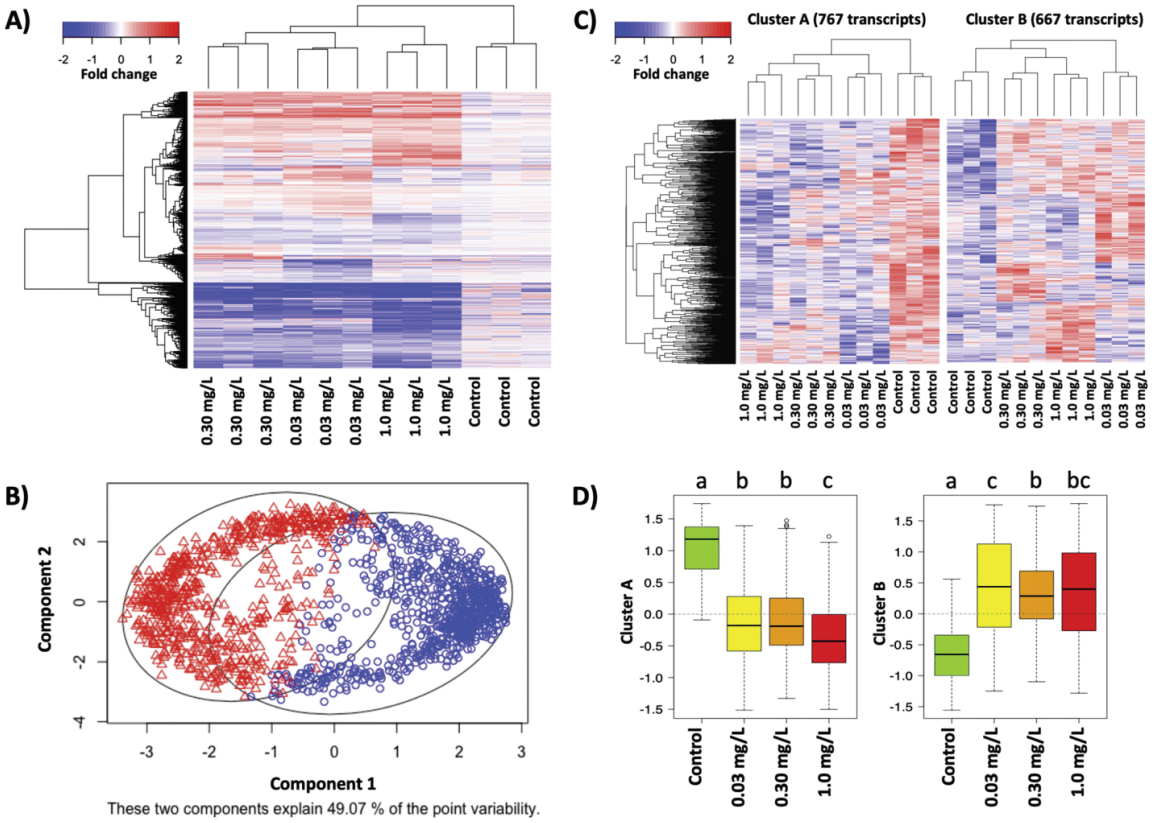

Fig. 2. Effects of PFOS on zebrafish embryo transcriptome. A) Heatmap showing concentration changes corresponding to the 1434 transcripts identified by ANOVA-PLS as differentially expressed genes (DEGs) in at least one of the experimental groups. Values were centered to the average of control samples and log2 transformed. Color scale ranges from blue (strongly underexpressed relative to control) to red (strongly overexpressed); white cells correspond to control values (fold change = 0). Both rows (genes) and columns (samples) were grouped by hierarchical clustering; the corresponding dendrograms are shown at the left and the top of the panel, respectively. B) Results from medoid PAM clustering of DEGs by PCA analysis showing the two defined clusters labeled in blue and red (clusters A and B, respectively). The two first components (PC1 and PC2) of the PCA explained 49.07% of total variability. C) Heatmaps of the genes classified in cluster A (left) and B (right) by the medoid PAM clustering of DEGs; legend as in Panel A. D) Normalized abundance values for all the genes included in each of the two clusters (cluster A at left, which contains the underexpressed genes due to PFOS exposure, and cluster B at right, where the genes that enhance their abundance among the exposure are placed). Low-case letters at the top of each graph indicate statistical differences (parametric ANOVA + Tukey's B post-hoc test with all pairwise comparisons, $p \leq 0.05$). Boxes include values between the 1st and 3rd quartiles, thick bars indicate average values and whiskers cover the total distribution, except for outliers (circles). (For interpretation of the references to color in this figure legend, the reader is referred to the web version of this article.)

expressed transcripts, respectively). Unexposed control samples appeared as a clearly differentiated group from the exposed ones. PAM clustering confirmed this rather gradual dose-response pattern by defining two clusters, A and B, corresponding to genes whose abundances decreased (767 genes) or increased (667 genes) upon PFOS exposure, respectively (Fig. 2B–D). Note that the samples of each exposure group clustered together in both clusters. Cluster A showed a clear separation between control and exposed samples, whereas the two highest doses (0.30 and 1.0 mg/L) separated from the 0.03 mg/L group. Cluster B shows a slightly different grouping of samples, as controls and the low dose (0.03 mg/L) clustered separately from the 0.30 and 1.0 mg/L groups. Fig. 2D shows the distribution of normalized expression values (mean = 0, standard deviation = 1) for all genes in both clusters and reflects the higher difference in the under-expression of the genes (cluster A) between non-treated (control) and treated samples than those among the different dose groups. The dose-response pattern is less evident in cluster B. We thus conclude that the LOAEC for transcriptomic effects of PFOS (at least, for the major part of it) is likely below 0.03 mg/L (30 ppb), as these samples separated themselves from controls. Moreover, we estimated 0.011 mg/L of PFOS (11 ppb) as PFOS transcriptomic PoD, about a third of the lowest concentration used in the transcriptomic study (Supplementary Fig. SF1B). This is >200 fold lower than the estimated PoD value for morphometric changes (Supplementary Fig. SF1B), and lower than the reported limit of detection for transcriptomic effects of PFOS by targeted analyses (0.10 mg/L, (Jantzen et al., 2016; Shi et al., 2008). RNA-seq transcriptomic data exposed in this study was confirmed by RT-qPCR (Supplementary Methods, Supplementary Fig. SF2, Supplementary Table ST3) showing a strong correlation between both techniques in several selected genes ($r^2 = 0.814$, $p < 10^{-4}$).

3.3. Functional analysis

DAVID functional analysis showed a relatively small subset of functional classes significantly enriched either in any of the two clusters or in the whole DEGs subset (Table 1, see also Fig. 3A and Supplementary Table ST4). Particularly notable is the case for over-represented transcripts (Cluster B), in which all significantly enriched functional classes were related to lipid transport and/or metabolism (Table 1). This is consistent with the known disruption of lipid homeostasis by PFOS and other structurally-related compounds in vertebrates (Das et al., 2017; Huang et al., 2016), and it shows a similar pattern as the lipid metabolism/transport transcriptomic effects induced by other EDCs like Bisphenol A (Martínez et al., 2018) (Supplementary Fig. SF3, $r^2 = 0.678$, $p < 10^{-4}$). The presence of yolk sac remains observed in the present study (Section 3.2.) is also in agreement with the alterations in the lipid homeostasis shown at the transcriptomic level.

Several functional modules associated to Cluster A were identified by DAVID analysis, although most of them corresponded to structural, rather than functional categories (Table 1, Fig. 3A). For example, the observed transcriptomic dysregulations in myosin, actin and tropomyosin transcripts (Supplementary Fig. SF4) are in agreement with the observed spinal deformities (Section 3.2.), which have been in turn related to alterations in myosin and other muscle fibers (Huang et al., 2010). As it can be observed in Supplementary Fig. SF4, genes in cluster A exhibited a classic dose-response pattern, increasing their expression according to the PFOS exposure. Nevertheless, the relationship between the dysregulation of these genes and the effects on the spinal cord and tail structure need to be confirmed by a further specific research.

Most enriched functional categories in Cluster A (KEGG or GO_BP terms) appeared related to the immunological system and/or pathogen response, including several cytokines, cytokine signaling-related proteins, proteases implicated to antigen presentation, or the JAK-STAT signaling pathway (Table 1). This is consistent with the known dysregulation of the immune system caused by PFOS and other perfluorinated substances, which includes changes in cytokines production (DeWitt et al., 2009; Lau et al., 2007; Peden-Adams et al., 2008; Suo et al., 2017). Structurally-defined modules (INTERPRO or GO_MF terms in Table 1) included a relatively large group of genes associated to the structural domain B30.2/SPRY and Zn-ion binding proteins, among

Table 1
David Functional Analysis[a] results for both gene clusters, individual and combined (only results with FDR ≤ 5%).

Category	Term	# of DEGs	Fold Enrichment	p value	FDR
Cluster 1 (underrepresented in treated samples relative to controls)					
INTERPRO	IPR001870:B30.2/SPRY domain	24	3.5	4.32E-07	6.66E-04
INTERPRO	IPR006574:SPRY-associated	20	3.4	9.36E-06	0.014
KEGG_PATHWAY	dre04630:Jak-STAT signaling pathway	12	5.2	1.59E-05	0.017
INTERPRO	IPR003877:SPla/RYanodine receptor SPRY	20	3.2	1.48E-05	0.023
INTERPRO	IPR001507:Zona pellucida domain	9	6.4	7.75E-05	0.120
GOTERM_BP_DIRECT	GO:0016567~protein ubiquitination	16	3.4	9.09E-05	0.133
INTERPRO	IPR003879:Butyrophylin-like	18	3.0	1.10E-04	0.169
GOTERM_BP_DIRECT	GO:0019885~antigen processing and presentation of endogenous peptide antigen via MHC class I	4	25.7	3.52E-04	0.515
INTERPRO	IPR013320:Concanavalin A-like lectin/glucanase	25	2.2	4.27E-04	0.656
GOTERM_MF_DIRECT	GO:0008270~zinc ion binding	47	1.6	0.002	2.160
KEGG_PATHWAY	dre04060:Cytokine-cytokine receptor interaction	11	3.2	0.002	2.341
INTERPRO	IPR011029:Death-like domain	9	3.7	0.003	4.393
GOTERM_BP_DIRECT	GO:0007160~cell-matrix adhesion	6	5.9	0.003	4.807
Cluster 2 (overrepresented in treated samples relative to controls)					
GOTERM_MF_DIRECT	GO:0008374~O-acyltransferase activity	5	11.5	7.98E-04	1.149
UP_KEYWORDS	Lipid transport	6	7.6	0.001	1.335
GOTERM_BP_DIRECT	GO:0006869~lipid transport	8	5.1	9.50E-04	1.408
KEGG_PATHWAY	dre00564:Glycerophospholipid metabolism	9	4.0	0.002	1.748
Clusters 1 + 2					
KEGG_PATHWAY	dre04060:Cytokine-cytokine receptor interaction	19	2.6	2.48E-04	0.285
KEGG_PATHWAY	dre04630:Jak-STAT signaling pathway	15	3.1	2.67E-04	0.307
GOTERM_MF_DIRECT	GO:0008374~O-acyltransferase activity	7	7.6	2.13E-04	0.324
UP_KEYWORDS	Signal	218	1.2	9.33E-04	1.178
GOTERM_CC_DIRECT	GO:0005615~extracellular space	40	1.7	0.001	1.531
GOTERM_MF_DIRECT	GO:0004888~transmembrane signaling receptor activity	24	2.1	0.001	2.160
GOTERM_BP_DIRECT	GO:0051607~defense response to virus	8	4.6	0.002	2.354
INTERPRO	IPR011029:Death-like domain	13	2.9	0.002	2.611

A complete version of this table is shown as Supplementary material (Table ST4).
[a] https://david.ncifcrf.gov

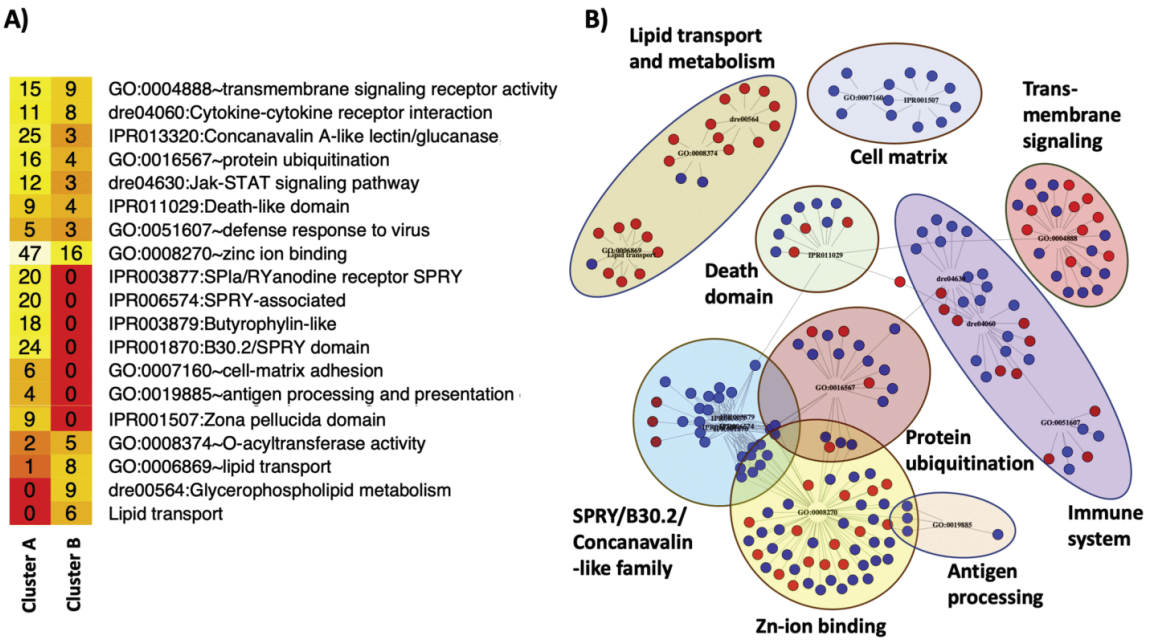

Fig. 3. Functional analyses of the genes categorized as DEGs, distributed in clusters as previously shown in Fig. 2. A) Distribution of DEGs among the two defined clusters (columns) and the different functional modules (rows). Only clusters with at least four hits in at least one of the clusters are shown. For simplicity, the "Signal" keyword module included in Table 1 was not considered in the figure. Numbers indicate the number of DEGs for each functional module classified in cluster A (left) or B (right). Cell colors represent the relative importance of transcripts associated to each pathway for each cluster (as a heat code: from red -less importance- to white -more importance-). Two cells with the same color correspond to identical fraction of DEGs (i.e. the same importance). Complete David Functional Analysis can be found at Table 1. B) Network representation of DEGs, which are represented by dots and colored as before (cluster A in blue and cluster B in red). Networking was carry out according to the adscription of the DEGs to functional modules (GO:biological process and KEGG databases were used, codes for each module are given as nodes). Color ellipses encircle groups of functional modules with particular interest and relevance (see Section 3.4). (For interpretation of the references to color in this figure legend, the reader is referred to the web version of this article.)

others. While the structural domain B30.2/SPRY have been reported to be involved in immunity and immunoglobulins (D'Cruz et al., 2013; Howe et al., 2016; Woo et al., 2006), zinc fingers (structural motif of the proteins which Zn binds to) have an extraordinary diversity of both structures and functions (Kluska et al., 2018; Laity et al., 2001).

Considering the whole DEG dataset, more general functions appear, including signaling, extracellular space and transmembrane receptor activity. Inspection of the genes identified by their structural, rather than functional characteristics, revealed the biological processes potentially affected by their de-regulation. These interdependences can be visualized in the network shown in Fig. 3B. For example, the structural class "IPR001507: Zona pellucida domain" shares some genes with the functional class "cell-matrix adhesion" (both in cluster A), suggesting alterations in cell-cell interactions. Similarly, the structural class "IPR011029: Death-like domain" may be related to programmed cell-death pathways, as most of the 13 genes identified as DEGs are also related to caspase recruitment, apoptosis, or TNF (tumor necrosis factor) activation (Table 1). This is consistent with previous studies in cells (Cui et al., 2017; Shi et al., 2008; Zhang et al., 2013) and zebrafish (Shi et al., 2008). Particularly noticeable is the structural-based module "IPR001870:B30.2/SPRY domain" that, together with closely-related structural terms (IPR003879 and IPR013320, among others), includes many components of the so-called TRIM protein family, a group of E3-ligase proteins functionally related to the innate immunity development (Versteeg et al., 2013) (Table 1). Most detected members of this family corresponded to the fish-specific finTRIM subfamily (FTR genes, Table 1), also putatively related to different aspects of the fish immune response (van der Aa et al., 2012). Also members of the TRIM family are the *bloodthirsty* (*btr*) genes, orthologous to the human TRIM39 protein and also potentially related with the above mentioned immune response (Luo et al., 2017; van der Aa et al., 2012; Zhang et al., 2015). All these genes appeared as down-regulated by the exposure to PFOS (Fig. 3, note that they are placed in cluster A).

Cell adhesion, another of the affected pathways in our study, is mediated by four major protein superfamilies (immunoglobulins, selectins, cadherins and integrins; a.k.a. CAMs). Immunoglobulins and selectins are involved in the immune response (Mashoof and Criscitiello, 2016; Roca et al., 2008; Sun et al., 2015); cadherins in the actin fibers linkeage through catenins (Li-Villarreal et al., 2015); and integrins facilitate the extracellular matrix adhesion, also activating the signaling transduction pathways including the apoptosis signals, among others (Mould et al., 2006). We observed that all those pathways were transcriptionally affected by PFOS (Table 1, Fig. 3). Although the data suggests the existence of a PFOS-induced initial toxic event related to cell adhesion and/or the signaling pathways, further studies are required in order to achieve a deeper comprehension about its mode of action.

It is remarkable how interweaved were the observed transcriptomics effects with themselves and with the phenotypic alterations, suggesting a common initial triggering point. For example, the structural and functional diversity of lectins (the above mentioned IPR013320 structural term is a subgroup of them) have been previously studied in teleost fish, showing their involvement not only in the immune response (Vasta et al., 2011), but also in lipid regulation (Cambi et al., 2005; Ng et al., 1989), and that lectin malfunction may result in bent tails and other skeletal muscle problems in zebrafish (Ahmed et al., 2009), which are similar to the ones observed in our exposed animals.

3.4. Toxicological relevance

Many animal and in vitro human systems indicate that exposure to PFOS may result in neurotoxicity, immunotoxicity, thyroid disruption, reproductive, cardiovascular and pulmonary toxicity, and diverse toxic effects in liver and kidneys (Das et al., 2017; DeWitt et al., 2009; Lau et al., 2007; Suo et al., 2017; Zeng et al., 2019). These studies suggest that PFOS represent a significant hazard for human health. This has been at least partially confirmed by the still scarce epidemiological studies, being water and food the two main sources of exposure (Zeng et al., 2019). In addition to their implication for human health, the wide use, high persistence, and bioaccumulative properties of PFOS and other PFAS implicate that they are ubiquitous in the environment, and in particular, in aquatic bodies. PFOS and other PFAS has been detected in fish and marine mammal and bird tissues at ng-μg/g ww levels (Ahrens and Bundschuh, 2014; Giesy and Kannan, 2001; Houde et al., 2011; Lau et al., 2007; Rodriguez-Jorquera et al., 2016). Both molecular and macroscopic effects have been reported for PFOS and other perfluoroorganic compounds in zebrafish embryos and adults (Chen et al., 2013; Cui et al., 2017; Fai Tse et al., 2016; Hagenaars et al., 2014; Lau et al., 2007; Shi et al., 2009). Similar effects have been reported in fathead minnows (*Pimephales promelas*) exposed to urban wastewaters presenting from ng to μg/L levels of different PFAS (Rodriguez-Jorquera et al., 2015). In addition, there is a growing evidence of toxic effects of perflouroorganic compounds in invertebrates and plants (Giesy et al., 2010; Li, 2009; Stylianou et al., 2019). Therefore, we consider that our findings reflect toxic effects relevant not only for human health, but also for the environment.

Lipid metabolism, immunological response and transmembrane/intracellular signaling appeared as the main cellular functions affected by PFOS exposure at the molecular level (Das et al., 2017; DeWitt et al., 2009; Lau et al., 2007; Suo et al., 2017). The favorite mechanism of action (MoA) proposed for PFOS toxicity involves its interaction with nuclear receptors intimately involved in metabolic regulation and immunological functions, like PPARα (peroxisome proliferator activating receptor), CAR (constitutive androstane receptor), PXR (pregnane X receptor) or FXR (farnesoid X receptor) (Lau et al., 2007; White et al., 2011). While our experimental approach does not allow the characterization of the molecular mechanisms underlying the observed changes, they are essentially consistent with this MoA, which explain the simultaneous deregulation of genes involved in lipid metabolism and immuno response, among others. The effect of PFOS on lipid metabolism (including glycerophospholipids) of zebrafish embryos was also observed at the metabolic level (Ortiz-Villanueva et al., 2018), and it is likely related to the observed changes in yolk sac absorption. Therefore, our data show essentially the same kind of responses at gene expression, metabolism and morphological level.

PFOS is usually found at low levels (in the range of ng/L) in surface waters (Kunacheva et al., 2011; Vedagiri et al., 2018), particularly those under the influence of sewage treatment plants (Rodriguez-Jorquera et al., 2015; Rodriguez-Jorquera et al., 2016). However, PFOS is considered a persistent pollutant and its high bioaccumulation and low elimination rates (Huang et al., 2010; Kannan et al., 2005) cause PFOS to be found at very high levels (0.05–5.0 mg/kg) in wildlife (Hoff et al., 2005). It has been reported a 10-fold bioaccumulation between the water and exposed-whole zebrafish larvae tissues in only 5 days of PFOS exposure (Huang et al., 2010). Our PoD values for PFOS estimated from either morphometric (2.53 mg/L) or transcriptional data (0.011 mg/L) were higher than the environmental limits established for drinking water (10^{-5}–10^{-4} mg/L) according to both EPA and EFSA, as well as other regulatory agencies (EC, 2004; Grandjean, 2018). Nevertheless, exposure routes for PFOS are diverse, and there are considerably higher legal limits for some purposes, like the 10 mg/kg limit for substances and preparations in the EU (EC, 2004). Regarding internal exposure levels, several studies have observed concentrations from 0.002 mg/L to 0.080 mg/L of PFOS in human serum of individuals from Asia, North America and Europe (Alexander et al., 2008; Jin et al., 2007; Vedagiri et al., 2018; Zeng et al., 2015) and even higher concentrations (0.145–0.381 mg/kg) in fish eggs (Kannan et al., 2005). This indicates that both humans and wildlife may be exposed to PFOS concentrations similar to or even higher than our calculated transcriptomic PoD value. Barring the need for dose-conversion and pharmacokinetics modeling to extrapolate the effects in zebrafish to humans, our results supported a very low safety margin, as they could imply that the immune system of exposed individuals, among others systems, could be affected at least at the transcriptomic level. In this regard, the suppression of immunological responses by different pollutants has been largely neglected until very recently, partially because the lack of an appropriate animal or cell models for its toxicological assessment (Möller et al., 2014; Rehberger et al., 2017; Segner et al., 2017). However, there is an increasing amount of evidence that some pollutants may indeed decrease the ability of fish and other vertebrates to fend off challenging infections (Fang et al., 2013; Quesada-Garcia et al., 2016). In the same direction, a report from the USA National Toxicology program also identified immunotoxicity as an emerging adverse effect of perfluorinated substances in humans (NPT, 2016). For all those reasons, we propose the inclusion of immunotoxicity tests in the existing zebrafish embryo testing schemes, which currently cover cardiovascular, nervous, neuromuscular, gastrointestinal and thyroid systems (Raldúa and Piña, 2014), to assess toxic effects of different substances in humans and other vertebrates.

4. Conclusions

Our results suggest a complex, multiple endocrine disruption-like toxic effects at concentrations well below the LOAEC/NOAEC for many of the macroscopic effects traditionally linked to PFOS toxicity in zebrafish embryos. While our results confirm the known effect of PFOS in the spinal cord, and its potential role as lipid disruptor, we found a significant decrease in the expression of many genes related to natural immunity and defense against infections, previously reported in other organisms. Therefore, we suggest that a common initial key event may trigger all observed adverse effects elicited by exposure to PFOS. We propose that the transcriptional pattern may be a marker for the immunotoxic effects of PFOS and other related substances in fish and other vertebrates, including humans. As the estimated PoD values for transcriptional changes occurred at concentrations already found in living organisms, including humans, our data suggest that current maximal tolerable levels may not protect adequately environmental and human health and might need to be revised.

Conflicts of interest

The authors declare that they have no conflicts of interest.

Acknowledgements

This work was supported by European Union's Seventh Framework Programme (FP/2007-2013)/ERC Grant Agreement n. 320737, and by the Spanish Ministry of Economy and Competitiveness (CTM2014-51985-R). AEC acknowledges the funding from ISCIII (Spanish Ministry of Economy and Competitiveness, grant number PT17/0009/0019), co-financed by the European Fund for Regional Development (FEDER). LNM was supported by a Beatriu de Pinos Postdoctoral Fellowship (2013BP-B-00088) funded by the Secretary for Universities and Research of the Department of Economy and Knowledge of the Government of Catalonia and the Cofund programme of the Marie Curie Actions of the 7th R&D Framework Programme of the European Union. RML was supported by an FPU Fellowship (FPU15/03332) from the Spanish Ministry of Education, Culture and Sport.

Appendix A. Supplementary data

Supplementary data to this article can be found online at https://doi.org/10.1016/j.scitotenv.2019.04.200.

References

Ahmed, H., Du, S.J., Vasta, G.R., 2009. Knockdown of a Galectin-1-like Protein in Zebrafish (*Danio rerio*) Causes Defects in Skeletal Muscle Development. 3 ed. pp. 277–283.

Ahrens, L., Bundschuh, M., 2014. Fate and effects of poly- and perfluoroalkyl substances in the aquatic environment: a review. Environ. Toxicol. Chem. 33, 1921–1929.

Alexander, J., Atli Auðunsson, G., Benford, D., Cockburn, A., Cravedi, J.-P., Dogliotti, E., Di Domenico, A., Luisa Fernández-Cruz, M., Fink-Gremmels, J., Fürst, P., Galli, C., Grandjean, P., Gzyl, J., Heinemeyer, G., Johansson, N., Mutti, A., Schlatter, J., van Leeuwen, R., van Peteghem, C., Verger, P., 2008. Perfluorooctane sulfonate (PFOS), perfluorooctanoic acid (PFOA) and their salts scientific opinion of the panel on contaminants in the food chain. EFSA J. 6, 1–131.

Ankley, G.T., Kuehl, D.W., Kahl, M.D., Jensen, K.M., Linnum, A., Leino, R.L., Villeneuve, D.A., 2005. Reproductive and developmental toxicity and bioconcentration of perfluorooctanesulfonate in a partial life-cycle test with the fathead minnow (Pimephales promelas). Environ. Toxicol. Chem. 24, 2316–2324.

Arvaniti, O.S., Stasinakis, A.S., 2015. Review on the occurrence, fate and removal of perfluorinated compounds during wastewater treatment. Sci. Total Environ. 524, 81–92.

Avdesh, A., Chen, M., Martin-Iverson, M.T., Mondal, A., Ong, D., Rainey-Smith, S., Taddei, K., Lardelli, M., Groth, D.M., Verdile, G., Martins, R.N., 2012. Regular care and maintenance of a zebrafish (Danio rerio) laboratory: an introduction. J. Vis. Exp. e4196.

Baker, M.E., Hardiman, G., 2014. Transcriptional analysis of endocrine disruption using zebrafish and massively parallel sequencing. J. Mol. Endocrinol. 52, R241–R256.

Bhat, V.S., Hester, S.D., Nesnow, S., Eastmond, D.A., 2013. Concordance of transcriptional and apical benchmark dose levels for conazole-induced liver effects in mice. Toxicol. Sci. 136, 205–215.

Caballero-Gallardo, K., Olivero-Verbel, J., Freeman, J.L., 2016. Toxicogenomics to evaluate endocrine disrupting effects of environmental chemicals using the zebrafish model. Current genomics 17, 515–527.

Cambi, A., Koopman, M., Figdor, C.G., 2005. How C-type lectins detect pathogens, pp. 481–488.

Chaparro-Ortega, A., Betancourt, M., Rosas, P., Vázquez-Cuevas, F.G., Chavira, R., Bonilla, E., Casas, E., Ducolomb, Y., 2018. Endocrine disruptor effect of perfluorooctane sulfonic acid (PFOS) and perfluorooctanoic acid (PFOA) on porcine ovarian cell steroidogenesis. Toxicol. in Vitro 46, 86–93.

Chen, Y., Reese, D.H., 2013. A screen for disruptors of the retinol (vitamin A) signaling pathway. Birth Defects Research Part B-Developmental and Reproductive Toxicology 98, 276–282.

Chen, J., Das, S.R., La Du, J., Corvi, M.M., Bai, C., Chen, Y., Liu, X., Zhu, G., Tanguay, R.L., Dong, Q., Huang, C., 2013. Chronic PFOS exposures induce life stage-specific behavioral deficits in adult zebrafish and produce malformation and behavioral deficits in F1 offspring. Environ. Toxicol. Chem. 32, 201–206.

Chen, J., Tanguay, R.L., Tal, T.L., Gai, Z., Ma, X., Bai, C., Tilton, S.C., Jin, D., Yang, D., Huang, C., Dong, Q., 2014. Early life perfluorooctanesulphonic acid (PFOS) exposure impairs zebrafish organogenesis. Aquat. Toxicol. 150, 124–132.

Corsini, E., Avogadro, A., Galbiati, V., dell'Agli, M., Marinovich, M., Galli, C.L., Germolec, D.R., 2011. In vitro evaluation of the immunotoxic potential of perfluorinated compounds (PFCs). Toxicol. Appl. Pharmacol. 250, 108–116.

Cui, Y., Lv, S., Liu, J., Nie, S., Chen, J., Dong, Q., Huang, C., Yang, D., 2017. Chronic perfluorooctanesulfonic acid exposure disrupts lipid metabolism in zebrafish. Human & Experimental Toxicology 36, 207–217.

Das, K.P., Wood, C.R., Lin, M.T., Starkov, A.A., Lau, C., Wallace, K.B., Corton, J.C., Abbott, B.D., 2017. Perfluoroalkyl acids-induced liver steatosis: effects on genes controlling lipid homeostasis. Toxicology 378, 37–52.

D'Cruz, A.A., Babon, J.J., Norton, R.S., Nicola, N.A., Nicholson, S.E., 2013. Structure and Function of the SPRY/B30.2 Domain Proteins Involved in Innate Immunity. Wiley-Blackwell, pp. 1–10.

van der Aa, L.M., Jouneau, L., Laplantine, E., Bouchez, O., Van Kemenade, L., Boudinot, P., 2012. FinTRIMs, fish virus-inducible proteins with E3 ubiquitin ligase activity. Developmental & Comparative Immunology 36, 433–441.

DeWitt, J.C., Shnyra, A., Badr, M.Z., Loveless, S.E., Hoban, D., Frame, S.R., Cunard, R., Anderson, S.E., Meade, B.J., Peden-Adams, M.M., Luebke, R.W., Luster, M.I., 2009. Immunotoxicity of Perfluorooctanoic Acid and Perfluorooctane Sulfonate and the Role of Peroxisome Proliferator-Activated Receptor Alpha. pp. 76–94.

DeWitt, J.C., Williams, W.C., Creech, N.J., Luebke, R.W., 2016. Suppression of antigen-specific antibody responses in mice exposed to perfluorooctanoic acid: role of PPAR alpha and T- and B-cell targeting. J. Immunotoxicol. 13, 38–45.

Dobin, A., Davis, C.A., Schlesinger, F., Drenkow, J., Zaleski, C., Jha, S., Batut, P., Chaisson, M., Gingeras, T.R., 2013. STAR: Ultrafast universal RNA-seq aligner. Bioinformatics 29, 15–21.

Du, G., Hu, J., Huang, H., Qin, Y., Han, X., Wu, D., Song, L., Xia, Y., Wang, X., 2013. Perfluorooctane sulfonate (PFOS) affects hormone receptor activity, steroidogenesis, and expression of endocrine-related genes in vitro and in vivo. Environ. Toxicol. Chem. 32, 353–360.

EC, 2004. In: Council, E.P.a (Ed.), Regulation (EC) no 850/2004 of the European Parliament and of the Council of 29 April 2004 on Persistent Organic Pollutants and Amending Directive 79/117/EEC. European Commission, Brussels (Belgium).

Edgar, R., Domrachev, M., Lash, A.E., 2002. Gene expression omnibus: NCBI gene expression and hybridization array data repository. Nucleic Acids Res. 30, 207–210.

EPA, R.A.F., 2012. Benchmark dose technical guidance. In: Agency, U.E.P. (Ed.), EPA/100/R-12/001. EPA, Washington, D.C.

EPA, R.A.F., 2018. In: Agency, U.S.E.P. (Ed.), Exposure to PFOS, PFHxS, or PFHxA, but Not GenX, Nafion BP1, or ADONA, Elicits Developmental Neurotoxicity in Larval Zebrafish.

de Esch, C., Slieker, R., Wolterbeek, A., Woutersen, R., de Groot, D., 2012. Zebrafish as potential model for developmental neurotoxicity testing: a mini review. Neurotoxicol. Teratol. 34, 545–553.

European Commission, D.E., 2000. Towards the Establishment of a Priority List of Substances for Further Evaluation of their Role in Endocrine Disruption.

Fai Tse, W.K., Li, J.W., Kwan Tse, A.C., Chan, T.F., Hin Ho, J.C., Sun Wu, R.S., Chu Wong, C.K., Lai, K.P., 2016. Fatty liver disease induced by perfluorooctane sulfonate: novel insight from transcriptome analysis. Chemosphere 159, 166–177.

Fang, C., Huang, Q.S., Ye, T., Chen, Y.J., Liu, L.P., Kang, M., Lin, Y., Shen, H.Q., Dong, S.J., 2013. Embryonic exposure to PFOS induces immunosuppression in the fish larvae of marine medaka. Ecotoxicol. Environ. Saf. 92, 104–111.

Farmahin, R., Williams, A., Kuo, B., Chepelev, N.L., Thomas, R.S., Barton-Maclaren, T.S., Curran, I.H., Nong, A., Wade, M.G., Yauk, C.L., 2017. Recommended approaches in the application of toxicogenomics to derive points of departure for chemical risk assessment. Arch. Toxicol. 91, 2045–2065.

Fresno, C., Balzarini, M.G., Fernandez, E.A., 2014. lmdme: linear models on designed multivariate experiments in R. J. Stat. Softw. 56, 1–16.

Giesy, J.P., Kannan, K., 2001. Global distribution of perfluorooctane sulfonate in wildlife. Environmental Science & Technology 35, 1339–1342.

Giesy, J.P., Naile, J.E., Khim, J.S., Jones, P.D., Newsted, J.L., 2010. Aquatic toxicology of perfluorinated chemicals. In: Whitacre, D.M. (Ed.), Reviews of Environmental Contamination and Toxicology. vol 202. Springer, New York, pp. 1–52.

Grandjean, P., 2018. Delayed discovery, dissemination, and decisions on intervention in environmental health: a case study on immunotoxicity of perfluorinated alkylate substances. Environ. Health 17, 62.

Hagenaars, A., Stinckens, E., Vergauwen, L., Bervoets, L., Knapen, D., 2014. PFOS affects posterior swim bladder chamber inflation and swimming performance of zebrafish larvae. Aquat. Toxicol. 157, 225–235.

Hill, A.J., Teraoka, H., Heideman, W., Peterson, R.E., 2005. Zebrafish as a model vertebrate for investigating chemical toxicity, pp. 6–19.

Hirose, Y., Simon, J.A., Ou, H.C., 2011. Hair cell toxicity in anti-cancer drugs: evaluating an anti-cancer drug library for independent and synergistic toxic effects on hair cells using the zebrafish lateral line. Jaro-Journal of the Association for Research in Otolaryngology 12, 719–728.

Hoff, P.T., Van Campenhout, K., Van De Vijver, K., Covaci, A., Bervoets, L., Moens, L., Huyskens, G., Goemans, G., Belpaire, C., Blust, R., De Coen, W., 2005. Perfluorooctane sulfonic acid and organohalogen pollutants in liver of three freshwater fish species in Flanders (Belgium): relationships with biochemical and organismal effects. Environ. Pollut. 137, 324–333.

Houde, M., De Silva, A.O., Muir, D.C.G., Letcher, R.J., 2011. Monitoring of perfluorinated compounds in aquatic biota: an updated review PFCs in aquatic biota. Environmental Science & Technology 45, 7962–7973.

Howe, K., Schiffer, P.H., Zielinski, J., Wiehe, T., Laird, G.K., Marioni, J.C., Soylemez, O., Kondrashov, F., Leptin, M., 2016. Structure and evolutionary history of a large family of NLR proteins in the zebrafish. Open Biol. 6, 160009.

Huang, H., Huang, C., Wang, L., Ye, X., Bai, C., Simonich, M.T., Tanguay, R.L., Dong, Q., 2010. Toxicity, uptake kinetics and behavior assessment in zebrafish embryos following exposure to perfluorooctanesulphonicacid (PFOS). Aquat. Toxicol. 98, 139–147.

Huang, S.S.Y., Benskin, J.P., Chandramouli, B., Butler, H., Helbing, C.C., Cosgrove, J.R., 2016. Xenobiotics produce distinct metabolomic responses in zebrafish larvae (Danio rerio). Environmental Science & Technology 50, 6526–6535.

Jantzen, C.E., Annunziato, K.A., Bugel, S.M., Cooper, K.R., 2016. PFOS, PFNA, and PFOA sublethal exposure to embryonic zebrafish have different toxicity profiles in terms of morphometrics, behavior and gene expression. Aquat. Toxicol. 175, 160–170.

Jensen, A.A., Leffers, H., 2008. Emerging Endocrine Disrupters: Perfluoroalkylated Substances. Int. J. Androl. 31, 161–169.

Jin, Y., Saito, N., Harada, K.H., Inoue, K., Koizumi, A., 2007. Historical trends in human serum levels of perfluorooctanoate and perfluorooctane sulfonate in Shenyang, China. Tohoku J. Exp. Med. 212, 63–70.

Kannan, K., Tao, L., Sinclair, E., Pastva, S.D., Jude, D.J., Giesy, J.P., 2005. Perfluorinated compounds in aquatic organisms at various trophic levels in a Great Lakes food chain. Arch. Environ. Contam. Toxicol. 48, 559–566.

Kato, K., Wong, L.-Y., Basden, B.J., Calafat, A.M., 2013. Effect of temperature and duration of storage on the stability of polyfluoroalkyl chemicals in human serum. Chemosphere 91, 115–117.

Kato, K., Ye, X., Calafat, A.M., 2015. PFASs in the General Population. pp. 51–76.

Kimmel, C.B., Ballard, W.W., Kimmel, S.R., Ullmann, B., Schilling, T.F., 1995. Stages of embryonic development of the zebrafish. Dev. Dyn. 203, 253–310.

Kluska, K., Adamczyk, J., Krężel, A., 2018. Metal binding properties, stability and reactivity of zinc fingers, pp. 18–64.

Kunacheva, C., Tanaka, S., Fujii, S., Boontanon, S.K., Musirat, C., Wongwattana, T., Shivakoti, B.R., 2011. Mass flows of perfluorinated compounds (PFCs) in central wastewater treatment plants of industrial zones in Thailand. Chemosphere 83, 737–744.

Lai, K.P., Ng, A.H.M., Wan, H.L., Wong, A.Y.M., Leung, C.C.T., Li, R., Wong, C.K.C., 2018. Dietary exposure to the environmental chemical, PFOS on the diversity of gut microbiota, associated with the development of metabolic syndrome. Front. Microbiol. 9, 11.

Laity, J.H., Lee, B.M., Wright, P.E., 2001. Zinc finger proteins: new insights into structural and functional diversity. Elsevier Current Trends 39–46.

Lau, C., 2015. Perfluorinated Compounds: An Overview. Humana Press, Cham, pp. 1–21.

Lau, C., Anitole, K., Hodes, C., Lai, D., Pfahles-Hutchens, A., Seed, J., 2007. Perfluoroalkyl acids: a review of monitoring and toxicological findings. Toxicol. Sci. 99, 366–394.
Li, M.H., 2009. Toxicity of perfluorooctane sulfonate and perfluorooctanoic acid to plants and aquatic invertebrates. Environ. Toxicol. 24, 95–101.
Li, B., Dewey, C.N., 2011. RSEM: accurate transcript quantification from RNA-Seq data with or without a reference genome. Bmc Bioinformatics 12, 323.
Li-Villarreal, N., Forbes, M.M., Loza, A.J., Chen, J., Ma, T., Helde, K., Moens, C.B., Shin, J., Sawada, A., Hindes, A.E., Dubrulle, J., Schier, A.F., Longmore, G.D., Marlow, F.L., Solnica-Krezel, L., 2015. Dachsous1b cadherin regulates actin and microtubule cytoskeleton during early zebrafish embryogenesis. Development 142, 2704–2718.
Loos, R., Carvalho, R., António, D.C., Comero, S., Locoro, G., Tavazzi, S., Paracchini, B., Ghiani, M., Lettieri, T., Blaha, L., Jarosova, B., Voorspoels, S., Servaes, K., Haglund, P., Fick, J., Lindberg, R.H., Schwesig, D., Gawlik, B.M., 2013. EU-wide monitoring survey on emerging polar organic contaminants in wastewater treatment plant effluents. Water Res. 47, 6475–6487.
Love, M.I., Huber, W., Anders, S., 2014. Moderated estimation of fold change and dispersion for RNA-seq data with DESeq2. Genome Biol. 15, 550.
Luo, K., Li, Y., Xia, L., Hu, W., Gao, W., Guo, L., Tian, G., Qi, Z., Yuan, H., Xu, Q., 2017. Analysis of the expression patterns of the novel large multigene TRIM gene family (finTRIM) in zebrafish. Fish & Shellfish Immunology 66, 224–230.
Lyu, X.-J., Li, W.-W., Lam, P.K.S., Yu, H.-Q., 2015. Insights into perfluorooctane sulfonate photodegradation in a catalyst-free aqueous solution. Sci. Rep. 5, 9353.
Martínez, R., Esteve-Codina, A., Herrero-Nogareda, L., Ortiz-Villanueva, E., Barata, C., Tauler, R., Raldúa, D., Piña, B., Navarro-Martín, L., 2018. Dose-dependent transcriptomic responses of zebrafish eleutheroembryos to bisphenol A. Environ. Pollut. 243, 988–997.
Mashoof, S., Criscitiello, M., 2016. Fish immunoglobulins. Biology 5, 45.
Möller, A.-M., Korytář, T., Köllner, B., Schmidt-Posthaus, H., Segner, H., 2014. The teleostean liver as an immunological organ: intrahepatic immune cells (IHICs) in healthy and benzo[a]pyrene challenged rainbow trout (Oncorhynchus mykiss). Developmental & Comparative Immunology 46, 518–529.
Mortazavi, A., Williams, B.A., McCue, K., Schaeffer, L., Wold, B., 2008. Mapping and quantifying mammalian transcriptomes by RNA-Seq. Nat. Methods 5, 621–628.
Mould, A.P., McLeish, J.A., Huxley-Jones, J., Goonesinghe, A.C., Hurlstone, A.F.L., Boot-Handford, R.P., Humphries, M.J., 2006. Identification of multiple integrin β1 homologs in zebrafish (Danio rerio). BMC Cell Biol. 7, 24.
Mushtaq, M.Y., Verpoorte, R., Kim, H.K., 2013. Zebrafish as a model for systems biology. Biotechnol. Genet. Eng. Rev. 29 (29), 187–205.
Ng, T.B., Li, W.W., Yeung, H.W., 1989. Effects of lectins with various carbohydrate binding specificities on lipid metabolism in isolated rat and hamster adipocytes. Int. J. Biochem. 21, 149–156.
NPT, National Toxicology Program, 2016. NTP Monograph: Immunotoxicity Associated with Exposure to Perfluorooctanoic Acid or Perfluorooctane Sulfonate. US Department of Human and Health Services.
OECD, 2002. Co-Operation on Existing Chemicals: Hazard Assessment of Perfluorooctane Sulfonate (PFOS) and its Salts. pp. 1–362.
OECD, 2013. Test No. 236: Fish Embryo Acute Toxicity (FET) Test. OECD Publishing.
Olsen, G.W., 2015. PFAS Biomonitoring in Higher Exposed Populations. Toxicological Effects of Perfluoroalkyl and Polyfluoroalkyl Substances. pp. 77–125.
Ortiz-Villanueva, E., Jaumot, J., Martinez, R., Navarro-Martin, L., Pina, B., Tauler, R., 2018. Assessment of endocrine disruptors effects on zebrafish (Danio rerio) embryos by untargeted LC-HRMS metabolomic analysis. Sci. Total Environ. 635, 156–166.
Paul, A.G., Jones, K.C., Sweetman, A.J., 2009. A first global production, emission, and environmental inventory for perfluorooctane sulfonate. Environmental Science & Technology 43, 386–392.
Peden-Adams, M.M., Keller, J.M., Eudaly, J.G., Berger, J., Gilkeson, G.S., Keil, D.E., 2008. Suppression of humoral immunity in mice following exposure to perfluorooctane sulfonate. Toxicol. Sci. 104, 144–154.
Phillips, J.R., Svoboda, D.L., Tandon, A., Patel, S., Sedykh, A., Mav, D., Kuo, B., Yauk, C.L., Yang, L., Thomas, R.S., Gift, J.S., Davis, J.A., Olysyzk, L., Merrick, B.A., Paules, R.S., Parham, F., Saddler, T., Shah, R.R., Auerbach, S.S., 2018. BMDExpress 2: enhanced transcriptomic dose-response analysis workflow. Bioinformatics https://doi.org/10.1093/bioinformatics/bty878 (Oxford, England).
Quesada-Garcia, A., Encinas, P., Valdehita, A., Baumann, L., Segner, H., Coll, J.M., Navas, J.M., 2016. Thyroid active agents T3 and PTU differentially affect immune gene transcripts in the head kidney of rainbow trout (Oncorynchus mykiss). Aquat. Toxicol. 174, 159–168.
R_Development_Core_Team, 2008. R: A Language and Environment for Statistical Computing. R Foundation for Statistical Computing, Vienna, Austria.
Raldúa, D., Piña, B., 2014. In vivo zebrafish assays for analyzing drug toxicity. Expert Opinion on Drug Metabolism and Toxicology 10, 685–697.
Raldua, D., Otero, D., Fabra, M., Cerda, J., 2008. Differential localization and regulation of two aquaporin-1 homologs in the intestinal epithelia of the marine teleost Sparus aurata. Am. J. Phys. Regul. Integr. Comp. Phys. 294, R993–R1003.
Rehberger, K., Werner, I., Hitzfeld, B., Segner, H., Baumann, L., 2017. 20 years of fish immunotoxicology – what we know and where we are. Crit. Rev. Toxicol. 47, 516–542.
Reuter, J.A., Spacek, D.V., Snyder, M.P., 2015. High-Throughput Sequencing Technologies.
Roca, F.J., Mulero, I., López-Muñoz, A., Sepulcre, M.P., Renshaw, S.A., Meseguer, J., Mulero, V., 2008. Evolution of the inflammatory response in vertebrates: fish TNF-alpha is a powerful activator of endothelial cells but hardly activates phagocytes. Journal of immunology (Baltimore, Md.: 1950) 181, 5071–5081.
Rodriguez-Jorquera, I.A., Kroll, K.J., Toor, G.S., Denslow, N.D., 2015. Transcriptional and physiological response of fathead minnows (Pimephales promelas) exposed to urban waters entering into wildlife protected areas. Environ. Pollut. 199, 155–165.
Rodriguez-Jorquera, I.A., Silva-Sanchez, C., Strynar, M., Denslow, N.D., Toor, G.S., 2016. Footprints of urban micro-pollution in protected areas: investigating the longitudinal distribution of perfluoroalkyl acids in wildlife preserves. PLoS One 11.
Rodriguez-Jorquera, I.A., Colli-Dula, R.C., Kroll, K., Jayasinghe, B.S., Marco, M.V.P., Silva-Sanchez, C., Toor, G.S., Denslow, N.D., 2019. Blood transcriptomics analysis of fish exposed to perfluoro alkyls substances: assessment of a non-lethal sampling technique for advancing aquatic toxicology research. Environmental Science & Technology 53, 1441–1452.
Sato, I., Kawamoto, K., Nishikawa, Y., Tsuda, S., Yoshida, M., Yaegashi, K., Saito, N., Liu, W., Jin, Y., 2009. Neurotoxicity of perfluorooctane sulfonate (PFOS) in rats and mice after single oral exposure. J. Toxicol. Sci. 34, 569–574.
Scholz, S., Mayer, I., 2008. Molecular biomarkers of endocrine disruption in small model fish. Mol. Cell. Endocrinol. 293, 57–70.
Segner, H., Verburg-van Kemenade, B.M.L., Chadzinska, M., 2017. The immunomodulatory role of the hypothalamus-pituitary-gonad axis: proximate mechanism for reproduction-immune trade offs? Developmental & Comparative Immunology 66, 43–60.
Shi, X.J., Du, Y.B., Lam, P.K.S., Wu, R.S.S., Zhou, B.S., 2008. Developmental toxicity and alteration of gene expression in zebrafish embryos exposed to PFOS. Toxicol. Appl. Pharmacol. 230, 23–32.
Shi, X., Yeung, L.W.Y., Lam, P.K.S., Wu, R.S.S., Zhou, B., 2009. Protein profiles in zebrafish (Danio rerio) embryos exposed to perfluorooctane sulfonate. Toxicol. Sci. 110, 334–340.
Spulber, S., Kilian, P., Ibrahim, W.N.W., Onishchenko, N., Ulhaq, M., Norrgren, L., Negri, S., Di Tuccio, M., Ceccatelli, S., 2014. PFOS induces behavioral alterations, including spontaneous hyperactivity that is corrected by dexamfetamine in zebrafish larvae. PLoS One 9, e94227.
Stegeman, J.J., Goldstone, J.V., Hahn, E., 2010. Perspectives on zebrafish as a model in environmental toxicology. In: StF. Perry, M.E., Farrell, A.P., Colin, J.B. (Eds.), Fish Physiology. Academic Press, pp. 367–439.
Stengel, D., Zindler, F., Braunbeck, T., 2017. An optimized method to assess ototoxic effects in the lateral line of zebrafish (Danio rerio) embryos. Comparative Biochemistry and Physiology Part C: Toxicology & Pharmacology 193, 18–29.
Strahle, U., Scholz, S., Geisler, R., Greiner, P., Hollert, H., Rastegar, S., Schumacher, A., Selderslaghs, I., Weiss, C., Witters, H., Braunbeck, T., 2012. Zebrafish embryos as an alternative to animal experiments–a commentary on the definition of the onset of protected life stages in animal welfare regulations. Reprod. Toxicol. 33, 128–132.
Stylianou, M., Bjornsdotter, M.K., Olsson, P.E., Jogsten, I.E., Jass, J., 2019. Distinct transcriptional response of Caenorhabditis elegans to different exposure routes of perfluorooctane sulfonic acid. Environ. Res. 168, 406–413.
Sun, G., Liu, K., Wang, X., Liu, X., He, Q., Hsiao, C.D., 2015. Identification and expression analysis of zebrafish (Danio rerio) E-selectin during embryonic development. Molecules 20, 18539–18550.
Suo, C., Fan, Z., Zhou, L., Qiu, J., 2017. Perfluorooctane sulfonate affects intestinal immunity against bacterial infection. Sci. Rep. 7, 5166.
Thienpont, B., Tingaud-Sequeira, A., Prats, E., Barata, C., Babin, P.J., Raldua, D., 2011. Zebrafish eleutheroembryos provide a suitable vertebrate model for screening chemicals that impair thyroid hormone synthesis. Environmental Science & Technology 45, 7525–7532.
Vasta, G.R., Nita-Lazar, M., Giomarelli, B., Ahmed, H., Du, S., Cammarata, M., Parrinello, N., Bianchet, M.A., Amzel, L.M., 2011. Structural and functional diversity of the lectin repertoire in teleost fish: relevance to innate and adaptive immunity. Dev. Comp. Immunol. 35, 1388–1399.
Vedagiri, U.K., Anderson, R.H., Loso, H.M., Schwach, C.M., 2018. Ambient levels of PFOS and PFOA in multiple environmental media. Remediation 28, 9–51.
Versteeg, G.A., Rajsbaum, R., Sanchez-Aparicio, M.T., Maestre, A.M., Valdiviezo, J., Shi, M., Inn, K.S., Fernandez-Sesma, A., Jung, J., Garcia-Sastre, A., 2013. The E3-ligase TRIM family of proteins regulates signaling pathways triggered by innate immune pattern-recognition receptors. Immunity 38, 384–398.
Webster, A.F., Chepelev, N., Gagne, R., Kuo, B., Recio, L., Williams, A., Yauk, C.L., 2015. Impact of genomics platform and statistical filtering on transcriptional benchmark doses (BMD) and multiple approaches for selection of chemical point of departure (PoD). PLoS One 10.
White, S.S., Fenton, S.E., Hines, E.P., 2011. Endocrine disrupting properties of perfluorooctanoic acid. J. Steroid Biochem. Mol. Biol. 127, 16–26.
Woo, J.S., Imm, J.H., Min, C.K., Kim, K.J., Cha, S.S., Oh, B.H., 2006. Structural and functional insights into the B30.2/SPRY domain. EMBO J. 25, 1353–1363.
Yang, L., Allen, B.C., Thomas, R.S., 2007. BMDExpress: a software tool for the benchmark dose analyses of genomic data. BMC Genomics 8.
Zeng, X.W., Qian, Z., Vaughn, M., Xian, H., Elder, K., Rodemich, E., Bao, J., Jin, Y.H., Dong, G.H., 2015. Human serum levels of perfluorooctane sulfonate (PFOS) and perfluorooctanoate (PFOA) in Uyghurs from Sinkiang-Uighur autonomous region, China: background levels study. Environ. Sci. Pollut. Res. 22, 4736–4746.
Zeng, Z.T., Song, B., Xiao, R., Zeng, G.M., Gong, J.L., Chen, M., Xu, P.A., Zhang, P., Shen, M.C., Yi, H., 2019. Assessing the human health risks of perfluorooctane sulfonate by in vivo and in vitro studies. Environ. Int. 126, 598–610.
Zhang, Y.H., Wang, J., Dong, G.H., Liu, M.M., Wang, D., Zheng, L., Jin, Y.H., 2013. Mechanism of perfluorooctanesulfonate (PFOS)-induced apoptosis in the immunocyte. J. Immunotoxicol. 10, 49–58.
Zhang, X., Zhao, H., Chen, Y., Luo, H., Yang, P., Yao, B., 2015. A zebrafish (Danio rerio) bloodthirsty member 20 with E3 ubiquitin ligase activity involved in immune response against bacterial infection. Biochem. Biophys. Res. Commun. 457, 83–89.

Supplemental information: scientific article III

Unravelling the mechanisms of PFOS toxicity by combining morphological and transcriptomic analyses in zebrafish embryos

Authors: R. Martínez, L. Navarro-Martín, C. Luccarelli, A.E. Codina, D. Raldúa, C. Barata, R. Tauler, B. Piña

Status: Published

Journal: Sci. Total Environ. 674 (2019) 462–471.

DOI: 10.1016/j.scitotenv.2019.04.200

Supplementary methods

Supp. method 1: RT-qPCR analysis

Total RNA from 9 replicates (10 larvae per replicate) was extracted using the Trizol method following the manufacturer protocol (Ambion, Thermo Fisher Scientific). Extracted concentrations were assessed with a NanoDrop® 8000 UV-Vis Spectrophotometer (Thermo Scientific) and genomic undesirable DNA was removed with Ambion™ DNase I (Thermo Fisher Scientific). RNA was reverse-transcribed to cDNA using Transcriptor First Strand cDNa Sythesis Kit (Roche Diagnostics) following manufacturer's protocols. A no-RT negative controls were also prepared by replacing the RT enzyme with water. To measure the relative mRNA abundances of target genes, quantitative real-time polymerase chain reactions (qRT-PCR) were carry out, using a LightCycler® 480 Real-Time PCR System (Roche Diagnostics, Mannheim, Germany). The amplification program consisted of 10 min at 95 °C, followed by 45 cycles (10 s at 95 °C, 30 s at 60 °C). After the amplification, a dissociation analysis was also programmed (obtaining a melting curve) to evaluate the specificity of the reaction. The amplification reaction efficiency for each gene was assessed (Supplementary Table ST3). Relative transcript abundance were calculated from maximum of the second derivative (Cp, calculated by technical duplicates) of their respective amplification curves. PPIAa was used as a reference gene. Cp values for target genes (Cp_{tg}) were normalized to the average Cp values of reference gene, following the equation: $\Delta Cp_{tg} = Cp_{PPIAa} - Cp_{tg}$. Transcript abundance changes in samples were calculated by the ΔΔCp method [1]: $\Delta\Delta Cp_{tg} = \Delta Cp_{tg}$ (control group) − ΔCp_{tg} (exposed group). From those ΔΔCptg values, fold-change ratios were obtained.

[1] M. W. Pfaffl, “A new mathematical model for relative quantification in real-time RT-PCR,” Nucleic Acids Res., 2001.

Supplementary Table ST1. RNA-Seq readings and mapping quality statistics.

Sample Barcode	Sample Name	Number of FLIs	Million read-pairs (or reads)	Yield (Gb)	Trimmed yield (Gb)	Avg PhiX error r1	Avg PhiX error r2	Organism	Reference	Avg % unique	Avg % unmapped	Avg % duplicate	Avg % difference r1	Avg % difference r2	Avg alignment insert size
AB3131	PFOS (2-5) Ctl R1	2	32.569	4.950	4.949	0.25	0.36	*Danio rerio*	drerio.GRCz10	80.60	2.06	18.38	1.31	1.33	144.00
AB3132	PFOS (2-5) 0,03ppm R1	1	41.359	6.287	6.286	0.17	0.31	*Danio rerio*	drerio.GRCz10	81.07	1.16	31.63	1.17	1.16	137.00
AB3133	PFOS (2-5) 0,3ppm R1	2	36.463	5.542	5.541	0.16	0.33	*Danio rerio*	drerio.GRCz10	79.42	1.82	21.92	1.26	1.26	141.00
AB3134	PFOS (2-5) 1ppm R1	2	42.264	6.424	6.422	0.17	0.34	*Danio rerio*	drerio.GRCz10	82.04	1.45	21.12	1.15	1.17	153.00
AB3139	PFOS (2-5) Ctl R3	2	39.487	6.002	6.000	0.17	0.34	*Danio rerio*	drerio.GRCz10	81.91	1.64	22.30	1.17	1.18	142.00
AB3140	PFOS (2-5) 0,03ppm R3	2	35.693	5.426	5.424	0.17	0.34	*Danio rerio*	drerio.GRCz10	83.27	1.52	22.27	1.18	1.20	148.00
AB3141	PFOS (2-5) 0,3ppm R3	1	37.656	5.724	5.717	0.14	0.28	*Danio rerio*	drerio.GRCz10	82.20	1.44	30.26	1.17	1.29	138.00
AB3142	PFOS (2-5) 1ppm R3	1	48.043	7.303	7.302	0.17	0.31	*Danio rerio*	drerio.GRCz10	83.20	1.16	30.91	1.24	1.23	137.00
AB3143	PFOS (2-5) Ctl R2	1	36.218	5.505	5.501	NA	NA	*Danio rerio*	drerio.GRCz10	82.41	1.53	31.48	1.13	1.15	151.00
AB3144	PFOS (2-5) 0,03ppm R2	1	38.790	5.896	5.892	NA	NA	*Danio rerio*	drerio.GRCz10	81.79	1.25	30.09	1.13	1.15	148.00
AB3145	PFOS (2-5) 0,3ppm R2	1	40.419	6.144	6.139	NA	NA	*Danio rerio*	drerio.GRCz10	85.39	1.33	32.59	1.16	1.20	153.00
AB3146	PFOS (2-5) 1ppm R2	2	36.776	5.590	5.589	0.16	0.33	*Danio rerio*	drerio.GRCz10	86.33	1.69	27.59	1.21	1.26	148.50

Column description	
Sample Barcode	Unique internal CNAG identifier of the sample
Sample Name	Sample name provided by the collaborator
Number of FLIs	Number of sequencing Flowcell Lane Index units for this sample (equivalent to the number of times the sample has been sequenced)
Million read-pairs (or reads)	Total million read-pairs (or reads for single-end runs) that passed Illumina filter
Yield (Gb)	Total yield in Gigabases from the read-pairs (or reads for single-end runs) that passed Illumina filter
Trimmed yield (Gb)	Trimmed yield in Gigabases from the read-pairs (or reads for single-end runs) that passed Illumina filter
Avg PhiX error r1	Average % mismatches between the spiked-in PhiX read 1 and the PhiX reference
Avg PhiX error r2	Average % mismatches between the spiked-in PhiX read 2 and the PhiX reference
Organism	Sample's organism according to submitter
Reference	Reference sequence (genome, transcriptome, contigs...) to which the reads have been mapped
Avg % unique	Average % of reads aligning to a single location in the reference
Avg % unmapped	Average % of reads not aligning to any location in the reference
Avg % duplicate	Average % of read-pairs (or reads, for single-end runs) that map exactly at the same location in the reference as another read-pair
Avg % difference r1	Average % mismatches between read 1 and the reference
Avg % difference r2	Average % mismatches between read 2 and the reference
Avg alignment insert size	Average mapping distance between read 1 and read 2

Supplementary Table ST2. Categorical morphological measurements in 5 dpf eleutheroembryos.

Group (mg/L of PFOS)	Scoliosis		Tail mal-formation (dorsoventral and lateral)	
	n/total	Statistical significance [a)]	n/total	Statistical significance [a)]
Control	0/50	n/a	4/100	n/a
0.10	0/50		4/100	
0.25	0/49		5/98	
0.50	0/50		6/100	
1.0	0/50		11/100	
2.5	1/50		17/100	**
5.0	1/50	**	42/100	***
7.5	18/48	***	45/96	***

a) Fisher exact probability test: $p < 0.05$ (*), $p < 0.01$ (**), $p < 0.001$ (***).

Supplementary Table ST3. Primers, efficiency and accession number for the genes measured with qRT-PCR (ppiaa, apoa4b.3, btr31, ccl20b, erap1a, erap2, spsb3b and stat1b).

Gene Name	Accesion nº	Description	Forward-primer	Reverse primer	Efficiency	R^2
ppiaa	NM_212758.1	peptidylprolyl isomerase Aa (cyclophilin A)	GGGTGGTAATGGAGCTGAGA	AATGGACTTGCCACCAGTTC	92.8%	>0.999
apoa4b.3	XM_001338001.6	apolipoprotein A-IV b, tandem duplicate 3	ACCAAATTAACTCTTCACAAACTTCG	ATGGCATGATAGGATGAATCGAT	92.3%	0.997
btr31	XM_005170606.2	bloodthirsty-related gene family, member 31	CATCATGCCTGCTCCTCACA	GCCGTGTCATGATCCAGAGTC	102.3%	0.982
ccl20b	NM_001113595.1	chemokine (C-C motif) ligand 20b	TGCAATCATTTTCCACACCG	CATAAGACCCGTTCTTGCGTC	98.5%	0.994
erap1a	XM_009305074.3	endoplasmic reticulum aminopeptidase 1a	CTCCGGGCTCCGCAGTAT	AGCAGTGGGACGTTCCTGTC	95.0%	0.996
erap2	NM_001123052.1	endoplasmic reticulum aminopeptidase 2	TCAGACCGGAGATTGCGTG	CCGTTCAGCCTTTTCCAAAC	103.7%	0.994
sps3b	XM_021470242.1	splA/ryanodine receptor domain and SOCS box containing 3b	ATATGATGGTTGGCATCGGG	CATCTGTGCCCAGCAGACTG	100.2%	0.993
stat1b	NM_200091.2	signal transducer and activator of transcription 1b	AGTGAAAGCTGTCGAGACGGA	CACCGAATGGATCTTGGGTT	103.2%	0.991

Supplementary Table ST4. David Functional Analysis[a)] results for both gene clusters, individual and combined (only results with FDR≤5%)

Category	Term	Genes	Count	Fold Enrichment	PValue	FDR
Cluster 1 (down-regulation)						
INTERPRO	IPR001870:B30.2/SPRY domain	SI:CH211-133H13.1, SPSB1, SI:DKEY-84H14.2, BTR26, BTR29, SI:CH211-247L8.8, SI:DKEY-3H2.3, SI:CH211-120G10.1, ZGC:174180, SI:CH211-76M11.8, TRIM109, SI:DKEY-222H21.8, BTR20, SI:CH211-255G12.8, RSPRY1, ZGC:194906, FTR37, SI:DKEY-61P9.9, FTR53, FTR35, FTR56, SPSB3B, FTR30, BTR31	24	3.5	4.32E-07	6.66E-04
INTERPRO	IPR006574:SPRY-associated	SI:CH211-133H13.1, SI:DKEY-84H14.2, BTR26, BTR29, SI:CH211-247L8.8, SI:DKEY-3H2.3, SI:CH211-120G10.1, ZGC:174180, SI:CH211-76M11.8, SI:DKEY-222H21.8, BTR20, SI:CH211-255G12.8, ZGC:194906, FTR37, SI:DKEY-61P9.9, FTR53, FTR35, FTR56, FTR30, BTR31	20	3.4	9.36E-06	0.014
KEGG_PATHWAY	dre04630:Jak-STAT signaling pathway	IRF9, SI:RP71-17I16.5, IFNPHI1, STAT1B, IL6ST, IL10RB, IL20RA, LEPA, IL19L, PIK3CD, SOCS3B, IL22RA2	12	5.2	1.59E-05	0.017
INTERPRO	IPR003877:SPla/RYanodine receptor SPRY	SI:CH211-133H13.1, SPSB1, SI:DKEY-84H14.2, BTR26, BTR29, SI:CH211-247L8.8, SI:DKEY-3H2.3, SI:CH211-120G10.1, ZGC:174180, SI:CH211-76M11.8, SI:DKEY-222H21.8, BTR20, SI:CH211-255G12.8, RSPRY1, ZGC:194906, SI:DKEY-61P9.9, FTR53, FTR56, BTR31, SPSB3B	20	3.2	1.48E-05	0.023
INTERPRO	IPR001507:Zona pellucida domain	ZP3C, SI:CH211-39F2.3, ZGC:66449, SI:CH73-181M17.1, SI:DKEY-239B22.1, SI:CH211-226H7.8, ZGC:153932, SI:CH211-226H7.5, SI:CH211-226H7.6	9	6.4	7.75E-05	0.120
GOTERM_BP_DIRECT	GO:0016567~protein ubiquitination	MKRN1, TRAF1, BTR26, CCNF, HACE1, UBOX5, ASB12A, ASB18, BTR20, UVSSA, KLHL26, CAND2, KLHL38B, FBXO32, SOCS3B, BTR31	16	3.4	9.09E-05	0.133
INTERPRO	IPR003879:Butyrophylin-like	SI:CH211-133H13.1, SI:DKEY-84H14.2, BTR26, BTR29, SI:CH211-247L8.8, SI:DKEY-3H2.3, SI:CH211-120G10.1, ZGC:174180, SI:CH211-76M11.8, TRIM109, SI:DKEY-222H21.8, BTR20, SI:CH211-255G12.8, ZGC:194906, SI:DKEY-61P9.9, FTR53, BTR31, FTR56	18	3.0	1.10E-04	0.169
GOTERM_BP_DIRECT	GO:0019885~antigen processing and presentation of endogenous peptide antigen via MHC class I	ERAP1A, ERAP1B, ERAP2, TAPBPL	4	25.7	3.52E-04	0.515
INTERPRO	IPR013320:Concanavalin A-like lectin/glucanase, subgroup	SI:CH211-133H13.1, SPSB1, SI:DKEY-84H14.2, BTR26, BTR29, SI:CH211-247L8.8, SI:DKEY-3H2.3, SI:CH211-120G10.1, ZGC:174180, SI:CH211-76M11.8, TRIM109, SI:DKEY-222H21.8, BTR20, SI:CH211-255G12.8, RSPRY1, ZGC:194906, FTR37, SI:DKEY-61P9.9, FTR53, FTR35, PROS1, FTR56, SPSB3B, FTR30, BTR31	25	2.2	4.27E-04	0.656
GOTERM_MF_DIRECT	GO:0008270~zinc ion binding	MKRN1, TRAF1, ZNFX1, ZRANB1B, ZMAT2, RORC, ISL1L, ADA, FANCL, BTR20, ZFAND5B, RSPRY1, CECR1A, SETMAR, SI:CH211-244B2.2, CCS, ERAP2, XAF1, ZGC:77880, TRIM63A, FTR79, NPLOC4, THRAA, ERAP1A, ERAP1B, BTR26, BTR29, SI:CH211-247L8.8, POLE, ESR1, SIRT5, PHF11, CXXC1A, UBOX5, RNF11A, CA4B, CSRP1B, TRIM109, BHMT, FTR37, RNF25, FTR35, FTR53, RNF26, BTR31, FTR30, FTR56	47	1.6	0.002	2.160
KEGG_PATHWAY	dre04060:Cytokine-cytokine receptor interaction	TNFB, IFNPHI1, CCL20B, CCL20A.3, IL6ST, IL10RB, IL20RA, LEPA, CCR6A, TNFRSF18, IL22RA2	11	3.2	0.002	2.341
INTERPRO	IPR011029:Death-like domain	IRAK3, SI:CH211-114L13.9, CARD9, CASP9, SI:DKEY-103E21.5, SI:DKEY-61P9.9, SI:DKEY-29H14.10, SI:CH211-171L17.4, ADGRG1	9	3.7	0.003	4.393
GOTERM_BP_DIRECT	GO:0007160~cell-matrix adhesion	SI:CH211-39F2.3, HPSE, SI:CH73-181M17.1, SI:DKEY-239B22.1, SI:CH73-329N5.6, EPDL1	6	5.9	0.003	4.807
Cluster 2 (up-regulation)						
GOTERM_MF_DIRECT	GO:0008374~O-acyltransferase activity	SOAT2, LCAT, GPAT2, YKT6, GPAM	5	11.5	7.98E-04	1.149
UP_KEYWORDS	Lipid transport	APOA4B.3, OSBPL2B, APOA4B.2, APOA4B.1, OSBPL10, OSBPL11	6	7.6	0.001	1.335
GOTERM_BP_DIRECT	GO:0006869~lipid transport	APOA4B.3, OSBPL2B, APOA4B.2, APOA4B.1, OSBPL10, APOBB.1, OSBPL11, VTG6	8	5.1	9.50E-04	1.408
KEGG_PATHWAY	dre00564:Glycerophospholipid metabolism	GPD2, PMT, PLA2G12A, LCAT, PTDSS1B, PLA2G12B, GPAT2, GPAT3, GPAM	9	4.0	0.002	1.748

Supplementary Table ST4. David Functional Analysis[a] results for both gene clusters, individual and combined (only results with FDR≤5%)

Clusters 1 + 2						
KEGG_PATHWAY	dre04060:Cytokine-cytokine receptor interaction	CCL20B, IL6ST, CCR6A, MET, IL2RGA, TNFB, IL12RB2, IFNPHI1, VEGFC, IL20RA, CCL20A.3, IL10RB, LEPA, TNFRSF18, TNFRSF19, TGFB1A, NGFRB, IL22RA2, THPO	19	2.6	2.48E-04	0.285
KEGG_PATHWAY	dre04630:Jak-STAT signaling pathway	STAT1B, IL6ST, PIK3CD, IL2RGA, IRF9, IL12RB2, SI:RP71-17I16.5, IFNPHI1, IL20RA, IL10RB, LEPA, IL19L, SOCS3B, THPO, IL22RA2	15	3.1	2.67E-04	0.307
GOTERM_MF_DIRECT	GO:0008374~O-acyltransferase activity	SOAT2, LCAT, NAA40, MBOAT4, GPAT2, YKT6, GPAM	7	7.6	2.13E-04	0.324
UP_KEYWORDS	Signal	LTBP1, IL6ST, SI:CH73-181M17.1, LHCGR, PDGFBA, EPDL1, B2M, SI:CH211-222K6.3, OGN, DEFBL1, LCAT, CFH, ZGC:153932, ERAP2, SERPINH1A, LAMB1A, SOSTDC1B, SI:DKEY-4C23.5, CCL34A.3, PKHD1L1, SI:CH211-145B13.6, ALPI.2, ZGC:100868, VEGFC, NPC2, ZGC:162608, SI:CH211-125E6.11, TGFB1A, ADAMTS5, UGT5G2, ZGC:77929, SI:RP71-1G18.7, IL17C, GNAIA, TMEM123, SI:CH1073-155H21.1, SI:CH1073-126C3.2, ZGC:163079, FREM2A, ZGC:123297, ADGRE14, APOBB.1, CYP2R1, HSPA13, MHC1ZBA, SI:CH211-134A4.3, SI:DKEY-112E17.1, LXN, NITR1B, LY86, NPNT, ZGC:171509, TAS1R3, SI:DKEY-84K17.2, CCL20A.3, PDPK1A, SCPP8, USP11, PRSS35, MBLAC1, SI:CH211-39F2.3, AVP, GIP, JKAMP, CNPY2, P4HA1B, SI:DKEY-162H11.3, CA4B, IL20RA, NITR13, FKBP14, TOR1L1, WNT9A, GPHA2, SI:CH73-334D15.1, ZGC:172053, HYAL2A, SEMA3GA, TFA, IL10RB, PLA2G12A, PLA2G12B, SEMA3GB, LY75, SI:DKEY-193C22.2, IGF3, STAB2, CLEC11A, ZGC:55621, KHK, CRFB15, FBLN2, SI:CH73-380L10.2, PCMTL, IGFBP1B, SEMA3FB, SI:CH211-207N23.2, SI:CH211-132G1.1, CCL20B, SI:CH211-132G1.4, IL2RGA, DICP2.2, VIPR2, MMP2, LYGL1, PRF1.1, CCL39.6, SI:CH211-125E6.5, SI:CH73-256J6.4, SI:CH211-133H13.1, SPARCL2, FZD7B, SI:DKEY-192K22.2, EPHB4B, ZGC:111983, SI:DKEY-88N24.8, MFAP5, PLXNC1, IGFBP5B, CTSS2.2, CTSS2.1, ITGB5, SI:CH211-145C1.1, SI:DKEY-247K7.2, IFNPHI1, SI:CH73-330K17.3, ANGPTL3, LOXL3A, HAVCR1, GNRH2, MPEG1.2, SI:CH73-329N5.6, SI:DKEY-239B22.1, MET, ADGRG1, SI:CH73-196I15.3, SI:CH211-76M11.8, SI:DKEY-37G12.1, CXCL19, ADGRF8, ITGA8, SI:DKEY-21E2.8, SLC8A2A, PCOLCE2B, IL22RA2, ANTXR1D, GM2A, HEXA, HDR,	218	1.2	9.33E-04	1.178
GOTERM_CC_DIRECT	GO:0005615~extracellular space	SERPINB1L1, SI:DKEY-23A13.6, CCL20B, IGFBP5B, LUM, CTSS2.2, ZGC:154142, CTSS2.1, ZGC:171509, SEMA3AB, PDGFBA, IGF2A, IL17C, TNFB, OGN, IFNPHI1, SEMA3GA, TFA, WNT3, SI:CH211-113A14.19, CCL20A.3, LEPA, CECR1A, C18H3ORF33, SEMA3GB, DIA1B, SERPINH1A, SOSTDC1B, SAAL1, INHA, IGF3, VEGFC, SI:CH73-36P18.5, CPAMD8, CTSD, CTSC, SI:CH73-380L10.2, TGFB1A, IGFBP1B, SEMA3FB	40	1.7	0.001	1.531
GOTERM_MF_DIRECT	GO:0004888~transmembrane signaling receptor activity	LY75, OR132-4, ADGRF6, SI:CH211-282J17.8, OR111-11, OR104-2, FZD7B, VIPR2, ADGRG1, OR103-2, SI:CH211-218M3.18, SI:DKEY-83F18.7, SI:CH211-225K7.3, ADGRE16, ADGRF8, OR105-1, ADGRE14, SI:CH211-225K7.5, ADGRE5B.2, SI:DKEY-23C22.5, SI:DKEY-88N24.8, PLA2R1, SI:CH211-282J17.1, OR126-3	24	2.1	0.001	2.160
GOTERM_BP_DIRECT	GO:0051607~defense response to virus	MXF, IFNPHI1, BNIP3LA, IFIT14, MXC, SI:CH73-236C18.8, LY86, MXA	8	4.6	0.002	2.354
INTERPRO	IPR011029:Death-like domain	DLG5B.1, SI:CH211-114L13.9, IRAK3, CARD9, CASP9, SI:DKEY-103E21.5, HDR, SI:DKEY-61P9.9, SI:CH211-66K16.2, SI:DKEY-29H14.10, SI:CH211-171L17.4, ADGRG1, NGFRB	13	2.9	0.002	2.611
GOTERM_BP_DIRECT	GO:0019885~antigen processing and presentation of endogenous peptide antigen via MHC class I	ERAP1A, ERAP1B, ERAP2, TAPBPL	4	12.8	0.003	4.194

[a] https://david.ncifcrf.gov

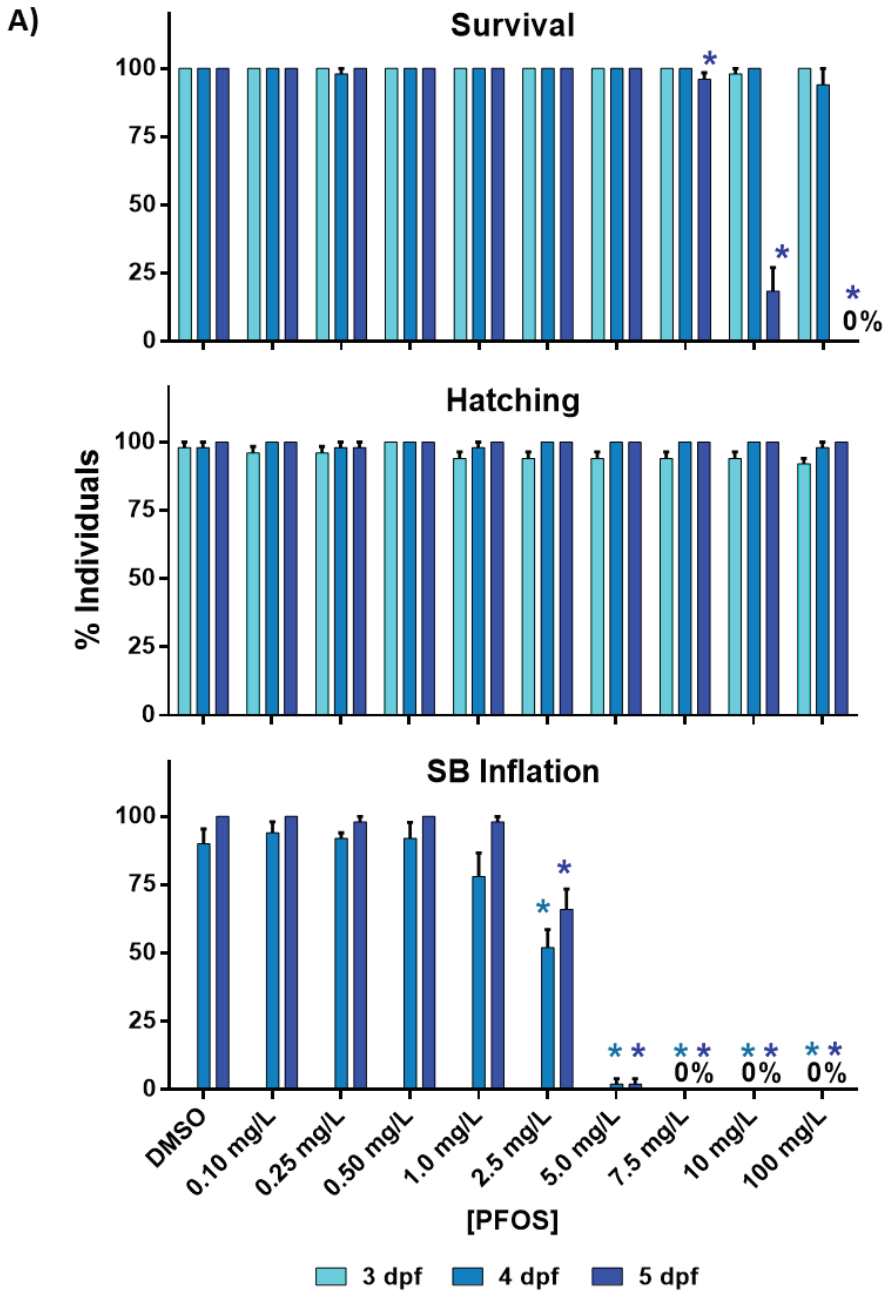

Supplementary Figure 1. Quantitative analysis of survival, morphometric and transcriptional data. A) Survival, hatching and swim bladder (SB) inflation rates of zebrafish embryos exposed to PFOS in the morphometric test. Measurements were taken at 3, 4 and 5 dpf. Bars represent the mean value ± SEM (standard error of the mean) for each group. Non-parametric test (Kruskal-Wallis with pairwise multiple comparisons, $p < 0.05$) was performed. Colored asterisks indicated statistical differences between exposed embryos and the corresponding control group for each age.

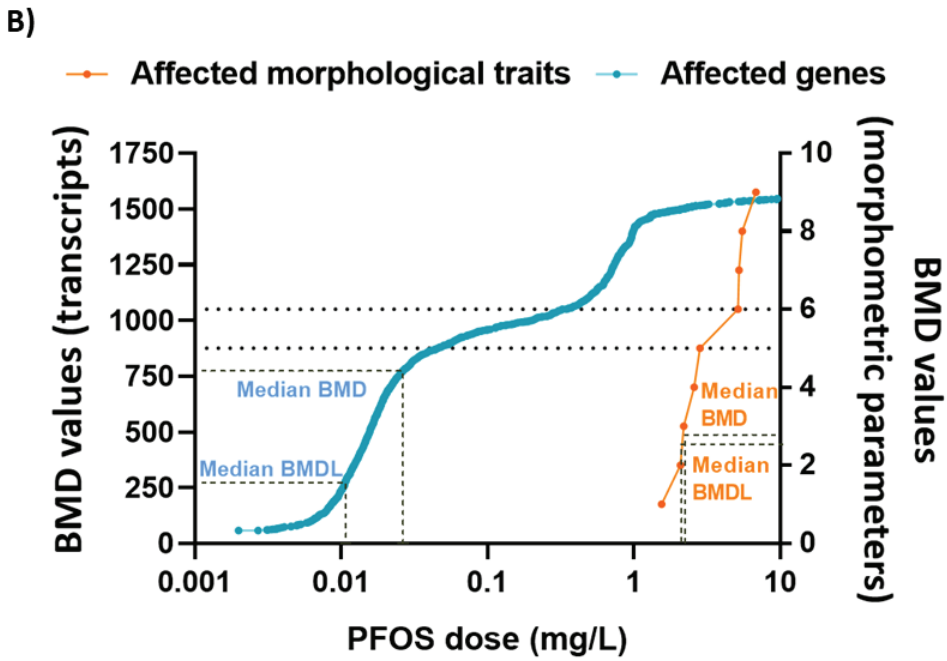

Supplementary Figure 1. Quantitative analysis of survival, morphometric and transcriptional data. B) Benchmark dose (BMD) analysis for morphometric and transcriptional changes. The graph shows accumulation plots of the best calculated BMD for each gene and morphological trait. BMD was calculated for each parameter by the BMDExpress software (https://www.sciome.com/bmdexpress/), using a combination third-order polynomial, third-order exponential and Hill equations, and choosing the best fitted model for each case separately. In case of the genes, only those with more than 100 counts between all the 12 replicates and a fold change > 1.5 or <0.75 were used. The median values of BMD and BMDL were calculated as 0.027 and 0.011 mg/L for the transcriptomic effects and 2.83 and 2.53 mg/L for the morphological effects, respectively. BMDL values were considered as PoD (Point of Departure) levels, doses at which negative effects started being significant). Dotted lines indicate the range coincidence of transcriptomic and morphological effects (in terms of % of affected genes/traits) between the most and less sensitive parameters.

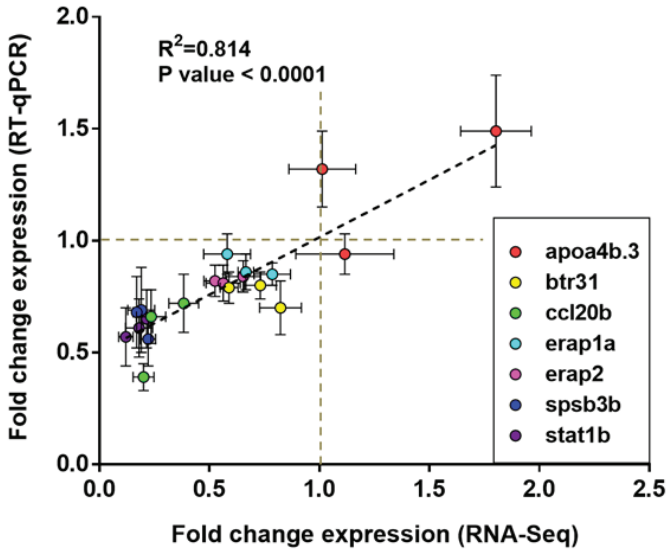

Supplementary Figure 2. Correlation between RNAs-Seq and RT-qPCR relative expression of some selected genes (apoa4b.3, btr31, ccl20b, erap1a, erap2, spsb3b and stat1b). Fold change expression data were used and a linear regression performed. Colored points represent the mean fold change ± SEM (standard error of the mean) of the three treatment groups (0.03, 0.3 and 1.0 mg/L of PFOS) per each gene. Three and nine replicates were used for RNA-Seq and RT-qPCR, respectively.

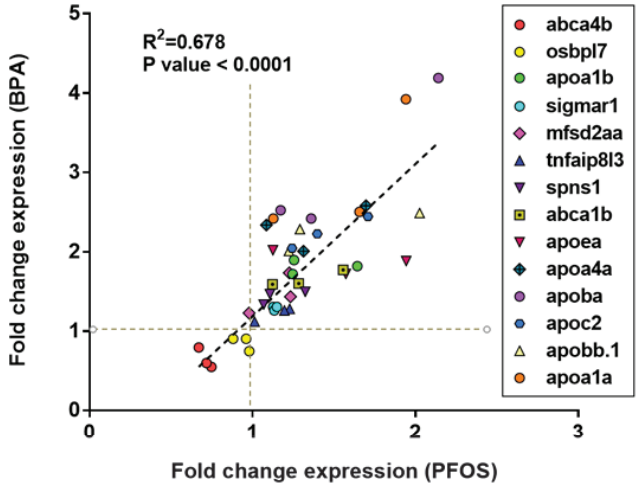

Supplementary Figure 3. Correlation of the relative expression (measured with RNASeq) of the differentially expressed genes (DEGs) related with lipid transport/metabolism between our PFOS exposure and a previous BPA exposure done in the same developmental timing and conditions [33]. For comparison, the most similar groups between exposures were linked with each other (controls between them –not used for the regression-, 1/40 LOAEC of BPA with 1/30 LOAEC of PFOS, 1/4 LOAEC of BPA with 1/3 LOAEC of PFOS and LOAEC of BPA with LOAEC of PFOS). Fold change expression data were used and a linear regression performed. Each point represents the mean value ± SEM (standard error of the mean) of the 3 transcriptomic replicates used in each exposure.

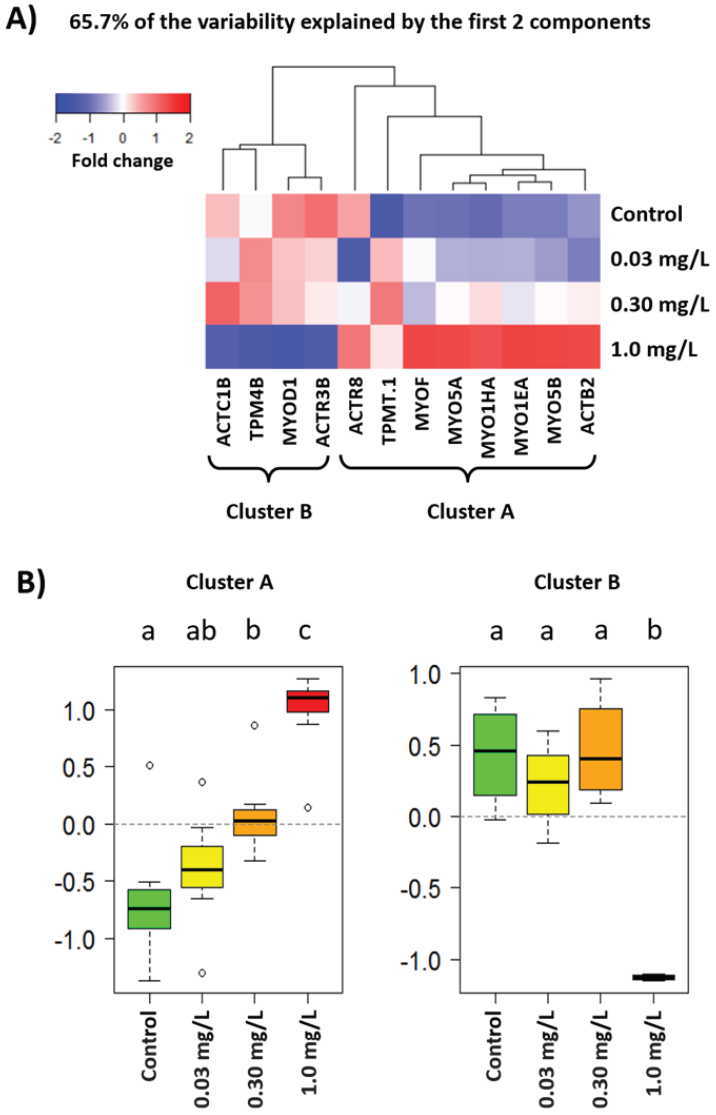

Supplementary Figure 4. Analyses of the myosines, tropomyosins and actins categorized as DEGs in the general transcriptomic analyses. A) Heatmap showing concentration changes corresponding to the 12 transcripts (only considering myosines, tropomyosins and actins) identified by ANOVA-PLS as differentially expressed genes (DEGs) in at least one of the experimental groups. Values were centered to the average of control samples and log2 transformed. The mean value of the 3 replicates is shown for each group. Color scale ranges from blue (strongly underexpressed relative to control) to red (strongly overexpressed); white cells correspond to control values (fold change = 0). Rows (genes) were grouped by hierarchical clustering and its corresponding dendrogram is shown at the top of the panel. The two clusters (A and B) determined in a posterior medoids PAM clustering analysis are indicated. B) Normalized abundance values for all the genes included in each of the two clusters (cluster A at left, which contains the overexpressed genes due to PFOS exposure, and cluster B at right, which contains the underexpressed genes). Low-case letters at the top of each graph indicate statistically different distributions (parametric ANOVA + Tukey's B post-hoc test with all pairwise comparisons, $p \leq 0.05$). Boxes include values between the 1st and 3rd quartiles, thick bars indicate average values and whiskers cover the total distribution, except for outliers (circles).

Scientific article IV

Transcriptomic effects of tributyltin (TBT) in zebrafish eleutheroembryos. A functional benchmark dose analysis

Authors: R. Martínez, A.E. Codina, C. Barata, R. Tauler, B. Piña, L. Navarro-Martín

Status: Published

Journal: *J Hazard Mater*. 398 (2020) 122881

DOI: 10.1016/j.jhazmat.2020.122881

Journal of Hazardous Materials 398 (2020) 122881

Contents lists available at ScienceDirect

Journal of Hazardous Materials

journal homepage: www.elsevier.com/locate/jhazmat

Transcriptomic effects of tributyltin (TBT) in zebrafish eleutheroembryos. A functional benchmark dose analysis

Rubén Martínez[a,b], Anna E. Codina[c,d], Carlos Barata[a], Romà Tauler[a], Benjamin Piña[a], Laia Navarro-Martín[a,*]

[a] Institute of Environmental Assessment and Water Research, IDAEA-CSIC, Barcelona, Catalunya, 08034, Spain
[b] Universitat de Barcelona (UB), Barcelona, Catalunya 08007, Spain
[c] CNAG-CRG, Centre for Genomic Regulation (CRG), Barcelona Institute of Science and Technology (BIST), Barcelona 08028, Spain
[d] Universitat Pompeu Fabra (UPF), Barcelona 08003, Spain

GRAPHICAL ABSTRACT

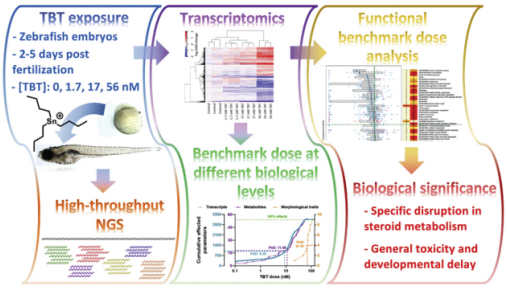

ARTICLE INFO

Editor: D. Aga

Keywords:
Tributyltin
Zebrafish
Endocrine disruption
RNA-Seq
Benchmark dose

ABSTRACT

Exposure to the antifouling tributyltin (TBT) has been related to imposex in mollusks and to obesogenicity, adipogenesis and masculinization in fish. To understand the underlying molecular mechanisms, we evaluated dose-response effects of TBT (1.7−56 nM) in zebrafish eleutheroembryos transcriptome exposed from 2 to 5 days post-fertilization. RNA-sequencing analysis identified 3238 differentially expressed transcripts in eleutheroembryos exposed to TBT. Benchmark dose analyses (BMD) showed that the point of departure (PoD) for transcriptomic effects (9.28 nM) was similar to the metabolomic PoD (11.5 nM) and about one order of magnitude lower than the morphometric PoD (67.9 nM) or the median lethal concentration (LC_{50}: 93.6 nM). Functional analysis of BMD transcriptomic data identified steroid metabolism and cholesterol and vitamin D_3 biosynthesis as the most sensitive pathways to TBT (< 50% PoD). Conversely, transcripts related to general stress and DNA damage became affected only at doses above the PoD. Therefore, our results indicate that

Abbreviations: ANOVA-PLS, Analysis of Variance-Partial Least Square; BMD, benchmark dose; BMDL, lower limit of the benchmark dose; BMDU, upper limit of the benchmark dose; DBT, dibutyltin; DEGs, differentially expressed genes; dpf, days post-fertilization; EC_{50}, half maximal effective concentration; EDC, endocrine disrupting chemical; hpf, hours post fertilization; KEGG, Kyoto Encyclopedia of Genes and Genomes; LC_{50}, median lethal concentration; LOAEC, lowest observed adverse effect concentration; LOECs, lowest observed effect concentrations; MIE, molecular initiating event; MoA, mode of action; NOECs, no observed effect concentrations; PAM, partition around medoids; PoD, point of departure; PPAR, peroxisome proliferator-activated receptors; RIN, RNA integrity number; RXR, retinoid X receptors; TBT, tributyltin; VDR, vitamin D receptors

* Corresponding author.
E-mail addresses: ruben1990martinez@hotmail.com (R. Martínez), anna.esteve@cnag.crg.eu (A.E. Codina), cbmqam@cid.csic.es (C. Barata), rtaqam@cid.csic.es (R. Tauler), bpcbmc@cid.csic.es (B. Piña), laianavarromartin@gmail.com (L. Navarro-Martín).

https://doi.org/10.1016/j.jhazmat.2020.122881
Received 14 February 2020; Received in revised form 3 April 2020; Accepted 4 May 2020
Available online 19 May 2020

transcriptomes can act as early molecular indicators of pollutant exposure, and illustrates their usefulness for the mechanistic identification of the initial toxic events. As the estimated molecular PoDs are close to environmental levels, we concluded that TBT may represent a substantial risk in some natural environments.

1. Introduction

Organotin compounds are organometallic chemicals based on several hydrocarbon chains which form direct Sn-C bonds with a central tin atom. Among them, TBT (tributyltin) compounds ($Sn(C_4H_9)_3^+ X^-$) show up as an important class of organotins, consisting in three butyl groups covalently bonded to a Sn^{4+} center atom (Davies, 2004). They possess several applications as disinfectants, microbiocides, fungicides and wood preservatives, and are used in water cooling towers, textiles products, sponges, foams, paper and building materials (U.S. Environmental Protection Agency, 2008). Precisely, its biocides properties triggered its worldwide use in anti-fouling paints in boats as a copolymer (Antizar-Ladislao, 2008; Yebra et al., 2004). Despite of the relative low solubility of organotins in water, they are able to reach the environment through a hydrolysis reaction of its copolymer that release tributyltin (TBT; $(C_4H_9)_3Sn^+$) (IMO, 2002; Takahashi, 2009). Despite the ban on organotin compounds and their inclusion in the Rotterdam Convention (Davies, 2004; IMO, 2002; Takahashi, 2009), their long half-life in sediments and their progressive release (Champ and Seligman, 1996), their current production in some countries, the poor regulation in water dumpings (Wang et al., 2019) and illegal uses (Bray, 2006; Ramaswamy et al., 2004) lead to the presence of concentrations high enough to be a matter of concern in different parts of the world (Castro and Fillmann, 2012; Langston et al., 2015). Total organotin concentrations range values of 1.76–486.62 ng Sn/g (dry weight) in Asian harbors (Wang et al., 2019), 43.9–63.5 ng Sn/L in some Asian rivers or 0.01–1.9 μg Sn/L (equivalent to 0.37 − 0.53 nM and to 0.08–16.0 nM of TBT, respectively) in coastal waters around the world (Li et al., 2019).

TBT is very toxic for marine organisms and shows endocrine disrupting properties, like promoting dysregulation of the synthesis of steroid hormones (Nakanishi, 2008). It can exert shell thickening and aberrant morphogenesis (imposex) in molluscs (Newman and McIntosh, 1993; Santillo and Langston, 2001) and obesogenicity, adipogenesis and masculinization in fish (Heindel and Blumberg, 2019; Lyssimachou et al., 2015; Santos et al., 2006). Although TBT is not usually included in the endocrine disrupting chemicals (EDCs) lists (ECHA (European Chemicals Agency), 2019; European Commission, 2007; Hass et al., 2018), many international agencies have recognized its EDC properties (Bergman et al., 2013; Demeneix and Slama, 2019; Gore et al., 2014). It has been proposed that the mode of action (MoA) of TBT is via covalent binding with retinoid X receptors (RXR) (le Maire et al., 2009). Although its effects at phenotypical, organismal and transcriptomic levels have been explained in other species (Baker and Hardiman, 2014; Cruz et al., 2015b; Zhang et al., 2018), not much is known on its transcriptomic effects in zebrafish eleutheroembryos. This fish species is considered an excellent vertebrate model for human and environmental toxicology, including endocrine disruption, thanks to its easy rearing and to the characteristics of their free-swimming late embryonic stages (Kimmel et al., 1995a; Parichy et al., 2009; Raldúa and Piña, 2014; Scholz and Mayer, 2008; Segner, 2009; Stegeman et al., 2010; Strähle et al., 2012).

Recent developments on high-throughput next generation sequencing (HT-NGS) technologies, especially RNA-Seq, has allowed to perform *in toto*, untargeted and integrative analyses of the effects of several EDCs in many organisms, including zebrafish (Caballero-Gallardo et al., 2016; Martínez et al., 2019b; Qian et al., 2014; Reuter et al., 2015; Wang et al., 2009; Zhao et al., 2014). Moreover, it has been observed that the phenotypical observations, as well as the metabolomic alterations produced by pollutants can be linked to transcriptomic dysregulation (Lee et al., 2017; Orlando et al., 2004; Ortiz-Villanueva et al., 2018), which usually is the first biological response to EDC exposure (Martínez et al., 2019b; Tu et al., 2019). The benchmark dose (BMD) concept defines the concentration that induces physiological changes that can be associated to an adverse effect. This concept has been applied to risk assessment since early 1980s (Davis et al., 2011; Filipsson et al., 2003), but only recently has been extended to transcriptomic responses, in order to: 1) detect the most sensitive pathways to EDC exposures using transcriptomic datasets (Wang et al., 2018), which could be used to identify primary response biomarkers of EDC exposures; 2) integrate data from different biological levels (Martínez et al., 2019b); and 3) determine the point of departure (PoD) of different structurally similar chemicals (Tu et al., 2019). However, the majority of studies evaluating transcriptomic points of departure have been done in adult animals and more studies based on early-stage exposures are needed (Pagé-Larivière et al., 2019).

In the present work, we exposed zebrafish eleutheroembryos from 2 to 5 days post-fertilization (dpf) to several TBT concentrations in a dose-response manner. We then studied the effects at the transcriptomic level using the benchmark dose approach, and analyzed the individual gene responses according to their functional annotation. Finally, we used this information, as well as published data from previous studies on the effects of TBT at morphological and metabolomical levels (Martínez et al., 2019a; Ortiz-Villanueva et al., 2018) to identify the different regulatory mechanisms responsible for the multiple toxic effects of TBT in zebrafish.

2. Materials and methods

2.1. Animals and rearing conditions

Zebrafish eggs were obtained by natural mating of adult individuals (wild-type *Danio rerio*, 12–18 months old) which were fed twice per day with dry flakes (TetraMin, Tetra, Germany). Mating was carried out in 4-L breeding tanks with six males and three females (2:1 proportion). A mesh bottom was placed for egg collection. Adults, eggs and embryos were maintained under standard conditions (28.0 ± 1.0 °C, photoperiod of 12L:12D) and kept in fish water which was composed of Instant Ocean (90 μg/mL, Aquarium Systems, Sarrebourg, France) and $CaSO_4{\cdot}2H_2O$ (100 μg/mL, Sigma-Aldrich, St.Louis. MO, USA), dissolved in reverse-osmosis purified water. Eggs were collected at 2 h post fertilization (hpf), rinsed and checked for fertilization. Embryos were placed in six multi-well plates at a density of 3.3 embryos/mL (10 individuals per well, in 3.0 mL) in clean fish water until the start of the exposures. Treatment assignment in the plates was randomized to avoid any possible bias. From now on, we will refer to hatched embryos that have not reach the stage of self-feeding (about 120 hpf in our conditions) as eleutheroembryos. All experimental procedures were carried out under the license DAMM 7669, 7964 from the competent authority in accordance with the institutional guidelines. They were approved by the Institutional Animal Care and Use Committees of the Research and Development Centre (CID) of the Spanish National Research Council (CSIC).

2.2. Zebrafish eleutheroembryos exposures to TBT

Tributyltin chloride (TBT, CAS-RN: 1461-22-9) was provided by Sigma-Aldrich (St. Louis, MO, USA). Stock solutions were prepared in dimethyl sulfoxide (DMSO) and stored at − 20 °C. During the exposure period, fresh experimental solutions were prepared every day by

dilution of the stock solutions in fish water (final DMSO concentration: 0.2% (v/v)). With the aim to avoid possible molecular events directly related with cellular/organism death processes, the exposure was set up using as a maximum TBT nominal concentration the previously reported lowest observed adverse effect concentration (LOAEC) in terms of survival, hatching or swim bladder inflation rates (100 nM) (Martínez et al., 2019a). Based on that, we chose to expose zebrafish eleutheroembryos to nominal concentrations of 0 (control; 0.2% DMSO), 3, 30 and 100 nM of TBT from 2 to 5 dpf. Exposures were carried out from 2 to 5 dpf to ensure that many of the endocrine systems were developed or under development (Löhr and Hammerschmidt, 2011) and also to avoid toxic effects at early embryonic developmental processes to focus the analysis on already differentiated cells and tissues. This exposure window has been used in the past in our laboratory (Martínez et al., 2019a,b, 2018; Ortiz-Villanueva et al., 2018) and it has been recognized as a good experimental window to study the effect of EDCs in zebrafish embryos by other researchers (Jarque et al., 2019). The present exposures occurred simultaneously with the ones from which metabolomic and morphometric data was obtained (Martínez et al., 2019a; Ortiz-Villanueva et al., 2018). TBT is stable in solution for at least some days (Cruz et al., 2015a; Jordão et al., 2016). Exposure medium was daily renewed and chemical analysis of TBT concentrations were measured as total Sn in the aqueous solutions by inductively coupled plasma mass spectrometry (ICP-MS) in laboratory ICP-MS/AES of IDAEA (Institute of Environmental Assessment and Water Research, Spain). From now on, we will refer to measured concentrations (nominal and measured TBT concentrations are reported at Supplementary Table ST1).

Anatomical development of embryos was followed daily during the exposure (Kimmel et al., 1995b) and survival (3, 4 and 5 dpf), hatching (3, 4 and 5 dpf) and swim bladder inflation rates (4 and 5 dpf) were recorded (210 embryos of each experimental condition were assessed by visual observation; Supplementary Table ST1). Replicates for each TBT condition (10 zebrafish eleutheroembryos per replicate) were collected, snap-frozen in dry ice and stored at −80 °C until further steps.

2.3. RNA extraction, library construction and high-throughput sequencing

Total RNA was extracted from independent pools of 10 eleutheroembryos using AllPrep DNA/RNA Mini Kit (Qiagen, CA, USA) as described by the manufacturer. RNA quality and concentrations were assessed with a NanoDrop® 8000 UV–Vis Spectrophotometer (Thermo Scientific). RNA preparations of three high quality replicates per condition were sent to the National Center for Genomic Analysis (CNAG, Barcelona, Spain) for high-throughput sequencing (RNA-Seq). Their quantity and quality were assessed by a Qubit® RNA BR Assay kit (Thermo Fisher Scientific) and RNA 6000 Nano Assay on a Bioanalyzer 2100 (Agilent Technologies), respectively. RNA concentrations ranged between 160 and 514 ng/μL, RNA integrity numbers (RIN) were higher than 8.5 and samples were free of genomic DNA. RNA-Seq libraries were prepared with the KAPA Stranded mRNA-Seq Kit Illumina® Platforms (Kapa Biosystems) with minor modifications. Briefly, 500 ng of total RNA as input material was poly(A) enriched with oligo-dT magnetic beads and fragmented (resulting RNA fragment size: 80–250 nt; major peak: 130 nt). The synthesis of the second strand cDNA was performed with dUTP instead of dTTP, to enhance strand specificity. A 3′ adenylation and ligation of indexed Illumina adapters were performed over the blunt-ended double-stranded cDNA. An enrichment step (15 PCR cycles) was carried out in the ligation product and validated on an Agilent 2100 Bioanalyzer with the DNA 7500 kit. Each final library was sequenced using TruSeq SBS Kit v3-HS (paired-end mode; 2 × 76bp as read length). We generated on average 42 million paired-end reads for each sample in a fraction of a sequencing lane on HiSeq2000 (Illumina). Image analysis, base calling and quality scoring of the run were processed using the manufacturer's software Real Time Analysis (RTA 1.13.48) and FASTQ sequence files were generated by the sequencing analysis software CASAVA. For each sample, more than a 98% of the obtained reads mapped properly to the reference genome (GRCz10). Most of them mapped to exonic regions and to protein-coding genes, with a total of 24,420 genes detected per sample. A full description of mapping quality statistics can be found in Supplementary Material.

2.4. Data analysis

2.4.1. Survival, hatching and swim bladder inflation rates

To determine differences in the survival, hatching and swim bladder inflation of the eleutheroembryos triggered by the TBT exposure, individual non-parametric Mann–Whitney–Wilcoxon tests against each control group (one per day) were performed over the percentages obtained (5 replicates per condition, 10 eleutheroembryos per replicate, $p \leq 0.05$). EC_{50} values (half maximal effective concentrations) were calculated by interpolation on the fitted curves (Hill equations with variable slope). GraphPad Prism version 8.1.2 (GraphPad Software, San Diego, California USA, www.graphpad.com) was used to perform all the statistical analyses and associated graphs.

2.4.2. RNA-Seq transcriptomic data

Reads obtained by RNA-Seq were aligned to the *Danio Rerio* reference genome (GRCz10) using the STAR software version 2.5.1b (Dobin et al., 2013). RSEM software version 1.2.28 (Li and Dewey, 2011) was used for the quantification of the genes annotated in GRCz10.84 (using default parameters). Counts were nor were normalized with the DESeq2 (v.1.10.1) R package (Love et al., 2014), which normalizes for sequencing depth and RNA composition using the median of ratios methodn. Afterwards, data was centered and scaled to the control set, log2 transformed and smoothed by loess function by *stats* package in R (R_Development_Core_Team, 2008) considering each TBT concentration (including control group) as a class. Statistical analysis to determine the differential expressed genes (DEGs) between all experimental conditions (adjusted p value < 0.05) was carried out by a ANOVA-PLS (Analysis of Variance-Partial Least Square) test using the *lmdme* package in R v. 1.0.136, R Core Team (Fresno et al., 2014). Briefly, this analysis consisted in a decomposition of the transcriptomic data matrix of all samples (normalized transcript values) through a linear model that considers the experimental design (TBT treatments), and builds a regression between the matrices obtained in the first linear decomposition (X) and a vector (y) defining defining the class membership of the samples (control, 1.7, 17 and 56 nM). This analysis allowed to identify 3238 differentially expressed genes (DEGs) that significantly described best the differences between groups ($p \leq 0.05$). Subsequently, hierarchical and PAM (partition around medoids) clustering analyses were both performed over the DEGs and plotted using the packages *gplots*, *fpc*, and *cluster* in R (Hennig, 2014; Maechler et al., 2019; Warnes et al., 2015). PAM analysis performed a principal component analysis (PCA) analyzing the covariance matrix of the variables and produced a 2D plot which showed the goodness of separation of the gene clusters (which are constructed minimizing the distances between the genes and the designated center points of k clusters). One-way ANOVAs followed by post hoc Tukey's B tests ($p < 0.05$) were used (using the *foreign* and *agricolae* packages in R (R Development Core Team, 2008, De Mendiburu, 2009) to assess statistically significant differences between the expression of all genes included in each cluster.

2.4.3. Benchmark doses and point of departures determination

Transcriptomic data obtained in the present study and metabolomic and morphometric data from analogous exposures done in our laboratory (Martínez et al., 2019a; Ortiz-Villanueva et al., 2018) were used to calculate benchmark doses (BMD) per each feature (transcript, metabolite or morphometric trait). In order to do that, measured TBT concentrations were used (see Section 2.2). The BMDExpress version 2.2

software (https://www.sciome.com/bmdexpress/) was used to carry out this analysis (Kuo et al., 2016; Phillips et al., 2018; Yang et al., 2007). Parameters of each data set (transcriptomic, metabolomic and morphometric) were individually adjusted to a mathematical model (linear, power, Hill, exponential (2nd, 3rd, 4th, 5th order) or polynomial (2nd, 3rd, 4th order)) and the best fitting was identified. The benchmark dose (BMD) of each of these parameters, as well as the upper and lower limits (BMDU and BMDL, respectively), were calculated using the best fitting model. Median BMDL for transcriptomic, metabolomic and morphometric datasets was calculated and assigned as the point of departure (PoD; i.e. the concentration from where it can be considered proved the existence of effects of the TBT) as it has been determined as a good estimation for a reference dose (Bhat et al., 2013; Farmahin et al., 2017; Webster et al., 2015).

2.4.4. Gene enrichment analysis

DAVID Bioinformatic Resources 6.8 (https://david.ncifcrf.gov/home.jsp) was used for the functional analysis of those genes with an individual BMD value equal or lower to the transcriptomic calculated PoD to assess the first metabolic pathways affected by the TBT. Gene enrichment analysis was performed in DAVID using the default *Danio rerio* background and setting the enrichment significances to a false discovery ratio (FDR) ≤5%. Afterwards, DEGs classified in each identified functional module (either from the GO:Biological Function and KEGG (Kyoto Encyclopedia of Genes and Genomes) datasets) were considered separately for the representation of their benchmark dose lower limits. Only pathways with at least five hits were represented, using the *gplots* package in R (R_Development_Core_Team, 2008). KEGG Mapper v4.1 (https://www.genome.jp/kegg/mapper.html) was used for the graphical representation of the under/overexpression of the genes involved in the steroid biosynthesis pathway (dre00100).

2.5. Open data

The transcriptomic dataset obtained in this study have been deposited in NCBI's Gene Expression Omnibus (Edgar et al., 2002) and are freely accessible through GEO Series accession number GSE139599 (https://www.ncbi.nlm.nih.gov/geo/query/acc.cgi?acc=GSE139599).

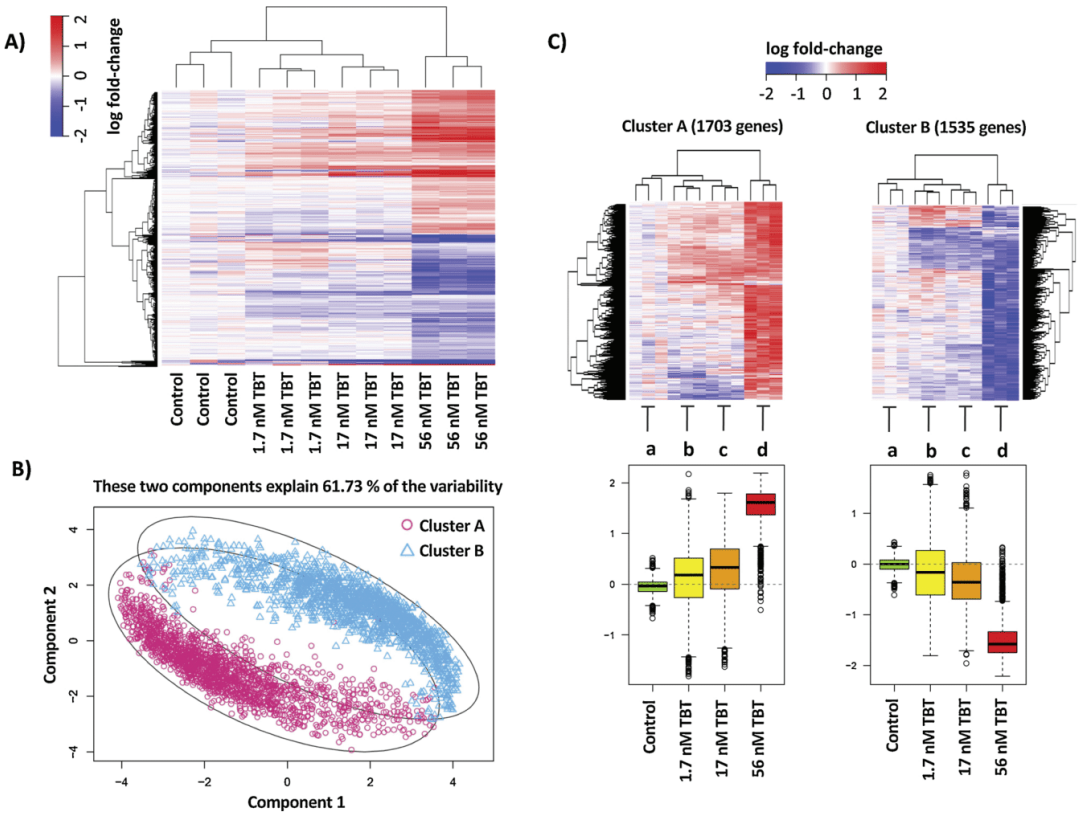

Fig. 1. (A) Heatmap corresponding to the 3238 transcripts identified as differentially expressed genes (DEGs) by ANOVA-PLS analysis. Represented values were normalized, centered to average values of control samples and then log2 transformed. Color scale ranges from blue (underrepresented DEGs) to red (overrepresented DEGs); white cells correspond to values identical to the average values of the controls. Both genes (rows) and samples (columns) were grouped by hierarchical clustering, illustrated by the dendrograms at the left and the top of the panel, respectively. (B) PCA analysis from PAM clustering of DEGs, showing the two defined clusters (cluster A, in magenta, and cluster B, in cyan). The two first components explained the 61.73% of total point variability. (C) Individual heatmaps of the DEGs classified by the PAM clustering in each cluster and distribution of their normalized abundance values. Low-case letters at the top of each group indicate statistically different distributions (determined by an ANOVA followed by a Tukey's B ($p \leq 0.05$) post-hoc test. Colored boxes included values between the 1 st and 3rd quartiles, means are indicated as thick bars and whiskers cover the total distribution, except for outliers (represented as circles). (For interpretation of the references to colour in this figure legend, the reader is referred to the web version of this article.)

3. Results

3.1. Survival, hatching and swim bladder inflation

No statistical differences on survival and hatching rates were detected between control and any TBT concentration group at any age. Conversely, a significant decrease in the swim bladder inflation rates were observed in the 56 nM of TBT group at 5 dpf. Complete results are reported in Supplementary Table ST1. The TBT concentration of 56 nM was categorized as the phenotypical LOAEC, as it was the lowest TBT level that exerted any adverse effect over these parameters at any age. This was in agreement with our previous results (Martínez et al., 2019a) and therefore 56 nM was selected as highest tested concentration for the present RNA-Seq transcriptomic study.

3.2. Determination and classification of DEGs

ANOVA-PLS analysis identified 3238 transcripts whose mRNA levels changed upon TBT treatment (DEGs) in at least one of the exposure groups (Supplementary Table ST2). Hierarchical clustering of samples closely reflected the experimental setup, as biological replicates for each different treatment group clustered together (Fig. 1A). Remarkably, the highest tested dose (56 nM of TBT) appeared as a clearly differentiated group from the rest of conditions, including controls. PAM clustering analysis defined the existence of two groups or clusters of DEGs (Fig. 1B). Cluster A (1703 genes) include genes whose relative abundances increased upon TBT exposure, while genes classified in cluster B (1535 genes) showed a decrease in abundance in TBT-treated samples (Fig. 1C). The distribution of normalized expression values (log fold-changes respect to the control group) denotes a clear dose-response pattern, being 56 nM the dose that presented the highest effects when compared to controls (boxplots in Fig. 1C).

3.3. Analysis of the different points of departure (PoDs) of TBT

The TBT transcriptomic PoD was estimated to be 9.28 nM (Fig. 2) using the median BMDL value of the transcripts as described in Section 2.4.3. It places itself between the low and medium doses used in this study, and it is comparable to the calculated PoD values for metabolite changes (11.48 nM), and well below the corresponding value for morphological traits (67.87 nM) (Fig. 2). Median of BMD doses (BMD) and BMD upper limits (BMDU) were, respectively, 14.52 and 29.82 nM for transcriptomics, 17.19 and 32.95 nM for metabolomics and 72.97 and 77.01 nM for morphometry. Note the similar slope of the cumulative plot at the three biological levels (Fig. 2). Summaries of the best fitted mathematical model for each individual parameter, as well its calculated BMD, BMDL and BMDU values are reported in the Supplementary Tables ST3–ST5 for the transcriptomic (only DEGs), metabolomic and morphometric data, respectively.

3.4. Identification of genes involved in molecular initiating events of TBT exposure

A DAVID functional analysis was performed with those genes with an individual BMD value equal or lower to the transcriptomic PoD (9.28 nM) to assess the first metabolic pathways affected by the TBT. Results obtained after the functional enrichment analysis (Supplementary Tables ST6) showed that most of the affected genes were related to general toxicity and/or pathways related to development: DNA-binding, domain transcription factors, transcription, nucleus, regulation of cell proliferation, cell cycle and differentiation, NAD(P)-binding domain, carbon metabolism, transferases, nucleotide binding, catalytic activity. Averaged BMDL values was estimated for DEGs included in each of these different functional modules (either from the GO:Biological Function and KEGG datasets), in order to identify molecular initiating events. Fig. 3 shows the distribution of these BMDL values, in which magenta and cyan dots represent the DEGs classified in clusters A (overrepresented) and B (underrepresented), respectively. The results show that functional pathways related to general development were particularly enriched in genes classified in cluster B (downregulated by TBT), while the pathways enriched in DEGs classified in cluster A (upregulated by TBT) were more related with immune and inflammatory response, glutathione metabolism, activation of GTPase activity and tRNA aminoacylation processes (Fig. 3; note the cell colors). Interestingly, the functional modules with the lowest estimated BMDL were steroid metabolism and biosynthesis pathways, schematically represented in Fig. 4 (map dre00100: steroid biosynthesis pathway, KEGG). The figure shows that genes codifying for the enzymes involved in the synthesis of cholesterol and vitamin D_3, starting at the squalene epoxidation step, were upregulated by TBT at similar concentrations of its PoD (1.7 nM and/or 17 nM of TBT; Fig. 4; red cells).

4. Discussion

Results from the functional benchmark dose analysis carried out in the present study suggested a general, rather unspecific toxicity pattern of TBT, since most of the affected molecular pathways were related to cell viability and development, except for the specific effect on the steroid metabolism. These results are in agreement with previous studies in fish showing the effect of TBT on DNA-related processes such as DNA repair (Soares et al., 2018; Zuo et al., 2012). On the other hand, our results also showed TBT effects in genes implicated in lipid metabolism and fatty acid biosynthesis pathways, which is consistent with an observed lipidic disruption previously reported in similar experimental setups (den Broeder et al., 2017). However, lipid dysregulation took place only at relatively high TBT concentrations, and it was limited to the transcriptomic level (Berto-Júnior et al., 2018; Grün, 2014; Ouadah-Boussouf and Babin, 2016; Tingaud-Sequeira et al., 2011). The induction of yolk-sac malabsorption syndrome or energy consumption dysregulation by TBT has not been found at this stage of development (5 dpf) (Liang et al., 2017; Martínez et al., 2019a), and obesogenic effects only appear at later larval stages (15 dpf, den Broeder et al., 2017). Interestingly, our results showed that the steroid biosynthesis pathways that lead to the synthesis of cholesterol and vitamin D_3

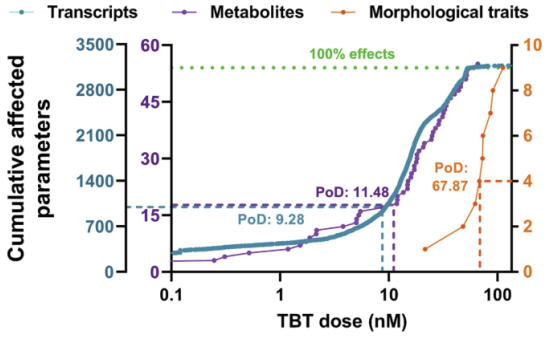

Fig. 2. Accumulation plot of BMD values for the parameters of the different biological levels of zebrafish eleutheroembryos exposed to TBT: transcriptomics (in blue), metabolomics (in purple) and morphometrics (in orange). Points represent the number of parameters with a BMD value lower than a specific TBT concentration. The best BMD value for each DEG/metabolite/morphological parameter was determined using the BMDExpress version 2.2 software (https://www.sciome.com/bmdexpress/) (Kuo et al., 2016; Phillips et al., 2018; Yang et al., 2007). The median BMDL values were used as PoD (point of departure) for the three biological levels and are interpolated in the graph as dotted lines. Green dotted line indicates the 100% of the studied parameters for each level (3238 differentially expressed genes, 55 metabolites and 9 morphological parameters). (For interpretation of the references to colour in this figure legend, the reader is referred to the web version of this article.)

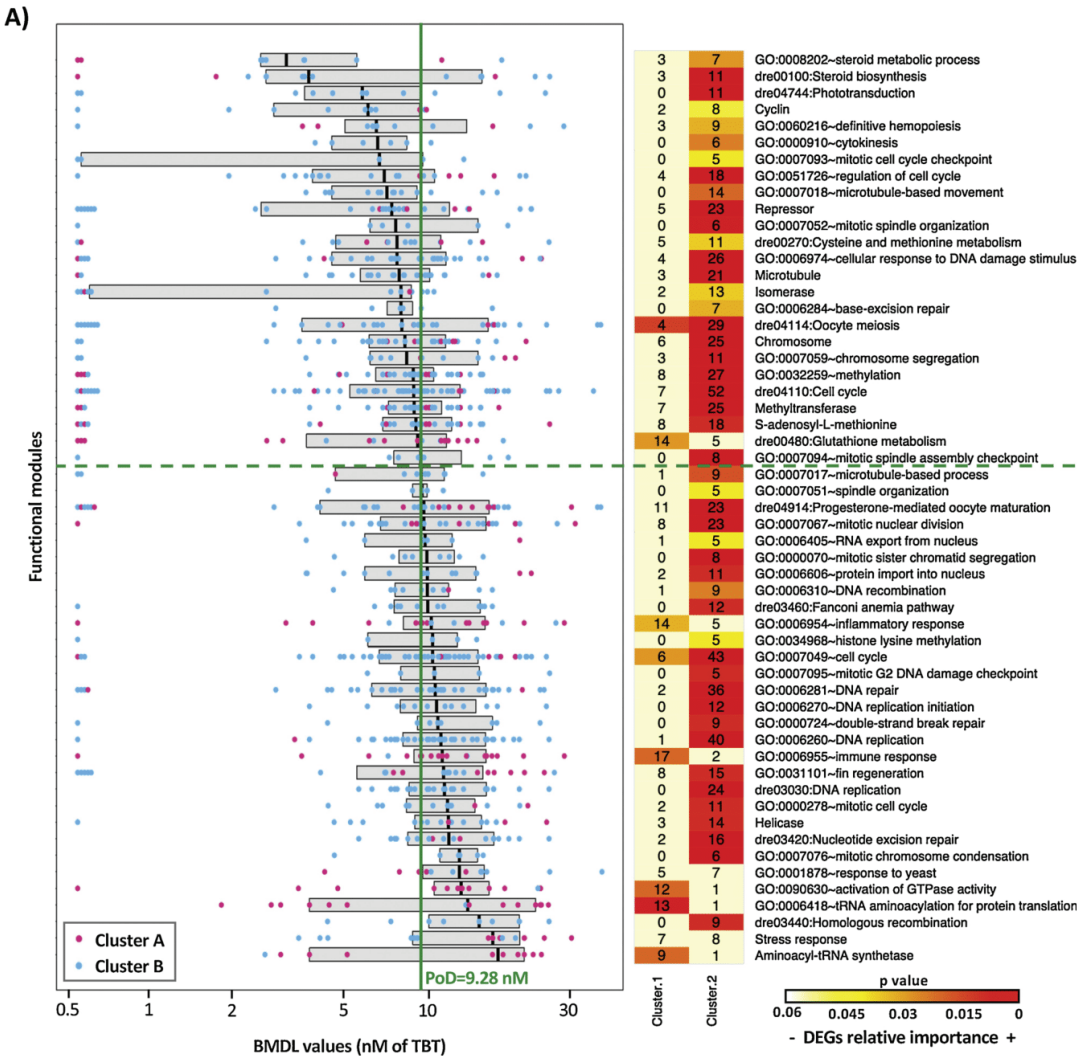

Fig. 3. BMDL values for individual DEGs, classified by their annotation to functional modules. For each module, grey box includes values between the 1 st and 3rd quartiles and a thick bar indicates the mean. Calculated BMDL of DEGs classified in cluster A and B are represented as magenta and cyan points, respectively. For helping visualization, green vertical line indicates the median BMDL considered as the transcriptomic point of departure (PoD) for TBT exposure (Fig. 2). Green dotted horizontal line separates the functional modules with median BMDL values higher or lower than global transcriptomic PoD. On the right, distribution of DEGs among the different functional modules (rows) and clusters (columns). Numbers express the absolute number of DEGs in each functional module and cluster, box colors indicate the relative importance of DEGs associated to each pathway for each cluster (from light-yellow -most- to red -less-; two cells of the same color correspond to an identical relative fraction of DEGs in both clusters). For simplification, only functional modules with at least 5 DEGs in at least one of the clusters were represented. Redundant functional modules were simplified to the one with the highest number of hits. (For interpretation of the references to colour in this figure legend, the reader is referred to the web version of this article.)

appeared as the modules that become affected at the lowest TBT concentrations. Since the cholesterol is a key molecule not only for cell membrane formation but also as a precursor for bile acids and steroid hormones synthesis (Anderson et al., 2011; Tokarz et al., 2013), we suggest that TBT exposure could lead important effects over the developing eleutheroembryos. Furthermore, cholesterol and its esters are important components of lipid droplets, which are the preferred form of storage for neutral lipids in the late larval, juvenile and adult stages (Flynn et al., 2009; Minchin and Rawls, 2011). Indeed, those effects in the cholesterol synthesis pathway observed at early stages of the eleutheroembryos development could be the cause of lipid disruptive effects observed later in life, as it has been observed in zebrafish (den Broeder et al., 2017; Lyssimachou et al., 2015). It has been previously reported that vitamin D_3 signaling is crucial for the normal development of the zebrafish during embryo stage, and that its dysregulation can lead a diapause-like arrest (endocrine-mediated developmental delay) in zebrafish embryos and eleutheroembryos (Craig et al., 2008; Romney et al., 2018). This is consistent with our observation that many development-related pathways (cell cycle, mitosis, microtubules, among others) were down-regulated in TBT-exposed embryos. These

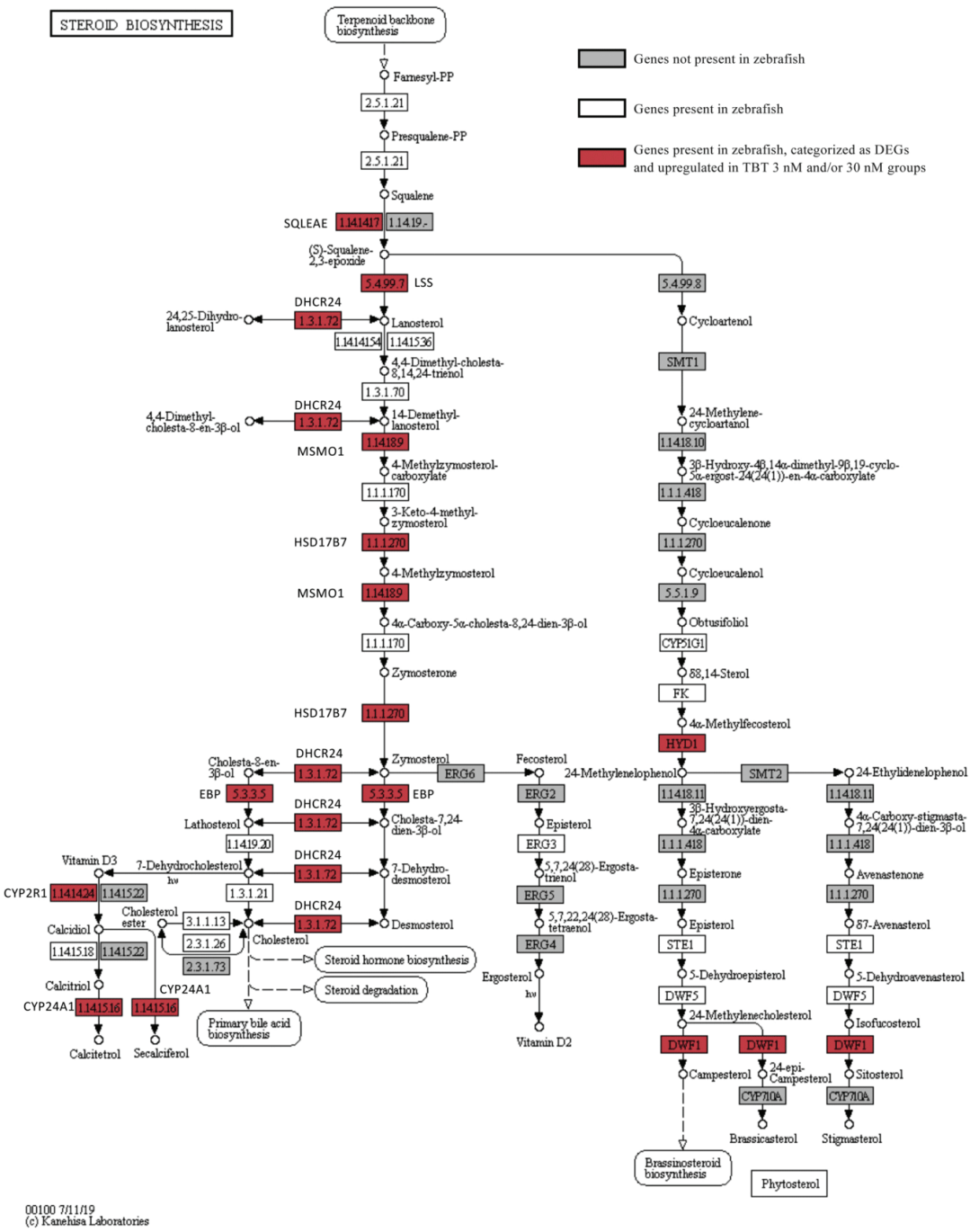

Fig. 4. Graphical representation of the steroid biosynthesis pathway (dre00100, Kyoto Encyclopedia of Genes and Genomes). Grey cells represent genes not present in zebrafish. Genes colored in white did not show changes on their mRNA levels in the 1.7 or 17 nM TBT exposure groups, those that showed overexpression in at least one of these concentrations are colored in red (eight genes in total). Those concentrations were chosen to represent the behaviour of the genes at concentrations close to the transcriptomic PoD (9.28 nM of TBT). (For interpretation of the references to colour in this figure legend, the reader is referred to the web version of this article.)

effects may well be related to previous observation that the morphometric effects of TBT were more related to a developmental delay than to a specific mode of action (Martínez et al., 2019a). Whether or not the developmental delay is mediated by a reduced cell proliferation rate should be further assessed.

A conceivable alternative explanation for the observed effect of TBT may be the release of Sn ion and the subsequent heavy metal poisoning in zebrafish embryos. TBT biodegradation in animal tissues has been suggested to undergo via hydroxylation followed by dealkylation to produce DBT (dibutyltin) and other metabolites, involving mostly cytochrome P450 enzymes (Beyer and Meador, 2011; Nesci et al., 2011). Although these reactions readily occur in zebrafish liver (McGinnis and Crivello, 2011), biotransformation of TBT has not ever been observed in embryos from different fish species, neither TBT biodegradation to inorganic tin ion ($Sn^{2+/4+}$) (Braunbeck et al., 1998). Thus, and although we cannot rule out a possible role for general metal poisoning effects, we propose that TBT exerted its early transcriptomic disrupting effects (mostly in the steroid related pathways) as such, without any significant influence from transformation products. Current evidences indicate the covalent binding of TBT to the retinoid X receptor (RXR) as the molecular initiating event (MIE) that trigger TBT adverse effects in many biological systems (De Voogt, 2015; le Maire et al., 2009). The TBT-RXR complex would form dysfunctional heterodimers with different receptors, including the peroxisome proliferator-activated receptors (PPAR-α, -γ, -δ) or vitamin D receptors (VDR), leading to molecular cascades of reactions that may explain the TBT disrupting properties (Grün, 2014; Huang and Chen, 2017; le Maire et al., 2009; Zhang et al., 2001). These RXRs heterodimers have been suggested to stimulate the steroid biosynthesis in cell cultures (Munetsuna et al., 2009), as well to be related with steroids, organism development, cholesterol, lipid metabolism, fatty acid biosynthesis, and immune response in different animal models (Evans and Mangelsdorf, 2014; Verhaegen, 2012). Therefore, our results are compatible with this proposed MIE for TBT, as all these metabolic pathways appeared as transcriptomically affected by TBT in our study.

Based on the integration of transcriptomic, metabolomic and morphometric data using BMD analysis, we can conclude that TBT exert a rapid and general toxicity in the exposed zebrafish eleutheroembryos. Whereas transcriptomic points of departure of other endocrine disrupting chemicals usually occur at concentrations at least 2–3 orders of magnitude lower than LC_{50} values (Martínez et al., 2019b, 2018; Weber et al., 2013), TBT altered the eleutheroembryo transcriptome and metabolome at only one order of magnitude below the estimated LC_{50}. This is in concordance with the fact that the PoD of TBT for morphological traits (67.87 nM) was found very close to lethal doses (LC_{50}: 93.63 nM; Martínez et al., 2019a). Nevertheless, our results support the idea that molecular analysis can be also used as early warning markers for toxicological studies. When comparing BMD results from our study at the transcriptome and metabolome levels, we also observed that both have similar PoDs. It has also been recently demonstrated that short-term transcriptomic PoDs are protective of chronic effects for fish exposed to EDCs, specifically to estrogenic compounds (Pagé-Larivière et al., 2019). Whereas the use of *-omics* technologies has been applied to study the mode of action and/or the MIE of pollutants (Brockmeier et al., 2017), the application of transcriptomic studies to chemical risk assessment is more limited (Harrill et al., 2019; Thomas et al., 2013). It should be noted in our results the similar slope of the cumulative effect plots of the BMD analysis done with the transcriptomic, metabolomic and morphometric data. As far as we know, not many studies have compared BMD analysis using data from different biological levels. Similar results were obtained in our laboratory in zebrafish eleutheroembryos exposed to PFOS when comparing transcriptomic and morphometric parameters using the BMD approach (Martínez et al., 2019b). We consider at least possible that the similar slopes of both curves may reflect the propagation of molecular events (transcriptome and metabolome) to higher levels of organization (morphology), although this assumption should be further explored. In summary, our results highlight the value of transcriptomic data and of the use of transcriptomic dose-response studies in environmental risk assessment.

A significant advance in the use of genomic data into risk assessment is due to the development of methods that integrate BMD approaches to analyze transcriptomic data. This method allows the identification of reference doses at which particular cellular responses are affected (Thomas et al., 2007). The study of the transcriptomic effects of TBT at the functional level using the BMD approach, instead of looking directly at the functionality of the DEGs, can also prevent the lack of reproducibility of specific identified DEGs as biomarkers between experiments or the lack of linkages with the phenotype, as have been observed in some clinical studies (Myers et al., 2015; Song et al., 2018). This is so because the effects of a pollutant on functional pathways are generally more robust than their effects on the expression of specific genes, whatever useful may they be for exposure and effect assessment studies. In addition, the application of benchmark dose approach in toxicology, chemical effects and risk assessment are nowadays preferred to other more conventional parameters as NOECs or LOECs (Altenburger et al., 2012; Escher et al., 2014; Mayfield and Skall, 2018) and allow us to compare different datasets at different doses, as previously reported (Tu et al., 2019). Finally, applying the BMD concept at the functional level allowed us to separate the initially affected pathways (steroid biosynthesis, in our case) from the ones disrupted at higher concentrations (cell viability, general development or lipid-related pathways, among others).

5. Conclusions

In summary, the present dose-response transcriptomic analysis allowed us to determine the most sensitive pathways affected by TBT, mostly related to the steroid biosynthesis, general cell viability and development. The transcriptomic effects in genes related to general toxicity may be related to a developmental delay induced by relatively high TBT concentrations, in agreement with previous morphometric results. Obesogenic effects, traditionally attributed to TBT, only appeared at concentrations relatively close to lethal levels. This is different from the typical pattern of toxic effects for most EDCs, like estrogenic compounds or thyroid disrupters, in which the earlier endocrine effects appear at concentrations two or three orders of magnitude lower than the $LC_{50,}$ suggesting than the toxic mode of action of TBT could differ from other EDCs. The present work contributes in the understanding of the environmental hazards associated to TBT and highlights the utility of using the benchmark dose approach with *-omic* datasets at the functional pathway level in environmental risk assessment.

CRediT authorship contribution statement

Rubén Martínez: Conceptualization, Data curation, Formal analysis, Investigation, Visualization, Writing - original draft, Writing - review & editing. **Anna E. Codina:** Data curation, Methodology. **Carlos Barata:** Funding acquisition, Writing - review & editing. **Romà Tauler:** Funding acquisition, Writing - review & editing. **Benjamin Piña:** Conceptualization, Data curation, Formal analysis, Funding acquisition, Project administration, Supervision, Visualization, Writing - original draft, Writing - review & editing. **Laia Navarro-Martín:** Conceptualization, Data curation, Formal analysis, Investigation, Project administration, Supervision, Visualization, Writing - original draft, Writing - review & editing.

Declaration of Competing Interest

The authors declare no conflicts of interest.

Acknowledgments

This work was supported by the European Research Council under the European Union's Seventh Framework Programme FP7-IDEAS-ERC/320737. Some parts of this study were also supported by grants from the Spanish Ministry of Economy and Competitiveness (CTQ2014-56777-R), from the Spanish Ministry of Science, Innovation and University (RTI2018- 096175-B-I00), and from the Spanish Ministry of Science and Innovation (Project CEX2018-000794-S). AEC acknowledges the funding from ISCIII (Spanish Ministry of Economy and Competitiveness, grant number PT17/0009/0019), co-financed by the European Fund for Regional Development (FEDER). RM was supported by a FPU predoctoral fellow from the Spanish Ministry of Education, Culture and Sport (ref. FPU15/03332). LNM was supported by a H2020-Marie Skłodowska-Curie Action MSCA-IF-RI- 2017 awarded by the European Commission (ref. 797725-EpiSTOX).

Appendix A. Supplementary data

Supplementary material related to this article can be found, in the online version, at doi:https://doi.org/10.1016/j.jhazmat.2020.122881.

References

Altenburger, R., Scholz, S., Schmitt-Jansen, M., Busch, W., Escher, B.I., 2012. Mixture toxicity revisited from a toxicogenomic perspective. Environ. Sci. Technol. 46, 2508–2522. https://doi.org/10.1021/es2038036.

Anderson, J.L., Carten, J.D., Farber, S.A., 2011. Zebrafish lipid metabolism: from mediating early patterning to the metabolism of dietary fat and cholesterol. Methods Cell Biol. 101, 111–141. https://doi.org/10.1016/B978-0-12-387036-0.00005-0.

Antizar-Ladislao, B., 2008. Environmental levels, toxicity and human exposure to tributyltin (TBT)-contaminated marine environment. A review. Environ. Int. 34, 292–308. https://doi.org/10.1016/j.envint.2007.09.005.

Baker, M.E., Hardiman, G., 2014. Transcriptional analysis of endocrine disruption using zebrafish and massively parallel sequencing. J. Mol. Endocrinol. 52, R241–R256. https://doi.org/10.1530/JME-13-0219.

Bergman, Å., Heindel, J.J., Jobling, S., Kidd, K.A., Zoeller, R.T., 2013. State of the Science of Endocrine Disrupting Chemicals 2012 - Summary for Decision Makers. WHOhttps://doi.org/10.1590/S1414-462X201300010003.

Berto-Júnior, C., de Carvalho, D.P., Soares, P., Miranda-Alves, L., 2018. Tributyltin and zebrafish: swimming in dangerous water. Front. Endocrinol. (Lausanne). 9, 152. https://doi.org/10.3389/fendo.2018.00152.

Beyer, W.N., Meador, J.P., 2011. Environmental Contaminants in Biota: Interpreting Tissue Concentrations. CRC Press.

Bhat, V.S., Hester, S.D., Nesnow, S., Eastmond, D.A., 2013. Concordance of transcriptional and apical benchmark dose levels for conazole-induced liver effects in mice. Toxicol. Sci. 136, 205–215. https://doi.org/10.1093/toxsci/kft182.

Braunbeck, T.(Thomas), Hinton, D.E., Streit, B., 1998. Fish Ecotoxicology. Birkhäuser Verlag, Basel, Switzerland.

Bray, S., 2006. Tributyltin pollution on a global scale. An overview of relevant and recent research: impacts and issues. Contract 54.

Brockmeier, E.K., Hodges, G., Hutchinson, T.H., Butler, E., Hecker, M., Tollefsen, K.E., Garcia-Reyero, N., Kille, P., Becker, D., Chipman, K., Colbourne, J., Collette, T.W., Cossins, A., Cronin, M., Graystock, P., Gutsell, S., Knapen, D., Katsiadaki, I., Lange, A., Marshall, S., Owen, S.F., Perkins, E.J., Plaistow, S., Schroeder, A., Taylor, D., Viant, M., Ankley, G., Falciani, F., 2017. The role of omics in the application of adverse outcome pathways for chemical risk assessment. Toxicol. Sci. 158, 252–262. https://doi.org/10.1093/toxsci/kfx097.

Caballero-Gallardo, K., Olivero-Verbel, J., Freeman, J.L., 2016. Toxicogenomics to evaluate endocrine disrupting effects of environmental chemicals using the zebrafish model. Curr. Genomics 17, 515–527. https://doi.org/10.2174/1389202917666160513105959.

Castro, Í.B., Fillmann, G., 2012. High tributyltin and imposex levels in the commercial muricid Thais chocolata from two Peruvian harbor areas. Environ. Toxicol. Chem. 31, 955–960. https://doi.org/10.1002/etc.1794.

Champ, M.A., Seligman, P.F., 1996. Organotin: Environmental Fate and Effects. Springer Science & Business Media.

Craig, T.A., Sommer, S., Sussman, C.R., Grande, J.P., Kumar, R., 2008. Expression and regulation of the vitamin D receptor in the zebrafish, Danio rerio. J. Bone Miner. Res. 23, 1486–1496. https://doi.org/10.1359/jbmr.080403.

Cruz, A., Anselmo, A.M., Suzuki, S., Mendo, S., 2015a. Tributyltin (TBT): a review on microbial resistance and degradation. Crit. Rev. Environ. Sci. Technol. 45, 970–1006. https://doi.org/10.1080/10643389.2014.924181.

Cruz, A., Rodrigues, R., Pinheiro, M., Mendo, S., 2015b. Transcriptomes analysis of Aeromonas molluscorum Av27 cells exposed to tributyltin (TBT): unravelling the effects from the molecular level to the organism. Mar. Environ. Res. 109, 132–139. https://doi.org/10.1016/j.marenvres.2015.06.017.

Davies, A.G., 2004. Organotin Chemistry, 2nd, Completely Revised and Updated Edition.

Davis, J.A., Gift, J.S., Zhao, Q.J., 2011. Introduction to benchmark dose methods and U.S. EPA's benchmark dose software (BMDS) version 2.1.1. Toxicol. Appl. Pharmacol. 254, 181–191. https://doi.org/10.1016/j.taap.2010.10.016.

De Mendiburu, F., 2009. Una Herramienta De Analisis Estadistico Para La Investigacion Agricola. Univ. Nac. Ing. Universidad Nacional de Ingeniería.

De Voogt, P., 2015. Reviews of Environmental Contamination and Toxicology 236https://doi.org/10.1007/978-3-319-20013-2.

Demeneix, B., Slama, R., 2019. Endocrine Disruptors: From Scientific Evidence to Human Health Protection Policy Department for Citizens' Rights and Constitutional Affairs.

den Broeder, M.J., Moester, M.J.B., Kamstra, J.H., Cenijn, P.H., Davidoiu, V., Kamminga, L.M., Ariese, F., De Boer, J.F., Legler, J., 2017. Altered adipogenesis in zebrafish larvae following high fat diet and chemical exposure is visualised by stimulated raman scattering microscopy. Int. J. Mol. Sci. 18, E894. https://doi.org/10.3390/ijms18040894.

Dobin, A., Davis, C.A., Schlesinger, F., Drenkow, J., Zaleski, C., Jha, S., Batut, P., Chaisson, M., Gingeras, T.R., 2013. STAR: ultrafast universal RNA-seq aligner. Bioinformatics 29, 15–21. https://doi.org/10.1093/bioinformatics/bts635.

ECHA (European Chemicals Agency), 2019. Endocrine Disruptor Assessment. https://echa.europa.eu/es/ed-assessment?p_p_id=disslists_WAR_disslistsportlet&p_p_lifecycle=0&p_p_state=normal&p_p_mode=view&p_p_col_id=column-1&p_p_col_pos=1&p_p_col_count=2&_disslists_WAR_disslistsportlet_dte_assessmentTo=&_disslists_WAR_disslistsportle.

Edgar, R., Domrachev, M., Lash, A.E., 2002. Gene Expression Omnibus: NCBI gene expression and hybridization array data repository. Nucleic Acids Res. 30, 207–210. https://doi.org/10.1093/nar/30.1.207.

Escher, B.I., Allinson, M., Altenburger, R., Bain, P.A., Balaguer, P., Busch, W., Crago, J., Denslow, N.D., Dopp, E., Hilscherova, K., Humpage, A.R., Kumar, A., Grimaldi, M., Jayasinghe, B.S., Jarosova, B., Jia, A., Makarov, S., Maruya, K.A., Medvedev, A., Mehinto, A.C., Mendez, J.E., Poulsen, A., Prochazka, E., Richard, J., Schifferli, A., Schlenk, D., Scholz, S., Shiraishi, F., Snyder, S., Su, G., Tang, J.Y.M., Burg, B.Van Der, Linden, S.C.V.Der, Werner, I., Westerheide, S.D., Wong, C.K.C., Yang, M., Yeung, B.H.Y., Zhang, X., Leusch, F.D.L., 2014. Benchmarking organic micropollutants in wastewater, recycled water and drinking water with in vitro bioassays. Environ. Sci. Technol. 48, 1940–1956. https://doi.org/10.1021/es403899t.

European Commission, 2007. Commission Staff Working Document on the Implementation for the "community Strategy for Endocrine Disrupters"- a Range of Substances Suspected of Interfering With the Hormone Systems of Humans and Wildlife. SEC (2007) 1635. Framework 1–37. https://doi.org/10.1017/CBO9781107415324.004.

Evans, R.M., Mangelsdorf, D.J., 2014. Nuclear receptors, RXR, and the big bang. Cell. 157, 255–266. https://doi.org/10.1016/j.cell.2014.03.012.

Farmahin, R., Williams, A., Kuo, B., Chepelev, N.L., Thomas, R.S., Barton-Maclaren, T.S., Curran, I.H., Nong, A., Wade, M.G., Yauk, C.L., 2017. Recommended approaches in the application of toxicogenomics to derive points of departure for chemical risk assessment. Arch. Toxicol. 91, 2045–2065. https://doi.org/10.1007/s00204-016-1886-5.

Filipsson, A.F., Sand, S., Nilsson, J., Victorin, K., 2003. The benchmark dose method–review of available models, and recommendations for application in health risk assessment. Crit. Rev. Toxicol. 33, 505–542. https://doi.org/10.1080/10408440390242360.

Flynn, E.J., Trent, C.M., Rawls, J.F., 2009. Ontogeny and nutritional control of adipogenesis in zebrafish (Danio rerio). J. Lipid Res. 50, 1641–1652. https://doi.org/10.1194/jlr.M800590-JLR200.

Fresno, C., Balzarini, M.G., Fernández, E.A., 2014. Lmdme : linear models on designed multivariate experiments in R. J. Stat. Softw. 56, 1–16. https://doi.org/10.18637/jss.v056.i07.

Gore, A.C., Crews, D., Doan, L.L., La Merrill, M., Patisaul, H., Zota, A., 2014. Introduction to Endocrine Disrupting Chemicals (EDCs)-A Guide for Public Interest Organizations and Policy-markers. Www.Endocrine.Org..

Grün, F., 2014. The obesogen tributyltin. Vitamins and Hormones. pp. 277–325. https://doi.org/10.1016/B978-0-12-800095-3.00011-0.

Harrill, J., Shah, I., Setzer, R.W., Haggard, D., Auerbach, S., Judson, R., Thomas, R.S., 2019. Considerations for strategic use of high-throughput transcriptomics chemical screening data in regulatory decisions. Curr. Opin. Toxicol. 15, 64–75. https://doi.org/10.1016/j.cotox.2019.05.004.

Hass, U., Christiansen, S., Andersen, D., Rosenberg, A., Egebjerg, K.M., Brandt, S., Nikolov, N.G., Holbech, H., Morthorst, J.E., 2018. List of endocrine disrupting chemicals.

Heindel, J.J., Blumberg, B., 2019. Environmental obesogens: mechanisms and controversies. Annu. Rev. Pharmacol. Toxicol. 59, 89–106. https://doi.org/10.1146/annurev-pharmtox-010818-021304.

Hennig, C., 2014. fpc: flexible procedures for clustering. http://cran.r-project.org/package=fpc.

Huang, Q., Chen, Q., 2017. Mediating roles of PPARs in the effects of environmental chemicals on sex steroids. PPAR Res. 2017, 3203161. https://doi.org/10.1155/2017/3203161.

IMO, 2002. Focus on IMO: anti-fouling systems. Int. Marit. Organ. 44, 1–31. https://doi.org/10.1097/TA.0b013e31817de3f4.

Jarque, S., Ibarra, J., Rubio-Brotons, M., García-Fernández, J., Terriente, J., 2019. Multiplex analysis platform for endocrine disruption prediction using zebrafish. Int. J. Mol. Sci. 20, E1739. https://doi.org/10.3390/ijms20071739.

Jordão, R., Garreta, E., Campos, B., Lemos, M.F.L., Soares, A.M.V.M., Tauler, R., Barata, C., 2016. Compounds altering fat storage in Daphnia magna. Sci. Total Environ. 545–546, 127–136. https://doi.org/10.1016/j.scitotenv.2015.12.097.

Kimmel, C.B., Ballard, W.W., Kimmel, S.R., Ullmann, B., Schilling, T.F., 1995a. Stages of embryonic development of the zebrafish. Dev. Dyn. 203, 253–310. https://doi.org/

10.1002/aja.1002030302.
Kimmel, C.B., Ballard, W.W., Kimmel, S.R., Ullmann, B., Schilling, T.F., 1995b. Stages of embryonic development of the zebrafish. Dev. Dyn. 203, 253–310. https://doi.org/10.1002/aja.1002030302.
Kuo, B., Francina Webster, A., Thomas, R.S., Yauk, C.L., 2016. BMDExpress Data Viewer - a visualization tool to analyze BMDExpress datasets. J. Appl. Toxicol. 36, 1048–1059. https://doi.org/10.1002/jat.3265.
Langston, W.J., Pope, N.D., Davey, M., Langston, K.M., O' Hara, S.C.M., Gibbs, P.E., Pascoe, P.L., 2015. Recovery from TBT pollution in english channel environments: a problem solved? Mar. Pollut. Bull. 95, 551–564. https://doi.org/10.1016/j.marpolbul.2014.12.011.
le Maire, A., Grimaldi, M., Roecklin, D., Dagnino, S., Vivat-Hannah, V., Balaguer, P., Bourguet, W., 2009. Activation of RXR-PPAR heterodimers by organotin environmental endocrine disruptors. EMBO Rep. 10, 367–373. https://doi.org/10.1038/embor.2009.8.
Lee, S.L.J., Horsfield, J.A., Black, M.A., Rutherford, K., Fisher, A., Gemmell, N.J., 2017. Histological and transcriptomic effects of 17α-methyltestosterone on zebrafish gonad development. BMC Genomics 18, 557. https://doi.org/10.1186/s12864-017-3915-z.
Li, B., Dewey, C.N., 2011. RSEM: accurate transcript quantification from RNA-Seq data with or without a reference genome. BMC Bioinformatics 12, 323. https://doi.org/10.1186/1471-2105-12-323.
Li, Z., Yu, D., Wangbao, G., Guangjun, W., Ermeng, Y., Jun, X., 2019. Aquatic ecotoxicology and water quality criteria of three organotin compounds: a review. Nat. Environ. Pollut. Technol. 18, 217–224.
Liang, X., Souders, C.L., Zhang, J., Martyniuk, C.J., 2017. Tributyltin induces premature hatching and reduces locomotor activity in zebrafish (Danio rerio) embryos/larvae at environmentally relevant levels. Chemosphere 189, 498–506. https://doi.org/10.1016/j.chemosphere.2017.09.093.
Löhr, H., Hammerschmidt, M., 2011. Zebrafish in endocrine systems: recent advances and implications for human disease. Annu. Rev. Physiol. 73, 183–211. https://doi.org/10.1146/annurev-physiol-012110-142320.
Love, M.I., Huber, W., Anders, S., 2014. Moderated estimation of fold change and dispersion for RNA-seq data with DESeq2. Genome Biol. 15, 550. https://doi.org/10.1186/s13059-014-0550-8.
Lyssimachou, A., Santos, J.G., André, A., Soares, J., Lima, D., Guimarães, L., Almeida, C.M.R., Teixeira, C., Castro, L.F.C., Santos, M.M., 2015. The mammalian "obesogen" tributyltin targets hepatic triglyceride accumulation and the transcriptional regulation of lipid metabolism in the liver and brain of zebrafish. PLoS One 10, e0143911. https://doi.org/10.1371/journal.pone.0143911.
Maechler, M., Rousseeuw, P., Struyf, A., Hubert, M., Hornik, K., Studer, M., Roudier, P., Gonzalez, J., Kozlowski, K., Schubert, E., 2019. Cluster: "Finding Groups in Data": Cluster Analysis Extended Rousseeuw Et al. https://cran.r-project.org/web/packages/cluster/index.html.
Martínez, R., Esteve-Codina, A., Herrero-Nogareda, L., Ortiz-Villanueva, E., Barata, C., Tauler, R., Raldúa, D., Piña, B., Navarro-Martín, L., 2018. Dose-dependent transcriptomic responses of zebrafish eleutheroembryos to Bisphenol A. Environ. Pollut. 243, 988–997. https://doi.org/10.1016/j.envpol.2018.09.043.
Martínez, R., Herrero-Nogareda, L., Van Antro, M., Campos, M.P., Casado, M., Barata, C., Piña, B., Navarro-Martín, L., 2019a. Morphometric signatures of exposure to endocrine disrupting chemicals in zebrafish eleutheroembryos. Aquat. Toxicol. 214, 105232. https://doi.org/10.1016/j.aquatox.2019.105232.
Martínez, R., Navarro-Martín, L., Luccarelli, C., Codina, A.E., Raldúa, D., Barata, C., Tauler, R., Piña, B., 2019b. Unravelling the mechanisms of PFOS toxicity by combining morphological and transcriptomic analyses in zebrafish embryos. Sci. Total Environ. 674, 462–471. https://doi.org/10.1016/j.scitotenv.2019.04.200.
Mayfield, D.B., Skall, D.G., 2018. Benchmark dose analysis framework for developing wildlife toxicity reference values. Environ. Toxicol. Chem. 37, 1496–1508. https://doi.org/10.1002/etc.4082.
McGinnis, C.L., Crivello, J.F., 2011. Elucidating the mechanism of action of tributyltin (TBT) in zebrafish. Aquat. Toxicol. 103, 25–31. https://doi.org/10.1016/j.aquatox.2011.01.005.
Minchin, J.E.N., Rawls, J.F., 2011. In vivo analysis of white adipose tissue in zebrafish. Methods in Cell Biology. Academic Press Inc, pp. 63–86. https://doi.org/10.1016/B978-0-12-381320-6.00003-5.
Munetsuna, E., Hojo, Y., Hattori, M., Ishii, H., Kawato, S., Ishida, A., Kominami, S.A.J., Yamazaki, T., 2009. Retinoic acid stimulates 17β-estradiol and testosterone synthesis in rat hippocampal slice cultures. Endocrinology 150, 4260–4269. https://doi.org/10.1210/en.2008-1644.
Myers, J.S., von Lersner, A.K., Robbins, C.J., Sang, Q.-X.A., 2015. Differentially expressed genes and signature pathways of human prostate cancer. PLoS One 10, e0145322. https://doi.org/10.1371/journal.pone.0145322.
Nakanishi, T., 2008. Endocrine disruption induced by organotin compounds; organotins function as a powerful agonist for nuclear receptors rather than an aromatase inhibitor. J. Toxicol. Sci. 33, 269–276. https://doi.org/10.2131/jts.33.269.
Nesci, S., Ventrella, V., Trombetti, F., Pirini, M., Borgatti, A.R., Pagliarani, A., 2011. Tributyltin (TBT) and dibutyltin (DBT) differently inhibit the mitochondrial Mg-ATPase activity in mussel digestive gland. Toxicol. In Vitro 25, 117–124. https://doi.org/10.1016/j.tiv.2010.10.001.
Newman, M.C., McIntosh, A.W., 1993. Metal ecotoxicology: concepts and applications. J. North Am. Benthol. Soc. 12, 106–107. https://doi.org/10.2307/1467696.
Orlando, E.F., Kolok, A.S., Binzcik, G.A., Gates, J.L., Horton, M.K., Lambright, C.S., Gray, L.E., Soto, A.M., Guillette, L.J., 2004. Endocrine-disrupting effects of cattle feedlot effluent on an aquatic sentinel species, the fathead minnow. Environ. Health Perspect. 112, 353–358. https://doi.org/10.1289/ehp.6591.
Ortiz-Villanueva, E., Jaumot, J., Martínez, R., Navarro-Martín, L., Piña, B., Tauler, R., 2018. Assessment of endocrine disruptors effects on zebrafish (Danio rerio) embryos by untargeted LC-HRMS metabolomic analysis. Sci. Total Environ. 635, 156–166. https://doi.org/10.1016/j.scitotenv.2018.03.369.
Ouadah-Boussouf, N., Babin, P.J., 2016. Pharmacological evaluation of the mechanisms involved in increased adiposity in zebrafish triggered by the environmental contaminant tributyltin. Toxicol. Appl. Pharmacol. 294, 32–42. https://doi.org/10.1016/j.taap.2016.01.014.
Pagé-Larivière, F., Crump, D., O'Brien, J.M., 2019. Transcriptomic points-of-departure from short-term exposure studies are protective of chronic effects for fish exposed to estrogenic chemicals. Toxicol. Appl. Pharmacol. 378, 114634. https://doi.org/10.1016/j.taap.2019.114634.
Parichy, D.M., Elizondo, M.R., Mills, M.G., Gordon, T.N., Engeszer, R.E., 2009. Normal table of postembryonic zebrafish development: staging by externally visible anatomy of the living fish. Dev. Dyn. 238, 2975–3015. https://doi.org/10.1002/dvdy.22113.
Phillips, J.R., Svoboda, D.L., Tandon, A., Patel, S., Sedykh, A., Mav, D., Kuo, B., Yauk, C.L., Yang, L., Thomas, R.S., Gift, J.S., Davis, J.A., Olszyk, L., Merrick, B.A., Paules, R.S., Parham, F., Saddler, T., Shah, R.R., Auerbach, S.S., 2018. BMDExpress 2: enhanced transcriptomic dose-response analysis workflow. Bioinformatics. 35, 1780–1782. https://doi.org/10.1093/bioinformatics/bty878.
Qian, X., Ba, Y., Zhuang, Q., Zhong, G., 2014. RNA-Seq technology and its application in fish transcriptomics. OMICS 18, 98–110. https://doi.org/10.1089/omi.2013.0110.
Raldúa, D., Piña, B., 2014. In vivo zebrafish assays for analyzing drug toxicity. Expert Opin. Drug Metab. Toxicol. 10, 685–697. https://doi.org/10.1517/17425255.2014.896339.
Ramaswamy, B.R., Tao, H., Hojo, M., 2004. Contamination and biomethylation of organotin compounds in pearl/fish culture areas in Japan. Anal. Sci. 20, 45–53. https://doi.org/10.2116/analsci.20.45.
Reuter, J.A., Spacek, D.V., Snyder, M.P., 2015. High-throughput sequencing technologies. Mol. Cell 58, 586–597. https://doi.org/10.1016/j.molcel.2015.05.004.
Romney, A.L.T., Davis, E.M., Corona, M.M., Wagner, J.T., Podrabsky, J.E., 2018. Temperature-dependent vitamin D signaling regulates developmental trajectory associated with diapause in an annual killifish. Proc. Natl. Acad. Sci. U. S. A. 115, 12763–12768. https://doi.org/10.1073/pnas.1804590115.
Santillo, D., Langston, W.J., 2001. Tributyltin (TBT) antifoulants: a tale of ships, snails and imposex. Late lessons from early Warn. precautionary Princ. 1896–2000.
Santos, M.M., Micael, J., Carvalho, A.P., Morabito, R., Booy, P., Massanisso, P., Lamoree, M., Reis-Henriques, M.A., 2006. Estrogens counteract the masculinizing effect of tributyltin in zebrafish. Comp. Biochem. Physiol. - C Toxicol. Pharmacol. 142, 151–155. https://doi.org/10.1016/j.cbpc.2005.11.014.
Scholz, S., Mayer, I., 2008. Molecular biomarkers of endocrine disruption in small model fish. Mol. Cell. Endocrinol. 293, 57–70. https://doi.org/10.1016/j.mce.2008.06.008.
Segner, H., 2009. Zebrafish (Danio rerio) as a model organism for investigating endocrine disruption. Comp. Biochem. Physiol. Part C Toxicol. Pharmacol. 149, 187–195. https://doi.org/10.1016/j.cbpc.2008.10.099.
Soares, J., Neuparth, T., Lyssimachou, A., Lima, D., André, A., Reis-Henriques, M.A., Castro, L.F.C., Carvalho, A.P., Monteiro, N.M., Santos, M.M., 2018. 17α-ethynilestradiol and tributyltin mixtures modulates the expression of NER and p53 DNA repair pathways in male zebrafish gonads and disrupt offspring embryonic development. Ecol. Indic. 95, 1008–1018. https://doi.org/10.1016/j.ecolind.2017.04.054.
Song, X.D., Song, X.X., Liu, G.B., Ren, C.H., Sun, Y.B., Liu, K.X., Liu, B., Liang, S., Zhu, M., 2018. Investigating multiple dysregulated pathways in rheumatoid arthritis based on pathway interaction network. J. Genet. 97, 173–178. https://doi.org/10.1007/s12041-018-0897-9.
Stegeman, J.J., Goldstone, J.V., Hahn, M.E., 2010. Perspectives on zebrafish as a model in environmental toxicology. Fish Physiol. Biochem. 29, 367–439. https://doi.org/10.1016/S1546-5098(10)02910-9.
Strähle, U., Scholz, S., Geisler, R., Greiner, P., Hollert, H., Rastegar, S., Schumacher, A., Selderslaghs, I., Weiss, C., Witters, H., Braunbeck, T., 2012. Zebrafish embryos as an alternative to animal experiments - A commentary on the definition of the onset of protected life stages in animal welfare regulations. Reprod. Toxicol. 33, 128–132. https://doi.org/10.1016/j.reprotox.2011.06.121.
Takahashi, K., 2009. Release rate of biocides from antifouling paints. Ecotoxicology of Antifouling Biocides. pp. 3–22. https://doi.org/10.1007/978-4-431-85709-9_1.
Thomas, R.S., Allen, B.C., Nong, A., Yang, L., Bermudez, E., Clewell, H.J., Andersen, M.E., 2007. A method to integrate benchmark dose estimates with genomic data to assess the functional effects of chemical exposure. Toxicol. Sci. 98, 240–248. https://doi.org/10.1093/toxsci/kfm092.
Thomas, R.R., Wesselkamper, S.C., Wang, N.C.Y., Zhao, J.J., Petersen, D.D., Lambert, J.C., Cote, I., Yang, L., Healy, E., Black, M.B., Clewell, H.J., Allen, B.C., Andersen, M.E., 2013. Temporal concordance between apical and transcriptional points of departure for chemical risk assessment. Toxicol. Sci. 134, 180–194. https://doi.org/10.1093/toxsci/kft094.
Tingaud-Sequeira, A., Ouadah, N., Babin, P.J., 2011. Zebrafish obesogenic test: a tool for screening molecules that target adiposity. J. Lipid Res. 52, 1765–1772. https://doi.org/10.1194/jlr.D017012.
Tokarz, J., Möller, G., Hrabě De Angelis, M., Adamski, J., 2013. Zebrafish and steroids: what do we know and what do we need to know? J. Steroid Biochem. 137, 165–173. https://doi.org/10.1016/j.jsbmb.2013.01.003.
Tu, W., Martínez, R., Navarro-Martin, L., Kostyniuk, D.J., Hum, C., Huang, J., Deng, M., Jin, Y., Chan, H.-M., Mennigen, J., 2019. Bioconcentration and metabolic effects of emerging PFOS alternatives in developing zebrafish. Environ. Sci. Technol. 53, 13427–13439. https://doi.org/10.1021/acs.est.9b03820.
U.S. Environmental Protection Agency, 2008. Reregistration Eligibility Decision for the Tributyltin Compounds: Bis(tributyltin) Oxide, Tributyltin Benzoate, and Tributyltin Maleate (case 2620). Washington, D.C.
Verhaegen, Y., 2012. Mode of Action, Concentrations and Effects of Tributyltin in Commons Shrimp Crangon crangon. Universiteit Gent.

Wang, Z., Gerstein, M., Snyder, M., 2009. RNA-Seq: a revolutionary tool for transcriptomics. Nat. Rev. Genet. 10, 57–63. https://doi.org/10.1038/nrg2484.

Wang, P., Xia, P., Yang, J., Wang, Z., Peng, Y., Shi, W., Villeneuve, D.L., Yu, H., Zhang, X., 2018. A reduced transcriptome approach to assess environmental toxicants using zebrafish embryo test. Environ. Sci. Technol. 52, 821–830. https://doi.org/10.1021/acs.est.7b04073.

Wang, X., Kong, L., Cheng, J., Zhao, D., Chen, H., Sun, R., Yang, W., Han, J., 2019. Distribution of butyltins at dredged material dumping sites around the coast of China and the potential ecological risk. Mar. Pollut. Bull. 138, 491–500. https://doi.org/10.1016/j.marpolbul.2018.11.043.

Warnes, G.R., Bolker, B., Bonebakker, L., Gentleman, R., Huber, W., Liaw, A., Lumley, T., Maechler, M., Magnusson, A., Moeller, S., Schwartz, M., Venables, B., 2015. Gplots: various R programming tools for plotting data. Compr. R Arch. Netw.

Weber, G.J., Sepúlveda, M.S., Peterson, S.M., Lewis, S.S., Freeman, J.L., 2013. Transcriptome alterations following developmental atrazine exposure in zebrafish are associated with disruption of neuroendocrine and reproductive system function, cell cycle, and carcinogenesis. Toxicol. Sci. 132, 458–466. https://doi.org/10.1093/toxsci/kft017.

Webster, A.F., Chepelev, N., Gagné, R., Kuo, B., Recio, L., Williams, A., Yauk, C.L., 2015. Impact of genomics platform and statistical filtering on transcriptional benchmark doses (BMD) and multiple approaches for selection of chemical point of departure (PoD). PLoS One 10, e0136764. https://doi.org/10.1371/journal.pone.0136764.

Yang, L., Allen, B.C., Thomas, R.S., 2007. BMDExpress: a software tool for the benchmark dose analyses of genomic data. BMC Genomics 8, 387. https://doi.org/10.1186/1471-2164-8-387.

Yebra, D.M., Kiil, S., Dam-Johansen, K., 2004. Antifouling technology - Past, present and future steps towards efficient and environmentally friendly antifouling coatings. Prog. Org. Coatings. 50, 75–104. https://doi.org/10.1016/j.porgcoat.2003.06.001.

Zhang, C., Baudino, T.A., Dowd, D.R., Tokumaru, H., Wang, W., MacDonald, P.N., 2001. Ternary complexes and cooperative interplay between NCoA-62/Ski-interacting protein and steroid receptor coactivators in vitamin D receptor-mediated transcription. J. Biol. Chem. 276, 40614–40620. https://doi.org/10.1074/jbc.M106263200.

Zhang, J., Zhang, C., Liu, M., Fan, M., Huang, M., 2018. Transcriptome analyses of sex differential gene expression in brains of rare minnow (Gobiocypris rarus) and effects of tributyltin exposure. Data Br. 18, 1193–1195. https://doi.org/10.1016/j.dib.2018.03.119.

Zhao, S., Fung-Leung, W.-P., Bittner, A., Ngo, K., Liu, X., 2014. Comparison of RNA-Seq and microarray in transcriptome profiling of activated T cells. PLoS One 9, e78644. https://doi.org/10.1371/journal.pone.0078644.

Zuo, Z., Wang, C., Wu, M., Wang, Y., Chen, Y., 2012. Exposure to tributyltin and triphenyltin induces DNA damage and alters nucleotide excision repair gene transcription in Sebastiscus marmoratus liver. Aquat. Toxicol. 122–123, 106–112. https://doi.org/10.1016/j.aquatox.2012.05.015.

R Development Core Team, 2008. R: A language and environment for statistical computing. R Foundation for Statistical Computing ISBN 3-900051-07-0.

Supplemental information: scientific article IV

Transcriptomic effects of tributyltin (TBT) in zebrafish eleutheroembryos. A functional benchmark dose analysis

Authors: R. Martínez, A.E. Codina, C. Barata, R. Tauler, B. Piña, L. Navarro-Martín

Status: Published

Journal: *J Hazard Mater*. 398 (2020) 122881

DOI: 10.1016/j.jhazmat.2020.122881

Supplemental table ST1. Survival, hatching and swim bladder inflation rates (%) at the different TBT concentration groups. Mean values ± SD (standard deviation) of each group are shown (n=5). Individual non-parametric Mann-Whitney-Wilcoxon tests against each control group (one per day) were performed. Significant differences (p<0.05) are marked with asterisks (*).

			Survival						Hatching				Swim bladder inflation (SBI)			
			3 dpf		4 dpf		5 dpf		3 dpf		4 dpf		5 dpf		4 dpf	5 dpf	
Stock solution (µM)	Nominal concentration (nM)	Measured concentration (nM)	% (Mean ± SEM)	St. sign.	% (Mean ± SEM)	St. sign.	% (Mean ± SEM)	St. sign.	% (Mean ± SEM)	St. sign.	% (Mean ± SEM)	St. sign.	% (Mean ± SEM)	St. sign.	% (Mean ± SEM)	St. sign.	% (Mean ± SEM)	St. sign.
(DMSO)	**0 (Control)**	**0 (Control)**	100.0 ± 0.0		100.0 ± 0.0		99.5 ± 1.8		66.4 ± 11.1		98.1 ± 3.1		99.0 ± 2.4		6.1 ± 7.4		69.0 ± 19.3	
1.5	**3.0**	**1.7**	100.0 ± 0.0		100.0 ± 0.0		98.5 ± 4.0		68.1 ± 18.3		100.0 ± 0.0		99.0 ± 3.7		7.2 ± 10.7		67.4 ± 18.5	
15	**30**	**17**	100.0 ± 0.0		99.5 ± 1.8		99.5 ± 1.8		64.0 ± 19		97.2 ± 6.1		99.5 ± 1.8		2.1 ± 4.2		44.2 ± 24.5	
50	**100**	**56**	100.0 ± 0.0		99.5 ± 1.8		98.1 ± 4.0		63.0 ± 10.3		95.7 ± 5.0		98.6 ± 2.9		1.0 ± 2.5		0.0 ± 0.0	*

Supplementary Table ST2. Summary of the fold-changes regarding the control group, p values and the cluster classification of the determined as differentially expressed genes (DEGs; 3238 genes) by ANOVA-PLS analysis.

See annexes

Supplementary Table ST3. Summary of the mathematical model chosen for the dose-response pattern of each gene expression, its calculated benchmark dose (BMD) and benchmark dose lower and upper confidence limits (BMDL and BMDU, respectively) used in the transcriptomic point of departure (PoD) analysis.

See annexes.

Supplementary Table ST4. Summary of the mathematical model chosen for the dose-response pattern of each metabolite amount, its calculated benchmark dose (BMD) and benchmark dose lower and upper confidence limits (BMDL and BMDU, respectively) used in the metabolomic point of departure (PoD) analysis. Data extracted from bibliography [1].

KEGG compund ID	Metabolite name	Best Model	BMD	BMDL	BMDU
C00157	PC(36:5)	Power model	3.532E-06	3.532E-06	3.538E-06
C01835	Maltotriose	Power model	9.162E-04	1.550E-07	5.691E-01
C06054	2-Oxo-3-hydroxy-4-phosphobutanoic acid	Power model	2.474E-01	4.771E-09	1.916E+01
C00020	Adenosine monophosphate	3º order polynomial	3.096E-01	2.134E-01	5.405E-01
C00020	Adenosine monophosphate	4º order exponential	5.200E-01	2.394E-01	1.834E+00
C04230	LysoPC(18:0)	2º order polynomial	1.183E+00	8.585E-01	1.804E+00
C00157	PC(32:1)	4º order exponential	1.530E+00	7.137E-01	3.461E+00
D01947	Glyceryl 1-monostearate	2º order polynomial	1.736E+00	1.241E+00	2.746E+00
-	Dehydrodiconiferyl alcohol	2º order polynomial	1.882E+00	1.339E+00	3.014E+00
-	Methylhexadecanoic acid	2º order polynomial	2.152E+00	1.517E+00	3.522E+00
C11133	Estrone glucuronide	2º order polynomial	2.169E+00	1.527E+00	3.566E+00
C00294	Inosine	2º order polynomial	3.802E+00	2.482E+00	7.860E+00
C00431	5-Aminopentanoate	2º order exponential	5.023E+00	3.266E+00	9.272E+00
C02237	5-Oxo-D-proline	4º order exponential	5.063E+00	1.511E+00	1.929E+01
C00031	α-D-Glucose	4º order exponential	5.307E+00	2.497E+00	1.605E+01
C00064	L-Glutamine	2º order polynomial	5.501E+00	3.310E+00	1.524E+01
C03684	6-Pyruvoyltetrahydropterin	2º order exponential	8.730E+00	5.458E+00	1.756E+01
C05468	5β-Cyprinolsulfate	2º order exponential	1.184E+01	7.028E+00	2.656E+01
C04230	LysoPC(16:0)	Linear model	1.198E+01	8.386E+00	2.008E+01
C00144	Guanosine monophosphate	2º order exponential	1.201E+01	7.375E+00	2.562E+01
C04230	LysoPC(22:6)	2º order exponential	1.361E+01	1.040E+01	1.893E+01
C00989	4-Hydroxybutanoic acid	2º order exponential	1.489E+01	1.119E+01	2.164E+01
C00127	Oxidized glutathione	Linear model	1.489E+01	1.017E+01	2.679E+01
C00073	L-Methionine	Linear model	1.507E+01	1.027E+01	2.724E+01
-	4-Aminohippuric acid	Linear model	1.602E+01	1.083E+01	2.971E+01
C04230	LysoPC(18:1)	2º order exponential	1.622E+01	1.204E+01	2.447E+01
C00366	Uric acid	Linear model	1.718E+01	1.148E+01	3.295E+01
C02237	5-Oxo-D-proline	Linear model	1.719E+01	1.149E+01	3.297E+01
C05669	β-Nitropropanoate	2º order exponential	1.790E+01	1.032E+01	4.596E+01
C00064	L-Glutamine	Linear model	1.819E+01	1.204E+01	3.597E+01
C00183	L-Valine	2º order exponential	1.820E+01	1.058E+01	4.620E+01
C00519	Hypotaurine	2º order exponential	1.905E+01	1.379E+01	3.115E+01
C02571	L-Acetylcarnitine	Linear model	2.076E+01	1.339E+01	4.476E+01
C00334	4-Aminobutanoate	Linear model	2.125E+01	1.364E+01	4.665E+01
C02737	PS(40:6)	2º order exponential	2.465E+01	1.346E+01	8.042E+01
C00025	L-Glutamate	Linear model	2.509E+01	1.547E+01	6.440E+01
-	6-Succinoaminopurine	Linear model	2.566E+01	1.573E+01	6.763E+01
C00318	L-Carnitine	Linear model	2.693E+01	1.629E+01	7.541E+01
C05926	Neopterin	2º order exponential	2.871E+01	1.892E+01	6.916E+01
C02737	PS(44:12)	2º order exponential	2.923E+01	1.503E+01	1.281E+02
C00300	Creatine	2º order exponential	3.129E+01	1.581E+01	1.567E+02
C01596	Maleamic acid	Linear model	3.190E+01	1.832E+01	1.198E+02
C00299	Uridine	Linear model	3.288E+01	1.869E+01	1.325E+02
C00073	L-Methionine	Linear model	3.383E+01	1.904E+01	1.467E+02
C00334	4-Aminobutanoate	Linear model	3.470E+01	1.936E+01	1.621E+02
C00245	Taurine	Linear model	3.711E+01	2.020E+01	2.201E+02
C00082	L-Tyrosine	2º order exponential	4.033E+01	2.388E+01	2.787E+02
C00300	Creatine	Linear model	4.413E+01	2.239E+01	1.311E+03
C01401	Alanine	2º order exponential	4.593E+01	2.040E+01	5.610E+05
C00475	Cytidine	Linear model	4.627E+01	2.300E+01	5.610E+07
C00082	L-Tyrosine	Power model	5.129E+01	1.706E+01	5.335E+01
C00262	Hypoxanthine	3º order exponential	5.212E+01	2.275E+01	5.535E+01
C00148	L-Proline	Power model	5.212E+01	1.484E+01	5.378E+01
C00043	Uridine diphosphate-N-acetylglucosamine	Linear model	6.016E+01	2.633E+01	5.610E+07
C00262	Hypoxanthine	2º order exponential	6.606E+01	2.484E+01	5.610E+05

[1] E. Ortiz-Villanueva, J. Jaumot, R. Martínez, L. Navarro-Martín, B. Piña, and R. Tauler, "Assessment of endocrine disruptors effects on zebrafish (Danio rerio) embryos by untargeted LC-HRMS metabolomic analysis," Sci. Total Environ., vol. 635, pp. 156–166, 2018.

Supplementary Table ST5. Summary of the mathematical model chosen for the dose-response pattern of each morphometric parameter, its calculated benchmark dose (BMD) and benchmark dose lower and upper confidence limits (BMDL and BMDU, respectively) used in the metabolomic point of departure (PoD) analysis. Data extracted from bibliography [1].

Parameter abbreviation	Morphometric parameter	Best Model	BMD	BMDL	BMDU
SBA	Swim bladder area	4º order polynomial	2.159E+01	1.915E+01	5.431E+01
EL	Eye length	3º order polynomial	4.832E+01	2.848E+01	5.817E+01
EW	Eye width	2º order polynomial	6.255E+01	5.483E+01	6.887E+01
ESD	Eye-snout distance	2º order polynomial	6.811E+01	6.318E+01	7.252E+01
YSA	Yolk sac area	Power model	7.297E+01	6.764E+01	8.072E+01
HW	Head width	2º order polynomial	7.353E+01	6.998E+01	7.701E+01
BL	Body length	3º order exponential	8.627E+01	8.457E+01	1.045E+02
IOD	Interocular distance	2º order polynomial	9.099E+01	8.660E+01	9.675E+01
HTA	Head-trunk angle	2º order polynomial	1.124E+02	9.863E+01	1.568E+02

[1] R. Martínez et al., "Morphometric signatures of exposure to endocrine disrupting chemicals in zebrafish eleutheroembryos," Aquat. Toxicol., vol. 214, p. 105232, Sep. 2019.

Supplementary Table ST6. Results from DAVID Functional Analysis[a)], FDR≤5%

See annexes

Supplementary material: sequencing information

Sample information

Name	Sample
AB3127	Ctrl R1
AB3107	Ctrl R2
AB3111	Ctrl R3
AB3128	3 nM TBT R1
AB3108	3 nM TBT R2
AB3112	3 nM TBT R3
AB3129	30 nM TBT R1
AB3109	30 nM TBT R2
AB3113	30 nM TBT R3
AB3130	100 nM TBT R1
AB3110	100 nM TBT R2
AB3114	100 nM TBT R3

FLI

Name	barcode	flowcell	library	lane
AB3107.156W.0	AB3107	C9JKUANXX	156W	2
AB3107.629V.0	AB3107	C9HUVANXX	629V	4
AB3108.157W.0	AB3108	C9JKUANXX	157W	2
AB3108.630V.0	AB3108	C9HUVANXX	630V	3
AB3109.158W.0	AB3109	C9JKUANXX	158W	2
AB3109.631V.0	AB3109	C9HUVANXX	631V	2
AB3110.693V.0	AB3110	C9HUVANXX	693V	2
AB3111.694V.0	AB3111	C9HUVANXX	694V	4
AB3112.695V.0	AB3112	C9HUVANXX	695V	4
AB3113.696V.0	AB3113	C9FGAANXX	696V	4
AB3114.697V.0	AB3114	C9HUVANXX	697V	5
AB3127.710V.0	AB3127	C9FGAANXX	710V	6
AB3127.710V.1	AB3127	C9HUVANXX	710V	2
AB3128.934V.1	AB3128	C9JT7ANXX	934V	7
AB3129.712V.0	AB3129	C9FGAANXX	712V	6
AB3129.712V.1	AB3129	C9HUVANXX	712V	2
AB3130.713V.1	AB3130	C9JT7ANXX	713V	7

PCR duplicates

Name	percent duplicates
AB3107.156W	11.177
AB3107.629V	22.129
AB3108.157W	18.283
AB3108.630V	23.363
AB3109.158W	19.776
AB3109.631V	24.066
AB3110.693V	23.405
AB3111.694V	22.472
AB3112.695V	25.79
AB3113.696V	22.896
AB3114.697V	25.263
AB3126.709V	25.286
AB3127.710V	23.923
AB3128.934V	28.763
AB3129.712V	25.123
AB3130.713V	28.201

Mapping Statistics

Name	total reads	paired mapped	percent paired mapped	single mapped	percent single mapped	unmapped	percent unmapped	split mapped	percent split mapped
AB3107.156W.0	29962712	28359952	100	0	0	1602760	5.349	3840238	14.232
AB3107.629V.0	88180284	83123764	100	0	0	5056520	5.734	10216031	13.846
AB3108.157W.0	47200368	44846336	100	0	0	2354032	4.987	5956057	14.656
AB3108.630V.0	67720506	63956758	100	0	0	3763748	5.558	8367412	15.026
AB3109.158W.0	51453278	49056156	100	0	0	2397122	4.659	6138770	14.234
AB3109.631V.0	80152074	76167552	100	0	0	3984522	4.971	9884032	14.76
AB3110.693V.0	82404600	78692866	100	0	0	3711734	4.504	9934359	14.562
AB3111.694V.0	80947298	76760856	100	0	0	4186442	5.172	10236503	14.879
AB3112.695V.0	88554360	84184422	100	0	0	4369938	4.935	11645064	15.659
AB3113.696V.0	65420440	62239030	100	0	0	3181410	4.863	8463945	15.47
AB3114.697V.0	75856448	71874108	100	0	0	3982340	5.25	10003588	15.392
AB3127.710V.0	46653386	43415088	100	0	0	3238298	6.941	5822440	15.043
AB3127.710V.1	30756348	28919232	100	0	0	1837116	5.973	3858649	14.952
AB3128.934V.1	128638644	122446476	100	0	0	6192168	4.814	18208412	15.911
AB3129.712V.0	46923230	44145302	100	0	0	2777928	5.92	6019838	15.32
AB3129.712V.1	30417042	28646796	100	0	0	1770246	5.82	3887322	15.225
AB3130.713V.1	95855960	90253826	100	0	0	5602134	5.844	12430271	15.416

Read Annotation

Name	exonic	percent exonic	intronic	percent intronic	intergenic	percent intergenic
AB3107.156W.0	23698462	87.827	769951	2.853	2598702	9.631
AB3107.629V.0	63759755	86.417	2223883	3.014	7991815	10.832
AB3108.157W.0	35701235	87.853	1304699	3.211	3748438	9.224
AB3108.630V.0	49053207	88.091	1734203	3.114	5029589	9.032
AB3109.158W.0	37418333	86.764	1488101	3.451	4338768	10.061
AB3109.631V.0	58777346	87.773	2164144	3.232	6184750	9.236
AB3110.693V.0	59668513	87.462	2094067	3.069	6629917	9.718
AB3111.694V.0	60161356	87.446	2694710	3.917	6122656	8.899
AB3112.695V.0	65817168	88.503	2706555	3.639	6018519	8.093
AB3113.696V.0	48579180	88.79	1617657	2.957	4646471	8.493
AB3114.697V.0	57945550	89.16	1973795	3.037	5232832	8.052
AB3127.710V.0	34269813	88.538	1259157	3.253	3271542	8.452
AB3127.710V.1	22819385	88.423	845882	3.278	2203761	8.539
AB3128.934V.1	103352293	90.31	3133126	2.738	8254608	7.213
AB3129.712V.0	34962557	88.975	1178853	3	3243799	8.255
AB3129.712V.1	22684846	88.847	773762	3.03	2132116	8.351
AB3130.713V.1	72178048	89.512	2345640	2.909	6288038	7.798

Genes

Name	genes detected	genes 25 percent expression
AB3107.156W.0	24030	68
AB3107.629V.0	25129	46
AB3108.157W.0	24668	39
AB3108.630V.0	25020	33
AB3109.158W.0	24661	36
AB3109.631V.0	25116	37
AB3110.693V.0	25067	32
AB3111.694V.0	25252	37
AB3112.695V.0	25294	27
AB3113.696V.0	24949	32
AB3114.697V.0	24988	32
AB3127.710V.0	24640	28
AB3127.710V.1	24230	28
AB3128.934V.1	25719	32
AB3129.712V.0	24673	26
AB3129.712V.1	24193	26
AB3130.713V.1	25222	23

Mapping ambiguity

Name	reads single gene pe	reads multiple gene pe	mapped unique reads	mapped ambigous reads	percent mapped unique reads	percent mapped ambigous reads	percent reads single gene pe	percent multiple gene pe
AB3107.156W.0	24655408	814898	26982966	1376986	95.14461096	4.855389036	96.80059596	3.199404043
AB3107.629V.0	69254194	2699186	73781518	9342246	88.76104071	11.23895929	96.24870159	3.75129841
AB3108.157W.0	38252136	1318752	40637668	4208668	90.61535819	9.384641813	96.66736819	3.332631808
AB3108.630V.0	53587018	2076238	55684700	8272058	87.06617055	12.93382945	96.2700026	3.729997397
AB3109.158W.0	40908368	1567862	43126574	5929582	87.91266482	12.08733518	96.3088485	3.691151498
AB3109.631V.0	64060864	2495000	66965276	9202276	87.91837763	12.08162237	96.25126946	3.74873054
AB3110.693V.0	65557696	2566928	68221846	10471020	86.69381288	13.30618712	96.2320115	3.767988503
AB3111.694V.0	65397804	2296144	68798634	7962222	89.62723657	10.37276343	96.60805128	3.391948716
AB3112.695V.0	71716778	2733378	74366786	9817636	88.33794214	11.66205786	96.32857989	3.671420111
AB3113.696V.0	52781464	1937376	54712638	7526392	87.9072794	12.0927206	96.45939863	3.540601372
AB3114.697V.0	62102532	2089808	64990374	6883734	90.4225121	9.577487904	96.74445892	3.255541082
AB3127.710V.0	37093050	1326276	38706390	4708698	89.15423597	10.84576403	96.54789363	3.45210637
AB3127.710V.1	24692262	887836	25807154	3112078	89.23872529	10.76127471	96.52919234	3.470807657
AB3128.934V.1	108307932	3581548	114441120	8005356	93.46215893	6.537841073	96.79903061	3.200969385
AB3129.712V.0	37675940	1396728	39294686	4850616	89.01215808	10.98784192	96.42530682	3.574693185
AB3129.712V.1	24439624	906596	25532508	3114288	89.12866905	10.87133095	96.42315107	3.576848934
AB3130.713V.1	77589686	2774850	80634704	9619122	89.3421449	10.6578551	96.54717101	3.452828994

Reads per chromosome (a)

Name	1	2	3	4	5	6	7	8	9	10	11	12	13
AB3107.156W.0	1332266	1252940	2250080	1103346	3250630	1579978	1446532	1157342	974426	962920	885408	1152964	996676
AB3107.629V.0	3477560	3319966	5899056	8244982	23776442	4140794	3844436	3064202	2567582	2519090	2325456	2989810	2587612
AB3108.157W.0	2062618	1813886	3619476	3460444	10302862	2523330	2135048	1620890	1444124	1338690	1208536	1866138	1382224
AB3108.630V.0	2764322	2483476	4917560	7115406	20795742	3403540	2896214	2179632	1946138	1799746	1627632	2479184	1818232
AB3109.158W.0	2126472	1888754	3661950	4899498	14879676	2627446	2163368	1705228	1634036	1373752	1301640	1830892	1549976
AB3109.631V.0	3299986	2975206	5708128	7886532	22793556	4083458	3395076	2667262	2530568	2136870	2027184	2817052	2370240
AB3110.693V.0	3331264	2914994	5841468	9419784	26993352	3826196	3381568	2651148	2319532	2231294	1943414	2647956	2239282
AB3111.694V.0	3447814	3102134	6394686	6865640	19202878	4201606	3553508	2711984	2482160	2277758	2014554	3020180	2178676
AB3112.695V.0	3779924	3260342	7410236	8156668	23697846	4808878	3909784	2812242	2639106	2245796	2067808	3513910	2420172
AB3113.696V.0	2780358	2398694	4955040	6592302	18579182	3469248	2768454	2123074	1852724	1674456	1566154	2410808	1816806
AB3114.697V.0	3420600	2935458	6185300	6292970	16189588	4084242	3270500	2452404	2041978	2047730	1747024	2776568	2100508
AB3127.710V.0	2034122	1733546	3664832	4367312	10873448	2590248	1951800	1433978	1261732	1210332	1040024	1854696	1174272
AB3127.710V.1	1358270	1151186	2445804	2895938	7193498	1726330	1300272	956852	843222	812522	696270	1236884	787584
AB3128.934V.1	6082328	5006390	11455156	6150518	17452712	7667800	6052350	4308180	4285630	3636300	3228300	5737398	3902216
AB3129.712V.0	2035766	1731834	3788134	4194870	11558350	2649586	1989298	1470930	1286088	1180638	1068010	1858892	1240656
AB3129.712V.1	1326258	1117556	2462872	2706572	7440320	1723112	1292518	957028	839860	769452	693180	1207654	808152
AB3130.713V.1	4350374	3453338	8220910	8845346	22913772	5168208	4085682	2903530	2433490	2411530	2010268	3768372	2453812

Reads per chromosome (b)

Name	14	15	16	17	18	19	20	21	22	23	24	25	MT
AB3107.156W.0	1110310	944088	1345974	1104806	749230	1706162	1140394	1003844	718750	1120284	679168	720474	712172
AB3107.629V.0	2918016	2483706	3555774	2958780	1984346	4521490	4067340	2652488	1898800	2959300	1785250	1895508	2015184
AB3108.157W.0	1682452	1360114	2045854	1553220	1042298	3050194	1971464	1418422	994900	1715708	954244	1009582	940226
AB3108.630V.0	2246302	1829838	2748226	2148790	1410676	4221620	3147168	1932120	1336560	2322798	1277672	1360098	1285876
AB3109.158W.0	1761718	1467026	2163956	1596300	1094782	3101592	2363816	1515550	1051982	1794986	1009592	1075902	1100364
AB3109.631V.0	2718002	2285918	3351126	2548758	1713054	4907576	3620366	2390720	1632320	2814566	1563404	1684466	1736654
AB3110.693V.0	2899504	2350910	3263810	2674330	1749880	4387782	3912290	2473402	1610192	2668734	1541992	1631574	1788630
AB3111.694V.0	2910482	2307902	3441256	2571582	1766430	5354112	3517972	2444914	1693770	2921310	1587818	1699034	1624886
AB3112.695V.0	3041164	2399312	3780746	2907022	1844132	6521714	3816138	2549146	1694130	3243388	1669134	1759942	1305612
AB3113.696V.0	2225038	1872424	2804956	2093172	1365852	4439434	2900230	1907276	1297436	2287080	1237342	1326426	984282
AB3114.697V.0	2925252	2183764	3428686	2332438	1621814	5655694	3034278	2332636	1469274	2828360	1417294	1528742	1511580
AB3127.710V.0	1609468	1221032	1937776	1241726	938384	3509188	1914140	1311286	912408	1678420	880326	914432	1148456
AB3127.710V.1	1076542	815570	1292696	820772	626898	2332478	1282654	870580	608314	1114044	590626	612110	776558
AB3128.934V.1	4725298	3697484	5972874	4359604	2851574	1E+07	4503488	3925280	2653460	5017616	2631818	2768268	2617604
AB3129.712V.0	1616146	1246658	2088864	1409930	962790	3533604	1878044	1349666	891004	1695148	868858	936486	1008814
AB3129.712V.1	1052768	810820	1354736	913894	623252	2281182	1222460	874104	579306	1097090	568142	604514	665092
AB3130.713V.1	3593960	2535806	4168922	2996264	1931222	7517688	3716806	2782026	1663658	3625780	1695300	1817458	2007570

Gene Biotypes

Name	protein coding	percent protein coding	three prime overlapping ncrna	percent 3prime overlapping ncrna	ig c gene	percent IG C gene	ig j gene	percent IG J gene	ig v gene	percent IG V gene	ig v pseud ogene	percent IG V pseudo gene	mt rrna	percent Mt rRNA	tr c gene	percent TR C gene	tr v gene	percent TR V gene	tr v pseud ogene	percent TR V pseudo gene	antisense	percent antisense
AB3107.156W.0	23710966	98.552	0	0	14	0	0	0	0	0	6	0	126948	0.528	0	0	16	0	0	0	36326	0.151
AB3107.629V.0	63871368	98.372	0	0	22	0	0	0	0	0	2	0	487952	0.752	0	0	38	0	0	0	91194	0.14
AB3108.157W.0	35815930	98.433	0	0	28	0	0	0	0	0	6	0	198224	0.545	0	0	48	0	0	0	47330	0.13
AB3108.630V.0	49186484	98.408	0	0	46	0	0	0	0	0	4	0	326866	0.654	0	0	46	0	0	0	56060	0.112
AB3109.158W.0	37641228	98.399	0	0	22	0	0	0	0	0	0	0	235312	0.615	0	0	34	0	0	0	49172	0.129
AB3109.631V.0	58989626	98.391	0	0	48	0	0	0	0	0	4	0	416930	0.695	0	0	46	0	0	0	67930	0.113
AB3110.693V.0	59809698	98.369	0	0	30	0	0	0	0	0	10	0	390680	0.643	0	0	46	0	0	0	68436	0.113
AB3111.694V.0	60952416	98.591	0	0	32	0	0	0	0	0	0	0	208874	0.338	0	0	58	0	0	0	69612	0.113
AB3112.695V.0	66545160	98.678	0	0	50	0	0	0	0	0	2	0	193998	0.288	0	0	56	0	0	0	65216	0.097
AB3113.696V.0	48804844	98.768	0	0	24	0	0	0	0	0	6	0	162072	0.328	0	0	52	0	0	0	49022	0.099
AB3114.697V.0	58036468	98.444	0	0	48	0	0	0	0	0	4	0	285740	0.485	0	0	52	0	0	0	60296	0.102
AB3127.710V.0	34226984	97.961	0	0	24	0	0	0	0	0	2	0	342104	0.979	0	0	50	0	0	0	36320	0.104
AB3127.710V.1	22791906	97.941	0	0	22	0	0	0	0	0	0	0	229246	0.985	0	0	34	0	0	0	25346	0.109
AB3128.934V.1	1.03E+08	98.454	0	0	98	0	0	0	0	0	6	0	586886	0.56	0	0	100	0	0	0	109956	0.105
AB3129.712V.0	34932086	98.279	0	0	24	0	0	0	0	0	2	0	247932	0.698	0	0	48	0	0	0	37248	0.105
AB3129.712V.1	22667350	98.256	0	0	22	0	0	0	0	0	0	0	161434	0.7	0	0	34	0	0	0	24746	0.107
AB3130.713V.1	71886284	98.064	0	0	56	0	0	0	0	0	0	0	625160	0.853	0	0	58	0	0	0	72178	0.098

Name	lincrna	percent lincRNA	mirna	percent miRNA	misc RNA	percent misc RNA	polymorphic pseudogene	percent polymorphic pseudogene	processed transcript	percent processed transcript	pseud ogene	percent pseudo gene	rrna	percent rRNA	sense intronic	percent sense intronic	sense overlapping	percent sense overlapping	snrna	percent snRNA	snorna	percent snoRNA
AB3107.156W.0	88994	0.37	258	0.001	220	0.001	5596	0.023	77884	0.324	566	0.002	196	0.001	580	0.002	146	0.001	26	0	176	0.001
AB3107.629V.0	228270	0.352	756	0.001	2366	0.004	14162	0.022	198592	0.306	1612	0.002	662	0.001	1346	0.002	342	0.001	42	0	474	0.001
AB3108.157W.0	170022	0.467	474	0.001	1230	0.003	8026	0.022	124448	0.342	768	0.002	228	0.001	728	0.002	242	0.001	30	0	298	0.001
AB3108.630V.0	206488	0.413	572	0.001	2402	0.005	10920	0.022	162926	0.326	1168	0.002	356	0.001	882	0.002	350	0.001	46	0	396	0.001
AB3109.158W.0	167856	0.439	468	0.001	1496	0.004	8226	0.022	129170	0.338	730	0.002	308	0.001	860	0.002	276	0.001	38	0	274	0.001
AB3109.631V.0	237830	0.397	640	0.001	2684	0.004	12798	0.021	192338	0.321	1244	0.002	464	0.001	1188	0.002	436	0.001	52	0	408	0.001
AB3110.693V.0	307558	0.506	880	0.001	2342	0.004	8128	0.013	184640	0.304	1152	0.002	470	0.001	1162	0.002	286	0	58	0	316	0.001
AB3111.694V.0	335236	0.542	756	0.001	2102	0.003	13820	0.022	200780	0.325	1636	0.003	652	0.001	1152	0.002	714	0.001	42	0	506	0.001
AB3112.695V.0	335456	0.497	780	0.001	2736	0.004	15446	0.023	237346	0.352	1422	0.002	548	0.001	1128	0.002	696	0.001	68	0	542	0.001
AB3113.696V.0	191368	0.387	580	0.001	1736	0.004	10112	0.02	165000	0.334	1186	0.002	368	0.001	1002	0.002	284	0.001	36	0	338	0.001
AB3114.697V.0	328480	0.557	848	0.001	1868	0.003	8652	0.015	198964	0.337	984	0.002	454	0.001	1138	0.002	290	0	42	0	306	0.001
AB3127.710V.0	191920	0.549	502	0.001	1252	0.004	6098	0.017	109896	0.315	862	0.002	234	0.001	694	0.002	374	0.001	50	0	384	0.001
AB3127.710V.1	129422	0.556	318	0.001	738	0.003	4054	0.017	73628	0.316	554	0.002	178	0.001	514	0.002	204	0.001	48	0	262	0.001
AB3128.934V.1	462446	0.441	1332	0.001	2580	0.002	22244	0.021	366932	0.35	1984	0.002	718	0.001	2100	0.002	716	0.001	154	0	962	0.001
AB3129.712V.0	180078	0.507	486	0.001	1654	0.005	6232	0.018	115616	0.325	710	0.002	218	0.001	678	0.002	258	0.001	40	0	304	0.001
AB3129.712V.1	119390	0.518	396	0.002	878	0.004	4196	0.018	76260	0.331	468	0.002	138	0.001	478	0.002	148	0.001	36	0	218	0.001
AB3130.713V.1	426388	0.582	1290	0.002	2930	0.004	9850	0.013	239794	0.327	1008	0.001	438	0.001	1302	0.002	362	0	76	0	516	0.001

Chapter III:

Changes in zebrafish eleutheroembryos' lipidome profile induced by bisphenol A.

BPA was the compound, between the three studied endocrine disrupting chemicals (EDCs), which had the higher effect in lipid metabolism both in transcriptome and in phenotype (with an exerted yolk sac malabsorption syndrome). Although some studies included effects of BPA in lipid metabolism in zebrafish at different stages [108,354]*, to our knowledge, no complete lipidomic study had been carried out about the effects on the zebrafish eleutheroembryos at the level of the different lipid families. For that reason, a deeper lipidomic study was carried out in zebrafish eleutheroembryos exposed to BPA (from concentrations high enough to elicit an increase in the yolk sac area). High performance thin layer chromatography (HPTLC) was used to assess the effects of BPA on the different lipid families (triglycerides, phosphatidylcholines, cholesterol esters…). Ultra-high performance liquid chromatography – mass spectrometry (UHPLC-MS) analysis not only confirmed the lipid families' results from HPTLC but also allowed us to discern the BPA effects on each specific lipid specie (considering each specific main fatty acids chain length and number of double bonds).*

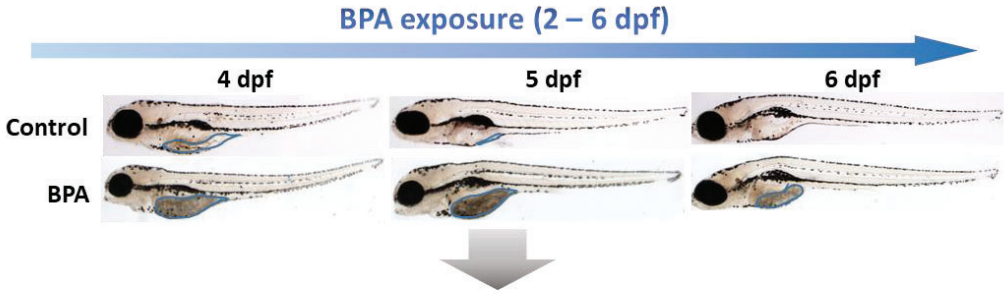

Lipidomic analysis

Thin layer chromatography

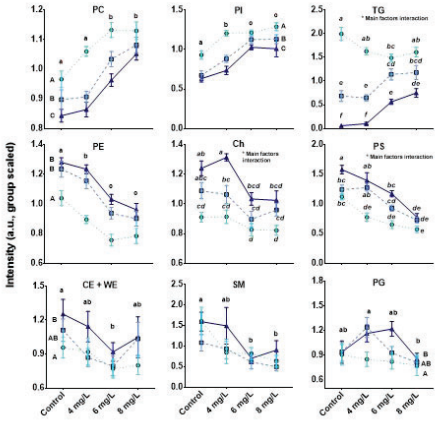

Ultra-high performance liquid chromatography – mass spectrometry

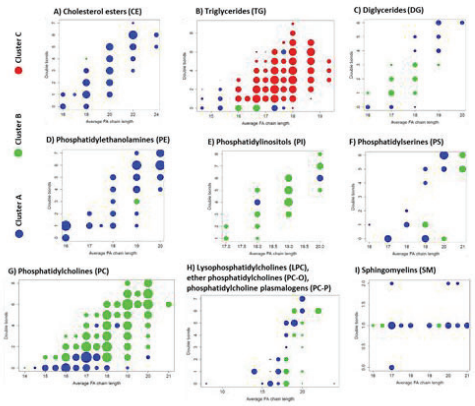

Biological interpretation and integration with transcriptomic results

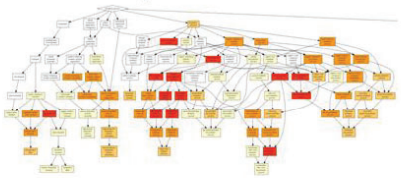

BPA mode of action proposal

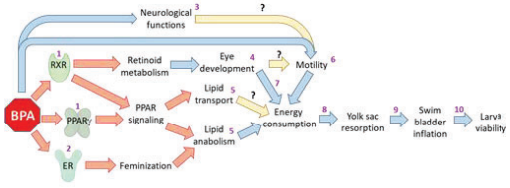

Main results

- BPA exerted a decrease of the lipid consumption, specifically in TG, DG, PI and PC, most of them related with energy obtainment (in the non-feeding eleutheroembryos).

- Most phospholipids (more related with structural functions) were only slightly or not altered.

- The consumption of the lipids and/or the BPA effects over them could be partially correlated with their physicochemical properties (fatty acid chain length and number of double bounds).

- Results are in agreement with morphometric, metabolomic and transcriptomic studies.

Scientific article V

Changes in lipid profiles induced by bisphenol A (BPA) in zebrafish eleutheroembryos during the yolk sac absorption stage

Authors: R. Martínez, L. Navarro-Martín, M. van Antro, I. Fuertes, M. Casado, C. Barata, B. Piña

Status: Published

Journal: Chemosphere. 246 (2020) 125704.

DOI: 10.1016/j.chemosphere.2019.125704

Chemosphere 246 (2020) 125704

Contents lists available at ScienceDirect

Chemosphere

journal homepage: www.elsevier.com/locate/chemosphere

Changes in lipid profiles induced by bisphenol A (BPA) in zebrafish eleutheroembryos during the yolk sac absorption stage

Rubén Martínez [a, b], Laia Navarro-Martín [a], Morgane van Antro [c], Inmaculada Fuertes [a], Marta Casado [a], Carlos Barata [a], Benjamin Piña [a, *]

[a] Institute of Environmental Assessment and Water Research, IDAEA-CSIC, Barcelona, Catalunya, 08034, Spain
[b] Universitat de Barcelona (UB), Barcelona, Catalunya, 08007, Spain
[c] Laboratory of Evolutionary and Adaptive Physiology, University of Namur, Namur, B5000, Belgium

HIGHLIGHTS

- BPA induces yolk-sac and lipid retention in late zebrafish eleutheroembryos.
- Most retained lipids were related to energy metabolism.
- Fate of individual lipids was determined by their physicochemical characteristics.
- Lipidomic changes were linked to most BPA adverse effects on fish eleutheroembryos.

GRAPHICAL ABSTRACT

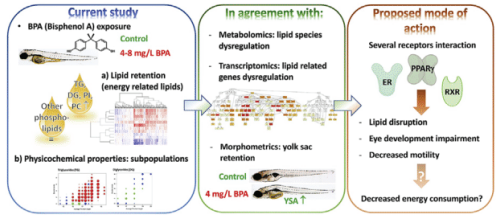

ARTICLE INFO

Article history:
Received 17 October 2019
Received in revised form
16 December 2019
Accepted 17 December 2019
Available online 20 December 2019

Handling Editor: David Volz

Keywords:
Endocrine disruption
Thin layer chromatography
Mass spectrometry
Yolk sac malabsorption
Adverse outcome pathway
Mode of action

ABSTRACT

Bisphenol A (BPA; 4,4'-(propane-2,2-diyl)diphenol) has been shown to act as an obesogen and to disrupt lipid metabolism in zebrafish eleutheroembryos (ZE). To characterize the consequences of this disruption, we performed a detailed lipidomic study using ZE exposed to different BPA concentrations (0, 4, 6 and 8 mg/L of BPA) from day 2 to up to day 6 post fertilization (dpf). Total lipids at 4, 5 and 6 dpf were extracted by Folch method and analyzed by high-performance thin layer chromatography (HPTLC) as wide-range preliminary screening. Selected conditions (0 and 6 mg/L of BPA) were used to obtain a high-quality lipid profile using ultra high-performance liquid chromatography/time-of-flight mass spectrometry (UHPLC-TOFMS). BPA exposed ZE exhibited increased amounts of triglycerides (TG), diglycerides (DG), phosphatidylcholines (PC) and phosphatidylinositols (PI), regarding the control group. Analysis of time- and BPA exposure-related patterns of specific lipid species showed a clear influence of unsaturation degree (mostly in DG and PC) and/or fatty acid chain length (mostly in TG and PC derivatives) on their response to the presence of BPA. A decreased yolk-sac and energy consumption in exposed individuals appeared as the main reason for the observed BPA-driven effects. Integration of these results with previous morphological, biochemical, transcriptomic, metabolomic and behavioral data suggests a disruption of different signalling pathways by BPA that starts at very low BPAconcentrations, whose effects propagate across different organization levels, and that cannot be only explained by the relatively weak estrogenic effect of BPA.

* Corresponding author. Institute of Environmental Assessment and Water Research, IDAEA-CSIC, Jordi Girona 18, 08034, Barcelona, Spain.
E-mail addresses: ruben1990martinez@hotmail.com (R. Martínez), laianavarromartin@gmail.com (L. Navarro-Martín), morgane.vanantro@student.unamur.be (M. van Antro), inmafuero@gmail.com (I. Fuertes), mcbbmc@cid.csic.es (M. Casado), cbmqam@cid.csic.es (C. Barata), bpcbmc@cid.csic.es (B. Piña).

https://doi.org/10.1016/j.chemosphere.2019.125704
0045-6535/

1. Introduction

Bisphenol A (BPA; 4,4'-(propane-2,2-diyl)diphenol) is a monomer used in the production of several plastics. Its estimated worldwide production for the past year (2018) was between 7.2 and 8.4 millions tons (Grand View Research Inc, 2015; Kadasala et al., 2016) and its release in the environment quantified in 450 tons/year (U S Environmental Protection Agency, 2010). Environmental BPA levels are usually low in surface waters (0–56 μg/L) (Corrales et al., 2015), although they can reach parts per million (ppm) levels in some landfill leachates or mill effluents (0–17 mg/L) (Canesi and Fabbri, 2015; Flint et al., 2012; Kolpin et al., 2002). BPA is classified as an endocrine disrupting chemical (EDC) in the TEDX list (https://endocrinedisruption.org/), as well as by the ECHA (European Chemicals Agency), WHO (World health Organization) and EPA (U.S. Environmental Protection Agency) (Bergman et al., 2013; European Chemicals Agency, 2017; U S Environmental Protection Agency, 2010). Traditionally, the research about its effects have been focused on its estrogenicity (Chen et al., 2002; Eramo et al., 2010; Moon, 2019) due to the fact that it acts as an agonist of estrogen receptors (ERs) (Heindel and Blumberg, 2019; Mu et al., 2018). Nevertheless, BPA is also known to interact with other receptors like the RXRs (retinoid X receptors) (Martínez et al., 2018), ERR-ϒ (estrogen-related receptor gamma) (Bergman et al., 2013; Tohmé et al., 2014) or the PPAR-ϒ (peroxisome proliferator-activated receptor gamma) (Martínez et al., 2018). Alteration of these non-estrogenic pathways by BPA has been also related to alterations in adipogenesis and obesity (Santangeli et al., 2018; vom Saal et al., 2012). Indeed, BPA has been considered as an obesogen not only in fish but also in rodents, aquatic invertebrates as *Daphnia magna*, and possibly even in humans (Jordão et al., 2016; Kim et al., 2019; Legeay and Faure, 2017; Maradonna and Carnevali, 2018; Rubin et al., 2019; Wang et al., 2013). Due to these disruptive effects, BPA has been banned for some uses and substituted during the past years by other compounds (mostly its derivatives which present similar adverse effects (Horan et al., 2018; Mesnage et al., 2017; Moon, 2019)). Regardless, it can be still found, among others, in bottles, food packaging, adhesives, beverage cans and epoxy resins (Almeida et al., 2018; Huang et al., 2012; Wang et al., 2015).

Zebrafish (*Danio rerio*) is considered a vertebrate model for the study of lipids and endocrine disruption because of its short life cycle, easy rearing, relatively large offspring, and its highly evolutionary conserved endocrine system and lipid metabolism compared with mammals (Hölttä-Vuori et al., 2010; Kimmel et al., 1995; Löhr and Hammerschmidt, 2011). Different aspects of lipid metabolism in zebrafish eleutheroembryos has been previously reported, including general lipidomic analyses (Fraher et al., 2016; Gorrochategui et al., 2017; Pirro et al., 2016) and studies on lipid trafficking from the yolk sac and on the expression of associated apolipoproteins (Hölttä-Vuori et al., 2010; Otis et al., 2015). Although some of these studies included the lipidomic effects of BPA in zebrafish at different stages (Riu et al., 2014; Santangeli et al., 2018), to our knowledge, no complete lipidomic study has yet been carried out about the effects of BPA on the early development of zebrafish at the level of the different lipid families.

Methodologies as HPTLC (high performance thin layer chromatography) or HPLC-MS (high performance liquid chromatography - mass spectrometry) are useful tools for lipidomic studies (Gorrochategui et al., 2017; Miyares et al., 2014). HPTLC exhibits better separation and resolution than the traditional thin layer chromatography and it is a cost-effective method with minimal sample cleaning requirements that allows an integrative quantitative analysis per each lipid family (Attimarad et al., 2011; John et al., 2015; Touchstone, 1995). Thus, it is an excellent screening tool before the performance of a more exhaustive lipidomic analysis as the HPLC-MS, which, although being more cost-expensive, allows the identification of each individual lipid inside each family, and it discriminates different fatty acids length and unsaturation number, exhibits lower limits of detection and quantification (LOD/LOQ, respectively), and reduces sample matrix effects (Cajka and Fiehn, 2014; Jurowski et al., 2017; Lydic and Goo, 2018).

The goal of the present study was to fill in the lack of information about the effects of BPA exposures on the lipidome profile during zebrafish early development, focusing on the behaviour of different lipid families and of individual lipid species, using both HPTLC and HPLC-MS to perform a detailed lipidomic analysis. With this purpose, zebrafish eleutheroembryos were exposed to different concentrations of BPA (0, 4, 6 and 8 mg/L) using as the lowest concentration the first one reported to have effects in yolk sac resorption (Martínez et al., 2019a) and in a specific time window, from 2 to 6 days post fertilization (dpf), in which embryos use the yolk sac as a reservoir of energy and proteins for its development. Combining this information with previously reported transcriptomic, metabolomic and morphometric data, we aim to characterize the obesogenic effects of BPA in fish and other vertebrates.

2. Materials and methods

2.1. Animals and rearing conditions

Zebrafish eggs, embryos and adult rearing and maintenance, as well as adult mating and eggs obtainment were performed as previously described (Martínez et al., 2019b). At 2 h post fertilization (hpf), the eggs were collected, rinsed and the fertilized ones were placed in 6-well multiplates at a density of 2 embryos/ml (10 individuals were placed in 5.0 ml of fish water per well). Embryos were kept in clean fish water until the start of the BPA exposures. All experimental procedures were performed under a license obtained from the local government (DAMM 7669, 7964), in accordance with the institutional guidelines and they were approved by the Institutional Animal Care and Use Committees of the Research and Development Centre (CID) of the Spanish National Research Council (CSIC). Although zebrafish developmental stages can be designated with different names (Belanger et al., 2010; Embry et al., 2010; Hahn et al., 2014; Parichy et al., 2009; Reed and Jennings, 2011; Wilson, 2012), in the present study we used the term "eleutheroembryos" indistinctly to refer to individuals at 4, 5 and 6 dpf, for clarity purposes.

2.2. Zebrafish eleutheroembryos exposure to BPA

2.2.1. Stocks solutions preparation

Bisphenol A (BPA, CAS-RN: 80-05-7, ≥99.0% purity, Sigma-Aldrich (St. Louis, MO, USA)) stock solutions were prepared in dimethyl sulfoxide (DMSO) and stored at −20 °C. Fresh experimental working solutions (final DMSO concentration: 0.2% (v/v)) were prepared daily by diluting the stock solutions with fish water until a final BPA concentration of 0 (control), 4, 6 and 8 mg/L was obtained. BPA concentration range was selected based in the minimum dose needed to affect the area of the yolk sac (4 mg/L) and the maximum acceptable dose in terms of lethality/malformations (8 mg/L) according to our previous studies (Martínez et al., 2019a).

2.2.2. Eleutheroembryos exposure and sampling

Zebrafish eleuthero/embryos were exposed to 0 (control), 4.0, 6.0 and 8.0 mg/L of BPA from 2 to 6 dpf. The exposure was initiated at 2 dpf to avoid the effect of the BPA on early embryonic developmental processes, allowing us to focus on its effects in the already differentiated tissues. To assure that zebrafish eleuthero/embryos were exposed appropriately to each BPA concentration and to avoid that BPA concentration decrease over time (which could occur due to the uptake and bioaccumulation of the pollutant by the individuals), all of the exposure media (including control group) were daily renewed. To avoid possible "tank" effects, the assignment of treatments was randomized in the 6-well multiplates.

Control and BPA exposed eleutheroembryos (4, 6 and 8 mg/L of BPA) were sampled at 4, 5 and 6 dpf, frozen in dry ice and stored at −80 °C until lipidomic analysis. The above sampling periods were selected to account for the period where the yolk sac (main lipid reservoir of the embryo) is almost completely depleted at 5 dpf in normal conditions (Flynn et al., 2009; Fraher et al., 2016). After the exposure, ten replicates per day and condition (5 eleutheroembryos per replicate) were collected for thin layer chromatography (see **2.4.2.**). Additionally, for the study of the yolk sac, 5 replicates (individual eleutheroembryo per replicate) per day and condition were sampled and fixed (see **2.3.**). During the exposure, mortality (3, 4, 5 and 6 dpf), hatching (3, 4, 5 and 6 dpf) and swim bladder inflation (4, 5 and 6 dpf) rates were recorded for each concentration (Supplementary Table ST1).

A detailed lipidomic study using mass spectrometry was performed in eleutheroembryos exposed to 6.0 mg/L of BPA, considered as the phenotypical lowest observed effect concentration (LOEC; see section 3.1.). Control and treated animals were sampled in duplicated (5 eleutheroembryos per replicate) at 4, 5, and 6 dpf, and stored as above.

2.3. Eleutheroembryo fixation and yolk sac measurements

Five replicates (individual larva) per each time (4, 5 and 6 dpf) and condition (control, 4.0, 6.0 and 8.0 mg/L of BPA) were sampled, fixed and analyzed. Eleutheroembryos were fixed in 4% paraformaldehyde (PFA) in PBS at 4 °C and gradually transferred to 90% glycerol for conservation and facilitation of eleutheroembryo placement under the microscope (Martínez et al., 2019a; Raldúa et al., 2008). Lateral image of each fixed larva was taken using a stereomicroscope Nikon SMZ1500 (Nikon Co., Tokyo, Japan) coupled with a Nikon digital Sight DS-Ri1 camera and the yolk sac area (YSA) was measured using the free graphical image analysis software ImageJ (National Institutes of Health, Bethesda, Maryland, USA) (Martínez et al., 2019a; Raldúa et al., 2008).

2.4. Lipidomic analysis

2.4.1. Lipid extraction

Zebrafish eleutheroembryos' total lipids were extracted using a modified Folch method (Christie and Han, 2010; Folch et al., 1957) with $CHCl_3$:MeOH (2:1 v/v) solution (containing 0.01% of BHT (dibutylhydroxytoluene) to avoid lipid oxidation). Extracted and dried lipid samples were stored for not more than 4 weeks at −80 °C until further analysis. A detailed and exhaustive protocol can be found in the **supplementary methods SM1 and SM2**.

2.4.2. High performance thin layer chromatography (HPTLC)

The analysis of lipid samples by high performance thin layer chromatography (HPTLC) was performed as previously described (Fuertes et al., 2018; Olsen and Henderson, 1989). Briefly, extracted samples were reconstituted in $CHCl_3$:MeOH (2:1 v/v) and spotted onto a thin 4 mm-length line in a pre-coated glass HPTLC silica gel 60 F_{254} plate (Merck; Darmstadt, Germany). Then, the HPTLC plate was double developed (firstly with a polar lipid eluent; and secondly with a neutral lipid eluent). The plate was dried, stained with the Fewster's dye and charred in a heater until visualization of the different lipid families occurred. A complete step to step protocol of the HPTLC loading performance, development and charring can be found in the **supplementary method SM3**. The quantitative analysis of the various lipid families represented by different brown-black spots in the plate was carried out by scanning densitometry. The plates were photographed on a Kodak Gel Logic 200 imaging system under white light and the intensity of the lipid spots from the corresponding chromatogram were measured using the imaging free software GelAnalyzer 2010a (http://www.gelanalyzer.com/). The identification of each lipid family in the plate was carried out according to the bibliography (Fuertes et al., 2018; Olsen and Henderson, 1989) as shown in Fig. F1A. Samples analyzed by HPTLC corresponded to 4, 5 and 6 dpf eleutheroembryos exposed to 0 (control), 4.0, 6.0 and 8.0 mg/L of BPA (n = 10 replicates per day and condition, 5 individuals per replicate).

2.4.3. Ultra-high performance liquid chromatography/time-of-flight mass spectrometry (UHPLC/TOFMS)

Lipidomic analyses of the lipid samples by Ultra-High Performance Liquid Chromatography/Time-Of-Flight Mass Spectrometry (UHPLC/TOFMS) were performed as previously described (Fuertes et al., 2018; Gorrochategui et al., 2014). Briefly: each sample was reconstituted in 300 μl of HPLC-grade methanol, vortexed and centrifuged during 5 min at 4 °C. 150 μl of the resultant solution was transferred to a mass chromatography vial with 20 μl of a lipid standard mix (final volume: 170 μl). Final amount of each lipid standard is reported at Supplementary Table ST2. Details about the instrumental, C8 column used, mobile phases and other chromatographic conditions and specifications can be found in Supplementary Table ST3. Individual lipid search was chosen roughly based in the detected lipids in previous lipidomic studies in zebrafish eleutheroembryos (Fraher et al., 2016) and the past experience of our group. The MassLynx™ V4.1 software (Waters, Massachusetts, USA) was used to perform the analyses, using the exact mass of each individual lipid as the searching motif, using a 0.05 Da window. Each lipid family was measured as a specific adduct and in a specific electro spray ionization (ESI) mode (positive or negative) chosen distinctly for each of them (reported at Supplementary Table ST2). The measured m/z ratio of the adduct, its retention time and its isotopic distribution were used for the identification. Generally, the accepted mass error in the m/z was 5 ppm; exceptionally, a slight higher error was accepted for the ones with the correct retention time pattern regarding its length and unsaturation degree and a correct isotopic distribution. All the identified lipids and its elemental composition, calculated and measured mass (m/z), retention time, error (ppm), double-bond equivalent (DBE) and mean amount (in pmol/eleutheroembryo) can be found at Supplementary Table ST4. Observed lipid families by UHPLC were: cholesterol esters (CE), triacylglycerols a.k.a. triglycerides (TG), diacylglycerols a.k.a. diglycerides (DG), phosphatidylethanolamines (PE), lysophosphatidylethanolamines (LPE), ether phosphatidylethanolamines (PE-O), phosphatidylethanolamine plasmalogens (PE-P), phosphatidylglycerols (PG), phosphatidylinositols (PI), phosphatidylserines (PS), phosphatidylcholines (PC), ether phosphatidylcholines (PC−O), phosphatidylcholine plasmalogens (PC−P) and sphingomyelins (SM). A scheme of the different lipid classes' chemical structures can be found in Supplementary Fig. SF1. The lipid annotation used consisted in the name of the lipid class followed by the number of the total number

of C atoms (taking into account all the fatty acid chains of the lipid) and the total number of unsaturations. Duplicate lipidomic analyses were performed per each time (4, 5 and 6 dpf) and condition (control and 6 mg/L of BPA).

2.5. Statistical analysis

2.5.1. Survival, hatching, swim bladder inflation and yolk sac area

With the aim to detect effects of the exposure to BPA in the survival, hatching and swim bladder inflation of the eleutheroembryos, individual non-parametric Mann-Whitney-Wilcoxon tests against each control group (one per day) were performed over the percentages obtained (6 replicates per condition, 10 eleutheroembryos per replicate, $p \leq 0.05$). Lipidomic responses across BPA treatments and time periods were analyzed by two way ANOVA, followed by a Tukey's post-hoc test (all pairwise comparisons, $p \leq 0.05$). Yolk sac area was expressed in mm^2. All the statistical analyses and the associated graphs were performed using GraphPad Prism version 8.1.2 for Windows (GraphPad Software, San Diego, California USA, www.graphpad.com).

2.5.2. HPTLC and UHPLC analyses

Lipid intensities (a.u.; arbitrary units) from the scanning densitometry (HPTLC) were normalized by sample (using the total phospholipids amount as reference value) and by lipid family (mean lipid family amount considering all the samples = 1.0). A more detailed description of the performed normalization can be found at **supplementary method SM4**. Differences in lipid intensities between the different conditions and days were analyzed by non-parametric Kruskal-Wallis tests with pairwise multiple comparisons. Differences were considered to be significant when $p < 0.05$. All the statistical analyses were carried out with SPSS 24.0 (Armonk, NY: IBM Corp., 2016) and the associated graphs were performed using GraphPad Prism version 8.1.2 for Windows (GraphPad Software, San Diego, California USA, www.graphpad.com).

For the mass spectrometry (UHPLC) analysis, each lipid total amount (pmol) per sample was calculated by comparison with its internal standard (using the relation of the peak areas extracted from the ion chromatograms). Afterwards, relative values were obtained by dividing the absolute values of each lipid and age by the mean of the control groups (each lipid independently; considering the three ages: 4, 5 and 6 dpf). Then, relative values were normalized by square-root transformation. Hierarchical clustering and PAM (partition around medoids) clustering analyses were performed to identify clusters of lipids with similar behaviour both during development and upon BPA exposure. Differences in the average amount of the lipids inside each cluster along the different groups were analyzed by a one-way ANOVA followed by a Tukey's post-hoc test with all pairwise comparisons, at the 5% confidence level. Those analyses, heatmap representations, and other statistics were performed in R using the R packages *stats*, *pheatmap*, *factoextra*, *FactoMineR*, *gplots*, *ggplot2*, *corrplot*, *fpc*, *fmsb*, *multcomp* and *cluster* (Bretz and Westfall, 2011; Hennig, 2014; Kassambara and Mundt, 2017; Lê et al., 2008; Maechler et al., 2019; Mevik and Wehrens, 2015; Nakazawa, 2018; R Development Core Team, 2008; Warnes et al., 2015; Wei et al., 2017; Wickham, 2011).

To study the correlation between the thin layer chromatography and mass spectrometry data, an analogous normalization was performed. The sum of all lipids from the same family obtained after UHPLC/TOFMS was obtained and afterwards, the normalization was performed similarly as done for the HPTLC data (**supplementary method SM4**).

Linear correlations between the HPTLC and UHPLC/TOFMS results, the yolk sac area (YSA) and the lipids amount, and YSA and lipid-related gene expression (extracted from the bibliography (Martínez et al., 2018)) were performed using Pearson correlation tests, at 5% confidence level. Gene expression values were obtained from reference (Martínez et al., 2018).

All statistical analyses and the associated graphs of the correlations were performed using GraphPad Prism version 8.1.2 for Windows (GraphPad Software, San Diego, California USA, www.graphpad.com). Raw and normalized data used in this study are reported in supplementary material and can be freely accessed at the repository digital. csic.es: https://digital.csic.es/handle/10261/192701?locale=en.

3. Results

3.1. Anatomical assessment of zebrafish eleutheroembryos

No statistical differences on survival or hatching rates were detected between control and BPA-exposed groups at any age or BPA concentration (Supplementary Table ST1). In contrast, a significant decrease in the swim bladder inflation rates were observed in the highest exposure group (8 mg/L of BPA) at 4, 5 and 6 dpf, and in the 6 mg/L group at 4 dpf, being consistent with our previous findings (Martínez et al., 2018). Exposure to BPA at concentrations of 6 mg/L or higher also resulted in a significant increase in yolk sac area (Fig. 1C), and for that reason was considered to be the lowest observed effect concentration (LOEC), in agreement with previous observations ((Martínez et al., 2018), Pearson correlation test: $r^2 = 0.99$, $p = 0.006$).

3.2. HPTLC results

Up to ten lipid families were identified by HPTLC in 4, 5 and 6 dpf eleutheroembryos treated with 0, 4, 6 and 8 mg/L BPA: cholesterol esters (CE) that eluted together with wax esters (WE), triglycerides (TG), cholesterol (Ch), phosphatidylethanolamines (PE), phosphatidylglycerols (PG), phosphatidylinositols (PI), phosphatidylserines (PS), phosphatidylcholines (PC) and sphingomyelins (SM) (Fig. F1). The amount of free fatty acids (FFA), which indicate lipid degradation, was negligible in all samples.

Total lipid analysis showed a relative decrease over time of the total fraction of PC, PI and TG in eleutheroembryos between 4 and 6 dpf and a relative enrichment in PE, Ch, PS, CE + WE, and PG (Fig. F1B) (Kruskal-Wallis test with pairwise multiple comparisons; $p \leq 0.05$). These results are in concordance with previously published mass spectrometry data ((Fraher et al., 2016), supplementary material, $r^2 \geq 0.78$; $p \leq 0.02$; except for the SM).

Exposure to BPA altered the lipid profile of the eleutheroembryos, as PC, PI and TG increased their relative abundances, henceforth reducing the relative amounts of other lipid groups (PE, PS, CE and SM; Fig. F1B). Note the differential effect of BPA on the TG relative amount at the 4 dpf age group (Fig. F1B). PG and the combined amount of CE + WE showed only minor changes both during development and upon BPA exposure (Fig. F1B).

3.3. Lipid analysis by UHPLC/TOFMS

A total of 267 individual lipids were identified and quantified by UHPLC/TOFMS high-throughput lipidomic analysis in control and 6 mg/L BPA exposed samples (Supplementary Table ST4). They could be divided into 15 different lipid families (ordered by number of measured lipids): 60 TGs, 56 PC, 21 PE, 20 CE, 18 PC-O, 17 DG, 15 PI, 14 SM, 13 PS, 13 LPC, 7 PE-O, 4 LPE, 4 PC-P, 3 PG and 2 PE-P. Considering the average molecular weight of the measured lipids (approximately 765 g/mol), the total lipid amount obtained per

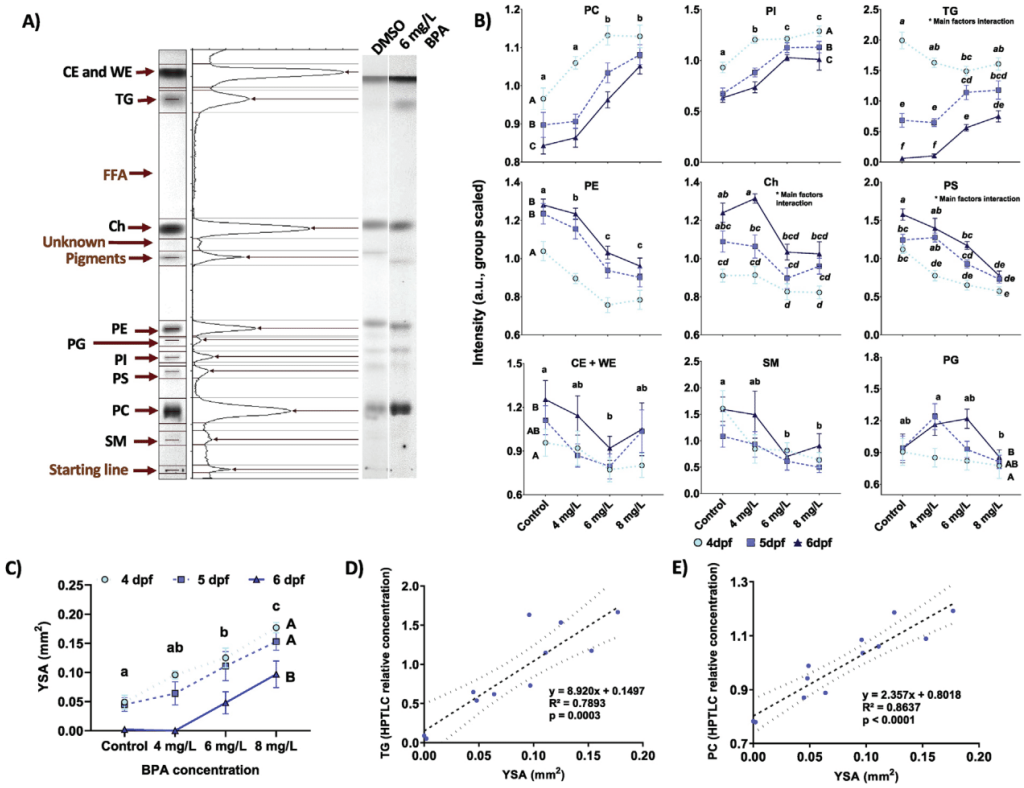

Fig. 1. A) Example of a high performance thin layer chromatography (HPTLC) analysis and the identification of each lipid family in the plate which was carry out according to the bibliography (Fuertes et al., 2018; Olsen and Henderson, 1989). Lipid classes detected by HPTLC were cholesterol esters (CE) that eluted together with wax esters (WE), triacylglycerols a.k.a. triglycerides (TG), cholesterol (Ch), phosphatidylethanolamines (PE), phosphatidylglycerols (PG), phosphatidylinositols (PI), phosphatidylserines (PS), phosphatidylcholines (PC) and sphingomyelins (SM). An unidentified spot and the pigments were not taken into account because their low interest in this study. Free fatty acid (FFA) amount were negligible indicating a low degradation of the samples. B) Relative lipid intensities of each lipid family obtained by high performance thin layer chromatography (HPTLC) for 0, 4, 6 and 8 mg/L of BPA exposed zebrafish eleutheroembryos at 4, 5 and 6 dpf. It needs to be highlighted the fact that due to the needed performed normalization in HPLTC, the intensities do not reflect the absolute effect of the time/treatment over each lipid family but the enrichment (lipid accumulation) or the decrease (lipid usage for energy or other purposes) of this lipid family regarding the total amount of lipids in the eleutheroembryos. Non-parametric Kruskal-Wallis test with pairwise multiple comparisons; $p \leq 0.05$) were performed for both factors (time and BPA exposure) and statistically different groups are indicated with different letters (low case or capital letters for differences between the exposure groups or the different ages, respectively, and italics for those which present main factors interaction). C) Yolk sac area (YSA) measurements of the eleutheroembryos exposed to BPA concentrations of 0 (control), 4.0, 6.0 and 8.0 mg/L at 4, 5 and 6 dpf. A parametric two-way ANOVA test (regarding time and exposure) followed by a Tukey's post-hoc test with all pairwise comparisons; $p \leq 0.05$) was performed and statistically different groups are indicated with different letters (low case or capital letters for BPA exposure and age groups' differences, respectively). D-E) Pearson correlation tests ($p < 0.05$) between the obtained absolute values of the YSA and the relative amount of TG and PC (respectively) measured by HPTLC.

individual (6.5 μg/eleutheroembryo) was very similar to other previously reported values for zebrafish embryos (Hachicho et al., 2015; Petersen and Kristensen, 1998); therefore, we can conclude that all the major lipids were measured.

Fig. F2A presents relative abundances for all 267 individual lipids in each sample. Hierarchical clustering analysis of these data reflected the experimental design, separating samples by age groups. Notably, control 5 dpf samples were grouped with the 6 dpf age group, whereas BPA-treated samples grouped with 4 dpf age group (Fig. F2A). Hierarchical clustering analysis of the lipid abundance by family (Fig. F2B) revealed 3 groups: the most abundant (PC, TG and PE); those with intermediate abundance (CE, PS, PI and SM) and the ones with minor contribution (PC−O, LPC, DG, PC-P, PG, PE-O, PE-P and LPE). PAM clustering analysis grouped the lipids into three clusters (Fig. F3A). Cluster A (130 lipids) corresponds to lipids that showed relatively minor variations between age groups and between treated and control samples (boxplots in Fig. F3B). Most CE (95.0%), DG (52.9%), PE (95.2%), LPE (75.0%), PE-O (100.0%), PE-P (100.0%), PG (100.0%), PS (69.2%), PC-O (83.3%), PC-P (75.0%) and SM (78.6%) were included in this cluster (Fig. F3C). Cluster B (89 lipids) includes lipids whose concentrations decrease with age, both in control and in treated samples, although the decrease was significantly weaker in the BPA-exposed groups (Fig. F3B). In fact, lipid concentrations were higher in BPA exposed individuals than in their control counterparts at any age. This cluster included most PI (86.7%), PC (73.2%) and LPC (84.6%), and a significant percentage of DG (47.1%) (Fig. F3C). Finally, cluster C (48 lipids) corresponds to lipids whose concentration decreased to almost undetectable levels at 5 and 6 dpf in control animals, and remained essentially stable in BPA-treated samples (Fig. F3B). It is remarkable that this cluster is exclusively composed by TG (80% of total TG, Fig. F3C). The classification of each individual lipid as well other detailed statistical analysis can be found in the Supplementary Table ST5. These results were in close agreement

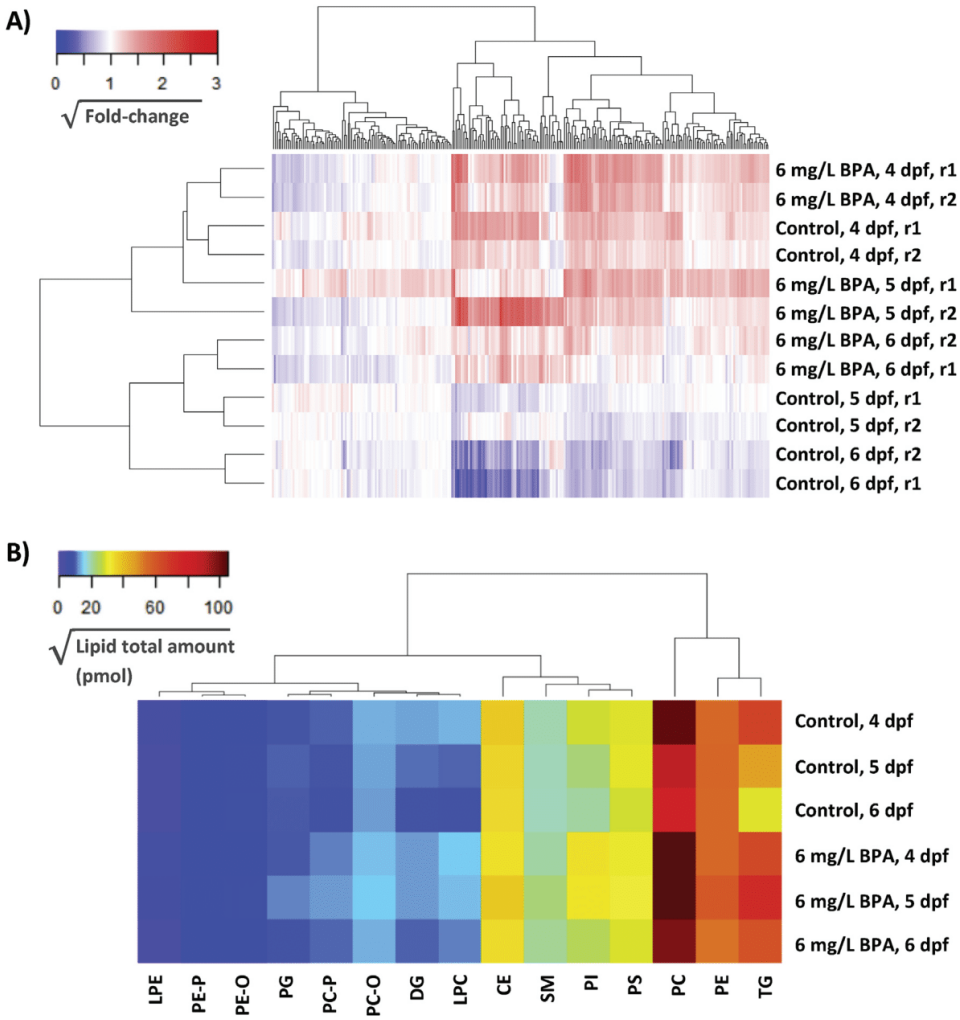

Fig. 2. A) Heatmap of the all the individual measured lipids by UHPLC/TOFMS: 267 lipids divided into 15 different lipid families: 60 TG, 56 PC, 21 PE, 20 CE, 18 PC-O, 17 DG, 15 PI, 14 SM, 13 PS, 13 LPC, 7 PE-O, 4 LPE, 4 PC-P, 3 PG and 2 PE-P. Hierarchical clustering for both lipids and samples cab be observed at the top and left of the graph, respectively. The data represent the square root of the fold-changes regarding the control groups' average (for each lipid): in red and blue, those lipids with fold-change higher or lower than 1.0, respectively. B) Heatmap of the absolute amount of each lipid family measured by UHPLC/TOFMS (obtained by summation of all specific lipid species inside the same family). Hierarchical clustering analysis of the lipid families are presented at the top of the heatmap. Square roots of the lipid total amounts (pmol) are represented and colored in a non-linear rainbow scale for helping the visualization of the lipid decreases in the different lipid families. (For interpretation of the references to color in this figure legend, the reader is referred to the Web version of this article.)

with the relative abundance data from both the HPTLC results and bibliographic HPLC/MS data ((Fraher et al., 2016), supplementary material, Supplementary Table ST6).

The tight distribution of the different lipid families among the three clusters was remarkable. Except for DG, at least 69% of the members of each family were included in a single cluster, and only four families (TG, DG, PC and PS) showed more than three members in more than one cluster (Supplementary Table ST5). A close inspection of the average fatty acid chain length and unsaturation degree show that the different clusters grouped lipids with similar characteristics within each family, as it is shown in Fig. F4.

The data suggests that the average fatty acid chain length and the level of unsaturation were the main factors to determine at which cluster a member of a given family belonged, driving the observed changes in its relative amount in any given condition (Supplementary Fig. SF2). For example, almost all TG included in clusters A and B (11 of 12 total species, respectively) contained either small-chain fatty acids (less than 16 carbons, on average) or totally saturated ones (Fig. F4). Similarly, most PC in cluster A contained fatty acids either totally saturated or with a single unsaturation (14 of 19 species with those characteristics; Fig. F4G, considering that the Y-axis represents the number of double bonds). DG clearly showed two subgroups of members (Fig. F4C) belonging to cluster A those fully saturated or with high levels of saturations (8 of 8 species), and to cluster B those with an intermedium unsaturation degree (1, 2 or 3 double bonds; 9 of 9

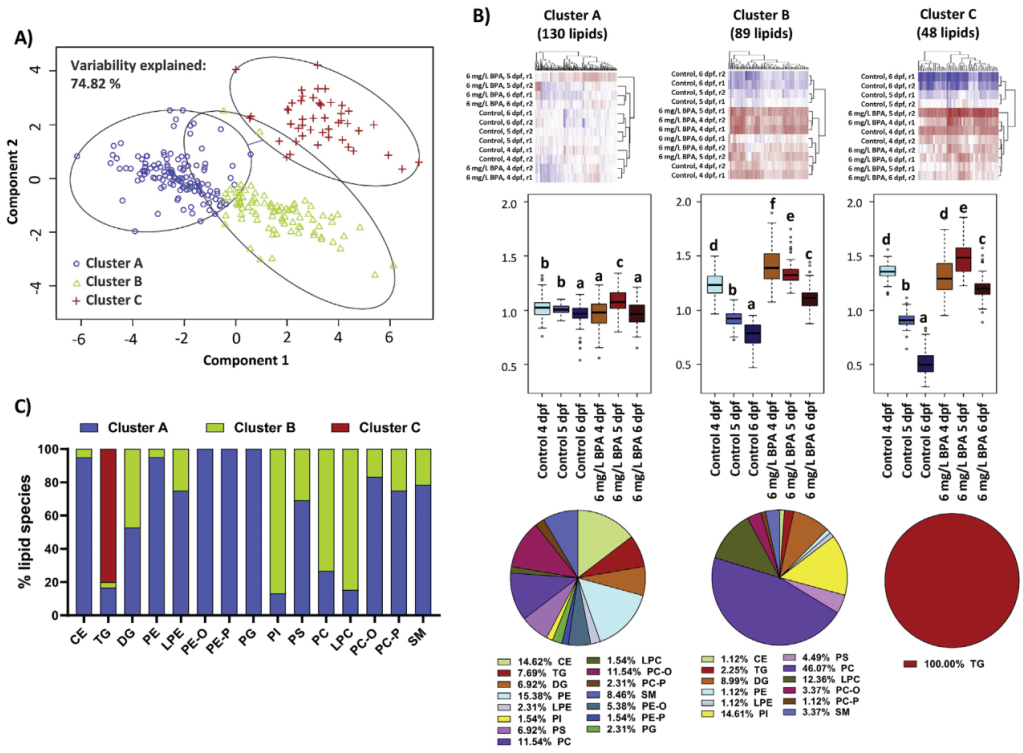

Fig. 3. A) PAM (partition around medoids) clustering analysis showing the presence of 3 different patterns in the lipids. Cluster A is shown in blue, cluster B in green and cluster C in red. First two principal components explained 74.82% of the total dataset variance. B) Heatmap and boxplots of the fold-changes normalized abundances and pie charts of the lipid families percentages for each of the three clusters defined in the PAM clustering analysis. In boxplots, differences in the average amount of the lipids inside each cluster along the different groups were analyzed by a one-way ANOVA by a Tukey's post-hoc test with all pairwise comparisons, $p \leq 0.05$. Different low case letters indicate statistically different groups. Average values and the 1st and 3rd quartiles are indicated by the thick bars, and the boxes, respectively. Total distribution is covered by the whiskers, except for the outliers (circles). C) Classification of the different lipid families' species (in percentage) among the three clusters defined in the PAM cluster analysis. Cluster A, B and C percentages are shown in blue, green and red, respectively. (For interpretation of the references to color in this figure legend, the reader is referred to the Web version of this article.)

species). The pattern for PS is somewhat complicated, but the adscription of the different members in cluster A or B is clearly determined by combination of the average FA chain length and the unsaturation degree (Fig. F4F). Interestingly, the abundance of PS lipids with very low or high unsaturation degree (0, 1, 5 or 6 double bonds) were much higher than those with an intermediate unsaturation degree (2, 3 or 4 double bonds). In addition, it could be observed that the phosphatidylcholine derivatives (LPC, PC-O and PC-P) exhibited a similar behaviour to that of PS lipids (Fig. F4H).

3.4. Lipid-related gene expression

Analysis of previous reported transcriptomic data (Martínez et al., 2018) from zebrafish eleutheroembryos treated with BPA (2–5 dpf) showed a clear dysregulation of genes related to lipid biosynthesis and catabolism (Supplementary Fig. SF3A and Table ST7). This effect took place even at lower concentrations (0.1–1 mg/L) than those that elicit a statistically significant increase of the yolk sac area (YSA), the main reservoir of the lipids (Supplementary Fig. SF3A). The transcriptomic data suggests a general upregulation of the lipid metabolism, including both the biosynthesis and catabolism, but that the imbalance in lipid metabolism by BPA was favorable to anabolic pathways. Forty-six differentially expressed genes (DEGs) were related to the lipid biosynthesis, compared with nineteen DEGs related to their catabolism and nine genes were involved in both pathways (Supplementary Fig. SF3A and Table ST7). The transcriptomic changes could be linearly correlated with the area of the yolk sac (Supplementary Fig. SF3B) which, in turn, correlated with the amount of remaining TG and PC (Fig. F1D-E). Transcripts involved in the lipid transport (essentially apolipoproteins) were also upregulated and their expression could be linearly correlated to the area of the yolk sac ($r^2 = 0.554$; $p < 0.0001$; Pearson correlation test; data not shown), which was extremely notable in case of the *apoa1a* and *apoba* ($r^2 = 0.893$; $p = 0.0004$).

4. Discussion

The major morphological effect of non-lethal BPA exposure in zebrafish eleutheroembryos was the permanence of a significant amount of yolk sac at up to 6 dpf, stage at which the yolk sac should have been completely reabsorbed in normal conditions. This effect has been previously observed (Martínez et al., 2019a, 2018) and it can be related to the presence of high amounts of TG, DG, PI, PC and LPC in BPA treated animals. Most of them are yolk sac-related lipids, as can be observed by their relative amount in the yolk sac and the rest of the body in unexposed conditions (Fraher et al., 2016). The yolk sac is the major reservoir of maternally deposited lipids and

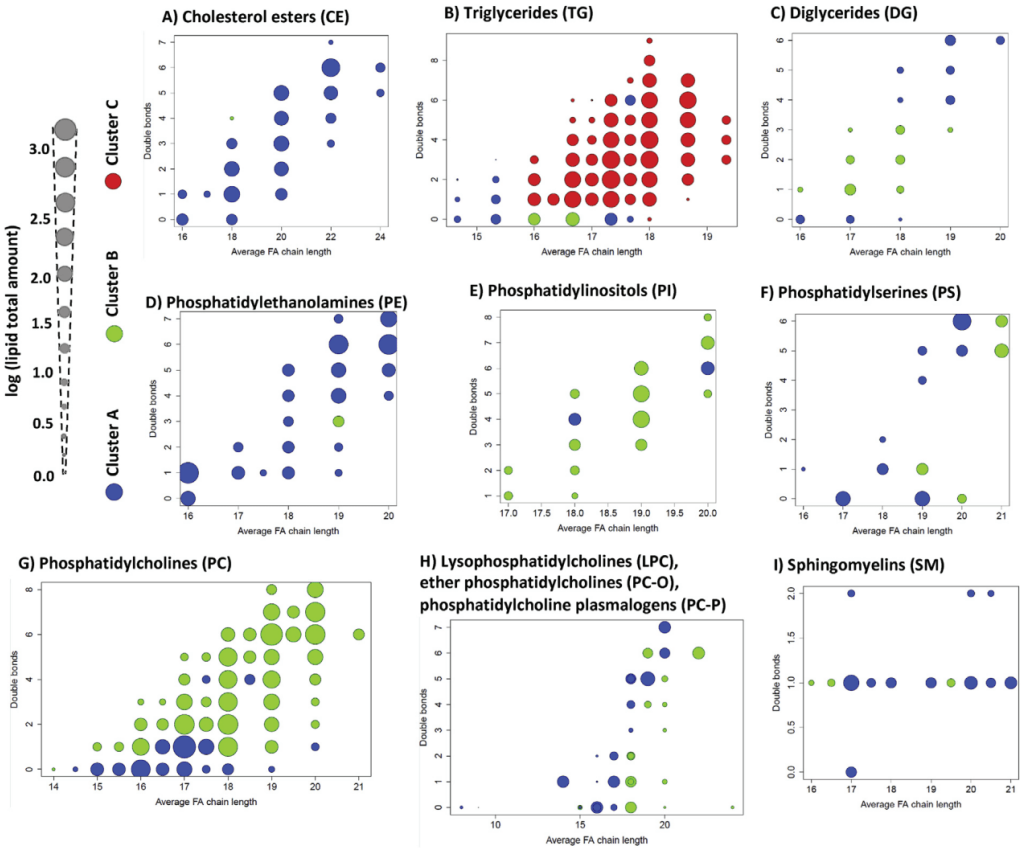

Fig. 4. Graphical representation of the lipid distribution regarding their unsaturation degree (Y-axis) and average FA chain length (X-axis) of the HPLC-TOFMS lipidomic dataset (lipids in control and 6 mg/L of BPA groups at 4, 5 and 6 dpf), divided per lipid family. Specific lipid species classified in the PAM clustering analysis (Fig. F3, Supplementary Table ST5) in cluster A, B and C are represented in blue, green and red color, respectively. The circumference size indicates the log-transformed total amount of each lipid (all samples average, in pmol). LPE, PE-O, PE-P and PG were not represented due to the low number of lipids in these families. (For interpretation of the references to color in this figure legend, the reader is referred to the Web version of this article.)

vitellogenin in the zebrafish eleuthero/embryo before reaching the self-feeding stage at 6 dpf, serving as main sources for energy and precursors for proteins, including lipoproteins (Babin et al., 2007; Fraher et al., 2016; Matsuda et al., 2011). Therefore, we interpret this apparent increase as a consequence of the inhibition of the consumption of the yolk sac lipids in the BPA exposed individuals and thereby, their reduced energy expenditure during these crucial embryonic stages. These results are in accordance with very recent studies in BPA-treated zebrafish (Ortiz-Villanueva et al., 2018; Santangeli et al., 2018). We also propose that part of the fatty acids from PC, LPC and PI are being consumed for energy acquirement, as: 1) their behaviour is similar to the one presented by the energy storage lipid families; 2) the lipid re-conversion both in the yolk sac and yolk syncytial layer is already activated (Miyares et al., 2014); and 3) their decrease in the yolk sac in normal conditions is not compensated by a similar increase in the rest of the body (Fraher et al., 2016).

In contrast, BPA exposure did not affect (or did it only slightly) the levels of CE, PE, PS, LPE, PE-O, PE-P, PG, PC-O, and SM. Most of these lipids are structural constituents of the biological membranes, whereas some of them are implicated in signalling or, in the case of SM, in myelination (Braverman and Moser, 2012; Dean and Lodhi, 2018; Lee et al., 2017; Nagan and Zoeller, 2001; Olsen and Færgeman, 2017; Pike, 2003; Quinn, 2014). This general lipid profile of BPA-exposed individuals, with only minor effects in the main "structural" lipid families (including those related to signalling or myelination) and larger effects in energy-storage lipids, does not correspond to a mere developmental delay. A previous detailed morphometric analysis reached the same conclusion, indicating that the exposed eleutheroembryos could also present a lower energy consumption (Martínez et al., 2019a). In addition, partial lipid results from a related metabolomic study (Ortiz-Villanueva et al., 2018) at lower BPA concentrations showed similar increase in some PC, DG and LPC, indicating that these effects are more related to a specific BPA mode of action than to a general toxic effect. Analysis of the behaviour of different molecular species within each lipid family revealed the presence of distinct subpopulations of TG, DG, PS, PC and phosphatidylcholine derivatives (LPC, PC-O and PC-P). We propose that these differential effects on the lipid subpopulations likely reflect the specific effect of BPA on storage lipids over structural ones. These subpopulations present different fatty acid chain lengths and/or unsaturation levels, reflecting the differential physicochemical requirements (fluidity, molecular weight) for structural and storage lipids. For example, we consider

it likely that the fraction of low fatty acid length or fully saturated TG that show a differentiated behaviour relative to the bulk TG may correspond to structural TG that do no form part, or do it only partially, to the yolk sac. In the same way, we propose that the subpopulations of PS, PC and PC derivatives that belonged to cluster A corresponded to structural lipids, whereas cluster B included molecular species mainly present in the yolk sac. It is revealing the case of DG, as they are intermediaries of both TG degradation and PC synthesis (Duncan et al., 2007; Gibellini and Smith, 2010; Kennedy and Weisst, 1956). This dual catabolic and anabolic role may be the reason for the peculiar distribution of DG molecular species between clusters A and B. Following this line of reasoning, we propose that cluster C corresponds to species exclusively present in the yolk sac and are only used for energy purposes, in this case, only TG.

In addition to the unsaturation degree and average FA length that triggered the clustering of the lipids, other differential physicochemical observations could be highlighted (see **supplemental material** for more information). For example, the lower abundance of the lipid species with an odd number of carbon atoms, the presence of neural/vision-related lipid species, or the different abundance patterns present in the lipid families did not trigger a different clustering of the lipids, indicating the lack of effects of the BPA exposure and/or the developmental stage over these characteristics.

The effects of BPA on both YSA and the levels of yolk sac-related lipids could be related to specific transcriptomic changes in genes implicated in lipid metabolism observed in a previous study (Martínez et al., 2018). BPA concentrations between 1 and 2 orders of magnitude below the ones required to induce morphological alterations (0.1 mg/L and 4.0 mg/L of BPA, respectively) induced a general upregulation of genes involved in lipid metabolism (Martínez et al., 2018), particularly those involved in lipid anabolism. This imbalance in favor of the biosynthesis and against lipid degradation could partially explain the reduction of lipid consumption in BPA-exposed zebrafish eleutheroembryos. We therefore propose that the dysregulation in gene expression may be part of the cause, rather than a consequence, of the effects of BPA on lipid levels and yolk sac resorption.

Gene ontology enrichment analysis (Supplementary Fig. SF4) identified genes involved in lipid transport, particularly in low and very-low density-lipoproteins, as strongly affected by BPA. These kind of lipoproteins contains a higher percentage of triglycerides (Feingold and Grunfeld, 2000; Garrett and Grisham, 2016) than high density lipoproteins, and therefore, they are supposed to be more implicated in energy metabolism. The *apoba* gene, one of the most affected apolipoproteins by BPA, codifies for the key protein implicated in formation of VLDL lipoproteins and chylomicrons (Cindrova-Davies et al., 2017; Young et al., 1995). In parallel, PC lipids, one of the families more retained in the BPA exposed individuals, are the major phospholipid component of the lipoproteins and the only one that is currently known to be essential for their assembly and secretion (Cole et al., 2012). In zebrafish eleutheroembryos, the apolipoprotein release by yolk syncytial layer (YSL) has been reported to be a key step for the transport of yolk lipids to the rest of the organism (Otis et al., 2015). In our case, the upregulation of apolipoproteins and its correlation with the increase of YSA at 5 and 6 dpf supports the idea that BPA did not impair lipid transport from the yolk to the rest of the body, and that the YS resorption impairment is more related to the lower eleutheroembryo energy consumption rate.

The observed lipidomic and transcriptomic effects of BPA in zebrafish embryos can be related to its known interaction with several nuclear receptors. BPA has been proposed to interact with the RXR/PPAR-ϒ receptor complex (cis-retinoic acid receptor/peroxisome proliferator-activated receptor gamma) (Huang and Chen, 2017; Riu et al., 2011) which is considered the master regulator of adipogenesis and lipid metabolism (Lempradl et al., 2015), activating transcription of apo- and lipoproteins in different model organisms (Dahabreh and Medh, 2012; Hai et al., 2015; Kersten, 2008; Shah et al., 2010). Similarly, zebrafish eleutheroembryos exposed to tributyltin (TBT), also considered as an obesogen and able to activate PPAR via RXR (Grün, 2014; le Maire et al., 2009) showed increased levels of some LPC and PC lipid species (Ortiz-Villanueva et al., 2018). In addition, the interaction of BPA with ERs (estrogen receptors) (Heindel and Blumberg, 2019; Mu et al., 2018) and ERR-ϒ (estrogen-related receptor gamma) (Bergman et al., 2013; Tohmé et al., 2014) could also participate in the effects of BPA on the lipid metabolism (Hao et al., 2013; Tohmé et al., 2014). All these signalling pathways are altered by BPA in zebrafish embryos (Martínez et al., 2018; Ortiz-Villanueva et al., 2017; Riu et al., 2011) and could be at least partially responsible for its obesogenic properties (Grün and Blumberg, 2007; Janesick and Blumberg, 2011).

The molecular and physiological mechanism of environmental obesogenicity are not completely understood yet (Heindel and Blumberg, 2019). Some of the proposed mechanisms include the differentiation and stimulation of adipocytes, increase lipid accumulation in liver, alteration of thermoregulation, or disruption of the hormonal regulation of appetite and satiety (Heindel and Blumberg, 2019). Adipocyte proliferation and activation is a common endpoint in laboratory tests for obesogenicity in animal models, including zebrafish (Riu et al., 2011; Maradonna and Carnevali, 2018). However, lipid accumulation in adipocytes does not occur in zebrafish larval after days 11–15 dpf, when adipocytes start differentiating (Riu et al., 2011; Imrie and Sadler, 2010). It is likely that the retention of yolk sac could not be assimilated to the accumulation of lipids in adipocytes, as the former only occur at BPA concentrations (from 4 mg/L on) far higher than the latter (0.1–0.2 mg/L BPA, Riu et al., 2011). Rather, we propose that the retention of the yolk sac may be related to a reduction of the energy consumption in treated embryos, an obesogenic mechanism also proposed for mammals, including humans (Heindel and Blumberg, 2019). Zebrafish eleutheroembryos exposed to BPA display a reduction on behavioral movement, which likely results in a lower energy consumption (Olsvik et al., 2019), as well as a specific reduction in eye development (Martínez et al., 2019a), being vision another important energy consumer (Emran et al., 2010). In this regard, one can hypothesize that yolk sac retention is a late manifestation of a series of toxic events that start by the activation of different nuclear receptors (RXR, PPARγ, ER) at low BPA concentrations (0.1 mg/L, Martínez el at, 2018), which progress through different molecular, biochemical, cellular, and behavioral events that finally result in macroscopic negative outcomes (yolk sac retention, swim bladder inflation, and, ultimately, death). This network of potential implications between the effects of BPA at the different complexity levels is shown in Fig. 5, which combines data from different sources and at different levels of organization. The figure is organized following an AOP (Adverse Outcome Pathway, Ankley et al., 2010) scheme, in which initial molecular events (interaction of BPA with different receptors) propagate the adverse responses to biochemical, cellular, tissue and organism levels.

5. Conclusions

BPA-treated eleutheroembryos showed higher retention of yolk sac and yolk-related lipids (mostly TG, DG, PI and PC) that their non-treated counterparts. On the other hand, CE, PE, PS, LPE, PE-O, PE-P, PG, PC-O, and SM lipid families (mostly related with structural

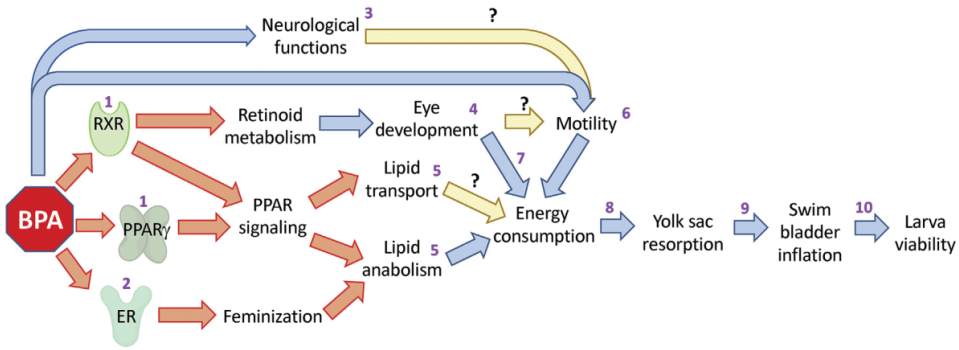

Fig. 5. Summary of potential adverse output pathways of BPA. The diagram summarizes the different outputs observed for the exposure to BPA of zebrafish embryos and their putative interconnections. We propose that BPA interact with ER, PPAR and RXR receptors, and that these interactions affects lipid metabolism, estrogenic responses and developmental processes, particularly in the eye development. These combined effects affect energy storage lipid consumption, by either disrupting lipid metabolism, reducing motility, reduction of vision function, or a combination of these. As a final consequence, there is a large excess of storage lipids (and of yolk sac) at the end of the eleutheroembryo stage, at which the early larva should be start actively feeding. We propose that the combined result should affect significantly the survival of the affected individuals. References: 1) (Martínez et al., 2018); 2) (Mu et al., 2018); 3) (Lam et al., 2011); 4) (Martínez et al., 2019a); 5) Present work; 6) (Olsvik et al., 2019); 7) (Emran et al., 2010); 8) (Sant and Timme-Laragy, 2018); 9) (Raldúa et al., 2008); 10) (Goolish and Okutake, 1999). Red and blue arrows show activation or inhibition of BPA in the pathway/effect/observation. (For interpretation of the references to color in this figure legend, the reader is referred to the Web version of this article.)

membranes and signalling functions) were only slightly or not affected both over the age or upon BPA exposure. Moreover, it could be observed that the differences in some lipid families' time- and BPA exposure-related patterns depended mostly on the unsaturation degree (mostly DG and PC) and fatty acid chain length (mostly TG and PC derivatives) of the lipids.

The presence of a significant portion of yolk sac in BPA-treated eleutheroembryos, and of its associated lipids, at developmental stages at which the feeding behaviour should be already activated appears as a major potential negative effect, as it interferes with other physiological key events, like swim bladder inflation. This specific "energy-storage" lipid retention in BPA exposed eleutheroembryos seems to be more related to a lower energy consumption and/or a favorable balance of the lipid dysregulation into the biosynthesis direction than to a lipid transport problem from the yolk sac. Energy-consuming functions like general motility or eye development have also been reported to be affected by BPA in similar studies and they may even be interconnected (low visual function may lead to low motility, for example).

In summary, the effects in lipid profile exerted by BPA in zebrafish eleutheroembryos seemed to be specific and not related to general baseline toxicity. The data also suggests that they are at least partially independent from estrogenic effects, which are the current basis for legal restrictions on BPA and on its derivatives. While other cellular targets, including different nuclear receptors, could not be discarded, activation of the PPAR/RXR complex and the downstream lipid metabolism genes appeared as good candidates to explain these estrogenic-independent effects. These conclusions are also based in previously reported transcriptomic, metabolomic and morphometric analyses of the effects of BPA in zebrafish eleutheroembryos, as well as in behavioural and molecular in vitro studies. In summary, the present study contributes in the understanding of the obesogenic properties of the BPA and its intercorrelated factors with the lipid metabolism.

Declaration of competing interest

The authors declare no conflicts of interest.

CRediT authorship contribution statement

Rubén Martínez: Conceptualization, Data curation, Formal analysis, Investigation, Methodology, Validation, Visualization, Writing - original draft, Writing - review & editing. **Laia Navarro-Martín:** Conceptualization, Investigation, Methodology, Supervision, Validation, Visualization, Writing - original draft, Writing - review & editing. **Morgane van Antro:** Data curation, Investigation, Methodology, Validation, Writing - review & editing. **Inmaculada Fuertes:** Data curation, Investigation, Methodology, Validation, Writing - review & editing. **Marta Casado:** Investigation, Methodology, Validation, Writing - review & editing. **Carlos Barata:** Funding acquisition, Project administration, Supervision, Visualization, Writing - review & editing. **Benjamin Piña:** Conceptualization, Formal analysis, Funding acquisition, Project administration, Supervision, Validation, Visualization, Writing - original draft, Writing - review & editing.

Acknowledgments

This work was supported by grants from the Spanish Ministry of Economy and Competitiveness (CTQ2014-56777-R) and the Spanish Ministry of Science, Innovation and University (RTI2018-096175-B-I00). RM was supported by a FPU predoctoral fellow from the Spanish Ministry of Education, Culture and Sport (ref. FPU15/03332). IF was supported by a FPI predoctoral fellow from the Spanish Ministry of Economy and Competitiveness (FPI-MICINN BES-2015-075023). We thank Juan Carlos Navarro and Josefina Casas for his valuable advice and expertise in the optimization of the thin-layer chromatography technique and liquid chromatography/mass spectrometry, respectively.

Appendix A. Supplementary data

Supplementary data to this article can be found online at https://doi.org/10.1016/j.chemosphere.2019.125704.

References

Almeida, S., Raposo, A., Almeida-González, M., Carrascosa, C., 2018. Bisphenol A: food exposure and impact on human health. Compr. Rev. Food Sci. Food Saf. 17,

1503–1517. https://doi.org/10.1111/1541-4337.12388.
Ankley, G.T., Bennett, R.S., Erickson, R.J., Hoff, D.J., Hornung, M.W., Johnson, R.D., Mount, D.R., Nichols, J.W., Russom, C.L., Schmieder, P.K., Serrrano, J.A., Tietge, J.E., Villeneuve, D.L., 2010. Adverse outcome pathways: a conceptual framework to support ecotoxicology research and risk assessment. Environ. Toxicol. Chem. https://doi.org/10.1002/etc.34.
Attimarad, M., Mueen Ahmed, K.K., Aldhubaib, B.E., Harsha, S., 2011. High-performance thin layer chromatography: a powerful analytical technique in pharmaceutical drug discovery. Pharm. Methods 2, 71–75. https://doi.org/10.4103/2229-4708.84436.
Babin, P.J., Carnevali, O., Lubzens, E., Schneider, W.J., 2007. Molecular aspects of oocyte vitellogenesis in fish. In: The Fish Oocyte. Springer, Netherlands, pp. 39–76. https://doi.org/10.1007/978-1-4020-6235-3_2.
Belanger, S.E., Balon, E.K., Rawlings, J.M., 2010. Saltatory ontogeny of fishes and sensitive early life stages for ecotoxicology tests. Aquat. Toxicol. 97, 88–95. https://doi.org/10.1016/j.aquatox.2009.11.020.
Bergman, Å., Heindel, J.J., Jobling, S., Kidd, K.A., Zoeller, R.T., 2013. State of the Science of Endocrine Disrupting Chemicals 2012 - Summary for Decision Makers. WHO. https://doi.org/10.1590/S1414-462X2013000100003.
Braverman, N.E., Moser, A.B., 2012. Functions of plasmalogen lipids in health and disease. Biochim. Biophys. Acta (BBA) - Mol. Basis Dis. https://doi.org/10.1016/j.bbadis.2012.05.008.
Bretz, F., Westfall, T.H.P., 2011. Multiple Comparisons Using R. CRC Press. https://doi.org/10.1128/AAC.03728-14.
Cajka, T., Fiehn, O., 2014. Comprehensive analysis of lipids in biological systems by liquid chromatography-mass spectrometry. TrAC Trends Anal. Chem. (Reference Ed.). https://doi.org/10.1016/j.trac.2014.04.017.
Canesi, L., Fabbri, E., 2015. Environmental effects of BPA: focus on aquatic species. Dose. Response. 13 https://doi.org/10.1177/1559325815598304, 1559325815598304.
Chen, M.Y., Ike, M., Fujita, M., 2002. Acute toxicity, mutagenicity, and estrogenicity of bisphenol-A and other bisphenols. Environ. Toxicol. 17, 80–86. https://doi.org/10.1002/tox.10035.
Christie, W.W., Han, X., 2010. Lipid Analysis : Isolation, Separation, Identification and Lipidomic Analysis. Oily Press, an imprint of PJ Barnes & Associates.
Cindrova-Davies, T., Jauniaux, E., Elliot, M.G., Gong, S., Burton, G.J., Charnock-Jones, D.S., 2017. RNA-seq reveals conservation of function among the yolk sacs of human, mouse, and chicken. Proc. Natl. Acad. Sci. 114, E4753–E4761. https://doi.org/10.1073/pnas.1702560114.
Cole, L.K., Vance, J.E., Vance, D.E., 2012. Phosphatidylcholine biosynthesis and lipoprotein metabolism. Biochim. Biophys. Acta Mol. Cell Biol. Lipids. https://doi.org/10.1016/j.bbalip.2011.09.009.
Corrales, J., Kristofco, L.A., Steele, W.B., Yates, B.S., Breed, C.S., Williams, E.S., Brooks, B.W., 2015. Global assessment of bisphenol A in the environment: review and analysis of its occurrence and bioaccumulation. Dose. Response 13. https://doi.org/10.1177/1559325815598308, 1559325815598308.
Dahabreh, D.F., Medh, J.D., 2012. Activation of peroxisome proliferator activated receptor-gamma results in an atheroprotective apolipoprotein profile in HepG2 cells. Adv. Biol. Chem. 218–225. https://doi.org/10.4236/abc.2012.23026, 02.
Dean, J.M., Lodhi, I.J., 2018. Structural and functional roles of ether lipids. Protein Cell. https://doi.org/10.1007/s13238-017-0423-5.
Duncan, R.E., Ahmadian, M., Jaworski, K., Sarkadi-Nagy, E., Sul, H.S., 2007. Regulation of lipolysis in adipocytes. Annu. Rev. Nutr. 27, 79–101. https://doi.org/10.1146/annurev.nutr.27.061406.093734.
Embry, M.R., Belanger, S.E., Braunbeck, T.A., Galay-Burgos, M., Halder, M., Hinton, D.E., Léonard, M.A., Lillicrap, A., Norberg-King, T., Whale, G., 2010. The fish embryo toxicity test as an animal alternative method in hazard and risk assessment and scientific research. Aquat. Toxicol. https://doi.org/10.1016/j.aquatox.2009.12.008.
Emran, F., Rihel, J., Adolph, A.R., Dowling, J.E., 2010. Zebrafish larvae lose vision at night. Proc. Natl. Acad. Sci. U.S.A. 107, 6034–6039. https://doi.org/10.1073/pnas.0914718107.
Eramo, S., Urbani, G., Sfasciotti, G.L., Brugnoletti, O., Bossù, M., Polimeni, A., 2010. Estrogenicity of bisphenol A released from sealants and composites: a review of the literature. Ann. Stomatol. 1, 14–21.
European Chemicals Agency, 2017. Member State Committee Support Document for Identification of 4,4'-isopropylidenediphenol (BPA, Bisphenol A) as a Substance of Very High Concern Because of its Endocrine Disrupting Properties Which Cause Probable Serious Effects to Human Health Which Give.
Feingold, K.R., Grunfeld, C., 2000. Introduction to Lipids and Lipoproteins. Endotext. MDText.com, Inc.
Flint, S., Markle, T., Thompson, S., Wallace, E., 2012. Bisphenol A exposure, effects, and policy: a wildlife perspective. J. Environ. Manag. 104, 19–34. https://doi.org/10.1016/j.jenvman.2012.03.021.
Flynn, E.J., Trent, C.M., Rawls, J.F., 2009. Ontogeny and nutritional control of adipogenesis in zebrafish (Danio rerio). J. Lipid Res. 50, 1641–1652. https://doi.org/10.1194/jlr.M800590-JLR200.
Folch, J., Lees, M., Sloane Stanley, G.H., 1957. A simple method for the isolation and purification of total lipides from animal tissues. J. Biol. Chem. 226, 497–509.
Fraher, D., Sanigorski, A., Mellett, N.A., Meikle, P.J., Sinclair, A.J., Gibert, Y., 2016. Zebrafish embryonic lipidomic analysis reveals that the yolk cell is metabolically active in processing lipid. Cell Rep. 14, 1317–1329. https://doi.org/10.1016/j.celrep.2016.01.016.
Fuertes, I., Jordão, R., Casas, J., Barata, C., 2018. Allocation of glycerolipids and glycerophospholipids from adults to eggs in Daphnia magna: perturbations by compounds that enhance lipid droplet accumulation. Environ. Pollut. 242, 1702–1710. https://doi.org/10.1016/j.envpol.2018.07.102.
Garrett, R.H., Grisham, C., 2016. Biochemistry, sixth ed. Biochemistry sixth ed.
Gibellini, F., Smith, T.K., 2010. The Kennedy pathway-de novo synthesis of phosphatidylethanolamine and phosphatidylcholine. IUBMB Life. https://doi.org/10.1002/iub.337.
Goolish, E.M., Okutake, K., 1999. Lack of gas bladder inflation by the larvae of zebrafish in the absence of an air-water interface. J. Fish Biol. 55, 1054–1063. https://doi.org/10.1006/jfbi.1999.1110.
Gorrochategui, E., Li, J., Fullwood, N.J., Ying, G.-G., Tian, M., Cui, L., Shen, H., Lacorte, S., Tauler, R., Martin, F.L., 2017. Diet-sourced carbon-based nanoparticles induce lipid alterations in tissues of zebrafish (Danio rerio) with genomic hypermethylation changes in brain. Mutagenesis 32, 91–103. https://doi.org/10.1093/mutage/gew050.
Gorrochategui, E., Pérez-Albaladejo, E., Casas, J., Lacorte, S., Porte, C., 2014. Perfluorinated chemicals: differential toxicity, inhibition of aromatase activity and alteration of cellular lipids in human placental cells. Toxicol. Appl. Pharmacol. 277, 124–130. https://doi.org/10.1016/j.taap.2014.03.012.
Grand View Research Inc, 2015. Bisphenol A (BPA) Market Analysis by Application (Polycarbonates, Epoxy Resins). Regional and Segment Forecasts to 2025 (San Francisco).
Grün, F., 2014. The obesogen tributyltin, in: Vitamins and Hormones, pp. 277–325. https://doi.org/10.1016/B978-0-12-800095-3.00011-0.
Grün, F., Blumberg, B., 2007. Perturbed nuclear receptor signaling by environmental obesogens as emerging factors in the obesity crisis. Rev. Endocr. Metab. Disord. https://doi.org/10.1007/s11154-007-9049-x.
Hachicho, N., Reithel, S., Miltner, A., Heipieper, H.J., Küster, E., Luckenbach, T., 2015. Body mass parameters, lipid profiles and protein contents of zebrafish embryos and effects of 2,4-dinitrophenol exposure. PLoS One 10, e0134755. https://doi.org/10.1371/journal.pone.0134755.
Hahn, M.E., McArthur, A.G., Karchner, S.I., Franks, D.G., Jenny, M.J., Timme-Laragy, A.R., Stegeman, J.J., Woodin, B.R., Cipriano, M.J., Linney, E., 2014. The transcriptional response to oxidative stress during vertebrate development: effects of tert-butylhydroquinone and 2,3,7,8-tetrachlorodibenzo-p-dioxin. PLoS One 9, e113158. https://doi.org/10.1371/journal.pone.0113158.
Hai, B., Ni, C., Xie, H., Guo, Z., Wu, M., Chen, Q., Zhou, Z., Fan, W., Zhou, H., 2015. Association between peroxisome proliferator-activated receptor and gene-gene interactions with the apolipoprotein A I/apolipoprotein B100 ratio. Zhonghua Xinxueguanbing Zazhi 43, 328–333.
Hao, R., Bondesson, M., Singh, A.V., Riu, A., McCollum, C.W., Knudsen, T.B., Gorelick, D.A., Gustafsson, J.Å., 2013. Identification of estrogen target genes during zebrafish embryonic development through transcriptomic analysis. PLoS One 8, e79020. https://doi.org/10.1371/journal.pone.0079020.
Heindel, J.J., Blumberg, B., 2019. Environmental obesogens: mechanisms and controversies. Annu. Rev. Pharmacol. Toxicol. 59, 89–106. https://doi.org/10.1146/annurev-pharmtox-010818-021304.
Hennig, C., 2014. fpc: flexible procedures for clustering. WWW Document. http://cran.r-project.org/package=fpc.
Hölttä-Vuori, M., Salo, V.T.V., Nyberg, L., Brackmann, C., Enejder, A., Panula, P., Ikonen, E., 2010. Zebrafish: gaining popularity in lipid research. Biochem. J. 429, 235–242. https://doi.org/10.1042/bj20100293.
Horan, T.S., Pulcastro, H., Lawson, C., Gerona, R., Martin, S., Gieske, M.C., Sartain, C.V., Hunt, P.A., 2018. Replacement bisphenols adversely affect mouse gametogenesis with consequences for subsequent generations. Curr. Biol. 28, 2948–2954. https://doi.org/10.1016/j.cub.2018.06.070 e3.
Huang, Q., Chen, Q., 2017. Mediating roles of PPARs in the effects of environmental chemicals on sex steroids. PPAR Res. 1–8. https://doi.org/10.1155/2017/3203161, 2017.
Huang, Y.Q., Wong, C.K.C., Zheng, J.S., Bouwman, H., Barra, R., Wahlström, B., Neretin, L., Wong, M.H., 2012. Bisphenol A (BPA) in China: a review of sources, environmental levels, and potential human health impacts. Environ. Int. 42, 91–99. https://doi.org/10.1016/j.envint.2011.04.010.
Imrie, D., Sadler, K.C., 2010. White adipose tissue development in zebrafish is regulated by both developmental time and fish size. Dev. Dynam. 239, 3013–3023.
Janesick, A., Blumberg, B., 2011. Minireview: PPARγ as the target of obesogens. J. Steroid Biochem. Mol. Biol. 127, 4–8. https://doi.org/10.1016/j.jsbmb.2011.01.005.
John, J., Reghuwanshi, A., Aravind, U.K., Aravindakumar, C.T., 2015. Development and validation of a high-performance thin layer chromatography method for the determination of cholesterol concentration. J. Food Drug Anal. 23, 219–224. https://doi.org/10.1016/j.jfda.2014.07.006.
Jordão, R., Garreta, E., Campos, B., Lemos, M.F.L., Soares, A.M.V.M., Tauler, R., Barata, C., 2016. Compounds altering fat storage in Daphnia magna. Sci. Total Environ. 545–546, 127–136. https://doi.org/10.1016/j.scitotenv.2015.12.097.
Jurowski, K., Kochan, K., Walczak, J., Barańska, M., Piekoszewski, W., Buszewski, B., 2017. Analytical techniques in lipidomics: state of the art. Crit. Rev. Anal. Chem. https://doi.org/10.1080/10408347.2017.1310613.
Kadasala, N.R., Narayanan, Badri, Liu, Yang, 2016. International trade regulations on BPA: global health and economic implications. Asian Dev. Policy Rev. 4, 134–142. https://doi.org/10.18488/journal.107/2016.4.4/107.4.134.142.
Kassambara, A., Mundt, F., 2017. factoextra: extract and visualize the results of multivariate data analyses [WWW Document]. https://cran.r-project.org/web/packages/factoextra/index.html.
Kennedy, E.P., Weisst, S.B., 1956. The function of cytidine coenzymes in the

biosynthesis of phospholipides. J. Biol. Chem. 222, 193–214.
Kersten, S., 2008. Peroxisome proliferator activated receptors and lipoprotein metabolism. PPAR Res. https://doi.org/10.1155/2008/132960.
Kim, K.Y., Lee, E., Kim, Y., 2019. The association between bisphenol A exposure and obesity in children - a systematic review with meta-analysis. Int. J. Environ. Res. Public Health. https://doi.org/10.3390/ijerph16142521.
Kimmel, C.B., Ballard, W.W., Kimmel, S.R., Ullmann, B., Schilling, T.F., 1995. Stages of embryonic development of the zebrafish. Dev. Dynam. 203, 253–310. https://doi.org/10.1002/aja.1002030302.
Kolpin, D.W., Furlong, E.T., Meyer, M.T., Thurman, E.M., Zaugg, S.D., Barber, L.B., Buxton, H.T., 2002. Pharmaceuticals, hormones, and other organic wastewater contaminants in U.S. streams, 1999-2000: a national reconnaissance. Environ. Sci. Technol. 36, 1202–1211. https://doi.org/10.1021/es011055j.
Lam, S.H., Hlaing, M.M., Zhang, X., Yan, C., Duan, Z., Zhu, L., Ung, C.Y., Mathavan, S., Ong, C.N., Gong, Z., 2011. Toxicogenomic and phenotypic analyses of bisphenol-a early-life exposure toxicity in zebrafish. PLoS One. https://doi.org/10.1371/journal.pone.0028273.
le Maire, A., Grimaldi, M., Roecklin, D., Dagnino, S., Vivat-Hannah, V., Balaguer, P., Bourguet, W., 2009. Activation of RXR-PPAR heterodimers by organotin environmental endocrine disruptors. EMBO Rep. 10, 367–373. https://doi.org/10.1038/embor.2009.8.
Lê, S., Josse, J., Husson, F., 2008. FactoMineR : an R package for multivariate analysis. J. Stat. Softw. 25, 1–18. https://doi.org/10.18637/jss.v025.i01.
Lee, J.M., Park, S.J., Im, D.S., 2017. Calcium signaling of lysophosphatidylethanolamine through LPA1 in human SH-SY5Y neuroblastoma cells. Biomol. Ther. 25, 194–201. https://doi.org/10.4062/biomolther.2016.046.
Legeay, S., Faure, S., 2017. Is bisphenol A an environmental obesogen? Fundam. Clin. Pharmacol. https://doi.org/10.1111/fcp.12300.
Lempradl, A., Pospisilik, J.A., Penninger, J.M., 2015. Exploring the emerging complexity in transcriptional regulation of energy homeostasis. Nat. Rev. Genet. 16, 665–681. https://doi.org/10.1038/nrg3941.
Löhr, H., Hammerschmidt, M., 2011. Zebrafish in endocrine systems: recent advances and implications for human disease. Annu. Rev. Physiol. 73, 183–211. https://doi.org/10.1146/annurev-physiol-012110-142320.
Lydic, T.A., Goo, Y.-H., 2018. Lipidomics unveils the complexity of the lipidome in metabolic diseases. Clin. Transl. Med. 7, 4. https://doi.org/10.1186/s40169-018-0182-9.
Maechler, M., Rousseeuw, P., Struyf, A., Hubert, M., Hornik, K., Studer, M., Roudier, P., Gonzalez, J., Kozlowski, K., Schubert, E., 2019. cluster: "Finding Groups in Data": cluster Analysis Extended Rousseeuw et al [WWW Document]. https://cran.r-project.org/web/packages/cluster/index.html.
Maradonna, F., Carnevali, O., 2018. Lipid metabolism alteration by endocrine disruptors in animal models: an overview. Front. Endocrinol. https://doi.org/10.3389/fendo.2018.00654.
Martínez, R., Esteve-Codina, A., Herrero-Nogareda, L., Ortiz-Villanueva, E., Barata, C., Tauler, R., Raldúa, D., Piña, B., Navarro-Martín, L., 2018. Dose-dependent transcriptomic responses of zebrafish eleutheroembryos to Bisphenol A. Environ. Pollut. https://doi.org/10.1016/j.envpol.2018.09.043.
Martínez, R., Herrero-Nogareda, L., Van Antro, M., Campos, M.P., Casado, M., Barata, C., Piña, B., Navarro-Martín, L., 2019a. Morphometric signatures of exposure to endocrine disrupting chemicals in zebrafish eleutheroembryos. Aquat. Toxicol. 214, 105232. https://doi.org/10.1016/j.aquatox.2019.105232.
Martínez, R., Navarro-Martín, L., Luccarelli, C., Codina, A.E., Raldúa, D., Barata, C., Tauler, R., Piña, B., 2019b. Unravelling the mechanisms of PFOS toxicity by combining morphological and transcriptomic analyses in zebrafish embryos. Sci. Total Environ. 674, 462–471. https://doi.org/10.1016/j.scitotenv.2019.04.200.
Matsuda, Y., Ito, Y., Hashimoto, H., Yokoi, H., Suzuki, T., 2011. Detection of vitellogenin incorporation into zebrafish oocytes by FITC fluorescence. Reprod. Biol. Endocrinol. 9 https://doi.org/10.1186/1477-7827-9-45.
Mesnage, R., Phedonos, A., Arno, M., Balu, S., Corton, J.C., Antoniou, M.N., 2017. Transcriptome profiling reveals bisphenol a alternatives activate estrogen receptor alpha in human breast cancer cells. Toxicol. Sci. 158, 431–443. https://doi.org/10.1093/toxsci/kfx101.
Mevik, B.-H., Wehrens, R., 2015. The pls package: principal component and partial least squares regression in R. J. Stat. Softw. 18, 1–23. https://doi.org/10.18637/jss.v018.i02.
Miyares, R.L., de Rezende, V.B., Farber, S.A., 2014. Zebrafish yolk lipid processing: a tractable tool for the study of vertebrate lipid transport and metabolism. Dis. Model. Mech. 7, 915–927. https://doi.org/10.1242/dmm.015800.
Moon, M.K., 2019. Concern about the safety of bisphenol A substitutes. Diabetes Metab. J. https://doi.org/10.4093/dmj.2019.0027.
Mu, X., Huang, Y., Li, Xuxing, Lei, Y., Teng, M., Li, Xuefeng, Wang, C., Li, Y., 2018. Developmental effects and estrogenicity of bisphenol A alternatives in a zebrafish embryo model. Environ. Sci. Technol. 52, 3222–3231. https://doi.org/10.1021/acs.est.7b06255.
Nagan, N., Zoeller, R.A., 2001. Plasmalogens: biosynthesis and functions. Prog. Lipid Res. https://doi.org/10.1016/S0163-7827(01)00003-0.
Nakazawa, M., 2018. fmsb: functions for medical statistics book with some demographic data [WWW Document]. https://cran.r-project.org/web/packages/fmsb/index.html.
Olsen, A.S.B., Færgeman, N.J., 2017. Sphingolipids: membrane microdomains in brain development, function and neurological diseases. Open Biol. https://doi.org/10.1098/rsob.170069.
Olsen, R.E., Henderson, R.J., 1989. The rapid analysis of neutral and polar marine lipids using double-development HPTLC and scanning densitometry. J. Exp. Mar. Biol. Ecol. 129, 189–197. https://doi.org/10.1016/0022-0981(89)90056-7.
Olsvik, P.A., Whatmore, P., Penglase, S.J., Skjærven, K.H., Anglès d'Auriac, M., Ellingsen, S., 2019. Associations between behavioral effects of bisphenol A and DNA methylation in zebrafish embryos. Front. Genet. 10, 184. https://doi.org/10.3389/fgene.2019.00184.
Ortiz-Villanueva, E., Jaumot, J., Martínez, R., Navarro-Martín, L., Piña, B., Tauler, R., 2018. Assessment of endocrine disruptors effects on zebrafish (Danio rerio) embryos by untargeted LC-HRMS metabolomic analysis. Sci. Total Environ. 635, 156–166. https://doi.org/10.1016/j.scitotenv.2018.03.369.
Ortiz-Villanueva, E., Navarro-Martín, L., Jaumot, J., Benavente, F., Sanz-Nebot, V., Piña, B., Tauler, R., 2017. Metabolic disruption of zebrafish (Danio rerio) embryos by bisphenol A. An integrated metabolomic and transcriptomic approach. Environ. Pollut. https://doi.org/10.1016/j.envpol.2017.07.095.
Otis, J.P., Zeituni, E.M., Thierer, J.H., Anderson, J.L., Brown, A.C., Boehm, E.D., Cerchione, D.M., Ceasrine, A.M., Avraham-Davidi, I., Tempelhof, H., Yaniv, K., Farber, S.A., 2015. Zebrafish as a model for apolipoprotein biology: comprehensive expression analysis and a role for ApoA-IV in regulating food intake. Dis. Model. Mech. 8, 295–309. https://doi.org/10.1242/dmm.018754.
Parichy, D.M., Elizondo, M.R., Mills, M.G., Gordon, T.N., Engeszer, R.E., 2009. Normal table of postembryonic zebrafish development: staging by externally visible anatomy of the living fish. Dev. Dynam. 238, 2975–3015. https://doi.org/10.1002/dvdy.22113.
Petersen, G.I., Kristensen, P., 1998. Bioaccumulation of lipophilic substances in fish early life stages. Environ. Toxicol. Chem.
Pike, L.J., 2003. Lipid rafts: bringing order to chaos. J. Lipid Res. 44, 655–667. https://doi.org/10.1194/jlr.R200021-JLR200.
Pirro, V., Guffey, S.C., Sepúlveda, M.S., Mahapatra, C.T., Ferreira, C.R., Jarmusch, A.K., Cooks, R.G., 2016. Lipid dynamics in zebrafish embryonic development observed by DESI-MS imaging and nanoelectrospray-MS. Mol. Biosyst. 12, 2069–2079. https://doi.org/10.1039/c6mb00168h.
Quinn, P.J., 2014. Sphingolipid symmetry governs membrane lipid raft structure. Biochim. Biophys. Acta Biomembr. 1838 https://doi.org/10.1016/j.bbamem.2014.02.021, 1922–1930.
R Development Core Team, 2008. R: a Language and Environment for Statistical Computing. R Foundation for Statistical Computing.
Raldúa, D., André, M., Babin, P.J., 2008. Clofibrate and gemfibrozil induce an embryonic malabsorption syndrome in zebrafish. Toxicol. Appl. Pharmacol. 228, 301–314. https://doi.org/10.1016/j.taap.2007.11.016.
Reed, B., Jennings, M., 2011. Guidance on the housing and care of Zebrafish Danio rerio. Res. Anim. Dep. Sci. Group, RSPCA 1–27.
Riu, A., Grimaldi, M., le Maire, A., Bey, G., Phillips, K., Boulahtouf, A., Perdu, E., Zalko, D., Bourguet, W., Balaguer, P., 2011. Peroxisome proliferator-activated receptor γ is a target for halogenated analogs of bisphenol A. Environ. Health Perspect. 119, 1227–1232. https://doi.org/10.1289/ehp.1003328.
Riu, A., Mccollum, C.W., Pinto, C.L., Grimaldi, M., Hillenweck, A., Perdu, E., Zalko, D., Bernard, L., Laudet, V., Balaguer, P., Bondesson, M., Gustafsson, J.A., 2014. Halogenated bisphenol-a analogs act as obesogens in zebrafish larvae (Danio rerio). Toxicol. Sci. 139, 48–58. https://doi.org/10.1093/toxsci/kfu036.
Rubin, B.S., Schaeberle, C.M., Soto, A.M., 2019. The case for BPA as an obesogen: contributors to the controversy. Front. Endocrinol. 10 https://doi.org/10.3389/fendo.2019.00030.
Sant, K.E., Timme-Laragy, A.R., 2018. Zebrafish as a model for toxicological perturbation of yolk and nutrition in the early embryo. Curr. Environ. Heal. Reports 5, 125–133. https://doi.org/10.1007/s40572-018-0183-2.
Santangeli, S., Notarstefano, V., Maradonna, F., Giorgini, E., Gioacchini, G., Forner-Piquer, I., Habibi, H.R., Carnevali, O., 2018. Effects of diethylene glycol dibenzoate and bisphenol A on the lipid metabolism of Danio rerio. Sci. Total Environ. 636, 641–655. https://doi.org/10.1016/j.scitotenv.2018.04.291.
Shah, A., Rader, D.J., Millar, J.S., 2010. The Effect of PPAR-α Agonism on Apolipoprotein Metabolism in Humans. https://doi.org/10.1016/j.atherosclerosis.2009.11.010. Atherosclerosis.
Tohmé, M., Prud'Homme, S.M., Boulahtouf, A., Samarut, E., Brunet, F., Bernard, L., Bourguet, W., Gibert, Y., Balaguer, P., Laudet, V., 2014. Estrogen-related receptor γ is an in vivo receptor of bisphenol A. FASEB J. 28, 3124–3133. https://doi.org/10.1096/fj.13-240465.
Touchstone, J.C., 1995. Thin-layer chromatographic procedures for lipid separation. J. Chromatogr. B Biomed. Sci. Appl. https://doi.org/10.1016/0378-4347(95)00232-8.
U.S. Environmental Protection Agency U S Environmental Protection Agency, 2010. Bisphenol-A action plan 1–22.
vom Saal, F.S., Nagel, S.C., Coe, B.L., Angle, B.M., Taylor, J.A., 2012. The estrogenic endocrine disrupting chemical bisphenol A (BPA) and obesity. Mol. Cell. Endocrinol. https://doi.org/10.1016/j.mce.2012.01.001.
Wang, J., Sun, B., Hou, M., Pan, X., Li, X., 2013. The environmental obesogen bisphenol A promotes adipogenesis by increasing the amount of 11β-hydroxysteroid dehydrogenase type 1 in the adipose tissue of children. Int. J. Obes. 37, 999–1005. https://doi.org/10.1038/ijo.2012.173.
Wang, S., Wang, L., Hua, W., Zhou, M., Wang, Q., Zhou, Q., Huang, X., 2015. Effects of bisphenol A, an environmental endocrine disruptor, on the endogenous hormones of plants. Environ. Sci. Pollut. Res. 22, 17653–17662. https://doi.org/10.1007/s11356-015-4972-y.
Warnes, G.R., Bolker, B., Bonebakker, L., Gentleman, R., Huber, W., Liaw, A., Lumley, T., Maechler, M., Magnusson, A., Moeller, S., Schwartz, M., Venables, B., 2015. gplots: various R programming tools for plotting data. Compr. R Arch. Netw.

Wei, T., Simko, V., Levy, M., Xie, Y., Jin, Y., Zemla, J., 2017. Corrplot: visualization of a correlation matrix [WWW Document]. https://cran.r-project.org/web/packages/corrplot/index.html.
Wickham, H., 2011. ggplot2. Wiley Interdiscip. Rev. Comput. Stat. 3, 180–185. https://doi.org/10.1002/wics.147.
Wilson, C., 2012. Aspects of larval rearing. ILAR J. https://doi.org/10.1093/ilar.53.2.169.
Young, S.G., Cham, C.M., Pitas, R.E., Burri, B.J., Connolly, A., Flynn, L., Pappu, A., Wong, J., Hamilton, R.L., Farese Jr., R.V., 1995. A genetic model of defective chylomicron formation: mice expressing apolipoprotein B in the liver, but not in the intestine. J. Clin. Investig. 96, 2932–2946. https://doi.org/10.1172/JCI118365.

Supplemental information: scientific article V

Changes in lipid profiles induced by bisphenol A (BPA) in zebrafish eleutheroembryos during the yolk sac absorption stage

Authors: R. Martínez, L. Navarro-Martín, M. van Antro, I. Fuertes, M. Casado, C. Barata, B. Piña

Status: Published

Journal: Chemosphere. 246 (2020) 125704.

DOI: 10.1016/j.chemosphere.2019.125704

Supplementary methods

SM1. Solutions preparation

a) Lipid extractant $CHCl_3$:MeOH (2:1) (NO BHT): 133.3 ml $CHCl_3$[a] and 66.6 ml MeOH[b].

b) Lipid extractant $CHCl_3$:MeOH (2:1) (BHT): 66.6 ml $CHCl_3$, 33.3 ml MeOH and 10 mg BHT[c].

c) Saline solution (0.88% KCl aqueous solution): 0.88 g KCl[d] in 100 ml mili-Q water.

d) Cleaning solution (for the TLCs): 170 ml C_6H_{14}[e] and 170 ml Et_2O[f].

e) Polar lipids eluent: 100 ml AcOMe[g], 100 ml iPrOH[h], 100 ml $CHCl_3$[a], 40 ml MeOH[b] and 36 ml of an aqueous solution (KCl 0,25%: 0,2 g KCl[d] in 80 ml mili-Q water).

f) Neutral lipids eluent: 340 ml C_6H_{14}[e], 60 ml Et_2O[f] and 6ml glacial AcOH[i].

g) Fewster solution (dye): 3% $Cu(AcO)_2$[j] and 8% H_3PO_4[k] aqueous solution (3,297 g of $Cu(AcO)_2$[j] and 9,41 ml H_3PO_4[j] 85%, fill up to 100 ml with mili-Q water).

[a] Chloroform, [b] methanol, [c] Butilhydrotoluene, [d] Potassium chloride, [e] hexane, [f] diethyl ether, [g] methyl acetate, [h] 2-isopropanol, [i] glacial acetic acid, [j] copper (II) acetate, [k] phosphoric acid.

SM2. Lipid extraction protocol (modified Folch method)

a) Put the frozen samples (-80 °C) into dry ice.

b) Add **0.75 ml** of $CHCl_3$:MeOH (2:1) + **BHT** to each one, add 2 iron beads and put them into ice.

c) Homogenize the samples in the tissuelyzer (**2 min, 50 Hz**).

d) Add **0.75 ml** of $CHCl_3$:MeOH (2:1) (**NO BHT)**.

e) Take the homogenized (~1.5 ml) with a glass pipette and put it in a new 2ml-Eppendorf.

f) Add **0,375 ml** of saline solution (*0.88% KCl*) and vortex the Eppendorfs. Two phases will separate (aqueous phase up, organic phase bottom).

g) Centrifuge the tubes at **4 ºC** during **5 min** at **maximum revolutions (≥ 12000 rpm)**.

h) Take the organic phase (bottom) with a glass pipette and put it in a new Eppendorf.

i) Evaporate it with a N_2 stream.

j) Resuspend the lipids in **0.8-1.0 ml** of $CHCl_3$:MeOH (2:1) (**NO BHT)**.

k) **Vortex** the Eppendorf very well to make sure that we collect all the lipids.

l) Take the resuspended lipid solution and put it in a glass chromatography vial.

m) Evaporate it with a N_2 stream.

n) Resuspend the lipids in **100 µl** of $CHCl_3$:MeOH (2:1) (**NO BHT)**.

o) **Vortex** the glass vial ensuring the complete lipid recollection.

p) Evaporate it with a N_2 stream.

q) Put the vials that have the dried lipids to the desiccator: **at vacuum, overnight** and in **darkness**.

SM3. Thin layer chromatography protocol

3.1. Plate cleaning:

a) Put 60-80 ml of cleaning solution (hexane:ether) into the bucket and close it.

b) Make a mark (a line) in the thin layer plate at 0,5 cm of one of the borders (it will be the upper border).

c) Put gently the plate into the bucket and run the plate to eliminate the impurities. Make sure the eluent arrive to the upper border (**~45 min**) and let it **5 additional minutes**.

d) Meanwhile, resuspend the dried lipids in 20 µl of $CHCl_3$:MeOH (2:1) (**NO BHT)**.

e) Once the elution is completed, take out the plate from the bucket and let it to dry in the fume hood for **10 min**.

f) Scratch with a scalpel the marked part of the plate where the impurities remains (perform it wearing a **mask**, **gently** and **over a filter paper**).

g) Put the scratched plate into a heater at **110 ºC** during **30 min**.

h) Take the plate off the heater and let it to cool down (a few minutes).

3.2. Sample spotting in the plate:

i) Turn 90° to the left the plate and mark it as follows:

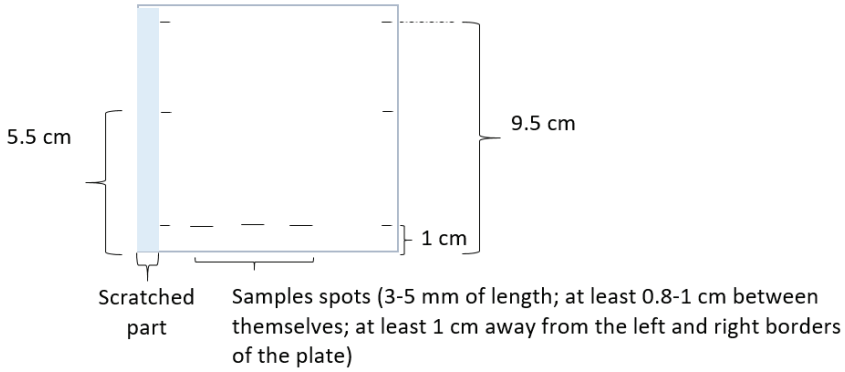

j) Take 1.5 µl of each sample (vortex each one very well just before taking the 1.5 µl) and put it in the plate gently:

I. Use a **Hamilton** pipette for make the spot.

II. Make it in **line** (3-5 mm).

III. Do not touch the plate (not so much) with the pipette (**avoid to scratch** the plate surface).

IV. Make the line as **thin** as possible (it would be necessary to do a few passes).

3.3. Plate running:

k) Put 60-80 ml of **polar** lipid eluent in the bucket.

l) Put the plate with the spotted samples into the bucket and run it to the first mark (5.5 cm) (**~15 min**).

m) Take the plate off the bucket and put it into the desiccator during **5 min at vacuum**.

n) Put 60-80 ml of **neutral** lipid eluent in the bucket.

o) Put the plate into the bucket and run it to the second mark (9.5 cm) (**~40 min**). **Make sure that the eluent does not pass the mark.**

p) Take away the plate and put it into the desiccator during **5 min at vacuum**.

3.4. Plate staining and charring:

q) Place the plate into a big cork box and wet it abundantly with the Fewster Solution (use a sprayer inside an extraction chamber).

r) Make sure, gently, that the back part of the plate are dry. The front part of the plate must not show water reflexes before start the next step.

s) When the plate is dry, put into the heater at **160 ºC** during **10 min***.

* If the spots are weakly marked, let the plate more time, but making sure that the background does not char.

t) Make a photo of the plate in the densitometer and keep it away from the light.

SM4. HPTLC-TOF and HPTLC results comparison

4.1. For HPLC-TOF results normalization:

1) $x_i = \sum_{j=1}^{n} y_j$

where “x” is the sum of all the lipids inside one lipid family (“i") in an specific sample, “n” the number of measured lipids in this family and “y_j” the absolute value (in pmol) of each specific lipid (PC 32:1, for example) measured in the sample.

$$2)\ z_i = \frac{x_i}{\frac{1}{n}\cdot\sum_{j=1}^{n} x_{i,j}}$$

where “x” is the sum of all the lipids inside one lipid family (“i") in an specific sample, “n” is the number of phospholipid families (5: PE, PI, PC, PG and PS) which are represented by “j”, and “z” is the lipid amount (of one specific lipid family) normalized by sample.

$$3)\ s_{i,j} = \frac{z_{i,j}}{\frac{1}{n}\cdot\sum_{j=1}^{n} z_{i,j}}$$

where “z” is the normalized lipid amount of one lipid family (“i") in an specific sample (“j”), “n” is the number of samples (all the different dpf ages) and “$s_{i,j}$” is the lipid amount (of an specific lipid family at an specific age) normalized by sample and lipid family.

4.2. For HPTLC results normalization:

$$4)\ u_i = \frac{t_i}{\frac{1}{n}\cdot\sum_{j=1}^{n} t_{i,j}}$$

where “t” is the intensity of the band corresponding to one lipid family (“i") in an specific sample, “n” is the number of phospholipid families (5: PE, PI, PC, PG and PS) which are represented by “j”, and “u” is the lipid amount (of one specific lipid family) normalized by sample.

$$5)\ v_{i,j} = \frac{u_{i,j}}{\frac{1}{n}\cdot\sum_{j=1}^{n} u_{i,j}}$$

where “u” is the normalized lipid amount of one lipid family (“i") in an specific sample (“j”), “n” is the number of samples and “$v_{i,j}$” is the lipid amount (of an specific lipid family “i” at an specific sample “j”) normalized by sample and lipid family.

4.3. For comparison between HPTLC-TOF and HPTLC results:

$$6)\ t_{i,j} = v_{i,j} \cdot \frac{s_{i,5dpf}}{v_{i,5dpf}}$$

where “t” is the final normalized lipid amount of one lipid family (“i") at an specific age (“j”) and “s” and “v” are the normalized lipid amounts (coming from HPTLC-TOF and HPTLC techniques, respectively) of one lipid family (“i") at 5 dpf (the common age at both experiments).

4.4. HPTLC validation and lipids families tendency over time:

Before performing the extensive lipidomic analysis, with the objective of validating the thin layer chromatography method for the study of zebrafish eleutheroembryos' lipids and to confirm the relative tendencies (accumulation or usage) of the several lipid families, a comparison between our HPTLC results (only control groups) and bibliographic HPLC/MS data [1] was performed. The specific normalization carried out to perform the data integration can be found at **supplementary method SM4**. As can be observed in the **supplementary methods figure SMF1**, a good correlation ($r^2 \geq 0.78$; $p \leq 0.02$; Pearson correlation test) between the relative amount of all the lipid families (except for the SM) and the time (1-6 dpf) could be stablished. The obtained tendencies (1-6 dpf) were equivalent with the ones obtained by thin layer chromatography (4-6 dpf): larvae were enriched over time in CE (and WE), Ch, PE, PG and PS meanwhile the total fraction of TAGs, PI and PC in the larvae (regarding the total amount of lipids) were decreased. We hypothesize that the uncorrelated tendency of the SM family is due to the low intensity of the band corresponding to the SM in HPTLC, allowing the increase of the variability in its measurements. Considering that the HPLC/MS results [1] corresponded to 1, 2, 3 and 5 dpf and the HPTLC results to 4, 5 and 6 dpf, that the day in common (5 dpf) was used to perform the normalization between techniques and that during the stages larvae do not have exogenous feeding that could alter drastically the lipid families relationship, we concluded that the above shown results revealed that the HPTLC methodology can reveal reliable results about the relative patterns of lipid families in zebrafish larvae samples and could be used as a non-expensive screening technique in lipidomic research (also generally confirmed by the comparison between our both HPTLC and UHPLC/TOFMS results, see **supplementary table ST5**).

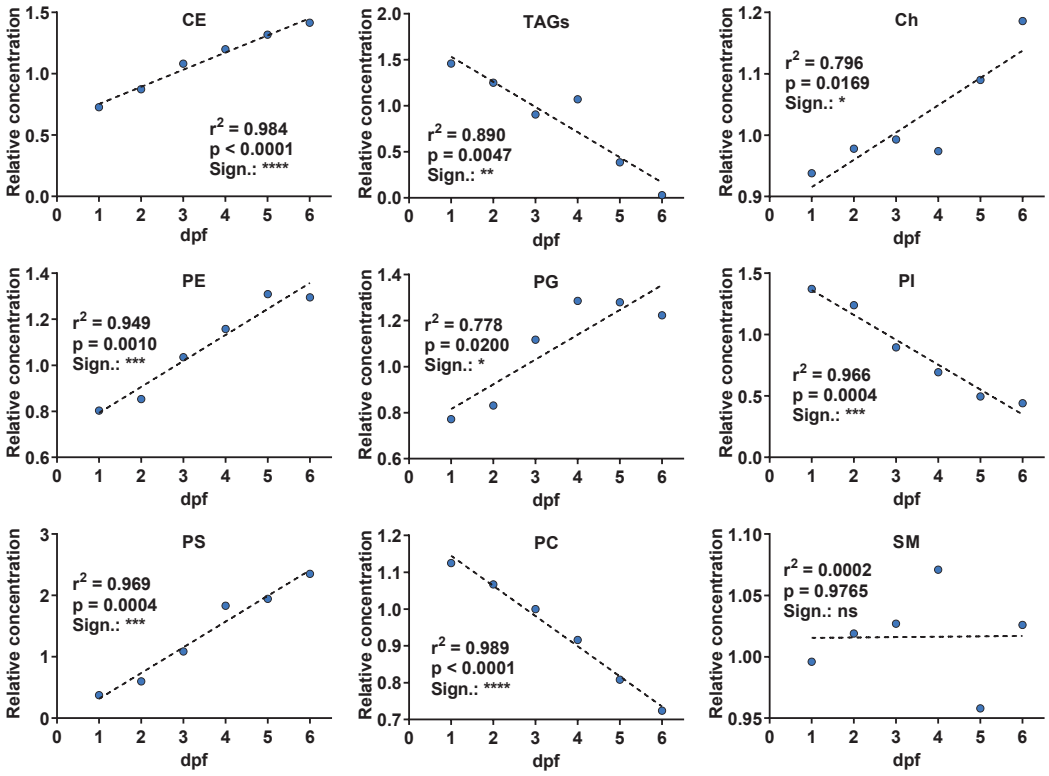

SMF1. Comparison between our HPTLC results (only control groups) and bibliographic HPLC/MS data [1]. The specific normalization carried out to perform the data integration can be found at **supplementary method SM4**. Pearson correlation tests were performed for all the lipid classes. In general, a good correlation between the relative amount of all the lipid families ($r^2 \geq 0.78$; $p \leq 0.02$; except for the SM) and the time (1-6 dpf) could be stablished. Significant correlations were specified by asterisks (* for $p<0.05$, ** for $p<0.01$, *** for $p<0.001$ and **** for $p<0.0001$). Common lipid families were CE (cholesterol esters), TAGs (triacylglycerols a.k.a. triglycerides), Ch (cholesterol), PG (phosphatidylglycerols), PE (phosphatidylethanolamines), PI (phosphatidylinositols), PS (phosphatidylserines), PC (phosphatidylcholines) and SM (sphingomyelins).

Supplementary observations

1. Lipid-related biological observations:

1.1. Lipid species with odd and even number of carbon atoms

Although the main and major fatty acid chains in the lipids of most species have an even number of carbon atoms, due to their biosynthetic processes (mostly between 16 and 22) [2], lipids with an average fatty acid chain length that implied some odd-numbered FA chain could be also detected (figure F4, supplemental table ST4). Their detection is in concordance with previous studies in zebrafish [1], their amount was mostly lower than the even-numbered lipids and their presence in zebrafish embryos can be mostly explained by maternal deposition which, in turn, can be justified by a dietary input (TetraMin Flakes -Tetra, Germany; http://www.tetra-fish.com-, [2]). Furthermore, they were clustered (**figure F4**) analogously as their neighbouring lipids, showing that they were not differentially affected by the BPA exposure neither by the time.

1.2. Lipid abundances patterns

It can be highlighted that there are 3 different patterns regarding the preponderance of the lipid species (**figure F4**): a) lipids of the CE, TG, DG, PI and PC families exhibited a higher abundance when both unsaturation degree and the average FA chain length were at intermedium levels, decreasing when at least one of them (or both) were very low or very high; b) lipids in PE, PS and PC derivatives (LPC, PC-O and PC-P) presented high abundances when their unsaturation degree was very low or high and low abundances when they presented an intermediate unsaturation degree. Finally, c) SM lipids mostly presented only 1 unsaturation (present in the sphingosine chain) showing that they are regularly composed by a totally saturated second chain. No specific pattern-dependent clustering could be observed, suggesting the lack of relation with the age or BPA effects. Nevertheless, the high similarity in the clustering and the lipid abundances patterns of PS and PC derivatives needs to be highlighted (**figure F4F, H**). The reason of the existence of this pattern (that has been also observed in the bibliography [1], [3], [4]), as far as we know, has not been explained although it could be a consequence of the different degree of unsaturations present in the different tissues of the eleutheroembryos. Although the pattern similarity between PS and PE lipid abundances could be easily explained by their interconversion by the PS synthase-

2 [5], the similarity with the PC derivatives (LPC, PC-O and PC-P) would need further studies as their conversion is not direct and it takes place via PE-PC-LPC [6], [7].

1.3. Vision/neural related lipid species

CE (**figure F4A**) are together with LPE and LPC the only lipid family with a singular fatty acid in their structure and thus, where a FA could be undoubtedly identified. Interestingly, the most abundant CE was CE 22:6 which contain the docosahexaenoic fatty acid (DHA; C22:6), a LC-PUFA (long chain – polyunsaturated fatty acid) extremely important in new forming tissues in the brain and in the retina of the zebrafish eleutheroembryos. At these stages of the zebrafish larvae, their neurovisual systems are very important due to its relative size with the whole body, and there is a demand of a relatively high amount of LC-PUFAs like EPA (eicosapentaenoic acid; C20:5) and DHA [8] compared with the rest of tissues. Both EPA and DHA could be not only detected in the CE lipid family but they were its 3rd and 1st most abundant fatty acids respectively (**supplemental table ST5**). DHA was also the 2nd and the 3rd most abundant fatty acid in the LPE and PLC lipid families, respectively (**supplemental table ST5**). Similarly, differences in the unsaturation degree and fatty acid chain length in the lipids (of the same family) of different tissues have been previously reported [9], [10]. In addition, in phosphatidylinositols, the major PI found in the eleutheroembryos was the 38:4 in concordance with the bibliography [10]. If it was mostly comprised by a stearic acid chain (C18:0) and arachidonic acid (20:4), similarly to the mammalians cells [9]–[12], should be further studied. It has been also reported that the PI of the brain are more enriched with stearoyl–arachidonoyl chains that the ones of the rest of the body and that the specific loss of arachidonic acid enrichment can lead to brain defects [12]. Nevertheless, although the BPA has been shown to affect vision-related genes [13], its effects over brain-related fatty acids needs to be further studied. As before, the lipid species clustered similarly as their neighbouring lipids suggesting that they are not differentially affected by the age nor BPA.

1.4. Lipid patterns comparison

In some families, the unsaturation degree and/or the average fatty acid chain length of their lipids exerted an effect over their classification in the PAM clustering analysis indicating that those factors could be relevant in their usage over the time and/or that those lipids could be

differentially affected by the BPA exposure. Similarly, the influence of the unsaturation degree and FA chain length in lipid processes like the lipid synthesis, degradation rate, serum concentration, oxidation, aging effects or the enzymatic activity over them have been previously described [14]–[19]. In this way, a creditable influence of these factors in the behavior (differentially affected by the time and/or the BPA exposure) of the lipids in our study could be taken into consideration (**figure F4**)).

· TG: their differential behavior based mostly in the length of the fatty acid chain (**figure F4B**; except the totally saturated TAGs). Similarly, in other mammals and bird studies, the length of the triglycerides have been related with different oxidation rates, transport pathways and lipid retention [20]–[22].

· DG: conversely, the behavior of DG (**figure F4C**) were mainly influenced by the number of unsaturations. We interpret the two classifications of DG as two subpopulations with different metabolic and/or functional roles, probably consequence of their role as intermediate metabolites in the TG lipolysis [23] and their signaling function (PKC activation) [12]. In fact, it has been previously reported that only the polyunsaturated DG (derived from the PIP_2 cycle) could be able to bind and activate PKC. On the other hand, low saturated DG could derived from the TG lipolysis.

· PC: similarly to DG, the behavior of the phosphatidylcholines were mostly influenced by the number of unsaturations, specifically the totally saturated (PCXX:0; **figure F4G**) and some mono-saturated species. Moreover, totally saturated PC presented a similar behaviour that saturated DG which showed a different behavior than the low-saturated lipids in their respective family. This concordance could be explained by their homeostasis [24]: *de novo* synthesis of phosphatidylcholines (the CDP-choline pathway, part of the Kennedy pathway [25], [26], which need a DG molecule) and/or their usage to the formation of new DG (by action of specific phospholipases [27]–[29]). As an example, as can be observed, the relative amount of the totally saturated DG (DG 32:0, 34:0 and 36:0) can be correlated with the correlative PC (PC 32:0, 34:0 and 36:0).

· PS and PC derivatives (LPC, PC-O and PC-P): their differential behavior based mostly in the length of the fatty acid chain (although its combination with the unsaturation degree needs to be

considered). Nevertheless, as far as we know, no biological processes affected differentially the PS based on their unsaturation degree or chain length.

[1] D. Fraher, A. Sanigorski, N. A. Mellett, P. J. Meikle, A. J. Sinclair, and Y. Gibert, "Zebrafish Embryonic Lipidomic Analysis Reveals that the Yolk Cell Is Metabolically Active in Processing Lipid," Cell Rep., vol. 14, no. 6, pp. 1317–1329, 2016.

[2] T. Řezanka and K. Sigler, "Odd-numbered very-long-chain fatty acids from the microbial, animal and plant kingdoms," Progress in Lipid Research, vol. 48, no. 3–4. Pergamon, pp. 206–238, 01-May-2009.

[3] E. Gorrochategui et al., "Diet-sourced carbon-based nanoparticles induce lipid alterations in tissues of zebrafish (Danio rerio) with genomic hypermethylation changes in brain," Mutagenesis, vol. 32, no. 1, pp. 91–103, 2017.

[4] H. Y. Kim, B. X. Huang, and A. A. Spector, "Phosphatidylserine in the brain: metabolism and function," Progress in Lipid Research, vol. 56, no. 1. NIH Public Access, pp. 1–18, Oct-2014.

[5] J. E. Vance, "Phospholipid synthesis and transport in mammalian cells," Traffic, vol. 16, no. 1, pp. 1–18, Jan. 2015.

[6] D. E. Vance and J. E. Vance, "Physiological consequences of disruption of mammalian phospholipid biosynthetic genes," Journal of Lipid Research, vol. 50, no. SUPPL. American Society for Biochemistry and Molecular Biology, p. S132, 2009.

[7] T. Harayama et al., "Lysophospholipid acyltransferases mediate phosphatidylcholine diversification to achieve the physical properties required in vivo," Cell Metab., vol. 20, no. 2, pp. 295–305, Aug. 2014.

[8] Ó. Monroig, J. Rotllant, E. Sánchez, J. M. Cerdá-Reverter, and D. R. Tocher, "Expression of long-chain polyunsaturated fatty acid (LC-PUFA) biosynthesis genes during zebrafish Danio rerio early embryogenesis," Biochim. Biophys. Acta - Mol. Cell Biol. Lipids, vol. 1791, no. 11, pp. 1093–1101, Nov. 2009.

[9] A. M. Hicks, C. J. DeLong, M. J. Thomas, M. Samuel, and Z. Cui, "Unique molecular signatures of glycerophospholipid species in different rat tissues analyzed by tandem mass spectrometry," Biochim. Biophys. Acta - Mol. Cell Biol. Lipids, vol. 1761, no. 9, pp. 1022–1029, Sep. 2006.

[10] A. Traynor-Kaplan et al., "Fatty-acyl chain profiles of cellular phosphoinositides," Biochim. Biophys. Acta - Mol. Cell Biol. Lipids, vol. 1862, no. 5, pp. 513–522, May 2017.

[11] M. R. Wenk et al., "Phosphoinositide profiling in complex lipid mixtures using electrospray ionization mass spectrometry," Nat. Biotechnol., vol. 21, no. 7, pp. 813–817, Jul. 2003.

[12] K. D'Souza and R. M. Epand, "Enrichment of phosphatidylinositols with specific acyl chains," Biochimica et Biophysica Acta - Biomembranes, vol. 1838, no. 6. Elsevier, pp. 1501–1508, 01-Jun-2014.

[13] R. Martínez et al., "Dose-dependent transcriptomic responses of zebrafish eleutheroembryos to Bisphenol A," Environ. Pollut., Dec. 2018.

[14] A. P. Rollón, Anaerobic digestion of fish processing wastewater with special emphasis on hydrolysis of suspended solids. A.A. Balkema, 1999.

[15] B. Selmi, E. Gontier, F. Ergan, and D. Thomas, "Effects of fatty acid chain length and unsaturation number on triglyceride synthesis catalyzed by immobilized lipase in solvent-free medium," Enzyme Microb. Technol., vol. 23, no. 3–4, pp. 182–186, Aug. 1998.

[16] C. E. Castuma and R. R. Brenner, "The influence of fatty acid unsaturation and physical properties of microsomal membrane phospholipids on UDP-glucuronyltransferase activity.," Biochem. J., vol. 258, no. 3, pp. 723–31, Mar. 1989.

[17] S. Grimsgaard, K. H. Bønaa, and K. S. Bjerve, "Fatty Acid Chain Length and Degree of Unsaturation Are Inversely Associated with Serum Triglycerides," 2000.

[18] A. Naudí, M. Jové, V. Ayala, M. Portero-Otín, G. Barja, and R. Pamplona, "Membrane lipid unsaturation as physiological adaptation to animal longevity," Frontiers in Physiology, vol. 4 DEC. Frontiers Media SA, p. 372, 17-Dec-2013.

[19] E. Rudolphi-Skórska, M. Filek, and M. Zembala, "The effects of the structure and composition of the hydrophobic parts of phosphatidylcholine-containing systems on phosphatidylcholine oxidation by ozone," J. Membr. Biol., vol. 250, no. 5, pp. 493–505, Oct. 2017.

[20] P. Schönfeld and L. Wojtczak, "Short- and medium-chain fatty acids in energy metabolism: the cellular perspective," J. Lipid Res., vol. 57, no. 6, pp. 943–954, 2016.

[21] A. T. Ward and R. R. Marquardt, "The effect of saturation, chain length of pure triglycerides, and age of bird on the utilization of rye diets," Poult. Sci., vol. 62, no. 6, pp. 1054–1062, Jun. 1983.

[22] M. H. Sung, F. H. Liao, and Y. W. Chien, "Medium-chain triglycerides lower blood lipids and body weight in streptozotocin-induced type 2 diabetes rats," Nutrients, vol. 10, no. 8, p. 963, Jul. 2018.

[23] R. E. Duncan, M. Ahmadian, K. Jaworski, E. Sarkadi-Nagy, and H. S. Sul, "Regulation of lipolysis in adipocytes," Annu. Rev. Nutr., vol. 27, no. 1, pp. 79–101, Aug. 2007.

[24] E. Sarri, A. Sicart, F. Lázaro-Diéguez, and G. Egea, "Phospholipid synthesis participates in the regulation of diacylglycerol required for membrane trafficking at the Golgi complex," J. Biol. Chem., vol. 286, no. 32, pp. 28632–28643, Aug. 2011.

[25] F. Gibellini and T. K. Smith, “The Kennedy pathway-de novo synthesis of phosphatidylethanolamine and phosphatidylcholine,” IUBMB Life, vol. 62, no. 6. John Wiley & Sons, Ltd, pp. 414–428, 01-Jun-2010.

[26] E. P. Kennedy and S. B. Weisst, “The function of cytidine coenzymes in the biosynthesis of phospholipides,” J. Biol. Chem., vol. 222, no. 1, pp. 193–214, 1956.

[27] T. Sakai, T. Sugiyama, Y. Banno, Y. Kato, and Y. Nozawa, “Involvement of phosphatidylcholine hydrolysis by phospholipase C in prostaglandin F2α-induced 1,2-diacylglycerol formation in osteoblast-like MC3T3-E1 cells,” J. Bone Miner. Metab., vol. 22, no. 3, pp. 198–206, May 2004.

[28] T. O. Eichmann and A. Lass, “DAG tales: the multiple faces of diacylglycerol - stereochemistry, metabolism, and signaling,” Cellular and Molecular Life Sciences, vol. 72, no. 20. Springer, pp. 3931–3952, Oct-2015.

[29] T. D. Pollard, J. Lippincott-Schwartz, W. C. Earnshaw, and G. T. Johnson, “Second messengers,” in Cell Biology (Third Edition), Elsevier, 2017, pp. 443–462.

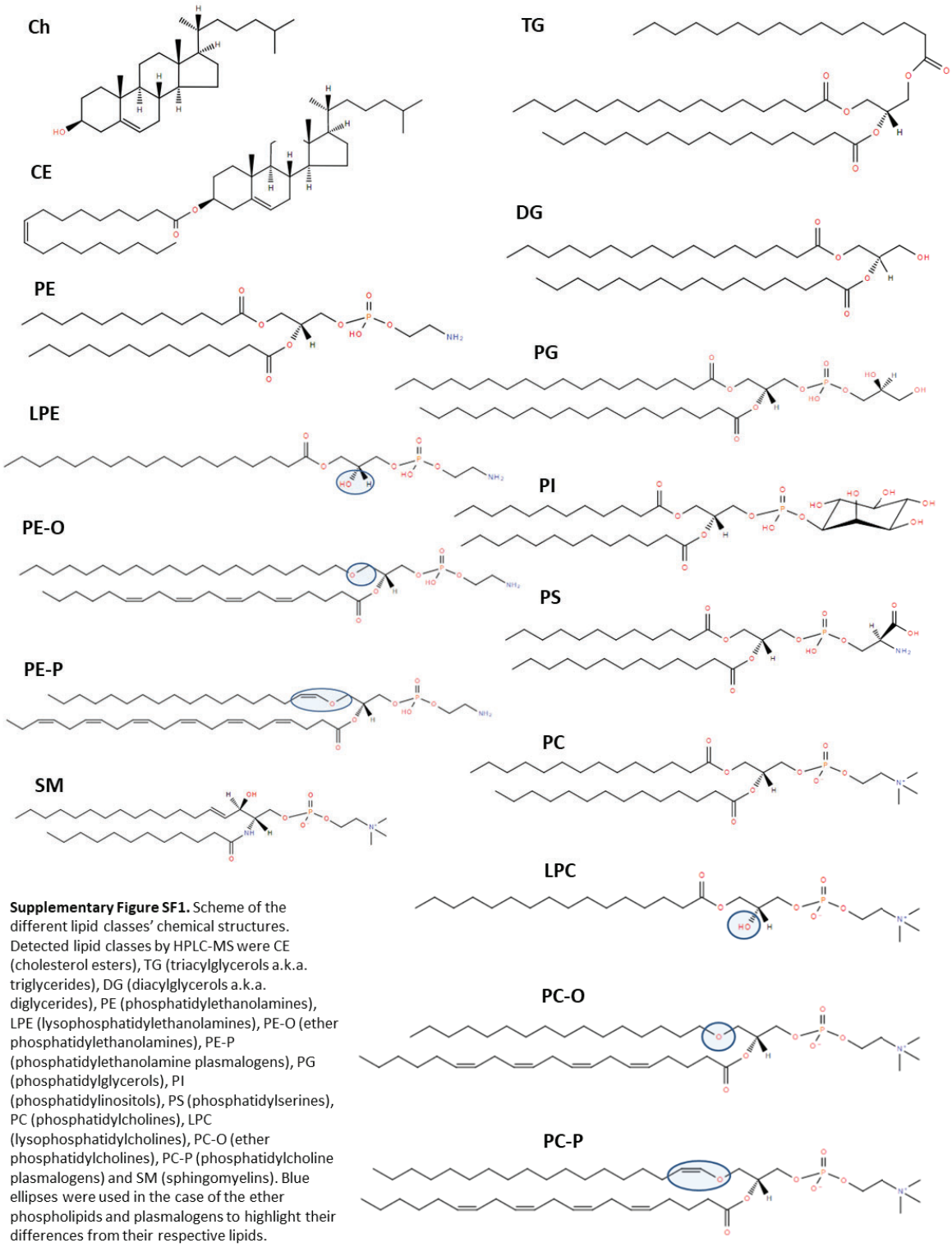

Supplementary Figure SF1. Scheme of the different lipid classes' chemical structures. Detected lipid classes by HPLC-MS were CE (cholesterol esters), TG (triacylglycerols a.k.a. triglycerides), DG (diacylglycerols a.k.a. diglycerides), PE (phosphatidylethanolamines), LPE (lysophosphatidylethanolamines), PE-O (ether phosphatidylethanolamines), PE-P (phosphatidylethanolamine plasmalogens), PG (phosphatidylglycerols), PI (phosphatidylinositols), PS (phosphatidylserines), PC (phosphatidylcholines), LPC (lysophosphatidylcholines), PC-O (ether phosphatidylcholines), PC-P (phosphatidylcholine plasmalogens) and SM (sphingomyelins). Blue ellipses were used in the case of the ether phospholipids and plasmalogens to highlight their differences from their respective lipids.

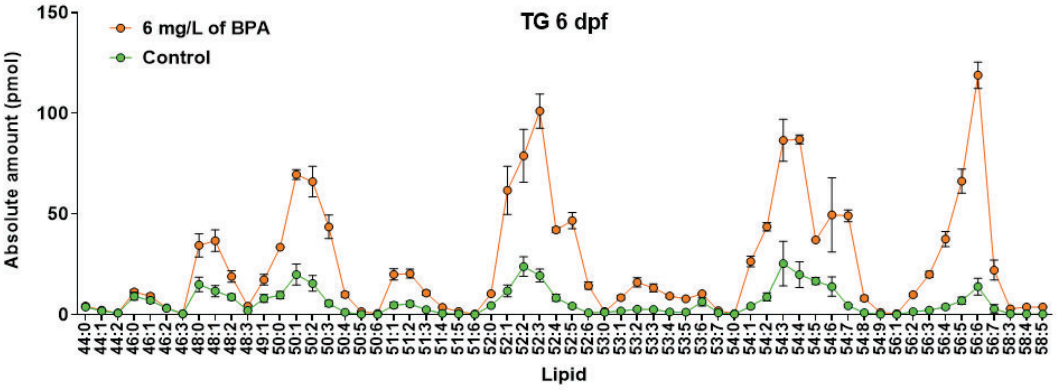

Figure SF2. Absolute amount (pmol/sample) of all the different detected and measured lipid species (by HPLC-TOFMS) in the TG family at both control and 6 mg/L of BPA-exposed groups at 6 dpf.

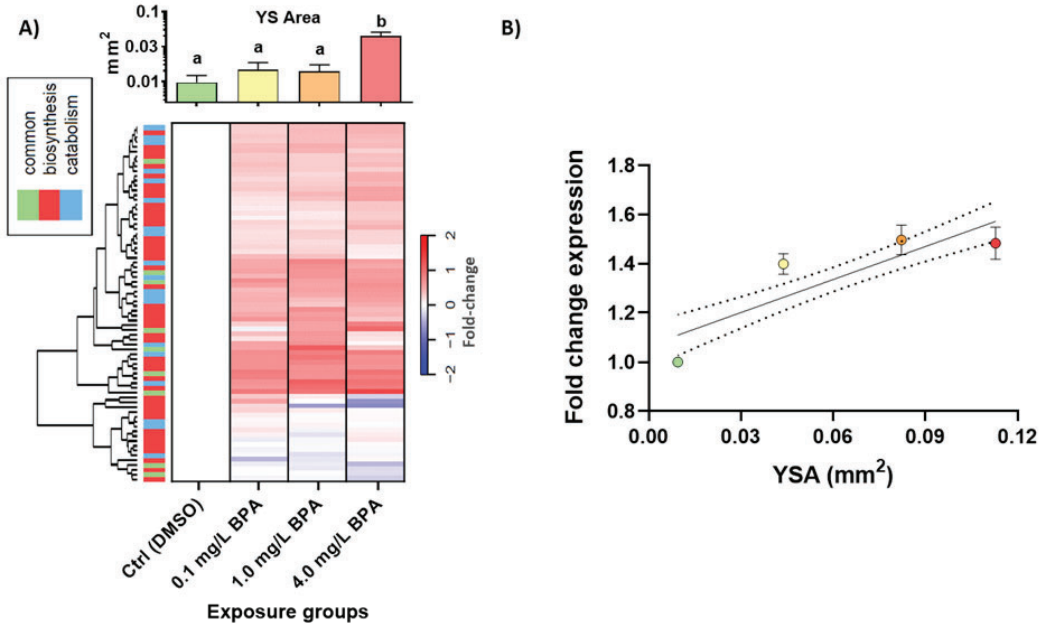

Supplementary Figure SF3. A) Bibliographic gene expression upregulation (fold-changes regarding the control group) of the lipid biosynthesis and catabolism related genes in the zebrafish eleutheroembryos exposed to different BPA concentrations and comparison with their yolk sac area (YSA) (Martínez et al., 2018). Upregulated genes are colored in red and downregulated ones in blue. Transcripts related with lipid biosynthesis, catabolism and common transcripts in both pathways are legend-indexed at left of the heatmap in red, blue and green, respectively. Gene selection was based in the pathway classification of the genes (zfin database; (Howe et al., 2012); http://zfin.org/) and the differential expression in (Martínez et al., 2018) (only differentially expressed genes (DEGs) were taken into account). A complete list of the transcripts and their pathway classification can be found in the supplemental table ST7. **B)** Pearson correlation test ($p < 0.0001$) between the fold-changes of lipid-related DEGs and the yolk sac area (YSA) of the eleutheroembryos.

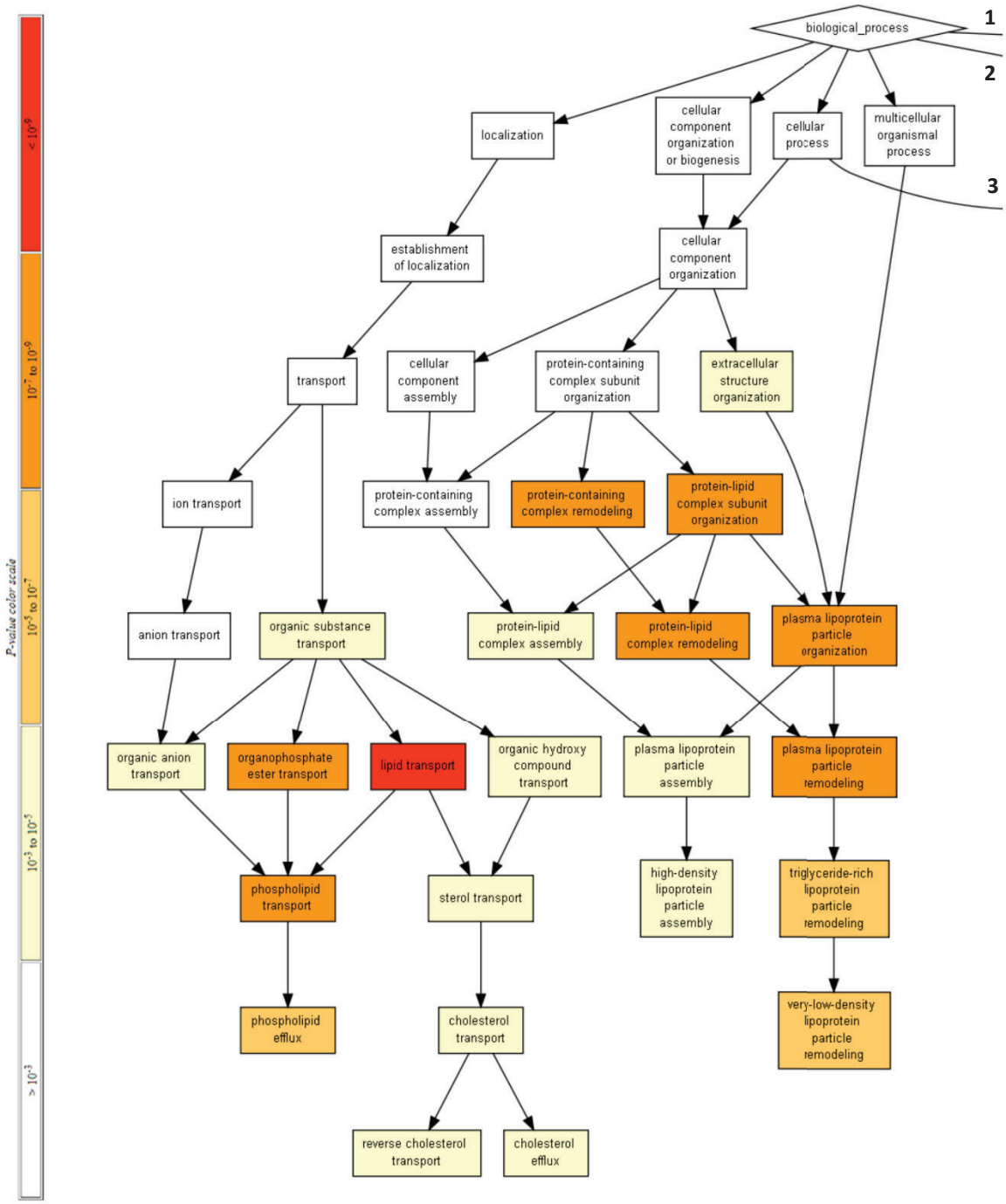

Supplementary figure SF4 (part I). Gene ontology enrichment analysis (performed by Gorilla -Gene Ontology enRIchment anaLysis and visuaLizAtion tool-; http://cbl-gorilla.cs.technion.ac.il/; (Eden et al., 2009)) using the bibliographic transcriptomic dataset of zebrafish eleutheroembryos exposed to BPA (Martínez et al., 2018). To perform the GO enrichment analysis, the list of the lipid related DEGs (differentially expressed genes) were used as a target list using the complete list of detected genes as the background list. Each square represents a different biological process.

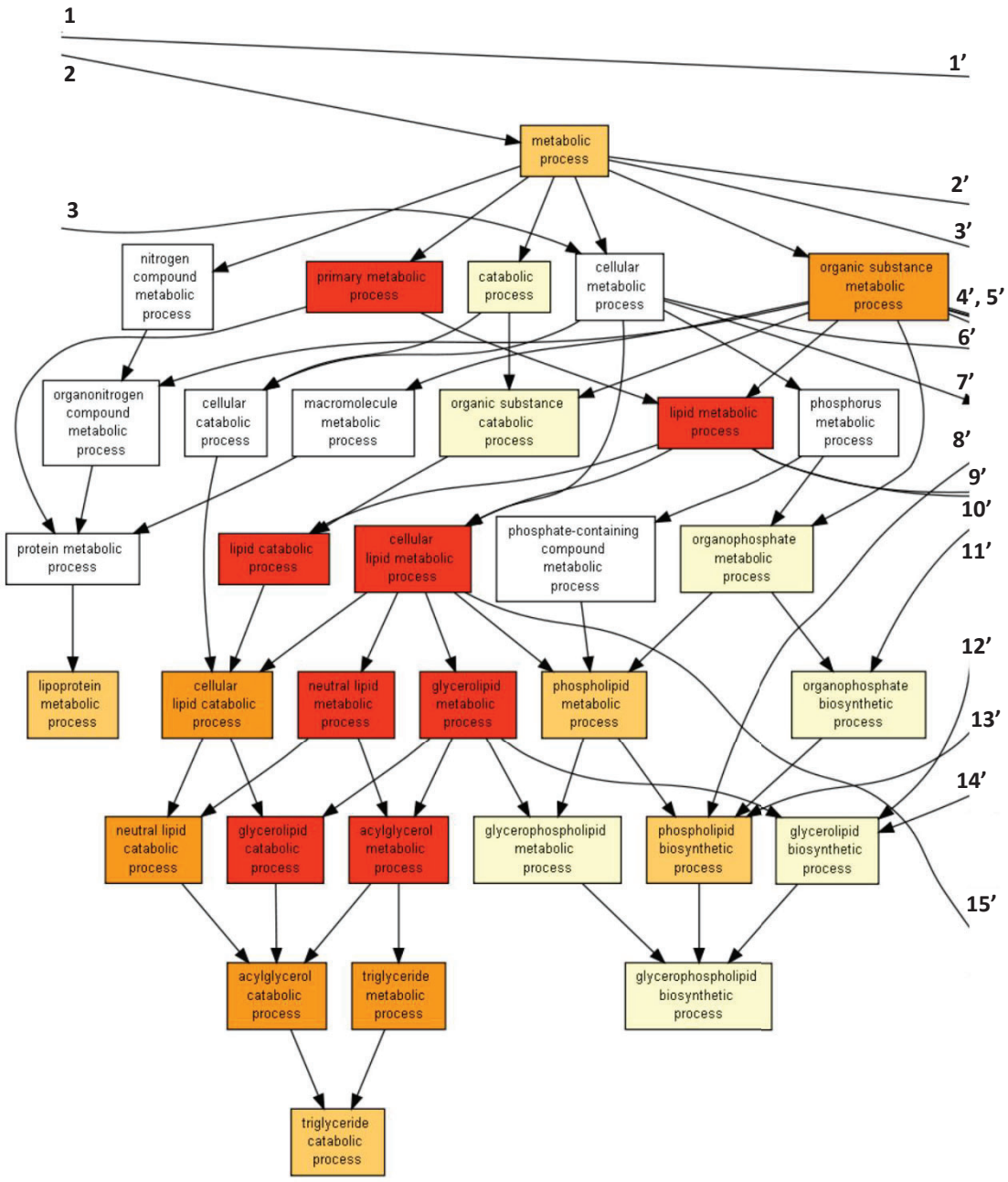

Supplementary figure SF4 (part II). Gene ontology enrichment analysis (performed by Gorilla -Gene Ontology enRIchment anaLysis and visuaLizAtion tool-; http://cbl-gorilla.cs.technion.ac.il/; (Eden et al., 2009)) using the bibliographic transcriptomic dataset of zebrafish eleutheroembryos exposed to BPA (Martínez et al., 2018). To perform the GO enrichment analysis, the list of the lipid related DEGs (differentially expressed genes) were used as a target list using the complete list of detected genes as the background list. Each square represents a different biological process.

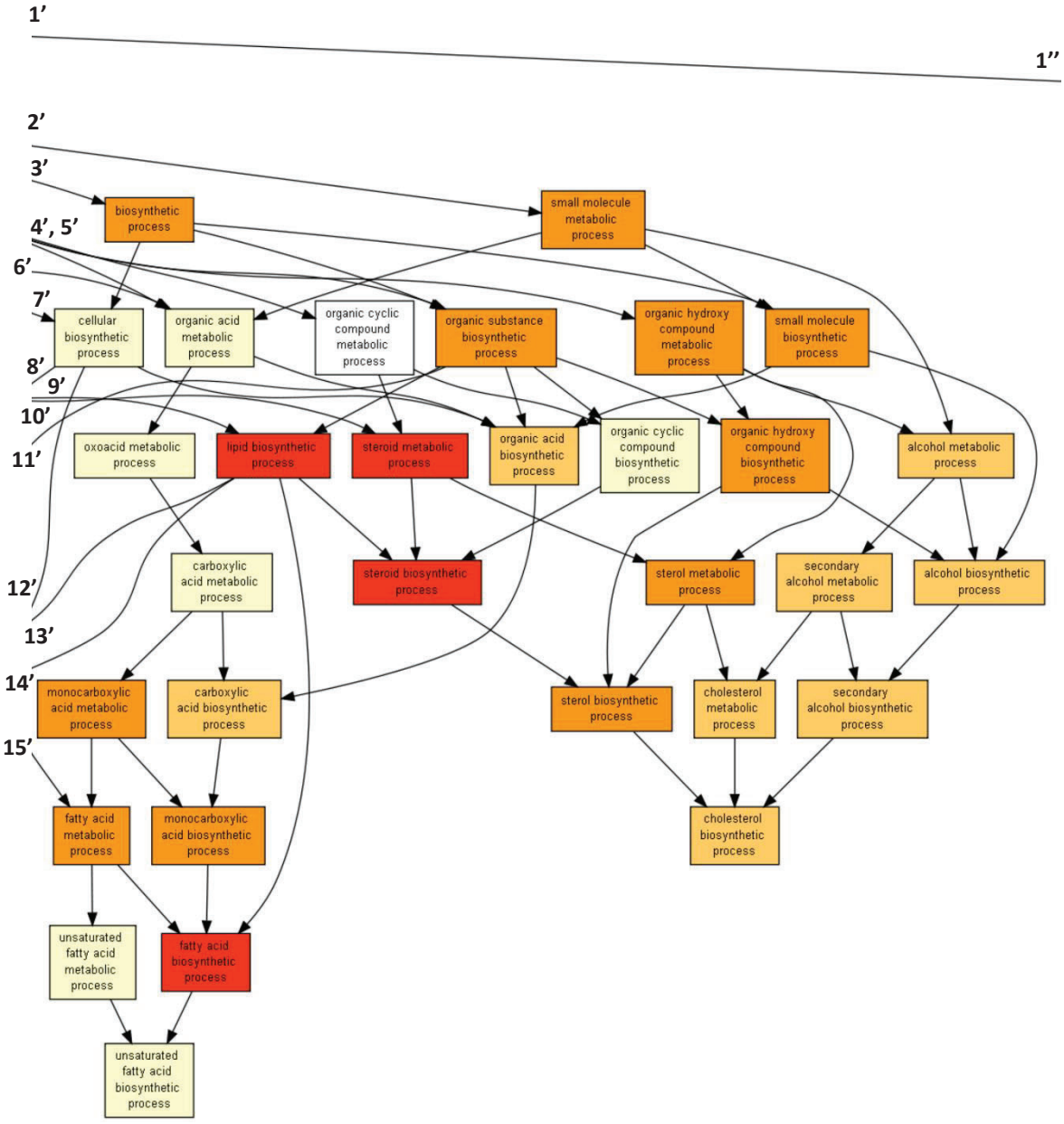

Supplementary figure SF4 (part III). Gene ontology enrichment analysis (performed by Gorilla -Gene Ontology enRIchment anaLysis and visuaLizAtion tool-; http://cbl-gorilla.cs.technion.ac.il/; (Eden et al., 2009)) using the bibliographic transcriptomic dataset of zebrafish eleutheroembryos exposed to BPA (Martínez et al., 2018). To perform the GO enrichment analysis, the list of the lipid related DEGs (differentially expressed genes) were used as a target list using the complete list of detected genes as the background list. Each square represents a different biological process.

Supplementary figure SF4 (part IV). Gene ontology enrichment analysis (performed by Gorilla -Gene Ontology enRIchment anaLysis and visuaLizAtion tool-; http://cbl-gorilla.cs.technion.ac.il/; (Eden et al., 2009)) using the bibliographic transcriptomic dataset of zebrafish eleutheroembryos exposed to BPA (Martínez et al., 2018). To perform the GO enrichment analysis, the list of the lipid related DEGs (differentially expressed genes) were used as a target list using the complete list of detected genes as the background list. Each square represents a different biological process.

Supplemental table ST1. Survival, hatching and swim bladder inflation rates (%). Mean values ± SD (standard deviation) of each group are shown (n=6). Mann-Whitney-Wilcoxon tests against each control group (one per day) were performed. Significant differences are marked with asterisks (* for p<0.05; ** for p<0.01; * for p<0.001; n/a: not applicable).**

			Survival							
			3 dpf		4 dpf		5 dpf		6 dpf	
Stock solution (mM)	Experimental solution (µM)	Experimental solution (mg/L)	% (Mean ± SD)	St. sign.	% (Mean ± SD)	St. sign.	% (Mean ± SD)	St. sign.	% (Mean ± SD)	St. sign.
(DMSO)	**0 (Control)**	**0 (Control)**	100.0 ± 0.0	n/a	100.0 ± 0.0	n/a	100.0 ± 0.0	n/a	100.0 ± 0.0	n/a
8.76	**17.5**	**4.0**	100.0 ± 0.0		98.8 ± 5.0		99.1 ± 3.0		100.0 ± 0.0	
13.14	**26.3**	**6.0**	99.4 ± 2.5		100.0 ± 0.0		100.0 ± 0.0		96.8 ± 4.9	
17.52	**35.0**	**8.0**	99.4 ± 2.5		100.0 ± 0.0		100.0 ± 0.0		88.0 ± 10.2	
			Hatching							
			3 dpf		4 dpf		5 dpf		6 dpf	
Stock solution (mM)	Experimental solution (µM)	Experimental solution (mg/L)	% (Mean ± SD)	St. sign.	% (Mean ± SD)	St. sign.	% (Mean ± SD)	St. sign.	% (Mean ± SD)	St. sign.
(DMSO)	**0 (Control)**	**0 (Control)**	86.4 ± 10.2	n/a	100.0 ± 0.0	n/a	100.0 ± 0.0	n/a	100.0 ± 0.0	n/a
8.76	**17.5**	**4.0**	94.4 ± 7.3		98.8 ± 5.0		100.0 ± 0.0		100.0 ± 0.0	
13.14	**26.3**	**6.0**	89.0 ± 10.1		99.4 ± 2.5		100.0 ± 0.0		100.0 ± 0.0	
17.52	**35.0**	**8.0**	67.5 ± 21.1		96.3 ± 6.2		100.0 ± 0.0		100.0 ± 0.0	
			Swim bladder inflation							
			3 dpf		4 dpf		5 dpf		6 dpf	
Stock solution (mM)	Experimental solution (µM)	Experimental solution (mg/L)	% (Mean ± SD)	St. sign.	% (Mean ± SD)	St. sign.	% (Mean ± SD)	St. sign.	% (Mean ± SD)	St. sign.
(DMSO)	**0 (Control)**	**0 (Control)**	-	n/a	74.6 ± 13.4	n/a	99.1 ± 3.0	n/a	98.3 ± 4.1	n/a
8.76	**17.5**	**4.0**	-		30.6 ± 18.5		98.2 ± 4.0		98.3 ± 4.1	
13.14	**26.3**	**6.0**	-		3.1 ± 4.7	***	68.7 ± 23.0		70.9 ± 21.4	
17.52	**35.0**	**8.0**	-		0.0 ± 0.0	***	6.6 ± 8.5	***	6.7 ± 8.2	**

Supplemental table ST2. Used internal standards, used ionization mode for measurements of each family, their elemental composition, measured and calculated mass (m/z), retention time (RT) in minutes, error (in ppm) between the measured and calculated mass, DBE (double bond equivalents) and total pmol added of each internal standard to each sample.

Lipid family	Internal Standard	Ionization	Elemental composition	Measured mass (m/z)	Calculated mass (m/z)	RT (minutes)	Error (ppm)	DBE	pmol added
CE	CE 17:0	$[M+NH_4]^+$	C44H82NO2	656.6368	656.6346	17.59	3.4	4.5	188.0
TAG	TAG C51:0 (1,2,3-17:0)	$[M+NH_4]^+$	C54H108NO6	866.8158	866.8177	18.13	-2.2	1.5	200.0
DAG	DAG 1,3-17:0 D5	$[M+NH_4]^+$	C37NO51H71D5	619.6021	619.6037	11.23	-2.6	0.5	166.0
PE	PE 16:0 D31-18:1	$[M-H]^-$	C39NO8P1H44D31	747.7159	747.7176	8.89	-2.3	3.5	133.0
LPE	LPE 17:1	$[M-H]^-$	C22H43NO7P	464.2781	464.2777	2.46	0.9	2.5	200.0
PG	PG 16:0 D31-18:1	$[M-H]^-$	C40O10P1H45D31	778.7120	778.7122	7.51	-0.3	3.5	125.0
PI	as PG	$[M-H]^-$	-	-	-	-	-	-	-
PS	PS 16:0 D31-18:1	$[M-H]^-$	C40NO10P1H44D31	791.7046	791.7074	8.23	-3.5	4.5	123.0
PC	PC 16:0 D31-18:1	$[M+H]^+$	C42NO8P1H52D31	791.7832	791.7802	8.90	3.8	2.5	126.0
LPC	LPC 17:0	$[M+H]^+$	C25H53NO7P	510.3549	510.3560	2.95	-2.2	0.5	120.0
SM	as PC	$[M+H]^+$	-	-	-	-	-	-	-

Supplemental table ST3. Relevant information about UHPLC-TOF characteristics, specifications and other chromatographic

System	Specifications
UHPLC system	Acquity UHPLC system (Waters Corp., Milford, MA, USA)
Chromatographic column	Acquity UPLC BEH C8 column (1.7mm particle size, 10x2.1 mm; Waters Ireland, Dublin, Ireland)
Ionization	Electro spray ionization (ESI) in positive and negative mode
Detector	Waters/LCT Premier XE time-of-flight (TOF) analyzer
Column temperature	30 °c
Flow rate	0.3 ml/min
Mobile phases	A) Methanol with 2 mM of ammonium formiate and 0.2% of formic acid B) Water with 2 of mM ammonium formiate and 0.2% of formic acid
Gradient	1) 80% of A --> 90% of A (in 3 min) 2) 90% of A (3 min) 3) 90% of A --> 99% of A (in 9 min) 4) 99% of A (3 min)

Supplemental table ST4. All the identified lipids in the study and its elemental composition, ionization mode where they were measured, calculated and measured mass (m/z), retention time (RT), error (ppm), double-bond equivalent (DBE) and mean amount (in pmol/larvae). Observed lipid families by UHPLC were: CE (cholesterol esters), TAGs (triacylglycerols a.k.a. triglycerides), DAGs (diacylglycerols a.k.a. diglycerides), PE (phosphatidylethanolamines), LPE (lysophosphatidylethanolamines), PE-O (ether phosphatidylethanolamines), PE-P (phosphatidylethanolamine plasmalogens), PG (phosphatidylglycerols), PI (phosphatidylinositols), PS (phosphatidylserines), PC (phosphatidylcholines), PC-O (ether phosphatidylcholines), PC-P (phosphatidylcholine plasmalogens) and SM (sphingomyelins). Each individual specie is annotated as <total fatty acyl chain length> : <total number of unsaturated bonds>.

Lipid family	Ionization	Lipid specie	Elemental composition	Calculated mass (m/z)	Measured mass (m/z)	RT (minutes)	Error (ppm)	DBE	Mean lipid amount (pmol/larvae)
CE	$[M+NH_4]^+$	16:0	C43H80NO2	642.6189	642.6196	17.15	1.1	4.5	19.6
		16:1	C43H78NO2	640.6033	640.6009	16.40	-3.7	5.5	5.2
		17:1	C44H80NO2	654.6189	654.6201	16.81	1.8	5.5	2.8
		18:0	C45H84NO2	670.6502	670.6519	18.25	2.5	4.5	11.0
		18:1	C45H82NO2	668.6346	668.6365	17.28	2.8	5.5	68.6
		18:2	C45H80NO2	666.6189	666.6215	16.59	3.9	6.5	46.1
		18:3	C45H78NO2	664.6033	664.6018	16.03	-2.3	7.5	6.9
		18:4	C45H76NO2	662.5876	662.5844	15.43	-4.8	8.5	0.6
		20:1	C47H86NO2	696.6659	696.6679	18.25	2.9	5.5	11.0
		20:2	C47H84NO2	694.6502	694.6495	17.47	-1.0	6.5	24.8
		20:3	C47H82NO2	692.6346	692.6343	16.81	-0.4	7.5	41.5
		20:4	C47H80NO2	690.6189	690.6176	16.27	-1.9	8.5	30.8
		20:5	C47H78NO2	688.6033	688.6057	15.71	3.5	9.5	49.1
		22:3	C49H86NO2	720.6659	720.6669	17.68	1.4	7.5	2.6
		22:4	C49H84NO2	718.6502	718.6528	17.03	3.6	8.5	7.9
		22:5	C49H82NO2	716.6346	716.6343	16.50	-0.4	9.5	30.0
		22:6	C49H80NO2	714.6189	714.6185	15.96	-0.6	10.5	149.2
		22:7	C49H78NO2	712.6033	712.6047	15.40	2.0	11.5	1.0
		24:5	C51H86NO2	744.6659	744.6680	17.28	2.8	9.5	3.4
		24:6	C51H84NO2	742.6502	742.6506	16.65	0.5	10.5	6.0
TAG	$[M+NH_4]^+$	44:0	C47H94NO6	768.7081	768.7076	15.57	-0.7	1.5	3.4
		44:1	C47H92NO6	766.6925	766.6922	15.02	-0.4	2.5	1.7
		44:2	C47H90NO6	764.6768	764.6741	14.52	-3.5	3.5	0.6
		46:0	C49H98NO6	796.7394	796.7422	16.21	3.5	1.5	9.8
		46:1	C49H96NO6	794.7238	794.7249	15.77	1.4	2.5	7.9
		46:2	C49H94NO6	792.7081	792.7044	15.33	-4.7	3.5	3.1
		46:3	C49H92NO6	790.6925	790.6917	14.86	-1.0	4.5	0.4
		48:0	C51H102NO6	824.7707	824.7742	16.90	4.2	1.5	24.0
		48:1	C51H100NO6	822.7551	822.7587	16.39	4.4	2.5	26.7
		48:2	C51H98NO6	820.7394	820.7413	15.87	2.3	3.5	18.9
		48:3	C51H96NO6	818.7238	818.7274	15.33	4.4	4.5	4.3
		49:1	C52H102NO6	836.7707	836.7717	16.71	1.2	2.5	14.7
		50:0	C53H106NO6	852.8020	852.8041	17.68	2.5	1.5	24.9
		50:1	C53H104NO6	850.7864	850.7895	17.06	3.6	2.5	62.7
		50:2	C53H102NO6	848.7707	848.7740	16.56	3.9	3.5	65.7
		50:3	C53H100NO6	846.7551	846.7592	16.06	4.8	4.5	31.3
		50:4	C53H98NO6	844.7394	844.7405	15.55	1.3	5.5	11.9
		50:5	C53H96NO6	842.7238	842.7250	15.11	1.4	6.5	1.3
		50:6	C53H94NO6	840.7081	840.7075	14.69	-0.7	7.5	0.6
		51:1	C54H106NO6	864.8020	864.8043	17.44	2.7	2.5	17.2
		51:2	C54H104NO6	862.7864	862.7897	16.90	3.8	3.5	19.7
		51:3	C54H102NO6	860.7707	860.7733	16.40	3.0	4.5	11.5
		51:4	C54H100NO6	858.7551	858.7576	15.90	2.9	5.5	4.3
		51:5	C54H98NO6	856.7394	856.7421	15.65	3.2	6.5	1.6
		51:6	C54H96NO6	854.7238	854.7263	15.27	2.9	7.5	0.3
		52:0	C55H110NO6	880.8333	880.8364	18.62	3.5	1.5	10.9
		52:1	C55H108NO6	878.8177	878.8219	17.84	4.8	2.5	53.4
		52:2	C55H106NO6	876.8020	876.8063	17.28	4.9	3.5	93.8
		52:3	C55H104NO6	874.7864	874.7897	16.71	3.8	4.5	102.9

Lipid family	Ionization	Lipid specie	Elemental composition	Calculated mass (m/z)	Measured mass (m/z)	RT (minutes)	Error (ppm)	DBE	Mean lipid amount (pmol/larvae)
TAG	$[M+NH_4]^+$	52:4	C55H102NO6	872.7707	872.7745	16.24	4.4	5.5	57.1
		52:5	C55H100NO6	870.7551	870.7585	15.77	3.9	6.5	38.7
		52:6	C55H98NO6	868.7394	868.7430	15.27	4.1	7.5	14.4
		53:0	C56H112NO6	894.8490	894.8483	19.19	-0.8	1.5	1.5
		53:1	C56H110NO6	892.8333	892.8349	18.28	1.8	2.5	7.0
		53:2	C56H108NO6	890.8177	890.8199	17.62	2.5	3.5	15.4
		53:3	C56H106NO6	888.8020	888.8044	17.06	2.7	4.5	13.9
		53:4	C56H104NO6	886.7864	886.7897	16.59	3.7	5.5	9.4
		53:5	C56H102NO6	884.7707	884.7731	16.23	2.7	6.5	7.3
		53:6	C56H100NO6	882.7551	882.7596	15.96	5.1	7.5	8.2
		53:7	C56H98NO6	880.7394	880.7422	15.46	3.2	8.5	1.8
		54:0	C57H114NO6	908.8646	908.8729	19.19	9.1	1.5	0.6
		54:1	C57H112NO6	906.8490	906.8497	18.75	0.8	2.5	21.9
		54:2	C57H110NO6	904.8333	904.8369	18.06	4.0	3.5	41.8
		54:3	C57H108NO6	902.8177	902.8138	17.44	-4.3	4.5	78.3
		54:4	C57H106NO6	900.8020	900.8049	17.03	3.2	5.5	83.6
		54:5	C57H104NO6	898.7864	898.7903	16.62	4.3	6.5	52.2
		54:6	C57H102NO6	896.7707	896.7744	16.27	4.1	7.5	50.8
		54:7	C57H100NO6	894.7551	894.7548	15.80	-0.3	8.5	36.0
		54:8	C57H98NO6	892.7394	892.7428	15.30	3.8	9.5	8.7
		54:9	C57H96NO6	890.7238	890.7278	14.77	4.5	10.5	1.3
		56:1	C59H116NO6	934.8803	934.8813	19.41	1.1	2.5	0.4
		56:2	C59H114NO6	932.8646	932.8676	18.94	3.2	3.5	9.7
		56:3	C59H112NO6	930.8490	930.8519	18.22	3.1	4.5	19.8
		56:4	C59H110NO6	928.8333	928.8346	17.79	1.4	5.5	31.0
		56:5	C59H108NO6	926.8177	926.8220	17.15	4.6	6.5	52.4
		56:6	C59H106NO6	924.8020	924.8066	16.68	5.0	7.5	84.8
		56:7	C59H104NO6	922.7864	922.7908	16.21	4.8	8.5	20.9
		58:3	C61H116NO6	958.8803	958.8784	19.19	-2.0	4.5	3.5
		58:4	C61H114NO6	956.8646	956.8686	18.56	4.2	5.5	4.0
		58:5	C61H114NO6	956.8646	956.8690	18.12	4.6	5.5	3.0
DAG	$[M+NH_4]^+$	32:0	C35H72NO5	586.5411	586.5404	9.97	-1.2	0.5	3.0
		32:1	C35H70NO5	584.5254	584.5271	9.16	2.9	1.5	1.0
		34:0	C37H76NO5	614.5724	614.5732	11.31	1.3	0.5	2.4
		34:1	C37H74NO5	612.5567	612.5557	10.44	-1.6	1.5	7.5
		34:2	C37H72NO5	610.5411	610.5431	9.60	3.3	2.5	2.8
		34:3	C37H70NO5	608.5254	608.5262	8.75	1.3	3.5	0.7
		36:0	C39H80NO5	642.6037	642.6047	12.48	1.6	0.5	0.6
		36:1	C39H78NO5	640.5880	640.5879	11.70	-0.2	1.5	2.1
		36:2	C39H76NO5	638.5724	638.5720	10.79	-0.6	2.5	4.1
		36:3	C39H74NO5	636.5567	636.5571	9.94	0.6	3.5	3.4
		36:4	C39H72NO5	634.5411	634.5397	9.60	-2.2	4.5	1.2
		36:5	C39H70NO5	632.5254	632.5273	8.72	3.0	5.5	1.7
		38:3	C41H78NO5	664.5880	664.5856	11.32	-3.6	3.5	1.1
		38:4	C41H76NO5	662.5724	662.5708	10.82	-2.4	4.5	7.4
		38:5	C41H74NO5	660.5567	660.5585	10.05	2.7	5.5	4.1
		38:6	C41H72NO5	658.5411	658.5397	9.35	-2.1	6.5	7.5
		40:6	C43H76NO5	686.5724	686.5725	10.62	0.1	6.5	4.5
PE	$[M-H]^-$	32:0	C37H73NO8P	690.5074	690.5049	4.97	-3.6	2.5	43.1
		32:1	C37H71NO8P	688.4917	688.4974	4.97	8.3	3.5	386.7
		34:1	C39H75NO8P	716.5230	716.5231	9.02	0.1	3.5	20.5
		34:2	C39H73NO8P	714.5074	714.5079	8.08	0.7	4.5	5.6
		35:1	C40H77NO8P	730.5387	730.5385	9.70	-0.3	3.5	2.5
		36:1	C41H79NO8P	744.5543	744.5545	10.33	0.3	3.5	19.5
		36:2	C41H77NO8P	742.5387	742.5366	9.49	-2.8	4.5	13.5
		36:3	C41H75NO8P	740.5230	740.5266	8.52	4.9	5.5	6.6
		36:4	C41H73NO8P	738.5074	738.5071	8.14	-0.4	6.5	15.5
		36:5	C41H71NO8P	736.4917	736.4896	7.29	-2.9	7.5	16.3
		38:1	C43H83NO8P	772.5856	772.5853	11.46	-0.4	3.5	2.9
		38:2	C43H81NO8P	770.5700	770.5703	10.58	0.4	4.5	3.8
		38:3	C43H79NO8P	768.5543	768.5521	9.93	-2.9	5.5	8.7
		38:4	C43H77NO8P	766.5387	766.5375	9.55	-1.6	6.5	53.6

Lipid family	Ionization	Lipid specie	Elemental composition	Calculated mass (m/z)	Measured mass (m/z)	RT (minutes)	Error (ppm)	DBE	Mean lipid amount (pmol/larvae)
PE	$[M-H]^-$	38:4	C43H77NO8P	766.5387	766.5375	9.55	-1.6	6.5	53.6
		38:5	C43H75NO8P	764.5230	764.5216	8.64	-1.8	7.5	41.8
		38:6	C43H73NO8P	762.5074	762.5077	7.95	0.4	8.5	201.4
		38:7	C43H71NO8P	760.4917	760.4951	6.73	4.5	9.5	3.8
		40:4	C45H81NO8P	794.5700	794.5687	10.43	-1.6	6.5	7.0
		40:5	C45H79NO8P	792.5543	792.5521	9.88	-2.8	7.5	26.7
		40:6	C45H77NO8P	790.5387	790.5422	9.33	4.4	8.5	309.7
		40:7	C45H75NO8P	788.5230	788.5202	8.36	-3.6	9.5	70.3
LPE	$[M-H]^-$	16:0	C21H43NO7P	452.2777	452.2811	2.62	7.5	1.5	0.9
		18:0	C23H47NO7P	480.3090	480.3081	3.28	-1.9	1.5	2.7
		18:1	C23H45NO7P	478.2934	478.2922	2.81	-2.5	2.5	0.5
		22:6	C27H43NO7P	524.2777	524.2758	2.34	-3.6	7.5	2.0
PE-O	$[M-H]^-$	34:2	C39H75NO7P	700.5281	700.5251	9.93	-4.3	3.5	2.1
		36:2	C41H79NO7P	728.5594	728.5616	11.05	3.0	3.5	12.8
		36:5	C41H73NO7P	722.5125	722.5095	9.02	-4.2	6.5	1.2
		36:6	C41H71NO7P	720.4968	720.4946	8.20	-3.1	7.5	0.3
		38:5	C43H77NO7P	750.5438	750.5423	9.99	-2.0	6.5	2.1
		40:6	C45H79NO7P	776.5594	776.5571	10.68	-3.0	7.5	1.7
		40:7	C45H77NO7P	774.5438	774.5425	10.14	-1.7	8.5	1.2
PE-P	$[M-H]^-$	38:5	C43H75NO7P	748.5281	748.5262	9.61	-2.5	7.5	1.3
		38:6	C43H73NO7P	746.5125	746.5134	8.83	1.2	8.5	18.0
PG	$[M-H]^-$	34:1	C40H76O10P	747.5176	747.5139	8.83	-4.9	3.5	21.8
		36:1	C42H80O10P	775.5489	775.5461	10.14	-3.6	3.5	15.5
		36:2	C42H78O10P	773.5333	773.5291	9.14	-5.4	4.5	5.1
PI	$[M-H]^-$	34:1	C43H80O13P	835.5337	835.5333	7.45	-0.5	4.5	4.8
		34:2	C43H78O13P	833.5180	833.5211	6.57	3.7	5.5	3.5
		36:1	C45H84O13P	863.5650	863.5647	8.86	-0.3	4.5	2.2
		36:2	C45H82O13P	861.5493	861.5465	7.98	-3.2	5.5	5.2
		36:3	C45H80O13P	859.5337	859.5347	6.98	1.2	6.5	10.1
		36:4	C45H78O13P	857.5180	857.5185	6.67	0.6	7.5	18.8
		36:5	C45H76O13P	855.5024	855.5026	6.01	0.2	8.5	6.6
		38:3	C47H84O13P	887.5650	887.5626	8.45	-2.7	6.5	11.3
		38:4	C47H82O13P	885.5493	885.5508	7.75	1.7	7.5	88.7
		38:5	C47H80O13P	883.5337	883.5362	7.12	2.8	8.5	73.2
		38:6	C47H78O13P	881.5180	881.5166	6.42	-1.6	9.5	33.0
		40:5	C49H84O13P	911.5650	911.5614	8.23	-3.9	8.5	3.6
		40:6	C49H82O13P	909.5493	909.5500	7.83	0.8	9.5	27.9
		40:7	C49H80O13P	907.5337	907.5358	6.86	2.3	10.5	23.1
		40:8	C49H78O13P	905.5180	905.5154	6.07	-2.9	11.5	2.9
PS	$[M-H]^-$	32:1	C38H71NO10P	732.4816	732.4874	8.14	7.9	4.5	1.1
		34:0	C40H77NO10P	762.5285	762.5305	11.21	2.6	3.5	44.5
		36:1	C42H79NO10P	788.5442	788.5431	9.77	-1.4	4.5	16.9
		36:2	C42H77NO10P	786.5285	786.5305	8.86	2.5	5.5	2.2
		38:0	C44H85NO10P	818.5911	818.5922	9.70	1.3	3.5	44.8
		38:1	C44H83NO10P	816.5755	816.5726	8.83	-3.6	4.5	13.3
		38:4	C44H77NO10P	810.5285	810.5286	8.92	0.1	7.5	5.7
		38:5	C44H75NO10P	808.5129	808.5095	8.14	-4.2	8.5	6.4
		40:0	C46H89NO10P	846.6224	846.6196	10.91	-3.3	3.5	5.2
		40:5	C46H79NO10P	836.5442	836.5448	9.30	0.7	8.5	15.4
		40:6	C46H77NO10P	834.5285	834.5315	8.73	3.6	9.5	155.2
		42:5	C48H83NO10P	864.5755	864.5748	8.67	-0.8	8.5	30.7
		42:6	C48H81NO10P	862.5598	862.5588	7.76	-1.2	9.5	14.7
PC	$[M+H]^+$	28:0	C36H73NO8P	678.5074	678.5052	6.02	-3.2	1.5	0.7
		29:0	C37H75NO8P	692.5230	692.5235	8.59	0.7	1.5	1.2
		30:0	C38H77NO8P	706.5387	706.5400	7.18	1.8	1.5	22.4
		30:1	C38H75NO8P	704.5230	704.5216	6.51	-2.0	2.5	4.9
		31:0	C39H79NO8P	720.5543	720.5571	7.91	3.9	1.5	21.5
		31:1	C39H77NO8P	718.5387	718.5413	7.12	3.6	2.5	6.3

Lipid family	Ionization	Lipid specie	Elemental composition	Calculated mass (m/z)	Measured mass (m/z)	RT (minutes)	Error (ppm)	DBE	Mean lipid amount (pmol/larvae)
PC	$[M+H]^+$	32:0	C40H81NO8P	734.5700	734.5721	8.59	2.9	1.5	183.2
		32:1	C40H79NO8P	732.5543	732.5530	7.72	-1.8	2.5	94.1
		32:2	C40H77NO8P	730.5387	730.5397	7.01	1.4	3.5	17.8
		32:3	C40H75NO8P	728.5230	728.5272	6.24	5.8	4.5	1.9
		33:0	C41H83NO8P	748.5856	748.5853	9.28	-0.4	1.5	20.1
		33:1	C41H81NO8P	746.5700	746.5712	8.34	1.6	2.5	47.4
		33:2	C41H79NO8P	744.5543	744.5561	7.65	2.4	3.5	13.7
		33:3	C41H77NO8P	742.5387	742.5359	6.65	-3.8	4.5	1.8
		34:0	C42H85NO8P	762.6013	762.5994	9.94	-2.5	1.5	46.3
		34:1	C42H83NO8P	760.5856	760.5866	9.06	1.3	2.5	669.5
		34:2	C42H81NO8P	758.5700	758.5726	8.09	3.4	3.5	223.8
		34:3	C42H79NO8P	756.5543	756.5546	7.18	0.4	4.5	46.8
		34:4	C42H77NO8P	754.5387	754.5405	6.56	2.4	5.5	10.4
		34:5	C42H75NO8P	752.5230	752.5229	6.02	-0.1	6.5	3.0
		35:0	C43H87NO8P	776.6169	776.6164	10.57	-0.6	1.5	3.4
		35:1	C43H85NO8P	774.6013	774.6027	9.60	1.8	2.5	56.3
		35:2	C43H83NO8P	772.5856	772.5844	8.80	-1.6	3.5	31.5
		35:3	C43H81NO8P	770.5700	770.5709	7.88	1.2	4.5	6.8
		35:4	C43H79NO8P	768.5543	768.5571	7.44	3.6	5.5	4.1
		35:5	C43H77NO8P	766.5387	766.5391	6.62	0.5	6.5	5.1
		36:0	C44H89NO8P	790.6326	790.6343	11.19	2.2	1.5	10.2
		36:1	C44H87NO8P	788.6169	788.6190	10.38	2.7	2.5	208.5
		36:2	C44H85NO8P	786.6013	786.6030	9.47	2.2	3.5	240.5
		36:3	C44H83NO8P	784.5856	784.5884	8.53	3.6	4.5	156.1
		36:4	C44H81NO8P	782.5700	782.5732	7.88	4.1	5.5	134.7
		36:5	C44H79NO8P	780.5543	780.5544	7.31	0.1	6.5	150.2
		36:6	C44H77NO8P	778.5387	778.5414	6.51	3.5	7.5	26.7
		37:4	C45H83NO8P	796.5856	796.5880	8.78	3.0	5.5	9.3
		37:5	C45H81NO8P	794.5700	794.5707	7.96	0.9	6.5	17.1
		37:6	C45H79NO8P	792.5543	792.5566	7.25,	2.9	7.5	22.7
		38:0	C46H93NO8P	818.6639	818.6675	12.35	4.4	1.5	1.7
		38:1	C46H91NO8P	816.6482	816.6487	11.41	0.6	2.5	22.4
		38:2	C46H89NO8P	814.6326	814.6339	10.63	1.6	3.5	40.0
		38:3	C46H87NO8P	812.6169	812.6193	9.85	3.0	4.5	63.7
		38:4	C46H85NO8P	810.6013	810.6039	9.34	3.2	5.5	106.7
		38:5	C46H83NO8P	808.5856	808.5895	8.35	4.8	6.5	50.9
		38:6	C46H81NO8P	806.5700	806.5728	7.94	3.5	7.5	510.9
		38:7	C46H79NO8P	804.5543	804.5550	6.82	0.9	8.5	75.6
		38:8	C46H77NO8P	802.5387	802.5410	6.02	2.9	9.5	6.9
		39:6	C47H83NO8P	820.5856	820.5888	8.58	3.9	7.5	51.6
		39:7	C47H81NO8P	818.5700	818.5703	7.75	0.4	8.5	16.8
		40:1	C48H95NO8P	844.6795	844.6830	12.48	4.1	2.5	3.8
		40:2	C48H93NO8P	842.6639	842.6632	11.70	-0.8	3.5	4.0
		40:3	C48H91NO8P	840.6482	840.6486	10.85	0.5	4.5	3.6
		40:4	C48H89NO8P	838.6326	838.6345	10.44	2.3	5.5	11.9
		40:5	C48H87NO8P	836.6169	836.6195	10.15	3.1	6.5	50.1
		40:6	C48H85NO8P	834.6013	834.6032	9.35	2.3	7.5	250.3
		40:7	C48H83NO8P	832.5856	832.5892	8.34	4.3	8.5	221.2
		40:8	C48H81NO8P	830.5700	830.5723	7.38	2.8	9.5	68.1
		42:6	C50H89NO8P	862.6326	862.6287	10.13	-4.5	7.5	10.3

Lipid family	Ionization	Lipid specie	Elemental composition	Calculated mass (m/z)	Measured mass (m/z)	RT (minutes)	Error (ppm)	DBE	Mean lipid amount (pmol/larvae)
LPC	$[M+H]^+$	14:1	C22H45NO7P	466.2934	466.2915	2.50	-4.1	1.5	15.9
		15:0	C23H49NO7P	482.3247	482.3260	3.26	2.7	0.5	1.0
		16:0	C24H51NO7P	496.3403	496.3398	2.57	-1.0	0.5	13.6
		18:0	C26H55NO7P	524.3716	524.3703	3.26	-2.5	0.5	7.5
		18:1	C26H53NO7P	522.3560	522.3541	2.73	-3.6	1.5	7.9
		18:2	C26H51NO7P	520.3403	520.3414	2.38	2.1	2.5	2.6
		20:0	C28H59NO7P	552.4029	552.4028	3.95	-0.2	0.5	0.5
		20:1	C28H57NO7P	550.3873	550.3854	3.31	-3.5	1.5	1.1
		20:3	C28H53NO7P	546.3560	546.3541	2.54	-3.5	3.5	0.6
		20:4	C28H51NO7P	544.3403	544.3348	2.32	-10.1	4.5	0.9
		20:5	C28H49NO7P	542.3247	542.3240	2.07	-1.3	5.5	1.3
		22:6	C30H51NO7P	568.3403	568.3395	2.32	-1.4	6.5	10.8
		24:0	C32H67NO7P	608.4655	608.4637	5.52	-3.0	0.5	0.4
PC-O	$[M+H]^+$	16:0	C24H53NO6P	482.3611	482.3617	3.05	1.2	-0.5	0.6
		18:0	C26H57NO6P	510.3924	510.3894	3.70	-5.9	-0.5	0.3
		30:0	C38H79NO7P	692.5594	692.5587	8.12	-1.0	0.5	0.4
		32:0	C40H83NO7P	720.5907	720.5883	9.53	-3.3	0.5	4.2
		32:1	C40H81NO7P	718.5751	718.5714	7.65	-5.1	1.5	0.5
		32:2	C40H79NO7P	716.5594	716.5576	6.56	-2.5	2.5	0.7
		34:0	C42H87NO7P	748.6220	748.6202	10.38	-2.4	0.5	1.7
		34:1	C42H85NO7P	746.6064	746.6042	9.94	-2.9	1.5	13.1
		34:2	C42H83NO7P	744.5907	744.5928	9.91	2.8	2.5	5.1
		36:1	C44H89NO7P	774.6377	774.6400	11.19	3.0	1.5	1.9
		36:2	C44H87NO7P	772.6220	772.6255	10.25	4.5	2.5	2.1
		36:3	C44H85NO7P	770.6064	770.6072	9.38	1.0	3.5	1.0
		36:4	C44H83NO7P	768.5907	768.5901	9.13	-0.8	4.5	5.1
		36:5	C44H81NO7P	766.5751	766.5784	8.28	4.3	5.5	10.2
		38:4	C46H87NO7P	796.6220	796.6227	10.00	0.9	4.5	2.7
		38:5	C46H85NO7P	794.6064	794.6082	9.22	2.3	5.5	4.2
		40:6	C48H87NO7P	820.6220	820.6217	10.22	-0.4	6.5	9.1
		40:7	C48H85NO7P	818.6064	818.6061	9.43	-0.4	7.5	15.3
PC-P	$[M+H]^+$	30:0	C38H77NO7P	690.5438	690.5394	7.56	-6.4	1.5	0.7
		36:5	C44H79NO7P	764.5594	764.5584	7.47	-1.3	6.5	3.6
		38:5	C46H83NO7P	792.5907	792.5940	8.88	4.2	6.5	34.0
		38:6	C46H81NO7P	790.5751	790.5776	8.81	3.2	7.5	8.0
SM	$[M+H]^+$	32:1	C37H76N2O6P	675.5441	675.5458	6.15	2.5	1.5	1.4
		33:1	C38H78N2O6P	689.5598	689.5616	6.68	2.6	1.5	3.3
		34:0	C39H82N2O6P	705.5911	705.5904	7.91	-1.0	0.5	12.1
		34:1	C39H80N2O6P	703.5754	703.5782	7.40	4.0	1.5	63.8
		34:2	C39H78N2O6P	701.5598	701.5731	6.82	19.0	2.5	2.7
		35:1	C40H82N2O6P	717.5911	717.5894	7.91	-2.4	1.5	5.2
		36:1	C41H84N2O6P	731.6067	731.6088	8.81	2.9	1.5	12.0
		38:1	C43H88N2O6P	759.6380	759.6409	10.16	3.8	1.5	10.9
		39:1	C44H90N2O6P	773.6537	773.6542	10.55	0.6	1.5	4.3
		40:1	C45H92N2O6P	787.6693	787.6709	11.41	2.0	1.5	23.5
		40:2	C45H90N2O6P	785.6537	785.6489	10.71	-6.1	2.5	3.2
		41:1	C46H94N2O6P	801.6850	801.6849	11.95	-0.1	1.5	7.5
		41:2	C46H92N2O6P	799.6693	799.6639	11.01	-6.8	2.5	2.2
		42:1	C47H96N2O6P	815.7006	815.7042	12.61	4.4	1.5	19.0

Supplemental table ST5. Each individual lipid classification in the PAM (partition around medoids) clustering analysis, their average fatty acid chain length, total number of unsaturations, average pmol/sample, normalized abundances and p values (one-way ANOVA followed by a Tukey's post-hoc test). Lipids are annotated as <lipid subclass> <total fatty acyl chain length> : <total number of unsaturated bonds>. Significant changes are specified by asterisks (* for p<0.05, ** for p<0.01, * for p<0.001).**

Lipid family	Lipid specie	Cluster	Average fatty acid chain length	Total number of unsaturations	Average pmol/ sample	Normalized abundances						p values						Significance
						Ctl 4dpf	Ctl 5dpf	Ctl 6dpf	6 mg/L BPA 4dpf	6 mg/L BPA 5dpf	6 mg/L BPA 6dpf	Ctl 4dpf	Ctl 5dpf	Ctl 6dpf	6 mg/L BPA 4dpf	6 mg/L BPA 5dpf	6 mg/L BPA 6dpf	
CE	CE 16:0	1	16.0	0	37.2	0.897	1.025	1.069	0.903	1.157	1.094	0.104	0.993	0.523	0.118	0.092	0.336	n.s.
	CE 16:1	1	16.0	1	13.6	0.988	0.966	1.043	0.819	1.015	0.963	0.746	0.999	0.286	0.069	0.486	0.973	n.s.
	CE 17:1	1	17.0	1	6.2	0.955	1.029	1.012	0.934	1.057	1.095	0.127	0.663	0.968	0.052	0.238	0.050	*
	CE 18:0	1	18.0	0	28.7	1.039	1.002	0.950	0.908	1.123	1.087	0.795	0.846	0.417	0.207	0.230	0.411	n.s.
	CE 18:1	1	18.0	1	180.3	1.053	0.995	0.949	0.987	1.144	1.013	0.615	0.625	0.228	0.538	0.072	0.851	n.s.
	CE 18:2	1	18.0	2	124.8	1.072	1.035	0.881	1.015	1.151	1.001	0.420	0.868	0.035	0.844	0.058	0.661	*
	CE 18:3	1	18.0	3	25.0	1.181	0.954	0.824	0.953	1.068	0.891	0.048	0.772	0.107	0.769	0.315	0.327	*
	CE 18:4	2	18.0	4	2.1	1.227	0.849	0.869	1.199	1.220	1.010	0.120	0.057	0.076	0.182	0.132	0.586	n.s.
	CE 20:1	1	20.0	1	40.2	1.183	0.946	0.829	0.897	1.040	0.956	0.071	0.770	0.174	0.440	0.520	0.846	n.s.
	CE 20:2	1	20.0	2	93.3	1.147	0.937	0.884	0.803	0.966	0.848	0.073	0.950	0.654	0.245	0.738	0.440	n.s.
	CE 20:3	1	20.0	3	136.9	1.076	0.985	0.929	0.809	0.952	0.826	0.138	0.538	0.997	0.209	0.805	0.272	n.s.
	CE 20:4	1	20.0	4	94.2	1.056	1.012	0.926	0.869	0.968	0.888	0.166	0.402	0.688	0.246	0.829	0.356	n.s.
	CE 20:5	1	20.0	5	130.9	1.058	0.907	1.024	1.093	1.103	0.942	0.498	0.068	0.960	0.210	0.162	0.174	n.s.
	CE 22:3	1	22.0	3	8.2	0.981	0.994	1.019	0.654	0.844	0.650	0.296	0.252	0.186	0.110	0.910	0.105	n.s.
	CE 22:4	1	22.0	4	23.9	1.009	0.975	1.007	0.770	0.886	0.860	0.328	0.529	0.340	0.136	0.722	0.525	n.s.
	CE 22:5	1	22.0	5	82.0	1.006	0.984	1.005	0.824	1.008	0.935	0.608	0.787	0.615	0.157	0.592	0.771	n.s.
	CE 22:6	1	22.0	6	386.7	1.029	0.987	0.983	1.000	1.076	0.971	0.763	0.770	0.720	0.912	0.342	0.603	n.s.
	CE 22:7	1	22.0	7	2.9	1.055	0.982	0.953	1.022	1.043	0.895	0.558	0.925	0.720	0.776	0.631	0.379	n.s.
	CE 24:5	1	24.0	5	9.0	0.953	0.924	1.106	0.699	0.955	0.901	0.776	0.993	0.116	0.066	0.756	0.835	n.s.
	CE 24:6	1	24.0	6	17.5	1.018	0.955	1.022	0.745	0.986	0.881	0.287	0.783	0.268	0.038	0.503	0.482	*
TAG	TAG 44:0	1	14.7	0	6.3	0.897	0.999	1.081	0.841	1.207	1.155	0.369	0.827	0.720	0.216	0.243	0.396	n.s.
	TAG 44:1	1	14.7	1	3.3	0.925	1.013	1.051	0.848	1.248	1.174	0.383	0.820	0.952	0.171	0.154	0.338	n.s.
	TAG 44:2	1	14.7	2	1.1	0.898	0.924	1.145	0.802	1.239	1.187	0.306	0.402	0.385	0.104	0.137	0.247	n.s.
	TAG 46:0	1	15.3	0	19.5	0.957	0.999	1.032	0.967	1.288	1.155	0.430	0.623	0.799	0.472	0.137	0.519	n.s.
	TAG 46:1	1	15.3	1	14.9	0.952	1.001	1.037	0.967	1.342	1.183	0.428	0.615	0.782	0.479	0.132	0.521	n.s.
	TAG 46:2	1	15.3	2	6.3	0.966	0.966	1.059	0.978	1.295	1.112	0.521	0.522	0.979	0.571	0.152	0.739	n.s.
	TAG 46:3	1	15.3	3	0.8	0.962	1.047	0.961	0.984	1.240	1.019	0.726	0.957	0.722	0.804	0.344	0.936	n.s.
	TAG 48:0	2	16.0	0	39.7	0.963	1.095	0.926	1.076	1.463	1.412	0.264	0.711	0.193	0.628	0.097	0.153	n.s.
	TAG 48:1	3	16.0	1	58.3	1.143	1.001	0.810	1.284	1.531	1.443	0.660	0.164	0.021	0.542	0.041	0.106	*
	TAG 48:2	3	16.0	2	46.6	1.219	0.894	0.834	1.392	1.577	1.230	0.884	0.162	0.104	0.323	0.084	0.842	n.s.
	TAG 48:3	3	16.0	3	10.9	1.219	0.893	0.834	1.404	1.546	1.190	0.844	0.168	0.108	0.270	0.094	0.964	n.s.
	TAG 49:1	3	16.3	1	37.7	1.151	0.975	0.834	1.106	1.398	1.235	0.833	0.402	0.122	0.950	0.123	0.478	n.s.
	TAG 50:0	2	16.7	0	67.9	1.180	1.038	0.706	1.130	1.326	1.321	0.494	0.400	0.003	0.886	0.053	0.057	**
	TAG 50:1	3	16.7	1	207.3	1.325	0.891	0.646	1.285	1.363	1.220	0.160	0.119	0.010	0.247	0.106	0.468	**
	TAG 50:2	3	16.7	2	187.6	1.356	0.861	0.614	1.495	1.660	1.279	0.486	0.124	0.023	0.197	0.062	0.739	*
	TAG 50:3	3	16.7	3	75.1	1.302	0.984	0.556	1.492	1.667	1.574	0.861	0.250	0.018	0.334	0.113	0.204	*
	TAG 50:4	3	16.7	4	36.1	1.496	0.753	0.404	1.745	1.795	1.243	0.339	0.097	0.015	0.087	0.066	0.989	*
	TAG 50:5	3	16.7	5	4.9	1.559	0.641	0.343	1.650	1.552	1.327	0.088	0.028	0.004	0.045	0.093	0.458	**
	TAG 50:6	3	16.7	6	1.9	1.456	0.813	0.395	1.842	1.628	1.211	0.400	0.159	0.018	0.052	0.165	0.961	*
	TAG 51:1	3	17.0	1	57.7	1.336	0.910	0.593	1.194	1.406	1.247	0.214	0.248	0.017	0.633	0.117	0.438	*
	TAG 51:2	3	17.0	2	62.2	1.335	0.899	0.614	1.303	1.497	1.212	0.318	0.214	0.024	0.398	0.091	0.710	*
	TAG 51:3	3	17.0	3	36.9	1.378	0.877	0.551	1.392	1.567	1.176	0.273	0.177	0.016	0.247	0.067	0.919	*
	TAG 51:4	3	17.0	4	14.1	1.439	0.838	0.441	1.502	1.624	1.148	0.254	0.182	0.016	0.172	0.078	0.939	*
	TAG 51:5	3	17.0	5	4.9	1.351	0.938	0.519	1.445	1.502	1.194	0.350	0.293	0.015	0.183	0.121	0.858	*
	TAG 51:6	3	17.0	6	1.1	1.406	0.823	0.535	1.420	1.576	1.138	0.312	0.210	0.039	0.290	0.117	0.961	*
	TAG 52:0	1	17.3	0	46.0	1.319	0.916	0.648	1.033	1.060	0.988	0.000	0.038	0.000	0.232	0.067	0.848	***
	TAG 52:1	3	17.3	1	192.3	1.350	0.928	0.525	1.172	1.317	1.210	0.140	0.359	0.012	0.594	0.187	0.450	*
	TAG 52:2	3	17.3	2	346.7	1.403	0.811	0.582	1.341	1.434	1.061	0.114	0.118	0.018	0.194	0.088	0.793	*
	TAG 52:3	3	17.3	3	319.0	1.392	0.840	0.548	1.488	1.633	1.254	0.348	0.122	0.017	0.183	0.065	0.765	*
	TAG 52:4	3	17.3	4	171.7	1.352	0.968	0.468	1.462	1.636	1.059	0.345	0.356	0.011	0.160	0.045	0.622	*
	TAG 52:5	3	17.3	5	94.5	1.317	1.024	0.437	1.369	1.857	1.469	0.760	0.365	0.012	0.605	0.035	0.361	*
	TAG 52:6	3	17.3	6	45.4	1.437	0.898	0.311	1.568	1.618	1.283	0.277	0.219	0.006	0.119	0.085	0.660	**
	TAG 53:0	1	17.7	0	5.2	1.155	0.977	0.840	0.935	1.031	0.980	0.005	0.827	0.010	0.243	0.304	0.874	**
	TAG 53:1	3	17.7	1	26.6	1.354	0.920	0.540	1.083	1.258	1.203	0.083	0.362	0.010	0.875	0.211	0.349	*
	TAG 53:2	3	17.7	2	56.0	1.403	0.878	0.482	1.266	1.435	1.188	0.134	0.224	0.010	0.391	0.104	0.656	*
	TAG 53:3	3	17.7	3	48.7	1.404	0.865	0.504	1.341	1.485	1.158	0.165	0.188	0.012	0.268	0.088	0.864	*
	TAG 53:4	3	17.7	4	33.4	1.419	0.874	0.438	1.364	1.484	1.181	0.148	0.201	0.008	0.226	0.088	0.768	**
	TAG 53:5	3	17.7	5	25.3	1.370	0.931	0.461	1.285	1.384	1.212	0.172	0.338	0.009	0.335	0.153	0.559	**
	TAG 53:6	1	17.7	6	21.7	1.100	0.936	0.933	0.987	1.201	1.212	0.798	0.412	0.402	0.620	0.365	0.330	n.s.
	TAG 53:7	3	17.7	7	4.9	1.163	0.996	0.777	1.171	1.347	1.172	0.723	0.518	0.084	0.689	0.175	0.682	n.s.
	TAG 54:0	3	18.0	0	2.3	1.242	1.053	0.524	0.950	1.228	0.887	0.138	0.654	0.024	0.847	0.157	0.563	*

Lipid family	Lipid specie	Cluster	Average fatty acid chain length	Total number of unsaturations	Average pmol/ sample	Normalized abundances						p values						Significance
						Ctl 4dpf	Ctl 5dpf	Ctl 6dpf	6 mg/L BPA 4dpf	6 mg/L BPA 5dpf	6 mg/L BPA 6dpf	Ctl 4dpf	Ctl 5dpf	Ctl 6dpf	6 mg/L BPA 4dpf	6 mg/L BPA 5dpf	6 mg/L BPA 6dpf	
TAG	TAG 54:2	3	18.0	2	149.7	1.356	0.938	0.516	1.192	1.369	1.161	0.125	0.353	0.009	0.515	0.110	0.646	**
	TAG 54:3	3	18.0	3	282.0	1.331	0.897	0.617	1.234	1.224	1.170	0.112	0.229	0.014	0.296	0.325	0.528	*
	TAG 54:4	3	18.0	4	279.0	1.332	0.940	0.557	1.287	1.380	1.182	0.195	0.293	0.010	0.292	0.126	0.662	*
	TAG 54:5	3	18.0	5	164.4	1.317	0.860	0.675	1.390	1.522	1.008	0.492	0.337	0.129	0.350	0.178	0.657	n.s.
	TAG 54:6	3	18.0	6	179.3	1.331	0.927	0.578	1.152	1.351	1.090	0.285	0.538	0.067	0.728	0.253	0.935	n.s.
	TAG 54:7	3	18.0	7	83.8	1.239	1.113	0.447	1.295	1.703	1.505	0.897	0.554	0.004	0.655	0.026	0.134	**
	TAG 54:8	3	18.0	8	28.6	1.437	0.872	0.391	1.513	1.567	1.208	0.229	0.200	0.009	0.138	0.095	0.838	**
	TAG 54:9	3	18.0	9	4.1	1.393	0.918	0.439	1.612	1.454	1.114	0.352	0.354	0.023	0.101	0.252	0.868	*
	TAG 56:1	3	18.7	1	1.6	1.388	0.920	0.438	0.959	1.239	1.136	0.014	0.429	0.002	0.638	0.086	0.306	**
	TAG 56:2	3	18.7	2	38.7	1.405	0.902	0.430	1.178	1.310	1.123	0.071	0.362	0.007	0.476	0.161	0.696	**
	TAG 56:3	3	18.7	3	78.6	1.437	0.875	0.378	1.222	1.373	1.146	0.075	0.290	0.006	0.409	0.126	0.676	**
	TAG 56:4	3	18.7	4	90.0	1.320	1.023	0.426	1.265	1.564	1.346	0.409	0.490	0.007	0.578	0.068	0.343	**
	TAG 56:5	3	18.7	5	153.0	1.305	1.036	0.433	1.237	1.514	1.361	0.390	0.537	0.006	0.619	0.075	0.258	**
	TAG 56:6	3	18.7	6	229.0	1.240	1.061	0.489	1.131	1.575	1.450	0.697	0.648	0.016	0.899	0.083	0.196	*
	TAG 56:7	3	18.7	7	77.3	1.350	0.944	0.384	1.307	1.294	1.164	0.193	0.517	0.010	0.261	0.286	0.648	*
	TAG 58:3	3	19.3	3	15.6	1.463	0.846	0.350	1.189	1.287	0.978	0.031	0.318	0.006	0.325	0.141	0.806	**
	TAG 58:4	3	19.3	4	16.9	1.473	0.850	0.297	1.230	1.373	1.099	0.049	0.277	0.004	0.340	0.110	0.800	**
	TAG 58:5	3	19.3	5	12.6	1.408	0.941	0.290	1.055	1.231	1.213	0.056	0.634	0.004	0.852	0.249	0.289	**
DAG	DAG 32:0	1	16.0	0	12.6	1.293	0.901	0.698	1.064	1.063	0.859	0.014	0.422	0.021	0.388	0.395	0.232	*
	DAG 32:1	2	16.0	1	3.7	1.307	0.877	0.700	1.267	1.170	0.908	0.052	0.196	0.022	0.084	0.278	0.286	*
	DAG 34:0	1	17.0	0	10.1	1.275	0.903	0.742	1.030	1.023	0.906	0.007	0.329	0.017	0.517	0.572	0.351	**
	DAG 34:1	2	17.0	1	29.3	1.337	0.861	0.634	1.238	1.216	0.943	0.091	0.278	0.035	0.228	0.276	0.544	*
	DAG 34:2	2	17.0	2	11.5	1.388	0.839	0.569	1.284	1.242	0.906	0.024	0.139	0.007	0.080	0.131	0.300	**
	DAG 34:3	2	17.0	3	2.7	1.396	0.874	0.505	1.340	1.329	0.952	0.010	0.075	0.001	0.022	0.026	0.250	***
	DAG 36:0	1	18.0	0	1.9	1.142	0.965	0.871	0.967	0.988	0.885	0.045	0.949	0.200	0.966	0.796	0.261	*
	DAG 36:1	2	18.0	1	7.9	1.282	0.920	0.697	1.176	1.159	0.995	0.047	0.274	0.013	0.210	0.265	0.675	*
	DAG 36:2	2	18.0	2	15.1	1.327	0.884	0.663	1.310	1.241	0.955	0.029	0.099	0.005	0.037	0.102	0.283	**
	DAG 36:3	2	18.0	3	13.5	1.393	0.831	0.582	1.342	1.276	0.927	0.012	0.051	0.002	0.023	0.059	0.208	**
	DAG 36:4	1	18.0	4	3.9	1.051	1.031	0.901	0.801	0.907	0.813	0.246	0.313	0.881	0.305	0.926	0.351	n.s.
	DAG 36:5	1	18.0	5	5.9	1.161	1.044	0.709	0.979	1.008	0.838	0.252	0.609	0.176	0.892	0.759	0.490	n.s.
	DAG 38:3	2	19.0	3	3.5	1.232	0.929	0.777	1.299	1.222	1.022	0.098	0.099	0.008	0.030	0.117	0.484	**
	DAG 38:4	1	19.0	4	14.9	0.841	1.068	1.071	0.746	0.971	0.887	0.136	0.038	0.035	0.012	0.468	0.428	*
	DAG 38:5	1	19.0	5	11.2	1.023	1.051	0.920	0.944	1.022	0.901	0.549	0.350	0.464	0.667	0.558	0.341	n.s.
	DAG 38:6	1	19.0	6	24.0	1.126	0.992	0.827	0.962	1.094	0.915	0.400	0.968	0.344	0.881	0.513	0.662	n.s.
	DAG 40:6	1	20.0	6	11.2	0.993	1.048	0.955	0.873	1.058	1.007	0.965	0.498	0.694	0.210	0.437	0.833	n.s.
PE	PE 32:0	1	16.0	0	100.7	0.977	1.010	1.011	0.975	1.109	0.970	0.570	0.984	0.964	0.547	0.104	0.486	n.s.
	PE 32:1	1	16.0	1	940.0	0.993	0.983	1.023	0.990	1.100	0.941	0.812	0.660	0.716	0.758	0.092	0.225	n.s.
	PE 34:1	1	17.0	1	59.1	1.065	1.004	0.924	1.056	1.007	0.875	0.203	0.777	0.271	0.254	0.736	0.078	n.s.
	PE 34:2	1	17.0	2	18.3	1.109	1.008	0.868	0.981	0.985	0.828	0.022	0.382	0.092	0.719	0.660	0.030	*
	PE 35:1	1	17.5	1	5.8	0.950	1.062	0.982	0.919	1.081	0.909	0.599	0.245	0.978	0.325	0.161	0.264	n.s.
	PE 36:1	1	18.0	1	46.1	0.979	1.025	0.994	1.005	1.070	0.960	0.604	0.704	0.827	0.996	0.237	0.387	n.s.
	PE 36:2	1	18.0	2	37.3	1.060	1.002	0.933	1.021	1.073	0.941	0.300	0.956	0.189	0.751	0.211	0.233	n.s.
	PE 36:3	1	18.0	3	20.2	1.128	1.008	0.841	1.103	1.101	0.902	0.078	0.919	0.018	0.149	0.156	0.082	*
	PE 36:4	1	18.0	4	37.1	0.941	1.059	0.996	0.883	0.968	0.918	0.616	0.041	0.392	0.087	0.853	0.300	*
	PE 36:5	1	18.0	5	43.1	1.029	1.057	0.906	1.017	1.007	0.961	0.629	0.383	0.211	0.757	0.870	0.606	n.s.
	PE 38:1	1	19.0	1	7.6	1.021	1.013	0.963	0.991	1.088	0.869	0.410	0.542	0.451	0.993	0.029	0.011	*
	PE 38:2	1	19.0	2	11.5	1.095	0.989	0.907	1.042	1.052	0.905	0.092	0.849	0.107	0.401	0.304	0.101	n.s.
	PE 38:3	2	19.0	3	28.4	1.213	0.923	0.820	1.245	1.186	0.903	0.032	0.080	0.009	0.016	0.060	0.051	**
	PE 38:4	1	19.0	4	115.9	0.908	1.053	1.032	0.914	0.988	0.947	0.129	0.078	0.167	0.161	0.721	0.505	n.s.
	PE 38:5	1	19.0	5	104.8	1.023	1.047	0.925	1.081	1.059	0.988	0.956	0.590	0.085	0.241	0.438	0.511	n.s.
	PE 38:6	1	19.0	6	505.0	1.014	1.021	0.964	1.012	1.080	0.973	0.951	0.852	0.414	0.984	0.244	0.514	n.s.
	PE 38:7	1	19.0	7	13.8	1.234	1.089	0.537	1.168	1.053	0.898	0.083	0.448	0.007	0.184	0.639	0.420	**
	PE 40:4	1	20.0	4	15.4	0.910	1.051	1.030	0.880	0.984	0.949	0.346	0.184	0.305	0.167	0.775	0.756	n.s.
	PE 40:5	1	20.0	5	66.1	1.023	1.023	0.950	1.067	1.109	0.983	0.958	0.965	0.245	0.511	0.208	0.498	n.s.
	PE 40:6	1	20.0	6	694.7	0.950	1.012	1.036	0.947	1.065	0.994	0.366	0.831	0.521	0.343	0.263	0.899	n.s.
	PE 40:7	1	20.0	7	198.2	1.089	1.005	0.895	1.070	1.118	0.954	0.266	0.774	0.060	0.414	0.131	0.262	n.s.
LPE	LPE 16:0	1	16.0	0	2.3	0.979	1.018	0.978	1.009	1.020	0.887	0.980	0.758	0.973	0.813	0.742	0.426	n.s.
	LPE 18:0	2	18.0	0	7.5	1.201	0.898	0.841	1.414	1.323	0.956	0.347	0.069	0.030	0.016	0.059	0.161	*
	LPE 18:1	1	18.0	1	1.3	1.038	0.967	0.990	1.181	1.107	0.948	0.993	0.427	0.588	0.141	0.446	0.324	n.s.
	LPE 22:6	1	22.0	6	5.0	1.057	0.980	0.955	1.212	1.188	0.950	0.998	0.471	0.347	0.171	0.237	0.323	n.s.
PE-O	PE-O 38:5/ PE-P 38:4	1	19.0	5	5.2	0.995	1.046	0.955	0.995	1.051	0.984	0.887	0.522	0.455	0.886	0.479	0.748	n.s.
	PE-O 40:7/ PE-P 40:6	1	20.0	7	28.5	0.909	1.078	1.005	0.821	1.020	0.904	0.494	0.110	0.486	0.084	0.367	0.455	n.s.
	PE-O 34:2/ PE-P 34:1	1	17.0	2	3.4	0.992	1.033	0.971	0.786	0.974	0.852	0.504	0.269	0.674	0.116	0.644	0.346	n.s.
	PE-O 36:2/ PE-P 36:1	1	18.0	2	0.8	1.064	0.981	0.952	0.948	1.146	0.944	0.515	0.775	0.547	0.519	0.146	0.489	n.s.

Lipid family	Lipid specie	Cluster	Average fatty acid chain length	Total number of unsaturations	Average pmol/ sample	Normalized abundances						p values						Significance
						Ctl 4dpf	Ctl 5dpf	Ctl 6dpf	6 mg/L BPA 4dpf	6 mg/L BPA 5dpf	6 mg/L BPA 6dpf	Ctl 4dpf	Ctl 5dpf	Ctl 6dpf	6 mg/L BPA 4dpf	6 mg/L BPA 5dpf	6 mg/L BPA 6dpf	
PE-O	PE-O 36:6/ PE-P 36:5	1	18.0	6	4.2	0.895	1.082	1.013	0.708	0.898	0.796	0.948	0.019	0.095	0.017	0.993	0.127	*
	PE-O 40:6/ PE-P 40:5	1	20.0	6	3.1	0.953	1.058	0.984	0.826	0.977	0.875	0.894	0.094	0.523	0.079	0.599	0.259	n.s.
PE-P	PE-P 38:5/ PE-O 38:6	1	19.0	5	2.9	0.862	1.073	1.051	0.721	0.925	0.830	0.261	0.006	0.011	0.003	0.710	0.083	**
	PE-P 38:6/ PE-O 38:7	1	19.0	6	43.2	1.007	1.012	0.978	1.024	1.155	0.980	0.791	0.844	0.519	0.974	0.112	0.534	n.s.
PG	PG 34:1	1	17.0	1	49.0	0.986	1.036	0.976	1.081	1.190	0.933	0.584	0.979	0.514	0.585	0.108	0.268	n.s.
	PG 36:1	1	18.0	1	33.3	0.915	1.059	1.019	0.863	1.090	0.933	0.440	0.351	0.634	0.187	0.211	0.572	n.s.
	PG 36:2	1	18.0	2	11.2	0.947	1.044	1.006	0.936	1.130	0.967	0.483	0.632	0.993	0.408	0.159	0.646	n.s.
PI	PI 34:1	2	17.0	1	12.0	1.290	0.871	0.750	1.729	1.565	1.279	0.715	0.015	0.004	0.005	0.030	0.787	**
	PI 34:2	2	17.0	2	10.6	1.388	0.831	0.618	1.736	1.534	1.095	0.017	0.001	0.000	0.000	0.001	0.116	***
	PI 36:1	2	18.0	1	5.0	1.161	0.929	0.877	1.451	1.562	1.185	0.814	0.098	0.058	0.106	0.035	0.947	*
	PI 36:2	2	18.0	2	14.9	1.365	0.826	0.672	1.686	1.582	1.158	0.073	0.001	0.000	0.001	0.002	0.446	***
	PI 36:3	2	18.0	3	32.2	1.500	0.724	0.470	1.898	1.673	1.080	0.005	0.000	0.000	0.000	0.000	0.066	***
	PI 36:4	1	18.0	4	44.4	1.058	1.006	0.929	1.234	1.256	1.008	0.742	0.319	0.072	0.073	0.047	0.332	*
	PI 36:5	2	18.0	5	15.6	1.114	0.985	0.882	1.333	1.323	1.147	0.875	0.193	0.047	0.089	0.102	0.875	*
	PI 38:3	2	19.0	3	33.9	1.446	0.749	0.577	1.768	1.748	1.138	0.100	0.004	0.001	0.003	0.003	0.388	***
	PI 38:4	2	19.0	4	215.7	1.100	0.970	0.920	1.269	1.355	1.005	0.952	0.066	0.022	0.032	0.005	0.151	**
	PI 38:5	2	19.0	5	191.1	1.212	0.928	0.814	1.527	1.421	1.047	0.479	0.018	0.003	0.002	0.010	0.166	**
	PI 38:6	2	19.0	6	80.7	1.124	0.976	0.882	1.347	1.316	1.096	0.996	0.126	0.027	0.036	0.060	0.750	*
	PI 40:5	2	20.0	5	9.7	1.291	0.855	0.769	1.601	1.536	1.164	0.296	0.004	0.001	0.002	0.005	0.633	**
	PI 40:6	1	20.0	6	62.0	1.024	1.013	0.961	1.118	1.238	1.118	0.521	0.445	0.196	0.645	0.095	0.640	n.s.
	PI 40:7	2	20.0	7	63.2	1.269	0.903	0.756	1.539	1.456	1.156	0.307	0.013	0.002	0.004	0.013	0.776	**
	PI 40:8	2	20.0	8	8.2	1.312	0.863	0.730	1.689	1.458	1.153	0.209	0.005	0.001	0.001	0.017	0.565	***
PS	PS 32:1	1	16.0	1	2.3	0.978	0.961	1.046	1.083	1.124	1.067	0.417	0.315	0.971	0.614	0.323	0.760	n.s.
	PS 34:0	1	17.0	0	109.3	1.013	1.017	0.970	1.055	1.051	1.025	0.647	0.806	0.030	0.119	0.167	0.870	*
	PS 36:1	1	18.0	1	32.1	0.848	1.087	1.045	0.807	1.029	0.987	0.160	0.159	0.334	0.075	0.437	0.801	n.s.
	PS 36:2	1	18.0	2	5.1	0.964	1.052	0.979	0.960	1.089	1.016	0.363	0.399	0.524	0.326	0.142	0.900	n.s.
	PS 38:0	1	19.0	0	118.1	1.102	0.987	0.899	1.223	1.181	1.016	0.355	0.055	0.003	0.004	0.016	0.177	**
	PS 38:1	2	19.0	1	36.8	1.221	0.952	0.774	1.477	1.341	1.062	0.051	0.002	0.000	0.000	0.001	0.068	***
	PS 38:4	1	19.0	4	10.6	0.758	1.094	1.101	0.557	0.800	0.846	0.254	0.027	0.024	0.009	0.488	0.876	**
	PS 38:5	1	19.0	5	14.2	0.874	1.041	1.073	0.728	0.918	0.876	0.669	0.261	0.168	0.102	0.998	0.684	n.s.
	PS 40:0	2	20.0	0	14.4	1.187	0.928	0.847	1.363	1.297	1.061	0.231	0.015	0.003	0.004	0.016	0.372	**
	PS 40:5	1	20.0	5	31.9	0.886	1.068	1.032	0.843	1.004	0.979	0.313	0.234	0.429	0.145	0.656	0.898	n.s.
	PS 40:6	1	20.0	6	365.9	0.955	1.027	1.013	0.880	1.052	0.958	0.718	0.523	0.650	0.186	0.335	0.752	n.s.
	PS 42:5	2	21.0	5	78.3	1.189	0.957	0.817	1.451	1.350	1.177	0.299	0.000	0.000	0.000	0.001	0.502	***
	PS 42:6	2	21.0	6	41.0	1.238	0.920	0.787	1.489	1.353	1.095	0.038	0.001	0.000	0.000	0.001	0.177	***
PC	PC 28:0	2	14.0	0	1.7	1.261	0.923	0.737	1.569	1.374	1.321	0.602	0.054	0.007	0.018	0.175	0.322	**
	PC 29:0	1	14.5	0	3.4	0.980	0.998	0.969	0.831	1.021	0.751	0.797	0.734	0.836	0.661	0.656	0.429	n.s.
	PC 30:0	1	15.0	0	57.7	1.058	1.021	0.912	1.050	1.174	1.018	0.744	0.763	0.067	0.849	0.055	0.729	n.s.
	PC 30:1	2	15.0	1	12.1	1.280	0.935	0.696	1.658	1.465	1.442	0.623	0.003	0.000	0.001	0.016	0.025	***
	PC 31:0	1	15.5	0	54.6	0.959	1.010	1.029	0.830	0.985	0.874	0.840	0.287	0.175	0.069	0.513	0.213	n.s.
	PC 31:1	2	15.5	1	16.1	1.131	0.985	0.865	1.243	1.278	1.161	0.720	0.063	0.004	0.054	0.023	0.396	**
	PC 32:0	1	16.0	0	488.1	0.993	1.019	0.986	0.890	1.006	0.854	0.608	0.387	0.682	0.336	0.488	0.162	n.s.
	PC 32:1	2	16.0	1	237.9	1.103	0.997	0.887	1.261	1.216	1.069	0.769	0.099	0.005	0.011	0.036	0.681	**
	PC 32:2	2	16.0	2	52.3	1.280	0.926	0.709	1.521	1.320	1.132	0.061	0.008	0.000	0.001	0.024	0.792	***
	PC 32:3	2	16.0	3	5.2	1.373	0.862	0.607	1.804	1.465	1.353	0.168	0.004	0.000	0.000	0.036	0.234	***
	PC 33:0	1	16.5	0	54.5	0.982	1.011	1.006	0.829	0.958	0.846	0.497	0.269	0.297	0.114	0.754	0.169	n.s.
	PC 33:1	1	16.5	1	103.8	0.971	1.002	1.025	1.054	1.133	1.035	0.278	0.552	0.832	0.761	0.130	0.978	n.s.
	PC 33:2	2	16.5	2	35.7	1.116	0.969	0.902	1.230	1.217	1.085	0.576	0.060	0.011	0.030	0.042	0.975	*
	PC 33:3	2	16.5	3	5.4	1.274	0.921	0.726	1.474	1.309	1.124	0.033	0.005	0.000	0.000	0.013	0.781	***
	PC 34:0	1	17.0	0	127.1	1.041	1.018	0.937	0.997	1.047	0.907	0.345	0.601	0.307	0.914	0.296	0.136	n.s.
	PC 34:1	1	17.0	1	1645.9	1.078	0.995	0.919	1.217	1.209	1.068	0.958	0.134	0.017	0.034	0.041	0.794	*
	PC 34:2	2	17.0	2	654.3	1.254	0.922	0.759	1.419	1.356	1.098	0.060	0.006	0.000	0.002	0.005	0.501	***
	PC 34:3	2	17.0	3	159.3	1.353	0.882	0.623	1.369	1.421	1.086	0.007	0.006	0.000	0.005	0.002	0.550	***
	PC 34:4	2	17.0	4	32.3	1.375	0.861	0.607	1.724	1.367	1.112	0.026	0.004	0.000	0.000	0.031	0.402	***
	PC 34:5	2	17.0	5	9.1	1.369	0.860	0.621	1.713	1.331	1.228	0.022	0.001	0.000	0.000	0.051	0.513	***
	PC 35:0	1	17.5	0	9.7	1.041	1.003	0.954	0.933	1.030	0.890	0.215	0.579	0.668	0.407	0.290	0.123	n.s.
	PC 35:1	1	17.5	1	142.0	1.072	0.978	0.944	1.129	1.190	1.070	0.846	0.084	0.028	0.167	0.023	0.889	*
	PC 35:2	2	17.5	2	89.8	1.231	0.930	0.785	1.389	1.355	1.103	0.057	0.003	0.000	0.001	0.002	0.516	***
	PC 35:3	2	17.5	3	19.9	1.228	0.919	0.806	1.383	1.277	1.055	0.074	0.012	0.001	0.002	0.022	0.338	**
	PC 35:4	1	17.5	4	9.9	1.039	1.021	0.936	1.083	1.162	1.121	0.709	0.504	0.065	0.691	0.115	0.317	n.s.
	PC 35:5	2	17.5	5	12.6	1.119	1.005	0.856	1.299	1.213	1.186	0.924	0.146	0.007	0.028	0.174	0.301	**
	PC 36:0	1	18.0	0	31.4	1.068	0.968	0.960	0.901	1.035	0.837	0.029	0.865	0.969	0.155	0.099	0.016	*
	PC 36:1	2	18.0	1	508.7	1.121	0.975	0.890	1.350	1.299	1.102	0.968	0.008	0.001	0.001	0.003	0.598	***
	PC 36:2	2	18.0	2	664.4	1.255	0.939	0.736	1.517	1.410	1.121	0.091	0.003	0.000	0.000	0.002	0.389	***

Lipid family	Lipid specie	Cluster	Average fatty acid chain length	Total number of unsaturations	Average pmol/ sample	Normalized abundances						p values						Significance
						Ctl 4dpf	Ctl 5dpf	Ctl 6dpf	6 mg/L BPA 4dpf	6 mg/L BPA 5dpf	6 mg/L BPA 6dpf	Ctl 4dpf	Ctl 5dpf	Ctl 6dpf	6 mg/L BPA 4dpf	6 mg/L BPA 5dpf	6 mg/L BPA 6dpf	
	PC 36:4	2	18.0	4	347.8	1.117	0.990	0.879	1.239	1.209	1.113	0.615	0.083	0.005	0.023	0.052	0.671	**
	PC 36:5	2	18.0	5	383.7	1.131	1.007	0.839	1.300	1.248	1.116	0.707	0.156	0.005	0.020	0.062	0.887	**
	PC 36:6	2	18.0	6	76.1	1.322	0.896	0.669	1.679	1.370	1.218	0.090	0.004	0.000	0.000	0.033	0.699	***
	PC 37:4	1	18.5	4	22.4	1.042	1.026	0.927	1.091	1.169	1.087	0.779	0.576	0.048	0.538	0.076	0.589	*
	PC 37:5	2	18.5	5	45.2	1.173	0.977	0.817	1.356	1.277	1.138	0.460	0.062	0.003	0.011	0.052	0.822	**
	PC 37:6	2	18.5	6	54.0	1.107	0.976	0.906	1.265	1.292	1.199	0.792	0.049	0.011	0.059	0.032	0.262	*
	PC 38:0	1	19.0	0	5.2	1.083	0.965	0.944	0.935	1.053	0.818	0.009	0.976	0.503	0.345	0.031	0.003	**
	PC 38:1	2	19.0	1	56.6	1.135	0.944	0.904	1.316	1.309	1.103	0.694	0.005	0.002	0.003	0.003	0.716	**
	PC 38:2	2	19.0	2	99.5	1.123	0.955	0.909	1.374	1.276	1.041	0.843	0.016	0.005	0.002	0.014	0.183	**
	PC 38:3	2	19.0	3	165.8	1.184	0.978	0.796	1.364	1.367	1.178	0.478	0.019	0.001	0.006	0.005	0.547	***
	PC 38:4	2	19.0	4	271.4	1.126	0.999	0.856	1.278	1.256	1.121	0.707	0.086	0.003	0.016	0.028	0.788	**
	PC 38:5	2	19.0	5	137.4	1.157	0.939	0.879	1.242	1.303	1.082	0.490	0.083	0.029	0.118	0.040	0.816	*
	PC 38:6	2	19.0	6	1276.4	1.126	0.976	0.883	1.279	1.295	1.133	0.849	0.042	0.005	0.024	0.016	0.752	**
	PC 38:7	2	19.0	7	205.9	1.175	1.012	0.770	1.346	1.236	1.120	0.205	0.077	0.000	0.002	0.034	0.835	***
	PC 38:8	2	19.0	8	20.6	1.315	0.917	0.653	1.596	1.327	1.175	0.085	0.015	0.000	0.001	0.068	0.880	***
	PC 39:6	2	19.5	6	129.7	1.131	0.977	0.875	1.290	1.292	1.136	0.813	0.056	0.007	0.027	0.025	0.760	**
	PC 39:7	2	19.5	7	44.3	1.207	0.936	0.816	1.437	1.376	1.147	0.336	0.006	0.001	0.002	0.005	0.904	***
	PC 40:1	1	20.0	1	9.7	1.102	0.948	0.939	1.203	1.245	1.034	0.645	0.037	0.029	0.044	0.014	0.400	*
	PC 40:2	2	20.0	2	10.6	1.233	0.901	0.815	1.477	1.440	1.120	0.231	0.002	0.000	0.001	0.002	0.421	***
	PC 40:3	2	20.0	3	10.0	1.247	0.887	0.810	1.453	1.394	1.146	0.074	0.001	0.000	0.000	0.001	0.810	***
	PC 40:4	2	20.0	4	31.0	1.216	0.965	0.764	1.497	1.348	1.218	0.397	0.008	0.000	0.001	0.014	0.374	***
	PC 40:5	2	20.0	5	133.7	1.182	0.971	0.811	1.389	1.287	1.110	0.495	0.097	0.007	0.015	0.085	0.857	**
	PC 40:6	2	20.0	6	632.3	1.161	0.954	0.861	1.363	1.346	1.155	0.566	0.002	0.000	0.001	0.001	0.687	***
	PC 40:7	2	20.0	7	570.9	1.203	0.952	0.803	1.466	1.372	1.173	0.422	0.005	0.000	0.001	0.005	0.815	***
	PC 40:8	2	20.0	8	173.0	1.151	0.902	0.927	1.365	1.306	1.120	0.580	0.001	0.002	0.001	0.004	0.834	***
	PC 42:6	2	21.0	6	28.8	1.246	0.864	0.834	1.437	1.378	1.147	0.133	0.002	0.001	0.002	0.006	0.942	**
LPC	LPC 14:1	1	14.0	1	35.4	0.966	1.029	1.003	1.009	1.122	1.005	0.399	0.919	0.763	0.843	0.161	0.794	n.s.
	LPC 15:0	2	15.0	0	2.9	1.234	0.883	0.800	1.468	1.311	0.947	0.293	0.088	0.032	0.017	0.114	0.197	*
	LPC 16:0	1	16.0	0	36.7	1.107	1.003	0.856	1.120	1.256	1.022	0.631	0.556	0.068	0.545	0.078	0.687	n.s.
	LPC 18:0	2	18.0	0	28.5	1.414	0.803	0.574	1.393	1.426	1.003	0.006	0.007	0.000	0.008	0.005	0.235	***
	LPC 18:1	2	18.0	1	26.2	1.338	0.847	0.693	1.571	1.292	0.998	0.012	0.004	0.000	0.000	0.031	0.083	***
	LPC 18:2	2	18.0	2	10.1	1.419	0.798	0.586	1.592	1.260	0.873	0.000	0.001	0.000	0.000	0.009	0.003	***
	LPC 20:0	2	20.0	0	1.3	1.290	0.896	0.720	1.499	1.628	1.353	0.357	0.001	0.000	0.004	0.001	0.084	***
	LPC 20:1	2	20.0	1	3.3	1.303	0.848	0.760	1.559	1.348	0.991	0.018	0.001	0.000	0.000	0.006	0.032	***
	LPC 20:3	2	20.0	3	2.2	1.333	0.882	0.658	1.497	1.267	0.992	0.011	0.012	0.000	0.001	0.042	0.123	***
	LPC 20:4	2	20.0	4	2.9	1.211	0.978	0.757	1.259	1.156	1.002	0.013	0.103	0.000	0.004	0.066	0.221	***
	LPC 20:5	2	20.0	5	5.1	1.339	0.873	0.655	1.394	1.160	0.938	0.012	0.056	0.002	0.006	0.251	0.173	**
	LPC 22:6	2	22.0	6	39.7	1.411	0.785	0.622	1.574	1.295	0.974	0.001	0.001	0.000	0.000	0.011	0.036	***
	LPC 24:0	2	24.0	0	1.6	1.363	0.837	0.662	1.280	1.330	1.048	0.002	0.004	0.000	0.012	0.004	0.499	***
PC-O	PC-O 16:0	1	8.0	0	1.7	1.076	1.008	0.906	1.093	1.167	1.104	0.785	0.426	0.044	0.591	0.122	0.485	*
	PC-O 18:0	1	9.0	0	0.7	1.138	0.955	0.887	1.164	1.206	1.076	0.418	0.188	0.055	0.277	0.134	0.952	n.s.
	PC-O 30:0	1	15.0	0	1.1	0.990	1.005	1.000	0.923	1.066	0.941	0.979	0.836	0.882	0.465	0.381	0.594	n.s.
	PC-O 32:0	1	16.0	0	10.0	0.910	1.036	1.044	0.774	0.909	0.862	0.859	0.139	0.118	0.067	0.847	0.396	n.s.
	PC-O 32:1/ PC-P 32:0	1	16.0	1	1.1	0.937	1.072	0.985	0.904	1.073	0.986	0.543	0.397	0.932	0.347	0.395	0.944	n.s.
	PC-O 32:2/ PC-P 32:1	1	16.0	2	1.4	0.841	1.100	1.036	0.802	1.156	0.860	0.414	0.382	0.641	0.295	0.231	0.484	n.s.
	PC-O 34:0	1	17.0	0	5.5	1.126	0.935	0.921	0.932	1.058	0.984	0.170	0.526	0.436	0.504	0.477	0.925	n.s.
	PC-O 34:1/ PC-P 34:0	1	17.0	1	34.0	1.107	0.955	0.927	1.217	1.215	1.053	0.513	0.023	0.010	0.015	0.016	0.551	**
	PC-O 34:2/ PC-P 34:1	1	17.0	2	11.3	1.033	0.963	1.001	1.147	1.224	1.145	0.447	0.108	0.239	0.377	0.076	0.395	n.s.
	PC-O 36:1/ PC-P 36:0	2	18.0	1	4.8	1.200	0.884	0.872	1.614	1.301	1.108	0.646	0.011	0.009	0.001	0.121	0.498	**
	PC-O 36:2/ PC-P 36:1	2	18.0	2	6.0	1.244	0.879	0.818	1.461	1.310	1.076	0.133	0.008	0.003	0.002	0.033	0.426	**
	PC-O 36:3/ PC-P 36:2	1	18.0	3	2.7	1.016	0.929	1.039	0.982	1.001	1.020	0.845	0.469	0.659	0.866	0.973	0.813	n.s.
	PC-O 36:4/ PC-P 36:3	1	18.0	4	9.9	0.868	1.020	1.095	0.912	1.025	0.982	0.082	0.535	0.092	0.245	0.487	0.981	n.s.
	PC-O 36:5/ PC-P 36:4	1	18.0	5	21.2	0.897	1.058	1.035	0.906	1.028	0.961	0.276	0.313	0.469	0.327	0.526	0.787	n.s.

Lipid family	Lipid specie	Cluster	Average fatty acid chain length	Total number of unsaturations	Average pmol/ sample	Normalized abundances						p values						Significance
						Ctl 4dpf	Ctl 5dpf	Ctl 6dpf	6 mg/L BPA 4dpf	6 mg/L BPA 5dpf	6 mg/L BPA 6dpf	Ctl 4dpf	Ctl 5dpf	Ctl 6dpf	6 mg/L BPA 4dpf	6 mg/L BPA 5dpf	6 mg/L BPA 6dpf	
PC-O	PC-O 38:5/ PC-P 38:4	1	19.0	5	13.0	1.052	1.074	0.840	0.977	0.800	0.872	0.252	0.182	0.335	0.667	0.189	0.511	n.s.
	PC-O 40:6/ PC-P 40:5	1	20.0	6	21.8	1.041	0.995	0.960	1.116	1.164	1.077	0.749	0.271	0.109	0.320	0.093	0.743	n.s.
	PC-O 40:7/ PC-P 40:6	1	20.0	7	37.0	1.059	0.970	0.966	1.137	1.226	1.074	0.840	0.147	0.131	0.325	0.046	0.971	*
PC-P	PC-P 30:0/ PC-O 30:1	1	15.0	0	1.6	0.993	1.002	0.998	0.969	1.104	1.089	0.728	0.795	0.767	0.551	0.416	0.508	n.s.
	PC-P 36:5/ PC-O 36:6	1	18.0	5	9.2	1.037	0.996	0.965	1.041	1.117	0.958	0.748	0.677	0.340	0.688	0.108	0.285	n.s.
	PC-P 38:5/ PC-O 38:6	1	19.0	5	82.7	1.081	0.980	0.932	1.171	1.240	1.128	0.913	0.154	0.056	0.260	0.063	0.577	n.s.
	PC-P 38:6/ PC-O 38:7	2	19.0	6	19.0	1.090	0.954	0.949	1.244	1.356	1.035	0.891	0.205	0.191	0.234	0.055	0.534	n.s.
SM	SM 32:1	2	16.0	1	4.0	1.290	0.886	0.735	1.506	1.399	1.206	0.148	0.007	0.001	0.003	0.019	0.635	***
	SM 33:1	2	16.5	1	8.7	1.149	0.961	0.867	1.233	1.258	1.145	0.429	0.043	0.005	0.054	0.030	0.463	**
	SM 34:0	1	17.0	0	25.5	0.956	1.013	1.029	0.947	1.085	1.177	0.310	0.766	0.938	0.264	0.498	0.091	n.s.
	SM 34:1	1	17.0	1	147.7	1.010	1.001	0.988	1.046	1.170	1.063	0.519	0.427	0.314	0.992	0.058	0.766	n.s.
	SM 34:2	1	17.0	2	7.4	1.076	1.021	0.885	1.045	1.090	0.963	0.482	0.928	0.175	0.714	0.393	0.565	n.s.
	SM 35:1	1	17.5	1	13.9	1.072	0.997	0.923	1.056	1.120	1.046	0.620	0.599	0.158	0.783	0.273	0.885	n.s.
	SM 36:1	1	18.0	1	23.9	0.927	1.041	1.027	0.927	1.131	1.142	0.224	0.913	0.942	0.224	0.253	0.208	n.s.
	SM 38:1	1	19.0	1	25.5	0.998	0.989	1.011	0.981	1.118	1.075	0.677	0.601	0.815	0.528	0.258	0.539	n.s.
	SM 39:1	2	19.5	1	10.8	1.098	0.954	0.922	1.236	1.266	1.083	0.968	0.257	0.174	0.245	0.171	0.931	n.s.
	SM 40:1	1	20.0	1	57.0	1.043	0.965	0.987	1.075	1.167	1.085	0.899	0.301	0.427	0.792	0.198	0.707	n.s.
	SM 40:2	1	20.0	2	7.8	1.059	0.976	0.960	1.130	1.186	1.079	0.936	0.291	0.221	0.428	0.165	0.865	n.s.
	SM 41:1	1	20.5	1	17.7	1.070	0.963	0.960	1.163	1.297	1.135	0.659	0.070	0.065	0.332	0.018	0.564	*
	SM 41:2	1	20.5	2	5.5	1.079	0.967	0.940	1.187	1.216	1.089	0.988	0.168	0.101	0.185	0.108	0.898	n.s.
	SM 42:1	1	21.0	1	42.4	1.015	1.003	0.980	1.078	1.234	1.117	0.334	0.246	0.138	0.896	0.022	0.425	*

Supplemental table ST6. Comparison between our both HPTLC and UHPLC/TOFMS results. Specific normalization carried out to perform the data integration can be found at supplementary method SM4. Pearson correlation tests were performed for all the lipid classes. Significant correlations are specified by asterisks (* for p<0.05, ** for p<0.01, * for p<0.001). Common lipid families were CE (cholesterol esters), TAGs (triacylglycerols a.k.a. triglycerides), PG (phosphatidylglycerols), PE (phosphatidylethanolamines), PI (phosphatidylinositols), PS (phosphatidylserines), PC (phosphatidylcholines) and SM (sphingomyelins).**

Lipid family	r^2	p	Significance
CE	0.918	0.0026	**
TAGs	0.426	0.1601	n.s.
PE	0.915	0.0028	**
PG	< 0.001	0.9917	n.s.
PI	0.845	0.0095	**
PS	0.865	0.0072	**
PC	0.871	0.0065	**
SM	0.053	0.6617	n.s.

Supplemental table ST7. Fold-change gene expression values extracted from the previous studies (Martínez et al., 2018) of zebrafish eleutheroembryos (5 dpf) exposed to 0, 0.1, 1.0 and 4.0 mg/L of BPA from 2 up to 5 dpf. Mean values and standard error of the mean (SEM) of each group are presented. Chosen genes were the differentially expressed genes (DEGs) related in the lipid biosynthesis pathway and catabolism, including those which are common in both pathways. Gene selection was based in the gene classification of zfin database (Howe et al., 2012; http://zfin.org/).

		Control		0.1 mg/L BPA		1.0 mg/L BPA		4.0 mg/l BPA	
Pathway	Gene	Mean	SEM	Mean	SEM	Mean	SEM	Mean	SEM
Biosynthesis	agpat9l	1.00	0.23	1.11	0.21	1.23	0.30	1.37	0.23
	anxa1c	1.00	0.12	1.24	0.12	0.56	0.08	0.48	0.15
	cdipt	1.00	0.22	1.07	0.17	1.14	0.26	1.31	0.24
	cga	1.00	0.23	1.31	0.31	1.71	0.38	2.30	0.49
	chpt1	1.00	0.16	1.42	0.20	1.58	0.33	1.47	0.20
	cyb5r2	1.00	0.13	1.88	0.25	2.68	0.72	2.37	0.41
	cyp7b1	1.00	0.32	1.35	0.34	1.31	0.41	1.43	0.35
	ddit3	1.00	0.15	1.01	0.18	0.88	0.13	0.81	0.10
	dgat1a	1.00	0.23	1.42	0.30	1.87	0.58	1.22	0.25
	dgat2	1.00	0.54	1.98	0.80	2.20	1.02	2.01	0.80
	dhcr7	1.00	0.28	1.51	0.43	2.01	0.64	1.46	0.33
	ebp	1.00	0.17	1.62	0.27	1.77	0.50	1.52	0.19
	elovl5	1.00	0.30	1.32	0.33	1.24	0.36	1.54	0.36
	elovl8b	1.00	0.15	1.78	0.23	1.67	0.41	1.99	0.50
	fads2	1.00	0.21	1.71	0.28	1.00	0.27	0.52	0.14
	faxdc2	1.00	0.22	1.63	0.41	1.99	0.53	1.63	0.37
	fgf1a	1.00	0.22	1.28	0.20	1.12	0.25	1.02	0.19
	gal3st2	1.00	0.21	1.08	0.16	0.85	0.21	1.12	0.17
	gpaa1	1.00	0.23	1.32	0.24	1.33	0.35	1.49	0.29
	hacd2	1.00	0.26	1.15	0.22	1.25	0.33	1.37	0.26
	hsd17b12b	1.00	0.18	1.31	0.20	1.46	0.37	1.53	0.29
	hsd3b7	1.00	0.24	1.23	0.24	1.49	0.39	1.67	0.31
	lias	1.00	0.20	1.18	0.19	1.12	0.23	1.33	0.23
	mecr	1.00	0.24	1.11	0.22	1.01	0.22	1.03	0.18
	mid1ip1b	1.00	0.18	0.93	0.13	0.95	0.14	0.76	0.10
	msmo1	1.00	0.17	1.46	0.22	1.42	0.34	1.08	0.15
	mvda	1.00	0.32	1.99	0.65	1.97	0.69	1.95	0.48
	mvk	1.00	0.19	1.52	0.24	1.36	0.38	1.59	0.22
	pcyt1bb	1.00	0.34	1.98	0.54	2.52	0.85	1.95	0.57
	pigb	1.00	0.21	1.21	0.18	1.21	0.27	1.25	0.19
	pigf	1.00	0.24	1.27	0.23	1.22	0.29	1.43	0.27
	pigs	1.00	0.25	1.35	0.27	1.37	0.34	1.71	0.40
	rdh10b	1.00	0.29	1.43	0.34	1.31	0.31	1.46	0.30
	rpe65a	1.00	0.39	0.67	0.20	0.87	0.32	1.03	0.29
	sdr42e2	1.00	0.59	2.28	0.98	1.95	0.83	2.33	1.04
	serac1	1.00	0.23	0.91	0.16	0.97	0.23	0.97	0.17
	sqlea	1.00	0.30	1.87	0.54	1.86	0.66	1.38	0.31
	st3gal4	1.00	0.22	1.18	0.21	1.30	0.32	1.26	0.20
	tamm41	1.00	0.26	1.16	0.22	0.93	0.24	1.07	0.21
	tecrb	1.00	0.17	1.18	0.18	1.26	0.25	1.12	0.14
	tecrl2b	1.00	0.06	1.37	0.11	1.13	0.06	0.77	0.09
	thnsl2	1.00	0.28	1.45	0.31	1.54	0.43	1.30	0.27
	tle3a	1.00	0.25	0.89	0.18	0.95	0.22	1.14	0.21
	tm7sf2	1.00	0.20	1.17	0.19	1.82	0.55	1.17	0.21
	yy1b	1.00	0.17	1.00	0.14	0.97	0.18	1.02	0.13
	zgc:162183	1.00	0.25	1.25	0.28	1.24	0.29	1.12	0.21

		Control		0.1 mg/L BPA		1.0 mg/L BPA		4.0 mg/l BPA	
Pathway	**Gene**	**Mean**	**SEM**	**Mean**	**SEM**	**Mean**	**SEM**	**Mean**	**SEM**
Catabolism	acat2	1.00	0.34	1.53	0.42	1.62	0.59	1.81	0.50
	bco1l	1.00	0.20	1.96	0.32	3.05	0.97	2.57	0.55
	crabp1b	1.00	0.24	1.37	0.25	1.33	0.27	1.32	0.23
	cyp26b1	1.00	0.24	1.16	0.24	1.41	0.39	1.72	0.37
	enpp6	1.00	0.20	1.17	0.21	1.32	0.25	1.27	0.19
	gdpd1	1.00	0.27	1.47	0.30	1.72	0.52	1.88	0.43
	gpcpd1	1.00	0.24	1.04	0.20	1.02	0.23	1.04	0.19
	hao1	1.00	0.39	2.01	0.59	2.32	0.83	2.31	0.73
	iah1	1.00	0.19	1.57	0.27	1.44	0.27	1.73	0.28
	lipea	1.00	0.20	0.96	0.14	0.84	0.16	0.94	0.16
	lipf	1.00	0.19	1.32	0.21	1.45	0.32	1.53	0.24
	naga	1.00	0.22	1.24	0.23	1.16	0.27	1.53	0.25
	neu1	1.00	0.25	1.24	0.24	1.29	0.31	1.56	0.28
	neu3.3	1.00	0.17	1.66	0.42	1.92	0.46	1.05	0.18
	pla2g12a	1.00	0.16	1.36	0.17	1.45	0.31	1.47	0.19
	plcd3a	1.00	0.16	1.07	0.14	1.07	0.18	0.99	0.11
	pnpla8	1.00	0.24	1.33	0.27	1.45	0.38	1.43	0.29
	sgpl1	1.00	0.23	1.51	0.39	1.89	0.51	1.79	0.39
	smpdl3b	1.00	0.16	1.62	0.37	2.18	0.56	1.73	0.35
Common	abhd2a	1.00	0.27	1.00	0.22	1.01	0.25	0.83	0.26
	apoa1a	1.00	0.13	2.42	0.43	2.50	0.65	3.92	0.70
	apoa1b	1.00	0.14	1.72	0.35	1.90	0.45	1.82	0.15
	apoa4a	1.00	0.32	2.34	0.04	2.01	0.42	2.58	0.10
	apoea	1.00	0.13	2.02	0.28	1.72	0.20	1.88	0.24
	cyp7a1	1.00	0.22	1.69	0.94	3.12	1.69	1.36	0.75
	lipca	1.00	0.21	0.92	0.53	1.72	1.13	2.83	0.85
	lpin1	1.00	0.20	0.90	0.33	0.90	0.22	0.67	0.07
	pld1a	1.00	0.25	1.36	0.25	1.32	0.44	1.38	0.27

Chapter IV:

Metabolism-related short- and long-term effects of BPA in zebrafish eleutheroembryos and juveniles. Implication of epigenetic mechanisms: DNA methylation and miRNAs.

Following the study focused on BPA, short- and long-term metabolic effects were assessed in BPA exposed individuals, which were placed in clean media from 6 dpf. Non-estrogenic effects of BPA were studied using an estrogenic control. Behavioral and gene expression were also assessed at both eleutheroembryo and juvenile stages. At the eleutheroembryo stage, two of the main epigenetic mechanisms were screened: DNA methylation and microRNAs (miRNAs). BisPCR^2 method (targeted bisulfite sequencing) was used to measure the DNA methylation of 4 selected genes (based in the results of the previous performed transcriptomic study): 2 non-affected and 2 of the most affected genes (cyp19a1b and aldh1a2). DNA methylation of these genes was compared with both their general expression and BPA under/over-expression effect. In addition, the expression of specific miRNAs (involved in the inhibition of the translation of genes related to lipids and energy homeostasis; and tissue-specific miRNAs) was assessed by qPCR.

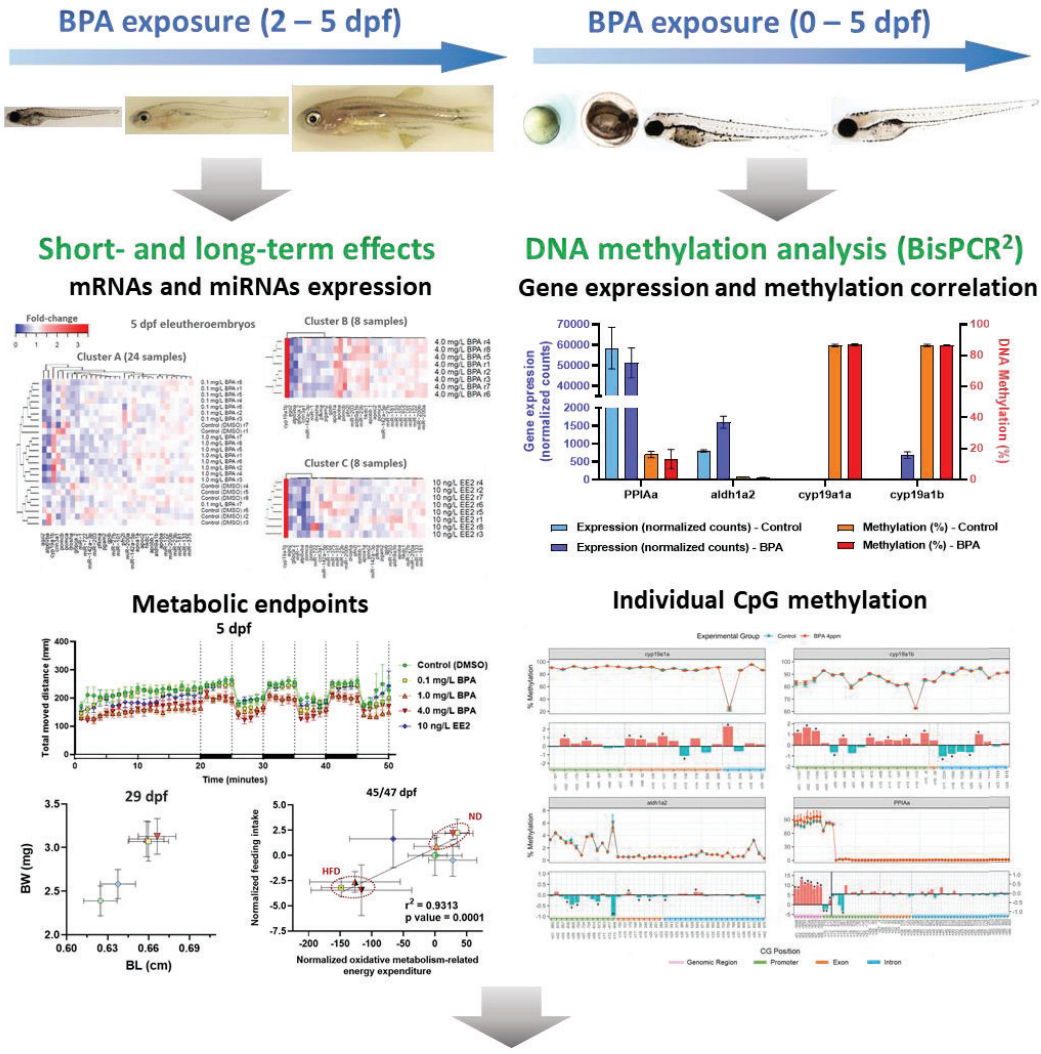

Main results

- Embryonic BPA exposure elicited an increase of weight and body mass index, behaviour changes and transcripts dysregulation still in juveniles.

- At 4-6 dpf, BPA exposure exerted a decrease in the feeding intake, motility, and disrupted the expression of homeostasis-related transcripts.

- miRNAs (specifically miR-1 and miR-23b) and DNA methylation at early stages were also altered. DNA methylation could be correlated with the expression of the respective genes.

- These epigenetic mechanisms could, at least partially, drive the observed long-term effects. If they remain altered at later developmental stages and whether they could explain the observed phenotypical alterations, it should be further studied.

Scientific article VI

Acute and long-term metabolic consequences of early developmental Bisphenol A exposure in zebrafish (*Danio rerio*)

Authors: R. Martínez, W. Tu, T. Eng, M. Allaire-Leung, B. Piña, L. Navarro-Martín, J.A. Mennigen

Status: Published

Journal: Chemosphere. 256 (2020) 127080.

DOI: 10.1016/j.chemosphere.2020.127080

Chemosphere 256 (2020) 127080

Contents lists available at ScienceDirect

Chemosphere

journal homepage: www.elsevier.com/locate/chemosphere

Acute and long-term metabolic consequences of early developmental Bisphenol A exposure in zebrafish (*Danio rerio*)

Rubén Martínez [a, b], Wenqing Tu [c], Tyler Eng [d], Melissa Allaire-Leung [d], Benjamin Piña [a], Laia Navarro-Martín [a], Jan A. Mennigen [d, *]

[a] Department of Environmental Chemistry, Institute of Environmental Assessment and Water Research, IDAEA-CSIC, Jordi Girona, Barcelona, Spain
[b] Department of Cellular Biology, Physiology and Immunology, Universitat de Barcelona (UB), Barcelona, Spain
[c] Research Institute of Poyang Lake, Jiangxi Academy of Sciences, Nanchang 330012, China
[d] Department of Biology, University of Ottawa, 20 Marie-Curie K1N 6N5, Ottawa, Ontario, Canada

HIGHLIGHTS

- Developmental BPA exposure results in acute, transient and long-term changes in zebrafish metabolism.
- Embryonic BPA exposure and juvenile nutritional challenge interact to affect locomotor behaviour.
- Most developmental BPA exposure effects are not mimicked by an estrogenic control.

GRAPHICAL ABSTRACT

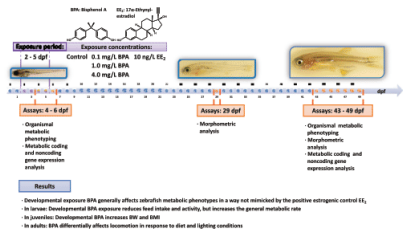

ARTICLE INFO

Article history:
Received 13 February 2020
Received in revised form
12 May 2020
Accepted 13 May 2020
Available online 18 May 2020

Handling Editor: David Volz

Keywords:
Estrogenic chemicals
Metabolic disruption
Plasticizer
BPA
microRNA
Metabolism

ABSTRACT

Bisphenol A (BPA) is an estrogenic contaminant linked to metabolic disruption. Developmental BPA exposure is of particular concern, as organizational effects may irreversibly disrupt metabolism at later life-stages. While BPA exposures in adult fish elicit metabolic perturbations similar to effects described in rodents, the metabolic effects of developmental BPA exposure in juvenile fish remain largely unknown. Following embryonic zebrafish exposure to BPA (0.1, 1 and 4 mg/L) and EE_2 (10 ng/L) from 2 to 5 dpf, we assessed the metabolic phenotype in larvae (4–6 dpf) and juveniles (43–49 dpf) which had been divided into regular-fed and overfed groups at 29 dpf. Developmental BPA exposure in larvae dose-dependently reduced food-intake and locomotion and increased energy expenditure. Juveniles (29 dpf) exhibited a transient increase in body weight after developmental BPA exposure and persistent diet-dependent locomotion changes (43–49 dpf). At the molecular level, glucose and lipid metabolism-related transcript abundance clearly separated BPA exposed fish from controls and EE_2 exposed fish at the larval stage, in juveniles on a regular diet and, to a lesser extent, in overfed juveniles. In general, the metabolic endpoints affected by BPA exposure were not mimicked by EE_2 treatment. We conclude that developmental BPA exposure elicits acute metabolic effects in zebrafish larvae and fewer transient and persistent effects in juveniles and that these metabolic effects are largely independent of BPA's estrogenicity.

1. Introduction

Bisphenol A (BPA) is a high production chemical with a global

* Corresponding author.
E-mail address: jan.mennigen@uottawa.ca (J.A. Mennigen).

https://doi.org/10.1016/j.chemosphere.2020.127080
0045-6535/

annual production volume of 9 million tonnes due to its wide use as a precursor in the fabrication of important plastics (Corrales et al., 2015; Gerona et al., 2020). Because of its high production volume, BPA is frequently detected in environments as well as wildlife and humans (Corrales et al., 2015; Gerona et al., 2020). To date, BPA is one of the most studied endocrine disrupting chemicals (EDCs) with well-described estrogenic effects affecting development of the adult reproductive phenotype (Howdeshell et al., 1999). Indeed, BPA exposure has raised concerns because of described developmental effects of BPA at concentrations below published regulatory limits, which has led to banning of BPA from infant plastic bottles in several countries (Onghena et al., 2014; Beal, 2018). In addition to early reports of effects of developmental BPA exposure on body weight in rodents (Howdeshell et al., 1999; Vom Saal et al., 2012), experimental evidence from rodent models as well as epidemiological evidence from human cohorts suggest wide-spread metabolism-disrupting effects of BPA, encompassing organizational as well as acute effects in central and peripheral regulation of organismal energy balance (Mackay et al., 2013; Ke et al., 2016; Stahlhut et al., 2018; Desai et al., 2018). Thus, given the well-described role of estrogen in the regulation of organismal energy balance (Mauvais-Jarvis et al., 2013), it has been postulated that BPA may act as metabolic disruptor via estrogenic signalling pathways (Vom Saal et al., 2012). (see Table 1)

In recent years, zebrafish are increasingly used as models for (estrogenic) EDCs (Segner, 2009), ecotoxicology (Dai et al., 2014) and human metabolic disease (Seth et al., 2013), as they allow for combining high-throughput organismal level metabolic phenotypization approaches with genetic and developmental tools available in zebrafish (Horzmann and Freeman, 2018). Here we take advantage of the zebrafish model to investigate the hypotheses that 1) developmental exposure to BPA in zebrafish alters the metabolic phenotype acutely 2) that developmental exposure to BPA alters developmental trajectories of metabolic phenotype emergence at baseline or in response to a subsequent metabolic challenge and 3) that metabolic effects of BPA in zebrafish are mediated by an estrogenic mode of action.

2. Materials and methods

2.1. BPA and EE_2 stock preparation and eleutheroembryo exposure

Bisphenol A (BPA, CAS-RN: 80-05-7, ≥99.0% purity) and 17α-ethynylestradiol (EE_2, CAS-RN: 57-63-6, ≥98.0% purity) were provided by Sigma-Aldrich (St. Louis, MO, USA). Stock solutions were prepared in DMSO and stored at 4 °C. Exposure solutions were prepared daily by dilution of stock solutions in system water with final DMSO concentration of 0.2% (*v*/*v*). Approximately 400 individuals were exposed in each treatment group (DMSO vehicle control, 0.1, 1.0 and 4.0 mg/L of BPA and 10 ng/L of EE_2) in eight replicate Petri dishes from 2 to 5 dpf, after which the larvae were raised in clean system water. In a recent global assessment of BPA concentrations in the environment, aquatic BPA concentrations up to 56 μg/L BPA have been reported in surface waters, while wastewater treatment plant (WWTP) effluent concentrations reached BPA concentrations up to 370 μg/L (Corrales et al., 2015). While the lowest BPA concentration of 0.1 mg/L used in our study therefore falls within the range of concentrations observed aquatic environments, it is to be noted that this reflects a high environmental concentration, as most BPA concentrations reported in surface waters and WWTP effluent are below 5 μg/L (Corrales et al., 2015). The remaining BPA concentrations used in our study (1 mg/L and 4 mg/L BPA lie in the same range as BPA concentrations reported from specific point sources, such as landfill leachates (Flint et al., 2012; Canesi and Fabbri, 2015). EE_2 was chosen as a positive estrogenic control to differentiate estrogenic effects of BPA from effects linked to non-estrogenic pathways, as it has been shown to exert its estrogenic effects at 10 ng/L in early stages of zebrafish individuals (Flint et al., 2012; Canesi and Fabbri, 2015; Thorpe et al., 2003). EE_2 is a highly potent and selective agonist of estrogen receptor in fish, exhibiting higher potency than the natural ligand estradiol (E_2) (Thorpe et al., 2003; Brion et al., 2012). Indeed, the 10 ng/L of EE_2 concentration used in our study represents a 5 fold higher concentration than the EE_2 estrogenic EC_{50} assessed in a transgenic zebrafish *cyp19a1b* GFP-based reporter assay (Brion et al., 2012), but falls well below (10-fold) EE_2 concentrations triggering adverse developmental effects on hatching in this model (Versonnen and Janssen, 2004). EE_2 is, in its own right, a pharmaceutical of concern in aquatic environments, with reported WWTP effluent concentrations up to 67 ng/L (Aris et al., 2014) and river water concentrations up to 15 ng/L (Shved et al., 2008). Therefore, in addition to serving as positive estrogenic control, EE_2, at the chosen concentration of 10 ng/L, also lies within an environmentally relevant range, allowing for an assessment of metabolic effects following developmental exposure to this aquatic contaminant. Finally, exposure concentrations of BPA and EE_2 and exposure duration replicate previously published studies in early developing zebrafish (Martínez et al., 2018, 2019a), allowing for better comparison.

Exposures started at 2 dpf to avoid potential effects of BPA and EE_2 on very early embryonic development (Tse et al., 2013), and to focus the study on effects on the already differentiated tissues of the larvae. From 6 dpf until the end of the study, larvae were fed twice daily with GEMMA Micro 75 food (Skretting, NB, Canada). From 30 dpf on, zebrafish of each treatment group were split in two subgroups and fed twice daily (normal diet, ND) or four times daily (high feeding diet, HFD) until the end of the study. Developmental stages of zebrafish described in this study are classified as embryonic (0–3 dpf), eleutheroembryonic (3–6 dpf), larval (6–30 dpf) and juvenile stages (>30dpf). All procedures performed in this study followed the guidelines of the Canadian Council on Animal Care (CCAC) for the use of animals in research approved by the University of Ottawa Animal Care Protocol Review Committee under protocol BL-3057.

2.2. Organismal-level metabolic phenotypization

2.2.1. Energy expenditure assay

A zebrafish energy expenditure assay was performed as previously described (Williams and Renquist, 2016; Reid et al., 2018; Tu et al., 2019). Briefly, zebrafish eleutheroembryos and juveniles were placed in 96- or 24-multiwell plates with 200 μL or 1.3 mL of Alamar Blue stock solution (AlamarBlue™ Cell Viability Reagent, Life Technologies, Eugene, OR, USA) per well, and fluorescence emission was measured over time to quantify cumulative $NADH_2$/$NADPH_2$ production as approximate measure of zebrafish oxidative metabolism (Williams and Renquist, 2016; Reid et al., 2018). Alamar Blue solution fluorescence was measured at 0, 24 and 48 h using a SpectraMax Gemini™ fluorescence reader (Molecular Devices, San Jose, CA, USA) with excitation and emission wavelengths of 530 and 590 nm, respectively.

2.3. Locomotor behaviour test

The locomotor behaviour of eleutheroembryos (5 dpf) and juveniles (43 dpf) were assessed in a 48 or 24-multiwell plate using ZebraBox® instrument (ViewPoint Life Science, Montreal, QC, Canada). Zebrafish were first incubated for 30–60 min to reduce sampling stress and then exposed to instantaneous 100% light/dark intensity changes with the following pattern (times in min, L, light,

Table 1
Related pathways and/or functions of the measured transcripts; primer sequences and SYBR-Green™-based real-time RT-PCR assay conditions used to quantify their relative abundance changes.

mRNA	Description	Related pathway/function	Efficiency (%)	R (Gerona et al., 2020)	Annealing Temp. (°C)	Amplicon size (nt)	Accesion Nº	Primer FW	Primer RV
ago2	argonaute RISC catalytic component 2	miRNA and pre-miRNA binding activity, pre-miRNA processing, RISC complex	105.2	0.980	60.0	144	XM_009294368.3	TGTCGTTGGCAGTATGGATG	GGTTTGAAGCGTGTGGATTT
aldh9a1b	aldehyde dehydrogenase 9 family, member A1b	NAD^+/NADH homeostasis	101.6	0.993	61.5	221	NM_201508.1	AGTGCTTTGTGGAGGAGAGC	TGGTAAAGACTCCTGCAGCG
apoa1a	apolipoprotein A-Ia	Lipid transport and homeostasis, lipoproteins, cholesterol binding and transfer activity	98.4	0.994	55.0	248	NM_131128.1	GAAGGCCTTCGAGTCCAACA	TCTGTGCGAATGTGGTCCTC
apoba	apolipoprotein Ba	Lipid and cholesterol transport, triglyceride mobilization	92.8	0.994	57.0	248	XM_689735.9	AGCTGAAGAACGCACTCTCC	GAACTTCAGGGCCGCATCTA
apobb.1	apolipoprotein Bb, tandem duplicate 1	Lipid transport and cellular response to xenobiotics	97.0	0.998	60.0	216	NM_001030062.1	TGGACATCGAAGCCAATGGA	GATCCCCATCCATCATGCCA
apoc2	apolipoprotein C-II	Lipoprotein catabolic process, chylomicrons, hemopoiesis	99.0	0.994	61.0	210	NM_001326448	GGAGAGCTTTCGTGTTCCCA	TCTTGAAAGATGCCGGCGTA
atp6v1ba	ATPase, H+ transporting, lysosomal, V1 subunit B, member a	ATP binding activity and ATP metabolic process, proton transmembrane transport	94.8	0.988	55.0	237	NM_182878.1	CATTGTCCCTCGTTGTTGTG	AGTTGTGCGCTTGTTGAATG
cnn3a	calponin 3, acidic a	Actin binding activity, actomyosin structure organisation, muscle contraction	96.3	0.984	59.0	239	NM_199753.1	GAGTACCAGGGCGAATACCA	TGACCGCATGGTTAGACAGA
cyp19a1b	cytochrome P450, family 19, subfamily A, polypeptide 1b	Estrogenicity, estradiol biosynthesis	96.2	0.991	53.0	181	NM_131642.2	GCAAAGGGGACAAACCTAATC	CCTTCGTCATCACCATAGCA
drosha	drosha ribonuclease III	miRNA biogenesis, angiogenesis, pri-miRNAs processing	92.3	0.985	60.0	153	NM_001110472.1	GGCAGAAATACGCTGAGGAG	GAGCAGGTCGGATACCAAAA
g6pca.2	glucose-6-phosphatase a, catalytic subunit, tandem duplicate 2	Gluconeogenesis, carbohydrate biosynthesis	99.5	0.993	61.0	111	NM_001163806.1	TCTGCATGAAAAGGTCTGGCT	ACACATCTTAGGGAGGGCAAA
gpib	glucose-6-phosphate isomerase b	Gluconeogenesis and glycolytic processes	98.3	0.998	61.0	254	NM_144764.2	CCGCACAAAGTTTTCCAGGG	AAGTTGATGAGGCCGTTGGT
hkdc1	hexokinase domain containing 1	Fructo-, gluco-, and manno-kinase activity, glucose homeostasis and glycolytic process	100.7	0.997	62.0	132	NM_001115125.1	TTCCAGTTGAAGCGGTGGTT	CCCTTCGAAGTAGCCGGTTT
pfkma	phosphofructokinase, muscle a	Canonical glycolysis	92.6	0.994	57.5	206	NM_001004575.2	CCCAGACTCTGCATGTGTGT	TGCTGACAACGTGCTCCATT
pfn2l	Pfn2l)	Actin binding activity, actin filament polymerization	94.7	0.985	60.0	164	NM_201466.2	ATGGAGGATCGCTCAACAAG	ACTAAAGGGGGCAAGGAAGA
pgam2	phosphoglycerate mutase 2 (muscle)	Myoblast fusion, musculature system	100.7	0.995	59.0	167	NM_201024.1	AGCCAAACATGGAGAGGAGC	TGGTGTCCTTCAAGCTCTCG
pomca	proopiomelanocortin a	Organismal response to stress, cortisol, stem cell differentiation	91.2	0.982	54.0	192	NM_181438.3	GCCCCTGAACAGATAGAGCC	CTCGTTATTTGCCAGCTCGC
pomcb	proopiomelanocortin b	Organismal response to stress, cortisol, stem cell differentiation	93.5	0.981	54.0	121	NM_001083051.1	TCCATCGAGCTCCAAAACCC	ACACTTTTACCGGTCTGCGT

D, darkness): 20L-5D-5L-5D-5L-5D-5L. The Viewpoint Zebralab® v3 quantization software was used to track the individual's movements and to perform the automated behavioural analysis to obtain the movement time and distance of a given larvae within three defined movement ranges (inactivity (<3 mm/s), small- (3–6 mm/s), and large- (6 mm/s) movements). The number of times that an individual transferred from one assigned movement range to another was also recorded.

2.3.1. Birefringence assay

To assess muscle sarcomere morphology in 5 dpf eleutheroembryos (n = 5 per treatment group), a birefringence assay was used as previously described (Berger et al., 2012; Smith et al., 2013). Briefly, 5–6 embryos of each treatment group were placed on a dissecting microscope (Olympus SZ61, Olympus Canada, Richmond Hill, ON, Canada) and an image obtained using a Lumenera Infinity 2 camera and Infinity Capture software (Teledyne Lumenera, Ottawa, ON, Canada) to measure animal surface. A subsequent second picture of the eleutheroembryos was taken immediately afterwards using two perpendicularly placed 77 mm circular polarizing lenses (77 mm circular polarizing lens (Amazon Basics, Amazon, Seattle, USA) to visualize and image birefringence created by sarcomeres. Care was taken to maintain eleutheroembryo position. Birefringence intensity was quantified using ImageJ software and normalized by larval surface area.

2.3.2. Feed-intake quantification

Feed-intake in 6 and 45 dpf zebrafish was measured as previously described (Tu et al., 2019). Briefly, zebrafish larvae or juveniles were fed *ad-libitum* with fluorescently labelled (4-(4-(didecylamino)styryl)-N-methylpyridinium iodide, Sigma-Aldrich, Canada) GEMMA Micro 75 food (Skretting, Saint Andrews Parish, NB, Canada). After a 1 h feeding period in darkness, individuals were collected, washed and homogenized in 300 μL of distilled water. 250 μL of each sample homogenate was transferred to a black 96-multiwell plate and the fluorescence was measured in a SpectraMax Gemini™ fluorescence reader (Molecular Devices, USA). Excitation and emission wavelengths (λ_{exc}, λ_{em}) were 485 nm and 535 nm, respectively. Zebrafish fed with unlabelled food were used in assays to obtain background fluorescence values used to normalize fluorescence readings.

2.3.3. Morphometric measurements

At 29 and 45 dpf, zebrafish were anesthetized with tricaine, slightly dried, weighed to determine body weight (BW), and body length (BL) measured by following the notochord of laterally positioned individuals on acquired images, and subsequently allowed to recover in an anesthetic-free system water filled tank. Individual body mass index (BMI) was calculated dividing its BW by the cube value of its BL.

2.3.4. Fluorescence imaging of neutral lipid deposition

Neutral lipid deposition was labelled and measured by Nile Red fluorophore (Minchin and Rawls, 2017). At 48 dpf, four juvenile zebrafish from each treatment group were placed in 5 mg/L Nile Red exposure solution for 30 min at 28.5 °C in darkness. Afterwards, individuals were rinsed twice with system water, anesthetized with tricaine and placed under a Nikon SMZ 1500 to obtaining capture images of the stained neutral lipids using the NIS Elements F software (Mississauga, ON, Canada). Fluorescence quantification was performed using ImageJ (National Institutes of Health, Bethesda, MD, USA).

2.4. Molecular profiling

2.4.1. Relative mRNA transcript quantification

Total RNA was extracted using the Trizol method following the manufacturer's protocol (Invitrogen, Oakville, ON, Canada) and retrotranscribed with the QuantiTech Reverse Transcription Kit (Qiagen, Toronto, ON, Canada) following the manufacturer's protocol. A negative control (noRT) was also generated to confirm the absence of genomic DNA. qRT-PCR reactions were performed in a CFX96 PCR instrument (Bio-Rad, Mississauga, ON, Canada) using the iTaq Universal SYBR Green Supermix (Bio-Rad Laboratories, Mississauga, ON, Canada). Relative changes in mRNA abundance of brain aromatase (*cyp19a1b*) was measured as a molecular marker of estrogenicity in larval zebrafish. In order to assess metabolic consequences of developmental BPA exposure at the molecular level, relative transcript abundance of transcripts involved in (glucose and lipid-dependent) energy metabolism were quantified, as these molecular metabolic pathways have been described as being disrupted at the transcript-level in acute exposure studies using mammalian models (Mackay et al., 2013; Chevalier et al., 2015; Marmugi et al., 2014; Tudurí et al., 2018; Shu et al., 2019). More specifically, several of the selected transcripts within these pathways also have well-described functions in energy metabolism by affecting central regulation of energy balance (proopiomelanocortins *pomca* and *pomcb*) (Löhr et al., 2018), lipid transport (apolipoproteins (*apo1a*; *apoba*; *apobb1*; *apoc2*) (Otis et al., 2015, 2019; Quinlivan and Farber, 2017), glycolysis (hexokinase domain containing 1 (*hkdc1*), glucose-6-phosphate isomerase b (*gpib*), phosphofructokinase muscle a (*pfkma*); phosphoglycerate mutase 2 muscle (*pgam2*) (Tixier et al., 2013; Lin et al., 2009; van Steijn et al., 2019), and gluconeogenesis (glucose-6-phosphatase (*gpca2*), NAD+/NADH homeostasis (aldehyde dehydrogenase 9 family, member A1b (*aldh9a1b*), and had previously been identified as candidate BPA responsive genes in developing zebrafish using a transcriptome-level screen using the same experimental design 24, thus allowing to not only validate, but also to assess the robustness of specific metabolic transcript changes across laboratories in this model. Finally, given the importance of miRNAs in teleost metabolic tissue differentiation and energy metabolism (Mennigen, 2016), transcripts of genes involved in canonical miRNA biogenesis (drosha ribonuclease 3 (*drosha*); argonaute 2 (*ago2*)) and tissue-specific miRNAs (see section below) were additionally quantified. Indeed, if and how developmental BPA exposure affects miRNA biogenesis and/or the expression of metabolic tissue-specific miRNAs is largely unknown and has not been characterized in non-mammalian species. Following the identification of a robust downregulation of muscle-specific miRNA-1, we secondarily decided to profile zebrafish validated *miR-1* target gene expression (calponin 3, acidic a (*cnn3a*); profilin 2 like (*pfn2l*), ATPase, H+ transporting, lysosomal, V1 subunit B, member a (*atp6v1ba*) all of which have been implicated in zebrafish muscle development (Mishima et al., 2009). Functions and/or related pathways of each transcript, and their specific primer sequences, efficiency and calibration curve correlation coefficients can be found in Table T1. Gene expression data were normalized using the NORMA-Gene approach as described by Heckmann et al. (2011).

2.4.2. Relative quantification of miRNAs

Reverse transcription of miRNAs was performed with the extracted total RNA using the miScript II reverse transcription kit (Qiagen, Toronto, ON, Canada) following the manufacturer's protocol. A RT-negative control was included. The specific miRNAs were quantified using the miRScript SYBR Green PCR kit (Qiagen, Toronto, ON, Canada) with miRNA-specific forward primers and a universal reverse primer (**Supplemental File SF1**). In order to

identify miRNAs that could be involved in the inhibition of the expression of genes related to lipid transport and glycolysis and gluconeogenesis pathways, zebrafish TargetScan algorithm (http://www.targetscan.org/fish_62/) was used to predict those miRNAs able to bind the 3′UTR of the above mentioned genes. miRNAs with higher scores in the prediction were selected for quantification (**Supplemental File SF2**). Additionally, we measured the expression of several metabolic tissue-specific miRNAs to monitor potential direct effects of BPA on zebrafish tissues with particular importance for energy metabolism: *miR-1* and *miR-133* for the skeletal muscle (Mishima et al., 2009), *miR-122* for the liver (Jopling, 2012) and *miR-375* for pancreas (Kloosterman et al., 2007). Relative fold changes in miRNA abundances were normalized using the NORMA-Gene approach as described by Heckmann et al. (2011).

2.5. In silico analysis of BPA and EE_2 molecular docking in zebrafish

To further assess potential differences in BPA and EE_2 estrogenicity, and to explore both compounds possible interactions with non-estrogenic receptors in the zebrafish model (estrogen-related receptor gamma (*esrrg*), molecular docking analyses were performed to investigate binding affinities *in silico*. The three-dimensional structures of zebrafish *essrg a* and *b* (*esrrga*/*esrrgb*; UniProtKB entries Q6Q6F4/Q5RJ38) and estrogen receptor 1 (*esr1*; UniProtKB entry P57717) were built by homology modelling strategy (PDB IDs 2GPU and 3ERT, respectively) using Modeller 9.14 software (Eswar et al., 2006). Docked active sites were defined as the ligand location of the template proteins and BPA and EE_2 were docked into them using AutoDock Vina (Trott and Olson, 2010). AutoDock Tools 1.5.6 package was used for generating the docking input files and the identification of the grid center. The superior pose with the lowest docked energy was selected and visually analyzed by Discovery Studio Visualizer 4.5 (San Diego, CA, USA).

2.6. Statistical analysis

All statistical analyses and the associated graphs were performed with the software GraphPad Prism version 8.1.2 (GraphPad Software, San Diego, California USA, www.graphpad.com). Partition around medoids (PAM) clustering analyses (Jin et al., 2010; Van der Laan et al., 2003) were performed for the transcripts and miRNAs datasets as well as partial least squares (PLS) regression analyses (Handbook of Partial Least, 2825; Helland, 1990). A principal component analysis (PCA) (Wold et al., 1987; Abdi and Williams, 2010) was performed integrating within-individual measurements at both ages (4–6 dpf and 43–49 dpf). PAM clustering, PLS and PCA analyses and their associated graphs as well as heatmaps were generated using the packages *gplots*, *ggplot2*, *fpc*, *cluster*, *factoextra*, *FactoMineR*, *stats*, *corrplot* and *fmsb* in R (R Development Core Team, 2008; Hennig, 2014; Warneset al., 2015; Maechleret al., 2019; Kassambara and Mundt, 2017; Lê et al., 2008; Mevik and Wehrens, 2015; Wickham, 2011; Nakazawa, 2018; Wei et al., 2017).

3. Results

3.1. BPA exposure acutely modulates the metabolic phenotype in eleutheroembryonic and larval zebrafish

3.1.1. Organism-level effects

3.1.1.1. Acute BPA exposure reduces feed intake and increases oxidative metabolism-related energy expenditure. Acute BPA exposure resulted in a dose-dependent reduction in feed intake in 6 dpf larvae treated with 4 mg/L of BPA compared to control (Fig. 1A; $p < 0.05$). No significant decrease in feed-intake was observed in the EE_2 treated group compared to control. Conversely, larvae exposed to either 1.0 or 4.0 mg/L of BPA, but not EE_2 increased their oxidative metabolism-related energy expenditure compared to the control (Fig. 1B; $p < 0.05$). Both feed intake and energy expenditure of control and BPA exposed zebrafish individuals (5–6 dpf) were not only linearly correlated with each other (Fig. 1C; $p = 0.016$), but also with increasing BPA exposure concentrations (**Supplemental File SF3A-B**; $p = 0.047$ and $p = 0.015$, respectively). As can be observed, individuals exposed to EE_2 did not follow this BPA concentration-dependent correlation.

3.2. BPA and EE_2 exposure reduce eleutheroembryo locomotion

Exposure to BPA and EE_2 decreased the total distance that 5 dpf eleutheroembryos moved during light and dark periods in the behavioural testing (Fig. 1D). While exposure to the lowest dose of BPA (0.1 mg/L) did not significantly change the total distance travelled by eleutheroembryos compared to the control group under light or dark conditions, 1.0 and 4.0 mg/L of BPA significantly decreased the total distance. Exposure to increasing BPA concentrations were only correlated with the observed decrease in swimming distance in the dark period (**Supplemental File SF3D**; 2° order polynomial, $p = 0.038$). Individuals exposed to 10 ng/L of EE_2 exhibited significantly decreased movement only during the dark periods.

3.2.1. Molecular-level effects

3.2.1.1. Molecular profiling of mRNA and miRNA transcripts reveals distinct clusters for exposure groups. PAM clustering analysis of mRNAs and miRNA expression in 5 dpf eleutheroembryos classified the replicates into three different expression clusters (Fig. 2A). Cluster A was characterized by slight or no changes in the expression of most genes and miRNAs. Both clusters B and C showed a high increase in the expression of *cyp19a1b*. Cluster B was additionally characterized by low expression of *ago2*, *atp6v1ba*, *g6pca.2*, *cnn3a1*, *drosha*, *pfkma*, *pgam2*, *gpib*, *miR-142a-3p* and *miR-1*, and high expression of *apoa1a* and *apoba*. Cluster C was characterized by low expression of *ago2*, *g6pca.2*, *atp6vba*, *pomca* and *miR-1*. Analysis of the data by hierarchical clustering closely reflected the experimental setup: All control, 0.1 mg/L BPA and 1.0 mg/L BPA exposure group replicates were represented in cluster A, all 4.0 mg/L of BPA exposure group replicates in cluster B, and all 10 ng/L EE_2 exposure group replicates were classified in cluster C (Fig. 2A and B). The specific clusters identified by PAM analysis effectively allow to separate cluster B from clusters A and C (Fig. 2C). Individual bar plots of mRNA and miRNAs expression profiles are reported in **Supplemental File SF4A** and **B**, respectively. Exposure to BPA reduced expression of *gpib*, *pgam2*, *ago2*, *drosha*, *atp6v1ba*, and *miR-1* and increased expression of *apoa1a*, *apoba*, *hkdc1*, *cyp19a1b* and *miR-23b*. Exposure to EE_2 reduced the expression of *ago2*, *atp6v1ba*, *g6pca.2*, *pomca* and *miR-1*, and increased the expression of *cyp19a1b*, *miR-122* and *miR-142a-5p*. Differential effects of BPA and EE_2 on mRNA and miRNA transcripts are reflected in the performed partial least square (PLS) analysis (**Supplemental File SF5A-C**). Gene expression profiling not only allows for a dose-dependent separation of BPA exposed groups from controls (component 1), but also reveals a separation of EE_2 exposed animals from other treatment groups (component 2).

3.3. Transient and persistent metabolic effects of developmental BPA and EE_2 exposures in juvenile zebrafish and responses to nutritional challenge

3.3.1. Organism-level effects

3.3.1.1. Developmental BPA exposure increases body weight and body mass index in 29 dpf juveniles. Juveniles which had been

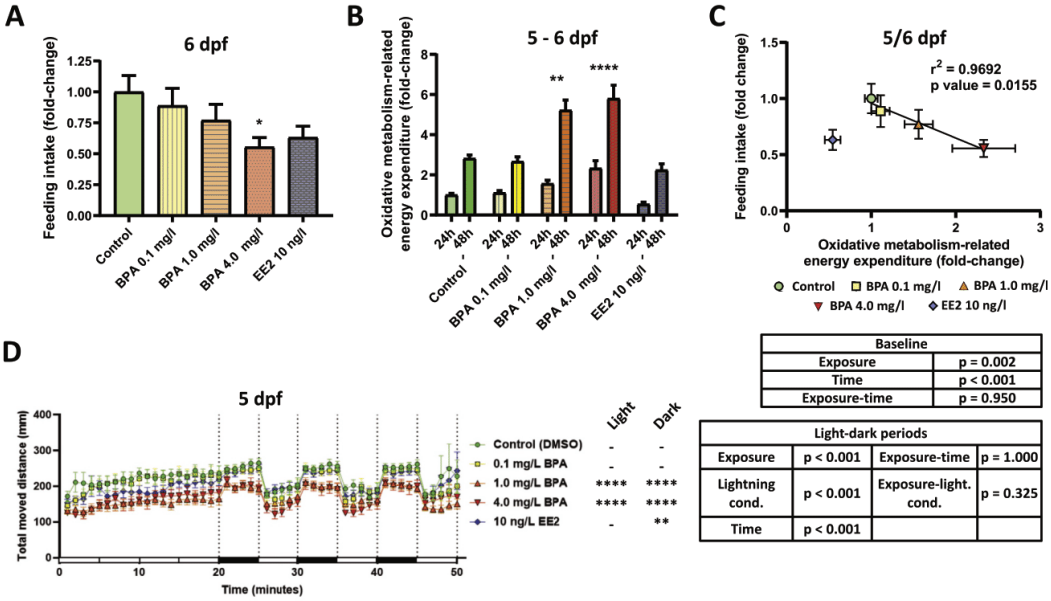

Baseline	
Exposure	p = 0.002
Time	p < 0.001
Exposure-time	p = 0.950

Light-dark periods			
Exposure	p < 0.001	Exposure-time	p = 1.000
Lightning cond.	p < 0.001	Exposure-light. cond.	p = 0.325
Time	p < 0.001		

Fig. 1. Organismal-level metabolic phenotype parameters in eleutheroembryos exposed to negative vehicle control, increasing concentration of BPA and a positive estrogenic control. Mean values and standard errors of the mean (S.E.M.) are shown: (**A**) Feed-intake (fold-change realttive to the control group) of 6 dpf eleutheroembryos. Asterisks represent groups statistically different from the control (ANOVA and Tukey's post-hoc test ($p \leq 0.05$). (**B**) Oxidative metabolism-related energy-expenditure (fold-change relative to control group values at 24 h) measured over 24 and 48 h time periods in 5/6 dpf eleutheroembryos/larvae. Asterisks represent groups statistically different from the control (repeated measurements ANOVA and Tukey's post-hoc test ($p \leq 0.05$)). (**C**) Linear regression between feed-intake and oxidative metabolism related energy expenditure in 5/6 dpf eleutheroembryos. (**D**) Total moved distance (mm) of 5 dpf eleutheroembryos White and black bars in the x-axis reflects light and dark conditions, respectively. Asterisks represent groups statistically different from the control (repeated measurements ANOVA and Tukey's post-hoc test (* for $p \leq 0.05$, ** for $p \leq 0.01$, *** for $p \leq 0.001$, and **** for $p \leq 0.0001$)).

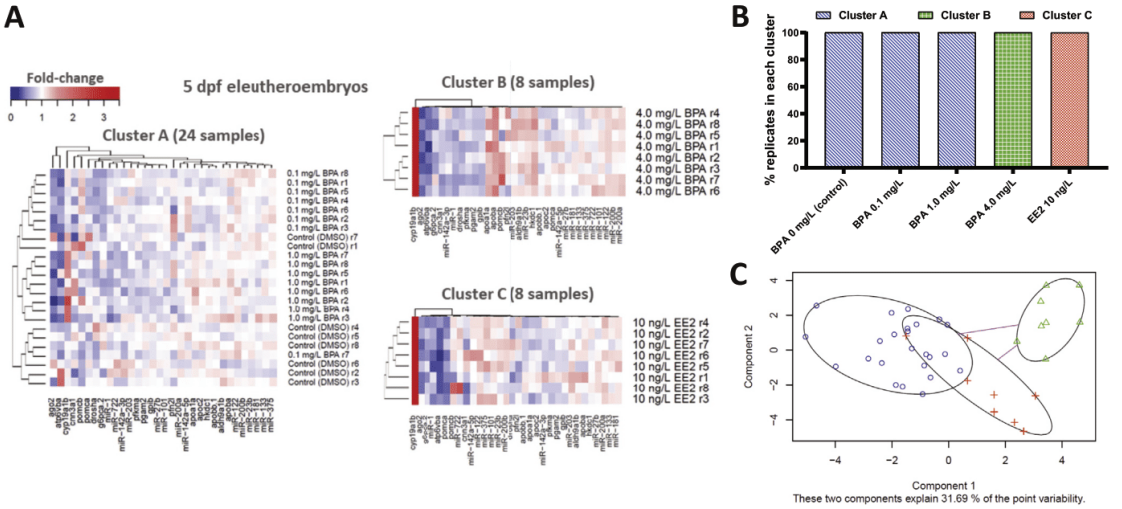

Fig. 2. (**A**) PAM clustering analysis-based heatmaps depicting expression clusters of relative mRNA and miRNA transcript abundance (fold-change values) in 5 dpf eleutheroembryos exposed to vehicle control, different concentrations of BPA or a positive estrogenic control. Higher or lower abundance (relative to control group) are indicated in red and blue, respectively. (**B**) Percentage of replicates within each experimental group classified in each cluster. (**C**) PAM clustering analysis results show two components which explain 31.69% of the variability. Transcripts classified in cluster A, B and C are represented by blue circles, green triangles and red crosses, respectively. (For interpretation of the references to colour in this figure legend, the reader is referred to the Web version of this article.)

developmentally exposed to BPA exhibited a significant increase in body weight compared to the control group at 29 dpf, irrespective of BPA exposure concentration (Fig. 3A). Individuals which had developmentally been exposed to EE_2 did not exhibit significant changes in body weight compared to either control groups. No significant difference in body length (BL) was identified between treatment groups (Fig. 3A). Body mass index (BMI) increased significantly only in individuals which had developmentally been exposed to 1 and 4.0 mg/L of BPA compared to control, while the BMI in EE_2 exposed fish was not significantly different from control group fish (Fig. 3A).

3.3.1.2. Developmental BPA or EE_2 exposure do not affect morphometric parameters in 45 dpf juveniles under different dietary regimes. The 14 d nutritional challenge (doubling of feeding) resulted in significant increases in BW, BL and BMI compared to fish maintained on a continuation of their regular dietary regime ($p < 0.0001$ in all cases, Fig. 3B). In 45 dpf juveniles neither an overall effect of developmental exposure, nor an interaction between developmental exposure and dietary regime were observed (Fig. 3B). No significant mortality was observed during the nutritional challenge (**Supplemental File SF6**), and juvenile zebrafish followed a common growth pattern ($BW = a \cdot BL^b$; $b = 3.26$), irrespective of developmental exposure in both dietary treatment groups (**Supplemental File SF7**).

3.3.1.3. Developmental BPA or EE_2 exposures do not affect feed-intake or oxidative metabolism-related energy expenditure in 45 dpf juveniles under different dietary regimes. Neither developmental exposure to BPA or EE_2 by itself ($p > 0.05$) nor developmental exposure in interaction with diet ($p > 0.05$) had any significant effect on juvenile feed-intake or oxidative metabolism related energy expenditure (Fig. 4A and B). As expected, in juveniles (45–48 dpf), significant increases in feed-intake and oxidative metabolism-related energy expenditure were observed in fish maintained on HFD compared to fish on the ND regime ($p < 0.05$). As in 5 dpf eleutheroembryos, a strong linear correlation ($p = 0.0001$) between the feed-intake and oxidative metabolism-related energy expenditure was evident in 45–47 dpf developmentally unexposed control and BPA exposed groups, but not EE_2 exposed groups (Fig. 4C). In order to account for diet-induced size differences on either parameter, feed-intake and oxidative metabolism-related energy-expenditure data (Fig. 4C) were normalized as previously described (Martínez et al., 2019a). Briefly, linear regressions were performed for the raw fluorescence readings of either dietary treatment control group values (ND and HFD separately) plotted over the body size of the individuals. Using the linear regression equations, theoretical values of feed-intake and oxidative metabolism-related energy expenditure were interpolated from BPA and EE_2 group fluorescence readings in either assay for ND and HFD groups. Finally, the differences between actually measured and interpolated values were calculated and results were centered to the mean of ND and HFD control groups, resulting in a value of 0 for each group. Following normalization, BPA exposed individuals challenged with HFD showed, in contrast to groups fed ND, a tendency for decreased feed intake and oxidative-metabolism related energy expenditure compared to control. Nevertheless, this effect was not significant ($p > 0.05$) and only revealed when the linear correlation was considered ($p = 0.0001$). No significant correlations between developmental BPA exposure concentration and feed-intake or oxidative-metabolism related energy expenditure was identified (**Supplemental File SF8A-D**).

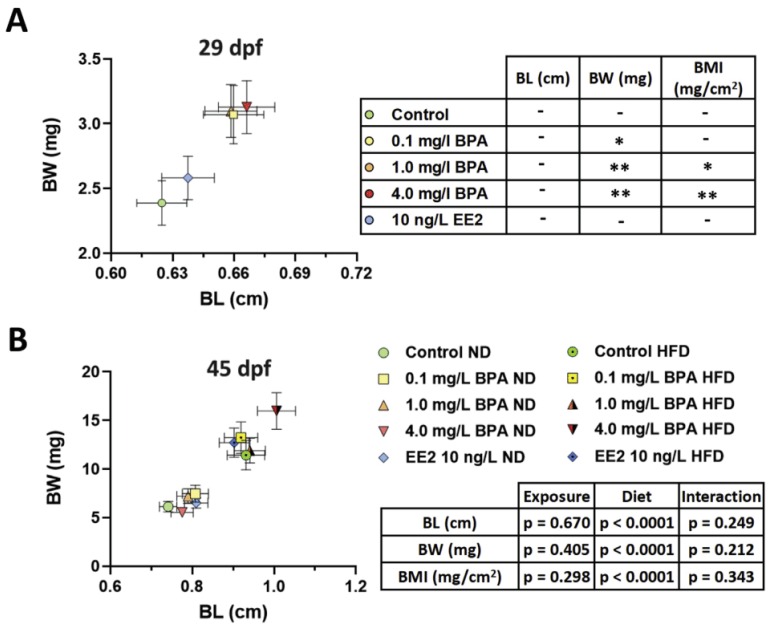

Fig. 3. Two dimensional plots of the body weight (BW) and body length (BL) of 29 dpf zebrafish juveniles (**A**) and 45 dpf juveniles (**B**). Mean values and standard errors of the mean (S.E.M.) are shown for BW and BL. For data obtained from 29 dpf zebrafish, asterisks represent groups statistically different from the control (ANOVA + Tukey's post-hoc test (* for $p \leq 0.05$, ** for $p \leq 0.01$, *** for $p \leq 0.001$, and **** for $p \leq 0.0001$)). For data obtained from 45 dpf zebrafish statistically differences were analyzed by two-way ANOVA to account for developmental exposure history and dietary treatment. P-values for each factor, as well as their interaction are reported, with a significance threshold of $p \leq 0.05$. For both developmental timepoints, body mass index (BMI) values were calculated from BW and BL values of each individual.

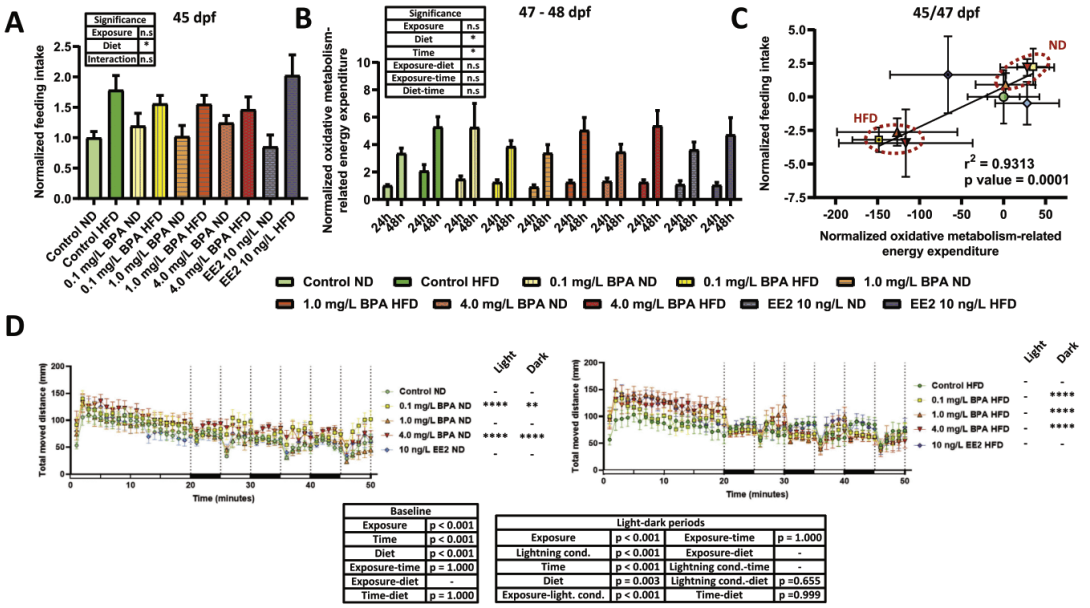

Fig. 4. Organismal-level metabolic phenotype parameters in juvenile zebrafish which had been developmentally exposed to negative vehicle control, different concentration of BPA or a positive estrogenic control. Mean values and standard errors of the mean (S.E.M.) are shown: feed-intake (normalized to the size of each individual and represented as fold-change relative to the ND control group) in 45 dpf juveniles (**A**). Data were analyzed by two-way ANOVA to account for exposure history and dietary groups. p-values for each factor, as well as their interaction are reported, with a significance threshold of $p \leq 0.05$. Normalized oxidative metabolism-related energy-expenditure (normalized to the size of each individual; fold-change relative to the ND control group at 24 h) measured over 24 and 48 h time periods in 47–48 dpf juveniles (**B**). Data were analyzed by three-way ANOVA to account for exposure history, dietary groups and assay length. p-values for each factor, as well as their interaction are reported, with a significance threshold of $p \leq 0.05$. Linear regression between feed-intake and oxidative metabolism related energy expenditure in juvenile zebrafish groups (**C**). In order to account for diet-induced size differences on either parameter, feed-intake and oxidative metabolism-related energy-expenditure data (Fig. 4C) were normalized as previously described 23. Briefly, linear regressions were performed for the raw fluorescence readings of either dietary treatment control group values (ND and HFD separately) plotted over the body size of the individuals. Using the linear regression equations, theoretical values of feed-intake and oxidative metabolism-related energy expenditure were interpolated from BPA and EE2 group fluorescence readings in either assay for ND and HFD groups. Finally, the differences between actually measured and interpolated values were calculated and results were centered to the mean of ND and HFD control groups, resulting in a value of 0 for each group. Total moved distance (mm) of 43 dpf juvenile groups maintained on ND or HFD regimes (**D**). White and black bars in the x-axis reflects light and dark conditions, respectively. Within each diet and light condition, asterisks represent statistically groups statistically different from the control (repeated measurements ANOVA + Tukey's post-hoc test ((* for $p \leq 0.05$, ** for $p \leq 0.01$, *** for $p \leq 0.001$, and **** for $p \leq 0.0001$)).

3.3.1.4. Persistent effects of developmental BPA and EE_2 on juvenile zebrafish locomotion. In 43 dpf juveniles, differences in locomotion parameters could be observed in response to developmental exposure to BPA and EE_2, which were furthermore dependent on diet and lighting conditions: ND-fed individuals exposed to 0.1 and 4.0 mg/L BPA travelled longer distances than the control group ($p < 0.05$), and this effect was significant during light and dark periods (Fig. 4D). Conversely, HFD-fed individuals which had developmentally been exposed to any BPA concentration had a decreased movement rate compared to control group individuals ($p < 0.05$), an effect which was, however, restricted to dark conditions. No significant effect of developmental EE_2 exposure on juvenile locomotion parameters was observed under any condition. No linear correlation between developmental BPA exposure concentration and swimming distance under light or dark periods was observed under ND or HFD, respectively (**Supplemental File SF8E-H**).

3.3.2. Molecular profiling

3.3.2.1. mRNAs and miRNAs expression of ND and HFD juveniles allows different clustering of exposure groups. In 49 dpf juveniles, PAM clustering analysis of the mRNAs classified the samples in three different groups (Fig. 5A). Clustering reflected the experimental setup as follows: ND and HFD control groups were classified mostly in clusters A and B, ND and HFD 0.1 mg/L of BPA were classified in clusters A and B (and partially C for the ND), ND and HFD 1.0 mg/L of BPA were mostly classified in clusters B and C, meanwhile both ND and HFD 4.0 mg/L of BPA replicates were classified all in cluster C (Fig. 5B). EE_2 replicates were classified mostly in cluster C (and some HFD replicates in B). Individual bar plots of the 49 dpf juvenile mRNAs abundances are reported in **Supplemental File SF9**. Exposure to BPA reduced mRNA abundance of *apoa1a, apoba, hkdc1, drosha, atp6v1ba,* and *ago2* within at least one concentration/diet group. Exposure to EE_2 reduced expression of *apoa1a, hkdc1, drosha, atp6v1ba,* and *ago2* in at least one of concentration/diet groups compared to controls).

3.4. Molecular docking analysis of BPA and EE2 with zebrafish estrogen receptors and estrogen-related receptors

Results from our *in silico* molecular docking analysis between BPA and EE_2 and zebrafish estrogen and estrogen-related receptors are visualized in Fig. 6A. Predicted key amino acid residues of ligand-receptor interactions (salt bridges, hydrogen bonds, dipole interactions, van der Waals forces) are visualized in Fig. 6B. Gibbs free energy of binding (ΔG_{bind}) were generally lower (more favorable) for EE_2 compared to BPA (Fig. 6C). Indeed, in the active site of the estrogen receptor (ERα), there were 11 amino acids (Leu^{44}, Met^{47}, Ala^{48}, Glu^{51}, Leu^{82}, Leu^{85}, Leu^{89}, Phe^{102}, Met^{119}, Hie^{222} and Leu^{223}) whose individual interaction with the EE_2 were lower

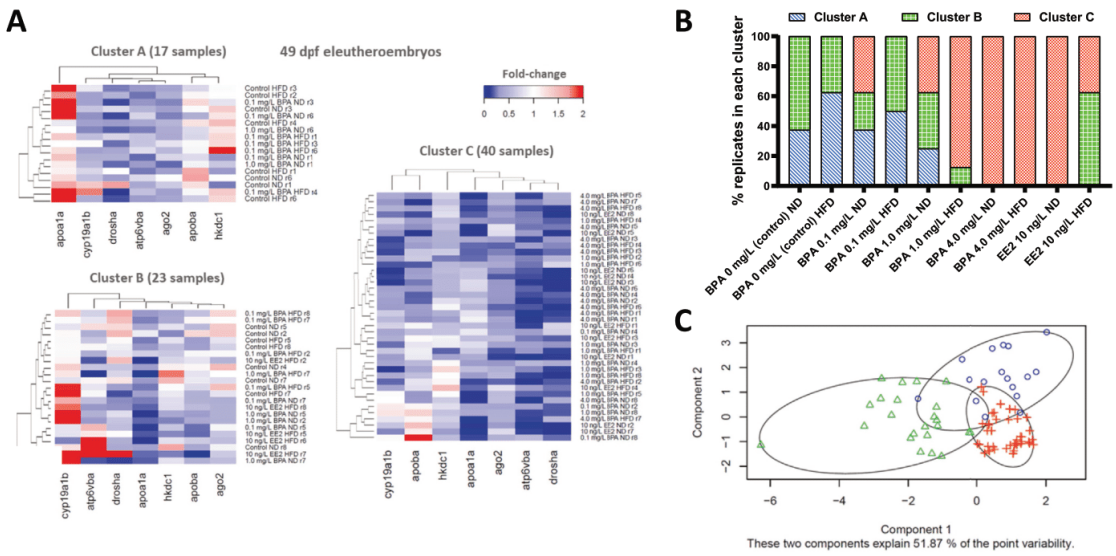

Fig. 5. PAM clustering analysis-based heatmaps depicting expression clusters of relative mRNA and miRNA transcript abundance (fold-change values) in 49 dpf juveniles which had been developmentally exposed to vehicle control, different concentrations of BPA or a positive estrogenic control (**A**). Higher or lower abundance (relative to control group) are indicated in red and blue, respectively. Percentage of replicates within each experimental group classified in each cluster (**B**). PAM clustering analysis results show two components which explain 51.87% of the variability (**C**). Transcripts classified in cluster A, B and C are represented by blue circles, green triangles and red crosses, respectively. (For interpretation of the references to colour in this figure legend, the reader is referred to the Web version of this article.)

than −1.0 kcal/mol meanwhile they were only five in case of the BPA (Leu^{44}, Met^{47}, Ala^{48}, Met^{119} and Leu^{223}). Five amino acids that interacted with BPA also interacted with the EE_2 whose higher affinity for the receptor is determined by additional interactions with other amino acids. Conversely, in case of the estrogen-related receptor gamma a (ESRRga), the affinity of the BPA and EE_2 is approximately the same, characterized by seven main interactions with amino acids for each of them. The amino acid residues Leu^{35}, Leu^{38}, Leu^{76}, Tyr^{93} and Phe^{202} were common for BPA and EE_2 binding. The BPA binding model for ESRRγa is specifically characterized by additionally established interactions with Cys^{36} and Ala^{39}, while the EE_2 binding model for ESRRγa predicts involvement of amino acid residues Met^{73} and Ile^{77}. Finally, in case of the estrogen-related receptor gamma b (ESRRγb), the predicted binding affinity for EE_2 is again higher compared to BPA with eight and three main identified amino acid residue interactions, respectively. Leu^{42}, Ala^{46} and Leu^{83} were the amino acid residues predicted to interacted with both ligands, Glu^{49}, Val^{87}, Phe^{100}, Leu^{116} and Leu^{119} were predicted to additionally interact with EE_2 only (**Supplemental File SF10**).

4. Discussion

4.1. Medium and high BPA as well as EE_2 exposures induce the estrogen-responsive cyp19a1b gene in acutely exposed eleutheroembryos

A strong and significant induction of brain aromatase *cyp19a1b*, a well-characterized molecular marker of estrogenic pathway activity exposure in zebrafish, was observed in zebrafish exposed to 4 mg/L BPA and 10 ng/L EE_2, but not 0.1 mg/L or 1 mg/L BPA, compared to control. The observed relative *cyp19a1b* transcript abundance not only strengthens between laboratory robustness of the observed estrogenic molecular response in eleutheroembryos under this experimental design (Martínez et al., 2018), but importantly validates that estrogenic signalling is activated in eleutheroembryos exposed to 4 mg/L and, to a lesser extent, in eleutheroembryos exposed to the positive estrogenic control (10 ng/L EE_2) in our experiment. The finding that much lower concentrations of EE_2 compared to BPA are sufficient to induce an estrogenic response is in line with previously reported weaker estrogenic activity of BPA compared to EE_2 in zebrafish embryos (Brion et al., 2012; Martínez et al., 2018) which may be linked to reported lower bioconcentration of BPA compared to EE_2 in zebrafish embryos at equal concentrations on the one hand (Wu et al., 2017; Souder and Gorelick, 2018), and the comparatively lower potency of BPA to activate zebrafish nuclear estrogen receptor α (Cosnefroy et al., 2012), which mediates estrogenic regulation of *cyp19a1b* in zebrafish (Cano-Nicolau et al., 2016), on the other. Together, the expression profile indicates the suitability of the experimental design to extrapolate potential estrogenic effects of BPA by dissociating metabolic effects in BPA groups without estrogenic response (0.1 mg/L and 1 mg/L) from metabolic effects in BPA groups with estrogenic response (4 mg/L BPA) as well as the positive estrogenic control group (10 ng/L EE_2).

4.2. BPA and EE2 acute exposures differentially alter eleutheroembryo metabolism at the organismal and molecular level

Acute organismal-level metabolic effects in BPA exposure eleutheroembryos were largely concentration-dependent, reaching significant differences compared to control groups in the high BPA exposure groups. The BPA-induced metabolic effects were not observed in EE_2 exposed animals, suggesting a contribution of non-estrogenic modes of action of BPA to eleutheroembryonic metabolic changes. The overall observed decrease in feed-intake which is inversely correlated increase in oxidative metabolic energy expenditure suggests that BPA, in a dose-dependent manner,

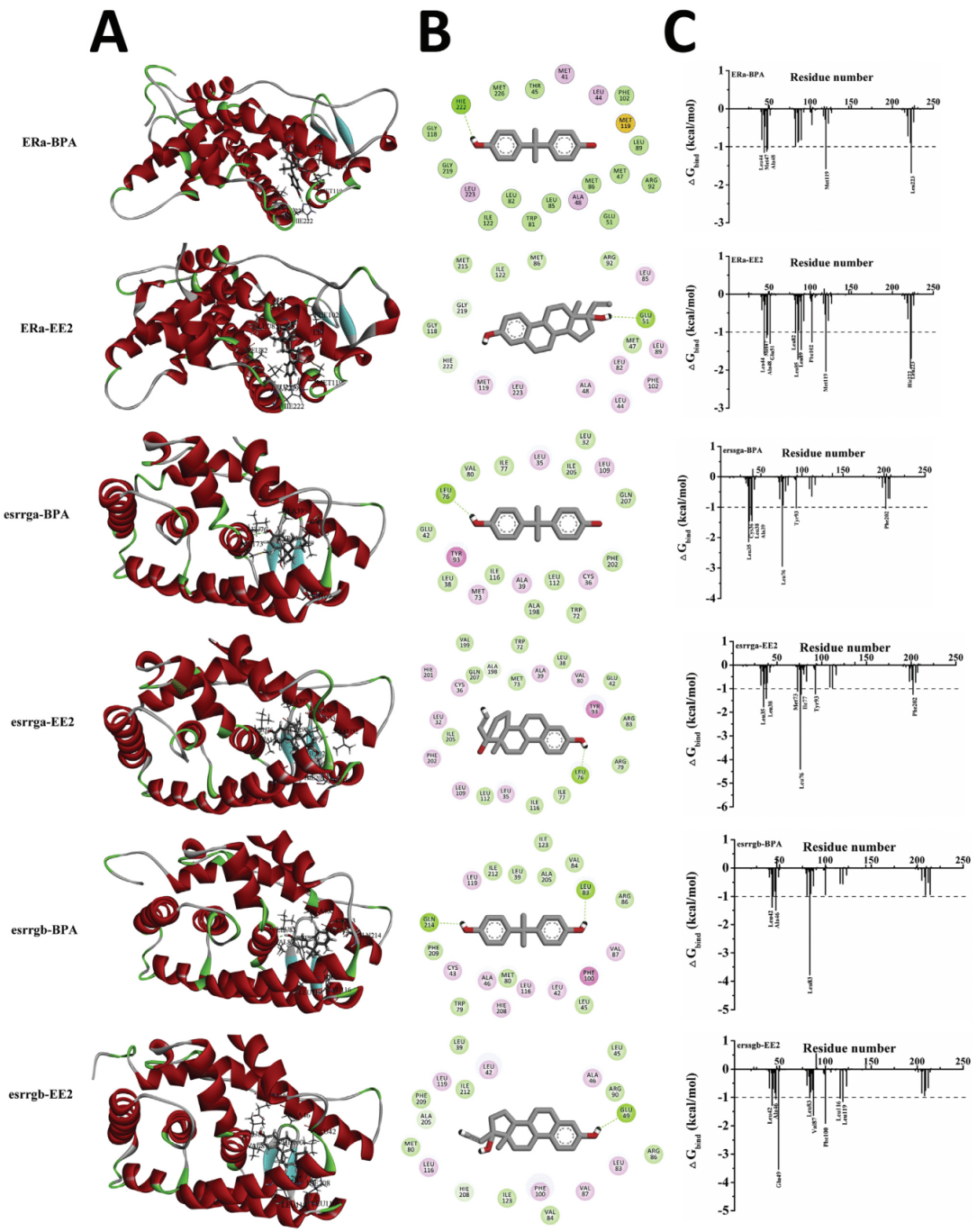

Fig. 6. Molecular docking of BPA and EE_2 with the estrogen receptor α and estrogen-related receptors γa and γb (**A**). Principal interactions of the ligand (BPA or EE_2) with the amino acid residues in the binding site of the receptor (**B**). Gibbs free energy of binding (ΔG_{bind}) per amino acid ordered by its residue number (**C**). Hie refers to histidine neutral ε-protonated.

promotes a negative energy balance in zebrafish exposed within the first week post-fertilization (2–5 dpf), at least in the final stages of yolk-sac resorption (5–6 dpf). It is important to note that the NADH/NADPH-based oxidative metabolism energy expenditure assay used in this study may be affected by additional (non-mitochondrial) cellular components affecting redox state, such as antioxidants (Rampersad, 2012). Because previous studies reported that BPA exposure in eleutheroembryos in the concentration range used in the current study reduced antioxidants (Wu et al., 2011), it is possible that such processes may have contributed to the increase in oxidative metabolism-related energy expenditure observed in BPA treated zebrafish to some extent. With regard to organism-level energy expenditure, we also observed a reduction of locomotor activity, although whether this represents a direct response to a negative energy balance cannot be causally resolved in the current study. It is plausible that the observed acute effects of BPA exposure on organismal energy expenditure are secondary to recently reported modes of action of BPA in developing zebrafish, which affect many components involved in eleutheroembryonic locomotion, such as brain neurogenesis (Kinch et al., 2016), motoneuronal (Morrice et al., 2018) and muscular (Tse et al., 2013; Wang et al., 2013) development. Interestingly, the experimental BPA exposure protocol resulted in a reduced yolk sac resorption (Martínez et al., 2019b), suggesting that metabolic substrate utilization from endogenous and exogenous feeding stages is potentially stage-dependently altered in eleutheroembryos exposed to 4 mg/L BPA.

The profiles of the underlying molecular mechanisms, specifically of protein-coding and non-coding (miRNA) transcripts relevant to energy metabolism in eleutheroembryos, are consistent with the proposed acute and specific metabolism-disrupting effects of BPA. The molecular-level effects in BPA-exposed eleutheroembryos were, once again, largely concentration-dependent, with the strongest effects observed in the highest BPA exposure group, and distinct from EE_2-dependent effects paralleling BPA exposure effects observed at the organismal level. Indeed, both groups with increased expression of the estrogenic marker *cyp19a1b*, 4 mg/L BPA and 10 ng/L EE_2, were characterized by separate expression clusters, while groups which did not display *cyp19a1b* induction compared to control (0.1 mg/L and 1 mg/L BPA) were found in the same expression cluster as the control group. This global pattern is based on changes at the individual gene expression level, as changes in several glucose and lipid metabolism-related transcript expression were specific to the 4 mg/L BPA exposure group. Specifically, eleutheroembryos exposed to 4 mg/L BPA significantly induced apolipoproteins *apoa1a*, *apoba* and the glycolytic enzyme *hkdc1* on the one hand and significantly reduced expression of muscle-specific glycolytic enzmyes glucose *gpib and pgam2* compared to control groups on the other. Interestingly, these targets not only confirm reported expression patterns in a recent transcriptomic screen under parallel exposure conditions in a different zebrafish strain (Martínez et al., 2018), but also point to potential specific metabolism-disrupting effects at the level of the yolk sac, digestive system, liver and muscle. The high-density lipoprotein and chylomicron component *apoa1a* is expressed in eleutheroembryo yolk sacs, intestine and liver, where it is functionally involved in lipid trafficking (Otis et al., 2015, 2019). Similarly, *apoba* is directly linked to microsomal triglyceride transfer protein lipid mobilization from eleutheroembryo yolk sacs (Quinlivan and Farber, 2017). While not measured in the current study, yolk sac dynamics and lipid profiles have indeed been shown to be affected by BPA in acutely exposed eleutheroembryos (Martínez et al., 2019b), suggesting that BPA exerts robust acute effect on eleutheroembryo lipid metabolism. Among BPA-responsive glucose-metabolism targets *hkdc1* are a recently characterized novel fifth hexokinase involved in embryonic whole body glucoregulation by promoting peripheral glucose uptake in mice (Ludvik et al., 2016), while *pgam2* encodes a muscle-specific phosphoglycerate mutase, a glycolytic enzyme linked to muscle development in zebrafish embryos (Tixier et al., 2013). Similarly, *gpib*, a glucosephosphate isomerase paralogue is predominantly expressed in zebrafish eleutheroembryonic muscle (Lin et al., 2009). Therefore, our study provides additional evidence for muscle (energy metabolism)-specific effects of BPA, as recently reported (Carnevali et al., 2019; Ahmed et al., 2020; Moreman et al., 2018).

In addition to these dose-dependent BPA-specific transcript changes, expression changes of components of the canonical miRNA biogenesis pathway was significantly reduced in all treatment groups compared to control. More specifically, the effects on the expression of argonaute protein 2 (*ago2*), a key mediator of the RISC-complex dependent posttranscriptional regulation of mRNAs, suggest that both BPA and EE_2 globally affect embryonic post-transcriptional regulation of gene expression by miRNAs. A similar pattern was observed for *drosha*, the rate-limiting enzyme in miRNA biogenesis (Kim et al., 2016), which exhibited significantly decreased abundance compared to controls, but only in 0.1 mg/L BPA treated eleutheroembryos. Together, these findings led us to investigate regulation of specific miRNAs, which were selected based on their known roles in metabolically important tissue-specific development (Mennigen, 2016), as well as from *in silico* predicted targeting of differentially regulated metabolic protein-coding transcripts. We observed a significant reduction of *miRNA-1* abundance in eleutheromebryos exposed to medium and high concentrations of BPA and EE_2. *miRNA-1* is a muscle-specifically expressed miRNA, which is critically involved in zebrafish muscle development (Mishima et al., 2009). Therefore, the *miRNA-1* expression profile, together with the identified gene expression changes in validated zebrafish *miRNA-1* targets (*pgam2, atp6v1ba*) involved in promoting muscle growth (Mishima et al., 2009) form a molecular expression profile indicative of BPA effects on muscle development. However, neither the birefringence assay to assess eleutheroembryonic muscle structure (Berger et al., 2012; Smith et al., 2013), nor the Seahorse assay to profile embryonic glycolysis via the extracellular acidification rate (ECAR) (Kumar et al., 2016; Bond et al., 2018), revealed significant effects of BPA or EE_2 treatments compared to control (**Supplementary File SF11A-B**), suggesting that in both cases observed molecular level effects do not translate into overt organismal level effects linked to gene-specific functions.

Finally, specific EE_2-dependent transcript responses were identified at the mRNA and miRNA transcript level, exemplified by a significant decrease in proopiomelanocortin b (*pomcb)* compared to control eleutheroembryos. Pomc neurons are, in addition to its role in the endocrine stress axis, critically involved in central feed-intake regulation and have been shown to be supressed by prenatal BPA and estrogen exposure in mice, leading to organizational re-programming of the central feeding circuitry (Mackay et al., 2013). In developing zebrafish, *pomcb* expression is restricted to the hypothalamus and pituitary (Liu et al., 2003), and our study indicates an estrogen-dependent regulation of *pomcb* in early development in zebrafish, also observed in mammalian models (Stincic et al., 2018). However, our study shows that, in contrast to mammals, this effect was neither mimicked by the weaker estrogen BPA, nor did it correlate with observed to acute or long-term feed-intake in zebrafish. It is however possible that hypothalamus-specific regulation of *pomcb* may be masked in whole embryo profiling.

At the miRNA level, we observed the estrogen-specific induction of *miRNA-122*, a liver-specific miRNA involved in zebrafish hepatic

development and lipid metabolism (Laudadio et al., 2012). This effect has been previously observed in adult zebrafish liver (Cohen and Smith, 2014), suggesting that this regulation occurs across different zebrafish life stages. Similar to the situation for muscle-specific *miRNA-1* [43], it is important to bear in mind that our experimental design cannot distinguish between allometric and physiological regulation dependent changes in liver-specific *miRNA-122* transcript abundance in the context of whole eleutheroembryos (Wienholds et al., 2005), and more detailed *in situ* hybridization studies would be necessary to differentiate between these possibilities.

Overall, consistent changes at both organismal and molecular level are clearly indicative of acute metabolic disruption in response to BPA exposure eleutheroembryos, with strong effects observed at the highest BPA exposure levels. These effects are, however, not mimicked by EE_2, as illustrated by integrated analysis of measured parameters, which not only differentiate BPA groups from controls in a dose-dependent manner, but also differentiate the highest BPA group from the positive estrogenic control group, both of which induced estrogenic reporter *cyp19a1b* expression.

4.3. Developmental BPA, but not EE_2 exposure induces significant transient weight gain in zebrafish larvae

At 29 dpf, developing zebrafish larvae exposed to any BPA concentration, but not EE_2 revealed a significant increase in body-weight compared to controls. Without any noticeable changes in standard length, this translated into a dose dependent increase in BMI compared to controls, reaching a significant increase in zebrafish larvae developmentally exposed to 1 and 4 mg/L BPA. These findings show that developmental exposure to BPA at any concentration tested, but not EE_2 increases body weight, indicative of an estrogen-independent mechanism. While not reported for BPA in zebrafish, this phenotype is in line with reported increases in body weight in zebrafish exposed to halogenated BPAs linked to PPARg-dependent increase in neutral lipid storage at 30 dpf (Riu et al., 2014). This finding is also in line with reported transient increase in the condition factor of rainbow trout reared from the highest BPA exposed eggs (nominal exposure 30 μg/mL, measured concentration 40 ng/egg) which was observed at 85 but not 112 dpf (Birceanu et al., 2015). However, it is opposite to reported decreases in body weight in the same species (Aluru et al., 2010). Directional differences in weight change in response to developmental BPA exposure are well-described in mammalian models (Le Corre et al., 2015; Rubin et al., 2009), and may be related to differences in exposures, species, sex or a receptor-based mode(s) of action, which may involve BPA-dependent sensitization to additional positive or negative developmental stimuli affecting subsequent body weight and growth trajectories.

4.4. Developmental BPA and EE_2 exposures differentially and diet-dependently affect locomotion parameters in zebrafish juveniles

Juveniles maintained on ND or HFD showed only few organismal level effects related to developmental BPA exposure. Animals under the HFD showed a significant increase in body weight, body length and BMI, but both parameters appeared unaffected by developmental BPA or EE_2 exposure under both dietary regimes. This suggests that previously observed increases in body weight related to BPA or EE_2 exposure were transitory in nature, and that they may indeed represent a period of compensatory growth, especially given the previously described negative effects on organismal and molecular parameters of energy balance during the acute BPA exposure period in eleutheroembryonic stages. A notable exception to the lack of long-term organism-level metabolic effects in juvenile zebrafish with developmental BPA exposure history is locomotion, which was significantly increased in juveniles with low and high BPA exposure history compared to the control group in light and dark conditions in the ND group, and significantly decreased in all BPA exposure juveniles under dark conditions in the HFD group. These results suggest that developmental BPA exposure consequences on locomotion behaviour are long-lasting, modulated by a nutritional challenge experienced in juveniles and manifest themselves in a light/dark-dependent fashion. Interestingly, recently reported transcriptomic responses in zebrafish eleutheroembryos exposed to the same exposure paradigm as in the current study revealed a significant enrichment for neurological and visual functions (Martínez et al., 2018) in line with recently reported effects of BPA on colour and light preference the same species (Li et al., 2017). Because zebrafish locomotion is an output dependent on multiple systems including sensory perception (The Behavioral Repertoire, 1007), it is feasible that developmental BPA exposure may lead to long-term alterations in sensory perception to affect locomotion. While BPA and estrogen-dependent effects on zebrafish locomotion have been described in response to acute and or chronic exposures across different life-stages in zebrafish (Wang et al., 2013; Li et al., 2017; Saili et al., 2013; Goundadkar and Katti, 2017; Olsvik et al., 2019), this study is, to our knowledge, the first to indicate long-lasting (1.5 mpf) consequences of developmental BPA exposure on zebrafish locomotion. While (estrogen-dependent) zebrafish and teleost neurogenesis is generally considered to be more plastic compared to mammalian model organisms (Diotel et al., 2013), the question of whether developmental BPA exposure has the potential to differentially organize neurocircuitry to mediate such long-lasting effects or whether central sensory or peripheral neuromuscular mechanisms are involved warrants further study. This is especially true in the light of recent finding that developmental exposure of zebrafish to estrogens has the potential to alter estrogen-responsiveness in adult zebrafish (Green et al., 2018). Interestingly, recent evidence does indeed suggest that developmental BPA exposure differentially affects methylated target genes with potential function in neurogenesis (Olsvik et al., 2019), and further longitudinal studies in zebrafish probing epigenetic mechanisms (Best et al., 2018) will likely provide additional insight into molecular underpinnings of the observed long-term effects following developmental BPA exposure on locomotion. In addition to these effects of BPA on zebrafish neurogenesis, high caloric intake in zebrafish has recently been demonstrated to impair neurogenesis in the adult zebrafish brain (Stankiewicz et al., 2019), raising the intriguing possibility that developmental BPA exposure interacts with caloric intake modulation at later life stages to alter neuronal plasticity and subsequent locomotion behaviour. This emerging hypothesis warrants additional rigorous testing in the zebrafish model.

4.5. Developmental BPA and EE2 induce acute and long-term gene expression changes in transcripts involved in energy metabolism and miRNA biogenesis

At the molecular level, lipid- and carbohydrate-metabolism-related gene expression decreased in zebrafish developmentally exposed to 1 mg/L and 4 mg/L BPA and EE_2 with differential effects in normally-fed and over-fed juveniles. While molecular changes in apolipoproteins in particular are indicative of alterations in lipid transport, they did not translate into organism-level effects on stored neutral lipids (**Supplementary File SF11C**). Components of the canonical miRNA biogenesis pathway were significantly reduced compared to control in all zebrafish with developmental BPA and EE_2 exposure history under a regular dietary regime, matching the profile in eleutheroembryos. Because *ago2* is a key

component in mediating miRNA-dependent post-transcriptional repression, possible long-term modulation of this pathway by estrogenic contaminants warrants further study. Collective analysis of protein-coding transcripts revealed a less divergent exposure group-specific cluster differentiation compared to acutely exposed eleutheroembryos, indicating a reduced impact of developmental exposure on metabolic gene expression in zebrafish over time.

4.6. Molecular modelling reinforces contribution of non-estrogenic modes of action of BPA on zebrafish metabolism

Because organismal and molecular level endpoints at different life-stages were appeared to both estrogen-dependent and independent, we used an *in silico* modelling approach to identify potential additional, non-estrogenic molecular modes of action of developmental BPA exposure in the zebrafish model. Indeed, while binding of BPA to zebrafish estrogen receptor α in particular has been confirmed experimentally (Cano-Nicolau et al., 2016; Le Fol et al., 2017; Pinto et al., 2019), albeit at a weaker affinity compared to the potent teleost estrogen receptor agonist EE_2, it is largely unknown whether additional receptor subtypes may be differentially affected by BPA and EE_2 in zebrafish. In mammalian model-systems, it is well known that BPA has the ability to bind to additional receptors (MacKay and Abizaid, 2018). A particularly interesting example is ERRg, which has not only been shown to bind to BPA with high affinity (Tohmé et al., 2014), but also to be critically involved in energy metabolism regulation (Stincic et al., 2018). Possible roles for ERRg (or other non-estrogen receptor targets) in mediating metabolic effects of BPA are furthermore supported by comparative studies revealing effects of BPA on lipid metabolism in the fruitfly (*Drosophila melanogaster*) (Williams et al., 2014), an invertebrate species which does not possess nuclear estrogen receptors but does possess a single estrogen-related receptor orthologous to human ERRg (Tennessen et al., 2011). Therefore, we comparatively analyzed BPA and EE_2 binding potential not only to zebrafish estrogen receptor α, the main postulated BPA target in zebrafish (Pinto et al., 2019), but also both paralogues of ERRg. This analysis supported experimentally established stronger binding between estrogen receptor alpha and EE_2 compared to BPA (Helland, 1990), confirming adequacy of the modelling approach. While the approach predicts less differential binding between EE_2 for ERRga (but not ERRgb), it does not provide evidence for likely BPA specific-activation of ERRg in zebrafish and can therefore not provide a single-receptor based explanation for the observed BPA-specific metabolic effects descried in our study.

4.7. Environmental implications

Although metabolic consequences of developmental BPA exposure manifested themselves at mg/L concentrations which exceed environmental concentrations in aquatic systems as such BPA concentrations are only found point source leachates (Jopling, 2012), several effects were observed following developmental BPA exposure concentrations of 0.1 mg/L, which lies within the range between the highest reported BPA surface (56 μg/L) and WWTP effluent concentrations (up to 370 μg/L) (Corrales et al., 2015) and therefore is informative in the discussion of environmental implications of this study. Importantly, the lowest dose of BPA tested was not sufficient to elicit a response in the estrogenic marker *cyp19a1b*, suggesting that metabolic effects observed were likely not mediated by transient developmental activation of estrogenic signalling pathways. Indeed, while metabolic consequences to developmental BPA exposure were generally dose-dependent, metabolic effects observed following developmental exposure to higher, estrogenic concentrations of BPA were not mimicked by EE_2 in early development, suggesting that metabolic effects following developmental BPA exposure in general were not dependent on estrogenic mode-of action. This is of importance for environmental risk assessment, as additive or synergistic effects of estrogenic contaminants have been reported in fish (Silva de Assis et al., 2013).

Irrespective of the mode of action, developmental exposure to 0.1 mg/L BPA was, similar to developmental exposure to higher BPA concentrations, sufficient to transiently increase larval body weight and differentially affect the locomotor phenotype in juveniles depending on nutrition and lighting conditions, two key environmental parameters. The observed transient increase on body weight warrants future investigation, as even moderate increases in fish bodyweight comparable to the transient increases in bodyweight (+20%) observed following developmental BPA exposure in our study, may affect interaction between conspecifics (Dai et al., 2014), interspecific competition and predator-prey dynamics (Nunn et al., 2012), as well as trophic network dynamics in aquatic ecosystems (Nunn et al., 2012). For example, bodyweight increases in male (+10%) and female (+20%) zebrafish were significantly associated with dominance status and increased reproductive success (Paull et al., 2010). Increased bodyweight in fish larvae has been linked to altered predation risk, as specific predator to prey mass ratios are widely observed and optimal foraging theory predicts that energetic gains, which increases with prey size, should be maximized in relation to energetic cost of capturing and handling, which also increases with prey size (Nunn et al., 2012). Conversely, increased larval size can affect selection of their prey, thus affecting multiple levels of trophic networks (Nunn et al., 2012).

In addition to body weight, locomotor behaviour of larval fish represents another important factor in predator-prey interactions, and many fish larvae of many species exhibit locomotor behaviour patterns influenced by specific environmental factors such as nutritional availability and daylight (Nunn et al., 2012). Therefore, the observed increase in locomotor activity in zebrafish developmentally exposed to 0.1 mg/L BPA and maintained on a normal diet, and the observed decrease in locomotor activity in the absence of light observed in zebrafish developmentally exposed to 0.1 mg/L BPA and maintained on a high feeding diet, suggest that transient BPA exposure may disrupt key locomotor behavioural responses important in predator-prey interactions. Disruption of increased zebrafish locomotion responses in dark phases of rapidly alternating light/dark tests have been interpreted as a potential interruption of the tendency of light seeking behaviour modulated by the stress axis (Burgess and Granato, 2007; Basnet et al., 2019). Given that decreased locomotion in developmentally contaminant-exposed larvae including including an environmental indicator fish larvae, the inland silverside (*Menidia beryllina*), has been shown to translate into differences in foraging success (Kasumyan, 2001) or predator evasion (Frank et al., 2019), future studies should explore this possibility for environmental concentrations of BPA. Foraging behaviour and predator evasion can be disrupted by contaminants at the level of locomotion capacity and sensory stimulus perception and integration (Kasumyan, 2001), and while our and previous studies (Martínez et al., 2018) have shown early developmental molecular signatures indicative of altered muscle development, such changes did not translate into morphological alterations in sarcomere structure as determined by birefringence assay. Therefore, in line with previously reported effects on genes enriched for neurological and visual functions (Martínez et al., 2018), and recently reported developmental consequences of low concentration BPA exposure on neurogenesis and behaviour (Kinch et al.,

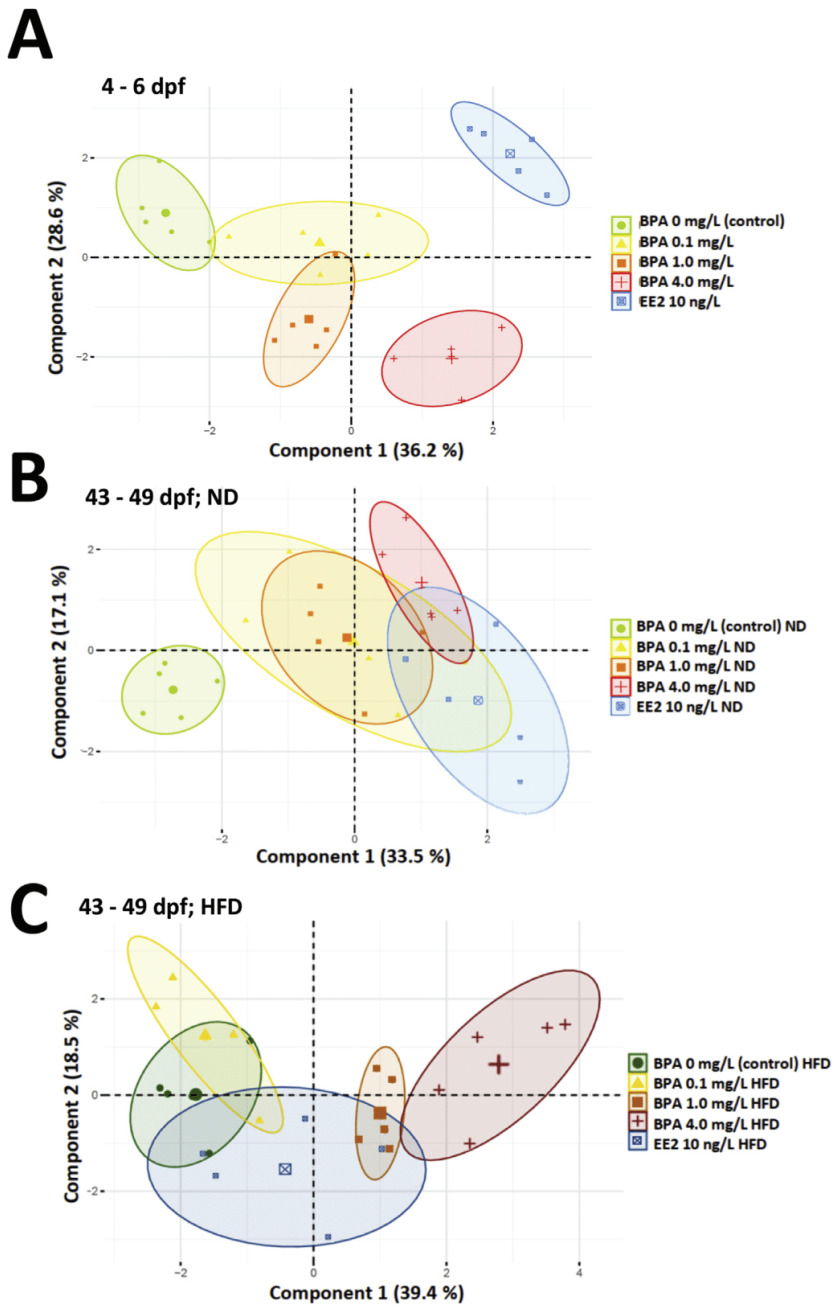

Fig. 7. Principal component analysis (PCA) at developmental stages (4–6 dpf and 43–49 dpf) used to integrating different organism-level and molecular-level parameters quantified in this study to assess effects on the metabolic phenotype. Oxidative metabolism-related energy expenditure, feed-intake, locomotion behaviour and gene expression data were used for both developmental stages. Oxygen consumption rate (OCR), extracellular acidification rate (ECAR), muscle bi-refringence were additionally used at the 4–6 dpf stage and body weight (BW), body length (BL) and neutral lipids stain intensity were additionally used at 43–49 dpf stage. In each case, two first components explained: 64.8% for 4–6 dpf eleutheroembryos (**A**); 50.6% for the 43–49 dpf juveniles maintained on ND (**B**); 57.9% for the 43–49 dpf juveniles maintained on HFD (**C**). In all cases, 5 replicates were generated by randomization using mean ± 2 S.E.M. for each parameter as limits. 70% confidence ellipses are shown.

2016), evidence suggests that observed locomotor changes may rather be linked to central integration and control of locomotion in response to environmental stimuli.

While our study focused on molecular and organismal level effects pertaining to the metabolic phenotype in larval zebrafish, the observed non-estrogen dependent transient increase in body weight and differential effects on locomotion in response to developmental BPA exposure raise concerns regarding possible impacts on organismal fitness at higher levels of biological organisation. We therefore propose that potential consequences of developmental BPA exposure on intra- and interspecific dynamics, as well as on trophic foodwebs should be prioritized both in laboratory settings, as well as in wild fish species in mesocosm settings to further link observed molecular and organismal level changes to possible ecological consequences. This is of particular importance for early fish development, when larvae are invariably most vulnerable to predation, competition, and environmental perturbations (Nunn et al., 2012).

5. Conclusions

Overall, our study supports both acute as well as long-term metabolism disrupting effects of BPA in zebrafish across development. As several organismal- or molecular-level metabolic effects in response to developmental BPA are largely different from effects in fish developmentally exposed to the positive estrogenic control EE_2, our study is suggestive of an involvement of receptors other than nuclear estrogen receptors. Our study reveals the strongest metabolic impact of BPA during acute eleutheroembryonic exposure, which is characterized by organismal level indices suggestive of negative influence on energy balance and alterations in lipid and carbohydrate metabolism. Observed longer-term effects following developmental BPA exposure are transitory (body weight) and generally less pronounced, with the exception of a persistent locomotory phenotype suggesting increased energy expenditure. Interestingly, this phenotype is differentially modulated by a nutritional challenge, revealing that developmental exposure history shapes adult metabolic challenge responses. Developmental BPA exposure-dependent changes in the expression of specific lipid- and carbohydrate metabolism-related genes persist in juveniles but compared to eleutheroembryonic patterns differ in directionality and their likely dependency on estrogenic signalling mechanisms. When analyzed integratively, the study of organismal and molecular-level parameters used to metabolically profile zebrafish allows for a clear separation of developmental exposure groups in a 70% confidence interval. This separation is strongest in acutely exposed eleutheroembryos where medium and high BPA exposure groups are dose-dependently separated from both negative vehicle control and positive estrogenic control groups (Fig. 7A). This result indicates that the eleutheroembryonic metabolic phenotype is differentially affected by estrogenic-response inducing BPA concentrations and EE_2, suggesting non estrogenic modes of action of BPA on the metabolic phenotype at these concentrations. ND-fed juvenile fish, all developmental exposure groups are distinguishable from the group developmentally exposed to negative vehicle control, but not each other, suggesting that developmental BPA exposure-dependent long-term affected parameters, such as locomotion behaviour and gene expression, are likely estrogen-dependent (Fig. 7B). Finally, in HD juveniles developmentally exposed to medium and high BPA are distinguishable from the negative vehicle control group, while juveniles developmentally-exposed to the positive estrogenic control are not distinguishable from any group with a 70% confidence interval (Fig. 7C). This suggests a slight interaction between developmental BPA exposure and juvenile dietary regime in low BPA and EE_2 groups.

Credit author statement

Study conception and design: RM, JAM, Acquisition of data: RM, MA-L, TE, Analysis and interpretation of data: RM, BP,LN-M, JAM, Drafting of manuscript: RM,JAM. Critical revision: RM,JAM,BP,LN-M. Funding Acquisition: JAM, RM,LN-M, BP.

Declaration of competing interest

The authors declare no conflicts of interest.

Acknowledgments

This work was supported by an NSERC-Discovery grant (#147476) and a Canadian Foundation for Innovation John R. Evans Leaders fund (#148035) awarded to JAM. RM was supported by an FPU predoctoral fellows from the Spanish Ministry of Education and Science (ref. FPU15/03332; EST18/00001).

Appendix A. Supplementary data

Supplementary data to this article can be found online at https://doi.org/10.1016/j.chemosphere.2020.127080.

References

Abdi, H., Williams, L.J., 2010. Principal component analysis. WIREs Computational Statistics 2, 433–459.
Ahmed, F., Chehadé, L., Garneau, L., Caron, A., Aguer, C., 2020. The effects of acute BPA exposure on skeletal muscle mitochondrial function and glucose metabolism. Mol. Cell. Endocrinol. 499, 110580.
Aluru, N., Leatherland, J.F., Vijayan, M.M., 2010. Bisphenol A in oocytes leads to growth suppression and altered stress performance in juvenile rainbow trout. PLoS ONE 5, e10741.
Aris, A.Z., Shamsuddin, A.S., Praveena, S.M., 2014. Occurrence of 17α-ethynylestradiol (EE2) in the environment and effect on exposed biota: a review. Environ. Int. 69, 104–119.
Basnet, R.M., Zizioli, D., Taweedet, S., Finazzi, D., Memo, M., 2019. Zebrafish larvae as a behavioral model in neuropharmacology. Biomedicines 7.
Beal, J.A., 2018. Baby bottles and bisphenol A (BPA): still a parental concern. MCN Am. J. Matern./Child Nurs. 43, 349.
Berger, J., Sztal, T., Currie, P.D., 2012. Quantification of birefringence readily measures the level of muscle damage in zebrafish. Biochem. Biophys. Res. Commun. 423, 785–788.
Best, C., et al., 2018. Epigenetics in teleost fish: from molecular mechanisms to physiological phenotypes. Comp. Biochem. Physiol. B Biochem. Mol. Biol. 224, 210–244.
Birceanu, O., Mai, T., Vijayan, M.M., 2015. Maternal transfer of bisphenol A impacts the ontogeny of cortisol stress response in rainbow trout. Aquat. Toxicol. 168, 11–18.
Bond, S.T., McEwen, K.A., Yoganantharajah, P., Gibert, Y., 2018. Live metabolic profile Analysis of zebrafish embryos using a Seahorse XF 24 extracellular flux analyzer. Methods Mol. Biol. 1797, 393–401.
Brion, F., et al., 2012. Screening estrogenic activities of chemicals or mixtures in vivo using transgenic (cyp19a1b-GFP) zebrafish embryos. PloS One 7.
Burgess, H.A., Granato, M., 2007. Modulation of locomotor activity in larval zebrafish during light adaptation. J. Exp. Biol. 210, 2526–2539.
Canesi, L., Fabbri, E., 2015. Environmental effects of BPA: focus on aquatic species. Dose Response 13, 1559325815598304.
Cano-Nicolau, J., et al., 2016. Estrogenic effects of several BPA analogs in the developing zebrafish brain. Front. Neurosci. 10, 112.
Carnevali, O., et al., 2019. Diets contaminated with Bisphenol A and Di-isononyl phtalate modify skeletal muscle composition: a new target for environmental pollutant action. Sci. Total Environ. 658, 250–259.
Chevalier, N., Fénichel, P., Bisphenol, A., 2015. Targeting metabolic tissues. Rev. Endocr. Metab. Disord. 16, 299–309.
Cohen, A., Smith, Y., 2014. Estrogen regulation of microRNAs, target genes, and microRNA expression associated with vitellogenesis in the zebrafish. Zebrafish 11, 462–478.
Corrales, J., et al., 2015. Global assessment of bisphenol A in the environment: review and analysis of its occurrence and bioaccumulation. Dose Response 13, 1559325815598308.
Le Corre, L., Besnard, P., Chagnon, M.-C.B.P.A., 2015. An energy balance disruptor. Crit. Rev. Food Sci. Nutr. 55, 769–777.

Cosnefroy, A., et al., 2012. Selective activation of zebrafish estrogen receptor subtypes by chemicals by using stable reporter gene assay developed in a zebrafish liver cell line. Toxicol. Sci. 125, 439–449.
Dai, Y.-J., et al., 2014. Zebrafish as a model system to study toxicology. Environ. Toxicol. Chem. 33, 11–17.
Desai, M., Ferrini, M.G., Jellyman, J.K., Han, G., Ross, M.G., 2018. In vivo and in vitro bisphenol A exposure effects on adiposity. J Dev Orig Health Dis 9, 678–687.
Diotel, N., et al., 2013. Effects of estradiol in adult neurogenesis and brain repair in zebrafish. Horm. Behav. 63, 193–207.
Eswar, N., et al., 2006. Comparative protein structure modeling using Modeller. *Curr Protoc Bioinformatics* **Chapter** 5. Unit-5.6.
Flint, S., Markle, T., Thompson, S., Wallace, E., 2012. Bisphenol A exposure, effects, and policy: a wildlife perspective. J. Environ. Manag. 104, 19–34.
Le Fol, V., et al., 2017. In vitro and in vivo estrogenic activity of BPA, BPF and BPS in zebrafish-specific assays. Ecotoxicol. Environ. Saf. 142, 150–156.
Frank, D.F., et al., 2019. Developmental exposure to environmentally relevant concentrations of bifenthrin alters transcription of mTOR and ryanodine receptor-dependent signaling molecules and impairs predator avoidance behavior across early life stages in inland silversides (Menidia beryllina). Aquat. Toxicol. 206, 1–13.
Gerona, R., Vom Saal, F.S., Hunt, P.A., 2020. BPA: have flawed analytical techniques compromised risk assessments? Lancet Diabetes Endocrinol 8, 11–13.
Goundadkar, B.B., Katti, P., 2017. Environmental estrogen(s) induced swimming behavioural alterations in adult zebrafish (Danio rerio). Environ. Toxicol. Pharmacol. 54, 146–154.
Green, J.M., et al., 2018. Early life exposure to ethinylestradiol enhances subsequent responses to environmental estrogens measured in a novel transgenic zebrafish. Sci. Rep. 8, 2699.
Handbook of Partial Least Squares - Concepts, Methods and Applications | Vincenzo Esposito Vinzi | Springer. https://www.springer.com/gp/book/9783540328254.
Heckmann, L.-H., Sørensen, P.B., Krogh, P.H., Sørensen, J.G., 2011. NORMA-Gene: a simple and robust method for qPCR normalization based on target gene data. BMC Bioinf. 12, 250.
Helland, I.S., 1990. Partial least squares regression and statistical models. Scand. J. Stat. 17, 97–114.
Hennig, C.. fpc: flexible procedures for clustering. " 2014. [Online]. Available: http://cran.r-project.org/package=fpc.
Horzmann, K.A., Freeman, J.L., 2018. Making waves: new developments in toxicology with the zebrafish. Toxicol. Sci. 163, 5–12.
Howdeshell, K.L., Hotchkiss, A.K., Thayer, K.A., Vandenbergh, J.G., vom Saal, F.S., 1999. Exposure to bisphenol A advances puberty. Nature 401, 763–764.
Jin, X., Han, J., 2010. K-medoids clustering. In: Sammut, C., Webb, G.I. (Eds.), Encyclopedia of Machine Learning. Springer US, pp. 564–565. https://doi.org/10.1007/978-0-387-30164-8_426. —.
Jopling, C., 2012. Liver-specific microRNA-122: biogenesis and function. RNA Biol. 9, 137–142.
Kassambara, A., Mundt, F., 2017. Factoextra: Extract and Visualize the Results of Multivariate Data Analyses [Online]. Available: https://cran.r-project.org/web/packages/factoextra/index.html.
Kasumyan, A.O., 2001. Effects of chemical pollutants on foraging behavior and sensitivity of fish to. Food Stimuli 41, 13.
Ke, Z.-H., et al., 2016. Bisphenol A exposure may induce hepatic lipid accumulation via reprogramming the DNA methylation patterns of genes involved in lipid metabolism. Sci. Rep. 6, 31331.
Kim, Y.-K., Kim, B., Kim, V.N., 2016. Re-evaluation of the roles of DROSHA, Exportin 5, and DICER in microRNA biogenesis. Proc. Natl. Acad. Sci. Unit. States Am. 113, E1881–E1889.
Kinch, C.D., Kurrasch, D.M., Habibi, H.R., 2016. Adverse morphological development in embryonic zebrafish exposed to environmental concentrations of contaminants individually and in mixture. Aquat. Toxicol. 175, 286–298.
Kloosterman, W.P., Lagendijk, A.K., Ketting, R.F., Moulton, J.D., Plasterk, R.H.A., 2007. Targeted inhibition of miRNA maturation with morpholinos reveals a role for miR-375 in pancreatic islet development. PLoS Biol. 5, e203.
Kumar, M.G., et al., 2016. Altered glycolysis and mitochondrial respiration in a zebrafish model of dravet syndrome. eNeuro 3.
Van der Laan, M., Pollard, K., Bryan, J., 2003. A new partitioning around medoids algorithm. J. Stat. Comput. Simulat. 73, 575–584.
Laudadio, I., et al., 2012. A feedback loop between the liver-enriched transcription factor network and miR-122 controls hepatocyte differentiation. Gastroenterology 142, 119–129.
S. Lê, J. Josse, and F. Husson, "FactoMineR : An R package for multivariate analysis," J. Stat. Software, vol. 25, no. 1, pp. 1–18, Mar. 2008.
Li, X., et al., 2017. Impact of low-dose chronic exposure to Bisphenol A (BPA) on adult male zebrafish adaption to the environmental complexity: disturbing the color preference patterns and reliving the anxiety behavior. Chemosphere 186, 295–304.
Lin, W.-W., Chen, L.-H., Chen, M.-C., Kao, H.-W., 2009. Differential expression of zebrafish gpia and gpib during development. Gene Expr. Patterns 9, 238–245.
Liu, N.-A., et al., 2003. Pituitary corticotroph ontogeny and regulation in transgenic zebrafish. Mol. Endocrinol. 17, 959–966.
Löhr, H., et al., 2018. Diet-induced growth is regulated via acquired leptin resistance and engages a pomc-somatostatin-growth hormone circuit. Cell Rep. 23, 1728–1741.
Ludvik, A.E., et al., 2016. HKDC1 is a novel hexokinase involved in whole-body glucose use. Endocrinology 157, 3452–3461.
MacKay, H., Abizaid, A., 2018. A plurality of molecular targets: the receptor ecosystem for bisphenol-A (BPA). Horm. Behav. 101, 59–67.
Mackay, H., et al., 2013. Organizational effects of perinatal exposure to bisphenol-A and diethylstilbestrol on arcuate nucleus circuitry controlling food intake and energy expenditure in male and female CD-1 mice. Endocrinology 154, 1465–1475.
Maechler, M., et al., 2019. "cluster: 'Finding Groups in Data': Cluster Analysis Extended Rousseeuw et al. " [Online]. Available: https://cran.r-project.org/web/packages/cluster/index.html.
Marmugi, A., et al., 2014. Adverse effects of long-term exposure to bisphenol A during adulthood leading to hyperglycaemia and hypercholesterolemia in mice. Toxicology 325, 133–143.
Martínez, R., et al., 2018. Dose-dependent transcriptomic responses of zebrafish eleutheroembryos to Bisphenol A. Environ. Pollut. 243, 988–997.
Martínez, R., et al., 2019. Morphometric signatures of exposure to endocrine disrupting chemicals in zebrafish eleutheroembryos. Aquat. Toxicol. 214, 105232.
Martínez, R., et al., 2019. Changes in lipid profiles induced by bisphenol A (BPA) in zebrafish eleutheroembryos during the yolk sac absorption stage. Chemosphere 246, 125704.
Mauvais-Jarvis, F., Clegg, D.J., Hevener, A.L., 2013. The role of estrogens in control of energy balance and glucose homeostasis. Endocr. Rev. 34 (3), 309–338. https://doi.org/10.1210/er.2012-1055.
Mennigen, J.A., 2016. Micromanaging metabolism-a role for miRNAs in teleost energy metabolism. Comp. Biochem. Physiol. B Biochem. Mol. Biol. 199, 115–125.
Mevik, B.-H., Wehrens, R., Jan. 2015. The pls package: principal component and partial least squares regression in R. J. Stat. Software 18 (2), 1–23.
Minchin, J.E.N., Rawls, J.F., 2017. A classification system for zebrafish adipose tissues. Dis Model Mech 10, 797–809.
Mishima, Y., et al., 2009. Zebrafish miR-1 and miR-133 shape muscle gene expression and regulate sarcomeric actin organization. Genes Dev. 23, 619–632.
Moreman, J., et al., 2018. Estrogenic mechanisms and cardiac responses following early life exposure to bisphenol A (BPA) and its metabolite 4-Methyl-2,4-bis(p-hydroxyphenyl)pent-1-ene (mbp) in zebrafish. Environ. Sci. Technol. 52, 6656–6665.
Morrice, J.R., Gregory-Evans, C.Y., Shaw, C.A., 2018. Modeling environmentally-induced motor neuron degeneration in zebrafish. Sci. Rep. 8, 1–11.
Nakazawa, M., 2018. Fmsb: Functions for Medical Statistics Book with Some Demographic Data [Online]. Available: https://cran.r-project.org/web/packages/fmsb/index.html.
Nunn, A.D., Tewson, L.H., Cowx, I.G., 2012. The foraging ecology of larval and juvenile fishes. Rev. Fish Biol. Fish. 22, 377–408.
Olsvik, P.A., et al., 2019. Associations between behavioral effects of bisphenol A and DNA methylation in zebrafish embryos. Front. Genet. 10, 184.
Onghena, M., et al., 2014. Development and application of a non-targeted extraction method for the analysis of migrating compounds from plastic baby bottles by GC-MS. Food Addit. Contam. Part A Chem Anal Control Expo Risk Assess 31, 2090–2102.
Otis, J.P., et al., 2015. Zebrafish as a model for apolipoprotein biology: comprehensive expression analysis and a role for ApoA-IV in regulating food intake. Dis Model Mech 8, 295–309.
Otis, J.P., Shen, M.-C., Caldwell, B.A., Reyes Gaido, O.E., Farber, S.A., 2019. Dietary cholesterol and apolipoprotein A-I are trafficked in endosomes and lysosomes in the live zebrafish intestine. Am. J. Physiol. Gastrointest. Liver Physiol. 316, 350–365. G–G.
Paull, G.C., et al., 2010. Dominance hierarchies in zebrafish (Danio rerio) and their relationship with reproductive success. Zebrafish 7, 109–117.
Pinto, C., et al., 2019. Differential activity of BPA, BPAF and BPC on zebrafish estrogen receptors in vitro and in vivo. Toxicol. Appl. Pharmacol. 380, 114709.
Quinlivan, V.H., Farber, S.A., 2017. Lipid uptake, metabolism, and transport in the larval zebrafish. Front. Endocrinol. 8, 319.
R Development Core Team, 2008. R: a Language and Environment for Statistical Computing.
Rampersad, S.N., 2012. Multiple applications of Alamar Blue as an indicator of metabolic function and cellular health in cell viability bioassays. Sensors 12, 12347–12360.
Reid, R.M., D'Aquila, A.L., Biga, P.R., 2018. The validation of a sensitive, non-toxic in vivo metabolic assay applicable across zebrafish life stages. Comp. Biochem. Physiol. C Toxicol. Pharmacol. 208, 29–37.
Riu, A., et al., 2014. Halogenated bisphenol-A analogs act as obesogens in zebrafish larvae (Danio rerio). Toxicol. Sci. 139, 48–58.
Rubin, B.S., Soto, A.M., Bisphenol, A., 2009. Perinatal exposure and body weight. Mol. Cell. Endocrinol. 304, 55–62.
Vom Saal, F.S., Nagel, S.C., Coe, B.L., Angle, B.M., Taylor, J.A., 2012. The estrogenic endocrine disrupting chemical bisphenol A (BPA) and obesity. Mol. Cell. Endocrinol. 354, 74–84.
Saili, K.S., Tilton, S.C., Waters, K.M., Tanguay, R.L., 2013. Global gene expression analysis reveals pathway differences between teratogenic and non-teratogenic exposure concentrations of bisphenol A and 17β-estradiol in embryonic zebrafish. Reprod. Toxicol. 38, 89–101.
Segner, H., 2009. Zebrafish (Danio rerio) as a model organism for investigating endocrine disruption. Comp. Biochem. Physiol. C Toxicol. Pharmacol. 149, 187–195.
Seth, A., Stemple, D.L., Barroso, I., 2013. The emerging use of zebrafish to model metabolic disease. Dis Model Mech 6, 1080–1088.
Shu, L., et al., 2019. Prenatal bisphenol A exposure in mice induces multitissue

multiomics disruptions linking to cardiometabolic disorders. Endocrinology 160, 409–429.
Shved, N., Berishvili, G., Baroiller, J.-F., Segner, H., Reinecke, M., 2008. Environmentally relevant concentrations of 17α-ethinylestradiol (EE2) interfere with the growth hormone (GH)/Insulin-Like growth factor (IGF)-I system in developing bony fish. Toxicol. Sci. 106, 93–102.
Silva de Assis, H.C., et al., 2013. Estrogen-like effects in male goldfish Co-exposed to fluoxetine and 17 alpha-ethinylestradiol. Environ. Sci. Technol. 47, 5372–5382.
Smith, L.L., Beggs, A.H., Gupta, V.A., 2013. Analysis of skeletal muscle defects in larval zebrafish by birefringence and touch-evoke escape response assays. JoVE, e50925. https://doi.org/10.3791/50925.
Souder, J.P., Gorelick, D.A., 2018. Assaying uptake of endocrine disruptor compounds in zebrafish embryos and larvae. Comp. Biochem. Physiol. C Toxicol. Pharmacol. 208, 105–113.
Stahlhut, R.W., et al., 2018. Experimental BPA exposure and glucose-stimulated insulin response in adult men and women. J Endocr Soc 2, 1173–1187.
Stankiewicz, A.J., et al., 2019. Cell kinetics in the adult neurogenic niche and impact of diet-induced accelerated aging. J. Neurosci. 39, 2810–2822.
van Steijn, L., Verbeek, F.J., Spaink, H.P., Merks, R.M.H., 2019. Predicting metabolism from gene expression in an improved whole-genome metabolic network model of Danio rerio. Zebrafish 16, 348–362.
Stincic, T.L., Grachev, P., Bosch, M.A., Rønnekleiv, O.K., Kelly, M.J., 2018. Estradiol drives the anorexigenic activity of proopiomelanocortin neurons in female mice. eNeuro 5.
Tennessen, J.M., Baker, K.D., Lam, G., Evans, J., Thummel, C.S., 2011. The Drosophila estrogen-related receptor directs a metabolic switch that supports developmental growth. Cell Metabol. 13, 139–148.
The behavioral Repertoire of larval zebrafish. Springer Nature Experiments, 2016. https://experiments.springernature.com/articles/10.1007/978-1-60761-922-2_12.
Thorpe, K.L., et al., 2003. Relative potencies and combination effects of steroidal estrogens in fish. Environ. Sci. Technol. 37, 1142–1149.
Tixier, V., et al., 2013. Glycolysis supports embryonic muscle growth by promoting myoblast fusion. Proc. Natl. Acad. Sci. Unit. States Am. 110, 18982–18987.
Tohmé, M., et al., 2014. Estrogen-related receptor γ is an in vivo receptor of bisphenol A. Faseb. J. 28, 3124–3133.
Trott, O., Olson, A.J., 2010. AutoDock Vina: improving the speed and accuracy of docking with a new scoring function, efficient optimization, and multithreading. J. Comput. Chem. 31, 455–461.
Tse, W.K.F., Yeung, B.H.Y., Wan, H.T., Wong, C.K.C., 2013. Early embryogenesis in zebrafish is affected by bisphenol A exposure. Biol Open 2, 466–471.
Tu, W., et al., 2019. Bioconcentration and metabolic effects of emerging PFOS alternatives in developing zebrafish. Environ. Sci. Technol. 53, 13427–13439.
Tudurí, E., et al., 2018. Timing of exposure and bisphenol-A: implications for diabetes development. Front. Endocrinol. 9.
Versonnen, B.J., Janssen, C.R., 2004. Xenoestrogenic effects of ethinylestradiol in zebrafish (Danio rerio). Environ. Toxicol. 19, 198–206.
Wang, X., et al., 2013. Bisphenol A affects axonal growth, musculature and motor behavior in developing zebrafish. Aquat. Toxicol. 142–143, 104–113.
Warnes, G.R., et al., 01-Jan. Gplots: Various R Programming Tools for Plotting Data. " *The Comprehensive R Archive Network (CRAN)*, pp. 1–66.
Wei, T., Simko, V., Levy, M., Xie, Y., Jin, Y., Zemla, J.. Corrplot: visualization of a correlation matrix. " 2017. [Online]. Available: https://cran.r-project.org/web/packages/corrplot/index.html.
Wickham, H., 2011. ggplot2. Wiley Interdiscip. Rev. Comput. Stat. 3 (2), 180–185.
Wienholds, E., et al., 2005. MicroRNA expression in zebrafish embryonic development. Science 309, 310–311.
Williams, S.Y., Renquist, B., 2016. J. High throughput Danio rerio energy expenditure assay. JoVE e53297. https://doi.org/10.3791/53297.
Williams, M.J., et al., 2014. Exposure to bisphenol A affects lipid metabolism in Drosophila melanogaster. Basic Clin. Pharmacol. Toxicol. 114, 414–420.
Wu, M., Xu, H., Shen, Y., Qiu, W., Yang, M., 2011. Oxidative stress in zebrafish embryos induced by short-term exposure to bisphenol A, nonylphenol, and their mixture. Environ. Toxicol. Chem. 30, 2335–2341.
Wold, S., Esbensen, K., Geladi, P., 1987. Princ. Compon. Anal. 16. http://pzs.dstu.dp.ua/DataMining/pca/bibl/Principal%20components%20analysis.pdf.
Wu, M., et al., 2017. Bioconcentration pattern and induced apoptosis of bisphenol A in zebrafish embryos at environmentally relevant concentrations. Environ. Sci. Pollut. Res. Int. 24, 6611–6621.

Supplemental information: scientific article VI

Acute and long-term metabolic consequences of early developmental Bisphenol A exposure in zebrafish (*Danio rerio*)

Authors: R. Martínez, W. Tu, T. Eng, M. Allaire-Leung, B. Piña, L. Navarro-Martín, J.A. Mennigen

Status: Published

Journal: Chemosphere. 256 (2020) 127080.

DOI: 10.1016/j.chemosphere.2020.127080

Supplemental File SF1. Target-scan fish predictions of interactions between mRNA transcripts and miRNAs profiled in this study.

miRNA	3' UTR binding site number	8mer	7mer-m8	7mer-1A	Target Scan Score	miRNA conserved across vertebrates	Targeted studied transcript	ENSEMBL ID	Tissue specific
dre-miR-1	5	0	2	3	-0.71	broadly conserved	cnn3a	ENSDARG00000008359.1	skeletal muscle[1]
dre-miR-1	2	1	1	0	-0.43	broadly conserved	atp6v1ba	ENSDARG00000013443.1	skeletal muscle[1]
dre-miR-1	1	1	0	0	-0.20	broadly conserved	pfn2l	ENSDARG00000012682.6	skeletal muscle[1]
dre-miR-1	1	1	0	0	-0.20	broadly conserved	pfn2l	ENSDARG00000012682.4	skeletal muscle[1]
dre-miR-1	1	1	0	0	-0.18	broadly conserved	pfn2l	ENSDARG00000012682.5	skeletal muscle[1]
dre-miR-1	1	1	0	0	-0.13	broadly conserved	pfn2l	ENSDARG00000012682.3	skeletal muscle[1]
dre-miR-1	1	1	0	0	-0.10	broadly conserved	pfn2l	ENSDARG00000012682.2	skeletal muscle[1]
dre-miR-1	1	1	0	0	-0.06	broadly conserved	pfn2l	ENSDARG00000012682.1	skeletal muscle[1]
dre-miR-1	1	0	0	1	-0.05	broadly conserved	cyp19a1b	ENSDARG00000009852.3	skeletal muscle[1]
dre-miR-1	1	0	0	1	-0.04	broadly conserved	cyp19a1b	ENSDARG00000009852.2	skeletal muscle[1]
dre-miR-1	1	0	0	1	-0.04	broadly conserved	cyp19a1b	ENSDARG00000009852.1	skeletal muscle[1]
dre-miR-101a	2	0	0	2	-0.28	broadly conserved	pomcb	ENSDARG00000069307.1	-
dre-miR-101a	2	0	0	2	-0.20	broadly conserved	pfkma	ENSDARG00000014179.1	-
dre-miR-101a	1	0	1	0	-0.17	broadly conserved	cyp19a1b	ENSDARG00000009852.3	-
dre-miR-101a	1	0	1	0	-0.17	broadly conserved	cyp19a1b	ENSDARG00000009852.1	-
dre-miR-101a	1	0	1	0	-0.17	broadly conserved	cyp19a1b	ENSDARG00000009852.2	-
dre-miR-101a	3	0	1	2	-0.15	broadly conserved	pomca	ENSDARG00000043135.1	-
dre-miR-101a	1	0	0	1	-0.14	broadly conserved	pomca	ENSDARG00000043135.2	-
dre-miR-122	1	0	1	0	-0.15	broadly conserved	atp6v1ba	ENSDARG00000013443.1	liver[2]
dre-miR-133a-5p	1	0	1	0	-0.30	broadly conserved	pfn2l	ENSDARG00000012682.4	skeletal muscle[1]
dre-miR-133a-5p	1	0	1	0	-0.30	broadly conserved	pfn2l	ENSDARG00000012682.6	skeletal muscle[1]
dre-miR-133a-5p	1	0	1	0	-0.29	broadly conserved	pfn2l	ENSDARG00000012682.5	skeletal muscle[1]
dre-miR-133a-5p	1	0	1	0	-0.26	broadly conserved	pfn2l	ENSDARG00000012682.3	skeletal muscle[1]
dre-miR-133a-5p	1	0	1	0	-0.24	broadly conserved	pfn2l	ENSDARG00000012682.2	skeletal muscle[1]
dre-miR-133a-5p	1	0	1	0	-0.22	broadly conserved	pfn2l	ENSDARG00000012682.1	skeletal muscle[1]
dre-miR-133a-5p	1	0	0	1	-0.18	broadly conserved	pomcb	ENSDARG00000069307.1	skeletal muscle[1]
dre-miR-133a-5p	1	0	0	1	-0.15	broadly conserved	cnn3a	ENSDARG00000008359.1	skeletal muscle[1]

[1] Y. Mishima et al., "Zebrafish miR-1 and miR-133 shape muscle gene expression and regulate sarcomeric actin organization," Genes Dev., vol. 23, no. 5, pp. 619–632, Mar. 2009.
[2] C. L. Jopling, "Liver-specific microRNA-122: biogenesis and function," RNA Biology, vol. 9, no. 2. Taylor & Francis, pp. 137–142, Feb-2012.

miRNA	3' UTR binding site number	8mer	7mer-m8	7mer-1A	Target Scan Score	miRNA conserved across vertebrates	Targeted studied transcript	ENSEMBL ID	Tissue specific
dre-miR-142a-3p	4	2	2	0	-1.13	broadly conserved	pfn2l	ENSDARG00000012682.6	-
dre-miR-142a-3p	4	2	2	0	-1.12	broadly conserved	pfn2l	ENSDARG00000012682.5	-
dre-miR-142a-3p	3	2	1	0	-0.99	broadly conserved	pfn2l	ENSDARG00000012682.8	-
dre-miR-142a-3p	4	2	2	0	-0.92	broadly conserved	pfn2l	ENSDARG00000012682.4	-
dre-miR-142a-3p	4	2	2	0	-0.88	broadly conserved	pfn2l	ENSDARG00000012682.3	-
dre-miR-142a-3p	4	2	2	0	-0.86	broadly conserved	pfn2l	ENSDARG00000012682.2	-
dre-miR-142a-3p	4	2	2	0	-0.85	broadly conserved	pfn2l	ENSDARG00000012682.1	-
dre-miR-142a-3p	3	2	1	0	-0.84	broadly conserved	pfn2l	ENSDARG00000012682.7	-
dre-miR-142a-3p	1	0	1	0	-0.19	broadly conserved	pfkma	ENSDARG00000014179.1	-
dre-miR-142a-3p	1	0	0	1	> -0.01	broadly conserved	pomca	ENSDARG00000043135.1	-
dre-miR-142a-5p	1	1	0	0	-0.17	poorly conserved	pfn2l	ENSDARG00000012682.6	-
dre-miR-142a-5p	1	1	0	0	-0.17	poorly conserved	pfn2l	ENSDARG00000012682.4	-
dre-miR-142a-5p	1	1	0	0	-0.15	poorly conserved	pfn2l	ENSDARG00000012682.5	-
dre-miR-142a-5p	1	1	0	0	-0.11	poorly conserved	pfn2l	ENSDARG00000012682.3	-
dre-miR-142a-5p	1	1	0	0	-0.07	poorly conserved	pfn2l	ENSDARG00000012682.2	-
dre-miR-142a-5p	4	0	3	1	-0.07	poorly conserved	pomca	ENSDARG00000043135.1	-
dre-miR-142a-5p	1	0	0	1	-0.04	poorly conserved	apoc2	ENSDARG00000092155.2	-
dre-miR-142a-5p	1	0	0	1	-0.04	poorly conserved	apoc2	ENSDARG00000092155.1	-
dre-miR-142a-5p	1	1	0	0	-0.04	poorly conserved	pfn2l	ENSDARG00000012682.1	-
dre-miR-144-3p	2	1	0	1	-0.44	broadly conserved	pomcb	ENSDARG00000069307.1	-
dre-miR-144-3p	1	1	0	0	-0.38	broadly conserved	pomca	ENSDARG00000043135.2	-
dre-miR-144-3p	2	0	2	0	-0.37	broadly conserved	cyp19a1b	ENSDARG00000009852.3	-
dre-miR-144-3p	2	2	0	0	-0.36	broadly conserved	pomca	ENSDARG00000043135.1	-
dre-miR-144-3p	2	0	2	0	-0.33	broadly conserved	cyp19a1b	ENSDARG00000009852.2	-
dre-miR-144-3p	2	0	2	0	-0.22	broadly conserved	cyp19a1b	ENSDARG00000009852.1	-
dre-miR-144-3p	2	0	0	2	-0.18	broadly conserved	pfkma	ENSDARG00000014179.1	-
dre-miR-144-3p	1	0	1	0	-0.04	broadly conserved	atp6v1ba	ENSDARG00000013443.1	-
dre-miR-181c-5p	1	0	1	0	-0.17	broadly conserved	apoa1a	ENSDARG00000012076.2	-
dre-miR-181c-5p	1	0	1	0	-0.17	broadly conserved	pfn2l	ENSDARG00000012682.4	-
dre-miR-181c-5p	1	0	1	0	-0.17	broadly conserved	pfn2l	ENSDARG00000012682.6	-
dre-miR-181c-5p	1	0	1	0	-0.16	broadly conserved	apoa1a	ENSDARG00000012076.1	-
dre-miR-181c-5p	1	0	1	0	-0.16	broadly conserved	pfn2l	ENSDARG00000012682.5	-
dre-miR-181c-5p	1	0	1	0	-0.14	broadly conserved	pfn2l	ENSDARG00000012682.3	-
dre-miR-181c-5p	1	0	1	0	-0.12	broadly conserved	pfn2l	ENSDARG00000012682.2	-
dre-miR-181c-5p	1	0	1	0	-0.10	broadly conserved	pfn2l	ENSDARG00000012682.1	-
dre-miR-181c-5p	1	0	1	0	-0.07	broadly conserved	pomcb	ENSDARG00000069307.1	-
dre-miR-181c-5p	1	0	0	1	-0.05	broadly conserved	pfkma	ENSDARG00000014179.2	-
dre-miR-181c-5p	1	0	0	1	-0.05	broadly conserved	pfkma	ENSDARG00000014179.1	-
dre-miR-181c-5p	2	1	1	0	> -0.05	broadly conserved	pomca	ENSDARG00000043135.1	-
dre-miR-200a-3p	1	0	1	0	-0.23	broadly conserved	apoa1a	ENSDARG00000012076.1	-
dre-miR-200a-3p	4	0	3	1	-0.19	broadly conserved	pomca	ENSDARG00000043135.1	-
dre-miR-200a-3p	1	0	1	0	-0.18	broadly conserved	cnn3a	ENSDARG00000008359.1	-
dre-miR-200b-3p	3	0	2	1	-0.42	broadly conserved	cyp19a1b	ENSDARG00000009852.3	-
dre-miR-200b-3p	3	0	2	1	-0.39	broadly conserved	cyp19a1b	ENSDARG00000009852.2	-
dre-miR-200b-3p	3	0	2	1	-0.27	broadly conserved	cyp19a1b	ENSDARG00000009852.1	-
dre-miR-200b-3p	1	1	0	0	-0.22	broadly conserved	cnn3a	ENSDARG00000008359.1	-

miRNA	3' UTR binding site number	8mer	7mer-m8	7mer-1A	Target Scan Score	miRNA conserved across vertebrates	Targeted studied transcript	ENSEMBL ID	Tissue specific
dre-miR-203a-3p	1	0	1	0	-0.13	broadly conserved	aldh9a1b	ENSDARG00000037061.1	-
dre-miR-203a-3p	2	0	2	0	> -0.04	broadly conserved	pomca	ENSDARG00000043135.1	-
dre-miR-203a-3p	1	0	1	0	> -0.02	broadly conserved	pfn2l	ENSDARG00000012682.5	-
dre-miR-203a-3p	1	0	1	0	> -0.02	broadly conserved	pfn2l	ENSDARG00000012682.6	-
dre-miR-203a-3p	1	0	1	0	> -0.02	broadly conserved	pfn2l	ENSDARG00000012682.1	-
dre-miR-203a-3p	1	0	1	0	> -0.02	broadly conserved	pfn2l	ENSDARG00000012682.2	-
dre-miR-203a-3p	1	0	1	0	> -0.02	broadly conserved	pfn2l	ENSDARG00000012682.3	-
dre-miR-203a-3p	1	0	1	0	> -0.02	broadly conserved	pfn2l	ENSDARG00000012682.4	-
dre-miR-23b	1	0	1	0	-0.19	broadly conserved	pomca	ENSDARG00000043135.2	-
dre-miR-23b	3	1	1	1	-0.19	broadly conserved	pomca	ENSDARG00000043135.1	-
dre-miR-27b-3p	2	0	0	2	-0.26	broadly conserved	aldh9a1b	ENSDARG00000037061.2	-
dre-miR-27b-3p	2	0	0	2	-0.25	broadly conserved	aldh9a1b	ENSDARG00000037061.1	-
dre-miR-27b-3p	2	0	1	1	-0.16	broadly conserved	pfn2l	ENSDARG00000012682.2	-
dre-miR-27b-3p	2	0	1	1	-0.14	broadly conserved	pfn2l	ENSDARG00000012682.1	-
dre-miR-27b-3p	1	0	0	1	-0.13	broadly conserved	pfkma	ENSDARG00000014179.1	-
dre-miR-27b-3p	1	0	0	1	-0.10	broadly conserved	aldh9a1b	ENSDARG00000037061.3	-
dre-miR-27b-3p	1	0	0	1	-0.02	broadly conserved	pfn2l	ENSDARG00000012682.4	-
dre-miR-27b-3p	1	0	0	1	-0.02	broadly conserved	pfn2l	ENSDARG00000012682.6	-
dre-miR-27b-3p	1	0	0	1	-0.01	broadly conserved	pfn2l	ENSDARG00000012682.5	-
dre-miR-27b-3p	1	0	0	1	> -0.01	broadly conserved	pfn2l	ENSDARG00000012682.3	-
dre-miR-27b-3p	1	0	0	1	> -0.01	broadly conserved	pomca	ENSDARG00000043135.1	-
dre-miR-375	1	0	0	1	-0.01	broadly conserved	pomca	ENSDARG00000043135.1	pancreas[3,4]
dre-miR-722	1	0	1	0	-0.07	broadly conserved	pfkma	ENSDARG00000014179.1	-
dre-miR-722	2	0	1	1	-0.03	broadly conserved	pomca	ENSDARG00000043135.1	-
dre-miR-722	1	0	0	1	-0.02	broadly conserved	pfn2l	ENSDARG00000012682.5	-
dre-miR-722	2	0	0	2	> -0.02	broadly conserved	pfn2l	ENSDARG00000012682.3	-
dre-miR-722	2	0	0	2	> -0.02	broadly conserved	pfn2l	ENSDARG00000012682.2	-
dre-miR-722	2	0	0	2	> -0.02	broadly conserved	pfn2l	ENSDARG00000012682.1	-
dre-miR-722	1	0	0	1	> -0.01	broadly conserved	apoa1a	ENSDARG00000012076.1	-
dre-miR-722	1	0	0	1	> -0.01	broadly conserved	hkdc1	ENSDARG00000038703.1	-
dre-miR-722	1	0	0	1	> -0.01	broadly conserved	hkdc1	ENSDARG00000038703.2	-

[3] W. P. Kloosterman, A. K. Lagendijk, R. F. Ketting, J. D. Moulton, and R. H. A. Plasterk, "Targeted inhibition of miRNA maturation with morpholinos reveals a role for miR-375 in pancreatic islet development," PLoS Biol., vol. 5, no. 8, pp. 1738–1749, Aug. 2007.

[4] Y. Liang, D. Ridzon, L. Wong, and C. Chen, "Characterization of microRNA expression profiles in normal human tissues," BMC Genomics, vol. 8, p. 166, Jun. 2007.

Supplemental File SF2. Primer sequences and SYBR-Green™-based real-time RT-PCR assay conditions used to quantify relative miRNA transcript abundance changes.

miRNA	Efficiency (%)	R^2	Annealing T (°C)	Size Amplicon (nt)	miRBase ID	NCBI gene ID	Primer FW
dre-miR-1	96.1	0.983	56.0	22	MIMAT0001768	494473	TGGAATGTAAAGAAGTATGTAT
dre-miR-101a	107.6	0.987	53.0	22	MIMAT0001814	100033623	TACAGTACTGTGATAACTGAAG
dre-miR-122	105.7	0.997	60.0	22	MIMAT0001818	100033627	TGGAGTGTGACAATGGTGTTTG
dre-miR-133a-5p	109.4	0.996	55.0	22	MIMAT0003404	100033653	AGCTGGTAAAATGGAACCAAAT
dre-miR-142a-3p	99.3	0.987	58.5	23	MIMAT0003160	100033664	TGTAGTGTTTCCTACTTTATGGA
dre-miR-142a-5p	105.6	0.981	57.5	21	MIMAT0001838	100033664	CATAAAGTAGAAAGCACTACT
dre-miR-144-3p	-	-	-	20	MIMAT0001841	100033668	TACAGTATAGATGATGTACT
dre-miR-181c-5p	99.7	0.991	53.0	22	MIMAT0001852	100033680	CACATTCATTGCTGTCGGTGGG
dre-miR-200a-3p	102.5	0.983	60.0	21	MIMAT0001861	100033692	TAACACTGTCTGGTAACGATG
dre-miR-200b-3p	102.4	0.992	54.5	22	MIMAT0001862	100033693	TAATACTGCCTGGTAATGATGA
dre-miR-203a-3p	99.8	0.984	54.5	22	MIMAT0001278	100033770	GTGAAATGTTTAGGACCACTTG
dre-miR-23b	96.5	0.984	51.0	22	MIMAT0001791	100033589	ATCACATTGCCAGGGATTACCA
dre-miR-27b-3p	101.3	0.986	60.0	21	MIMAT0001797	100033600	TTCACAGTGGCTAAGTTCTGC
dre-miR-375	96.5	0.985	56.0	22	MIMAT0001876	100271844	TTTGTTCGTTCGGCTCGCGTTA
dre-miR-722	101.0	0.981	58.0	22	MIMAT0003748	100033732	TTTTGCAGAAACGTTTCAGATT

Supplemental File SF3. Correlations between BPA exposure concentration and organism-level metabolic phenotype parameters in 5 dpf eleutheroembryos: feed-intake (**A**), oxidative metabolism-related energy expenditure (**B**), locomotion in light (**C**) and locomotion in dark (**D**). Four different dose-response curves for monotonic and non-monotonic patterns were considered (linear, 2º order polynomial, sigmoidal and Gaussian) to account for non-monotonic dose responses as previously described [113]. A likelihood ratio test (LRT) against an intercept-only null model was used to examine the better fit-model, which is reported in each graph, as its correlation coefficient r^2 and p-values. $p \leq 0.05$ identifies correlations with significantly better fits than the null model.

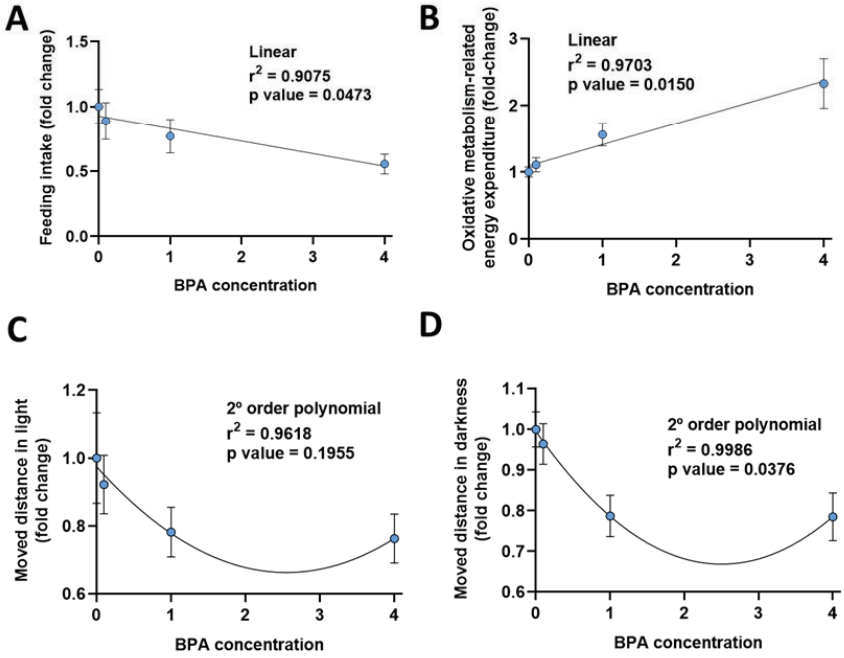

Supplemental File SF4. Individual relative mRNA (**A**) and miRNA (**B**) transcript abundance changes (fold-change) in exposure groups normalized to control group in 5dpf eleutheroembryos. Individual datapoints as well as average abundance is shown in addition to S.E.M. Data were analyzed by ANOVA and Tukey's post-hoc tests were used to identify identify significant differences relative to the negative control group: * for $p \leq 0.05$; ** for $p \leq 0.01$; *** for $p \leq 0.001$; **** for $p \leq 0.0001$.

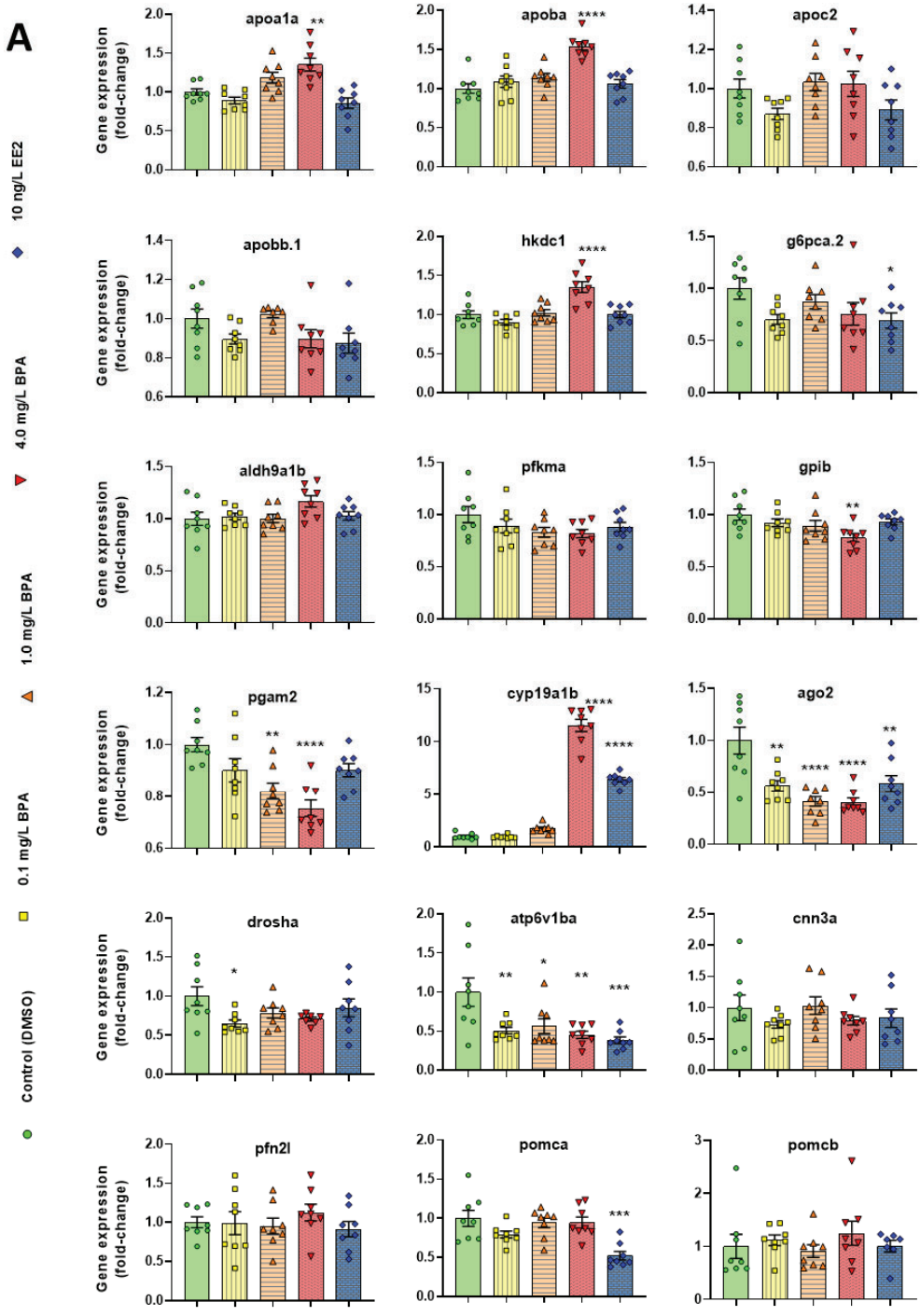

Supplemental File SF4. Individual relative mRNA (**A**) and miRNA (**B**) transcript abundance changes (fold-change) in exposure groups normalized to control group in 5dpf eleutheroembryos. Individual datapoints as well as average abundance is shown in addition to S.E.M. Data were analyzed by ANOVA and Tukey's post-hoc tests were used to identify identify significant differences relative to the negative control group: * for $p \leq 0.05$; ** for $p \leq 0.01$; *** for $p \leq 0.001$; **** for $p \leq 0.0001$.

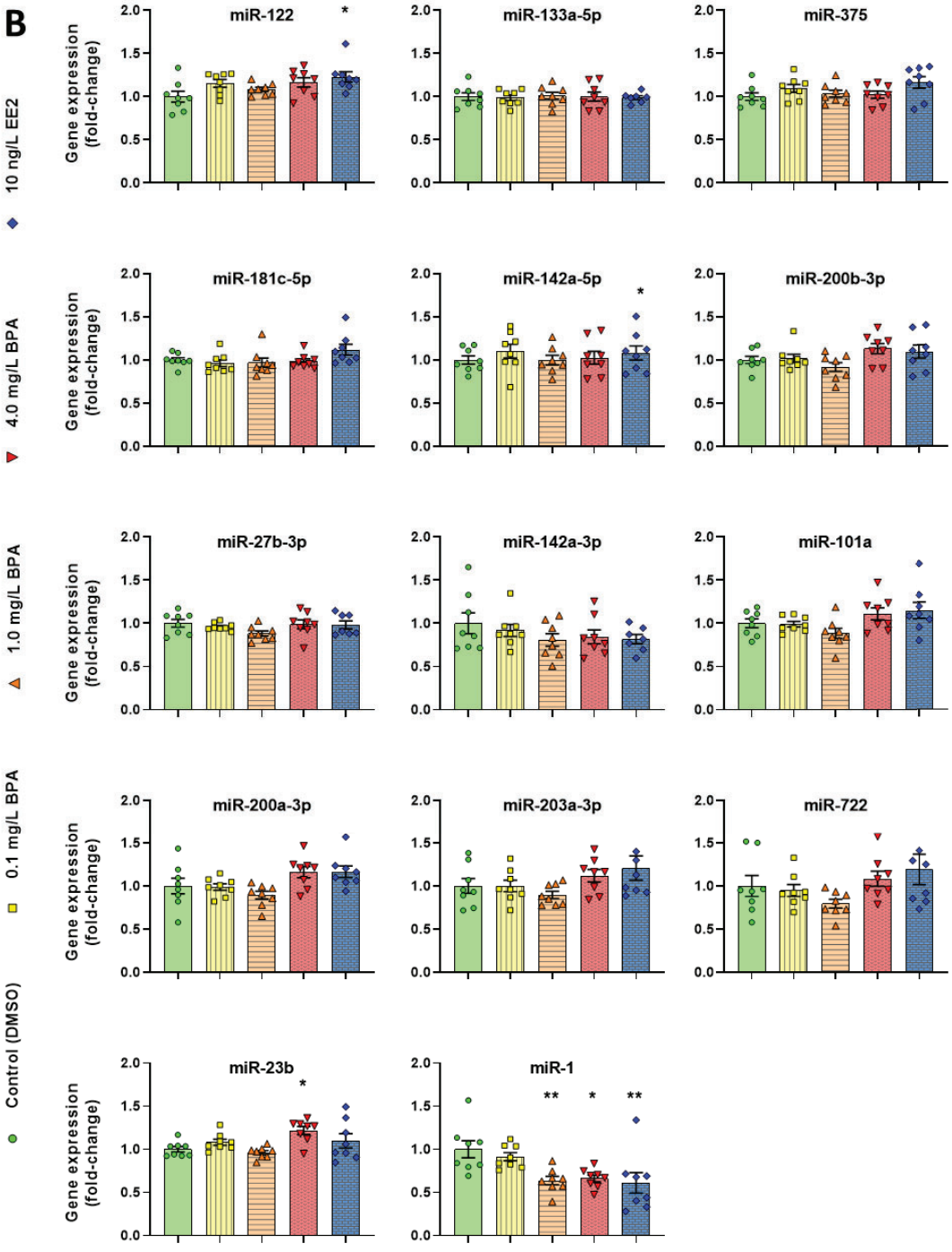

Supplemental File SF5. Heatmap of mRNA and miRNA transcripts in different developmental exposure groups of 5 dpf eleutheroembryos (**A**) and 49 dpf juveniles with different developmental exposure history and dietary treatment (**B**). Fold-change values compared to the control group are represented, and higher or lower relative abundance indicated in red and blue, respectively. Partial Least Squares (PLS) analyses of 5 dpf eleutheroembryos (**C**), and ND-fed (**D**) or HFD-fed (**E**) 49 dpf juveniles. Gene expression of each dataset was used as observable variables (matrix X) and the group classification as predicted variables (matrix Y). The first two components explained 26 % of the X-matrix and an 85 % of the Y-matrix (**C**); 49 % of the X matrix and 86 % of the Y-matrix (**D**), and a 52 % of the X-matrix and a 34 % of the Y-matrix (**E**). Small colored features represent the individual replicates; bigger features represent the mean of each condition.

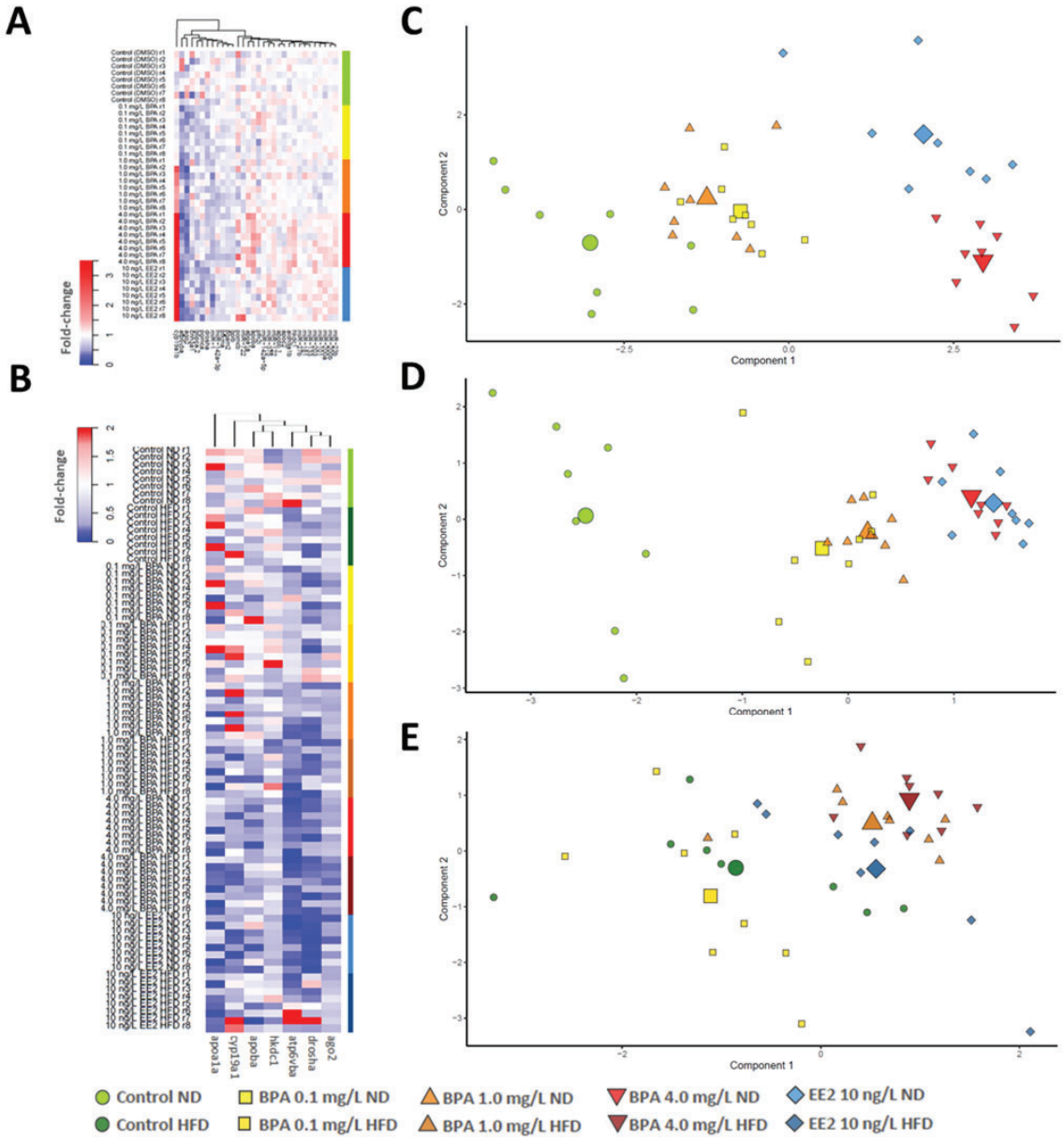

Supplemental File SF6. Average survival (%) before (29 dpf; **A**) and following (37 dpf; **B**) dietary treatments. Data were analyzed by ANOVA and two-way ANOVA respectively, with a significance threshold set at $p \leq 0.05$.

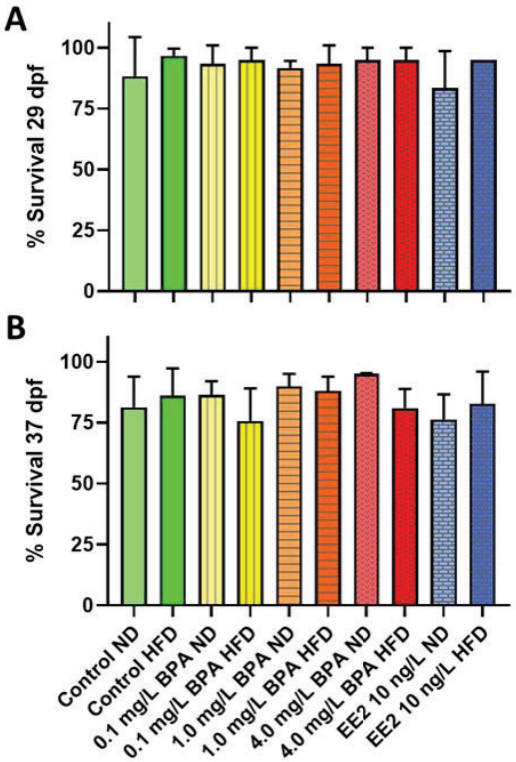

Supplemental File SF7. Overall (**A**) and group-dependent (**B**) exponential correlations between body weight and body length in juvenile zebrafish. Individual fish data are represented.

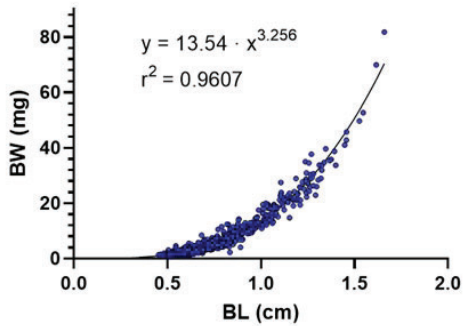

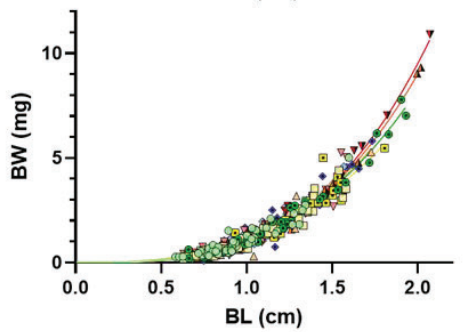

45 dpf	b value	Confidence intervals
Ctl ND	3.198	2.926 to 3.478
Ctl HFD	2.958	2.791 to 3.134
0.1 mg/L BPA ND	2.92	2.633 to 3.228
0.1 mg/L BPA HFD	2.755	2.418 to 3.118
1.0 mg/L BPA ND	3.127	2.877 to 3.382
1.0 mg/L BPA HFD	3.161	3.057 to 3.266
4.0 mg/L BPA ND	3.294	3.002 to 3.611
4.0 mg/L BPA HFD	3.254	3.032 to 3.482
EE2 10 ng/L ND	3.069	2.825 to 3.322
EE2 10 ng/LHFD	2.912	2.616 to 3.236

Supplemental File SF8. Correlations between BPA exposure concentration and organism-level metabolic phenotype parameters in juvenile zebrafish on ND and HFD diets: oxidative metabolism-related energy expenditure (**A-B**), feed intake (**C-D**), locomotion in light (**E-F**) locomotion in dark (**G-H**). Four different dose-response curves for monotonic and non monotonic patterns were considered (linear, 2º order polynomial, sigmoidal and Gaussian) as previously described [113]. A likelihood ratio test (LRT) against an intercept-only null model was used to examine the better fit-model, which is reported in each graph, as its correlation coefficient r^2 and p-values. $p \leq 0.05$ identifies correlations significantly better fits than the null model.

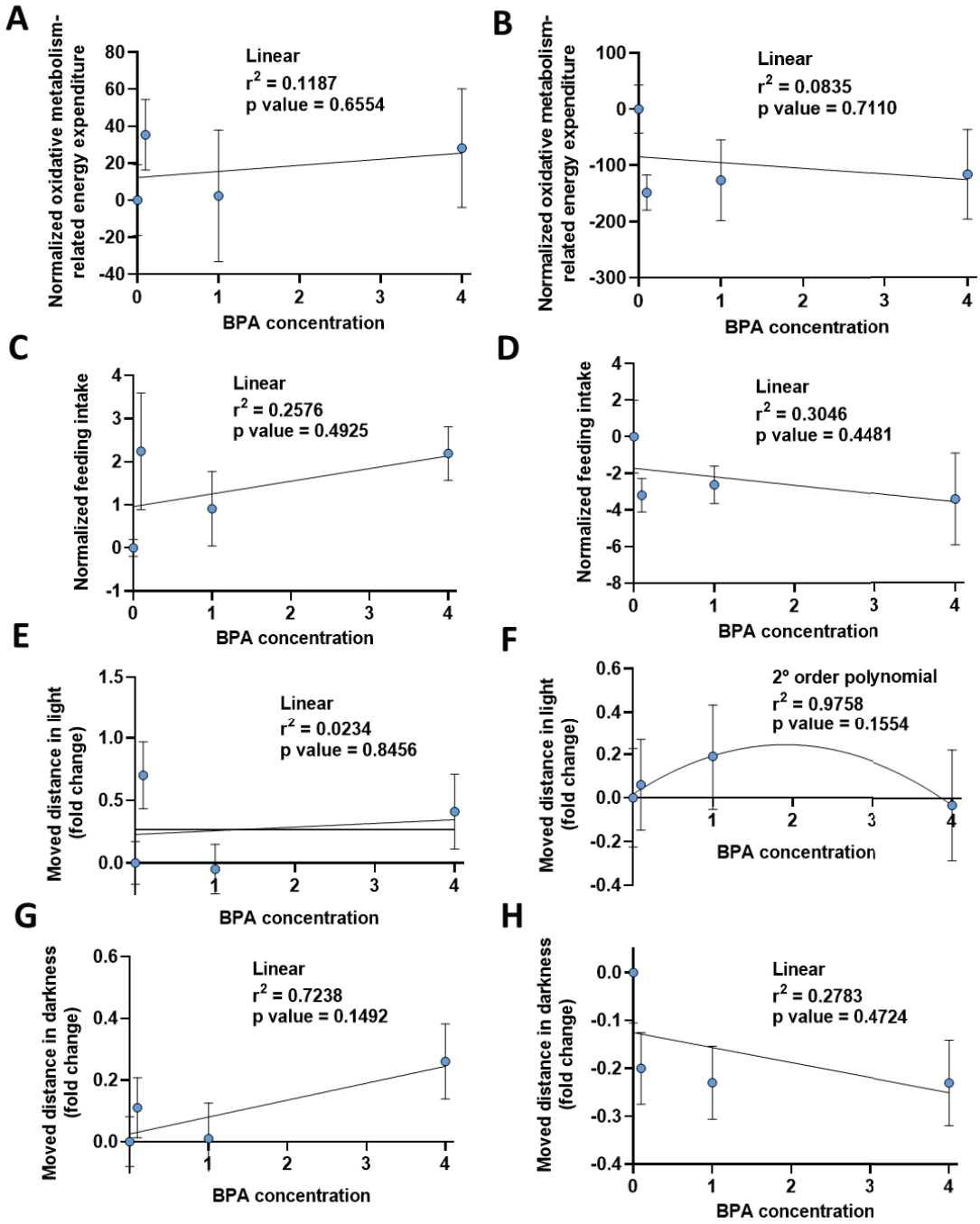

Supplemental File SF9. Individual relative mRNA transcript abundance changes (fold-change) in exposure groups normalized to control group in 49 dpf juvenile zebrafish. Individual datapoints as well as average abundance is shown in addition to S.E.M. Data were analyzed by ANOVA and Tukey's post-hoc tests were used to identify significant differences relative to the negative control group. Signifcant differences were indicated as follows: * for $p \leq 0.05$; ** for $p \leq 0.01$; *** for $p < 0.001$; **** for $p < 0.0001$.

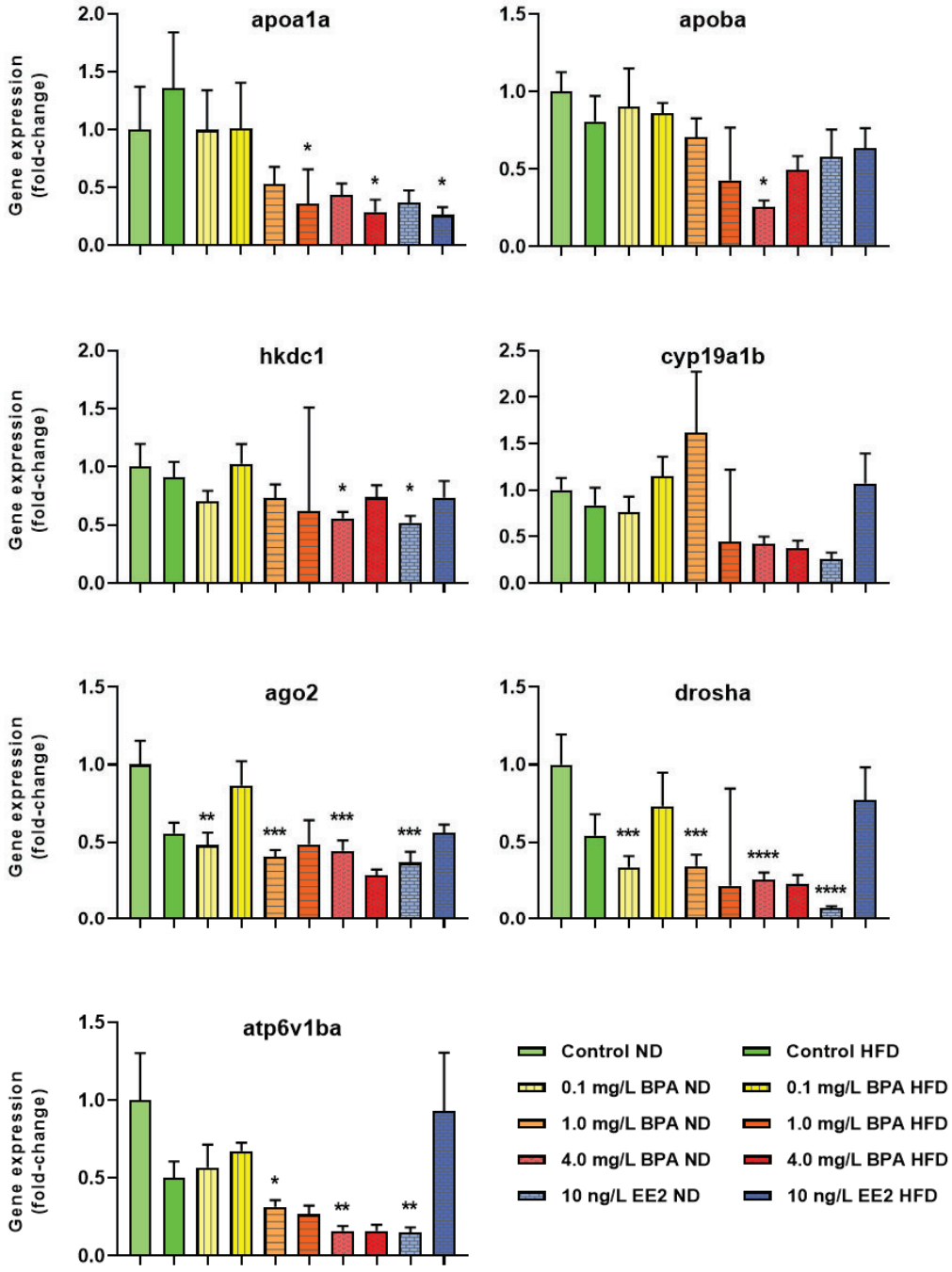

Supplemental File SF10. Root-mean-square deviation of atomic positions (RMSD) used to validate the molecular docking of the different receptors with BPA (in red) and EE2 (in black). Values were below 3 Ångstroms indicating appropriateness of calculations.

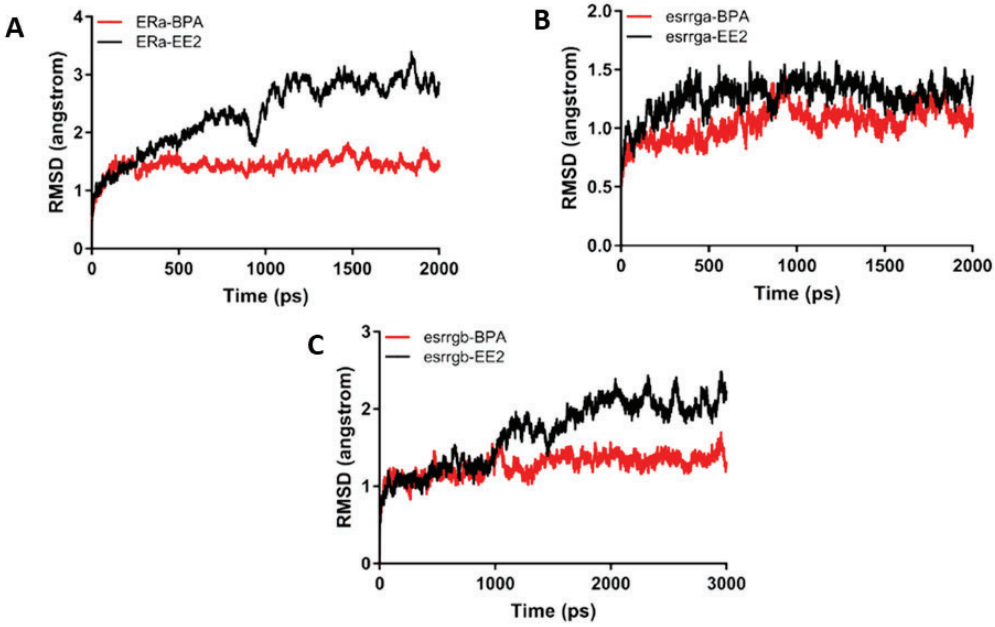

Supplemental File SF11. Additional assays conducted in eleutheroembryos and juvenile zebrafish: Relative muscle birefringence / surface area normalized to control in 5 dpf eleutheroembryos (**A**). Average data and S.E.M. are shown and data was analyzed by ANOVA ($p > 0.05$; no statistical difference). Two- dimensional plot of oxygen consumption rate (OCR) and extracellular acidification rate (ECAR) in 5 dpf eleutheroembryos (**B**). Individual ANOVAs were performed for OCR and ECR ($p > 0.05$; no statistical differences). Nile red-stained neutral lipid / surface area in 45 dpf juvenile zebrafish (**C**). A two-way ANOVA was performed against control group ($p > 0.05$; no statistical differences for developmental exposure history, dietary treatment and their interaction).

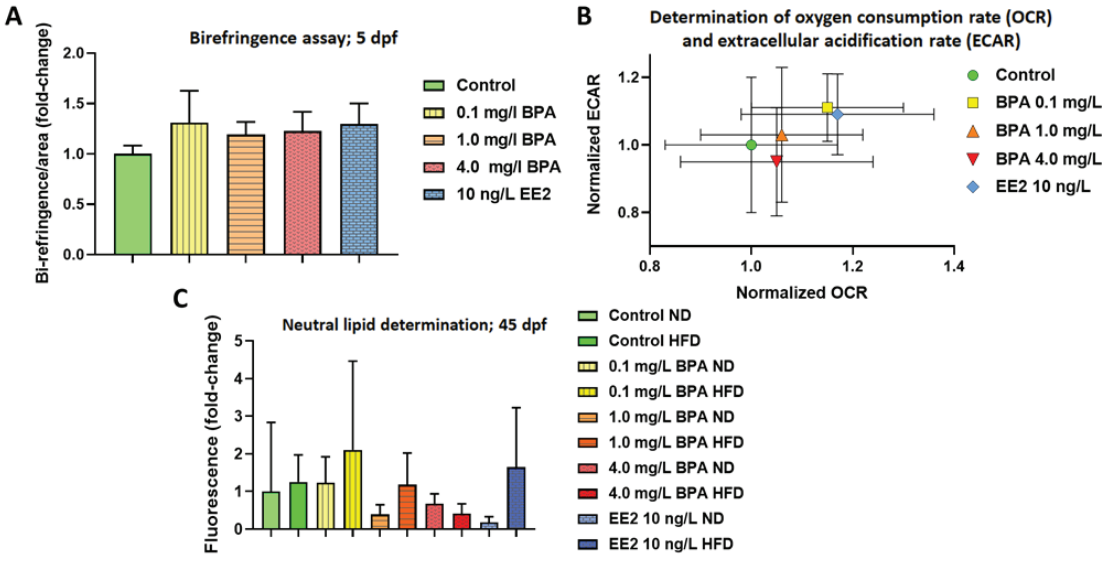

Scientific article VII

Alterations of DNA methylation levels of key genes related to BPA exposures in zebrafish embryos

Authors: R. Martínez, S. Heath, R. Tauler, B. Piña, L. Navarro-Martín

Status: In preparation

Journal: -

DOI: -

Alterations of DNA methylation levels of key genes related to BPA exposures in zebrafish embryos

Rubén Martínez[1,2], Simon Heath[3,4], Romà Tauler[1], Benjamin Piña[1], Laia Navarro-Martín[1]*

[1] Institute of Environmental Assessment and Water Research, IDAEA-CSIC, Barcelona, Catalunya, 08034, Spain
[2] Universitat de Barcelona (UB), Barcelona, Catalunya, 08007, Spain
[3] CNAG-CRG, Centre for Genomic Regulation (CRG), Barcelona Institute of Science and Technology (BIST), Barcelona, 08028, Spain
[4] Universitat Pompeu Fabra (UPF), Barcelona, 08003, Spain

* Corresponding author: Laia Navarro-Martín, Institute of Environmental Assessment and Water Research, IDAEA-CSIC, Jordi Girona 18, 08034 Barcelona, Spain TEL. +34 93 4006100, ext 1503; E-mail: laianavarromartin@gmail.com

Abstract

An emerging concern related to endocrine disrupting chemicals (EDCs) is their ability to modify cellular regulatory mechanisms long after the exposure occurred, via epigenetics. Previous studies showed BPA treatment elicit alterations in both DNA methylation and transcript levels for several genes in zebrafish embryos, although the possible functional relationship between both effects is still unknown. In the present study, we studied methylation patterns of four genes in zebrafish embryos exposed to 17.5 µM of BPA in a 0-5 dpf time window, using the BisPCR^2 method. Selected genes included cytochrome P450a1b (*cyp19a1b*) and aldehyde dehydrogenase 1a2 (*aldh1a2*), whose transcription levels were significantly increased upon BPA treatment, and two control genes, *ppiaa* and *cyp19a1a*, whose expression remained unaltered by the treatment. Our results revealed significant differences ranging from 0.1 to 2 % in the DNA methylation in several CpG positions. In BPA-exposed eleutheroembryos, we observed: 1) A significant *aldh1a2* hypomethylation (mostly in its promoter region), which correlated with its increased gene expression; 2) No effects in gene expression or DNA methylation in *ppiaa*; 3) Hypermethylation of *cyp19a1b* promoter region and hypomethylation of its first intron; 4) A general hypermethylation of *cyp19a1a*, which remained silent in both control and treated samples. Our results indicate a complex regulation mechanism for BPA-responsive genes, and suggest the need for integrative transcriptomic and epigenetic platforms to develop cost-effective high-throughput screenings to identify and better understand the epigenetic signatures of exposure to EDCs and their epigenetic mode of action.

1. Introduction

An emerging interest related to substances of very high concern, such as the endocrine disrupting chemicals (EDCs), is that they are able to modify cellular regulatory mechanisms long after the actual exposure occurred. Long-term effects are thought to be mediated by epigenetics (Barouki et al., 2018; Csoka and Szyf, 2009), although is not clear if it happens through chromatin packaging changes (via DNA methylation or histone modifications) and/or modulation of miRNAs abundance. Commonly, epigenetic modifications are maintained after cell divisions and they exert a key role in the formation of natural phenotypes. When they are environmentally-induced (e.g. after the exposure to an endocrine disruptor or temperature changes), they can lead to several adverse effects and they can even be inherited between generations (Guerrero-Bosagna and Skinner, 2012; Kamstra et al., 2017; Navarro-Martín et al., 2011; Skinner et al., 2010). Indeed, changes in certain regions of the methylome has been reported after the exposure to several EDCs (Awada et al., 2019; Olsvik et al., 2019a; Senyildiz et al., 2017; T. Zhang et al., 2018; Zhang et al., 2012; Y. Zhang et al., 2018). This could lead, in turn, to changes in the transcriptome, as DNA methylation of a gene has been traditionally inversed related with its expression (Du et al., 2012; Phillips Theresa, 2008). All these matters are studied by environmental epigenetics, field in which zebrafish (*Danio rerio*) has arisen itself during last years as an excellent model (Kamstra et al., 2015).

Bisphenol A (BPA) is a monomer worldwide used in plastics, but its use has been progressively partially banned, due to its numerous adverse effects (estrogenicity, obesogenicity, reproductive functions disruption or effects on glucose homeostasis, among others) (Alonso-Magdalena et al., 2010; Horan et al., 2018; Martínez et al., 2018; Mesnage et al., 2017; Moon, 2019; Rubin and Soto, 2009). Nevertheless, BPA is still used for some purposes and its production and release to the environment were estimated to be between 7.2 and 8.4 millions tons, and 450 tons/year, respectively (Grand View Research Inc, 2015; Kadasala et al., 2016; U S Environmental Protection Agency, 2010). After it was reported that BPA could induce obesity in mice via hypomethylation of agouti gene (Dolinoy et al., 2007), other studies demonstrated that BPA could affect DNA methylation also in other species (Mileva et al., 2014; Singh and Li, 2012). For example, developmental BPA exposure could be linked to changes in DNA methylation of *grin2b* (an important gene for neuronal function) in rats and humans in a sexual dimorphic fashion (Alavian-Ghavanini et al., 2018), or to several genes in the hypothalamus and hippocampus of adult rats (Cheong et al., 2018). In fish, it was reported the hypermethylation of *star* and *hsd11b2* and hypomethylation of *hsd3b* (steroids-related genes) in female rare minnow (*Gobiocypris rarus*), when exposed to 15 µg/L of BPA, were significantly correlated to their mRNA levels and to ER-EREs (estrogen receptor - estrogen response elements) interactions (T. Zhang et al., 2018). Also, it was reported a reduction in global DNA methylation in zebrafish testes and ovaries following exposure to 1 mg/L BPA (Laing et al., 2016), and heavy alterations in the expression of *dnmts*

(transcripts that encoded for DNA methyltransferases, key proteins in methylation maintenance and de novo methylation) after exposure to 5 µg/L BPA (Santangeli et al., 2016). Zebrafish embryos exposed to 0.1 nM - 30 µM of BPA presented alterations of methylation patterns of genes associated with the nervous system development, which could be linked with abnormal swimming activity (Olsvik et al., 2019a). Interestingly, alteration of vison-related genes was also found in zebrafish embryos exposed to 0.1 - 4.0 mg/L BPA (Martínez et al., 2018), which in turn could explain the observed alterations in swimming behavior (Martínez et al., 2020; Olsvik et al., 2019a). In addition, another study found that embryos exposed to 0.1 - 8.0 mg/L BPA showed alterations in craniofacial parameters (including eye size), and induced yolk sac malabsorption syndrome (Martínez et al., 2019a) which could be explained by a decreased energy expenditure due to the lower locomotor activity (Olsvik et al., 2019a).

Methylome effects of exposures to EDCs can be studied following two approaches, which are both very valuable depending on which is the research question to answer. Whole genome bisulfite sequencing (WGBS) studies DNA methylation changes in a holistic manner, but offers low coverage at the CpG level, which in most cases means that evaluation of methylation levels needs to be performed at the region level. This approach results in the detection of methylation differences usually higher than 10% (Chandra et al., 2018; Olsvik et al., 2019b)) making it less sensitive to small changes. Conversely to WGBS, the use of the BisPCR^2 method (Bernstein et al., 2015), which is based in targeted bisulfite sequencing, permits higher sequence depth allowing for high individual CpG coverage and is capable to detect smaller percentage methylation change in very specific genomic regions (Kitraki et al., 2015).

With the aim to better understand the model of action of BPA at the epigenetic level, we have studied DNA methylation levels of two key genes identified to be over-expressed in BPA exposed zebrafish embryos (Martínez et al., 2018; Ortiz-Villanueva et al., 2017): 1) cytochrome P450 a1b (*cyp19a1b*), responsible for the biosynthesis of estrogens from androgens, and involved in the response to estrogenic compounds (such as BPA); and 2) aldehyde dehydrogenase 1a2 (*aldh1a2*), which catalyzes the synthesis of retinoic acid (RA) from retinaldehyde and a key player in the retinol pathway. In addition, we also studied two genes that were not affected by BPA exposures at the transcriptomic level: 1) *cyp19a1a* (a *cyp19a1b* homologous and highly expressed in gonads), but which is not yet expressed at the studied stage (Yin et al., 2017); and 2) peptidylprolyl isomerase Aa (*ppiaa*), which is widely expressed through development and in adults stages, and which is generally used as a reference gene (Fuller-Carter et al., 2015; Sato and Takeda, 2013).

2. Materials and methods

2.1. Animal maintenance and rearing conditions

All adult wild-type zebrafish (*Danio rerio*, 12-18 months old), obtained eggs by natural mating, and developing embryos were kept and reared under controlled standard conditions

(28.5 ± 1.0 °C, 12 L:12D photoperiod) in fish water as has been previously described (Martínez et al., 2019b). Eggs were collected and rinsed at 2 hours post fertilization (hpf) and fertilized ones were randomly placed in 6 multi-well plates at a density of 10 individuals per well in 3 ml of exposure solution (see section 2.2.). Experimental procedures were carried out following the institutional guidelines under a license from the local government (DAMM 7669, 7964) and were approved by the Institutional Animal Care and Use Committee (IACUC) at the Research and Development Centre (CID) of the Spanish National Research Council (CSIC).

2.2. BPA solutions preparation, zebrafish eggs/embryos exposure and sample collection

Bisphenol A (4,4'-(propane-2,2-diyl)diphenol; CAS-RN: 80-05-7; ≥99.0% purity) was provided by Sigma-Aldrich (St. Louis, MO, USA). High concentration stocks were performed in dimethyl sulfoxide (DMSO) and stored at 4 ºC. Fresh working solutions were newly prepared (by dilution of stocks in fish water) with a final DMSO concentration of 0.2% (v/v) and daily changed. In each 6-multiplate well 3 ml of a BPA solution and 10 eggs were placed at 2 hpf. Indeed, zebrafish eggs/embryos were exposed to 0.2 % of DMSO (as control group) or to 4 mg/L (17.5 µM) of BPA (as treated group) from 0 to 5 days post fertilization (dpf). Treated group BPA concentration was chosen based on the lowest observed effect concentration (LOEC) of gross morphological effects previously reported in an analogous exposure (Ortiz-Villanueva et al., 2017). A total of 10 biological replicates (8 zebrafish embryos per replicate) were collected, instantly frozen with dry ice and stored at -80 ºC.

2.3. Target genes and selected CpG positions

Four genes were selected based on abundance and BPA effects at the mRNA levels (Martínez et al., 2018; Ortiz-Villanueva et al., 2017), expecting that they would reflect different methylation status: 1) *cyp19a1b* (lowly expressed in controls and affected by BPA), 2) *aldh1a2* (highly expressed in controls and affected by BPA); 3) *cyp19a1a* (lowly expressed in controls and not affected by BPA); 4) *ppiaa* (highly expressed in controls and not affected by BPA). Promoter, first exon and first intron regions covering approximately 1500-3000 bp of each gene were selected and CpG positions located based in the *Danio rerio* reference genome GRCz10. Primers were designed on those regions using MethPrimer v1.1 software (Li and Dahiya, 2002) resulting in the analysis of a total of 25 amplicons, ranging from 133-348 bp, containing 141 CpG different positions (supplemental table ST1). A summary of the amplicons and CpG positions is shown in figure 1.

2.4. DNA extraction, sample preparation and deep sequencing

Sample DNA was extracted with the AllPrep DNA/RNA Mini Kit (Qiagen). To evaluate bisulfite conversion, standards were generated following Kamstra and collaborators methodology (Kamstra et al., 2017). Briefly, a DNA pool (generated by mixing the DNA of several random

samples) was used to generate 0% and 100% methylated standards. 0% methylated standard was

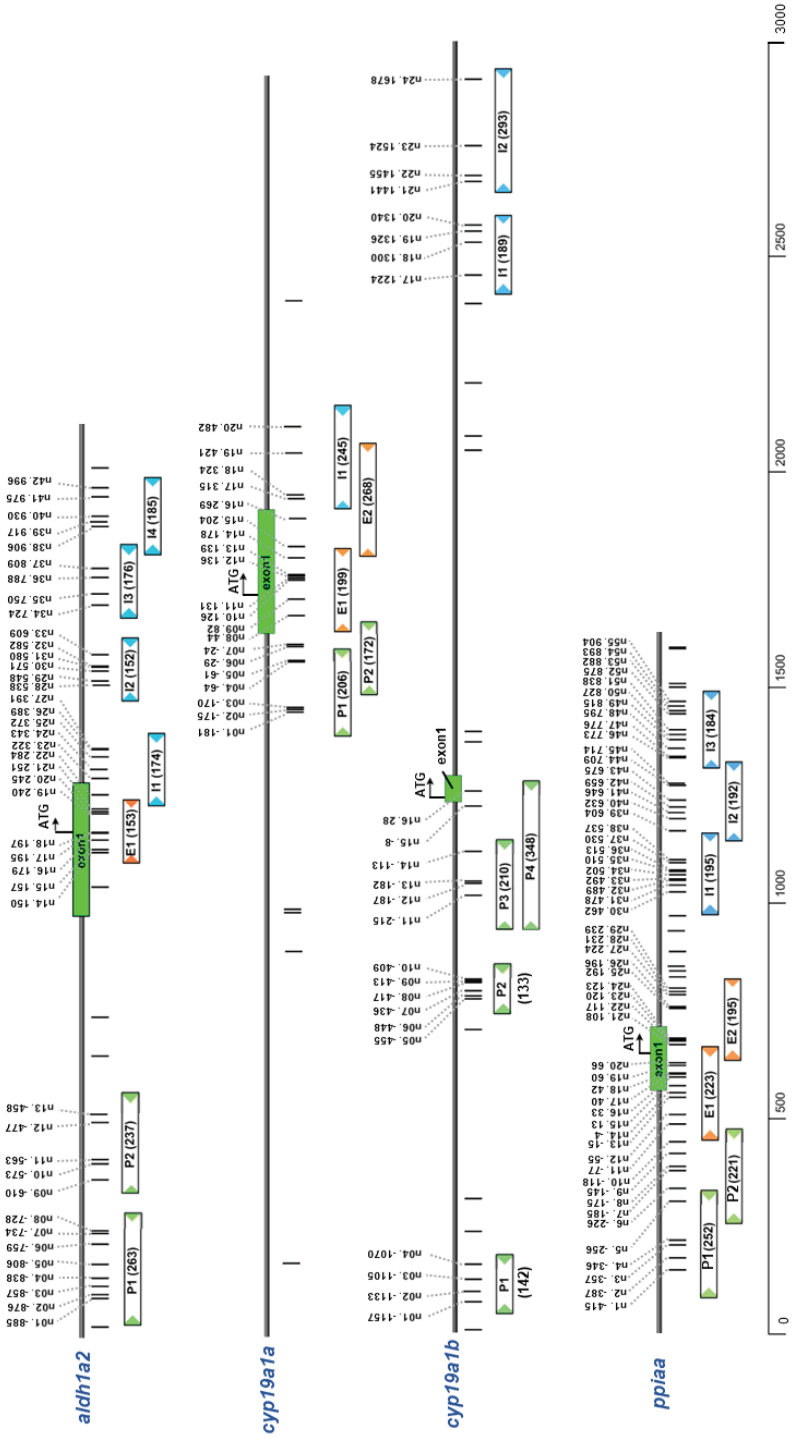

Figure 1. Scheme of the close regions (approximately ± 1500 base pairs) of the transcription starting site (TSS) of the four studied genes: *aldh1a2*, *cyp19a1a*, *cyp19a1b* and *ppiaa*. Each CpG position is represented by a vertical black line. Shortcut numeration and the relative position regarding the TSS has been added to those CpG positions amplified in this study. Amplicons in the promoter, exon and intron are labelled in green, orange and blue, respectively. Name assignment and length of each amplicon are indicated inside the box that represent each of them.

generated by REPLI-g Mini Kit (Qiagen) while CpG Methyltransferase (M.SssI) (Thermo Fisher Scientific) was used to obtain the 100% methylated standard. A 50% standard was generated by mixing same amounts of 0 and 100% standards. Both standards and samples were treated with bisulfite (which transforms all non-methylated cytosines to uracils) with EZ DNA Methylation-Gold™ Kit (Zymo Research). Afterwards, BisPCR^2 method (Bernstein et al., 2015) adapted by (Kamstra et al., 2017) was used for targeted bisulfite next generation sequencing. Briefly, DNA sequencing libraries were carried out following two rounds of PCR (PCR#1 and PCR#2) for target enrichment and sample Illumina barcoding (Bernstein et al., 2015), respectively. PCR conditions, primers used, as well other specifications are reported in supplemental tables ST1 and ST2. See supplementary material for a more detailed protocol. The final generated pool was sequenced at the Center for Genomic Regulation-National Center for Genomics Analysis (CRG-CNAG). Paired-end sequencing was performed on the Illumina MiSeq with a sequencing depth of 25.3 million. Pool of 25 libraries was sequenced with 15% PhiX Control v3 spike in (Illumina) using the 600-cycle MiSeq Reagent Kit v3 (Illumina) sequencing kit format following the manufacturer's protocol for paired end sequencing 2x300 with a simple 6bp index. Image analysis, base calling and quality scoring of the run were processed using the manufacturer's software Real Time Analysis (RTA 1.18.54) and followed by generation of FASTQ sequence files.

2.5. Bioinformatic analysis to determine methylation status of each CpG

Both read ends were trimmed to 125 bp as the sequences after this point showed extensive adaptor contamination. The trimmed reads were then mapped to the *D. rerio* reference genome (GRCz10) using the gem3 mapper in bisulfite mapping option (see (Merkel et al., 2019) for more details). Reads with mapping qualities (MAPQ) >=20 and that overlapped the target regions (given by the amplicons) were identified and each CpG methylation in these reads extracted using a custom script. This script worked by generating a table of all CpGs in the target regions. For each read overlapping a target region, the methylation status at each CpG position was recorded as methylated, non-methylated or unknown.

2.6. Statistics

For each CpG position, methylation percentage was calculated and differences were assessed by an exact Fisher test using the sum of the counts for each condition (considering methylation/unmethylation and control/treated). Statistics were performed in R (R Development Core Team, 2008) with the packages *factoextra* and *stats*. SeqBuilder Pro ® (DNAStar v.15, Madison, Wisconsin, USA, www.dnastar.com) software was used to generate diagrams of genomic regions and CpG positions. Remaining figures were performed in R (with the packages gplots and ggplot2) or GraphPad Prism version 8.1.2 (GraphPad Software, San Diego, California USA, www.graphpad.com).

3. Results

3.1. BPA effects on DNA methylation levels of individual CpG positions

Counts of methylated and unmethylated cytosine per each CpG position can be found in supplementary table ST3 for all samples and standards. First of all, we verified a high performance on the bisulfite conversion since DNA methylation average levels for all tested regions of the 0, 50 and 100% methylated standards were 0.56, 50.2 and 95.7%, respectively. DNA methylation levels were generally uniform across the entire gene regions, with some exceptions (Figure 2 upper panel per gene and supplementary figure SF1) : 1) In the case of *cyp19a1a*, DNA methylation ranged from 85.8 to 95.7% in all positions except for CpG position +315 (the very first CpG position of the first intron) that presented a methylation around 24%; 2) Methylation levels of *cyp19a1b* were a little more variable ranging from 79.2 to 95.2%, with position -113 showing a drop on DNA methylation to 62.6%. In general, variability in methylation percentage of *aldh1a2* was higher in the positions found in the promoter region (values ranging from 0.8 to

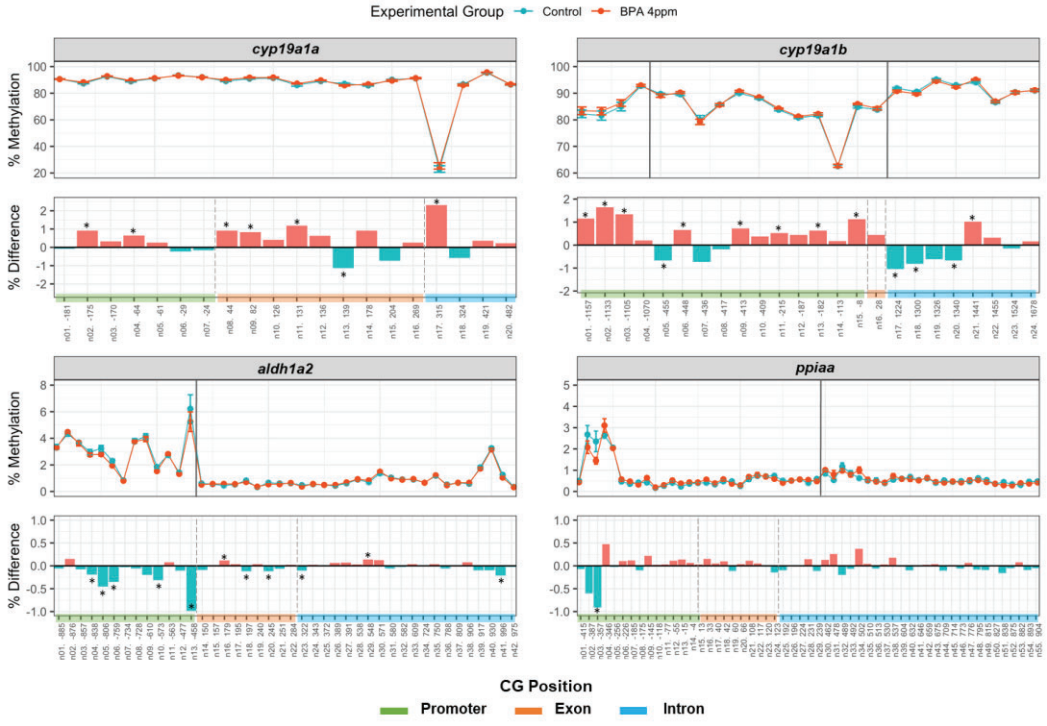

Figure 2. Percentage of methylation of each individual CpG position in the *aldh1a2*, *cyp19a1a*, *cyp19a1b* and *ppiaa* genes (upper panels). Continuous lines separates not consecutives CpGs. Red and blue bars (bottom panels) represent a hypermethylation in the treated and in the control group, respectively. Statistical differences (marked by an asterisk) were assessed by an exact Fisher test using the sum of the counts for each condition (10 replicates per condition, considering methylation/unmethylation and control/treated). Promoters, exons and introns are labelled in green, orange and blue, respectively, and are separated by dotted lines.

6.2%) than in the rest of the gene (ranging from 0.3 to 3.3%). Similarly, DNA methylation levels for *ppiaa* were slightly higher in the first part of the promoter region (with CpGs that reached methylation levels up to 3.1%) while the rest of the gene showed very low levels of methylation, from 0.2 to 1.2%.

Our results also revealed significant differences between control and BPA exposed eleutheroembryos mostly ranging from 0.1 to 2.2% of DNA methylation in several CpG positions (figure 2, bottom panel per gene). As it can be observed, BPA-exposed individuals presented a general *cyp19a1a* hypermethylation across the promoter, first exon and intron regions (6 significantly hypermethylated CpGs and only one hypomethylated CpG). Similarly, most of the significant differences in the DNA methylation levels of the *cyp19a1b* promoter corresponded to hypermethylated CpGs (8 out of 9) in the treated individuals. Nevertheless, DNA methylation levels of CpGs located close to the start of the first intron were mostly hypomethylated. On the other hand, BPA exposed individuals showed a general hypomethylation of *aldh1a2* (9 of the 11 significantly altered CpGs were hypomethylated), mostly in the promoter region. Interestingly, only a single CpG position in the ppiaa far promoter was differentially hypomethylated in BPA-treated samples, even considering that the high occurrence CpG of the *ppiaa* gene allowed us to study up to 55 different positions.

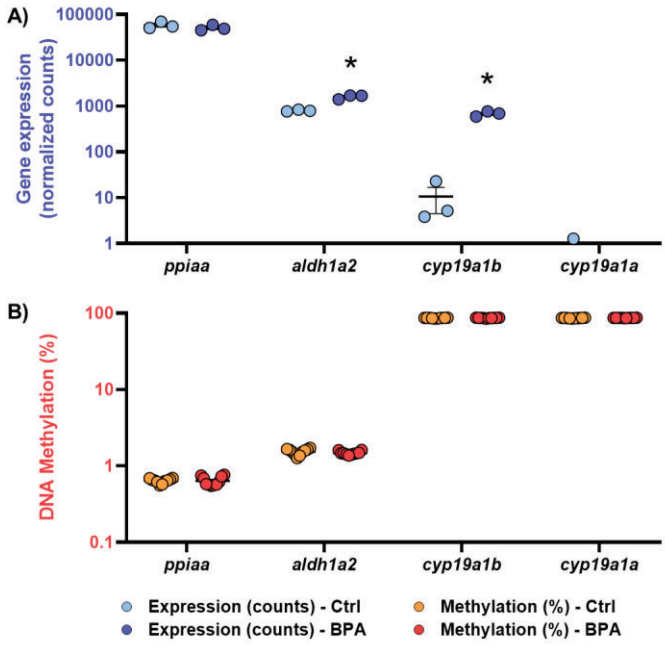

Figure 3. Gene expression (A, normalized counts, three replicates per condition) by RNA-Seq of *aldh1a2*, *cyp19a1a*, *cyp19a1b* and *ppiaa* (Ortiz-Villanueva et al., 2017) and their methylation status (B, percentage levels, 10 replicates per condition) both for control and BPA-exposed groups. Asterisk indicates statistically significant differences (t-test, $p < 0.05$) between treatments.

3.2. Correlation between averaged methylation levels and transcript abundance

Transcriptomic data obtained simultaneously in our laboratory (Ortiz-Villanueva et al., 2017) was used to test possible correlations between DNA methylation and transcript abundance (see figures 3 and 4). A general inverse relationship between gene expression and DNA methylation was observed (figure 3). For example, the studied regions of *ppiaa* and *aldh1a2* were found largely unmethylated (methylation average levels were 0.6% and 1.5%, respectively), whereas their basal transcript amount were extremely high (approximately 55000 and 1200 normalized

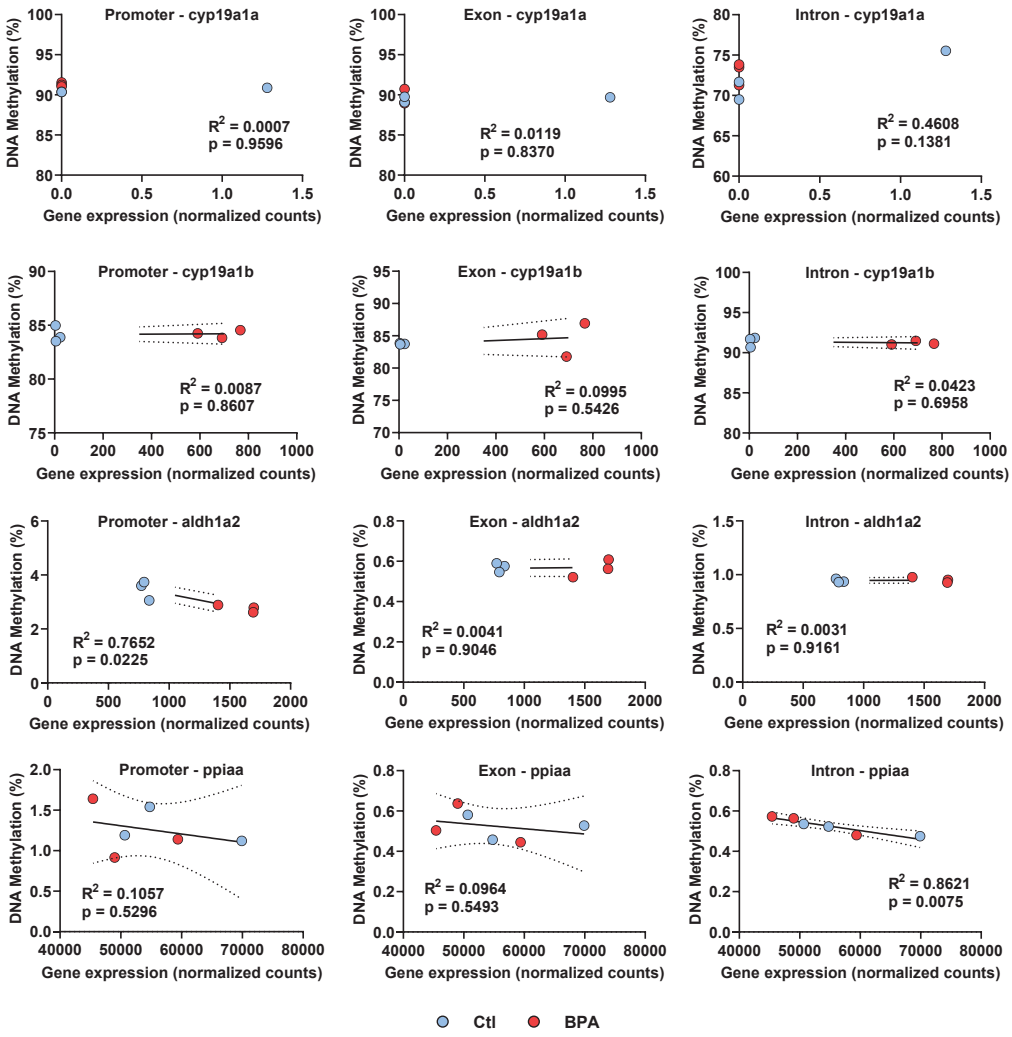

Figure 4. Linear regressions between gene expression (x axis) of *aldh1a2*, *cyp19a1a*, *cyp19a1b* and *ppiaa* (Ortiz-Villanueva et al., 2017) and their methylation levels (y axis) by promoter, exon and intron regions. Blue and red circles indicate control and BPA-exposed replicates, respectively. Only the three corresponding replicates in both studies (which were simultaneously DNA/RNA extracted) were considered.

counts, respectively, considering both control and BPA conditions). On the other hand, both *cyp19a1b* and *cyp19a1a* were highly methylated (86.5% and 86.6% of methylation, respectively) while their transcript abundance in control samples was very low. Gene expression of *cyp19a1a* was virtually null, both in controls and exposed individuals (less than one normalized count per sample). In the case of *cyp19a1b*, its expression was also extremely low in control samples (average of 11 normalized counts per sample) although it was highly increased in the exposed ones (around 700 normalized counts per sample). Nevertheless, the increased expression of neither *aldh1a2* nor *cyp19a1b* could be correlated by a statistically significant change in the general methylation levels of the respective genes. Only when the analysis was focused on specific genome regions, some significant correlations between methylation levels and transcript abundance could be reported, as for the *aldh1a2* promoter and *ppiaa* first intron (figure 4, $p < 0.05$).

4. Discussion

4.1. Usefulness of targeted bisulfite sequencing

Our results revealed significant differences mostly ranging from 0.1 to 2 in the % of DNA methylation in several CpG positions of the four analyzed genes (*aldh1a2*, *ppiaa*, *cyp19a1a* and *cyp19a1b*). These differences might seem small when compared to other WGBS studies (Chandra et al., 2018; Kitraki et al., 2015; Olsvik et al., 2019a), but it needs to be considered the higher sequence depth achieved by the BisPCR^2 method used in the present study, which permits a high sequencing coverage for each CpG and allows to detect lower methylation differences. Indeed, detection of small differences in methylation data and at specific CpGs (DMC) using small sample size still remain a challenge using whole genome sequencing technologies, due to the low achieved sequence depth (Lee and Morris, 2016). In addition, as pools of whole embryo samples were analyzed (containing many different tissues and cell types), the use of a targeted sequencing method permits to detect effects which might be masked by the complexity of the sample using untargeted approaches. This highlights the usefulness of studies looking for the effects of pollutants on DNA methylation levels of key genes involved in the mode of action of these pollutants.

4.2. Gene expression and methylation status relationships

4.2.1. *aldh1a2*

BPA exerts methylation changes in genes related to axons, synaptic development and neurons (Olsvik et al., 2019a). Retinoid metabolism appears to be crucial in several of these systems, like nervous system development or vision, in addition to more general functions, like embryonic development or apoptosis in many animals (Blomhoff and Blomhoff, 2006; Maden, 2001), including zebrafish (Grandel et al., 2002). Indeed, BPA was also shown to alter the retinoid

metabolism (Ortiz-Villanueva et al., 2017), probably via RXR-RAR (le Maire et al., 2009; Sharma et al., 2018). In previous studies from our group (Martínez et al., 2019a, 2018; Ortiz-Villanueva et al., 2017), BPA-exposed zebrafish eleutheroembryos showed alterations in the visual system as well as decreased whole body total retinol levels and an increased abundance of transcripts involved in the pathway that catalyzes the synthesis of retinoic acid (RA) from retinol, including *aldh1a2*. *aldh1a2* is a widely expressed transcript found in several tissues of the zebrafish eleutheroembryos, including the yolk, intestine, swim bladder, fins or spinal cord, among others (Alexa et al., 2009; Pittlik and Begemann, 2012). Therefore, considering that we are studying pools of whole-body embryos, the presence of this transcript in several tissues seems to be reflected by relatively high transcript abundance (approximately 800 counts in controls) associated with a very low DNA methylation (1.6%). On the other hand, several CpGs of *aldh1a2* were hypomethylated in the BPA-exposed samples especially in the promoter region, which methylation could be inversely correlated with the increase in *aldh1a2* transcript levels. This relationship (an overexpression of a gene mediated by a decreased methylation in its promoter) has been widely described and has constituted the standard model for the effects of DNA methylation in gene transcription during several years (Anastasiadi et al., 2018; Du et al., 2012; Farthing et al., 2008; García-Cardona et al., 2014; Phillips Theresa, 2008). Our results suggest that BPA could be modulating *aldh1a2* transcription through changes in its promoter methylation, but further studies are needed to confirm this result at a functional level.

4.2.2. *ppiaa*

It has been found that *ppiaa* is widely expressed across different organs in zebrafish individuals and that its transcript abundance remains constant when those are exposed to different experimental conditions, to the point of being commonly used as a housekeeping gene in qPCR analyses (Castanheira Néia et al., 2018; Fuller-Carter et al., 2015; Martínez et al., 2019b; Sato and Takeda, 2013). Our results confirmed that its expression was extremely high in eleutheroembryos (approximately 55000 counts) and that it was not altered by BPA exposure, while its general methylation was extremely low (0.6%). We also observed no changes in DNA methylation levels after BPA exposure in any of the regions studied (promoter, first exon, first intron), except for one hypomethylated CpG position found in the promoter. Interestingly, we found an inverse correlation between gene expression levels and first intron methylation in all studied samples (BPA exposed and controls). Previous studies demonstrated that, in some cases, the inverted correlation between gene expression and DNA methylation levels is not observed in the promoter region, but rather in the gene body (Lou et al., 2014) or the first intron (Anastasiadi et al., 2018). This suggests that the expression of *ppiaa* could be mediated by the methylation of its first intron, which is not altered by environmental stressors. To our knowledge, no study has previously reported the correlation between the methylation of *ppiaa* and its transcript abundance in any organism. Further studies should be carried out to discard or confirm this observation.

4.2.3. Brain and gonad aromatases (*cyp19a1b* and *cyp19a1a*)

Estrogenicity and induction of aromatase in zebrafish are widely known effects of BPA (Awada et al., 2019; Pinto et al., 2019). Zebrafish (as other teleost fish) possess two isoforms of the cytochrome P450 aromatase, *cyp19a1a* and *cyp19a1b*, which are mainly expressed in gonads and brain, respectively, and codify for two structurally different proteins (Piferrer and Blázquez, 2005). Aromatase is a key enzyme responsible for the conversion of androgens to estrogens, hormones that play an important role in neurogenesis and control of reproduction. Thus, a thigh control in the regulation of transcription of these two genes that share the same function is crucial. The first study that showed differences on methylation levels of *cyp19a1a* and *cyp19a1b* between gonads and brains, also demonstrated that environmental factors, such as temperature, can modulate specific changes in DNA methylation of *cyp19a1a*, but not *cyp19a1b* (Navarro-Martín et al., 2011). On the other hand, it has been also reported that BPA can bind estrogen receptors (ERs), interacting with the estrogen responsive elements (EREs) in promoter regions of genes which are naturally regulated by estradiol (E2), like *cyp19a1b*, increasing, in this way, their expression (Acconcia et al., 2015; Menuet et al., 2005). In turn, both ER and *cyp19a1b* increase their expression by activation of ER by estrogens and several estrogenic endocrine disruptors (including BPA), resulting in a positive auto-regulatory loop (Acton, 2013; Brion et al., 2012).

At the transcriptomic level, *cyp19a1b* was found to be the most affected transcript (increased up to 64 times) by 17.5 µM BPA in zebrafish exposed from 0 to 5 dpf (Ortiz-Villanueva et al., 2017). It is well known that expression of *cyp19a1b* in zebrafish is mainly located in brain glial cells (Brion et al., 2012; Le Page et al., 2006; Menuet et al., 2005; Pellegrini et al., 2007), which, in the case of zebrafish start differentiating between 36-50 hpf and are active, at least at 4 dpf (Baraban et al., 2019; Brösamle and Halpern, 2002). Indeed, profiles of *cyp19a1b* transcript abundance show that it starts to get expressed between 24 and 48 hpf (Brion et al., 2012; Lassiter and Linney, 2007; Mouriec et al., 2009). Our results showed that whole-body eleutheroembryos had elevated average DNA methylation levels (86.5%) along with very low transcript *cyp19a1b* abundance in control individuals. Considering that we analyzed pools of whole-body eleutheroembryos, which contain many different tissues, we propose that resulting averaged methylation levels arise from highly methylated *cyp19a1b* copies in the majority of the tissues except for glial cells, where we would expect lower methylation levels permitting its expression. Our results shown that exposure to BPA highly increased *cyp19a1b* expression, as has been previously reported for other estrogenic compounds (Brion et al., 2012). We propose that BPA-induced increase in transcript levels might be possible by a combination of the presence of the active transcriptional machinery (transcription factors and cofactors) as well as low gene DNA methylation levels in zebrafish glial cells at this developmental stage (5 dpf). Differentially methylated cytosines after exposure to BPA were observed in our study for the case of *cyp19a1b*, with promoter hypermethylation and first intron hypomethylation. As exposed in section 4.2.2., it has been reported that in some cases

the inverted correlation between gene expression and DNA methylation is better observed in first intron (Anastasiadi et al., 2018), but also that promoter hypermethylation could be associated to increased transcriptional activity and gene expression (Smith et al., 2020). Our results suggest that this could be an alternative mechanism of BPA-mediated transcription regulation of this gene. Nevertheless, no significant correlation was found between changes in *cyp19a1b* transcript abundance and methylation levels in any of the regions studied (promoter, first exon and intron). We suggest that the implication of other mechanisms that regulate the transcription (for example, via ER-ERE activation) and the low number of cells that express *cyp19a1b* prevent to stablish significant linear correlations.

Similar to *cyp19a1b*, averaged DNA methylation levels of *cyp19a1a* were found to be around 86.6%. It is known that *cyp19a1a*, unlike *cyp19a1b*, does not contain ERE binding sites in its promoter (Gupta, 2017), which impedes transcription activation mediated by the binding of BPA with ERs (Acconcia et al., 2015). Similarly, early larval estrogen exposure in the European sea bass (*Dicentrarchus labrax*) did not affect *cyp19a1a* expression levels neither promoter DNA methylation in adult gonads suggesting that a possible change in *cyp19a1a* by estrogens could be indirectly mediated due a feminization process (Navarro-Martín et al., 2011, 2009) rather than to a direct mechanism. Transcription of *cyp19a1a* is accepted to occur mainly in the granulosa cells of the follicle of the ovaries and its expression in zebrafish does not start until 10-12 dpf (Lau et al., 2016; Yin et al., 2017). Although primordial germ cells (PGC) migrate to the gonadal ridge in zebrafish during the first 24 hpf, their number is negligible and the transcripts involved in sex determination, PGC meiosis, and gonad differentiation do not start until 8-13 dpf (Mcarthur et al., 2020; Pandian, 2012; Schartl and Herpin, 2018; Wang et al., 2017), indicating that gonadal formation hasn't start yet at 5 dpf. In our study, we observed that exposure to BPA provoked a general hypermethylation of *cyp19a1a*, but that this was not translated to changes in transcript abundance (which was virtually null) as shown by (Ortiz-Villanueva et al., 2017). All together (lack of EREs in *cyp19a1a*, lack of the existence of any cell types with an active transcription machinery for *cyp19a1a*…) may explain the lack of the effects of BPA in *cyp19a1a* transcript abundance. On the other hand, and since *cyp19a1a* is key gene during gonadal differentiation, whether or not the observed DNA methylation changes in *cyp19a1a* are maintained and could lead to changes in transcript abundance later in development is an interesting matter for further study. For example, estrogen-independently hypermethylation of *cyp19a1a* promoter could be related with decreased expression in sea bass (Navarro-Martín et al., 2011). Finally, whether the methylation changes in *cyp19a1a* exerted by BPA in the present study are triggered by its estrogenic effects or by other of its mechanisms of action is still unclear.

4.3. Gene expression regulatory mechanisms via DNA methylation

Cell studies have reported how, in general terms, genes rich in CpG islands (CGI+) are more expressed than the ones with low (CGI−) (Beck et al., 2018). These CGIs serve as "landing sites"

for the transcription factors (TF) as most of the TF binding sites are rich in CpGs (Deaton and Bird, 2011; Illingworth and Bird, 2009). It has been reported that most targets for each TF are CGI+ genes, not CGI− genes (Beck et al., 2018), suggesting that CGI+ genes could initiate the transcription from multiple positions and be less sensible to changes than CGI− genes (Beck et al., 2018; Illingworth and Bird, 2009). CGI+ genes are located predominantly in the center of the nucleus, together with the transcription factories, but also with Polycomb bodies, which can regulate their transcription via methylation and/or Polycomb repressive complex (PRC) (Beck et al., 2018; Deaton and Bird, 2011). In the other hand, CGI− genes are mainly located in the periphery (forming heterochromatin), they are less expressed, and their transcription seems to be mediated via internalization to the nuclear center by local enhancer–promoter interactions (Beck et al., 2018).

Related to these findings, we can suggest that this is the case for the genes analyzed in the present study, as global gene expression and number of CpGs seemed to have a direct relationship: *ppiaa* (a gene found to be highly expressed and stable during development and under different experimental conditions), is by far the one most enriched in CpG positions when compared to the rest. Enrichment in CpG positions was followed by *aldh1a2*, which had intermediate expression levels that were affected by BPA exposure. Finally, *cyp19a1b* and *cyp19a1a* presented only a third of the CpG positions than *ppiaa* (covering a similar size on the genome) and a very low basal gene expression. Although only *cyp19a1b* presented differences at the gene expression level, we suggest that BPA-, hormonal- or developmental-mediated regulation of transcription of both genes might be also mediated by local enhancer-promoter interactions.

A recently published study have shown that exposure to BPA did not alter global methylation levels in zebrafish embryos but did show methylation changes in certain sites of the genome (Olsvik et al., 2019a). While other studies reported poor correlations between gene expression levels and the global methylation of entire CpG islands (Illingworth and Bird, 2009), several linear correlations could be stablished with the methylation of certain CpGs of particular gene regions (Simó-Mirabet et al., 2020). This suggests that environmental stressors could also modulated gene expression via methylation of only certain regions or even only some CpGs of the target genes, in addition to a general hypo/hypermethylation mechanism. Further studies should be carried out to increase the comprehension of these phenomena, as probably it would depend on each specific gene and its transcription factors.

5. Conclusions

Based on our results, we can conclude that BPA-mediated effects of *aldh1a2* expression might be regulated by changes in methylation levels, but further studies are needed to evaluate its causality. Furthermore, the fact that changes in DNA methylation and transcriptomic levels caused by exposure to EDCs, are not always correlated, suggests that gene transcription is

regulated at different levels (epigenome, expression of transcription factors…), which may explain this variability in the observed effects.

Conflicts of interest

The authors declare no conflicts of interest.

Acknowledgments

This work was supported by the European Research Council under the European Union's Seventh Framework Programme (FP/ 2007-2013)/ERC Grant Agreement n. 320737. SH acknowledges the funding from ISCIII (Spanish Ministry of Economy and Competitiveness, grant number PT17/0009/0019), co-financed by the European Fund for Regional Development (FEDER). LNM was supported by a H2020-Marie Skłodowska-Curie Action MSCA-IF-RI-2017 awarded by the European Commission (ref. 797725-EpiSTOX). RM was supported by a FPU predoctoral fellow from the Spanish Ministry of Education, Culture and Sport (ref. FPU15/03332).

Bibliography

Acconcia, F., Pallottini, V., Marino, M., 2015. Molecular mechanisms of action of BPA. Dose-Response 13. https://doi.org/10.1177/1559325815610582

Acton, Q.A., 2013. Connective tissue cells—advances in research and application: 2013 edition.

Alavian-Ghavanini, A., Lin, P.-I., Lind, P.M., Risén Rimfors, S., Halin Lejonklou, M., Dunder, L., Tang, M., Lindh, C., Bornehag, C.-G., Rüegg, J., 2018. Prenatal bisphenol A exposure is linked to epigenetic changes in glutamate receptor subunit gene Grin2b in female rats and humans. Sci. Rep. 8, 11315. https://doi.org/10.1038/s41598-018-29732-9

Alexa, K., Choe, S.K., Hirsch, N., Etheridge, L., Laver, E., Sagerström, C.G., 2009. Maternal and zygotic aldh1a2 activity is required for pancreas development in zebrafish. PLoS One 4, e8261. https://doi.org/10.1371/journal.pone.0008261

Alonso-Magdalena, P., Vieira, E., Soriano, S., Menes, L., Burks, D., Quesada, I., Nadal, A., 2010. Bisphenol A exposure during pregnancy disrupts glucose homeostasis in mothers and adult male offspring. Environ. Health Perspect. 118, 1243–50. https://doi.org/10.1289/ehp.1001993

Anastasiadi, D., Esteve-Codina, A., Piferrer, F., 2018. Consistent inverse correlation between DNA methylation of the first intron and gene expression across tissues and species. Epigenetics and Chromatin 11, 1–17. https://doi.org/10.1186/s13072-018-0205-1

Awada, Z., Nasr, R., Akika, R., Cahais, V., Cuenin, C., Zhivagui, M., Herceg, Z., Ghantous, A., Zgheib, N.K., 2019. DNA methylome-wide alterations associated with estrogen receptor-dependent effects of bisphenols in breast cancer. Clin. Epigenetics 11, 138. https://doi.org/10.1186/s13148-019-0725-y

Baraban, M., Retamal, M.A., Ortiz, F.C., 2019. Physiology of myelin forming cells, from myelination to neural modulators. Front. Cell. Neurosci. 13. https://doi.org/10.3389/fncel.2019.00475

Barouki, R., Melén, E., Herceg, Z., Beckers, J., Chen, J., Karagas, M., Puga, A., Xia, Y., Chadwick, L., Yan, W., Audouze, K., Slama, R., Heindel, J., Grandjean, P., Kawamoto, T., Nohara, K., 2018. Epigenetics as a mechanism linking developmental exposures to long-term toxicity. Environ. Int. https://doi.org/10.1016/j.envint.2018.02.014

Beck, S., Rhee, C., Song, J., Lee, B.K., LeBlanc, L., Cannon, L., Kim, J., 2018. Implications of CpG islands on chromosomal architectures and modes of global gene regulation. Nucleic Acids Res. 46, 4382–4391. https://doi.org/10.1093/nar/gky147

Bernstein, D.L., Kameswaran, V., Le Lay, J.E., Sheaffer, K.L., Kaestner, K.H., 2015. The BisPCR2 method for targeted bisulfite sequencing. Epigenetics Chromatin 8, 27. https://doi.org/10.1186/s13072-015-0020-x

Blomhoff, R., Blomhoff, H.K., 2006. Overview of retinoid metabolism and function. J. Neurobiol. https://doi.org/10.1002/neu.20242

Brion, F., Le Page, Y., Piccini, B., Cardoso, O., Tong, S.K., Chung, B. chu, Kah, O., 2012. Screening estrogenic activities of chemicals or mixtures in vivo using transgenic (cyp19a1b-GFP) zebrafish embryos. PLoS One 7, e36069. https://doi.org/10.1371/journal.pone.0036069

Brösamle, C., Halpern, M.E., 2002. Characterization of myelination in the developing zebrafish. Glia 39, 47–57. https://doi.org/10.1002/glia.10088

Castanheira Néia, V.B.M.J., Ambrosio-Albuquerque, E.P., de Lima Figueiredo, I., da Silva, T.C., Lewandowski, V., De Almeida, F.L.A., Ribeiro, R.P., Visentainer, J.E.L., Visentainer, J.V., 2018. Effect of peanut addition to the cafeteria diet on adiposity and inflammation in Zebrafish (Danio rerio). Food Agric. Immunol. 29, 762–775. https://doi.org/10.1080/09540105.2018.1445702

Chandra, A., Senapati, S., Roy, S., Chatterjee, G., Chatterjee, R., 2018. Epigenome-wide DNA methylation regulates cardinal pathological features of psoriasis. Clin. Epigenetics 10, 108. https://doi.org/10.1186/s13148-018-0541-9

Cheong, A., Johnson, S.A., Howald, E.C., Ellersieck, M.R., Camacho, L., Lewis, S.M., Vanlandingham, M.M., Ying, J., Ho, S.M., Rosenfeld, C.S., 2018. Gene expression and DNA methylation changes in the hypothalamus and hippocampus of adult rats developmentally exposed to bisphenol A or ethinyl estradiol: a CLARITY-BPA consortium study. Epigenetics 13, 704–720. https://doi.org/10.1080/15592294.2018.1497388

Csoka, A.B., Szyf, M., 2009. Epigenetic side-effects of common pharmaceuticals: A potential new field in medicine and pharmacology. Med. Hypotheses 73, 770–780. https://doi.org/10.1016/j.mehy.2008.10.039

Deaton, A.M., Bird, A., 2011. CpG islands and the regulation of transcription. Genes Dev. 25, 1010–1022. https://doi.org/10.1101/gad.2037511

Dolinoy, D.C., Huang, D., Jirtle, R.L., 2007. Maternal nutrient supplementation counteracts bisphenol A-induced DNA hypomethylation in early development. Proc. Natl. Acad. Sci. U. S. A. 104, 13056–13061. https://doi.org/10.1073/pnas.0703739104

Du, X., Han, L., Guo, A.Y., Zhao, Z., 2012. Features of methylation and gene expression in the promoter-associated CpG islands using human methylome data. Comp. Funct. Genomics 2012. https://doi.org/10.1155/2012/598987

Farthing, C.R., Ficz, G., Ng, R.K., Chan, C.F., Andrews, S., Dean, W., Hemberger, M., Reik, W., 2008. Global mapping of DNA methylation in mouse promoters reveals epigenetic reprogramming of pluripotency genes. PLoS Genet. 4. https://doi.org/10.1371/journal.pgen.1000116

Fuller-Carter, P.I., Carter, K.W., Anderson, D., Harvey, A.R., Giles, K.M., Rodger, J., 2015. Integrated analyses of zebrafish miRNA and mRNA expression profiles identify miR-29b and miR-223 as potential regulators of optic nerve regeneration. BMC Genomics 16, 1–19. https://doi.org/10.1186/s12864-015-1772-1

García-Cardona, M.C., Huang, F., García-Vivas, J.M., López-Camarillo, C., Del Río Navarro, B.E., Navarro Olivos, E., Hong-Chong, E., Bolaños-Jiménez, F., Marchat, L.A., 2014. DNA methylation of leptin and adiponectin promoters in children is reduced by the combined presence of obesity and insulin resistance. Int. J. Obes. 38, 1457–1465. https://doi.org/10.1038/ijo.2014.30

Grand View Research Inc, 2015. Bisphenol A (BPA) market analysis by application (polycarbonates, epoxy resins). Regional and segment forecasts to 2025. San Francisco.

Grandel, H., Lun, K., Rauch, G.J., Rhinn, M., Piotrowski, T., Houart, C., Sordino, P., Küchler, A.M., Schulte-Merker, S., Geisler, R., Holder, N., Wilson, S.W., Brand, M., 2002. Retinoic acid signalling in the zebrafish embryo is necessary during presegmentation stages to pattern the anterior-posterior axix of the CNS and to induce a pectoral fin bud. Development 129, 2851–2865.

Guerrero-Bosagna, C., Skinner, M.K., 2012. Environmentally induced epigenetic transgenerational inheritance of phenotype and disease. Mol. Cell. Endocrinol. https://doi.org/10.1016/j.mce.2011.10.004

Gupta, R.C., 2017. Reproductive and developmental toxicology, Reproductive and Developmental Toxicology. https://doi.org/10.1016/b978-0-407-02301-7.50017-3

Horan, T.S., Pulcastro, H., Lawson, C., Gerona, R., Martin, S., Gieske, M.C., Sartain, C. V., Hunt, P.A.,

2018. Replacement bisphenols adversely affect mouse gametogenesis with consequences for subsequent generations. Curr. Biol. 28, 2948-2954.e3. https://doi.org/10.1016/j.cub.2018.06.070

Illingworth, R.S., Bird, A.P., 2009. CpG islands - "A rough guide." FEBS Lett. https://doi.org/10.1016/j.febslet.2009.04.012

Kadasala, N.R., Narayanan, ---Badri, Liu, ---Yang, 2016. International trade regulations on BPA: global health and economic implications. Asian Dev. Policy Rev. 4, 134–142. https://doi.org/10.18488/journal.107/2016.4.4/107.4.134.142

Kamstra, J.H., Aleström, P., Kooter, J.M., Legler, J., 2015. Zebrafish as a model to study the role of DNA methylation in environmental toxicology. Environ. Sci. Pollut. Res. 22, 16262–16276. https://doi.org/10.1007/s11356-014-3466-7

Kamstra, J.H., Sales, L.B., Aleström, P., Legler, J., 2017. Differential DNA methylation at conserved non-genic elements and evidence for transgenerational inheritance following developmental exposure to mono(2-ethylhexyl) phthalate and 5-azacytidine in zebrafish. Epigenetics Chromatin 10, 20. https://doi.org/10.1186/s13072-017-0126-4

Kitraki, E., Nalvarte, I., Alavian-Ghavanini, A., Rüegg, J., 2015. Developmental exposure to bisphenol A alters expression and DNA methylation of Fkbp5, an important regulator of the stress response. Mol. Cell. Endocrinol. 417, 191–199. https://doi.org/10.1016/j.mce.2015.09.028

Laing, L. V, Viana, J., Dempster, E.L., Trznadel, M., Trunkfield, L.A., Uren Webster, T.M., van Aerle, R., Paull, G.C., Wilson, R.J., Mill, J., Santos, E.M., 2016. Bisphenol A causes reproductive toxicity, decreases dnmt1 transcription, and reduces global DNA methylation in breeding zebrafish (Danio rerio). Epigenetics 11, 526–538. https://doi.org/10.1080/15592294.2016.1182272

Lassiter, C.S., Linney, E., 2007. Embryonic expression and steroid regulation of brain aromatase cyp19a1b in zebrafish (Danio rerio). Zebrafish 4, 49–57. https://doi.org/10.1089/zeb.2006.9995

Lau, E.S.-W., Zhang, Z., Qin, M., Ge, W., 2016. Knockout of zebrafish ovarian aromatase gene (cyp19a1a) by TALEN and CRISPR/Cas9 leads to all-male offspring due to failed ovarian differentiation. Sci. Rep. 6, 37357. https://doi.org/10.1038/srep37357

le Maire, A., Grimaldi, M., Roecklin, D., Dagnino, S., Vivat-Hannah, V., Balaguer, P., Bourguet, W., 2009. Activation of RXR-PPAR heterodimers by organotin environmental endocrine disruptors. EMBO Rep. 10, 367–373. https://doi.org/10.1038/embor.2009.8

Le Page, Y., Scholze, M., Kah, O., Pakdel, F., 2006. Assessment of Xenoestrogens Using Three Distinct Estrogen Receptors and the Zebrafish Brain Aromatase Gene in a Highly Responsive Glial Cell System. Environ. Health Perspect. 114, 752–758. https://doi.org/10.1289/ehp.8141

Lee, W., Morris, J.S., 2016. Identification of differentially methylated loci using wavelet-based functional mixed models. Bioinformatics 32, 664–672. https://doi.org/10.1093/bioinformatics/btv659

Li, L.C., Dahiya, R., 2002. MethPrimer: designing primers for methylation PCRs. Bioinformatics 18, 1427–1431. https://doi.org/10.1093/bioinformatics/18.11.1427

Maden, M., 2001. Role and distribution of retinoic acid during CNS development. Int. Rev. Cytol. https://doi.org/10.1016/S0074-7696(01)09010-6

Martínez, R., Esteve-Codina, A., Herrero-Nogareda, L., Ortiz-Villanueva, E., Barata, C., Tauler, R., Raldúa, D., Piña, B., Navarro-Martín, L., 2018. Dose-dependent transcriptomic responses of zebrafish eleutheroembryos to Bisphenol A. Environ. Pollut. 243, 988–997. https://doi.org/10.1016/j.envpol.2018.09.043

Martínez, R., Herrero-Nogareda, L., Van Antro, M., Campos, M.P., Casado, M., Barata, C., Piña, B., Navarro-Martín, L., 2019a. Morphometric signatures of exposure to endocrine disrupting chemicals in zebrafish eleutheroembryos. Aquat. Toxicol. 214, 105232. https://doi.org/10.1016/j.aquatox.2019.105232

Martínez, R., Navarro-Martín, L., Luccarelli, C., Codina, A.E., Raldúa, D., Barata, C., Tauler, R., Piña, B., 2019b. Unravelling the mechanisms of PFOS toxicity by combining morphological and transcriptomic analyses in zebrafish embryos. Sci. Total Environ. 674, 462–471. https://doi.org/10.1016/j.scitotenv.2019.04.200

Martínez, R., Tu, W., Eng, T., Allaire-Leung, M., Piña, B., Navarro-Martín, L., Mennigen, J.A., 2020. Acute and long-term metabolic consequences of early developmental Bisphenol A exposure in zebrafish (Danio rerio). Chemosphere 256, 127080.

https://doi.org/10.1016/j.chemosphere.2020.127080

Mcarthur, K.L., Chow, D.M., Fetcho, J.R., 2020. The zebrafish in biomedical research: biology, husbandry, diseases, and research applications. https://doi.org/10.1016/B978-0-12-812431-4.00046-4

Menuet, A., Pellegrini, E., Brion, F., Gueguen, M.M., Anglade, I., Pakdel, F., Kah, O., 2005. Expression and estrogen-dependent regulation of the zebrafish brain aromatase gene. J. Comp. Neurol. 485, 304–320. https://doi.org/10.1002/cne.20497

Merkel, A., Fernández-Callejo, M., Casals, E., Marco-Sola, S., Schuyler, R., Gut, I.G., Heath, S.C., 2019. GemBS: High throughput processing for DNA methylation data from bisulfite sequencing. Bioinformatics 35, 737–742. https://doi.org/10.1093/bioinformatics/bty690

Mesnage, R., Phedonos, A., Arno, M., Balu, S., Corton, J.C., Antoniou, M.N., 2017. Transcriptome profiling reveals bisphenol a alternatives activate estrogen receptor alpha in human breast cancer cells. Toxicol. Sci. 158, 431–443. https://doi.org/10.1093/toxsci/kfx101

Mileva, G., Baker, S.L., Konkle, A.T.M., Bielajew, C., 2014. Bisphenol-A: Epigenetic reprogramming and effects on reproduction and behavior. Int. J. Environ. Res. Public Health. https://doi.org/10.3390/ijerph110707537

Moon, M.K., 2019. Concern about the safety of bisphenol A substitutes. Diabetes Metab. J. https://doi.org/10.4093/dmj.2019.0027

Mouriec, K., Lareyre, J.J., Tong, S.K., Le Page, Y., Vaillant, C., Pellegrini, E., Pakdel, F., Chung, B.C., Kah, O., Anglade, I., 2009. Early regulation of brain aromatase (cyp19a1b) by estrogen receptors during zebrafish development. Dev. Dyn. 238, 2641–2651. https://doi.org/10.1002/dvdy.22069

Navarro-Martín, L., Blázquez, M., Piferrer, F., 2009. Masculinization of the European sea bass (Dicentrarchus labrax) by treatment with an androgen or aromatase inhibitor involves different gene expression and has distinct lasting effects on maturation. Gen. Comp. Endocrinol. 160, 3–11. https://doi.org/10.1016/j.ygcen.2008.10.012

Navarro-Martín, L., Viñas, J., Ribas, L., Díaz, N., Gutiérrez, A., Di Croce, L., Piferrer, F., 2011. DNA methylation of the gonadal aromatase (cyp19a) promoter is involved in temperature-dependent sex ratio shifts in the European sea bass. PLoS Genet. 7, e1002447. https://doi.org/10.1371/journal.pgen.1002447

Olsvik, P.A., Whatmore, P., Penglase, S.J., Skjærven, K.H., Anglès d'Auriac, M., Ellingsen, S., 2019a. Associations between behavioral effects of bisphenol A and DNA methylation in zebrafish embryos. Front. Genet. 10, 184. https://doi.org/10.3389/fgene.2019.00184

Olsvik, P.A., Whatmore, P., Penglase, S.J., Skjærven, K.H., D'Auriac, M.A., Ellingsen, S., 2019b. Associations between behavioral effects of bisphenol A and DNA methylation in zebrafish embryos. Front. Genet. 10. https://doi.org/10.3389/fgene.2019.00184

Ortiz-Villanueva, E., Navarro-Martín, L., Jaumot, J., Benavente, F., Sanz-Nebot, V., Piña, B., Tauler, R., 2017. Metabolic disruption of zebrafish (Danio rerio) embryos by bisphenol A. An integrated metabolomic and transcriptomic approach. Environ. Pollut. 231, 22–36. https://doi.org/10.1016/j.envpol.2017.07.095

Pandian, T.J., 2012. Genetic Sex Differentiation in Fish, Genetic Sex Differentiation in Fish. https://doi.org/10.1201/b12296

Pellegrini, E., Mouriec, K., Anglade, I., Menuet, A., Le Page, Y., Gueguen, M.M., Marmignon, M.H., Brion, F., Pakdel, F., Kah, O., 2007. Identification of aromatase-positive radial glial cells as progenitor cells in the ventricular layer of the forebrain in zebrafish. J. Comp. Neurol. 501, 150–167. https://doi.org/10.1002/cne.21222

Phillips Theresa, 2008. The role of methylation in gene expression [WWW Document]. Nat. Educ. URL https://www.nature.com/scitable/topicpage/the-role-of-methylation-in-gene-expression-1070/ (accessed 4.30.20).

Piferrer, F., Blázquez, M., 2005. Aromatase distribution and regulation in fish, in: Fish Physiology and Biochemistry. Springer, pp. 215–226. https://doi.org/10.1007/s10695-006-0027-0

Pinto, C., Hao, R., Grimaldi, M., Thrikawala, S., Boulahtouf, A., Aït-Aïssa, S., Brion, F., Gustafsson, J.Å., Balaguer, P., Bondesson, M., 2019. Differential activity of BPA, BPAF and BPC on zebrafish estrogen receptors in vitro and in vivo. Toxicol. Appl. Pharmacol. 380, 114709. https://doi.org/10.1016/j.taap.2019.114709

Pittlik, S., Begemann, G., 2012. New sources of retinoic acid synthesis revealed by live imaging of an Aldh1a2-GFP reporter fusion protein

throughout zebrafish development. Dev. Dyn. 241, 1205–1216. https://doi.org/10.1002/dvdy.23805

R Development Core Team, 2008. R: a language and environment for statistical computing, R Foundation for Statistical Computing.

Rubin, B.S., Soto, A.M., 2009. Bisphenol A: Perinatal exposure and body weight. Mol. Cell. Endocrinol. 304, 55–62. https://doi.org/10.1016/j.mce.2009.02.023

Santangeli, S., Maradonna, F., Gioacchini, G., Cobellis, G., Piccinetti, C.C., Dalla Valle, L., Carnevali, O., 2016. BPA-induced deregulation of epigenetic patterns: effects on female zebrafish reproduction. Sci. Rep. 6. https://doi.org/10.1038/srep21982

Sato, A., Takeda, H., 2013. Neuronal subtypes are specified by the level of neurod expression in the zebrafish lateral line. J. Neurosci. 33, 556–562. https://doi.org/10.1523/JNEUROSCI.4568-12.2013

Schartl, M., Herpin, A., 2018. Sex determination in vertebrates, in: Encyclopedia of Reproduction. pp. 159–167. https://doi.org/10.1016/B978-0-12-809633-8.20551-7

Senyildiz, M., Karaman, E.F., Bas, S.S., Pirincci, P.A., Ozden, S., 2017. Effects of BPA on global DNA methylation and global histone 3 lysine modifications in SH-SY5Y cells: an epigenetic mechanism linking the regulation of chromatin modifiying genes. Toxicol. Vitr. 44, 313–321. https://doi.org/10.1016/j.tiv.2017.07.028

Sharma, S., Ahmad, S., Khan, M.F., Parvez, S., Raisuddin, S., 2018. In silico molecular interaction of bisphenol analogues with human nuclear receptors reveals their stronger affinity vs. classical bisphenol A. Toxicol. Mech. Methods 28, 660–669. https://doi.org/10.1080/15376516.2018.1491663

Simó-Mirabet, P., Perera, E., Calduch-Giner, J.A., Pérez-Sánchez, J., 2020. Local DNA methylation helps to regulate muscle sirtuin 1 gene expression across seasons and advancing age in gilthead sea bream (Sparus aurata). Front. Zool. 17, 15. https://doi.org/10.1186/s12983-020-00361-1

Singh, S., Li, S.S.L., 2012. Epigenetic effects of environmental chemicals bisphenol A and phthalates. Int. J. Mol. Sci. https://doi.org/10.3390/ijms130810143

Skinner, M.K., Manikkam, M., Guerrero-Bosagna, C., 2010. Epigenetic transgenerational actions of environmental factors in disease etiology. Trends Endocrinol. Metab. https://doi.org/10.1016/j.tem.2009.12.007

Smith, J., Sen, S., Weeks, R.J., Eccles, M.R., Chatterjee, A., 2020. Promoter DNA hypermethylation and paradoxical gene activation. Trends in Cancer 6, 392–406. https://doi.org/10.1016/j.trecan.2020.02.007

U S Environmental Protection Agency, 2010. U.S. Environmental Protection Agency. Bisphenol-A action plan 1–22.

Wang, X., Chen, S., Zhang, W., Ren, Y., Zhang, Q., Peng, G., 2017. Dissection of larval zebrafish gonadal tissue. J. Vis. Exp. 2017. https://doi.org/10.3791/55294

Yin, Y., Tang, H., Liu, Y., Chen, Y., Li, G., Liu, X., Lin, H., 2017. Targeted disruption of aromatase reveals dual functions of cyp19a1a during sex differentiation in zebrafish. Endocrinology 158, 3030–3041. https://doi.org/10.1210/en.2016-1865

Zhang, T., Guan, Y., Wang, S., Wang, L., Cheng, M., Yuan, C., Liu, Y., Wang, Z., 2018. Bisphenol A induced abnormal DNA methylation of ovarian steroidogenic genes in rare minnow Gobiocypris rarus. Gen. Comp. Endocrinol. 269, 156–165. https://doi.org/10.1016/j.ygcen.2018.09.009

Zhang, X.F., Zhang, L.J., Feng, Y.N., Chen, B., Feng, Y.M., Liang, G.J., Li, L., Shen, W., 2012. Bisphenol A exposure modifies DNA methylation of imprint genes in mouse fetal germ cells. Mol. Biol. Rep. 39, 8621–8628. https://doi.org/10.1007/s11033-012-1716-7

Zhang, Y., Guan, Y., Fan, X., Wu, L., Wang, Z., 2018. Bisphenol A regulates rare minnow testicular vitellogenin expression via reducing its promoter Er recruitment. Ecotoxicol. Environ. Saf. 147, 423–429. https://doi.org/10.1016/j.ecoenv.2017.09.001

Supplemental information: scientific article VII

Alterations of DNA methylation levels of key genes related to BPA exposures in zebrafish embryos

Authors: R. Martínez, S. Heath, R. Tauler, B. Piña, L. Navarro-Martín

Status: In preparation

Journal: -

DOI: -

Supplementary methods

SM1. BisPCR^2 method (PCR#1 and PCR#2 rounds)

h) A 0 % methylated standard was prepared from a sample pool using the REPLI-g Mini Kit (Qiagen) following the manufacturer's protocol.

i) A 100 % methylated standard was prepared from a sample pool using a CpG Methyltransferase (M.SssI) (Thermo Fisher Scientific) following the manufacturer's protocol.

j) Both 0 and 100 % methylated standards were cleaned with the Genomic DNA Clean & Concentrator™-10 kit (Zymo Research) following the manufacturer's protocol.

k) A 50 % methylated standard was prepared by mixing 0 and 100 % standards (1:1).

l) A sodium bisulfite conversion was applied over 500 ng of each sample and standard (where all non-methylated cytosines are converted to uracils) with EZ DNA Methylation-Gold™ Kit (Zymo Research).

m) PCR#1 round was performed over each sample and standard for each one of the selected amplicons (supplemental table ST1).

n) Gross amplicon amount per sample was measured by gel densitometry:

   a. Gel: 2 % of agarose in 1X TAE (Tris-acetate-EDTA) buffer. RedSafe™ Nucleic Acid Staining Solution (iNtRON Biotechnology) was used as loading dye. MassRuler DNA Ladder Mix (Thermo Fisher Scientific) was used as a reference for the size of the bands.

   b. Measurements: gels were photographed on a Kodak Gel Logic 200 imaging system under UV light and the intensities of the bands corresponding to the amplicons were measured using the imaging free software GelAnalyzer 2010a (www.gelanalyzer.com).

o) For each sample and standard, a mix of all of its amplicons was performed considering the above measured intensities, with the goal to have the same amount of each amplicon in the amplicon pool. A total of 23 pools (20 samples and 3 standards were obtained).

p) Each pool was cleaned using the DNA Clean & Concentrator™-5 kit (Zymo Research) following the manufacturer's protocol.

q) PCR#2 round was performed over each sample and standard pool (see primers and temperature conditions at supplemental tables ST1 and ST2).

r) Each sample and standard pool amplification products from the PCR were cleaned as in i) and their concentration measured by a NanoDrop® 8000 UV-Vis Spectrophotometer (Thermo Scientific).

s) A final pool was generated by mixing all samples and standards pool amplification products considering their concentrations (with the goal to have the same DNA amount coming from each sample in the pool).

t) Final pool was sequenced at the Center for Genomic Regulation-National Center for Genomics Analysis (CRG-CNAG) with a sequencing depth of 25.3 million and the counts for every CpG position and for every methylation pattern were obtained.

Supplementary figures

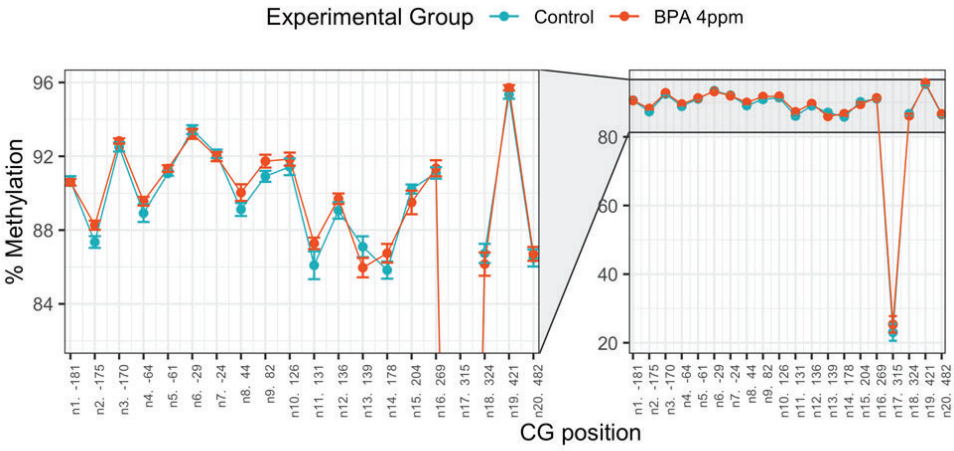

Supplementary figure SF1. Percentage of methylation of each individual CpG position in the *cyp19a1a* gene. Enlargement view of the high methylated CpG positions.

Supplemental table ST1. BisPCR conditions, CpG number, size and used primers for each measured amplicon. For the primers, complementary sequence to the amplicon is expressed in black, and overhangs in blue/green. Dark blue/green sequence express complementarity with the primers used in PCR#2.

aldh1a2

Amplicon	CpG number	PCR size	PCR size (PCR#1, with overhangs)	PCR size (PCR#2, with barcoding)	T of PCR#1	[primers] (nM) in PCR#1	T of PCR#2	[primers] (nM) in the PCR#2)
aldh1a2 P1	8	263	330	385	58	250	68-->56 ºC	250
aldh1a2 P2	5	237	304	359	58	250	68-->56 ºC	250
aldh1a2 E1	8	153	220	275	58	250	68-->56 ºC	250
aldh1a2 I1	6	174	241	296	58	250	68-->56 ºC	250
aldh1a2 I2	6	152	219	274	58	250	68-->56 ºC	250
aldh1a2 I3	4	176	243	298	58	250	68-->56 ºC	250
aldh1a2 I4	5	185	252	307	54	150	68-->56 ºC	250

PPIAa

Amplicon	CpG number	PCR size	PCR size (PCR#1, with overhangs)	PCR size (PCR#2, with barcoding)	T of PCR#1	[primers] (nM) in PCR#1	T of PCR#2	[primers] (nM) in the PCR#2)
PPIAa P1	5	252	319	374	58	250	68-->56 ºC	250
PPIAa P2	6	221	288	343	58	250	68-->56 ºC	250
PPIAa E1	10	223	290	345	58	250	68-->56 ºC	250
PPIAa E2	9	195	262	317	62	200	68-->56 ºC	250
PPIAa I1	9	195	262	317	58	250	68-->56 ºC	250
PPIAa I2	7	192	259	314	58	250	68-->56 ºC	250
PPIAa I3	10	184	251	306	62	200	68-->56 ºC	250

cyp19a1a

Amplicon	CpG number	PCR size	PCR size (PCR#1, with overhangs)	PCR size (PCR#2, with barcoding)	T of PCR#1	[primers] (nM) in PCR#1	T of PCR#2	[primers] (nM) in the PCR#2)
cyp19a1a P1	5	206	273	328	58	250	68-->56 ºC	250
cyp19a1a P2	4	172	239	294	58	250	68-->56 ºC	250
cyp19a1a E1	7	199	266	321	60	250	68-->56 ºC	250
cyp19a1a E2	5	268	335	390	58	250	68-->56 ºC	250
cyp19a1a I1	4	245	312	367	58	250	68-->56 ºC	250

cyp19a1b

Amplicon	CpG number	PCR size	PCR size (PCR#1, with overhangs)	PCR size (PCR#2, with barcoding)	T of PCR#1	[primers] (nM) in PCR#1	T of PCR#2	[primers] (nM) in the PCR#2)
cyp19a1b P1	4	142	209	264	58	250	68-->56 ºC	250
cyp19a1b P2	6	133	200	255	54	150	68-->56 ºC	250
cyp19a1b P3	4	210	277	332	58	500	68-->56 ºC	250
cyp19a1b P4	6	348	415	470	58	250	68-->56 ºC	250
cyp19a1b I1	4	189	256	311	58	250	68-->56 ºC	250
cyp19a1b I2	4	293	360	415	58	250	68-->56 ºC	250

Supplemental table ST1 (continuation). BisPCR conditions, CpG number, size and used primers for each measured amplicon. For the primers, complementary sequence to the amplicon is expressed in black, and overhangs in blue/green. Dark blue/green sequence express complementarity with the primers used in PCR#2.

aldh1a2

Amplicon	Forward PCR#1 primer	Reverse PCR#1 primer
aldh1a2 P1	ACACTCTTTCCCTACACGACGCTCTTCCGATCTGAGTGTTAAAAGTTTTTTAGATGGTTTT	GTGACTGGAGTTCAGACGTGTGCTCTTCCGATCTATCAACCAATATTTCTCTCCACCTA
aldh1a2 P2	ACACTCTTTCCCTACACGACGCTCTTCCGATCTTAGTGTTGGTTTATTGTGGTTGAAA	GTGACTGGAGTTCAGACGTGTGCTCTTCCGATCTCTAAAATACAATTTCCATACTTTATTAACA
aldh1a2 E1	ACACTCTTTCCCTACACGACGCTCTTCCGATCTTATAGGAAGGATTTTAAAGTTGTAAT	GTGACTGGAGTTCAGACGTGTGCTCTTCCGATCTCATCAAATAAAAAAATACCATAAAC
aldh1a2 I1	ACACTCTTTCCCTACACGACGCTCTTCCGATCTTGGTATTTTTTTATTTGATGTTTTTAT	GTGACTGGAGTTCAGACGTGTGCTCTTCCGATCTATTTAAATCTCTCATATACTTTCCCCTC
aldh1a2 I2	ACACTCTTTCCCTACACGACGCTCTTCCGATCTTAGATTTGTTTTTGGATATGTTTTTG	GTGACTGGAGTTCAGACGTGTGCTCTTCCGATCTAATTAACACAAATAAAATTTATTTAACATT
aldh1a2 I3	ACACTCTTTCCCTACACGACGCTCTTCCGATCTAATGGAGTTATATAGATTATTGAAGTTTAT	GTGACTGGAGTTCAGACGTGTGCTCTTCCGATCTATATTTTAATCACAAATATTAATCTTATCC
aldh1a2 I4	ACACTCTTTCCCTACACGACGCTCTTCCGATCTGATAAGATTAATATTTGTGATTAAAATATA	GTGACTGGAGTTCAGACGTGTGCTCTTCCGATCTAATAAATTAACTATCTTACATTCCTTC

PPIAa

Amplicon	Forward PCR#1 primer	Reverse PCR#1 primer
PPIAa P1	ACACTCTTTCCCTACACGACGCTCTTCCGATCTTATATGTAGTTTTGAAAATATTGAAATATT	GTGACTGGAGTTCAGACGTGTGCTCTTCCGATCTATAATAACAAACAAACACTAACACAC
PPIAa P2	ACACTCTTTCCCTACACGACGCTCTTCCGATCTTTTTAAATTTTGGAAAATTATTGAATAAAA	GTGACTGGAGTTCAGACGTGTGCTCTTCCGATCTAACACATAAATAAACCAATCAAATATCC
PPIAa E1	ACACTCTTTCCCTACACGACGCTCTTCCGATCTGGATATTTGATTGGTTTATTTATGTGTTAT	GTGACTGGAGTTCAGACGTGTGCTCTTCCGATCTAAAAACACTTTAAACCTTACCATAACTTTA
PPIAa E2	ACACTCTTTCCCTACACGACGCTCTTCCGATCTAAAGAATTTAAAGTTATGGTAAGGTTTAAA	GTGACTGGAGTTCAGACGTGTGCTCTTCCGATCTACAAAACAACTTCCTCAAAAAAAAC
PPIAa I1	ACACTCTTTCCCTACACGACGCTCTTCCGATCTGTTTGTGATTTTTGTAAGTTAGAAGTTAAG	GTGACTGGAGTTCAGACGTGTGCTCTTCCGATCTATACACATTATTAAACAACCCTTTTT
PPIAa I2	ACACTCTTTCCCTACACGACGCTCTTCCGATCTAAAGGGTTGTTTAATAATGTGTATT	GTGACTGGAGTTCAGACGTGTGCTCTTCCGATCTCATTACAATAAACCCATAAAATAACTACAA
PPIAa I3	ACACTCTTTCCCTACACGACGCTCTTCCGATCTTATTTTATGGGTTTATTGTAATGTG	GTGACTGGAGTTCAGACGTGTGCTCTTCCGATCTACTACTAATTAAAAACAAATTCAACTC

cyp19a1a

Amplicon	Forward PCR#1 primer	Reverse PCR#1 primer
cyp19a1a P1	ACACTCTTTCCCTACACGACGCTCTTCCGATCTTATTTTTTGTTTGTTTGTAGGTTTGAT	GTGACTGGAGTTCAGACGTGTGCTCTTCCGATCTCCTTATATACTCCTTTATATCCTTCAAC
cyp19a1a P2	ACACTCTTTCCCTACACGACGCTCTTCCGATCTTTGAAGTTTTGATGAAAATTTAGAGAT	GTGACTGGAGTTCAGACGTGTGCTCTTCCGATCTCCCAACAACTACATAAAACTCAATC
cyp19a1a E1	ACACTCTTTCCCTACACGACGCTCTTCCGATCTTGATTGAGTTTTATGTAGTTGTTGG	GTGACTGGAGTTCAGACGTGTGCTCTTCCGATCTCATTATCCTAAACCCTTTCAATACC
cyp19a1a E2	ACACTCTTTCCCTACACGACGCTCTTCCGATCTGTATTGAAAGGGTTTAGGATAATG	GTGACTGGAGTTCAGACGTGTGCTCTTCCGATCTCCTATAACAATAAAAATAAATTTACC
cyp19a1a I1	ACACTCTTTCCCTACACGACGCTCTTCCGATCTTTAGGTTAGTTGGATTTGTTTTAGA	GTGACTGGAGTTCAGACGTGTGCTCTTCCGATCTTCCTTTTATTAACATATAATTAAATTCATT

cyp19a1b

Amplicon	Forward PCR#1 primer	Reverse PCR#1 primer
cyp19a1b P1	ACACTCTTTCCCTACACGACGCTCTTCCGATCTGGATTTTTATTTTGAAAAATAATTAGTTA	GTGACTGGAGTTCAGACGTGTGCTCTTCCGATCTATAAACAAAAAACTAACAAAAAACC
cyp19a1b P2	ACACTCTTTCCCTACACGACGCTCTTCCGATCTTTTATTAGGTTTAAAGTTTTTTTAAATAAA	GTGACTGGAGTTCAGACGTGTGCTCTTCCGATCTACCAAAAATATAAAAAATAAAAACAATATT
cyp19a1b P3	ACACTCTTTCCCTACACGACGCTCTTCCGATCTATGAAAGATTGGATTTGGAATTAAG	GTGACTGGAGTTCAGACGTGTGCTCTTCCGATCTAAAAACTCAAAACAATCCAACAAAC
cyp19a1b P4	ACACTCTTTCCCTACACGACGCTCTTCCGATCTATGAAAGATTGGATTTGGAATTAAG	GTGACTGGAGTTCAGACGTGTGCTCTTCCGATCTTCTAAACATACAACTCAAACCTACC
cyp19a1b I1	ACACTCTTTCCCTACACGACGCTCTTCCGATCTTGGATATTTTTGTTTTATAGAATTAAAATA	GTGACTGGAGTTCAGACGTGTGCTCTTCCGATCTAAAAAAAACTACACTATATCCTACCC
cyp19a1b I2	ACACTCTTTCCCTACACGACGCTCTTCCGATCTTTGAGTTTAAGTATATTAAATTTAAAG	GTGACTGGAGTTCAGACGTGTGCTCTTCCGATCTACTAATAATACACTACTCTATAAATCCC

Supplemental table ST2. Used primers (with the barcode) for each sample. Dark blue/green sequence express complementarity with the primers used in PCR#1. Underlined

		Samples	Illumina multiplex index
Universal forward PCR#2 primer	AATGATACGGCGACCACCGAGATCT**ACACTCTTTCCCTACACGAC**	ALL samples	Universal
Reverse PCR#2 primers	CAAGCAGAAGACGGCATACGAGAT**CGTGAT**GTGACTGGAGTTCAGACGTGT	Control r1	1
	CAAGCAGAAGACGGCATACGAGAT**ACATCG**GTGACTGGAGTTCAGACGTGT	Control r2	2
	CAAGCAGAAGACGGCATACGAGAT**GCCTAA**GTGACTGGAGTTCAGACGTGT	Control r3	3
	CAAGCAGAAGACGGCATACGAGAT**TGGTCA**GTGACTGGAGTTCAGACGTGT	Control r4	4
	CAAGCAGAAGACGGCATACGAGAT**CACTGT**GTGACTGGAGTTCAGACGTGT	Control r5	5
	CAAGCAGAAGACGGCATACGAGAT**ATTGGC**GTGACTGGAGTTCAGACGTGT	Control r6	6
	CAAGCAGAAGACGGCATACGAGAT**GATCTG**GTGACTGGAGTTCAGACGTGT	Control r7	7
	CAAGCAGAAGACGGCATACGAGAT**TCAAGT**GTGACTGGAGTTCAGACGTGT	Control r8	8
	CAAGCAGAAGACGGCATACGAGAT**CTGATC**GTGACTGGAGTTCAGACGTGT	Control r9	9
	CAAGCAGAAGACGGCATACGAGAT**AAGCTA**GTGACTGGAGTTCAGACGTGT	Control r10	10
	CAAGCAGAAGACGGCATACGAGAT**GTAGCC**GTGACTGGAGTTCAGACGTGT	4 mg/L BPA r1	11
	CAAGCAGAAGACGGCATACGAGAT**TACAAG**GTGACTGGAGTTCAGACGTGT	4 mg/L BPA r2	12
	CAAGCAGAAGACGGCATACGAGAT**TTGACT**GTGACTGGAGTTCAGACGTGT	4 mg/L BPA r3	13
	CAAGCAGAAGACGGCATACGAGAT**GGAACT**GTGACTGGAGTTCAGACGTGT	4 mg/L BPA r4	14
	CAAGCAGAAGACGGCATACGAGAT**TGACAT**GTGACTGGAGTTCAGACGTGT	4 mg/L BPA r5	15
	CAAGCAGAAGACGGCATACGAGAT**GGACGG**GTGACTGGAGTTCAGACGTGT	4 mg/L BPA r6	16
	CAAGCAGAAGACGGCATACGAGAT**CTCTAC**GTGACTGGAGTTCAGACGTGT	4 mg/L BPA r7	17
	CAAGCAGAAGACGGCATACGAGAT**GCGGAC**GTGACTGGAGTTCAGACGTGT	4 mg/L BPA r8	18
	CAAGCAGAAGACGGCATACGAGAT**TTTCAC**GTGACTGGAGTTCAGACGTGT	4 mg/L BPA r9	19
	CAAGCAGAAGACGGCATACGAGAT**GGCCAC**GTGACTGGAGTTCAGACGTGT	4 mg/L BPA r10	20
	CAAGCAGAAGACGGCATACGAGAT**CGAAAC**GTGACTGGAGTTCAGACGTGT	Standard 0%	21
	CAAGCAGAAGACGGCATACGAGAT**CGTACG**GTGACTGGAGTTCAGACGTGT	Standard 50%	22
	CAAGCAGAAGACGGCATACGAGAT**CCACTC**GTGACTGGAGTTCAGACGTGT	Standard 100%	23

Supplementary table ST3. Raw counts of methylated and no methylated CpGs of samples (control and BPA exposed) and standards. Number of chromosome of each gene are indicated, as well as the position in the genome of each CpG, and its shorcut and amplicon where it was amplified.

See annexes

V. General discussion

"Research is to see what everybody has seen and think what nobody has thought"

Albert Szent-Györgyi

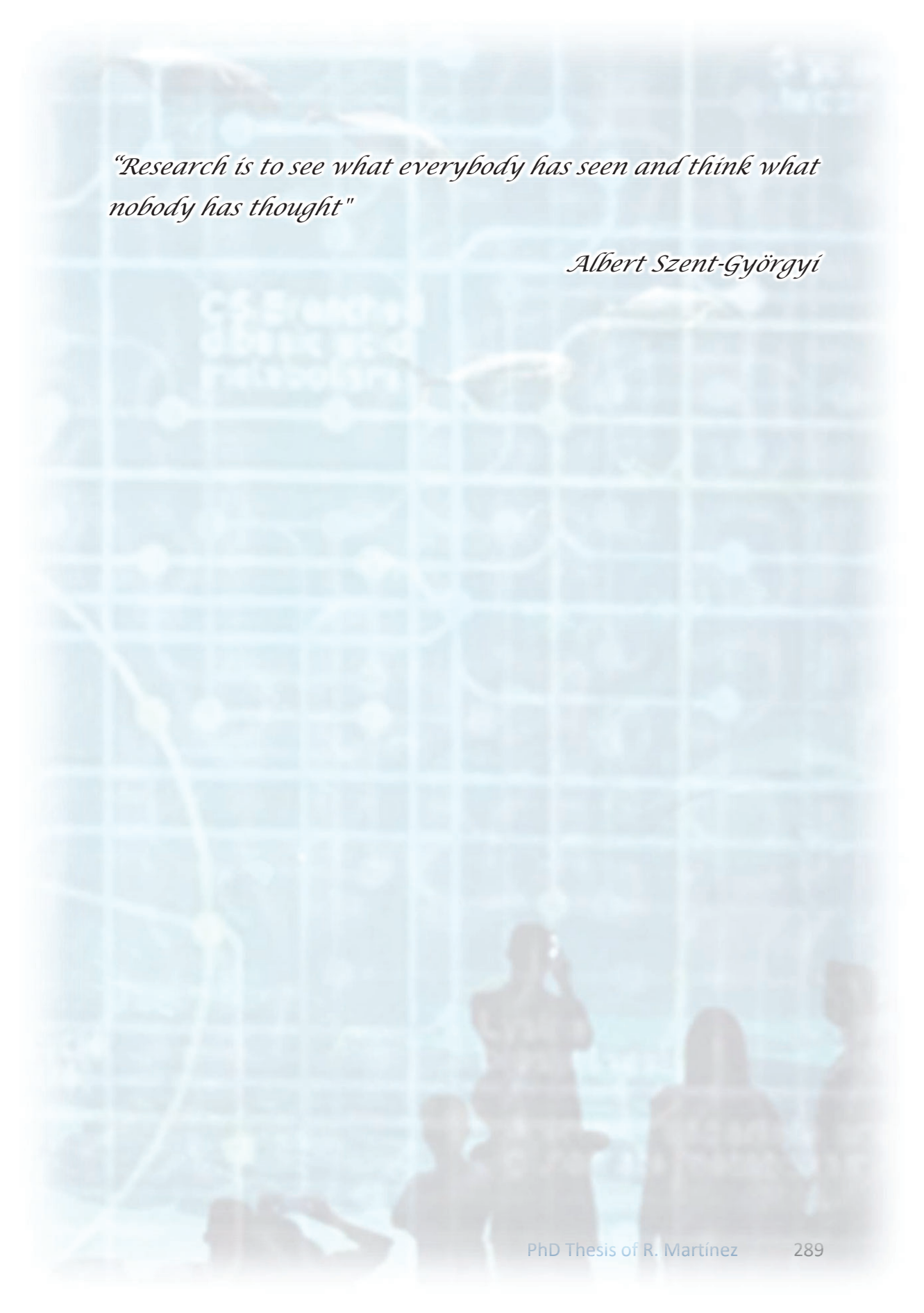

The integration and data fusion of the results (of BPA, PFOS and TBT) from this Thesis at different possible levels allow us not only to discern new aspects of their specific endocrine disruption from a general toxicity, but also to identify the early affected pathways and the degree of endocrine disruption (regarding other adverse effects) exerted by each of them. It also allows comparison between the different modes of action of these three compounds that, while all altering the lipid metabolism, they exert very different phenotypical manifestations in the zebrafish eleutheroembryos.

I. Endocrine disruption and general toxicity

A crucial question needs to be considered when endocrine disruption is studied: if the endocrine disruptor concentration is too high, the EDC could transcriptomically affect a large number of biological pathways, either directly (those ones deregulated due to the mode of action of the EDC) or indirectly (via compensation mechanisms or simply general toxicity). In this situation, how to assess the MIE and the truly mechanism of action of an endocrine disruptor?

The main difference between an endocrine disruptor and other xenobiotics lacking endocrine disrupting properties is their capacity to affect the endocrine systems at very low concentrations regarding its lethality and independently from its general toxicity. Therefore, if a given xenobiotic only "disrupts" the endocrine system at concentrations close to its lethal dose, it could not be considered an endocrine disrupting chemical, since its main mechanism of action does not imply the direct disruption of endocrine-related pathways. The benchmark dose (BMD) concept is a very useful approach to discern between the different mechanisms of action of an endocrine disruptor and its side effects due to a general toxicity. The determination of the point of departure of the different affected pathways (combining the individual calculated BMD for each gene in those pathways) would allow us to assess which are the first ones to be deregulated, and therefore, to propose a possible MOA and/or MIE for a given or suspected endocrine disruptor. For that reason, and since the functional analysis of the DEGs using a BMD

approach was only carried out for TBT (chapter II, article IV), we show here a similar analysis for BPA and PFOS.

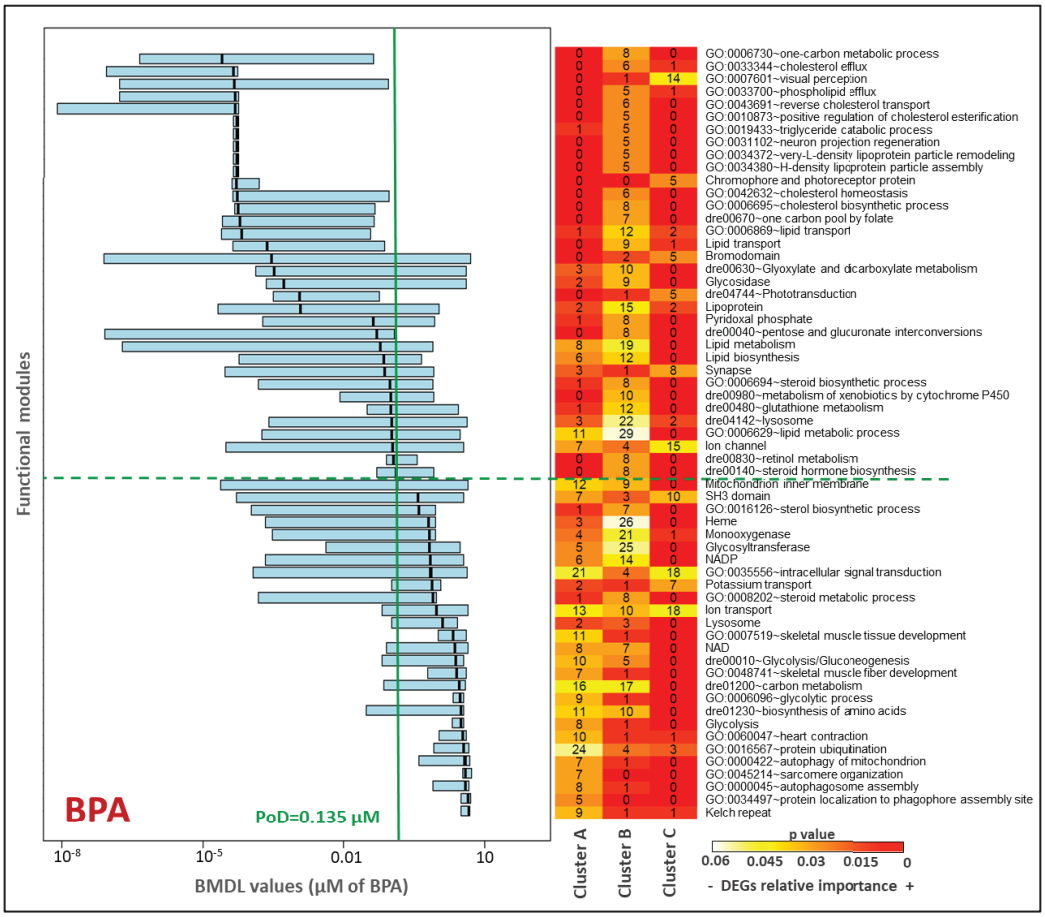

Figure V.1.: BMDL values for individual DEGs, classified by their annotation to functional modules, in BPA exposure (chapter II, article II). For each module, grey-blue box includes values between the 1st and 3rd quartiles and a thick bar indicates the mean. For helping visualization, green vertical line indicates the median BMDL considered as the transcriptomic point of departure (PoD) for BPA exposure (chapter II, article II). Green dotted horizontal line separates the functional modules with median BMDL values higher or lower than global transcriptomic PoD. On the right, distribution of DEGs among the different functional modules (rows) and clusters (columns). Numbers express the absolute number of DEGs in each functional module and cluster, box colors indicate the relative importance of DEGs associated to each pathway for each cluster (from light-yellow -most- to red -less-; two cells of the same color correspond to an identical relative fraction of DEGs in both clusters). For simplification, only functional modules with at least 5 DEGs in at least one of the clusters were represented. Redundant functional modules were simplified to the one with the highest number of hits.

In the case of BPA (figure V.1.), results from the BMD analysis showed that the pathways affected at the lowest concentrations were the ones related with lipids (cholesterol, phospholipids, lipoproteins, triglycerides, lipid transport and metabolism…) and visual perception. Retinol and steroid-related processes were altered by BPA even at the lowest tested dose (0.44 µM). These observations agree with the proposed mode of action of BPA, implicating not only signalling by PPAR-γ and ER, but also acting via RAR and/or RXR, among others. They are also consistent with the phenotypical effects observed by us and others. For example, we observed that eleutheroembryos exposed to BPA from 2 to 5 dpf presented yolk sac malabsorption syndrome, lipidome disruption and the decrease of eye width (chapter I, II and III, articles I and II and V). A possible visual impairment should be further studied and its relationship with the decreased mobility presented by the exposed eleutheroembryos (chapter IV, article VI; [193]). Thus, our results are consistent with the endocrine disruption and obesogenic properties reported for BPA (chapter II, article II; [145,355,356]). Other processes affected at higher doses were those related with energy balance, muscle development or heart contraction. That was confirmed by the dysregulation of several transcripts involved in energy homeostasis and miRNA(s) involved in muscle and heart (chapter IV, article VI).

The most sensitive pathways to PFOS were those related to cell-cell interactions, cell adhesion, immune response, zinc fingers, apoptosis, cytokines, and others (figure V.2.). Lipid transport and glycerophospholipid metabolism pathways were also affected at PFOS concentrations clearly below lethality levels. Our results showed that scoliosis and kyphosis were among the main morphological effects of PFOS in the eleutheroembryos (chapter I, article I). This could be related to the observed deregulation of transcripts involved in muscle structure and functioning, like myosin or actin genes (chapter II, article III). Although it could be considered as a wide spectrum of effects, many transcriptional changes seem to have a common origin. Cell adhesion, the affected pathway with the lowest PoD, is commonly mediated by four major protein superfamilies (immunoglobulins, selectins, cadherins and integrins) globally known as cell adhesion molecules or CAMs, and located on the cell surface. They have been related

to processes like immune response, actin fibers linkage, and signal transduction (including apoptosis signals). Other affected pathways with low PoD are related to lectins -also involved in immune response-, lipid regulation and skeletal muscle (chapter II, article III). All these CAMs-related pathways were affected by PFOS.

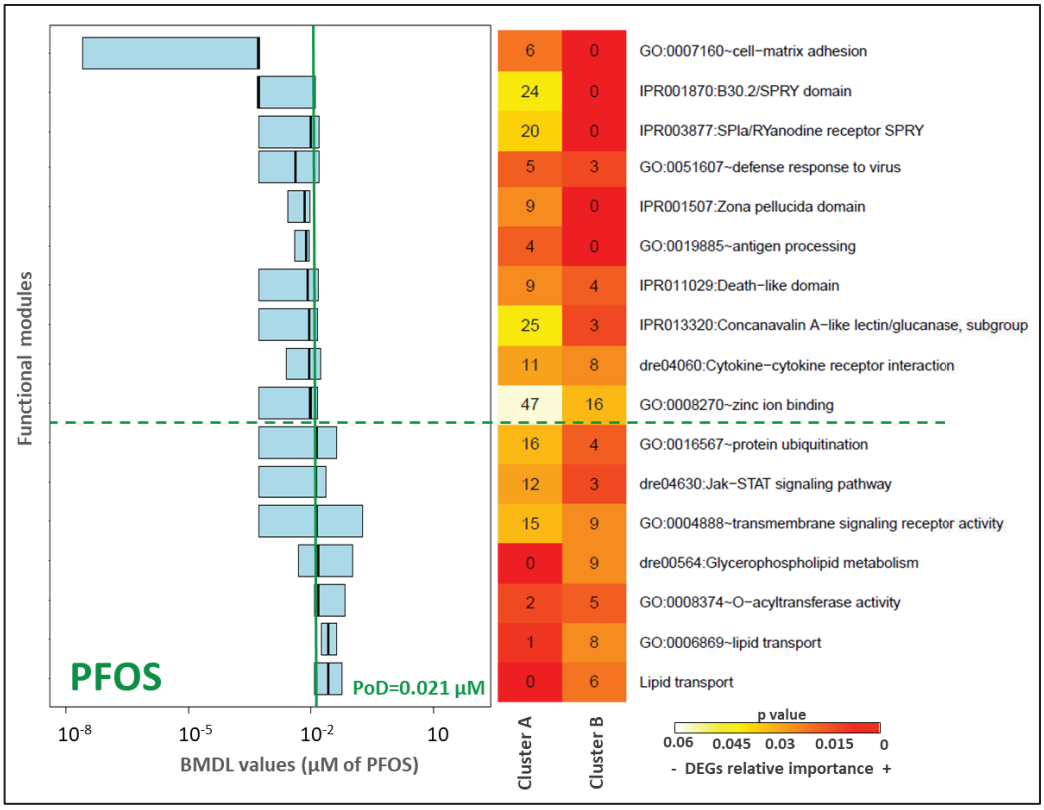

Figure V.2.: BMDL values for individual DEGs, classified by their annotation to functional modules, in PFOS exposure (chapter II, article III). Graphical features are analogous to the ones explained in figure V.1. legend.

While PFOS can partially bind/activate several nuclear receptors (androgen receptors -AR-, ER, TR, PPAR- γ...) [357,358], it has been proposed that its binding to PPAR-α is the most important molecular event to explain its dysregulatory effects [357,359,360]. Natural ligands of PPAR-α are fatty acids, with which PFOS shares many structural chemical features, like amphiphilicity (polar head and a large non-polar carbon chain). It has been reported in different models that PPAR-α activators can not only inhibit cell

adhesion via cytokines [361], but that they are also involved in immune response and changes in immunoglobulins, selectins and integrins [362–364]. Moreover, it has been also observed that PPAR-α activation induces lipid catabolism (free fatty acid oxidation and supressed lipogenesis) via heterodimerization with FXR receptors [362,365]. A further, non-receptor mediated direct mechanism for PFOS toxicity needs to be also considered, as PFOS may integrate directly into cell- and mitochondrial membranes, altering their fluidity and permeability [366]. These mechanisms and effects agree with both functional transcriptomic analysis and phenotypic results. PFOS exposed individuals presents lower yolk sac area (YSA) than they should have considering their size (chapter I, article I), indicating a higher nutrient expenditure. Similarly, in mammals, PFOS elicits an unwarranted extra heat production via uncoupling protein 1 (UCP1) in brown adipose tissue, resulting in a higher energy expenditure [367]. Nevertheless, although zebrafish has UCP1 orthologue, its lack of brown adipose tissue and of both general and specific cranial heat production (observed in some fish), suggest that the energy expenditure is used for other purposes [368].

In summary, we consider that endocrine disrupting properties of PFOS seem to be limited to lipid metabolism in our experimental conditions. Moreover, its effects would not be truly obesogenic-like, but rather “pseudo-anorexic", via the suggested increase in lipid oxidation and energy expenditure.

Finally, TBT exerted a clear disruption in the steroid biosynthesis and metabolism since these pathways showed the lowest PoD in exposed eleutheroembryos (chapter II, article IV; figure V.3.). Most of other affected pathways were related with cell division (microtubule, cell cycle, mitotic cell cycle, chromosome, methylation…), which can be correlated with a general developmental delay at phenotypic level. As previously reported (chapter II, article IV), all these transcriptomic effects can be explained by the binding of TBT to RXR receptors, which heterodimerize with VDR and RAR, affecting in this way steroid production (via cholesterol and vitamin D_3 pathways) and immune response (in this last case, only disrupted at higher doses). Phototransduction pathway, also disrupted at relatively low concentrations, can also be explained by RAR-RXR

heterodimers [369,370]. On the other hand, lipid related disruption, which could originate via heterodimerization with PPAR-γ, is only affected at relatively high TBT concentrations and, consistently, its lipid-related morphological effects were mainly non-specific (chapter II, article IV). Yolk sac area increased in the individuals exposed to TBT in a way that could be explained by a mere developmental delay (chapter I, article I).

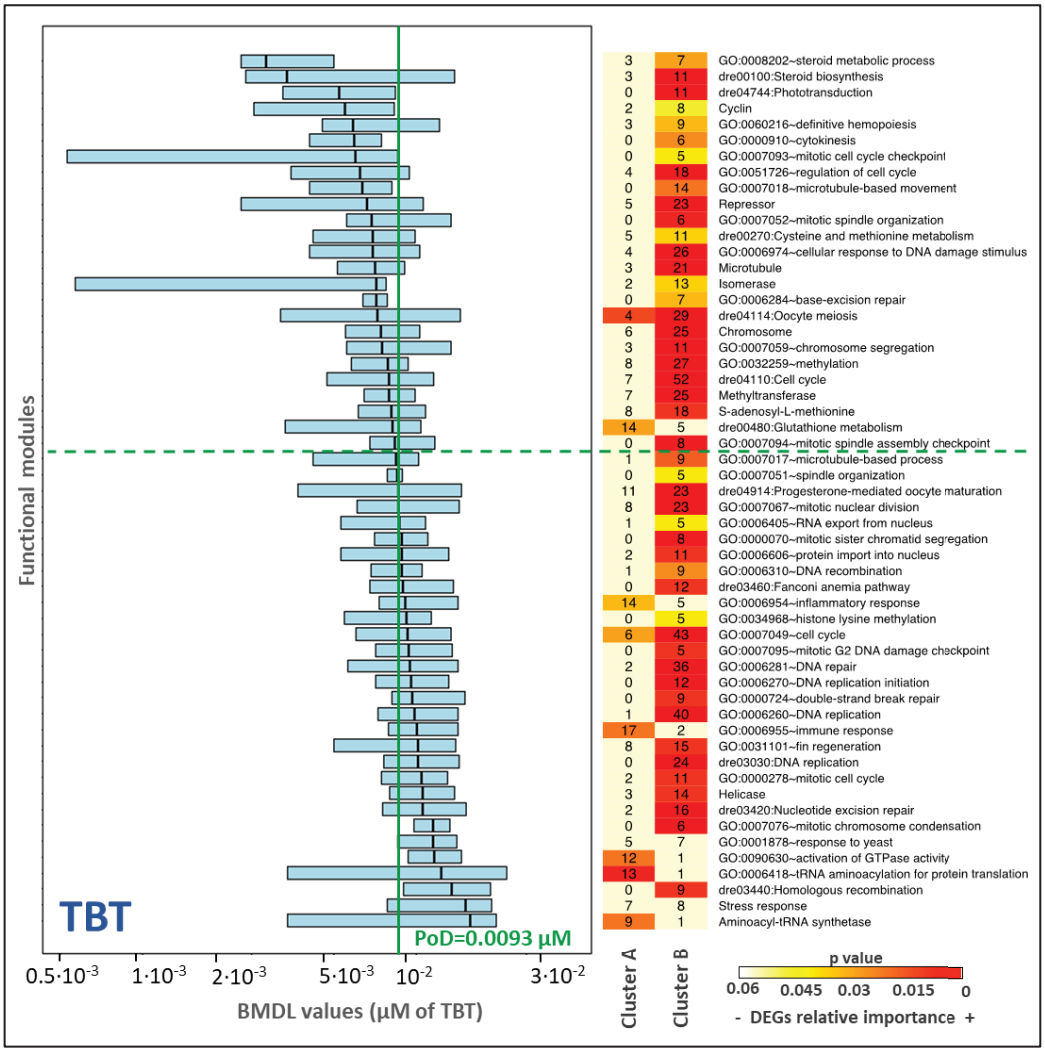

Figure V.3. (adapted from [371]): BMDL values for individual DEGs, classified by their annotation to functional modules, in TBT exposure (chapter II, article IV). Graphical features are analogous to the ones explained in figure V.1. legend.

Therefore, in our conditions, obesogenic properties exerted by TBT are limited to transcriptomic level and at high TBT concentrations, suggesting that the activation of RXR receptors could be less important for the lipidomic effects than the activation of PPAR-γ receptors (like BPA) via the PPAR-RXR complex.

II. Integrative analysis of BPA, PFOS, and TBT

a) Transcriptomic, metabolomic and morphometric point of departure (PoD) analysis

When an organism is exposed to any xenobiotic, including endocrine disruptors, the magnitude of the effects depends on the studied endpoint at a specific biological level, with further influence from other variables like dose and time of exposure. In many cases, and after the molecular initiation event (MIE) takes place, subsequent molecular interactions result in the deregulation of different transcripts. Consequently, the levels of the codified proteins may also change when translation rate becomes adapted to the new transcriptome situation. As a general rule, transcript and protein amounts can change by even several orders of magnitude [36], showing $\log_2$ fold changes values between -5 and +5 [372–375]. Finally, the subsequent changes in enzyme levels and activities would modify the synthesis and degradation pathway rates for different metabolites, the concentration of which becomes also deregulated. Conversely to transcripts or proteins, metabolites usually change by relative small factors, showing $\log_2$ fold changes values between -2 and +2 [36,68,135,376,377]. As a rule, these three molecular levels (transcripts, proteins, metabolites) are the first ones to be affected and detected both in time and/or concentration. Next, sometimes almost simultaneously, specific directly-related endpoints as behaviour, via neurotransmitters, become altered. Subsequently, cell and tissue deregulations take place and physiologic effects can be detected. Finally, organ and organism effects (known as apical phenotypes) become evident at different levels, ending up with severe, vital effects, like malformations or mortality, if the exposure dose is high enough. Morphological alterations commonly change in one order of magnitude or less [140].

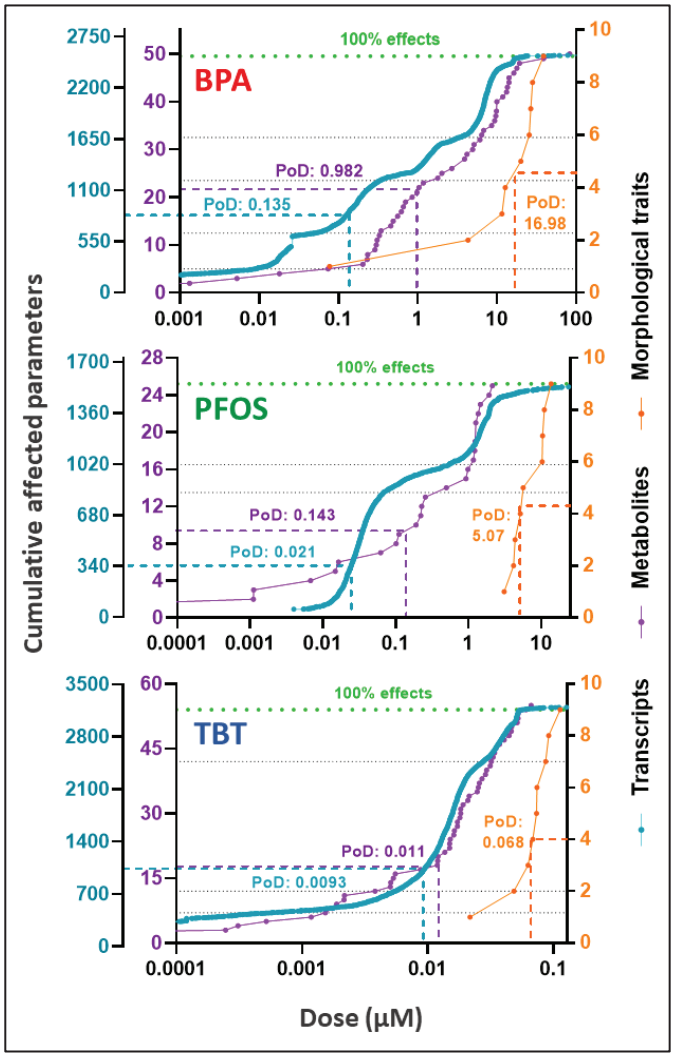

Figure V.4.: BPA, PFOS and TBT cumulative plots indicating the number of affected parameters (genes, metabolites and morphological traits) by exposure doses. This analysis has been done following the benchmark dose (BMD) approach. Transcripts, metabolites and morphological traits are shown in blue, purple and orange, respectively. Point of departure values (PoD) were calculated as the median of all the benchmark dose lower limits (BMDLs) in each biological level, as described herein [378–380].

Consistent with these general principles, we have compared transcriptomic and metabolomic points of departure (PoD) from our studies (chapter I and II: articles I, II, III and IV; [68]), and have found that they are similar, differing a maximum of one order of magnitude for all three cases (BPA, PFOS and TBT, figure V.4.). On the other hand,

adverse effects at morphological level required significantly higher exposure doses. The ratio between the smaller molecular PoD (characteristically, the transcriptomic one) and the morphologic PoD varies 126 times for BPA, 237 times for PFOS and 7 times in the case of TBT. Although that could indicate a different mechanism of toxicity for TBT (related to a heavy metal poisoning by Sn), further research on this matter should be carried out (chapter II; article IV).

Text box V.1.

· Apical endpoint: traditionally, gross whole-organism adverse outcome of exposure to a toxic, as developmental anomalies, reproduction problems, organ malformations, or death.

· Point of departure (PoD): regarding a biological level or endpoint, threshold reference value at which it can be considered that adverse effects start to take place. Also known as the general BMD (benchmark dose) for this specific endpoint. PoD are commonly calculated using the median of the BMDL (lower limit of the BMD calculations) obtained for each variable in a certain biological level.

Among the three studied compounds, TBT was the most toxic one: LC_{50} values (2-5 dpf of exposure; at 5 dpf) for TBT was 0.17 µM, while the corresponding values were 18.2 and 79.9 µM for PFOS and BPA, respectively. Similarly, the lowest concentration for adverse effects to occur at any of the three studied biological levels (figure V.5., A) corresponded to TBT, followed by PFOS and BPA, in that order. Nevertheless, when comparing results using equilethal concentrations as reference (x % of the LC_{50}), we observed that PoDs at all tested biological levels were higher for TBT than in BPA and PFOS, which in fact were both very similar to each other (figure V.5., B). This indicates that the individuals exposed to TBT only started to present adverse effects at concentrations closer to lethality, compared with BPA and PFOS, which elicited adverse effects at much lower relative concentrations, especially at transcriptomic and metabolomic levels. At this point, it needs to be highlighted the difference between equilethal and equitoxic concentrations. By definition, while the first term refers to the concentrations of different compounds exerting the same mortality level, the second

one indicates those concentrations that exerted the same severity of a given specific adverse effect. Absolute values of equilethal and equitoxic doses, as well as the ratio between them, may be very different for certain endocrine disruptors and other stressors [381–383]. Indeed, a recent study demonstrates how equilethal concentrations of certain perfluorinated compounds (PFOS among them), exert very different degrees of affection in the several studied endpoints [384]. That is not only affected by the mechanism of action of each EDC, but also by their relative potency as agonist or antagonist of the target receptor(s). Indeed, in our case, the TBT was the one with lower equitoxicity at same equilethal concentrations.

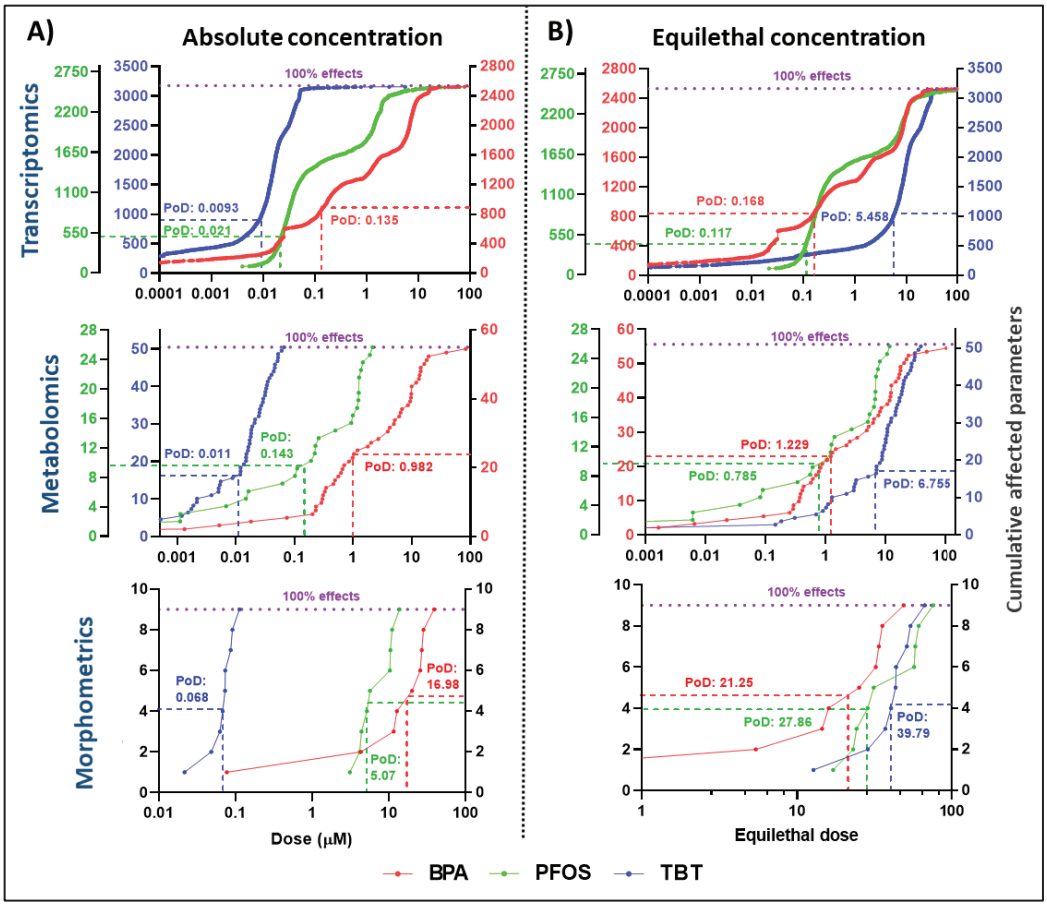

Figure V.5.: BMD cumulative plots of the affected parameters (transcripts, metabolites and morphological traits) regarding the absolute (A) and equilethal (B) dose of BPA, PFOS and TBT. BPA, PFOS and TBT values are shown in red, green and blue, respectively.

b) Comparative functional analysis

A deeper view of the differences between toxic mechanisms for the three compounds came from combined comparative functional analysis of transcriptomic data. Figure V.6. shows the hierarchical clustering of differentially expressed genes (DEGs; VIII.2.annex table 1) after the combined normalization of the three datasets.

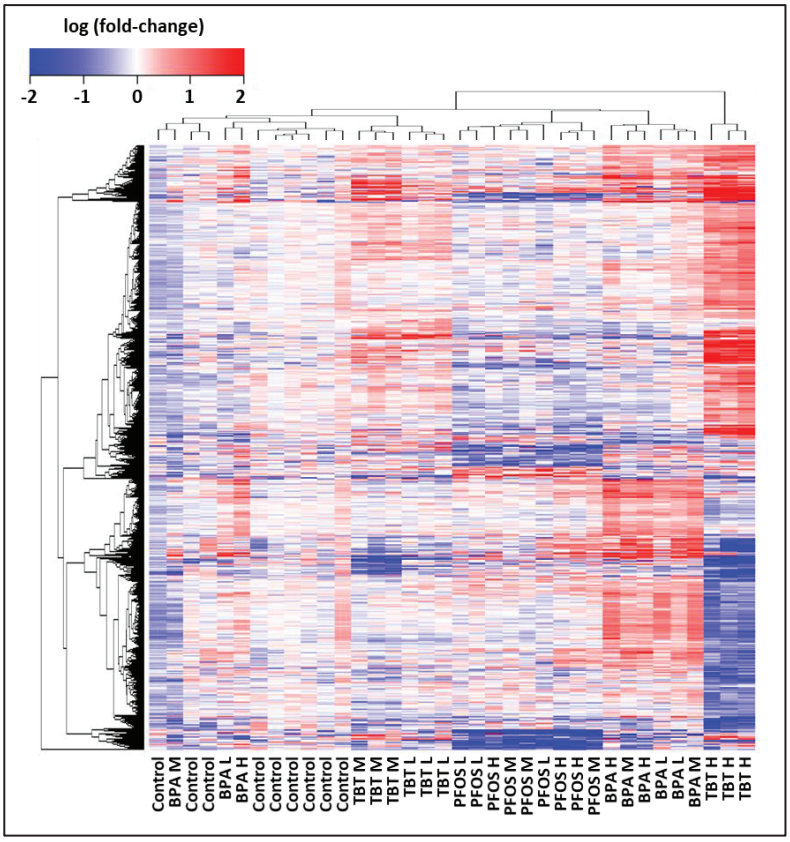

Figure V.6.: Heatmap of the differentially expressed genes (DEGs) of the BPA, PFOS and TBT exposed groups' samples. Transcripts counts were normalized by pqn (probabilistic quotient normalization) and fold-changes regarding the mean of the control groups for each dataset (BPA, PFOS and TBT) were calculated (to avoid any possible bias due to zebrafish batches). Then, an ANOVA-PLS was performed and genes with p adjusted values < 0.001 were considered as DEGs (3132 genes). Hierarchical clustering of both samples and DEGs are shown in the columns and rows, respectively. Data are represented as fold-changes values, log transformed and scaled relative to control mean values. L, M and H correspond to the low, medium and high exposure concentration of each EDC, respectively.

A principal component analysis (PCA) of the normalized transcriptomic data defined two components explaining 50.9 % of the total variability. The score plot in figure V.7. shows the separation of samples from all three treatments, and the separation of the highest dose treatments from control samples. PC1 (34.9% of observed variation) separates TBT from the rest of samples, whereas PC2 (16.0% of observed variation) separates all three compounds (figure V.7.).

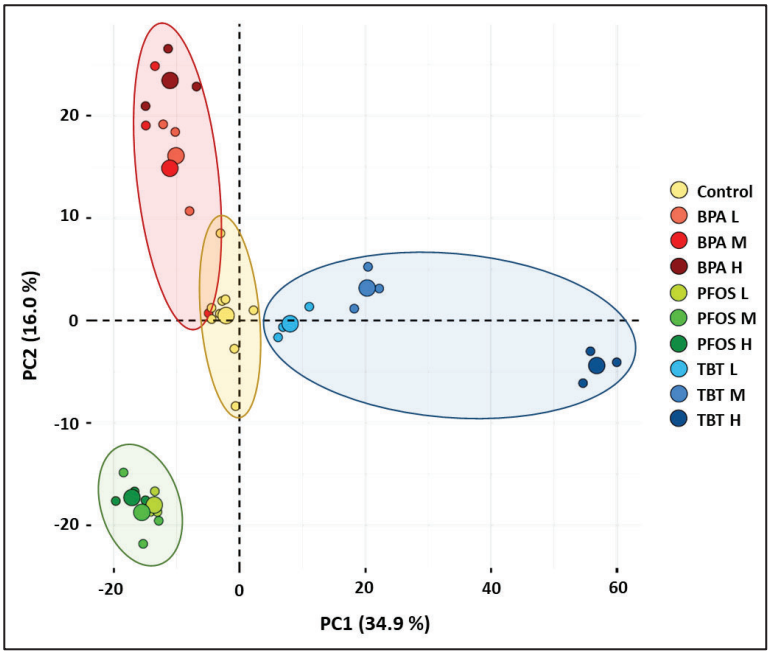

Figure V.7.: principal component analysis (PCA) of the obtained DEGs (3132). Scores of the samples in the first two components (which explain 50.9% of the total variability) are shown. L, M and H correspond to the low, medium and high exposure concentration of each EDC, respectively.

Text box V.2.

· Hierarchical clustering: method of cluster analysis which goal is to build a hierarchy of clusters, obtaining a dendrogram-like classification. Briefly, hierarchical clustering assigns each sample/variable (the classification is performed for both samples and variables) to its own group. Iteration process is then performed, where the two most similar groups are joined in each step, and that continues until only one final cluster is obtained.

· PAM (partition around medoids) clustering: clustering algorithm that classifies the datapoints in several medoids (or clusters). Briefly: after performing a PCA, the PAM algorithm analyzes the covariance matrix to search k representative objects (medoids or clusters) that explain the structure of the data. Each observation is assigned to its nearest cluster. Iteration process is then performed to choose the number and position of medoids that minimizes the sum of pairwise dissimilarities.

· Transcript amount: quantity of mRNAs in a cell, tissue or organism at a specific time.

· Gene expression: all the processes by which a functional product (usually a protein) is synthesized from the information contained in the genes. Nevertheless, the term is commonly confused with "transcript amount" and indistinctly used, and some terms like "differentially expressed genes" are used to refer to significant changes in transcript amount.

PAM (partition around medoids) clustering of the genes reports the group of transcripts that similarly change, and their comparison among exposure groups can provide us valuable information. Cluster A includes those genes overrepresented in BPA-treated samples, not affected by PFOS exposure and underrepresented in TBT-treated samples (figure V.8.). It includes a vast collection of genes involved in growth and development (VIII.2.annex table 2): DNA replication, cell cycle, cell division, chromosome, mitosis, microtubules… As previously reported (chapter I and II; articles I and IV; [140,371]), TBT morphological effects could be correlated to a general developmental delay. The transcriptomic results from TBT-treated samples showed deregulation of cholesterol and vitamin D_3-related pathways, and it is known that D_3 signaling is crucial for the normal development of the zebrafish during embryo stage, which would support the conclusions from the morphological data. The deregulation of this pathway can be explained by the binding of TBT to retinoid X receptors (RXR) which can heterodimerize with vitamin D receptors (VDR) [385–387]. On the other hand, it has been reported the binding of BPA to the estrogen receptor alpha (ERα) [388]. This binding can activate the extra-nuclear signaling pathways of kinase/mitogen-activated protein kinase (ERK/MAPK) and phosphatidyl-inositol-3-kinase/AKT (PI3K/AKT), which can enhance cell proliferation [388–391], and could explain the activation of its related transcriptomic pathways.

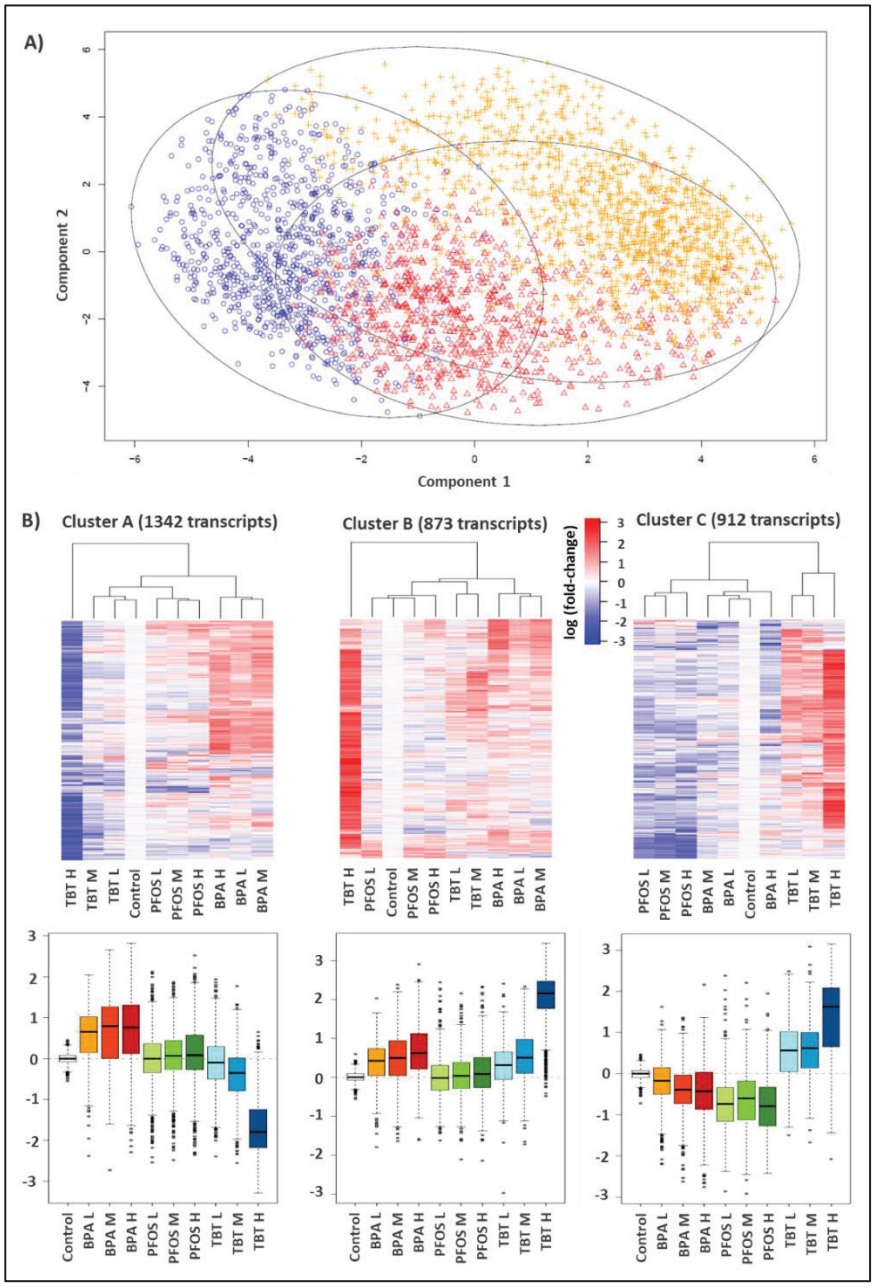

Figure V.8.: A) Score plot of the partition around medoids (PAM) clustering. Two first components explained 34.24% of the total variability. Yellow crosses, red triangles and blue circles indicates the genes of the clusters A, B and C, respectively. B) PAM clusters and boxplots of differentially expressed genes (3132) from all combined datasets (BPA, PFOS and TBT). Data are represented as fold-change values, log transformed and scaled relative to control mean values. L, M and H correspond to low, medium and high exposure concentrations of each EDC, respectively.

Cluster B grouped genes overrepresented in eleutheroembryos exposed to BPA and TBT, with small changes in PFOS-exposed ones. Genes in this cluster were mainly involved in oxygen transportation and energy homeostasis (globins, heme binding, mitochondrion, cell redox, carbohydrate metabolism…) and lipids (lipid binding and transport, cholesterol, low and high density lipoproteins, chylomicrons, cholesterol, triglycerides…), among others. While up-regulation of lipid-related pathways can be simply explained by the activation of the PPAR-γ-RXR complex, the energy homeostasis involves many biological pathways and several nuclear receptors have been reported to be implied, as PPAR (α, β, γ), ER, estrogen-related receptors (ERR), thyroid receptors (TR), liver X receptors (LXR), farnesoid X receptors (FXR), or constitutive androstane receptors (CAR) [392–395]. As previously reported, both BPA and TBT can activate PPAR-γ-RXR complex via PPAR-γ and RXR, respectively, while PFOS has been proposed to bind PPARα, CAR, pregnane X receptor (PXR) or FXR (chapter II, articles II, III and IV).

Cluster C includes genes strongly overrepresented in TBT-treated samples and underrepresented in PFOS-treated ones. Most of the genes in this cluster were related to glycolysis, cell adhesion, immune response and cytokines, among other functions. The ability of PFOS to down-regulated these pathways has been already shown and agrees with the bibliography (chapter II, article III). Nevertheless, it can be also observed a dose-response down-regulation of these genes in the case of BPA exposed individuals and up-regulation for those exposed to TBT. It has been reported that both PPAR (activated by BPA) and LXR (activated by PFOS) receptors can repress the inflammatory response and thus, the immune response [396,397]. On the other hand, different cell and mice studies reported that the activation of RXR receptors (proposed molecular initiation event of TBT) activates inflammatory and immune responses and upregulates chemokine expression. Nevertheless, it has been proposed that this effect is not mediated by PPAR-RXR heterodimer but by others, like retinoid acid receptor (RAR)-RXR or RXR-VDR heterodimers [398–402]. This fact could explain the general upregulation of the cluster C genes by TBT.

c) Identification by *omics* of endocrine disruption taking place at early life stages and at low EDC doses

Phenotypic alterations by EDCs at different biological levels and developmental stages, and/or at high effector concentrations may be traced down to transcriptomic alterations at early life stages and at lower doses. Table V.1. shows a list of several of these possible correlations for zebrafish embryos exposed to BPA, PFOS, or TBT.

Endocrine disruptor	Early transcriptomic alteration	Phenotype at higher concentrations or later in life
BPA	Lipid metabolism (chapter II, article II).	- Yolk sac malabsorption (chapter I, article I). - TG, DG, PC and PI decreased consumption (chapter III, article V). - Higher body weight and body mass index in juveniles (chapter IV, article VI).
	Visual perception (chapter II, article II).	- Decreased eye width (chapter II, article II). - Decreased mobility (likely related) (chapter IV, article VI).
	Steroid hormone biosynthesis (chapter II, article II).	- Bibliography (adult exposure): decreased testosterone and increased 17β-estradiol and vitellogenin levels [403].
PFOS	Apoptosis (chapter II, article III).	- Bibliography: Increased apoptotic cells [404].
	Immune response (chapter II, article III).	- Bibliography (similar doses but chronic exposure): disrupted activities of immune-related enzymes [405].
	Myosins, actins and tropomyosins (chapter II, article III).	- Scoliosis and kyphosis (chapter I, article I).
	Lipid transport (at slightly higher concentrations) (chapter II, article III).	- Decreased relative yolk sac area regarding eleutheroembryo size (suggested increased energy consumption) (chapter I, article I).
TBT	Steroid metabolism (chapter II, article IV).	- Bibliography (adult exposure): decreased plasma level of 17β-estradiol, increased cortisol levels [406]. - Bibliography (chronic exposure): masculinization (male biased population) [407].
	Cell cycle (chapter II, article IV).	- Developmental delay (chapter I, article I).

Table V.1.: summary of the main transcriptomic disruptions exerted by BPA, PFOS and TBT in zebrafish eleutheroembryos (exposed from 2-5 dpf) and phenotype alterations observed later in life and/or at higher doses.

A fundamental question is whether or not the alterations due to EDCs may propagate in time even when the effector has been removed. In the case of BPA, we observed mid-range persistence of the increase of weight and body mass index, of behaviour changes and of transcript dysregulation in juveniles exposed during the period from 2 to 5 dpf, and led in clean water from 6 dpf until 29-47 dpf (chapter IV, article VI). As explained in the introduction, these long-term effects can be, at least partially, mediated by epigenetic mechanisms (as miRNAs or DNA methylation). Consistently with this hypothesis, exposed eleutheroembryos (5 dpf) showed an increase of *miR-23b* and a decrease of miR-1 (chapter IV, article VI). *miR-1* is involved in muscle and heart [408,409], and although no effects in eleutheroembryonic muscle structure could be observed, their motility was decreased. *miR-23b* is predicted to target proopiomelanocortin A (*pomca*), which has been related with food intake and obesity [410]. Nevertheless, its role in adiposity in zebrafish is unclear [411]. On the other hand, we investigated the correlation between the general methylation status of a gene and its expression levels (chapter IV, article VII). The effects of the BPA exposure in the expression of some of the most affected genes (*cyp19a1b* and *aldh1a2*) could be partially explained by its exerted changes in the methylation of those gene, although other mechanisms needed also to be considered (chapter IV, article VII). If these epigenetic changes remain altered at later developmental stages and whether they could explain the observed phenotypical alterations, it is a matter that should be further studied.

Regarding the integration of data from several organismal levels, although the early detection of adverse effects, classically by transcriptomics, is usually the most informative analysis (even before more evident alterations can be noticed), phenotypic effects can be eventually used to clarify the functional analysis of the transcriptomic data. This exemplifies the usefulness of the combination of different *omics* and/or integrative analyses' information in environmental risk assessment, for the study of the different EDC mechanisms of action. For example, the potential biological meaning of the dysregulations of muscle-related transcripts by PFOS treatment may be easily understood after the observed scoliosis and kyphosis presented by the treated individuals (chapter II, article III).

III. Proposed adverse outcome pathways for BPA, PFOS and TBT

Considering all the results obtained in this thesis and bibliographic information, we summarize and/or propose the adverse outcome pathways of BPA, PFOS and TBT in the figures V.9., V.10. and V.11., respectively.

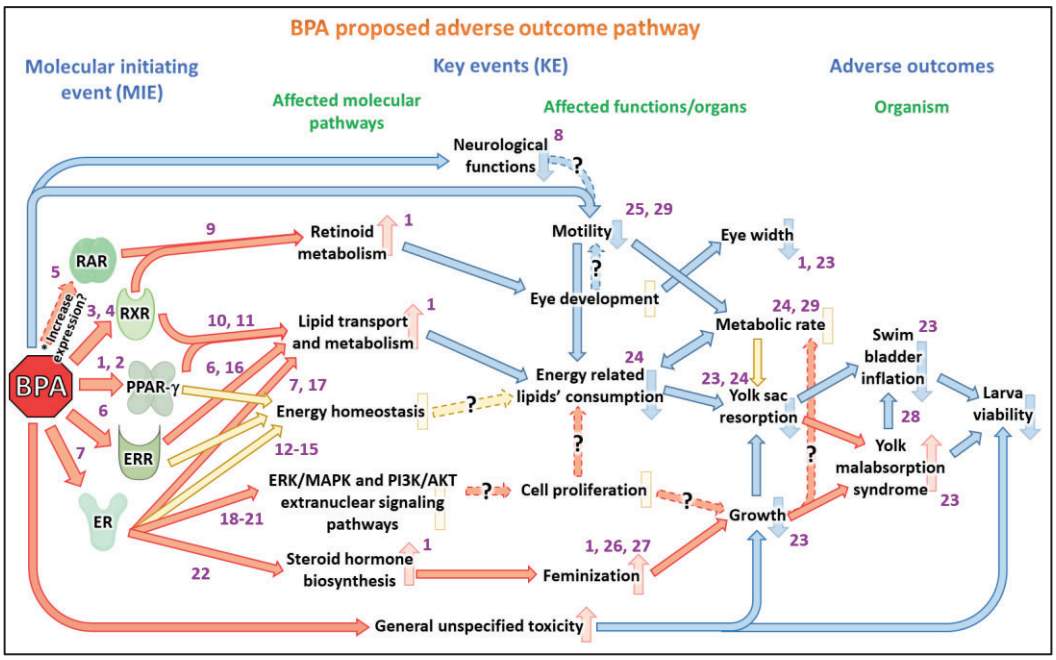

Figure V.9. (adapted from [75]): adverse outcome pathway (AOP) for BPA in zebrafish eleutheroembryos. Red and blue arrows connecting observations represent an exerted agonism/activation/increase and antagonism/inhibition/decrease, respectively (predicted by logic and/or observed in any animal model). Red and blue arrows in each observation represent an observed decrease/increase in this endpoint (observed in zebrafish). Yellow arrows both between observations and in at observation itself, represent uncertain effect and/or non monotonic effect. Numbers in purple indicate the references that reported: the interaction of BPA with nuclear receptors (in general), relation between receptors and biological pathways (in general), and direct effects of BPA (specifically in zebrafish embryos/larvae). References: 1) [71]; 2) [412]; 3) [413]; 4) [414]; 5) [415]; 6) [335]; 7) [416]; 8) [351]; 9) [417]; 10) [418]; 11) [419]; 12) [392]; 13) [393]; 14) [394]; 15) [395]; 16) [420]; 17) [97]; 18) [388]; 19) [389]; 20) [390]; 21) [391]; 22) [421]; 23) [140]; 24) [75]; 25) [193]; 26) [422]; 27) [423]; 28) [424]; 29) [425].

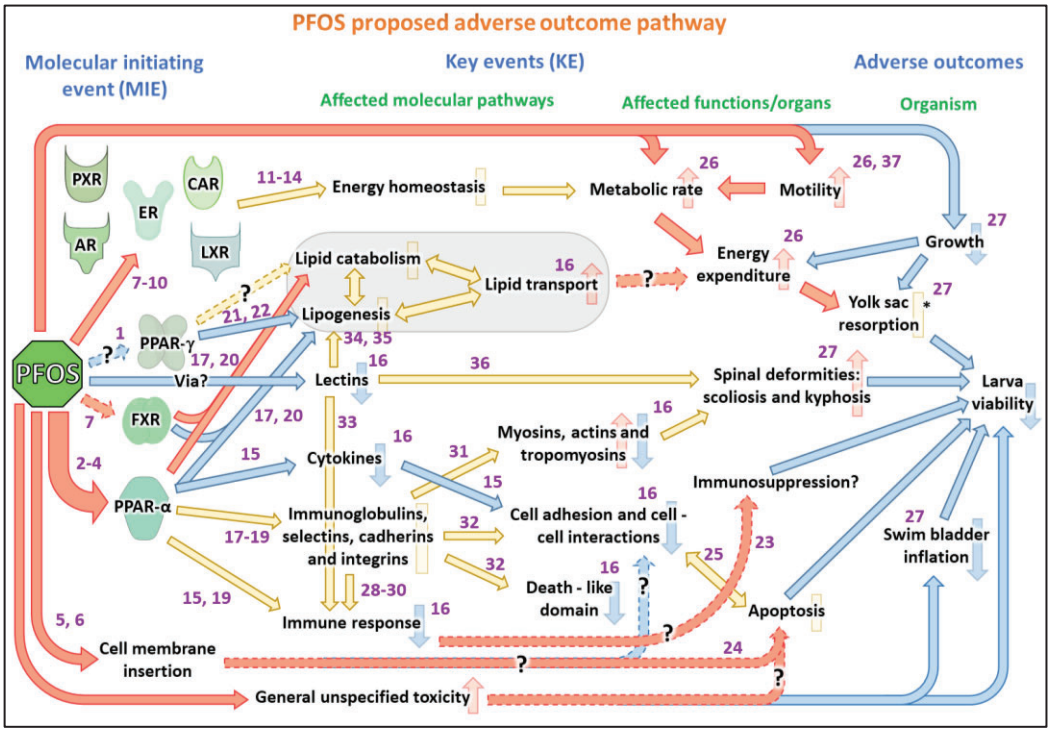

Figure V.10.: adverse outcome pathway (AOP) for PFOS in zebrafish eleutheroembryos. Red and blue arrows connecting observations represent an exerted agonism/activation/increase and antagonism/inhibition/decrease, respectively (predicted by logic and/or observed in any animal model). Red and blue arrows in each observation represent an observed decrease/increase in this endpoint (observed in zebrafish). Yellow arrows both between observations and in at observation itself, represent uncertain effect and/or non monotonic effect. Numbers in purple indicate the references that reported: the interaction of PFOS with nuclear receptors (in general), relation between receptors and biological pathways (in general), and direct effects of PFOS (specifically in zebrafish embryos/larvae). References: 1) [426]; 2) [357]; 3) [359]; 4) [360]; 5) [366]; 6) [427]; 7) [428]; 8) [429]; 9) [430]; 10) [358]; 11) [392]; 12) [393]; 13) [394]; 14) [395]; 15) [361]; 16) [72]; 17) [362]; 18)[363]; 19) [364]; 20) [365]; 21) [114]; 22) [431], 23) [432]; 24) [433]; 25) [434]; 26) [384]; 27) [140]; 28) [435]; 29) [436]; 30) [437]; 31) [438]; 32) [439]; 33) [440]; 34) [441]; 35) [442]; 36) [443]; 37) [444]. *Yolk resorption: although the yolk sac area of PFOS-exposed individuals is higher than the one of control group, it is far lower than the one that should correspond for their size, indicating a higher consumption of the yolk sac.

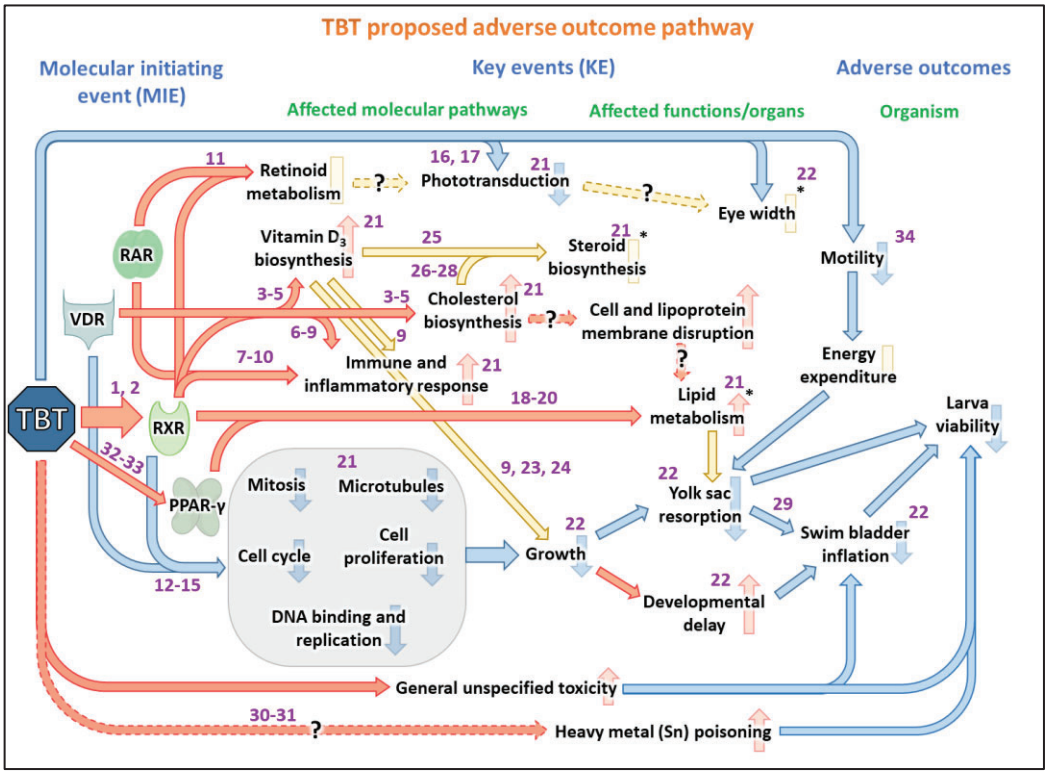

Figure V.11.: adverse outcome pathway (AOP) for TBT in zebrafish eleutheroembryos. Red and blue arrows connecting observations represent an exerted agonism/activation/increase and antagonism/inhibition/decrease, respectively (predicted by logic and/or observed in any animal model). Red and blue arrows in each observation represent an observed decrease/increase in this endpoint (observed in zebrafish). Yellow arrows both between observations and in at observation itself, represent uncertain effect and/or non monotonic effect. Numbers in purple indicate the references that reported: the interaction of TBT with nuclear receptors (in general), relation between receptors and biological pathways (in general), and direct effects of TBT (specifically in zebrafish embryos/larvae). References: 1) [445]; 2) [446]; 3) [385]; 4) [386]; 5) [387]; 6) [398]; 7) [399]; 8) [400]; 9) [401]; 10) [402], 11) [417]; 12) [447]; 13) [448]; 14) [449]; 15) [91]; 16) [369]; 17) [370]; 18) [450]; 19) [451]; 20) [114]; 21) [371]; 22) [140]; 23) [452]; 24) [453]; 25) [454]; 26) [455]; 27) [456]; 28) [457]; 29) [424]; 30) [458]; 31) [340]; 32) [459]; 33) [460]; 34) [461]. *Lipid metabolism: only at very high concentrations and/or later in life. *Eye width: higher eye width regarding the one that they should have considering the developmental delay. *Steroid biosynthesis: hormetic response based on the concentration.

Although there are evidences that all BPA, PFOS and TBT can alter lipid metabolism, they show very diverse spectra of effects on the lipid-related pathways. These differences could be explained by their proposed different molecular initiation events. A summary

of the effects of BPA, PFOS and TBT in lipid metabolism of zebrafish eleutheroembryos is shown in figure V.12.

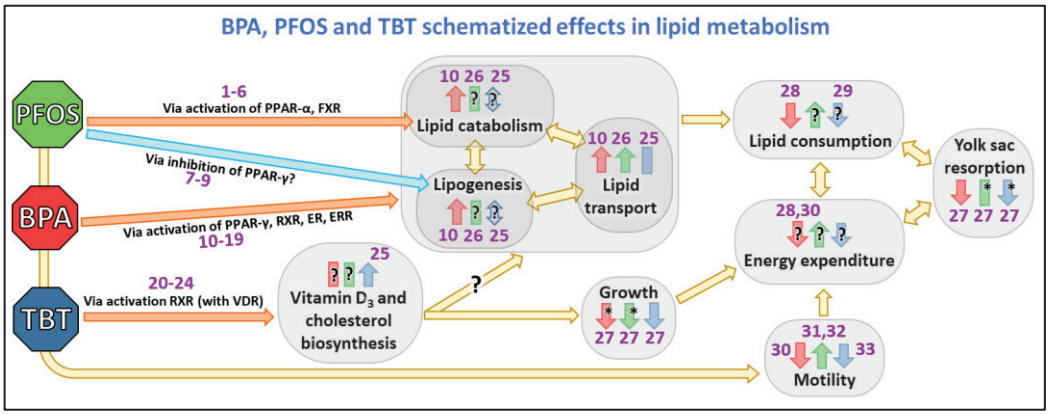

Figure V.12.: summary of the effects of BPA, PFOS and TBT in lipid metabolism of zebrafish eleutheroembryos. Orange and cyan arrows connecting observations represent an exerted agonism/activation/increase and antagonism/inhibition/decrease, respectively (predicted by logic and/or observed in any animal model). Yellow arrows between observations represent uncertain effect and/or non-monotonic effect. In each observation, red, green and blue arrows represent the direct observed effect of BPA, PFOS and TBT, respectively: up-arrow indicates an increase, down-arrow indicates a decrease, and a rectangle indicates no effect. Not known effects are indicated by an interrogation mark. Numbers in purple indicate the references that reported: the interaction of BPA with nuclear receptors (in general), relation between receptors and biological pathways (in general), and direct effects of BPA (specifically in zebrafish embryos/larvae). References: 1) [428]; 2) [357]; 3) [359]; 4) [360]; 5) [362]; 6) [365]; 7) [426]; 8) [114]; 9) [431]; 10) [71]; 11) [412]; 12) [335]; 13) [416]; 14) [413]; 15) [414]; 16) [418]; 17) [419]; 18) [420]; 19) [97]; 20) [445]; 21) [446]; 22) [385]; 23) [386]; 24) [387]; 25) [371]; 26) [72]; 27) [140]; 28) [75]; 29) [68]; 30) [425]; 31) [384]; 32) [444]; 33) [461]. *Growth: in case of BPA and PFOS, the decrease is nonspecific, due to general toxicity at high doses. *Yolk sac resorption: BPA elicits yolk sac malabsorption syndrome; PFOS-exposed individuals present a YS lower than they should by their size; and TBT triggers a decrease of the consumption that could be explained by a mere developmental delay.

In our system, PFOS inhibits lipid accumulation, which could be related to the activation of lipid catabolism through inhibition of PPAR-γ and activation of PPAR-α and, probably, FXR. The macroscopic effects of BPA are the opposite, exerting a yolk sac malabsorption syndrome and lipid accumulation in the embryos. We propose that these effects are brought about by activation of PPAR-γ, together with the simultaneous activation of RXR,

ERR and ER. Finally, TBT seems to act as a pure RXR activator, although its simultaneous activation of PPAR-γ needs to be also considered [459,460]. The obesogenic effects of TBT exposed embryos is relatively mild and, in any case, far weaker than the effects triggered by BPA. It is thus possible that the simultaneous activation of independent signalling cascades by BPA (RXR + PPAR-γ; ERR; ER) may be the responsible for its strong obesogenic effects in zebrafish embryos. All the proposed involved regulatory elements are present in all vertebrates and functional through all life stages, so these findings may be relevant for the obesogenic effects of these compounds in other species, including humans.

IV. Impacts and future research

The integration of transcriptomic and integrative analyses at other biological levels allowed us to propose adverse outcome pathways for endocrine disruption mediated by BPA, PFOS and TBT. The analysis can be used to define a reduced number of specific targeted assays to either confirm or disprove different aspects of the AOPs, like the identification of MIE or key events. The use of transcriptomic data for routine screening assays has been considered to complement current methods in human and environmental risk assessment and regulatory toxicology [206,462,463]. Dose-response transcriptomic assays for mandatory compounds' toxicity tests (as OCDE guidelines) are considered for both substituting different animal tests and detecting unexpected adverse effects. For example, the existing bans and restrictions on the use of BPA and PFOS has fuelled their substitution by different alternatives, like BPF, BPAF, and BPS, or F53-B and Cl-PFESAs, respectively. Nevertheless, the toxic and endocrine disruptive effects of some of these alternatives are similar to, or even worse than the ones elicited by the restricted compounds [308–310,314,384,464]. Therefore, transcriptomic analyses (and its data fusion with other *omics* or integrative analyses) may represent a good alternative to complement the lack of toxicological information from new products or their mixes or to characterize adverse effects of environmental samples with unknown composition. As they provide mechanisms of action, possible target receptors,

and biological pathways, they may facilitate the development of suitable phenotypic approaches that could be ultimately be used at large scale.

Considering the results obtained in this thesis, we propose the next goals to be achieved in future research:

- Assessment of lipidomic and long-term metabolic effects of PFOS and TBT in eleutheroembryos to complete the characterization of their metabolic toxicity.

- Determination of epigenetic changes exerted by BPA at later developmental stages and elucidation of whether or not they could explain the observed phenotypical alterations. The analysis could be extended to PFOS and TBT.

- Inter- and trans-generational untargeted *omic* studies performance to complement the bibliographic information from the targeted inter/transgenerational studies that have been performed during last years.

- Integration of *omic* technologies with dose-response experimental setups and benchmark dose analyses to stablish reference safety concentrations of exposure of other endocrine disruptors.

VI. Conclusions

"There are two possible outcomes: if the result confirms the hypothesis, then you've made a measurement. If the result is contrary to the hypothesis, then you've made a discovery"

Enrico Fermi

This thesis contributed to the understanding of the modes of action and effects of BPA, PFOS and TBT in zebrafish eleutheroembryos, which could be also extrapolated to other animal models and to humans. Information at different biological levels was integrated to achieve a higher comprehension of observed different phenomena. The study was also further focused in BPA. The conclusions of the thesis could be summarized as follows:

1) BPA, PFOS, and TBT elicited specific effects in exposed zebrafish eleutheroembryos that can be referred to their respective modes of action and molecular initiation events.

2) BPA effects were far beyond its alleged estrogenic potential, showing a very complex pattern of toxic effects that also included lipid and visual disruption, obesogenic effects, and yolk sac malabsorption (retention of lipids mainly related with energy obtainment).

3) Macroscopic and molecular effects of PFOS included muscle-skeletal alterations (scoliosis and kyphosis), immunosuppression, and disruption of the system related to cell adhesion molecules (CAMs).

4) TBT appeared as a strong toxicant, with a low median lethal concentration, and inducing a general developmental delay (diapause-arrest effect). At very low concentrations, it affected steroids' and cell cycle metabolic pathways.

5) All three toxicants altered lipid metabolism, although with a different extension and consequences. The strongest obesogenic effect was exerted by BPA, whereas PFOS seemed to have “anti-obesogenic”, anorexic-like properties. Comparatively TBT exerted mild effects on lipid metabolic pathways and were only observed at concentrations close to lethality.

6) Persisting effects of BPA, including higher body weight and body mass index, impaired behaviour, and specific changes in gene expression, were observed later in development after exposure cessation. At the molecular level, alterations in the epigenome were observed by a decrease of *miR-1* and increase of *miR-23b* amounts, and differential DNA methylation of certain regions of *aldh1a2*, *cyp19a1a* and *cyp19a1b*.

7) The integration of data at the different biological levels allowed to propose AOPs for each toxicant, showing the intricate network of molecular and macroscopic effects leading to their respective adverse outcomes.

8) Analysis of the proposed AOPs identified the interaction of the tested compounds with different nuclear receptors as the likely MIE for all three compounds. In general terms, the proposed molecular targets can be divided into different broad categories: those related to estrogenic effects (ER, ERR), those interacting with PPAR and/or RXR systems (PPARα, PPARγ, RXR, RAR, VDR) and those related with energy homeostasis (CAR, LXR, PXR). The differential affinity of the three compounds for these receptors may determine their toxic effects at molecular, structural, and behavioural levels.

VII. References

"Be less curious about people and more curious about ideas"

Marie Skłodowska Curie

1. Brand A, Allen L, Altman M, Hlava M, Scott J. Beyond authorship: Attribution, contribution, collaboration, and credit. Learn Publ. 2015;28: 151–155. doi:10.1087/20150211
2. Spengler JD, Sexton K. Indoor air pollution: a public health perspective. Science (80-). 1983;221: 9–17. doi:10.1126/science.6857273
3. Humphreys DR. Agricultural expansion and tropical deforestation: poverty, international trade and land use. Forestry. 2002;75: 214–214. doi:10.1093/forestry/75.2.214
4. Yang B, Nielsen AB, Ljung K, Fahlgren E, Hormes A, Hammarlund D. Quantitative landscape reconstruction and erosion history during the past 1,100 years in the Skogaryd Research Catchment, southern Sweden. Veg Hist Archaeobot. 2020; 1–14. doi:10.1007/s00334-020-00770-6
5. Bhagwat S. The history of deforestation and forest fragmentation: a global perspective. Global Forest Fragmentation. 2014. pp. 5–19. doi:10.1079/9781780642031.0005
6. Martínez Cortizas A, López-Merino L, Bindler R, Mighall T, Kylander ME. Early atmospheric metal pollution provides evidence for Chalcolithic/Bronze Age mining and metallurgy in Southwestern Europe. Sci Total Environ. 2016;545–546: 398–406. doi:10.1016/j.scitotenv.2015.12.078
7. Hillman AL, Abbott MB, Valero-Garcés BL, Morellon M, Barreiro-Lostres F, Bain DJ. Lead pollution resulting from Roman gold extraction in northwestern Spain. Holocene. 2017;27: 1465–1474. doi:10.1177/0959683617693903
8. Hong S, Candelone JP, Patterson CC, Boutron CF. Greenland ice evidence of hemispheric lead pollution two millennia ago by Greek and Roman civilizations. Science (80-). 1994;265: 1841–1843. doi:10.1126/science.265.5180.1841
9. Massard-Guilbaud G, Mathis CF. A brief introduction to the history of pollution: from local to global. Microbial Ecotoxicology. Springer International Publishing; 2017. pp. 3–15. doi:10.1007/978-3-319-61795-4_1
10. Schwarzenbach RP, Egli T, Hofstetter TB, von Gunten U, Wehrli B. Global water pollution and human health. Annu Rev Environ Resour. 2010;35: 109–136. doi:10.1146/annurev-environ-100809-125342
11. Stanek LW, Brown JS, Stanek J, Gift J, Costa DL. Air pollution toxicology-a brief review of the role of the science in shaping the current understanding of air pollution health risks. Toxicological Sciences. 2011. pp. S8–S27. doi:10.1093/toxsci/kfq367
12. Rodríguez Eugenio N, Michael McLaughlin F, Bazza Z, Ronald Vargas F, Kohlschmid E, Oxana Perminova F, et al. Soil pollution: a hidden reality. Food and Agriculture Organization of the United Nations. 2018. Available: www.fao.org/
13. Tchounwou PB, Yedjou CG, Patlolla AK, Sutton DJ. Heavy metal toxicity and the environment. EXS. 2012. pp. 133–164. doi:10.1007/978-3-7643-8340-4_6
14. EPA. Global anthropogenic non-CO2 greenhouse gas emissions : 1990 - 2030. Off Atmos Programs Clim Chang Div US Environ Prot Agency. 2011; 1990–2030. Available: http://www.epa.gov/climatechange/EPAactivities/economics/nonco2projections.html.
15. Crippa M, Oreggioni G, D G, Muntean M, Schaaf E, Lo Vullo E, et al. Fossil CO2 and GHG emissions of all world countries - 2019 Report. 2019. doi:10.2760/687800
16. Klimont Z, Kupiainen K, Heyes C, Purohit P, Cofala J, Rafaj P, et al. Global anthropogenic emissions of particulate matter including black carbon. Atmos Chem Phys. 2017;17: 8681–8723. doi:10.5194/acp-17-8681-2017
17. Larson SJ, Capel PD, Majewski MS. Pesticides in surface waters, Distribution, trends and governing factors. Ann Arbor Press. 1997.
18. Mateo-Sagasta J, Marjani S, Turral H, Burke J. Water pollution from agriculture: a global

review. FAO y IWMI. 2017. doi:http://www.fao.org/3/a-i7754e.pdf
19. Rezania S, Park J, Md Din MF, Mat Taib S, Talaiekhozani A, Kumar Yadav K, et al. Microplastics pollution in different aquatic environments and biota: a review of recent studies. Marine Pollution Bulletin. Elsevier Ltd; 2018. pp. 191–208. doi:10.1016/j.marpolbul.2018.05.022
20. Kanan S, Samara F. Dioxins and furans: a review from chemical and environmental perspectives. Trends in Environmental Analytical Chemistry. Elsevier B.V.; 2018. pp. 1–13. doi:10.1016/j.teac.2017.12.001
21. Ahmed F, Fakhruddin ANM. A review on environmental contamination of petroleum hydrocarbons and its biodegradation. Int J Environ Sci Nat Resour. 2018;11: 1–7. doi:10.19080/IJESNR.2018.11.555811
22. Rebello S, Asok AK, Mundayoor S, Jisha MS. Surfactants: toxicity, remediation and green surfactants. Environmental Chemistry Letters. Springer Verlag; 2014. pp. 275–287. doi:10.1007/s10311-014-0466-2
23. Larsson DGJ. Pollution from drug manufacturing: review and perspectives. Philosophical Transactions of the Royal Society B: Biological Sciences. Royal Society of London; 2014. doi:10.1098/rstb.2013.0571
24. European Commission. What are the health costs of environmental pollution? 2018. doi:10.2779/88198
25. Landrigan PJ, Fuller R, Acosta NJR, Adeyi O, Arnold R, Basu N (Nil), et al. The Lancet Commission on pollution and health. Lancet (London, England). 2018;391: 462–512. doi:10.1016/S0140-6736(17)32345-0
26. UN (United Nations) S of the SC (SSC). Stockholm convention on persistent organic pollutions (POPs). 2017.
27. Vasseur P, Cossu-Leguille C. Linking molecular interactions to consequent effects of persistent organic pollutants (POPs) upon populations. Chemosphere. 2006. pp. 1033–1042. doi:10.1016/j.chemosphere.2005.05.043
28. Alexander DE. Bioaccumulation, bioconcentration, biomagnification. Environmental Geology. Kluwer Academic Publishers; 2006. pp. 43–44. doi:10.1007/1-4020-4494-1_31
29. Neely WB (Wesley B. Chemicals in the environment: distribution, transport, fate, analysis. M. Dekker; 1980.
30. Fernández M del C. The role of persistent organic pollutants on Prochlorococcus photosynthetic capability under the global change scenario. 2016. Available: http://hdl.handle.net/2117/96401
31. Sauvé S, Desrosiers M. A review of what is an emerging contaminant. Chemistry Central Journal. 2014. doi:10.1186/1752-153X-8-15
32. Geissen V, Mol H, Klumpp E, Umlauf G, Nadal M, van der Ploeg M, et al. Emerging pollutants in the environment: A challenge for water resource management. Int Soil Water Conserv Res. 2015;3: 57–65. doi:10.1016/j.iswcr.2015.03.002
33. EPA. SAB advisory on aquatic life water quality criteria for contaminants of emerging concern. 2008; EPA-SAB-09-007. Available: http://yosemite.epa.gov/sab/SABPRODUCT.NSF/b5d8a1ce9b07293485257375007012b7/E37FB6980DCDD9B585257532005F6F2C/$File/EPA-SAB-09-007-unsigned.pdf
34. Richardson SD, Ternes TA. Water analysis: emerging contaminants and current issues. Analytical Chemistry. 2018. pp. 398–428. doi:10.1021/acs.analchem.7b04577
35. Ravindra, Arya P, Haq SA. Effects of xenobiotics and their biodegradation in marine life. Smart Bioremediation Technologies. Elsevier; 2019. pp. 63–81. doi:10.1016/b978-0-12-818307-6.00004-4
36. Piña B, Raldúa D, Barata C, Portugal J, Navarro-Martín L, Martínez R, et al. Functional data analysis: omics for environmental risk assessment. Comprehensive Analytical Chemistry. 2018. pp. 583–611.

doi:10.1016/bs.coac.2018.07.007
37. Tolleson WH. Mechanistic ecotoxicology and environmental toxicology. J Environ Sci Heal Part C. 2018;36: 164–166. doi:10.1080/10590501.2018.1492201
38. Damiani G. Ecotoxicology and ecosystems health. Ann Ist Super Sanita. 2002;38: 155–9. Available: http://www.ncbi.nlm.nih.gov/pubmed/12387139
39. Muralikrishna I V., Manickam V. Environmental risk assessment. Environmental Management. Elsevier; 2017. pp. 135–152. doi:10.1016/B978-0-12-811989-1.00008-7
40. Linkov I, Loney D, Cormier S, Satterstrom FK, Bridges T. Weight-of-evidence evaluation in environmental assessment: review of qualitative and quantitative approaches. Science of the Total Environment. 2009. pp. 5199–5205. doi:10.1016/j.scitotenv.2009.05.004
41. Cothern CR. Comparative environmental risk assessment. Comparative Environmental Risk Assessment. CRC Press; 2018. doi:10.1201/9781351070805
42. Carson R, Darling L, Darling L. Silent spring. Riverside Press (Cambridge M., editor. 1962.
43. Christie DA, Tansey EM. Environmental toxicology: the legacy of Silent Spring. History of Medicine. 2002.
44. Balaguer P, Delfosse V, Grimaldi M, Bourguet W. Structural and functional evidences for the interactions between nuclear hormone receptors and endocrine disruptors at low doses. Comptes Rendus - Biologies. Elsevier Masson SAS; 2017. pp. 414–420. doi:10.1016/j.crvi.2017.08.002
45. Groh KJ, Carvalho RN, Chipman JK, Denslow ND, Halder M, Murphy CA, et al. Development and application of the adverse outcome pathway framework for understanding and predicting chronic toxicity: II. A focus on growth impairment in fish. Chemosphere. Elsevier Ltd; 2015. pp. 778–792. doi:10.1016/j.chemosphere.2014.10.006
46. Enoch SJ, Cronin MTD, Ellison CM. The use of a chemistry-based profiler for covalent DNA binding in the development of chemical categories for read-across for genotoxicity. ATLA Alternatives to Laboratory Animals. 2011. pp. 131–145. doi:10.1177/026119291103900206
47. Allen TEH, Goodman JM, Gutsell S, Russell PJ. A history of the molecular initiating event. Chemical Research in Toxicology. American Chemical Society; 2016. pp. 2060–2070. doi:10.1021/acs.chemrestox.6b00341
48. Sachana M. Adverse outcome pathways and their role in revealing biomarkers. Biomarkers in Toxicology. 2019. pp. 163–170. doi:10.1016/b978-0-12-814655-2.00009-8
49. Willett C. Adverse outcome pathways. Encyclopedia of Toxicology. Elsevier; 2014. pp. 95–99. doi:10.1016/B978-0-12-386454-3.01244-6
50. Allen TEH, Goodman JM, Gutsell S, Russell PJ. Defining molecular initiating events in the adverse outcome pathway framework for risk assessment. Chem Res Toxicol. 2014;27: 2100–2112. doi:10.1021/tx500345j
51. Ankley GT, Bennett RS, Erickson RJ, Hoff DJ, Hornung MW, Johnson RD, et al. Adverse outcome pathways: a conceptual framework to support ecotoxicology research and risk assessment. Environmental Toxicology and Chemistry. 2010. pp. 730–741. doi:10.1002/etc.34
52. OECD. Users' handbook supplement to the guidance document for developing and assessing adverse outcome pathways. 2016. doi:10.1787/5jlv1m9d1g32-en
53. Epa U, of Research O. Adverse outcome pathway (AOP) research brief. 2017. Available: https://www.epa.gov/chemical-research
54. Knöbel M, Busser FJM, Rico-Rico Á, Kramer NI, Hermens JLM, Hafner C, et al. Predicting adult fish acute lethality with the zebrafish embryo: relevance of test duration,

endpoints, compound properties, and exposure concentration analysis. Environ Sci Technol. 2012;46: 9690–9700. doi:10.1021/es301729q
55. Suter GW, Rosen AE, Linder E, Parkhurst DF. Endpoints for responses of fish to chronic toxic exposures. Environ Toxicol Chem. 1987;6: 793–809. doi:10.1002/etc.5620061009
56. Porte C, van den Brink N, van der Oost R. Biomarkers in environmental assessment. Ecotoxicological Testing of Marine and Freshwater Ecosystems. CRC Press; 2005. pp. 87–152. doi:10.1201/9781420037500.ch3
57. Peakall D. Animal biomarkers as pollution indicators. Choice Rev Online. 1992;30: 30-1502-30–1502. doi:10.5860/CHOICE.30-1502
58. OECD. Test No. 236: fish embryo acute toxicity (FET) test. OECD Guidel Test Chem. 2013. doi:10.1787/9789264203709-en
59. Trevan JW. The error of determination of toxicity. Proc R Soc London Ser B, Contain Pap a Biol Character. 1927;101: 483–514. doi:10.1098/rspb.1927.0030
60. OECD. Test No 234: fish sexual development test. OECD Guidel Test Chem. OECD; 2011 Jul. doi:10.1787/9789264122369-en
61. OECD. Test No. 424: neurotoxicity study in rodents. OECD Guidel Test Chem. OECD; 2006 Jul. doi:10.1787/9789264071025-en
62. OECD. Test No. 451: carcinogenicity studies. OECD Guidel Test Chem. OECD; 2018 Jun. doi:10.1787/9789264071186-en
63. OECD. Test No. 493: performance-based test guideline for human recombinant estrogen receptor (hrER) in vitro assays to detect chemicals with ER binding affinity. OECD Guidel Test Chem. 2014. Available: https://www.oecd.org/env/test-no-493-performance-based-test-guideline-for-human-recombinant-estrogen-receptor-hrer-in-vitro-assays-to-detect-chemicals-9789264242623-en.htm
64. OECD. Test No. 456: H295R steroidogenesis assay. OECD Guidel Test Chem. OECD; 2011 Jul. doi:10.1787/9789264122642-en
65. Choudhuri S, Patton GW, Chanderbhan RF, Mattia A, Klaassen CD. From classical toxicology to Tox21: some critical conceptual and technological advances in the molecular understanding of the toxic response beginning from the last quarter of the 20th century. Toxicol Sci. 2018;161: 5–22. doi:10.1093/toxsci/kfx186
66. Bedia C, Cardoso P, Dalmau N, Garreta-Lara E, Gómez-Canela C, Gorrochategui E, et al. Applications of metabolomics analysis in environmental research. Comprehensive Analytical Chemistry. Elsevier B.V.; 2018. pp. 533–582. doi:10.1016/bs.coac.2018.07.006
67. Liu X, Ser Z, Cluntun AA, Mentch SJ, Locasale JW. A strategy for sensitive, large scale quantitative metabolomics. J Vis Exp. 2014. doi:10.3791/51358
68. Ortiz-Villanueva E, Jaumot J, Martínez R, Navarro-Martín L, Piña B, Tauler R. Assessment of endocrine disruptors effects on zebrafish (Danio rerio) embryos by untargeted LC-HRMS metabolomic analysis. Sci Total Environ. 2018;635: 156–166. doi:10.1016/j.scitotenv.2018.03.369
69. Pradas I, Huynh K, Cabré R, Ayala V, Meikle PJ, Jové M, et al. Lipidomics reveals a tissue-specific fingerprint. Front Physiol. 2018;9. doi:10.3389/fphys.2018.01165
70. Mulvey C, Thur B, Crawford M, Godovac-Zimmermann J. How many proteins are missed in quantitative proteomics based on MS/MS sequencing methods? Proteomics Insights. 2010;3: 61–66. doi:10.4137/PRI.S5882
71. Martínez R, Esteve-Codina A, Herrero-Nogareda L, Ortiz-Villanueva E, Barata C, Tauler R, et al. Dose-dependent transcriptomic responses of zebrafish eleutheroembryos to Bisphenol A. Environ Pollut. 2018;243: 988–997. doi:10.1016/j.envpol.2018.09.043
72. Martínez R, Navarro-Martín L, Luccarelli C, Codina AE, Raldúa D, Barata C, et al.

Unravelling the mechanisms of PFOS toxicity by combining morphological and transcriptomic analyses in zebrafish embryos. Sci Total Environ. 2019;674: 462–471. doi:10.1016/j.scitotenv.2019.04.200

73. Che N, Ma Y, Ruan H, Xu L, Wang X, Yang X, et al. Integrated semi-targeted metabolomics analysis reveals distinct metabolic dysregulation in pleural effusion caused by tuberculosis and malignancy. Clin Chim Acta. 2018;477: 81–88. doi:10.1016/j.cca.2017.12.003
74. Fraher D, Sanigorski A, Mellett NA, Meikle PJ, Sinclair AJ, Gibert Y. Zebrafish embryonic lipidomic analysis reveals that the yolk cell is metabolically active in processing lipid. Cell Rep. 2016;14: 1317–1329. doi:10.1016/j.celrep.2016.01.016
75. Martínez R, Navarro-Martín L, van Antro M, Fuertes I, Casado M, Barata C, et al. Changes in lipid profiles induced by bisphenol A (BPA) in zebrafish eleutheroembryos during the yolk sac absorption stage. Chemosphere. 2020;246. doi:10.1016/j.chemosphere.2019.125704
76. Ben-Shlomo R, Shanas U. Genetic ecotoxicology of asbestos pollution in the house mouse Mus musculus domesticus. Environ Sci Pollut Res. 2011;18: 1264–1269. doi:10.1007/s11356-011-0481-9
77. Pavkovic M, Pantano L, Gerlach C V., Brutus S, Boswell SA, Everley RA, et al. Multi omics analysis of fibrotic kidneys in two mouse models. Sci data. 2019;6: 92. doi:10.1038/s41597-019-0095-5
78. Breton J, Massart S, Vandamme P, De Brandt E, Pot B, Foligné B. Ecotoxicology inside the gut: impact of heavy metals on the mouse microbiome. BMC Pharmacol Toxicol. 2013;14: 62. doi:10.1186/2050-6511-14-62
79. Scholz S, Fischer S, Gündel U, Küster E, Luckenbach T, Voelker D. The zebrafish embryo model in environmental risk assessment - Applications beyond acute toxicity testing. Environmental Science and Pollution Research. 2008. pp. 394–404. doi:10.1007/s11356-008-0018-z
80. Stegeman JJ, Goldstone J V., Hahn ME. Perspectives on zebrafish as a model in environmental toxicology. Fish Physiology. 2010. pp. 367–439. doi:10.1016/S1546-5098(10)02910-9
81. Tanguay RL. The rise of zebrafish as a model for toxicology. Toxicological Sciences. 2018. pp. 3–4. doi:10.1093/toxsci/kfx295
82. Anzenbacher P, Anzenbacherová E. Cytochromes P450 and metabolism of xenobiotics. Cellular and Molecular Life Sciences. Birkhauser Verlag Basel; 2001. pp. 737–747. doi:10.1007/PL00000897
83. Combarnous Y, Diep Nguyen TM. Comparative overview of the mechanisms of action of hormones and endocrine disruptor compounds. Toxics. MDPI AG; 2019. doi:10.3390/toxics7010005
84. De Coster S, Van Larebeke N. Endocrine-disrupting chemicals: associated disorders and mechanisms of action. Journal of Environmental and Public Health. Hindawi Publishing Corporation; 2012. doi:10.1155/2012/713696
85. Papalou O, Kandaraki EA, Papadakis G, Diamanti-Kandarakis E. Endocrine disrupting chemicals: an occult mediator of metabolic disease. Frontiers in Endocrinology. Frontiers Media S.A.; 2019. p. 112. doi:10.3389/fendo.2019.00112
86. Bertoli S, Leone A, Battezzati A. Human bisphenol A exposure and the “diabesity phenotype.” Dose-Response. 2015;13. doi:10.1177/1559325815599173
87. Hertz-Picciotto I, Sass JB, Engel S, Bennett DH, Bradman A, Eskenazi B, et al. Organophosphate exposures during pregnancy and child neurodevelopment: recommendations for essential policy reforms. PLoS Med. 2018;15: e1002671. doi:10.1371/journal.pmed.1002671
88. European-Parliament. Endocrine disruptors: from scientific evidence to human health protection. Isbn 978-92-846-4671-5. 2019. doi:10.2861/802173 | QA-01-

19-272-EN-N
89. Liew Z, Goudarzi H, Oulhote Y. Developmental exposures to perfluoroalkyl substances (PFASs): an update of associated health outcomes. Current environmental health reports. NLM (Medline); 2018. pp. 1–19. doi:10.1007/s40572-018-0173-4
90. Lauretta R, Sansone A, Sansone M, Romanelli F, Appetecchia M. Endocrine disrupting chemicals: effects on endocrine glands. Frontiers in Endocrinology. Frontiers Media S.A.; 2019. p. 178. doi:10.3389/fendo.2019.00178
91. Evans RM, Mangelsdorf DJ. Nuclear receptors, RXR, and the big bang. Cell. Cell Press; 2014. pp. 255–266. doi:10.1016/j.cell.2014.03.012
92. Tabb MM, Blumberg B. New modes of action for endocrine-disrupting chemicals. Molecular Endocrinology. Oxford Academic; 2006. pp. 475–482. doi:10.1210/me.2004-0513
93. Roig B, Mnif W, Hadj Hassine AI, Zidi I, Bayle S, Bartegi A, et al. Endocrine disrupting chemicals and human health risk assessment: a critical review. Crit Rev Environ Sci Technol. 2013;43: 2297–2351. doi:10.1080/10643389.2012.672076
94. Yang O, Kim HL, Weon J-I, Seo YR. Endocrine-disrupting chemicals: review of toxicological mechanisms using molecular pathway analysis. J Cancer Prev. 2015;20: 12–24. doi:10.15430/JCP.2015.20.1.12
95. Heindel JJ, Blumberg B. Environmental obesogens: mechanisms and controversies. Annu Rev Pharmacol Toxicol. 2019;59: 89–106. doi:10.1146/annurev-pharmtox-010818-021304
96. Maradonna F, Carnevali O. Lipid metabolism alteration by endocrine disruptors in animal models: an overview. Frontiers in Endocrinology. Frontiers Media S.A.; 2018. doi:10.3389/fendo.2018.00654
97. Heindel JJ, Schug TT. The obesogen hypothesis: current status and implications for human health. Curr Environ Heal Reports. 2014;1: 333–340. doi:10.1007/s40572-014-0026-8
98. Darbre PD. Endocrine disruption and human health. Endocrine Disruption and Human Health. Elsevier Inc.; 2015. doi:10.1016/C2013-0-19087-3
99. Shahnazaryan U, Wójcik M, Bednarczuk T, Kuryłowicz A. Role of obesogens in the pathogenesis of obesity. Medicina (Lithuania). MDPI AG; 2019. doi:10.3390/medicina55090515
100. Janesick AS, Blumberg B. Obesogens: an emerging threat to public health. American Journal of Obstetrics and Gynecology. Mosby Inc.; 2016. pp. 559–565. doi:10.1016/j.ajog.2016.01.182
101. Jordão R, Casas J, Fabrias G, Campos B, Piña B, Lemos MFL, et al. Obesogens beyond vertebrates: Lipid perturbation by tributyltin in the crustacean Daphnia magna. Environ Health Perspect. 2015;123: 813–819. doi:10.1289/ehp.1409163
102. Lyssimachou A, Santos JG, André A, Soares J, Lima D, Guimarães L, et al. The mammalian "obesogen" tributyltin targets hepatic triglyceride accumulation and the transcriptional regulation of lipid metabolism in the liver and brain of zebrafish. PLoS One. 2015;10. doi:10.1371/journal.pone.0143911
103. Schmidt JS, Schaedlich K, Fiandanese N, Pocar P, Fischer B. Di(2-ethylhexyl) Phthalate (DEHP) impairs female fertility and promotes adipogenesis in C3H/N mice 105. EnvironHealth Perspect. 2012.
104. Hao C, Cheng X, Guo J, Xia H, Ma X. Perinatal exposure to diethyl-hexyl-phthalate induces obesity in mice. Front Biosci - Elit. 2013;5 E: 725–733. doi:10.2741/e653
105. Zhang H yu, Xue W yan, Li Y yuan, Ma Y, Zhu Y shuang, Huo W qian, et al. Perinatal exposure to 4-nonylphenol affects adipogenesis in first and second generation rats offspring. Toxicol Lett. 2014;225: 325–332. doi:10.1016/j.toxlet.2013.12.011

106. MacKay H, Patterson ZR, Abizaid A. Perinatal exposure to low-dose bisphenol-A disrupts the structural and functional development of the hypothalamic feeding circuitry. Endocrinology. 2017;158: 768–777. doi:10.1210/en.2016-1718
107. den Broeder MJ, Moester MJB, Kamstra JH, Cenijn PH, Davidoiu V, Kamminga LM, et al. Altered adipogenesis in zebrafish larvae following high fat diet and chemical exposure is visualised by stimulated raman scattering microscopy. Int J Mol Sci. 2017;18. doi:10.3390/ijms18040894
108. Riu A, McCollum CW, Pinto CL, Grimaldi M, Hillenweck A, Perdu E, et al. Halogenated Bisphenol-A analogs act as obesogens in zebrafish larvae (Danio rerio). Toxicol Sci. 2014;139: 48–58. doi:10.1093/toxsci/kfu036
109. Mentor A, Brunström B, Mattsson A, Jönsson M. Developmental exposure to a human relevant mixture of endocrine disruptors alters metabolism and adipogenesis in zebrafish (Danio rerio). Chemosphere. 2020;238: 124584. doi:10.1016/j.chemosphere.2019.124584
110. Lempradl A, Pospisilik JA, Penninger JM. Exploring the emerging complexity in transcriptional regulation of energy homeostasis. Nat Rev Genet. 2015;16: 665–681. doi:10.1038/nrg3941
111. Den Broeder MJ, Kopylova VA, Kamminga LM, Legler J. Zebrafish as a model to study the role of peroxisome proliferating-activated receptors in adipogenesis and obesity. PPAR Res. 2015;2015: 1–11. doi:10.1155/2015/358029
112. Ibabe A, Bilbao E, Cajaraville MP. Expression of peroxisome proliferator-activated receptors in zebrafish (Danio rerio) depending on gender and developmental stage. Histochem Cell Biol. 2005;123: 75–87. doi:10.1007/s00418-004-0737-2
113. Kersten S. Peroxisome proliferator activated receptors and lipoprotein metabolism. PPAR Research. Hindawi; 2008. p. 132960. doi:10.1155/2008/132960
114. Walczak R, Tontonoz P. PPARadigms and PPARadoxes: expanding roles for PPARgamma in the control of lipid metabolism. J Lipid Res. 2002;43: 177–86. Available: http://www.ncbi.nlm.nih.gov/pubmed/11861659
115. Berger J, Moller DE. The mechanisms of action of PPARs. Annu Rev Med. 2002;53: 409–435. doi:10.1146/annurev.med.53.082901.104018
116. Chiarelli F, Marzio D Di. Peroxisome proliferator-activated receptor-γ agonists and diabetes: Current evidence and future perspectives. Vasc Health Risk Manag. 2008;4: 297. Available: https://www.ncbi.nlm.nih.gov/pmc/articles/PMC2496982/
117. Cindrova-Davies T, Jauniaux E, Elliot MG, Gong S, Burton GJ, Charnock-Jones DS. RNA-seq reveals conservation of function among the yolk sacs of human, mouse, and chicken. Proc Natl Acad Sci. 2017;114: E4753–E4761. doi:10.1073/pnas.1702560114
118. Dahabreh DF, Medh JD. Activation of peroxisome proliferator activated receptor-gamma results in an atheroprotective apolipoprotein profile in HepG2 cells. Adv Biol Chem. 2012;02: 218–225. doi:10.4236/abc.2012.23026
119. Hai B, Ni C, Xie H, Guo Z, Wu M, Chen Q, et al. Association between peroxisome proliferator-activated receptor and gene-gene interactions with the apolipoprotein A I/apolipoprotein B100 ratio. Zhonghua Xin Xue Guan Bing Za Zhi. 2015;43: 328–33. Available: http://www.ncbi.nlm.nih.gov/pubmed/26082365
120. Feingold KR, Grunfeld C. Introduction to lipids and lipoproteins. Endotext. MDText.com, Inc.; 2000. Available: http://www.ncbi.nlm.nih.gov/pubmed/26247089
121. Miyares RL, de Rezende VB, Farber SA.

Zebrafish yolk lipid processing: a tractable tool for the study of vertebrate lipid transport and metabolism. Dis Model Mech. 2014;7: 915–927. doi:10.1242/dmm.015800
122. Otis JP, Zeituni EM, Thierer JH, Anderson JL, Brown AC, Boehm ED, et al. Zebrafish as a model for apolipoprotein biology: comprehensive expression analysis and a role for ApoA-IV in regulating food intake. Dis Model Mech. 2015;8: 295–309. doi:10.1242/dmm.018754
123. Schlegel A. Zebrafish models for dyslipidemia and atherosclerosis research. Frontiers in Endocrinology. Frontiers Media S.A.; 2016. p. 159. doi:10.3389/fendo.2016.00159
124. Oka T, Nishimura Y, Zang L, Hirano M, Shimada Y, Wang Z, et al. Diet-induced obesity in zebrafish shares common pathophysiological pathways with mammalian obesity. BMC Physiol. 2010;10: 21. doi:10.1186/1472-6793-10-21
125. Caballero-Gallardo K, Olivero-Verbel J, Freeman JL. Toxicogenomics to evaluate endocrine disrupting effects of environmental chemicals using the zebrafish model. Curr Genomics. 2016;17: 515–527. doi:10.2174/1389202917666160513105959
126. Soh J, Gordon PMK, Sensen CW. Genome annotation. Genome Annotation. 2016. doi:10.1201/9781315226828-5
127. Campos B, Fletcher D, Piña B, Tauler R, Barata C. Differential gene transcription across the life cycle in Daphnia magna using a new all genome custom-made microarray. BMC Genomics. 2018;19. doi:10.1186/s12864-018-4725-7
128. Hamilton F. An account of the fishes found in the river Ganges and its branches. Edinburgh :Hurst, Robinson, and Co.,1822.; 1822. doi:https://doi.org/10.5962/bhl.title.59540
129. Whiteley AR, Bhat A, Martins EP, Mayden RL, Arunachalam M, Uusi-HeikkilÎ S, et al. Population genomics of wild and laboratory zebrafish (Danio rerio). Mol Ecol. 2011;20: 4259–4276. doi:10.1111/j.1365-294X.2011.05272.x
130. Cavalieri V, Spinelli G. Environmental epigenetics in zebrafish. Epigenetics and Chromatin. BioMed Central Ltd.; 2017. doi:10.1186/s13072-017-0154-0
131. Shehwana H, Konu O. Comparative transcriptomics between zebrafish and mammals: a roadmap for discovery of conserved and unique signaling pathways in physiology and disease. Front Cell Dev Biol. 2019;7: 5. doi:10.3389/fcell.2019.00005
132. Hermsen SAB, Piersma AH. Implementation of transcriptomics in the zebrafish embryotoxicity test. Toxicogenomics-Based Cellular Models. Elsevier; 2014. pp. 127–141. doi:10.1016/B978-0-12-397862-2.00007-3
133. Link V, Shevchenko A, Heisenberg CP. Proteomics of early zebrafish embryos. BMC Dev Biol. 2006;6: 1. doi:10.1186/1471-213X-6-1
134. Lucitt MB, Price TS, Pizarro A, Wu W, Yocum AK, Seiler C, et al. Analysis of the zebrafish proteome during embryonic development. Mol Cell Proteomics. 2008;7: 981–994. doi:10.1074/mcp.M700382-MCP200
135. Huang SM, Xu F, Lam SH, Gong Z, Ong CN. Metabolomics of developing zebrafish embryos using gas chromatography- and liquid chromatography-mass spectrometry. Mol Biosyst. 2013;9: 1372–1380. doi:10.1039/c3mb25450j
136. Dhillon SS, Torell F, Donten M, Lundstedt-Enkel K, Bennett K, Rännar S, et al. Metabolic profiling of zebrafish embryo development from blastula period to early larval stages. Monleon D, editor. PLoS One. 2019;14: e0213661. doi:10.1371/journal.pone.0213661
137. Yamakawa N, Vanbeselaere J, Chang LY, Yu SY, Ducrocq L, Harduin-Lepers A, et al. Systems glycomics of adult zebrafish identifies organ-specific sialylation and glycosylation patterns. Nat Commun.

2018;9: 1–14. doi:10.1038/s41467-018-06950-3

138. Alexeyenko A, Wassenberg DM, Lobenhofer EK, Yen J, Linney E, Sonnhammer ELL, et al. Dynamic zebrafish interactome reveals transcriptional mechanisms of dioxin toxicity. PLoS One. 2010;5. doi:10.1371/journal.pone.0010465
139. Teixidó E, Kießling TR, Krupp E, Quevedo C, Muriana A, Scholz S. Automated morphological feature assessment for zebrafish embryo developmental toxicity screens. Toxicol Sci. 2019;167: 438–449. doi:10.1093/toxsci/kfy250
140. Martínez R, Herrero-Nogareda L, Van Antro M, Campos MP, Casado M, Barata C, et al. Morphometric signatures of exposure to endocrine disrupting chemicals in zebrafish eleutheroembryos. Aquat Toxicol. 2019;214: 105232. doi:10.1016/j.aquatox.2019.105232
141. Santoro MM. Zebrafish as a model to explore cell metabolism. Trends in Endocrinology and Metabolism. Elsevier Inc.; 2014. pp. 546–554. doi:10.1016/j.tem.2014.06.003
142. Skinner AMJ, Watt PJ. Strategic egg allocation in the zebra fish, Danio rerio. Behav Ecol. 2007;18: 905–909. doi:10.1093/beheco/arm059
143. Spence R, Smith C. Mating preference of female zebrafish, Danio rerio, in relation to male dominance. Behav Ecol. 2006;17: 779–783. doi:10.1093/beheco/arl016
144. Löhr H, Hammerschmidt M. Zebrafish in endocrine systems: recent advances and implications for human disease. Annu Rev Physiol. 2011;73: 183–211. doi:10.1146/annurev-physiol-012110-142320
145. Jarque S, Ibarra J, Rubio-Brotons M, García-Fernández J, Terriente J. Multiplex analysis platform for endocrine disruption prediction using zebrafish. Int J Mol Sci. 2019;20: 1739. doi:10.3390/ijms20071739
146. Hölttä-Vuori M, Salo VT V., Nyberg L, Brackmann C, Enejder A, Panula P, et al. Zebrafish: gaining popularity in lipid research. Biochem J. 2010;429: 235–242. doi:10.1042/bj20100293
147. Raldúa D, Piña B. In vivo zebrafish assays for analyzing drug toxicity. Expert Opin Drug Metab Toxicol. 2014;10: 685–697. doi:10.1517/17425255.2014.896339
148. Strähle U, Scholz S, Geisler R, Greiner P, Hollert H, Rastegar S, et al. Zebrafish embryos as an alternative to animal experiments - A commentary on the definition of the onset of protected life stages in animal welfare regulations. Reprod Toxicol. 2012;33: 128–132. doi:10.1016/j.reprotox.2011.06.121
149. Howe K, Clark MD, Torroja CF, Torrance J, Berthelot C, Muffato M, et al. The zebrafish reference genome sequence and its relationship to the human genome. Nature. 2013;496: 498–503. doi:10.1038/nature12111
150. Varshney GK, Lu J, Gildea DE, Huang H, Pei W, Yang Z, et al. A large-scale zebrafish gene knockout resource for the genome-wide study of gene function. Genome Res. 2013;23: 727–735. doi:10.1101/gr.151464.112
151. Nasevicius A, Ekker SC. Effective targeted gene “knockdown” in zebrafish. Nat Genet. 2000;26: 216–220. doi:10.1038/79951
152. Limited GR. Zebrafish Mutation Project. 2013 [cited 14 Feb 2020]. Available: https://www.sanger.ac.uk/sanger/Zebrafish_Zmpbrowse
153. Hahn ME, McArthur AG, Karchner SI, Franks DG, Jenny MJ, Timme-Laragy AR, et al. The transcriptional response to oxidative stress during vertebrate development: effects of tert-butylhydroquinone and 2,3,7,8-tetrachlorodibenzo-p-dioxin. PLoS One. 2014;9: e113158. doi:10.1371/journal.pone.0113158
154. Belanger SE, Balon EK, Rawlings JM. Saltatory ontogeny of fishes and sensitive early life stages for ecotoxicology tests.

Aquat Toxicol. 2010;97: 88–95. doi:10.1016/j.aquatox.2009.11.020
155. Embry MR, Belanger SE, Braunbeck TA, Galay-Burgos M, Halder M, Hinton DE, et al. The fish embryo toxicity test as an animal alternative method in hazard and risk assessment and scientific research. Aquatic Toxicology. Elsevier; 2010. pp. 79–87. doi:10.1016/j.aquatox.2009.12.008
156. Flynn EJ, Trent CM, Rawls JF. Ontogeny and nutritional control of adipogenesis in zebrafish (Danio rerio). J Lipid Res. 2009;50: 1641–1652. doi:10.1194/jlr.M800590-JLR200
157. Kimmel CB, Ballard WW, Kimmel SR, Ullmann B, Schilling TF. Stages of embryonic development of the zebrafish. Dev Dyn. 1995;203: 253–310. doi:10.1002/aja.1002030302
158. Howe DG, Bradford YM, Conlin T, Eagle AE, Fashena D, Frazer K, et al. ZFIN, the Zebrafish Model Organism Database: increased support for mutants and transgenics. Nucleic Acids Res. 2012;41: D854–D860. doi:10.1093/nar/gks938
159. Wilson C. Aspects of larval rearing. ILAR Journal. Narnia; 2012. pp. 169–178. doi:10.1093/ilar.53.2.169
160. Reed B, Jennings M. Guidance on the housing and care of Zebrafish Danio rerio. Res Anim Dep Sci Group, RSPCA. 2011; 1–27.
161. Parichy DM, Elizondo MR, Mills MG, Gordon TN, Engeszer RE. Normal table of postembryonic zebrafish development: staging by externally visible anatomy of the living fish. Dev Dyn. 2009;238: 2975–3015. doi:10.1002/dvdy.22113
162. Parichy DM, Turner JM. Zebrafish puma mutant decouples pigment pattern and somatic metamorphosis. Dev Biol. 2003;256: 242–257. doi:10.1016/S0012-1606(03)00015-0
163. Lanham KA, Peterson RE, Heideman W. Sensitivity to dioxin decreases as zebrafish mature. Toxicol Sci. 2012;127: 360–370. doi:10.1093/toxsci/kfs103
164. Norrgren L. Fish models for ecotoxicology. Acta Vet Scand. 2012;54: S14. doi:10.1186/1751-0147-54-s1-s14
165. Bradford Y, Conlin T, Dunn N, Fashena D, Frazer K, Howe DG, et al. ZFIN: enhancements and updates to the zebrafish model organism database. Nucleic Acids Res. 2011;39: D822. doi:10.1093/nar/gkq1077
166. Dupont C, Armant DR, Brenner CA. Epigenetics: definition, mechanisms and clinical perspective. Seminars in Reproductive Medicine. NIH Public Access; 2009. pp. 351–357. doi:10.1055/s-0029-1237423
167. Chen Z, Li S, Subramaniam S, Shyy JY-J, Chien S. Epigenetic regulation: a new frontier for biomedical engineers. Annu Rev Biomed Eng. 2017;19: 195–219. doi:10.1146/annurev-bioeng-071516-044720
168. Turner BM. Cellular memory and the histone code. Cell. Cell Press; 2002. pp. 285–291. doi:10.1016/S0092-8674(02)01080-2
169. Heard E, Martienssen RA. Transgenerational epigenetic inheritance: myths and mechanisms. Cell. Cell Press; 2014. pp. 95–109. doi:10.1016/j.cell.2014.02.045
170. Navarro-Martín L, Viñas J, Ribas L, Díaz N, Gutiérrez A, Di Croce L, et al. DNA methylation of the gonadal aromatase (cyp19a) promoter is involved in temperature-dependent sex ratio shifts in the European sea bass. Whitelaw E, editor. PLoS Genet. 2011;7: e1002447. doi:10.1371/journal.pgen.1002447
171. McCullough S, Dolinoy D. Toxicoepigenetics. Toxicoepigenetics. Elsevier; 2019. doi:10.1016/c2015-0-04098-9
172. McCullough SD, Dhingra R, Fortin MC, Diaz-Sanchez D. Air pollution and the epigenome: a model relationship for the exploration of toxicoepigenetics. Current Opinion in Toxicology. Elsevier B.V.; 2017. pp. 18–25. doi:10.1016/j.cotox.2017.07.001

173. Lauschke VM, Barragan I, Ingelman-Sundberg M. Pharmacoepigenetics and toxicoepigenetics: novel mechanistic insights and therapeutic opportunities. Annu Rev Pharmacol Toxicol. 2018;58: 161–185. doi:10.1146/annurev-pharmtox-010617-053021
174. Horsthemke B. A critical view on transgenerational epigenetic inheritance in humans. Nature Communications. Nature Publishing Group; 2018. pp. 1–4. doi:10.1038/s41467-018-05445-5
175. Perez MF, Lehner B. Intergenerational and transgenerational epigenetic inheritance in animals. Nature Cell Biology. Nature Publishing Group; 2019. pp. 143–151. doi:10.1038/s41556-018-0242-9
176. Alonso-Magdalena P, Rivera FJ, Guerrero-Bosagna C. Bisphenol-A and metabolic diseases: epigenetic, developmental and transgenerational basis. Environ Epigenetics. 2016;2. doi:10.1093/eep/dvw022
177. Lombó M, Fernández-Díez C, González-Rojo S, Navarro C, Robles V, Herráez MP. Transgenerational inheritance of heart disorders caused by paternal bisphenol A exposure. Environ Pollut. 2015;206: 667–678. doi:10.1016/j.envpol.2015.08.016
178. Mørkve Knudsen T, Rezwan FI, Jiang Y, Karmaus W, Svanes C, Holloway JW. Transgenerational and intergenerational epigenetic inheritance in allergic diseases. J Allergy Clin Immunol. 2018;142: 765–772. doi:10.1016/j.jaci.2018.07.007
179. O'Brien J, Hayder H, Zayed Y, Peng C. Overview of microRNA biogenesis, mechanisms of actions, and circulation. Frontiers in Endocrinology. Frontiers Media S.A.; 2018. doi:10.3389/fendo.2018.00402
180. Brennecke J, Stark A, Russell RB, Cohen SM. Principles of microRNA-target recognition. PLoS Biology. Public Library of Science; 2005. pp. 0404–0418. doi:10.1371/journal.pbio.0030085
181. Fabian MR, Sonenberg N, Filipowicz W. Regulation of mRNA translation and stability by microRNAs. Annu Rev Biochem. 2010;79: 351–379. doi:10.1146/annurev-biochem-060308-103103
182. Martinez R, Vera-Chang MN, Haddad M, Zon J, Navarro-Martin L, Trudeau VL, et al. Developmental fluoxetine exposure in zebrafish reduces offspring basal cortisol concentration via life stage-dependent maternal transmission. Rosenfeld CS, editor. PLoS One. 2019;14: e0212577. doi:10.1371/journal.pone.0212577
183. Vera-Chang MN, Moon TW, Trudeau VL. Cortisol disruption and transgenerational alteration in the expression of stress-related genes in zebrafish larvae following fluoxetine exposure. Toxicol Appl Pharmacol. 2019;382: 114742. doi:10.1016/j.taap.2019.114742
184. Rodgers AB, Morgan CP, Leu NA, Bale TL. Transgenerational epigenetic programming via sperm microRNA recapitulates effects of paternal stress. Proc Natl Acad Sci U S A. 2015;112: 13699–13704. doi:10.1073/pnas.1508347112
185. Song Y, Zhang C, Zhang J, Jiao Z, Dong N, Wang G, et al. Localized injection of miRNA-21-enriched extracellular vesicles effectively restores cardiac function after myocardial infarction. Theranostics. 2019;9: 2346–2360. doi:10.7150/thno.29945
186. Brown RAM, Richardson KL, Kalinowski FC, Epis MR, Horsham JL, Kabir TD, et al. Evaluation of microRNA delivery in vivo. Methods in Molecular Biology. Humana Press Inc.; 2018. pp. 155–178. doi:10.1007/978-1-4939-7435-1_12
187. Wang TY, Zhang J, Zhu J, Lian HY, Yuan HJ, Gao M, et al. Expression profiles and function analysis of microRNAs in postovulatory aging mouse oocytes. Aging (Albany NY). 2017;9: 1186–1201. doi:10.18632/aging.101219
188. Li E, Zhang Y. DNA methylation in mammals. Cold Spring Harb Perspect Biol. 2014;6. doi:10.1101/cshperspect.a019133
189. Goll MG, Halpern ME. DNA methylation in

zebrafish. Progress in Molecular Biology and Translational Science. Elsevier B.V.; 2011. pp. 193–218. doi:10.1016/B978-0-12-387685-0.00005-6

190. Snape A. MBDs mediate methylation, deacetylation and transcriptional repression. Trends in Genetics. Elsevier Ltd; 2000. p. 20. doi:10.1016/S0168-9525(99)01925-3
191. Anastasiadi D, Esteve-Codina A, Piferrer F. Consistent inverse correlation between DNA methylation of the first intron and gene expression across tissues and species. Epigenetics and Chromatin. 2018;11. doi:10.1186/s13072-018-0205-1
192. Baccarelli A, Bollati V. Epigenetics and environmental chemicals. Current Opinion in Pediatrics. NIH Public Access; 2009. pp. 243–251. doi:10.1097/MOP.0b013e32832925cc
193. Olsvik PA, Whatmore P, Penglase SJ, Skjærven KH, D'Auriac MA, Ellingsen S. Associations between behavioral effects of bisphenol A and DNA methylation in zebrafish embryos. Front Genet. 2019;10. doi:10.3389/fgene.2019.00184
194. Doshi T, Mehta SS, Dighe V, Balasinor N, Vanage G. Hypermethylation of estrogen receptor promoter region in adult testis of rats exposed neonatally to bisphenol A. Toxicology. 2011;289: 74–82. doi:10.1016/j.tox.2011.07.011
195. Cheong A, Johnson SA, Howald EC, Ellersieck MR, Camacho L, Lewis SM, et al. Gene expression and DNA methylation changes in the hypothalamus and hippocampus of adult rats developmentally exposed to bisphenol A or ethinyl estradiol: a CLARITY-BPA consortium study. Epigenetics. 2018;13: 704–720. doi:10.1080/15592294.2018.1497388
196. Sen A, Heredia N, Senut MC, Hess M, Land S, Qu W, et al. Early life lead exposure causes gender-specific changes in the DNA methylation profile of DNA extracted from dried blood spots. Epigenomics. 2015;7: 379–393. doi:10.2217/epi.15.2
197. Ortega-Recalde O, Day RC, Gemmell NJ, Hore TA. Zebrafish preserve global germline DNA methylation while sex-linked rDNA is amplified and demethylated during feminisation. Nat Commun. 2019;10: 1–10. doi:10.1038/s41467-019-10894-7
198. Nilsson EE, Sadler-Riggleman I, Skinner MK. Environmentally induced epigenetic transgenerational inheritance of disease. Environ Epigenetics. 2018;4. doi:10.1093/eep/dvy016
199. Carvan MJ, Kalluvila TA, Klingler RH, Larson JK, Pickens M, Mora-Zamorano FX, et al. Mercury-induced epigenetic transgenerational inheritance of abnormal neurobehavior is correlated with sperm epimutations in zebrafish. Freedman JH, editor. PLoS One. 2017;12: e0176155. doi:10.1371/journal.pone.0176155
200. Kamstra JH, Hurem S, Martin LM, Lindeman LC, Legler J, Oughton D, et al. Ionizing radiation induces transgenerational effects of DNA methylation in zebrafish. Sci Rep. 2018;8. doi:10.1038/s41598-018-33817-w
201. Seisenberger S, Peat JR, Hore TA, Santos F, Dean W, Reik W. Reprogramming DNA methylation in the mammalian life cycle: building and breaking epigenetic barriers. Philosophical Transactions of the Royal Society B: Biological Sciences. Royal Society; 2013. doi:10.1098/rstb.2011.0330
202. Messerschmidt DM. Should I stay or should I go, protection and maintenance of DNA methylation at imprinted genes. Epigenetics. 2012;7: 969–975. doi:10.4161/epi.21337
203. Gorrochategui E, Jaumot J, Lacorte S, Tauler R. Data analysis strategies for targeted and untargeted LC-MS metabolomic studies: overview and workflow. TrAC - Trends in Analytical Chemistry. Elsevier B.V.; 2016. pp. 425–442. doi:10.1016/j.trac.2016.07.004
204. Ankley GT, Daston GP, Degitz SJ, Denslow ND, Hoke RA, Kennedy SW, et al.

Toxicogenomics in regulatory ecotoxicology. Environmental Science and Technology. 2006. pp. 4055–4065. doi:10.1021/es0630184

205. Kamstra JH, Aleström P, Kooter JM, Legler J. Zebrafish as a model to study the role of DNA methylation in environmental toxicology. Environ Sci Pollut Res. 2015;22: 16262–16276. doi:10.1007/s11356-014-3466-7
206. Schirmer K, Fischer BB, Madureira DJ, Pillai S. Transcriptomics in ecotoxicology. Anal Bioanal Chem. 2010;397: 917–923. doi:10.1007/s00216-010-3662-3
207. Calzolai L, Ansorge W, Calabrese E, Denslow N, Part P, Lettieri T. Transcriptomics and proteomics. Applications to ecotoxicology. Comp Biochem Physiol - Part D Genomics Proteomics. 2007;2: 245–249. doi:10.1016/j.cbd.2007.04.007
208. Sepúlveda MS, Ralston-Hooper KJ, Sanchez BC, Hopf-Jannasch A, Baker SD, Diaz N, et al. Use of proteomic and metabolomic techniques in ecotoxicological research. General, Applied and Systems Toxicology. Chichester, UK: John Wiley & Sons, Ltd; 2011. doi:10.1002/9780470744307.gat215
209. Viant MR. Applications of metabolomics to the environmental sciences. Metabolomics. 2009. pp. 1–2. doi:10.1007/s11306-009-0157-3
210. Taylor NS, White TA, Viant MR. Defining the baseline and oxidant perturbed lipidomic profiles of Daphnia magna. Metabolites. 2017;7. doi:10.3390/metabo7010011
211. Fuertes I, Jordão R, Casas F, Barata C. Allocation of glycerolipids and glycerophospholipids from adults to eggs in Daphnia magna: perturbations by compounds that enhance lipid droplet accumulation. Environ Pollut. 2018;242: 1702–1710. doi:10.1016/j.envpol.2018.07.102
212. Horiuchi R, Nakajima Y, Kashiwada S, Miyanishi N. Effects of silver nanocolloids on plant complex type N-glycans in Oryza sativa roots. Sci Rep. 2018;8. doi:10.1038/s41598-018-19474-z
213. Iida M, Takemoto K. A network biology-based approach to evaluating the effect of environmental contaminants on human interactome and diseases. Ecotoxicol Environ Saf. 2018;160: 316–327. doi:10.1016/j.ecoenv.2018.05.065
214. Gonzalez P, Pierron F. Omics in aquatic ecotoxicology. Aquatic Ecotoxicology. Elsevier; 2015. pp. 183–203. doi:10.1016/B978-0-12-800949-9.00008-5
215. Teixido E, Kießling T, Leuthold D, Scholz S. Effect signatures in zebrafish embryos exposed to compounds with potential developmental toxicity. Reprod Toxicol. 2017;72: 49. doi:10.1016/j.reprotox.2017.06.179
216. Franzosa EA, Sirota-Madi A, Avila-Pacheco J, Fornelos N, Haiser HJ, Reinker S, et al. Gut microbiome structure and metabolic activity in inflammatory bowel disease. Nat Microbiol. 2019;4: 293–305. doi:10.1038/s41564-018-0306-4
217. Pinu FR, Beale DJ, Paten AM, Kouremenos K, Swarup S, Schirra HJ, et al. Systems biology and multi-omics integration: viewpoints from the metabolomics research community. Metabolites. 2019;9. doi:10.3390/metabo9040076
218. Misra BB, Langefeld C, Olivier M, Cox LA. Integrated omics: tools, advances and future approaches. J Mol Endocrinol. 2018; R21–R45. doi:10.1530/jme-18-0055
219. Tini G, Marchetti L, Priami C, Scott-Boyer MP. Multi-omics integration - A comparison of unsupervised clustering methodologies. Brief Bioinform. 2018;20: 1269–1279. doi:10.1093/bib/bbx167
220. Taguchi Y h. Multiomics data analysis using tensor decomposition based unsupervised feature extraction: – comparison with DIABLO–. Lecture Notes in Computer Science (including subseries Lecture Notes in Artificial Intelligence and

Lecture Notes in Bioinformatics). Cold Spring Harbor Laboratory; 2019. pp. 565–574. doi:10.1007/978-3-030-26763-6_54
221. Raldúa D, Casado M, Prats E, Faria M, Puig-Castellví F, Pérez Y, et al. Targeting redox metabolism: the perfect storm induced by acrylamide poisoning in the brain. Sci Rep. 2020;10: 312. doi:10.1038/s41598-019-57142-y
222. Bartlett JMS, Stirling D. A short history of the polymerase chain reaction. Methods Mol Biol. 2003;226: 3–6. doi:10.1385/1-59259-384-4:3
223. Bhagavan N V., Ha CE. Essentials of medical biochemistry. Essentials of Medical Biochemistry. 2011. doi:10.1016/C2009-0-00064-6
224. Zhang G, Brown EW, González-Escalona N. Comparison of real-time PCR, reverse transcriptase real-time PCR, loop-mediated isothermal amplification, and the FDA conventional microbiological method for the detection of Salmonella spp. in produce. Appl Environ Microbiol. 2011;77: 6495–6501. doi:10.1128/AEM.00520-11
225. Menezes A. Steps for a Successful qPCR Experiment. 2015. Available: https://eu.idtdna.com/pages/education/decoded/article/successful-qpcr
226. Boulter N, Suarez FG, Schibeci S, Sunderland T, Tolhurst O, Hunter T, et al. A simple, accurate and universal method for quantification of PCR. BMC Biotechnol. 2016;16: 27. doi:10.1186/s12896-016-0256-y
227. Čikoš Š, Bukovská A, Koppel J. Relative quantification of mRNA: Comparison of methods currently used for real-time PCR data analysis. BMC Mol Biol. 2007;8: 113. doi:10.1186/1471-2199-8-113
228. Pfaffl MW. Relative quantification. Real-time PCR. 2007. pp. 64–82.
229. Pfaffl MW. A new mathematical model for relative quantification in real-time RT-PCR. Nucleic Acids Res. 2001;29: 45e – 45. doi:10.1093/nar/29.9.e45
230. Livak KJ, Schmittgen TD. Analysis of relative gene expression data using real-time quantitative PCR and the 2-ΔΔCT method. Methods. 2001;25: 402–408. doi:10.1006/meth.2001.1262
231. Heckmann LH, Sørensen PB, Krogh PH, Sørensen JG. NORMA-Gene: A simple and robust method for qPCR normalization based on target gene data. BMC Bioinformatics. 2011;12: 250. doi:10.1186/1471-2105-12-252
232. Jou WM, Haegeman G, Ysebaert M, Fiers W. Nucleotide sequence of the gene coding for the bacteriophage MS2 coat protein. Nature. 1972;237: 82–88. doi:10.1038/237082a0
233. Fiers W, Contreras R, Duerinck F, Haegeman G, Iserentant D, Merregaert J, et al. Complete nucleotide sequence of bacteriophage MS2 RNA: Primary and secondary structure of the replicase gene. Nature. 1976;260: 500–507. doi:10.1038/260500a0
234. Padmanabhan R, Padmanabhan R, Wu R. Nucleotide sequence analysis of DNA: IX. Use of oligonucleotides of defined sequence as primers in DNA sequence analysis. Biochem Biophys Res Commun. 1972;48: 1295–1302. doi:10.1016/0006-291X(72)90852-2
235. Sanger F, Nicklen S, Coulson AR. DNA sequencing with chain-terminating inhibitors. Proc Natl Acad Sci U S A. 1977;74: 5463–5467. doi:10.1073/pnas.74.12.5463
236. Heather JM, Chain B. The sequence of sequencers: The history of sequencing DNA. Genomics. Academic Press Inc.; 2016. pp. 1–8. doi:10.1016/j.ygeno.2015.11.003
237. Raghavendra P, Pullaiah T. Pathogen identification using novel sequencing methods. Advances in Cell and Molecular Diagnostics. Elsevier; 2018. pp. 161–202. doi:10.1016/B978-0-12-813679-9.00007-5
238. Maxam AM, Gilbert W. A new method for sequencing DNA. Proc Natl Acad Sci U S A. 1977;74: 560–564.

doi:10.1073/pnas.74.2.560
239. Nyrén P, Pettersson B, Uhlén M. Solid phase DNA minisequencing by an enzymatic luminometric inorganic pyrophosphate detection assay. Anal Biochem. 1993;208: 171–175. doi:10.1006/abio.1993.1024
240. Muir P, Li S, Lou S, Wang D, Spakowicz DJ, Salichos L, et al. The real cost of sequencing: Scaling computation to keep pace with data generation. Genome Biol. 2016;17. doi:10.1186/s13059-016-0917-0
241. National Human Genome Research Institute. DNA Sequencing Costs: Data | NHGRI. In: National Human Genome Research Institute [Internet]. 2019 [cited 5 Feb 2020]. Available: https://www.genome.gov/about-genomics/fact-sheets/DNA-Sequencing-Costs-Data
242. Richards S. Arthropod genome sequencing and assembly strategies. Methods in Molecular Biology. Humana Press Inc.; 2019. pp. 1–14. doi:10.1007/978-1-4939-8775-7_1
243. Singh S. The hundred-dollar genome: a health care cart before the genomic horse. CMAJ. Canadian Medical Association; 2018. p. E514. doi:10.1503/cmaj.69259
244. Costa V, Angelini C, De Feis I, Ciccodicola A. Uncovering the complexity of transcriptomes with RNA-Seq. Journal of Biomedicine and Biotechnology. 2010. doi:10.1155/2010/853916
245. Gerstein MB, Rozowsky J, Yan KK, Wang D, Cheng C, Brown JB, et al. Comparative analysis of the transcriptome across distant species. Nature. 2014;512: 445–448. doi:10.1038/nature13424
246. Velculescu VE, Zhang L, Zhou W, Vogelstein J, Basrai MA, Bassett DE, et al. Characterization of the yeast transcriptome. Cell. 1997;88: 243–251. doi:10.1016/S0092-8674(00)81845-0
247. Metzker ML. Sequencing technologies the next generation. Nature Reviews Genetics. 2010. pp. 31–46. doi:10.1038/nrg2626
248. Lowe R, Shirley N, Bleackley M, Dolan S, Shafee T. Transcriptomics technologies. PLoS Comput Biol. 2017;13. doi:10.1371/journal.pcbi.1005457
249. Song Y, Xu X, Wang W, Tian T, Zhu Z, Yang C. Single cell transcriptomics: moving towards multi-omics. Analyst. Royal Society of Chemistry; 2019. pp. 3172–3189. doi:10.1039/c8an01852a
250. Kanter I, Kalisky T. Single cell transcriptomics: methods and applications. Frontiers in Oncology. Frontiers Research Foundation; 2015. doi:10.3389/fonc.2015.00053
251. Read J, Brenner S. Microarray technology. Encyclopedia of Genetics. Elsevier; 2001. p. 1191. doi:10.1006/rwgn.2001.2095
252. Fuertes I, Vila-Costa M, Asselman J, Piña B, Barata C. Data processing for RNA/DNA sequencing. Reference Module in Chemistry, Molecular Sciences and Chemical Engineering. Elsevier; 2020. doi:10.1016/B978-0-12-409547-2.14595-0
253. Alpern D, Gardeux V, Russeil J, Mangeat B, Meireles-Filho ACA, Breysse R, et al. BRB-seq: ultra-affordable high-throughput transcriptomics enabled by bulk RNA barcoding and sequencing. Genome Biol. 2019;20: 71. doi:10.1186/s13059-019-1671-x
254. Williams CR, Baccarella A, Parrish JZ, Kim CC. Trimming of sequence reads alters RNA-Seq gene expression estimates. BMC Bioinformatics. 2016;17. doi:10.1186/s12859-016-0956-2
255. Ranganathan S, Nakai K, Schönbach C, Gribskov M. Encyclopedia of Bioinformatics and Computational Biology. Encyclopedia of Bioinformatics and Computational Biology. Elsevier; 2019. doi:10.1016/c2016-1-00174-8
256. Conesa A, Madrigal P, Tarazona S, Gomez-Cabrero D, Cervera A, McPherson A, et al. A survey of best practices for RNA-seq data analysis. Genome Biology. BioMed Central Ltd.; 2016. doi:10.1186/s13059-016-0881-8

257. Rolim AEH, Henrique-Araújo R, Ferraz EG, de Araújo Alves Dultra FK, Fernandez LG. Lipidomics in the study of lipid metabolism: current perspectives in the omic sciences. Gene. Elsevier; 2015. pp. 131–139. doi:10.1016/j.gene.2014.10.039
258. Fahy E, Cotter D, Sud M, Subramaniam S. Lipid classification, structures and tools. Biochim Biophys Acta - Mol Cell Biol Lipids. 2011;1811: 637–647. doi:10.1016/j.bbalip.2011.06.009
259. Liebisch G, Vizcaíno JA, Köfeler H, Trötzmüller M, Griffiths WJ, Schmitz G, et al. Shorthand notation for lipid structures derived from mass spectrometry. J Lipid Res. 2013;54: 1523–1530. doi:10.1194/jlr.M033506
260. Schwaiger M, Schoeny H, El Abiead Y, Hermann G, Rampler E, Koellensperger G. Merging metabolomics and lipidomics into one analytical run. Analyst. 2019;144: 220–229. doi:10.1039/c8an01219a
261. Blanco A, Blanco G. Lipids. Medical Biochemistry. Elsevier; 2017. pp. 99–119. doi:10.1016/B978-0-12-803550-4.00005-7
262. Engelking LR. Overview of lipid metabolism. Textbook of Veterinary Physiological Chemistry. Elsevier; 2015. pp. 340–344. doi:10.1016/b978-0-12-391909-0.50053-0
263. De Carvalho CCCR, Caramujo MJ. The various roles of fatty acids. Molecules. MDPI AG; 2018. doi:10.3390/molecules23102583
264. Itoh Y, Kawamata Y, Harada M, Kobayashi M, Fujii R, Fukusumi S, et al. Free fatty acids regulate insulin secretion from pancreatic β cells through GPR40. Nature. 2003;422: 173–176. doi:10.1038/nature01478
265. Van Meer G, Voelker DR, Feigenson GW. Membrane lipids: Where they are and how they behave. Nature Reviews Molecular Cell Biology. NIH Public Access; 2008. pp. 112–124. doi:10.1038/nrm2330
266. Cole LK, Vance JE, Vance DE. Phosphatidylcholine biosynthesis and lipoprotein metabolism. Biochimica et Biophysica Acta - Molecular and Cell Biology of Lipids. 2012. pp. 754–761. doi:10.1016/j.bbalip.2011.09.009
267. Merolli A, Santin M. Role of phosphatidyl-serine in bone repair and its technological exploitation. Molecules. Multidisciplinary Digital Publishing Institute (MDPI); 2009. pp. 5367–5381. doi:10.3390/molecules14125367
268. Clarke JH. Lipid signalling: picking out the PIPs. Current Biology. Cell Press; 2003. pp. R815–R817. doi:10.1016/j.cub.2003.09.054
269. Krawitz PM, Höchsmann B, Murakami Y, Teubner B, Krüger U, Klopocki E, et al. A case of paroxysmal nocturnal hemoglobinuria caused by a germline mutation and a somatic mutation in PIGT. Blood. 2013;122: 1312–1315. doi:10.1182/blood-2013-01-481499
270. Morita SY, Terada T. Enzymatic measurement of phosphatidylglycerol and cardiolipin in cultured cells and mitochondria. Sci Rep. 2015;5: 1–15. doi:10.1038/srep11737
271. Lund P. Molecular chaperones in the cell. Frontiers in molecular biology. 2001. Available: https://books.google.es/books?id=5_m2vxkfz3kC&pg=PA44&lpg=PA44&dq=pe+chaperone&source=bl&ots=Y8XGuVp4S0&sig=ACfU3U3-HirfXoVhl8F0i39neCzd79F0Gw&hl=es&sa=X&ved=2ahUKEwjEqcbyt5XoAhVFxoUKHZuyAwEQ6AEwBHoECAkQAQ#v=onepage&q=pechaperone&f=false
272. Aguilera-Méndez A, Álvarez-Delgado C, Hernández-Godinez D, Fernandez-Mejia C. Hepatic diseases related to triglyceride metabolism. Mini-Reviews Med Chem. 2013;13: 1691–1699. doi:10.2174/1389557511313120001
273. Hodgkin MN, Pettitt TR, Martin A, Michell RH, Pemberton AJ, Wakelam MJO. Diacylglycerols and phosphatidates: Which molecular species are intracellular messengers? Trends Biochem Sci. 1998;23:

200–204. doi:10.1016/S0968-0004(98)01200-6

274. Chrast R, Saher G, Nave KA, Verheijen MHG. Lipid metabolism in myelinating glial cells: lessons from human inherited disorders and mouse models. Journal of Lipid Research. American Society for Biochemistry and Molecular Biology; 2011. pp. 419–434. doi:10.1194/jlr.R009761

275. Alonso MA, Millán J. The role of lipid rafts in signalling and membrane trafficking in T lymphocytes. Journal of Cell Science. J Cell Sci; 2001. pp. 3957–3965.

276. Stephenson DJ, Hoeferlin LA, Chalfant CE. Lipidomics in translational research and the clinical significance of lipid-based biomarkers. Translational Research. Mosby Inc.; 2017. pp. 13–29. doi:10.1016/j.trsl.2017.06.006

277. Wollam J, Antebi A. Sterol regulation of metabolism, homeostasis, and development. Annu Rev Biochem. 2011;80: 885–916. doi:10.1146/annurev-biochem-081308-165917

278. Tabas I. Cholesterol in health and disease. J Clin Invest. 2002;110: 583–590. doi:10.1172/jci16381

279. Luo J, Yang H, Song BL. Mechanisms and regulation of cholesterol homeostasis. Nature Reviews Molecular Cell Biology. Nature Research; 2019. pp. 1–21. doi:10.1038/s41580-019-0190-7

280. Boyd GS, McNamara B, Suckling KE, Tocher DR. Cholesterol metabolism in the adrenal cortex. J Steroid Biochem. 1983;19: 1017–1027. doi:10.1016/0022-4731(83)90048-1

281. Gorrochategui E, Li J, Fullwood NJ, Ying G-G, Tian M, Cui L, et al. Diet-sourced carbon-based nanoparticles induce lipid alterations in tissues of zebrafish (Danio rerio) with genomic hypermethylation changes in brain. Mutagenesis. 2017;32: 91–103. doi:10.1093/mutage/gew050

282. Stahl E. History of the development of thin-layer chromatography. Thin-Layer Chromatography. Berlin, Heidelberg: Springer Berlin Heidelberg; 1965. pp. 1–4. doi:10.1007/978-3-662-01031-0_1

283. Touchstone JC. Thin-layer chromatographic procedures for lipid separation. Journal of Chromatography B: Biomedical Sciences and Applications. Elsevier; 1995. pp. 169–195. doi:10.1016/0378-4347(95)00232-8

284. Sherma J, Fried B. Handbook of thin-layer chromatography. 2005. Available: https://books.google.es/books?hl=es&lr=&id=s2nzNmEntZAC&oi=fnd&pg=PP1&dq=basics+of+thin+layer+chromatography&ots=MPjEaD1vK8&sig=wsf4ezx4YAZI2l_ILt0kmUiPvzw#v=onepage&q=basics of thin layer chromatography&f=false

285. Attimarad M, Mueen Ahmed KK, Aldhubaib BE, Harsha S. High-performance thin layer chromatography: A powerful analytical technique in pharmaceutical drug discovery. Pharm Methods. 2011;2: 71–75. doi:10.4103/2229-4708.84436

286. John J, Reghuwanshi A, Aravind UK, Aravindakumar CT. Development and validation of a high-performance thin layer chromatography method for the determination of cholesterol concentration. J Food Drug Anal. 2015;23: 219–224. doi:10.1016/j.jfda.2014.07.006

287. Folch J, Lees M, Sloane Stanley GH. A simple method for the isolation and purification of total lipides from animal tissues. J Biol Chem. 1957;226: 497–509. Available: http://www.ncbi.nlm.nih.gov/pubmed/13428781

288. Olsen RE, Henderson RJ. The rapid analysis of neutral and polar marine lipids using double-development HPTLC and scanning densitometry. J Exp Mar Bio Ecol. 1989;129: 189–197. doi:10.1016/0022-0981(89)90056-7

289. Churchward MA, Brandman DM, Rogasevskaia T, Coorssen JR. Copper (II) sulfate charring for high sensitivity on-plate

fluorescent detection of lipids and sterols: quantitative analyses of the composition of functional secretory vesicles. J Chem Biol. 2008;1: 79–87. doi:10.1007/s12154-008-0007-1

290. Karger BL. HPLC: Early and recent perspectives. Journal of Chemical Education. 1997. pp. 45–48. doi:10.1021/ed074p45

291. Nováková L, Svoboda P, Pavlík J. Ultra-high performance liquid chromatography. Liquid Chromatography: Fundamentals and Instrumentation: Second Edition. Elsevier; 2017. pp. 719–769. doi:10.1016/B978-0-12-805393-5.00029-4

292. Taleuzzaman M, Ali S, Gilani S, Imam I, Hafeez A. Ultra performance liquid chromatography (UPLC) - A review. Austin J Anal Pharm Chem. 2015;2: 1056–1060. Available: https://austinpublishinggroup.com/analytical-pharmaceutical-chemistry/fulltext/ajapc-v2-id1056.php

293. Cajka T, Fiehn O. Comprehensive analysis of lipids in biological systems by liquid chromatography-mass spectrometry. TrAC - Trends in Analytical Chemistry. NIH Public Access; 2014. pp. 192–206. doi:10.1016/j.trac.2014.04.017

294. Jurowski K, Kochan K, Walczak J, Barańska M, Piekoszewski W, Buszewski B. Analytical techniques in lipidomics: state of the art. Critical Reviews in Analytical Chemistry. Taylor & Francis; 2017. pp. 418–437. doi:10.1080/10408347.2017.1310613

295. Lydic TA, Goo Y-H. Lipidomics unveils the complexity of the lipidome in metabolic diseases. Clin Transl Med. 2018;7: 4. doi:10.1186/s40169-018-0182-9

296. Gorrochategui Matas E. Assessment of the lipidomic effects of environmental pollutants on exposed organisms using chemometric and analytical methods. TDX (Tesis Dr en Xarxa). 2018 [cited 9 Feb 2020]. Available: http://diposit.ub.edu/dspace/handle/2445/122292%0Ahttp://www.tesisenred.net/handle/10803/544130

297. Chen C, Tan R, Wong L, Fekete R, Halsey J. Quantitation of microRNAs by real-time RT-qPCR. Methods Mol Biol. 2011;687: 113–134. doi:10.1007/978-1-60761-944-4_8

298. Garate X, La Greca A, Neiman G, Blüguermann C, Santín Velazque NL, Moro LN, et al. Identification of the miRNAome of early mesoderm progenitor cells and cardiomyocytes derived from human pluripotent stem cells. Sci Rep. 2018;8: 1–14. doi:10.1038/s41598-018-26156-3

299. Agarwal V, Bell GW, Nam JW, Bartel DP. Predicting effective microRNA target sites in mammalian mRNAs. Elife. 2015;4. doi:10.7554/eLife.05005

300. Olova N, Krueger F, Andrews S, Oxley D, Berrens R V., Branco MR, et al. Comparison of whole-genome bisulfite sequencing library preparation strategies identifies sources of biases affecting DNA methylation data. Genome Biol. 2018;19: 33. doi:10.1186/s13059-018-1408-2

301. Kernaleguen M, Daviaud C, Shen Y, Bonnet E, Renault V, Deleuze JF, et al. Whole-genome bisulfite sequencing for the analysis of genome-wide dna methylation and hydroxymethylation patterns at single-nucleotide resolution. Methods in Molecular Biology. Humana Press Inc.; 2018. pp. 311–349. doi:10.1007/978-1-4939-7774-1_18

302. Chandra A, Senapati S, Roy S, Chatterjee G, Chatterjee R. Epigenome-wide DNA methylation regulates cardinal pathological features of psoriasis. Clin Epigenetics. 2018;10: 108. doi:10.1186/s13148-018-0541-9

303. Kitraki E, Nalvarte I, Alavian-Ghavanini A, Rüegg J. Developmental exposure to bisphenol A alters expression and DNA methylation of Fkbp5, an important regulator of the stress response. Mol Cell Endocrinol. 2015;417: 191–199. doi:10.1016/j.mce.2015.09.028

304. Lantz-Mcpeak S, Guo X, Cuevas E, Dumas M, Newport GD, Ali SF, et al. Developmental

toxicity assay using high content screening of zebrafish embryos. J Appl Toxicol. 2015;35: 261–272. doi:10.1002/jat.3029

305. Detrich HW, Westerfield M, Zon LI. Essential zebrafish methods : cell and developmental biology. Reliable lab solutions. 2009. Available: https://books.google.es/books?id=euS0OV2sxO0C&pg=PA467&lpg=PA467&dq=morphometric+zebrafish+pca&source=bl&ots=pgwlfLj2v_&sig=ACfU3U0jHuDmm2TrCVGkDHcmqPcbFVfNPQ&hl=es&sa=X&ved=2ahUKEwiqsceTifLoAhWMDWMBHZ1sC0kQ6AEwE3oECAwQPA#v=onepage&q=morphometric zebrafis
306. Hanif MA, Siddik MAB, Islam MA, Chaklader MR, Nahar A. Multivariate morphometric variability in sardine, Amblygaster clupeoides (Bleeker, 1849), from the Bay of Bengal coast, Bangladesh. J Basic Appl Zool. 2019;80: 53. doi:10.1186/s41936-019-0110-6
307. Anumudu C, Mojekwu T. Advanced techniques for morphometric analysis in fish. J Aquac Res Dev. 2015;06: 1–6. doi:10.4172/2155-9546.1000354
308. Horan TS, Pulcastro H, Lawson C, Gerona R, Martin S, Gieske MC, et al. Replacement bisphenols adversely affect mouse gametogenesis with consequences for subsequent generations. Curr Biol. 2018;28: 2948-2954.e3. doi:10.1016/j.cub.2018.06.070
309. Mesnage R, Phedonos A, Arno M, Balu S, Corton JC, Antoniou MN. Transcriptome profiling reveals bisphenol a alternatives activate estrogen receptor alpha in human breast cancer cells. Toxicol Sci. 2017;158: 431–443. doi:10.1093/toxsci/kfx101
310. Moon MK. Concern about the safety of bisphenol A substitutes. Diabetes and Metabolism Journal. Korean Diabetes Association; 2019. pp. 46–48. doi:10.4093/dmj.2019.0027
311. Davies AG. Organotin chemistry, 2nd, completely revised and updated edition. 2004. Available: https://www.wiley.com/en-us/Organotin+Chemistry%2C+2nd%2C+Completely+Revised+and+Updated+Edition-p-9783527310234
312. IMO. Focus on IMO: Anti-fouling systems. Int Marit Organ. 2002;44: 1–31. doi:10.1097/TA.0b013e31817de3f4
313. Takahashi K. Release rate of biocides from antifouling paints. Ecotoxicology of Antifouling Biocides. 2009. pp. 3–22. doi:10.1007/978-4-431-85709-9_1
314. Paul AG, Jones KC, Sweetman AJ. A first global production, emission, and environmental inventory for perfluorooctane sulfonate. Environ Sci Technol. 2009. doi:10.1021/es802216n
315. Kadasala NR, Narayanan B, Liu Y. International trade regulations on BPA: global health and economic implications. Asian Dev Policy Rev. 2016;4: 134–142. doi:10.18488/journal.107/2016.4.4/107.4.134.142
316. Champ MA, Seligman PF. Organotin: environmental fate and effects. Springer Science & Business Media; 1996. Available: https://books.google.com/books?id=kA9AkPpAkxgC&pgis=1
317. Wang X, Kong L, Cheng J, Zhao D, Chen H, Sun R, et al. Distribution of butyltins at dredged material dumping sites around the coast of China and the potential ecological risk. Mar Pollut Bull. 2019; 491–500. doi:10.1016/j.marpolbul.2018.11.043
318. Bray S. Tributyltin pollution on a global scale. An overview of relevant and recent research: impacts and issues. Contract. 2006; 54.
319. Ahrens L, Bundschuh M. Fate and effects of poly- and perfluoroalkyl substances in the aquatic environment: a review. Environ Toxicol Chem. 2014;33: 1921–1929. doi:10.1002/etc.2663
320. Talsness CE, Andrade AJM, Kuriyama SN, Taylor JA, vom Saal FS. Components of plastic: experimental studies in animals and relevance for human health. Philos Trans R

Soc B Biol Sci. 2009;364: 2079–2096. doi:10.1098/rstb.2008.0281
321. Langston WJ, Pope ND, Davey M, Langston KM, O' Hara SCM, Gibbs PE, et al. Recovery from TBT pollution in english channel environments: a problem solved? Mar Pollut Bull. 2015;95: 551–564. doi:10.1016/j.marpolbul.2014.12.011
322. Rodriguez-Jorquera IA, Kroll KJ, Toor GS, Denslow ND. Transcriptional and physiological response of fathead minnows (Pimephales promelas) exposed to urban waters entering into wildlife protected areas. Environ Pollut. 2015;199: 155–165. doi:10.1016/j.envpol.2015.01.021
323. Corrales J, Kristofco LA, Steele WB, Yates BS, Breed CS, Williams ES, et al. Global assessment of bisphenol A in the environment: review and analysis of its occurrence and bioaccumulation. Dose Response. 2015;13: 1559325815598308. doi:10.1177/1559325815598308
324. Canesi L, Fabbri E. Environmental effects of BPA: focus on aquatic species. Dose Response. 2015;13: 1559325815598304. doi:10.1177/1559325815598304
325. Flint S, Markle T, Thompson S, Wallace E. Bisphenol A exposure, effects, and policy: a wildlife perspective. J Environ Manage. 2012;104: 19–34. doi:10.1016/j.jenvman.2012.03.021
326. Li Z, Yu D, Wangbao G, Guangjun W, Ermeng Y, Jun X. Aquatic ecotoxicology and water quality criteria of three organotin compounds: a review. Nat Environ Pollut Technol. 2019;18: 217–224. Available: www.neptjournal.com
327. Gianguzza A. Organotin - environmental fate and effects. Mar Chem. 1997;57: 133. doi:10.1016/s0304-4203(97)88167-4
328. Suja F, Pramanik BK, Zain SM. Contamination, bioaccumulation and toxic effects of perfluorinated chemicals (PFCs) in the water environment: a review paper. Water Sci Technol. 2009;60: 1533–1554. doi:10.2166/wst.2009.504
329. Chen H, Zhang C, Han J, Yu Y, Zhang P. PFOS and PFOA in influents, effluents, and biosolids of Chinese wastewater treatment plants and effluent-receiving marine environments. Environ Pollut. 2012;170: 26–31. doi:10.1016/j.envpol.2012.06.016
330. Coggan TL, Moodie D, Kolobaric A, Szabo D, Shimeta J, Crosbie ND, et al. An investigation into per- and polyfluoroalkyl substances (PFAS) in nineteen Australian wastewater treatment plants (WWTPs). Heliyon. 2019;5. doi:10.1016/j.heliyon.2019.e02316
331. vom Saal FS, Nagel SC, Coe BL, Angle BM, Taylor JA. The estrogenic endocrine disrupting chemical bisphenol A (BPA) and obesity. Molecular and Cellular Endocrinology. NIH Public Access; 2012. pp. 74–84. doi:10.1016/j.mce.2012.01.001
332. Penza M, Jeremic M, Marrazzo E, Maggi A, Ciana P, Rando G, et al. The environmental chemical tributyltin chloride (TBT) shows both estrogenic and adipogenic activities in mice which might depend on the exposure dose. Toxicol Appl Pharmacol. 2011;255: 65–75. doi:10.1016/j.taap.2011.05.017
333. Chen J, Wang X, Ge X, Wang D, Wang T, Zhang L, et al. Chronic perfluorooctanesulphonic acid (PFOS) exposure produces estrogenic effects in zebrafish. Environ Pollut. 2016;218: 702–708. doi:10.1016/j.envpol.2016.07.064
334. Mu X, Huang Y, Li X, Lei Y, Teng M, Li X, et al. Developmental Effects and Estrogenicity of Bisphenol A Alternatives in a Zebrafish Embryo Model. Environ Sci Technol. 2018;52: 3222–3231. doi:10.1021/acs.est.7b06255
335. Tohmé M, Prud'Homme SM, Boulahtouf A, Samarut E, Brunet F, Bernard L, et al. Estrogen-related receptor γ is an in vivo receptor of bisphenol A. FASEB J. 2014;28: 3124–3133. doi:10.1096/fj.13-240465
336. Huang Q, Chen Q. Mediating roles of PPARs in the effects of environmental chemicals on sex steroids. PPAR Res.

2017;2017: 1–8. doi:10.1155/2017/3203161
337. Holtcamp W. Obesogens: an environmental link to obesity. Environ Health Perspect. 2012;120: a62-8. doi:10.1289/ehp.120-a62
338. Thayer KA, Heindel JJ, Bucher JR, Gallo MA. Role of environmental chemicals in diabetes and obesity: A national toxicology program workshop review. Environmental Health Perspectives. 2012. doi:10.1289/ehp.1104597
339. Lima D, Castro LFC, Coelho I, Lacerda R, Gesto M, Soares J, et al. Effects of tributyltin and other retinoid receptor agonists in reproductive-related endpoints in the zebrafish (Danio rerio). J Toxicol Environ Heal - Part A Curr Issues. 2015;78: 747–760. doi:10.1080/15287394.2015.1028301
340. McGinnis CL, Crivello JF. Elucidating the mechanism of action of tributyltin (TBT) in zebrafish. Aquat Toxicol. 2011;103: 25–31. doi:10.1016/j.aquatox.2011.01.005
341. Tse WKF, Yeung BHY, Wan HT, Wong CKC. Early embryogenesis in zebrafish is affected by bisphenol A exposure. Biol Open. 2013;2: 466–71. doi:10.1242/bio.20134283
342. Wang J, Wang X, Xiong C, Liu J, Hu B, Zheng L. Chronic bisphenol A exposure alters behaviors of zebrafish (Danio rerio). Environ Pollut. 2015;206: 275–281. doi:10.1016/j.envpol.2015.07.015
343. Vogs C, Johanson G, Näslund M, Wulff S, Sjödin M, Hellstrandh M, et al. Toxicokinetics of perfluorinated alkyl acids influences their toxic potency in the zebrafish embryo (Danio rerio). Environ Sci Technol. 2019;53: 3898–3907. doi:10.1021/acs.est.8b07188
344. Jantzen CE, Annunziato KM, Cooper KR. Behavioral, morphometric, and gene expression effects in adult zebrafish (Danio rerio) embryonically exposed to PFOA, PFOS, and PFNA. Aquat Toxicol. 2016;180: 123–130. doi:10.1016/j.aquatox.2016.09.011
345. Chen J, Tanguay RL, Tal TL, Gai Z, Ma X, Bai C, et al. Early life perfluorooctanesulphonic acid (PFOS) exposure impairs zebrafish organogenesis. Aquat Toxicol. 2014;150: 124–132. doi:10.1016/j.aquatox.2014.03.005
346. Saili KS, Tilton SC, Waters KM, Tanguay RL. Global gene expression analysis reveals pathway differences between teratogenic and non-teratogenic exposure concentrations of bisphenol A and 17β-estradiol in embryonic zebrafish. Reprod Toxicol. 2013;38: 89–101. doi:10.1016/j.reprotox.2013.03.009
347. Renaud L, Silveira WA da, Hazard ES, Simpson J, Falcinelli S, Chung D, et al. The plasticizer bisphenol A perturbs the hepatic epigenome: a systems level analysis of the miRNome. Genes (Basel). 2017;8: 269. doi:10.3390/genes8100269
348. Huang L, Zuo Z, Zhang Y, Wang C. Toxicogenomic analysis in the combined effect of tributyltin and benzo[a]pyrene on the development of zebrafish embryos. Aquat Toxicol. 2015;158: 157–164. doi:10.1016/j.aquatox.2014.10.024
349. Fai Tse WK, Li JW, Kwan Tse AC, Chan TF, Hin Ho JC, Sun Wu RS, et al. Fatty liver disease induced by perfluorooctane sulfonate: novel insight from transcriptome analysis. Chemosphere. 2016;159: 166–177. doi:10.1016/j.chemosphere.2016.05.060
350. Villeneuve DL, Garcia-Reyero N, Escalon BL, Jensen KM, Cavallin JE, Makynen EA, et al. Ecotoxicogenomics to support ecological risk assessment: a case study with bisphenol A in fish. Environ Sci Technol. 2012;46: 51–9. doi:10.1021/es201150a
351. Lam SH, Hlaing MM, Zhang X, Yan C, Duan Z, Zhu L, et al. Toxicogenomic and phenotypic analyses of bisphenol-a early-life exposure toxicity in zebrafish. PLoS One. 2011;6. doi:10.1371/journal.pone.0028273
352. Ortiz-Villanueva E, Navarro-Martín L, Jaumot J, Benavente F, Sanz-Nebot V, Piña B, et al. Metabolic disruption of zebrafish (Danio rerio) embryos by bisphenol A. An integrated metabolomic and transcriptomic approach. Environ Pollut. 2017;231: 22–36.

doi:10.1016/j.envpol.2017.07.095
353. Davis JA, Gift JS, Zhao QJ. Introduction to benchmark dose methods and U.S. EPA's benchmark dose software (BMDS) version 2.1.1. Toxicology and Applied Pharmacology. Academic Press; 2011. pp. 181–191. doi:10.1016/j.taap.2010.10.016
354. Santangeli S, Notarstefano V, Maradonna F, Giorgini E, Gioacchini G, Forner-Piquer I, et al. Effects of diethylene glycol dibenzoate and bisphenol A on the lipid metabolism of Danio rerio. Sci Total Environ. 2018;636: 641–655. doi:10.1016/j.scitotenv.2018.04.291
355. Delfosse V, Grimaldi M, le Maire A, Bourguet W, Balaguer P. Nuclear receptor profiling of bisphenol-A and its halogenated analogues. Vitamins and Hormones. Academic Press Inc.; 2014. pp. 229–251. doi:10.1016/B978-0-12-800095-3.00009-2
356. Ngo MT, Doan TTP, Nguyen CT, Vo DTN, Do CHL, Le NP. Chronic exposure of µg/L range bisphenol A to adult zebrafish (Danio rerio) leading to adipogenesis. AIP Conference Proceedings. American Institute of Physics Inc.; 2017. p. 020028. doi:10.1063/1.5000196
357. Vanden Heuvel JP, Thompson JT, Frame SRSR, Gillies PJ. Differential activation of nuclear receptors by perfluorinated fatty acid analogs and natural fatty acids: A comparison of human, mouse, and rat peroxisome proliferator-activated receptor-α, -β, and -γ, liver X receptor-β, and retinoid X receptor-α. Toxicol Sci. 2006;92: 476–489. doi:10.1093/toxsci/kfl014
358. Kang JS, Ahn TG, Park JW. Perfluorooctanoic acid (PFOA) and perfluooctane sulfonate (PFOS) induce different modes of action in reproduction to Japanese medaka (Oryzias latipes). J Hazard Mater. 2019;368: 97–103. doi:10.1016/j.jhazmat.2019.01.034
359. DeWitt JC, Shnyra A, Badr MZ, Loveless SE, Hoban D, Frame SR, et al. Immunotoxicity of perfluorooctanoic acid and perfluorooctane sulfonate and the role of peroxisome proliferator-activated receptor alpha. Critical Reviews in Toxicology. 2009. pp. 76–94. doi:10.1080/10408440802209804
360. Viberg H, Eriksson P. Perfluorooctane sulfonate and perfluorooctanoic acid. Reproductive and Developmental Toxicology. Elsevier; 2017. pp. 811–827. doi:10.1016/b978-0-12-804239-7.00043-3
361. Marx N, Sukhova GK, Collins T, Libby P, Plutzky J. PPARalpha activators inhibit cytokine-induced vascular cell adhesion molecule-1 expression in human endothelial cells. Circulation. 1999;99: 3125–31. doi:10.1161/01.cir.99.24.3125
362. Kim YS, Lee H-M, Kim JK, Yang C-S, Kim TS, Jung M, et al. PPAR-α activation mediates innate host defense through induction of TFEB and lipid catabolism. J Immunol. 2017;198: 3283–3295. doi:10.4049/jimmunol.1601920
363. Kintscher U, Lyon C, Wakino S, Bruemmer D, Feng X, Goetze S, et al. PPARalpha inhibits TGF-beta-induced beta5 integrin transcription in vascular smooth muscle cells by interacting with Smad4. Circ Res. 2002;91: e35-44. doi:10.1161/01.res.0000046017.96083.34
364. Cao H, Wen G, Li H. Role of peroxisome proliferator-activated receptor α in atherosclerosis. Mol Med Rep. 2014;9: 1755–1760. doi:10.3892/mmr.2014.2020
365. Jiao Y, Lu Y, Li XY. Farnesoid X receptor: a master regulator of hepatic triglyceride and glucose homeostasis. Acta Pharmacologica Sinica. Nature Publishing Group; 2015. pp. 44–50. doi:10.1038/aps.2014.116
366. Hu W yue, Jones PD, DeCoen W, King L, Fraker P, Newsted J, et al. Alterations in cell membrane properties caused by perfluorinated compounds. Comp Biochem Physiol Part C Toxicol Pharmacol. 2003;135: 77–88. doi:10.1016/S1532-0456(03)00043-7
367. Shabalina IG, Kalinovich A V., Cannon B, Nedergaard J. Metabolically inert

perfluorinated fatty acids directly activate uncoupling protein 1 in brown-fat mitochondria. Arch Toxicol. 2016;90: 1117–1128. doi:10.1007/s00204-015-1535-4

368. Jastroch M, Wuertz S, Kloas W, Klingenspor M. Uncoupling protein 1 in fish uncovers an ancient evolutionary history of mammalian nonshivering thermogenesis. Physiol Genomics. 2005;22: 150–156. doi:10.1152/physiolgenomics.00070.2005
369. Al Tanoury Z, Piskunov A, Rochette-Egly C. Vitamin A and retinoid signaling: genomic and nongenomic effects. Journal of Lipid Research. American Society for Biochemistry and Molecular Biology; 2013. pp. 1761–1775. doi:10.1194/jlr.R030833
370. Kiser PD, Golczak M, Palczewski K. Chemistry of the retinoid (visual) cycle. Chemical Reviews. American Chemical Society; 2014. pp. 194–232. doi:10.1021/cr400107q
371. Martínez R, Codina AE, Barata C, Tauler R, Piña B, Navarro-Martín L. Transcriptomic effects of tributyltin (TBT) in zebrafish eleutheroembryos. A functional benchmark dose analysis. J Hazard Mater. 2020;398: 122881. doi:10.1016/j.jhazmat.2020.122881
372. Armant O, Gourain V, Etard C, Strähle U. Whole transcriptome data analysis of zebrafish mutants affecting muscle development. Data Br. 2016;8: 61–68. doi:10.1016/j.dib.2016.05.007
373. Yuan W, Jiang S, Sun D, Wu Z, Wei C, Dai C, et al. Transcriptome profiling analysis of sex-based differentially expressed mRNAs and lncRNAs in the brains of mature zebrafish (Danio rerio). BMC Genomics. 2019;20: 830. doi:10.1186/s12864-019-6197-9
374. Dong X, Qiu X, Meng S, Xu H, Wu X, Yang M. Proteomic profile and toxicity pathway analysis in zebrafish embryos exposed to bisphenol A and di-n-butyl phthalate at environmentally relevant levels. Chemosphere. 2018;193: 313–320. doi:10.1016/j.chemosphere.2017.11.042
375. Low LWL, Tate S, Gunaratne J, Carney TJ. Confirming gene mutation by CRISPR-Cas9 at the protein level and identifying proteome-wide changes. 2020. Available: https://sciex.com/x116737
376. Faria M, Ziv T, Gómez-Canela C, Ben-Lulu S, Prats E, Novoa-Luna KA, et al. Acrylamide acute neurotoxicity in adult zebrafish. Sci Rep. 2018;8: 1–14. doi:10.1038/s41598-018-26343-2
377. Jia J, Qin J, Yuan X, Liao Z, Huang J, Wang B, et al. Microarray and metabolome analysis of hepatic response to fasting and subsequent refeeding in zebrafish (Danio rerio). BMC Genomics. 2019;20: 919. doi:10.1186/s12864-019-6309-6
378. Bhat VS, Hester SD, Nesnow S, Eastmond DA. Concordance of transcriptional and apical benchmark dose levels for conazole-induced liver effects in mice. Toxicol Sci. 2013;136: 205–215. doi:10.1093/toxsci/kft182
379. Farmahin R, Williams A, Kuo B, Chepelev NL, Thomas RS, Barton-Maclaren TS, et al. Recommended approaches in the application of toxicogenomics to derive points of departure for chemical risk assessment. Arch Toxicol. 2017;91: 2045–2065. doi:10.1007/s00204-016-1886-5
380. Webster AF, Chepelev N, Gagné R, Kuo B, Recio L, Williams A, et al. Impact of genomics platform and statistical filtering on transcriptional benchmark doses (BMD) and multiple approaches for selection of chemical point of departure (PoD). PLoS One. 2015;10: e0136764. doi:10.1371/journal.pone.0136764
381. Mackillop WJ. The non-lethal effects of ionizing radiation and hyperthermia on colony growth in a human bladder cancer cell line. Cancer Lett. 1985;27: 315–322. doi:10.1016/0304-3835(85)90190-9
382. Walsh GM, Fink GB. Comparative toxicity and distribution of endrin and dieldrin after intravenous administration in mice. Toxicol

Appl Pharmacol. 1972;23: 408–416. doi:10.1016/0041-008X(72)90043-9
383. O'Brien RD, Metcalf RL. Toxic phosphorus esters. Chemistry, metabolism, and biological effects. Q Rev Biol. 1963;38: 213–214. doi:10.1086/403846
384. Tu W, Martínez R, Navarro-Martin L, Kostyniuk DJ, Hum C, Huang J, et al. Bioconcentration and Metabolic Effects of Emerging PFOS Alternatives in Developing Zebrafish. Environ Sci Technol. 2019;53: 13427–13439. doi:10.1021/acs.est.9b03820
385. Orlov I, Rochel N, Moras D, Klaholz BP. Structure of the full human RXR/VDR nuclear receptor heterodimer complex with its DR3 target DNA. EMBO J. 2012;31: 291–300. doi:10.1038/emboj.2011.445
386. Kollitz EM, Hawkins MB, Whitfield GK, Kullman SW. Functional diversification of vitamin D receptor paralogs in teleost fish after a whole genome duplication event. Endocrinology. 2014;155: 4641–4654. doi:10.1210/en.2014-1505
387. Zhang C, Baudino TA, Dowd DR, Tokumaru H, Wang W, MacDonald PN. Ternary complexes and cooperative interplay between NCoA-62/Ski-interacting protein and steroid receptor coactivators in vitamin D receptor-mediated transcription. J Biol Chem. 2001;276: 40614–40620. doi:10.1074/jbc.M106263200
388. Acconcia F, Pallottini V, Marino M. Molecular mechanisms of action of BPA. Dose-Response. 2015;13. doi:10.1177/1559325815610582
389. Livezey M, Kim JE, Shapiro DJ. A new role for estrogen receptor a in cell proliferation and cancer: Activating the anticipatory unfolded protein response. Frontiers in Endocrinology. Frontiers Media S.A.; 2018. doi:10.3389/fendo.2018.00325
390. JavanMoghadam S, Weihua Z, Hunt KK, Keyomarsi K. Estrogen receptor alpha is cell cycle-regulated and regulates the cell cycle in a ligand-dependent fashion. Cell Cycle. 2016;15: 1579–1590. doi:10.1080/15384101.2016.1166327
391. Osborne CK, Shou J, Massarweh S, Schiff R, Come S, Santen R, et al. Crosstalk between estrogen receptor and growth factor receptor pathways as a cause for endocrine therapy resistance in breast cancer. Clinical Cancer Research. 2005. Available: https://clincancerres.aacrjournals.org/lens/clincanres/11/2/865s
392. Giguère V. Transcriptional control of energy homeostasis by the estrogen-related receptors. Endocrine Reviews. Oxford Academic; 2008. pp. 677–696. doi:10.1210/er.2008-0017
393. Francis GA, Fayard E, Picard F, Auwerx J. Nuclear receptors and the control of metabolism. Annu Rev Physiol. 2003;65: 261–311. doi:10.1146/annurev.physiol.65.092101.142528
394. Feige JN, Auwerx J. Transcriptional coregulators in the control of energy homeostasis. Trends in Cell Biology. 2007. pp. 292–301. doi:10.1016/j.tcb.2007.04.001
395. Wieneke N, Hirsch-Ernst KI, Kuna M, Kersten S, Püschel GP. PPARα-dependent induction of the energy homeostasis-regulating nuclear receptor NR1i3 (CAR) in rat hepatocytes: potential role in starvation adaptation. FEBS Lett. 2007;581: 5617–5626. doi:10.1016/j.febslet.2007.11.011
396. Huang W, Glass CK. Nuclear receptors and inflammation control: molecular mechanisms and pathophysiological relevance. Arteriosclerosis, Thrombosis, and Vascular Biology. NIH Public Access; 2010. pp. 1542–1549. doi:10.1161/ATVBAHA.109.191189
397. Le Menn G, Neels JG. Regulation of immune cell function by PPARs and the connection with metabolic and neurodegenerative diseases. International Journal of Molecular Sciences. 2018. doi:10.3390/ijms19061575
398. Alameda Serrano D, Ricote Pacheco M. Regulación transcripcional de la inflamación

en macrófagos por el Receptor X de Retinoides. Universidad Autónoma de Madrid. 2014. Available: http://hdl.handle.net/10486/662592

399. Núñez V, Alamedaa D, Rico D, Mota R, Gonzalo P, Cedenilla M, et al. Retinoid X receptor α controls innate inflammatory responses through the up-regulation of chemokine expression. Proc Natl Acad Sci U S A. 2010;107: 10626–10631. doi:10.1073/pnas.0913545107
400. Coleman DJ, Garcia G, Hyter S, Jang HS, Chagani S, Liang X, et al. Retinoid-X-Receptors (α/β) in melanocytes modulate innate immune responses and differentially regulate cell survival following UV irradiation. Steingrimsson E, editor. PLoS Genet. 2014;10: e1004321. doi:10.1371/journal.pgen.1004321
401. Spilianakis CG, Lee GR, Flavell RA. Twisting the Th1/Th2 immune response via the retinoid X receptor: lessons from a genetic approach. European Journal of Immunology. John Wiley & Sons, Ltd; 2005. pp. 3400–3404. doi:10.1002/eji.200535588
402. Raverdeau M, Mills KHG. Modulation of T cell and innate immune responses by retinoic acid. J Immunol. 2014;192: 2953–2958. doi:10.4049/jimmunol.1303245
403. Zhao F, Wei P, Wang J, Yu M, Zhang X, Tian H, et al. Estrogenic effects associated with bisphenol A exposure in male zebrafish (Danio rerio) is associated with changes of endogenous 17β-estradiol and gene specific DNA methylation levels. Gen Comp Endocrinol. 2017;252: 27–35. doi:10.1016/j.ygcen.2017.07.032
404. Shi X, Du Y, Lam PKS, Wu RSS, Zhou B. Developmental toxicity and alteration of gene expression in zebrafish embryos exposed to PFOS. Toxicol Appl Pharmacol. 2008;230: 23–32. doi:10.1016/j.taap.2008.01.043
405. Guo J, Wu P, Cao J, Luo Y, Chen J, Wang G, et al. The PFOS disturbed immunomodulatory functions via nuclear Factor-κB signaling in liver of zebrafish (Danio rerio). Fish Shellfish Immunol. 2019;91: 87–98. doi:10.1016/j.fsi.2019.05.018
406. Liu ZH, Li YW, Hu W, Chen QL, Shen YJ. Mechanisms involved in tributyltin-enhanced aggressive behaviors and fear responses in male zebrafish. Aquat Toxicol. 2020;220: 105408. doi:10.1016/j.aquatox.2020.105408
407. McAllister BG, Kime DE. Early life exposure to environmental levels of the aromatase inhibitor tributyltin causes masculinisation and irreversible sperm damage in zebrafish (Danio rerio). Aquat Toxicol. 2003;65: 309–316. doi:10.1016/S0166-445X(03)00154-1
408. Mishima Y, Abreu-Goodger C, Staton AA, Stahlhut C, Shou C, Cheng C, et al. Zebrafish miR-1 and miR-133 shape muscle gene expression and regulate sarcomeric actin organization. Genes Dev. 2009;23: 619–632. doi:10.1101/gad.1760209
409. Li J, Dong X, Wang Z, Wu J. MicroRNA-1 in cardiac diseases and cancers. Korean J Physiol Pharmacol. 2014;18: 359–363. doi:10.4196/kjpp.2014.18.5.359
410. Rubinstein M, Low MJ. Molecular and functional genetics of the proopiomelanocortin gene, food intake regulation and obesity. FEBS Letters. Wiley Blackwell; 2017. pp. 2593–2606. doi:10.1002/1873-3468.12776
411. Shi C, Lu Y, Zhai G, Huang J, Shang G, Lou Q, et al. Hyperandrogenism in POMCa-deficient zebrafish enhances somatic growth without increasing adiposity. J Mol Cell Biol. 2019 [cited 5 May 2020]. doi:10.1093/jmcb/mjz053
412. Ahmed S, Atlas E. Bisphenol S- and bisphenol A-induced adipogenesis of murine preadipocytes occurs through direct peroxisome proliferator-activated receptor gamma activation. Int J Obes. 2016;40: 1566–1573. doi:10.1038/ijo.2016.95
413. Boucher JG, Husain M, Rowan-Carroll A,

Williams A, Yauk CL, Atlas E. Identification of mechanisms of action of bisphenol A-induced human preadipocyte differentiation by transcriptional profiling. Obesity. 2014;22: 2333–2343. doi:10.1002/oby.20848

414. Sharma S, Ahmad S, Khan MF, Parvez S, Raisuddin S. In silico molecular interaction of bisphenol analogues with human nuclear receptors reveals their stronger affinity vs. classical bisphenol A. Toxicol Mech Methods. 2018;28: 660–669. doi:10.1080/15376516.2018.1491663

415. Nishizawa H, Morita M, Sugimoto M, Imanishi S, Manabe N. Effects of in utero exposure to bisphenol A on mRNA expression of arylhydrocarbon and retinoid receptors in murine embryos. J Reprod Dev. 2005;51: 315–324. doi:10.1262/jrd.16008

416. Mu X, Huang Y, Li X, Lei Y, Teng M, Li X, et al. Developmental effects and estrogenicity of bisphenol A alternatives in a zebrafish embryo model. Environ Sci Technol. 2018;52: 3222–3231. doi:10.1021/acs.est.7b06255

417. Inoue D, Sei K, Ike M. Disruption of retinoic acid receptor signaling by environmental pollutants. Journal of Health Science. 2010. pp. 221–230. doi:10.1248/jhs.56.221

418. Gervois P, Torra IP, Fruchart JC, Staels B. Regulation of lipid and lipoprotein metabolism by PPAR activators. Clinical Chemistry and Laboratory Medicine. Walter de Gruyter and Co.; 2000. pp. 3–11. doi:10.1515/CCLM.2000.002

419. Ahmadian M, Suh JM, Hah N, Liddle C, Atkins AR, Downes M, et al. PPARγ signaling and metabolism: The good, the bad and the future. Nat Med. 2013;19: 557–566. doi:10.1038/nm.3159

420. Bergman Å, Heindel JJ, Jobling S, Kidd KA, Zoeller RT. State of the science of endocrine disrupting chemicals 2012 - summary for decision makers. WHO. 2013. doi:10.1590/S1414-462X2013000100003

421. Sanderson JT. The steroid hormone biosynthesis pathway as a target for endocrine-disrupting chemicals. Toxicological Sciences. 2006. pp. 3–21. doi:10.1093/toxsci/kfl051

422. Cano-Nicolau J, Vaillant C, Pellegrini E, Charlier TD, Kah O, Coumailleau P. Estrogenic effects of several BPA analogs in the developing zebrafish brain. Front Neurosci. 2016;10: 112. doi:10.3389/fnins.2016.00112

423. Le Fol V, Aït-Aïssa S, Sonavane M, Porcher JM, Balaguer P, Cravedi JP, et al. In vitro and in vivo estrogenic activity of BPA, BPF and BPS in zebrafish-specific assays. Ecotoxicol Environ Saf. 2017;142: 150–156. doi:10.1016/j.ecoenv.2017.04.009

424. Raldúa D, André M, Babin PJ. Clofibrate and gemfibrozil induce an embryonic malabsorption syndrome in zebrafish. Toxicol Appl Pharmacol. 2008;228: 301–314. doi:10.1016/j.taap.2007.11.016

425. Martínez R, Tu W, Eng T, Allaire-Leung M, Piña B, Navarro-Martín L, et al. Acute and long-term metabolic consequences of early developmental Bisphenol A exposure in zebrafish (Danio rerio). Chemosphere. 2020;256: 127080. doi:10.1016/j.chemosphere.2020.127080

426. Zeng Z, Song B, Xiao R, Zeng G, Gong J, Chen M, et al. Assessing the human health risks of perfluorooctane sulfonate by in vivo and in vitro studies. Environment International. Elsevier Ltd; 2019. pp. 598–610. doi:10.1016/j.envint.2019.03.002

427. Liao TT, Shi YL, Jia JW, Jia RW, Wang L. Sensitivity of morphological change of Vero cells exposed to lipophilic compounds and its mechanism. J Hazard Mater. 2010;179: 1055–1064. doi:10.1016/j.jhazmat.2010.03.113

428. Lau C, Anitole K, Hodes C, Lai D, Pfahles-Hutchens A, Seed J. Perfluoroalkyl acids: A review of monitoring and toxicological findings. Toxicological Sciences. Oxford University Press; 2007. pp. 366–394.

doi:10.1093/toxsci/kfm128
429. White SS, Fenton SE, Hines EP. Endocrine disrupting properties of perfluorooctanoic acid. J Steroid Biochem Mol Biol. 2011;127: 16–26. doi:10.1016/j.jsbmb.2011.03.011
430. Knutsen HK, Alexander J, Barregård L, Bignami M, Brüschweiler B, Ceccatelli S, et al. Risk to human health related to the presence of perfluorooctane sulfonic acid and perfluorooctanoic acid in food. EFSA J. 2018;16. doi:10.2903/j.efsa.2018.5194
431. Lodhi IJ, Yin L, Jensen-Urstad APL, Funai K, Coleman T, Baird JH, et al. Inhibiting adipose tissue lipogenesis reprograms thermogenesis and PPARγ activation to decrease diet-induced obesity. Cell Metab. 2012;16: 189–201. doi:10.1016/j.cmet.2012.06.013
432. DeWitt JC, Blossom SJ, Schaider LA. Exposure to per-fluoroalkyl and polyfluoroalkyl substances leads to immunotoxicity: epidemiological and toxicological evidence. J Expo Sci Environ Epidemiol. 2019;29: 148–156. doi:10.1038/s41370-018-0097-y
433. Zhang Y, Chen X, Gueydan C, Han J. Plasma membrane changes during programmed cell deaths. Cell Res. 2018;28: 9–21. doi:10.1038/cr.2017.133
434. Suzanne M, Steller H. Letting go: modification of cell adhesion during apoptosis. Journal of Biology. BioMed Central; 2009. p. 49. doi:10.1186/jbiol152
435. Roca FJ, Mulero I, López-Muñoz A, Sepulcre MP, Renshaw SA, Meseguer J, et al. Evolution of the inflammatory response in vertebrates: fish TNF-alpha is a powerful activator of endothelial cells but hardly activates phagocytes. J Immunol. 2008;181: 5071–81. doi:10.4049/jimmunol.181.7.5071
436. Mashoof S, Criscitiello M. Fish immunoglobulins. Biology (Basel). 2016;5: 45. doi:10.3390/biology5040045
437. Sun G, Liu K, Wang X, Liu X, He Q, Hsiao C Der. Identification and expression analysis of zebrafish (Danio rerio) E-selectin during embryonic development. Molecules. 2015;20: 18539–18550. doi:10.3390/molecules201018539
438. Li-Villarreal N, Forbes MM, Loza AJ, Chen J, Ma T, Helde K, et al. Dachsous1b cadherin regulates actin and microtubule cytoskeleton during early zebrafish embryogenesis. Development. 2016;143: 1832–1832. doi:10.1242/dev.138859
439. Mould AP, McLeish JA, Huxley-Jones J, Goonesinghe AC, Hurlstone AFL, Boot-Handford RP, et al. Identification of multiple integrin β1 homologs in zebrafish (Danio rerio). BMC Cell Biol. 2006;7: 24. doi:10.1186/1471-2121-7-24
440. Vasta GR, Nita-Lazar M, Giomarelli B, Ahmed H, Du S, Cammarata M, et al. Structural and functional diversity of the lectin repertoire in teleost fish: Relevance to innate and adaptive immunity. Dev Comp Immunol. 2011;35: 1388–1399. doi:10.1016/j.dci.2011.08.011
441. Cambi A, Koopman M, Figdor CG. How C-type lectins detect pathogens. Cellular Microbiology. 2005. pp. 481–488. doi:10.1111/j.1462-5822.2005.00506.x
442. Ng TB, Li WW, Yeung HW. Effects of lectins with various carbohydrate binding specificities on lipid metabolism in isolated rat and hamster adipocytes. Int J Biochem. 1989;21: 149–156. doi:10.1016/0020-711X(89)90103-1
443. Ahmed H, Du SJ, Vasta GR. Knockdown of a galectin-1-like protein in zebrafish (Danio rerio) causes defects in skeletal muscle development. Glycoconjugate Journal. 2009. pp. 277–283. doi:10.1007/s10719-008-9178-9
444. Gaballah S, Swank A, Sobus JR, Howey XM, Schmid J, Catron T, et al. Evaluation of developmental toxicity, developmental neurotoxicity, and tissue dose in zebrafish exposed to GenX and other PFAS. Environ Health Perspect. 2020;128: 047005. doi:10.1289/EHP5843
445. De Voogt P. Reviews of environmental

contamination and toxicology. Reviews of Environmental Contamination and Toxicology. 2015. doi:10.1007/978-3-319-20013-2

446. le Maire A, Grimaldi M, Roecklin D, Dagnino S, Vivat-Hannah V, Balaguer P, et al. Activation of RXR-PPAR heterodimers by organotin environmental endocrine disruptors. EMBO Rep. 2009;10: 367–373. doi:10.1038/embor.2009.8
447. Soares J, Neuparth T, Lyssimachou A, Lima D, André A, Reis-Henriques MA, et al. 17α-ethynilestradiol and tributyltin mixtures modulates the expression of NER and p53 DNA repair pathways in male zebrafish gonads and disrupt offspring embryonic development. Ecol Indic. 2018;95: 1008–1018. doi:10.1016/j.ecolind.2017.04.054
448. Zuo Z, Wang C, Wu M, Wang Y, Chen Y. Exposure to tributyltin and triphenyltin induces DNA damage and alters nucleotide excision repair gene transcription in Sebastiscus marmoratus liver. Aquat Toxicol. 2012;122–123: 106–112. doi:10.1016/j.aquatox.2012.05.015
449. Verhaegen Y. Mode of action, concentrations and effects of tributyltin in commons shrimp Crangon crangon. Universiteit Gent. 2012. Available: https://biblio.ugent.be/publication/2753445
450. Keller H, Dreyer C, Medin J, Mahfoudi A, Ozato K, Wahli W. Fatty acids and retinoids control lipid metabolism through activation of peroxisome proliferator-activated receptor-retinoid X receptor heterodimers. Proc Natl Acad Sci U S A. 1993;90: 2160–2164. doi:10.1073/pnas.90.6.2160
451. Varga T, Czimmerer Z, Nagy L. PPARs are a unique set of fatty acid regulated transcription factors controlling both lipid metabolism and inflammation. Biochimica et Biophysica Acta - Molecular Basis of Disease. Elsevier; 2011. pp. 1007–1022. doi:10.1016/j.bbadis.2011.02.014
452. Craig TA, Sommer S, Sussman CR, Grande JP, Kumar R. Expression and regulation of the vitamin D receptor in the zebrafish, Danio rerio. J Bone Miner Res. 2008;23: 1486–1496. doi:10.1359/jbmr.080403
453. Romney ALT, Davis EM, Corona MM, Wagner JT, Podrabsky JE. Temperature-dependent vitamin D signaling regulates developmental trajectory associated with diapause in an annual killifish. Proc Natl Acad Sci U S A. 2018;115: 12763–12768. doi:10.1073/pnas.1804590115
454. Hong SH, Lee JE, An SM, Shin YY, Hwang DY, Yang SY, et al. Effect of vitamin d3 on biosynthesis of estrogen in porcine granulosa cells via modulation of steroidogenic enzymes. Toxicol Res. 2017;33: 49–54. doi:10.5487/TR.2017.33.1.049
455. Rone MB, Fan J, Papadopoulos V. Cholesterol transport in steroid biosynthesis: role of protein-protein interactions and implications in disease states. Biochimica et Biophysica Acta - Molecular and Cell Biology of Lipids. NIH Public Access; 2009. pp. 646–658. doi:10.1016/j.bbalip.2009.03.001
456. Anderson JL, Carten JD, Farber SA. Zebrafish lipid metabolism: from mediating early patterning to the metabolism of dietary fat and cholesterol. Methods Cell Biol. 2011;101: 111–41. doi:10.1016/B978-0-12-387036-0.00005-0
457. Tokarz J, Möller G, Hrabě De Angelis M, Adamski J. Zebrafish and steroids: what do we know and what do we need to know? Journal of Steroid Biochemistry and Molecular Biology. Pergamon; 2013. pp. 165–173. doi:10.1016/j.jsbmb.2013.01.003
458. Braunbeck T (Thomas), Hinton DE, Streit B. Fish ecotoxicology. Birkhäuser Verlag; 1998. Available: https://books.google.es/books?id=AS7HYknQewAC&pg=PA269&lpg=PA269&dq=tbt+dbt+biotransformation+fish&source=bl&ots=AEThlCB4vc&sig=ACfU3U1UuBVTtYjswX0fYfFpLkFCjb9gpw&hl=es&sa=X&ved=2ahUKEwj

1ovX0nILlAhXC7eAKHWopBvwQ6AEwEHoECAgQAQ#v=onepage&q=tbt dbt biotransf
459. Li X, Ycaza J, Blumberg B. The environmental obesogen tributyltin chloride acts via peroxisome proliferator activated receptor gamma to induce adipogenesis in murine 3T3-L1 preadipocytes. J Steroid Biochem Mol Biol. 2011;127: 9–15. doi:10.1016/j.jsbmb.2011.03.012
460. Li X, Ycaza J, Blumberg B. Structure-dependent activation of peroxisome proliferator-activated receptor (PPAR) γ by organotin compounds. J Steroid Biochem Mol Biol. 2011;127: 9–15. doi:10.1016/j.cbi.2009.03.006
461. Liang X, Souders CL, Zhang J, Martyniuk CJ. Tributyltin induces premature hatching and reduces locomotor activity in zebrafish (Danio rerio) embryos/larvae at environmentally relevant levels. Chemosphere. 2017;189: 498–506. doi:10.1016/j.chemosphere.2017.09.093
462. Milan M, Pauletto M, Boffo L, Carrer C, Sorrentino F, Ferrari G, et al. Transcriptomic resources for environmental risk assessment: a case study in the Venice lagoon. Environ Pollut. 2015;197: 90–98. doi:10.1016/j.envpol.2014.12.005
463. Harrill J, Shah I, Setzer RW, Haggard D, Auerbach S, Judson R, et al. Considerations for strategic use of high-throughput transcriptomics chemical screening data in regulatory decisions. Current Opinion in Toxicology. Elsevier B.V.; 2019. pp. 64–75. doi:10.1016/j.cotox.2019.05.004
464. Deng M, Wu Y, Xu C, Jin Y, He X, Wan J, et al. Multiple approaches to assess the effects of F-53B, a Chinese PFOS alternative, on thyroid endocrine disruption at environmentally relevant concentrations. Sci Total Environ. 2018;624: 215–224. doi:10.1016/j.scitotenv.2017.12.101

VIII. Annexes

"[...] Art is I: Science is We"

Claude Bernard

Due to their size, large supplementary tables both from results and discussion sections are linked below to external data files. At least three links are provided for each table to assure the access to the information across time.

VIII.1. Annexes from results section

VIII.1.1. Chapter II, article II

Supplementary Table ST2. Results from DAVID Functional Analysis [a)], FDR≤5%

https://www.dropbox.com/s/z8ikklbi6v7oa41/1-s2.0-S0269749118319948-mmc3.xlsx?dl=0

https://drive.google.com/file/d/1ZH1Hnk7T3LLUCDiORwyTHI7y4csnW118/view?usp=sharing

https://mega.nz/file/tlwBHB6a#-S9yiMhbp1hT7_5Ev1l8VUV-GsLZU5p1mpUjWCTxXdc

VIII.1.2. Chapter II, article IV

Supplementary Table ST2. Summary of the fold-changes regarding the control group, p values and the cluster classification of the determined as differentially expressed genes (DEGs; 3238 genes) by ANOVA-PLS analysis.

https://ars.els-cdn.com/content/image/1-s2.0-S0304389420308700-mmc2.xlsx (ST2)

https://www.dropbox.com/s/xdj1ul0u9projcn/1-s2.0-S0304389420308700-mmc2.xlsx?dl=0 (ST2)

https://drive.google.com/file/d/1Z6RlMJ9f4-DINvb3oox2tIvDzbVDgyKc/view?usp=sharing

https://mega.nz/file/phR2XQlA#zczFWR2F9q-UGxU4PjPsI2rieb_U8p90lVBDJvQoNhQ

Supplementary Table ST3. Summary of the mathematical model chosen for the dose-response pattern of each gene expression, its calculated benchmark dose (BMD) and benchmark dose lower and upper confidence limits (BMDL and BMDU, respectively) used in the transcriptomic point of departure (PoD) analysis.

https://ars.els-cdn.com/content/image/1-s2.0-S0304389420308700-mmc2.xlsx (ST3)

https://www.dropbox.com/s/xdj1ul0u9projcn/1-s2.0-S0304389420308700-mmc2.xlsx?dl=0 (ST3)

https://drive.google.com/file/d/1ebZrk999JWSCOR2ptpVOgtZbl1xBC0Jt/view?usp=sharing

https://mega.nz/file/UpBEyAoL#OfZa80-hqTY4khaao50puB-pw_k20MHNxmLCsMOgUgE

Supplementary Table ST6. Results from DAVID Functional Analysis [a)], FDR≤5%

https://ars.els-cdn.com/content/image/1-s2.0-S0304389420308700-mmc2.xlsx (ST6)

https://www.dropbox.com/s/xdj1ul0u9projcn/1-s2.0-S0304389420308700-mmc2.xlsx?dl=0 (ST6)

https://drive.google.com/file/d/1UMzuWSlA6_t6tAaopU4OJE-Xt8uVIuLH/view?usp=sharing

https://mega.nz/file/Z1REgC5L#wvHeYafwL1Gw6e9ifSrds1H394hFOO6Poo-UafVJtag

VIII.1.3. Chapter IV, article VII

Supplementary table ST3. Raw counts of methylated and no methylated CpGs of samples (control and BPA exposed) and standards. Number of chromosome of each gene are indicated, as well as the position in the genome of each CpG, and its shorcut and amplicon where it was amplified.

https://www.dropbox.com/s/m4h6uftiygvc8ol/Martinez%20et%20al%202020%20BPA%20DNA%20methylation_supplementary%20table%203.xlsx?dl=0

https://drive.google.com/file/d/1Mqs3wnrdNqWGRsiKg4QP_XMvytga9ncC/view?usp=sharing

https://mega.nz/file/gsIkyKTY#NB-G1oKIEqDYy_54lwTUz3UnZQ7pvyqYUXwK4dCArUY

VIII.2. Annexes from discussion section

Annex table 1. Differentially expressed genes (DEGs) of the BPA, PFOS and TBT exposed groups' samples.

https://www.dropbox.com/s/6m8o0hv3hinptwx/Thesis_supp.tables_links.xlsx?dl=0 (DEGs)

https://drive.google.com/file/d/1x5l3rwaIIHFNKNiUiPaVmkj-wke8AD1I/view?usp=sharing

https://mega.nz/file/pI5myaib#JQw0nYVGPKPmmSSdOjCBR7uhle2udDoCe_UQfTQ-gKU

Annex table 2. DAVID functional analysis of the differentially expressed genes (DEGs) classified in clusters A, B and C in the performed partition around medoids (PAM) analysis.

https://www.dropbox.com/s/6m8o0hv3hinptwx/Thesis_supp.tables_links.xlsx?dl=0 (Cluster A, B, C)

https://drive.google.com/file/d/1XmN5n8Fr04RFeaVFtaim6SDL6DtDufp2/view?usp=sharing

https://mega.nz/file/E140SCDY#jSBrrTHMsDV4fFdBB-E10JDN8Qq9R-FfWpLoH3S6RNw

UNIVERSITAT DE BARCELONA

idaea
INSTITUTE OF ENVIRONMENTAL ASSESSMENT AND WATER RESEARCH

EXCELENCIA SEVERO OCHOA

CSIC
CONSEJO SUPERIOR DE INVESTIGACIONES CIENTÍFICAS